NASA Technical Memorandum 100544

AVSCOM
Technical Memorandum 88-B-007

INFLOW MEASUREMENT MADE WITH A LASER VELOCIMETER ON A HELICOPTER MODEL IN FORWARD FLIGHT

Volume IV TAPERED PLANFORM BLADES AT AN ADVANCE RATIO OF 0.15

Susan L. Althoff and Joe W. Elliott
Aerostructures Directorate
USAARTA-AVSCOM
Langley Research Center
Hampton, Virginia

Richard H. Sailey
PRC Kentron Inc.
Aerospace Technologies Division
Hampton, Virginia

April 1988

National Aeronautics and Space Administration

Langley Research Center
Hampton, Virginia 23665-5225

SUMMARY

An experimental investigation was conducted in the 14- by 22-Foot Subsonic Tunnel at NASA Langley Research Center to measure the inflow into a scale model helicopter rotor in forward flight ($\mu_\infty = 0.15$). The measurements were made with a two-component Laser Velocimeter (LV) one chord above the plane formed by the path of the rotor tips (tip path plane). A conditional sampling technique was employed to determine the position of the rotor at the time that each velocity measurement was made so that the azimuthal fluctuations in velocity could be determined. Measurements were made at a total of 146 separate locations in order to clearly define the inflow character. This data is presented herein without analysis. In order to increase the availability of the resulting data, both the mean and azimuthally dependent values are included as part of this report on two 5.25 inch floppy disks in Microsoft Corporation MS-DOS format.

INTRODUCTION

One of the problems confronting the helicopter industry is the lack of detailed information about the velocity fluctuations around and through rotating blades. This information is needed for two reasons: to ensure a more complete understanding of the flowfield environment associated with a thrusting rotor and to provide data for the validation of rapidly emerging computational codes. One explanation for the lack of available data is the absence, until recent years, of a suitable device for making such measurements. Making measurements of the velocity around a system of rotating blades requires an accurate, nonintrusive measurement capability that presents a minimum risk to the systems involved. The Laser Velocimeter (LV), which uses high energy light beams to measure velocities, is ideally suited to this task.

The Laser Velocimeter has been successfully used to measure specific areas and localized phenomena within the rotor disk (refs. 1 through 3). In addition, the hotwire anemometer and pressure probes, both having directional measuring limitations, have been employed in similar programs (refs. 4 and 5). This is, however, the first time that a comprehensive program has been undertaken to map the flow into the complete rotor disk. This investigation has been conducted to measure the flow into a representative rotor system as a function of azimuth using a two-component (streamwise and vertical direction) LV system.

NOTATION

A_0 — constant term in Fourier series of blade feathering (collective) at $r/R = 0.75$, deg

A_1 — coefficient of cosine term in Fourier series of blade feathering, deg

B_1 — coefficient of sine term in Fourier series of blade feathering, deg

C_D — rotor drag coefficient, $D/\rho\, \pi R^2\, V_{tip}^2$

C_Q — rotor torque coefficient, $M_Z/\rho\, \pi R^3\, V_{tip}^2$

C_T — rotor thrust coefficient, $T/\rho\, \pi R^2\, V_{tip}^2$

D — rotor drag, positive to the rear

M_Z — rotor torque, ft/lbf

Q	rotor torque, in-lbf
q	dynamic pressure, lbf/ft^2
r	local radius of the rotor system, ft
R	rotor radius, ft
T	thrust produced by the rotor, lbf
U_∞	tunnel free-stream velocity, positive downstream, ft/sec
U	free-stream component of velocity, positive downstream, ft/sec
u_i	induced component of velocity parallel to the tip path plane (positive flow downstream), ft/sec
v_i	induced component of velocity normal to the tip path plane (positive flow up), ft/sec
V	vertical component of velocity, positive up, ft/sec
V_{tip}	rotor blade tip velocity (ΩR), ft/sec
Greek	
α	angle between rotor disk and free-stream velocity (positive nose up), deg
λ	inflow ratio normal to tip path plane (positive up), $(U_\infty \sin(\alpha) + v_i)/V_{tip}$
λ_i	induced inflow ratio normal to tip path plane (positive up), $(v_i)/V_{tip}$
μ_∞	rotor advance ratio, $U_\infty \cos(\alpha)/V_{tip}$
μ	inflow ratio parallel to tip path plane (positive downstream), $(U_\infty \cos(\alpha) + u_i)/V_{tip}$
μ_i	induced inflow ratio parallel to tip path plane (positive downstream) u_i/V_{tip}
Ω	rotor rotational speed, radians/sec
ψ	rotor azimuth measured from downstream position, positive counterclockwise, as viewed from above, deg
ρ	air density, slugs/ft^3
θ	blade pitch angle at a specific azimuth (positive nose up), deg, $\theta = A_0 - A_1 \cos\psi - B_1 \sin\psi$
$\overline{xx}$	mean value

EXPERIMENTAL APPARATUS

The experimental apparatus used in this investigation included the NASA Langley Research Center 14- by 22-Foot Subsonic Tunnel, the 2-Meter Rotor Test System (2MRTS), and a two-component laser velocimeter system.

The 14- by 22-Foot Subsonic Tunnel is an atmospheric, closed-circuit wind tunnel of conventional design with enhancements for the testing of powered and high-lift configurations (ref. 6). The tunnel is shown in figure 1. When the tunnel is operated in the open configuration, the walls and ceiling of the test section are lifted out of the flow, leaving only a solid floor and a flow collector. In this configuration, the tunnel can be driven to about 170 knots. This investigation was conducted with the tunnel in the open configuration to allow complete optical access to the rotor flowfield.

The 2MRTS is a general purpose rotorcraft model testing system which was mounted on a strut in the forward part of the test section (see fig. 2). The system consists of a 29-horsepower electric drive motor and 90° speed-reducing transmission, a blade pitch remote control system, and two six-component strain gage balances used for measuring forces and moments on the rotor system and fuselage shell. The four-bladed rotor hub is fully articulated with viscous dampers for lead-lag motion and coincident flap and lag hinges. A more detailed description of the 2MRTS can be found in reference 7. The fuselage which was used for this test was a generic high-speed helicopter configuration. The characteristics of the tapered rotor blades used during this investigation can be found in table 1. The rotor blade planform is shown in figure 3. No attempt was made to dynamically scale the rotor blades; rather, they were very rigid to provide a general research capability.

The LV system used in this investigation was designed to measure the instantaneous components of velocity in the longitudinal (free stream) and vertical directions. The LV system is described in reference 8. The system is comprised of four subsystems: optics, traverse, data acquisition, and seeding. The optics subsystem, which is shown in figure 4, operates in backscatter mode and at high power (4 watts in all lines) in order to accommodate the long focal lengths needed to scan the wide test section. The transmitting and receiving optics packages are augmented by a zoom lens system consisting of a 3-in. clear aperture negative lens and a 12-in. clear aperture positive lens. Bragg cells in each of the optical paths provide a directional measurement capability. The velocity measurements are made at a point in space where the four beams cross, called the sample volume. The length of the sample volume (transverse to the flow direction) increases as the sample volume is moved away from the optics assembly. The sample volume length, over the 10- to 20-foot focal length of the system, is less than 1 cm and has a constant diameter of 0.2 mm.

The traverse subsystem provides five degrees of freedom in positioning the sample volume and is controlled by the same computer that is used for data acquisition. Translation of the sample volume in the horizontal and vertical direction is accomplished by displacing the entire optics platform. Translation along the lateral axes is accomplished by displacing the negative lens located in the zoom lens assembly, thus refocusing the sample volume along the axes of optical transmission. The other two degrees of freedom, pan and tilt, are implemented by rotating the final mirror about its vertical and horizontal axes in order to change the direction of optical transmission. The total range of the traversing system is 7 ft vertically, 6 ft streamwise, 16.5 ft laterally, and 10° in both pan and tilt. Measurements can be made outside of this envelope by repositioning the optics platform, which is mounted on wheels to facilitate such relocations. For this study the traversing system was positioned to the left of the test section when looking downstream as shown in figure 5.

The data acquisition subsystem is shown schematically in figure 6 and interfaces with the optical signal processing equipment to receive two channels of raw LV data and up to five channels of auxiliary data. In this investigation, four of the auxiliary channels were used for the acquisition of data relative to blade position. Two of the channels (one each for the U and V components) measured the azimuthal position of the rotor shaft and the other two measured the lead/lag and flapping motion. The system converts the raw LV data to engineering units and determines the statistical characteristics of the acquired data so that the test results can be evaluated during the acquisition process. The raw data, the data which have been converted to engineering units, and 64 parameters from the tunnel static data acquisition system are written to magnetic tape for later analysis. The final function performed by the data system is to control the five degree-of-freedom scan system.

The seeding subsystem, shown schematically in figure 7, is a solid particle, liquid dispensing system (ref. 9). Polystyrene latex microspheres are suspended in a mixture containing, by volume, 50 percent water and 50 percent ethyl alcohol. The advantages of the polystyrene particles are their low density, high reflectivity, and precise particle size. The particles used in this investigation were 1.7 microns in diameter with a standard deviation of 0.0239 microns. The particle mixture is pumped to an array of 32 nozzles where compressed air is used to atomize the mixture. These nozzles are mounted on a frame 8 feet wide by 6 feet high which is suspended on cables in the settling chamber of the tunnel. The low vapor pressure of water/alcohol mixture allows it to evaporate as it travels the 85 feet from the settling chamber to the test section. This process provides isolated single particles in the flowfield whose velocities are measured as they pass through the sample volume. The local fluid velocity is inferred from the seed particle velocity.

ERROR ANALYSIS

The overall LV system error is obtained by summing the error of all of the components that contribute to an error in the velocity measurement. The error sources are summarized in the table below, and are defined in references 10 and 11. The resulting total bias error of -0.81 to 1.82 percent is obtained by adding the percents contributed by each error source. The total random error of 1.12 percent is obtained by taking the square root of the sum of the squared percents of the random sources. Taking the square root of the sum of the squares of the random and bias errors gives a total system error of 1.38 percent to 2.14 percent.

Error source	Bias error	Random error
Cross beam angle measurement	±0.81	N/A
Diverging fringes	A	A
Time jitter	N/A	N/A
Clock synchronization	0.51	±0.51
Quantization	A	±1.00
Velocity bias	B	B
Bragg bias	B	B
Velocity gradient	B	B
Particle lag	±0.50	B
Total error	-0.81 to 1.82	1.12

A Not measured
B Negligible
N/A Not applicable

TEST PROCEDURES

In all cases, measurements were made at azimuthal increments of 30° from $\psi = 0$, at 3.0 in. (approximately one chord) above the plane formed by the tips of the blades. Measurements were made from a radial location of $r/R = 0.4$ to $r/R = 1.1$, with the majority of the measurement locations concentrated toward the outboard portion of the disk. Figure 8 shows the measurement locations superimposed on the rotor disk. During the test, the rotor tip path plane was maintained at -3° relative to the free stream by zeroing the blade flapping relative to the shaft and setting the shaft angle to -3°. The operating tip speed for the test was held at 624 ft/sec (2200 rpm), the nominal tunnel speed was 94 ft/sec ($\mu_\infty = 0.15$), and the nominal rotor thrust coefficient was 0.0064. Table 2 lists the nominal test conditions and selected test parameters. The LV data acquisition process consisted of placing the sample volume at the measurement location and acquiring data for a period of 1 minute or until 4096 velocity measurements were made in either the longitudinal or the vertical component. During this process, conditional sampling techniques were employed to permanently associate each measured velocity with the location of the rotor blades at the time when the measurement was made. At the conclusion of the process, the measurement location was changed and the acquisition process was repeated.

DATA REDUCTION

Independent velocity measurements in the free stream and vertical direction were made at each measurement location. At the same instant in time that a velocity measurement was made, the location of the blades was recorded for that velocity component. The maximum time required to acquire these data was 1 minute (2200 rotor revolutions for this test) and the minimum approximately 20 sec. These data, collected over many revolutions, were sorted into 128 equally spaced azimuth segments (2.81° wide) that are representative of blade position and include corrections for blade lead/lag motion. The velocity value assigned to each interval at a measurement location is the arithmetic mean of all the measurements that were taken in the respective 2.81° wide azimuthal range. The results of this sorting process provide the azimuthally dependent velocity data. The "mean velocity" value refers to the velocity calculated from the arithmetic mean of all the measurements made at a single measurement location.

EXPERIMENTAL RESULTS

Table 3 lists the measurement locations, the mean and standard deviation of the two components of induced inflow velocity, and the number of measurements in each of the measured components (U and V). In figure 9 the mean longitudinal induced component of velocity, μ_i, with a band of ± one standard deviation is plotted vs. blade radius for each radial scan. The standard deviation represents the fluctuation in velocity at a given measurement location; it is not an indication of the error in the mean measurements. The size of the symbols used for plotting the mean velocity values is an approximation of the calculated error in the measurements. Figure 10 presents in the same format the mean normal induced component of velocity, λ_i. The same data without the ± one standard deviation is presented in a contour plot format in figures 11 and 12 in order to show more clearly the interactions over the whole disk (viewed from above). The format of each of the figures (13 through 158) is the induced velocity vs. azimuth at the top of the figure, the number of measurements that went into determining the velocity value for each azimuth segment in the center, and an order ratio analysis of the azimuthal variation at the bottom of the figure.

The figure numbers for the azimuthal and radial measurement locations are indicated below.

Azimuth / r/R	0	30	60	90	120	150	180	210	240	270	300	330
0.40	--	23	36	--	59	72	84	97	109	122	133	146
0.50	13	24	37	47	60	73	85	98	110	123	134	147
0.60	14	25	38	48	61	74	86	99	111	124	135	148
0.70	15	26	39	49	62	75	87	--	112	125	136	149
0.74	16	27	40	50	63	76	88	100	113	126	137	150
0.78	17	28	41	51	64	77	89	101	114	127	138	151
0.82	18	29	42	52	65	78	90	102	115	128	139	152
0.86	19	30	43	53	66	79	91	103	116	129	140	153
0.90	20	31	44	54	67	80	92	104	117	130	141	154
0.94	21	32	45	55	68	81	93	105	118	131	142	155
0.98	22	33	--	56	69	82	94	106	119	132	143	156
1.04	--	34	--	57	70	83	95	107	120	--	144	157
1.10	--	35	46	58	71	--	96	108	121	--	145	158

The mean and standard deviation of the induced inflow velocities (table 3) and the azimuthally dependent induced inflow velocities (figs. 13 through 158) are included on 5.25 flexible disk in the pocket on the inside of the rear cover of this report. The details of the data format and the file structure are located in the file "README.DOC". The disk format is 360 kbyte double-sided, written using the Microsoft Corporation MS-DOS operating system.

CONCLUDING REMARKS

The Laser Velocimeter provides an effective system for making measurements in the dynamic environment associated with rotor blades. It has been used on numerous occasions to measure the localized flow phenomena encountered in such flows. This investigation demonstrates the use of a matured LV system to map the flow into a representative rotor in forward flight by making velocity measurements at 146 locations above the rotor disk. These measurements provide both the mean and azimuthally dependent velocity values, and they provide a detailed look at the nature of this flow.

REFERENCES

1. Landgrebe, A. J.; and Johnson, B. V.: Measurement of Model Helicopter Rotor Flow Velocities With a Laser Doppler Velocimeter. American Helicopter Society Journal, Vol. 19, July 1974, pp. 39-43.

2. Biggers, J. C.; and Orloff, K. L.: Laser Velocimeter Measurements of the Helicopter Rotor-Induced Flowfield. American Helicopter Society, Annual National V/STOL Forum, 30th, Washington, D.C., May 7-9, 1974.

3. Owen, F. K.; and Taubert, M. E.: Measurement and Prediction of Model-Rotor Flowfields. AIAA 18th Fluid Dynamics, Plasmadynamics and Laser Conference, Cincinnati, Ohio, July 16-18, 1985.

4. Tangler, J. L.; Wohlfeld, R. M.; and Miley, S. J.: An Experimental Investigation of Vortex Stability, Tip Shapes, Compressibility and Noise for Hovering Models. NASA CR-2305, September 1973.

5. Junker, B.: Investigations of Blade-Vortices in the Rotor Downwash. Twelfth European Rotorcraft Forum, Garmish-Partenkirchen, Federal Republic of Germany, September 22-25, 1986.

6. Applin, Z. T.: Flow Improvements in the Circuit of the Langley 4- by 7-Meter Tunnel. NASA TM-85662, December 1983.

7. Phelps, A. E., III; and Berry, J. D.: Description of the U.S. Army 2-Meter Rotor Test System. NASA TM-87762, AVSCOM TM 86-B-4, January 1987.

8. Sellers, W. L.; and Elliott, J. W.: Applications of a Laser Velocimeter in the Langley 4- by 7-Meter Tunnel. Proceedings of the Workshop on Flow Visualization and Laser Velocimetry for Wind Tunnels. NASA CP-2243, March 1982, pp. 283-293.

9. Elliott, J. E.; and Nichols, C. E.: Seeding Systems for Use With a Laser Velocimeter in Large Scale Wind Tunnels. Proceedings of the Workshop on Wind Tunnel Seeding Systems for Laser Velocimeters, NASA CP-2393, March 1985, pp. 93-103.

10. Young, W. H.; Meyers, J. F.; and Hepner, T. E.: Laser Velocimeter Systems Analysis to a Flow Survey Above a Stalled Wing. NASA TN D-8408, August 1977.

11. Dring, R. P.: Sizing Criteria for Laser Anemometry Particles. Journal of Fluid Engineering, Vol. 104, March 1982, pp. 15-17.

TABLE 1.- 2MRTS ROTOR AND BLADE CHARACTERISTICS

Hub type	Fully articulated
Number of blades	4
Airfoil section	NACA 0012
Hinge offset, in., r/R	2.00,0.06
Root cutout, in., r/R	8.25,0.24
Pitch-flap coupling angle, deg	0.0
Twist linear, deg	-13.0
Radius, R, in.	32.50
Rotor solidity, bc/πR	0.0977
Blade stiffness	
Flapwise, lb-in	13000
Torsional, lb-in	12750
Blade weight, grams	222.0
Lead/lag damping, in-lb/deg/sec	182.4

TABLE 2.- NOMINAL ROTOR CONTROL AND PERFORMANCE PARAMETERS

C_T	0.0064
C_Q	0.000369
C_D	0.00
α, deg	-3.04
Coning, deg	1.5
AO, deg	6.26
A_1, deg	-2.08
B_1, deg	1.96
μ_∞	0.15
U, ft/sec	94.1
V_{tip}, ft/sec	624.0
Lag, deg	0.95

TABLE 3.- INFLOW VELOCITY SUMMARY

		μ_1			λ_1		
ψ	r/R	Mean	Standard deviation	# measurements	Mean	Standard deviation	# measurements
0	.50	.0226	.0086	765	-.0418	.0092	1181
0	.60	.0178	.0076	778	-.0473	.0096	1085
0	.60	.0179	.0128	815	-.0519	.0104	1067
0	.70	.0122	.0097	813	-.0554	.0106	1006
0	.74	.0108	.0102	727	-.0562	.0104	892
0	.78	.0086	.0102	849	-.0584	.0102	1015
0	.82	.0056	.0098	741	-.0583	.0105	943
0	.86	.0041	.0083	373	-.0569	.0090	430
0	.90	.0002	.0098	345	-.0579	.0088	367
0	.94	-.0001	.0092	263	-.0579	.0074	299
0	.98	-.0022	.0111	172	-.0573	.0075	205
30	.40	.0282	.0121	309	-.0385	.0106	384
30	.50	.0229	.0111	445	-.0479	.0117	544
30	.50	.0238	.0111	450	-.0488	.0121	558
30	.60	.0186	.0109	197	-.0564	.0118	208
30	.70	.0121	.0103	317	-.0594	.0115	321
30	.74	.0095	.0104	273	-.0580	.0119	281
30	.78	.0072	.0105	385	-.0601	.0106	393
30	.82	.0067	.0106	386	-.0585	.0101	404
30	.86	.0031	.0093	461	-.0592	.0085	490
30	.90	.0005	.0100	493	-.0585	.0072	491
30	.94	0.0000	.0082	389	-.0577	.0056	388
30	.98	-.0013	.0093	454	-.0568	.0060	501
30	1.04	-.0053	.0086	322	-.0541	.0054	400
30	1.10	-.0050	.0084	252	-.0518	.0043	311
60	.40	.0236	.0161	425	-.0356	.0087	546
60	.50	.0245	.0128	430	-.0404	.0083	608
60	.60	.0198	.0130	602	-.0406	.0069	844
60	.70	.0179	.0106	499	-.0414	.0070	703
60	.74	.0150	.0098	399	-.0403	.0067	554
60	.78	.0149	.0135	397	-.0419	.0062	441
60	.82	.0132	.0107	256	-.0417	.0068	371
60	.86	.0125	.0081	294	-.0406	.0065	442
60	.90	.0112	.0091	204	-.0350	.0076	338
60	.94	.0095	.0073	168	-.0323	.0068	254
60	1.10	.0014	.0085	541	.0644	.0055	696
90	.50	.0234	.0098	120	-.0286	.0084	213
90	.60	.0284	.0142	233	-.0263	.0071	315
90	.70	.0261	.0133	325	-.0204	.0087	471
90	.74	.0260	.0110	431	-.0173	.0087	677
90	.78	.0242	.0121	513	-.0121	.0072	825
90	.82	.0221	.0122	711	-.0029	.0110	1222
90	.86	.0183	.0097	803	.0044	.0095	1454
90	.90	.0154	.0118	658	.0138	.0069	1007
90	.94	.0132	.0115	706	.0285	.0094	1298

TABLE 3.- Continued

ψ	r/R	μ_1 Mean	μ_1 Standard deviation	μ_1 # measurements	λ_1 Mean	λ_1 Standard deviation	λ_1 # measurements
90	.98	.0065	.0106	852	.0296	.0053	1482
90	1.04	.0029	.0101	741	.0226	.0055	1293
90	1.10	-.0006	.0094	917	.0181	.0048	1521
120	.40	.0247	.0141	275	-.0211	.0079	391
120	.50	.0268	.0126	203	-.0155	.0077	296
120	.60	.0260	.0120	240	-.0064	.0082	341
120	.70	.0210	.0148	453	.0046	.0085	620
120	.74	.0183	.0100	377	.0084	.0075	597
120	.78	.0169	.0190	404	.0119	.0063	533
120	.82	.0151	.0139	369	.0143	.0051	512
120	.86	.0127	.0113	341	.0163	.0064	527
120	.90	.0050	.0122	387	.0175	.0058	609
120	.94	.0012	.0098	398	.0162	.0048	599
120	.98	.0002	.0120	484	.0141	.0050	765
120	1.04	-.0005	.0103	451	.0113	.0048	777
120	1.10	-.0018	.0114	542	.0090	.0047	807
150	.40	.0222	.0125	206	-.0127	.0074	323
150	.50	.0232	.0135	323	-.0068	.0069	433
150	.60	.0239	.0143	329	.0015	.0098	511
150	.70	.0226	.0140	333	.0086	.0050	470
150	.74	.0146	.0120	300	.0114	.0059	491
150	.78	.0151	.0147	235	.0137	.0061	359
150	.82	.0125	.0162	313	.0138	.0064	449
150	.86	.0099	.0111	175	.0144	.0052	345
150	.90	.0077	.0119	143	.0126	.0044	242
150	.94	.0057	.0175	294	.0116	.0045	428
150	.98	.0020	.0130	226	.0113	.0049	393
150	1.04	.0028	.0144	137	.0083	.0046	226
180	.40	.0169	.0062	482	-.0138	.0088	438
180	.50	.0195	.0062	510	-.0093	.0085	450
180	.60	.0198	.0066	488	-.0026	.0103	438
180	.70	.0183	.0069	509	.0068	.0086	472
180	.74	.0151	.0065	419	.0086	.0087	411
180	.78	.0134	.0070	721	.0117	.0091	728
180	.82	.0118	.0069	975	.0125	.0080	933
180	.86	.0076	.0070	1024	.0133	.0074	992
180	.90	.0047	.0072	644	.0131	.0068	596
180	.94	.0025	.0066	370	.0128	.0066	361
180	.98	.0032	.0062	1913	.0124	.0065	1822
180	1.04	-.0006	.0057	2271	.0111	.0063	2094
180	1.10	-.0004	.0052	2110	.0089	.0067	2009
210	.40	.0152	.0068	621	-.0152	.0076	518
210	.50	.0194	.0073	388	-.0133	.0097	358
210	.60	.0195	.0077	266	-.0065	.0112	244
210	.74	.0201	.0066	779	.0043	.0085	677

TABLE 3.- Continued

ψ	r/R	μ_1 Mean	μ_1 Standard deviation	μ_1 # measurements	λ_1 Mean	λ_1 Standard deviation	λ_1 # measurements
210	.78	.0186	.0072	1043	.0070	.0108	1001
210	.82	.0167	.0077	1063	.0101	.0104	1000
210	.86	.0135	.0082	1163	.0108	.0096	1116
210	.90	.0096	.0079	1202	.0121	.0085	1147
210	.94	.0068	.0075	1280	.0127	.0077	1205
210	.98	.0055	.0071	1137	.0122	.0064	1024
210	1.04	.0026	.0062	956	.0101	.0072	903
210	1.10	-.0003	.0064	1310	.0083	.0073	1198
240	.40	.0122	.0090	219	-.0178	.0058	328
240	.50	.0123	.0098	816	-.0189	.0070	1053
240	.60	.0150	.0111	814	-.0164	.0090	1070
240	.70	.0142	.0123	702	-.0103	.0107	894
240	.74	.0156	.0115	772	-.0068	.0099	993
240	.78	.0161	.0109	782	-.0040	.0100	964
240	.82	.0174	.0101	945	.0011	.0086	1167
240	.86	.0163	.0112	1026	.0066	.0104	1242
240	.90	.0148	.0106	1058	.0096	.0091	1250
240	.94	.0113	.0103	992	.0120	.0073	1167
240	.98	.0091	.0090	803	.0133	.0057	982
240	1.04	.0060	.0074	443	.0131	.0043	505
240	1.10	.0022	.0087	170	.0111	.0041	198
270	.40	.0112	.0089	744	-.0168	.0048	903
270	.50	.0133	.0103	880	-.0212	.0064	1043
270	.60	.0136	.0102	580	-.0229	.0069	709
270	.70	.0147	.0099	1033	-.0240	.0080	1267
270	.74	.0137	.0109	948	-.0232	.0080	1165
270	.78	.0133	.0095	807	-.0215	.0086	1034
270	.82	.0141	.0103	708	-.0190	.0086	877
270	.86	.0145	.0100	556	-.0156	.0077	665
270	.90	.0135	.0084	308	-.0093	.0077	383
270	.94	.0110	.0072	227	-.0013	.0067	286
270	.98	.0100	.0070	200	.0073	.0062	249
300	.40	.0183	.0093	537	-.0152	.0064	678
300	.50	.0175	.0089	832	-.0220	.0064	1031
300	.60	.0157	.0093	252	-.0273	.0074	294
300	.70	.0136	.0094	1387	-.0328	.0081	1741
300	.74	.0145	.0089	1086	-.0343	.0082	1399
300	.78	.0120	.0094	814	-.0358	.0081	1005
300	.82	.0101	.0089	704	-.0377	.0084	852
300	.86	.0102	.0092	465	-.0375	.0072	588
300	.90	.0084	.0088	279	-.0378	.0069	359
300	.94	.0058	.0097	192	-.0362	.0065	249
300	.98	.0038	.0088	113	-.0347	.0060	160
300	1.02	.0003	.0103	73	-.0236	.0076	99
300	1.10	-.0013	.0092	130	.0060	.0068	156
330	.40	.0220	.0077	769	-.0221	.0075	1184

TABLE 3.- Concluded

		μ_1			λ_1		
ψ	r/R	Mean	Standard deviation	# measurements	Mean	Standard deviation	# measurements
330	.50	.0203	.0072	616	-.0268	.0076	833
330	.60	.0175	.0084	396	-.0320	.0087	514
330	.70	.0149	.0079	330	-.0375	.0091	425
330	.74	.0127	.0073	264	-.0390	.0086	313
330	.78	.0094	.0072	139	-.0411	.0090	172
330	.82	.0081	.0068	424	-.0428	.0079	523
330	.86	.0074	.0077	246	-.0438	.0079	293
330	.90	.0050	.0078	241	-.0443	.0069	304
330	.94	.0034	.0068	257	-.0448	.0059	346
330	.98	.0010	.0076	288	-.0444	.0053	334
330	1.04	-.0018	.0076	331	-.0424	.0042	378
330	1.10	-.0039	.0075	425	-.0402	.0044	495

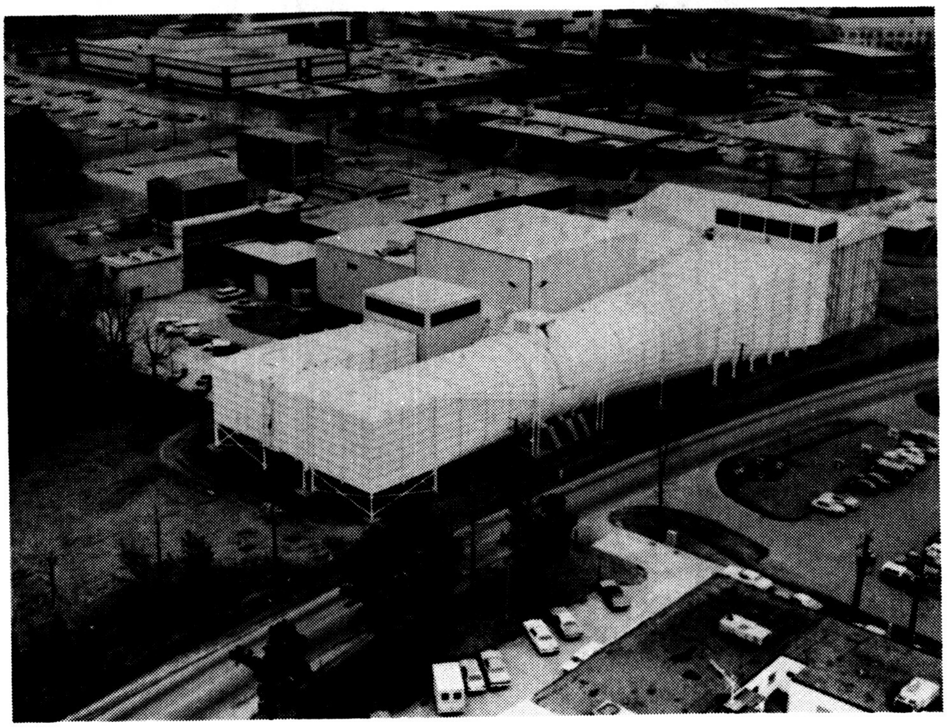

(a) Aerial view

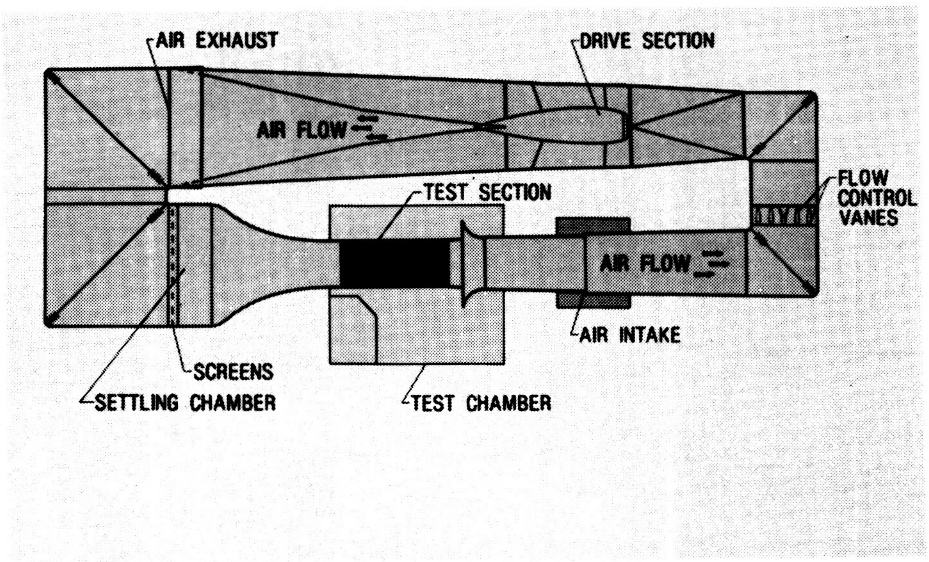

(b) Schematic

Figure 1.- 14 × 22 Foot Subsonic Tunnel.

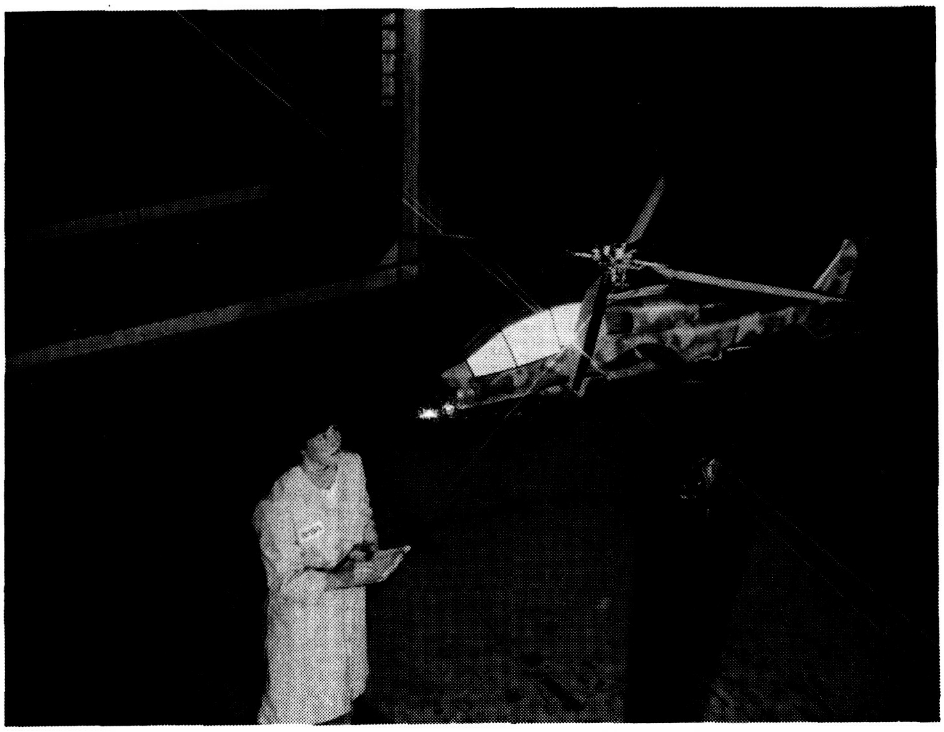

Figure 2.- 2MRTS mounted in forward bay of the test section using generic high-speed fuselage.

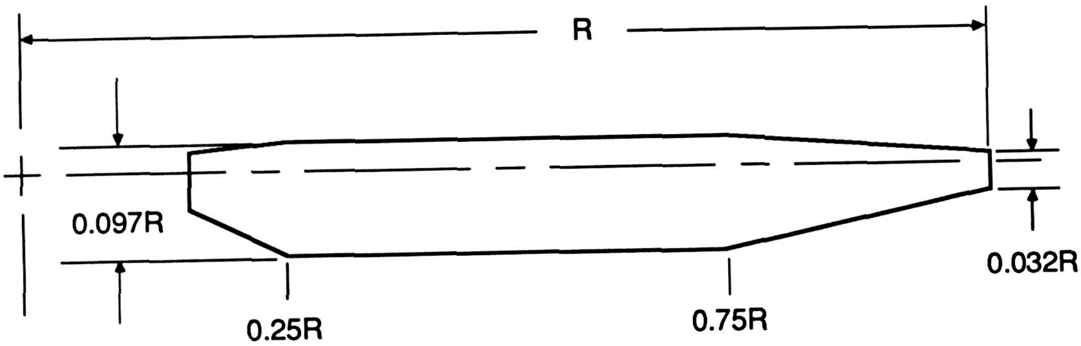

Figure 3.- Rotor blade planform. R = 32.5 inches.

ORIGINAL PAGE IS
OF POOR QUALITY

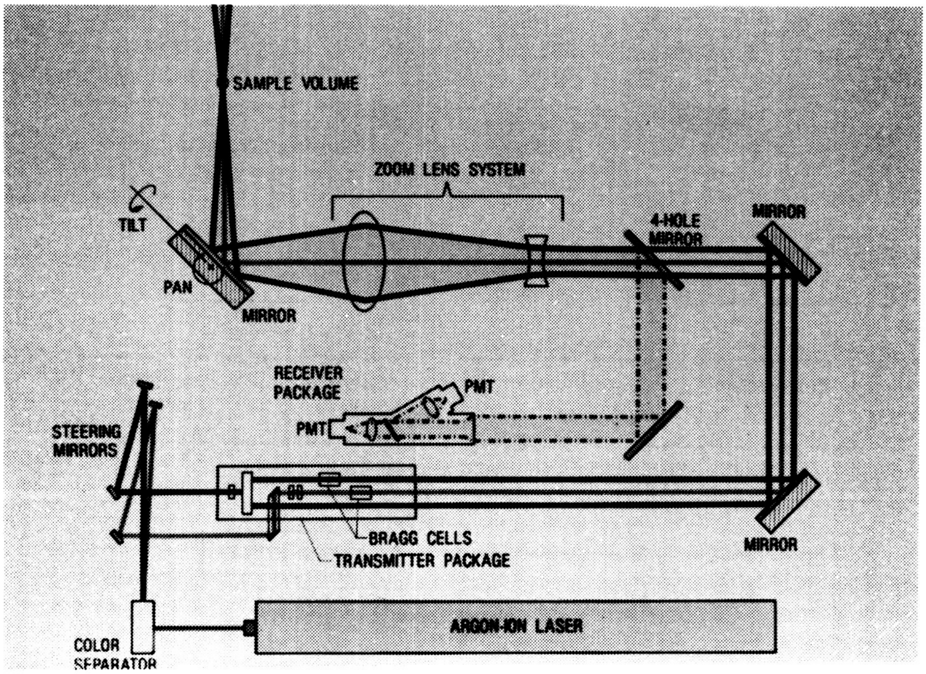

Figure 4.- Schematic diagram of Laser Velocimeter Optics Subsystem.

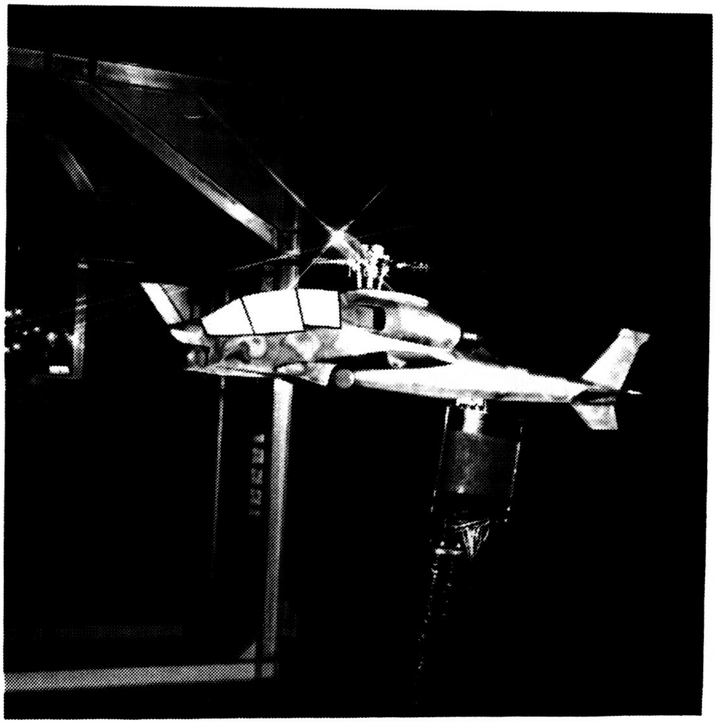

Figure 5.- Laser Velocimeter positioned in test chamber. 2MRTS with generic high speed fuselage

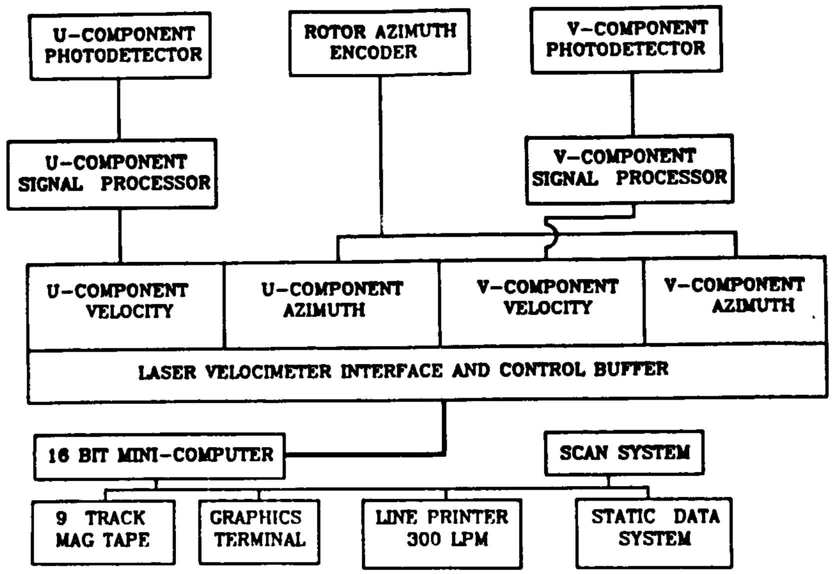

Figure 6.- Schematic view of data aquisition and control subsystem.

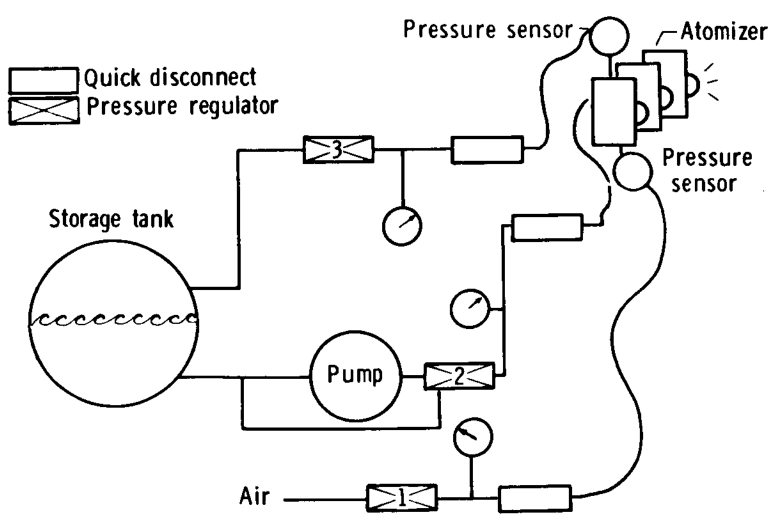

Figure 7.- Schematic of Seeding system.

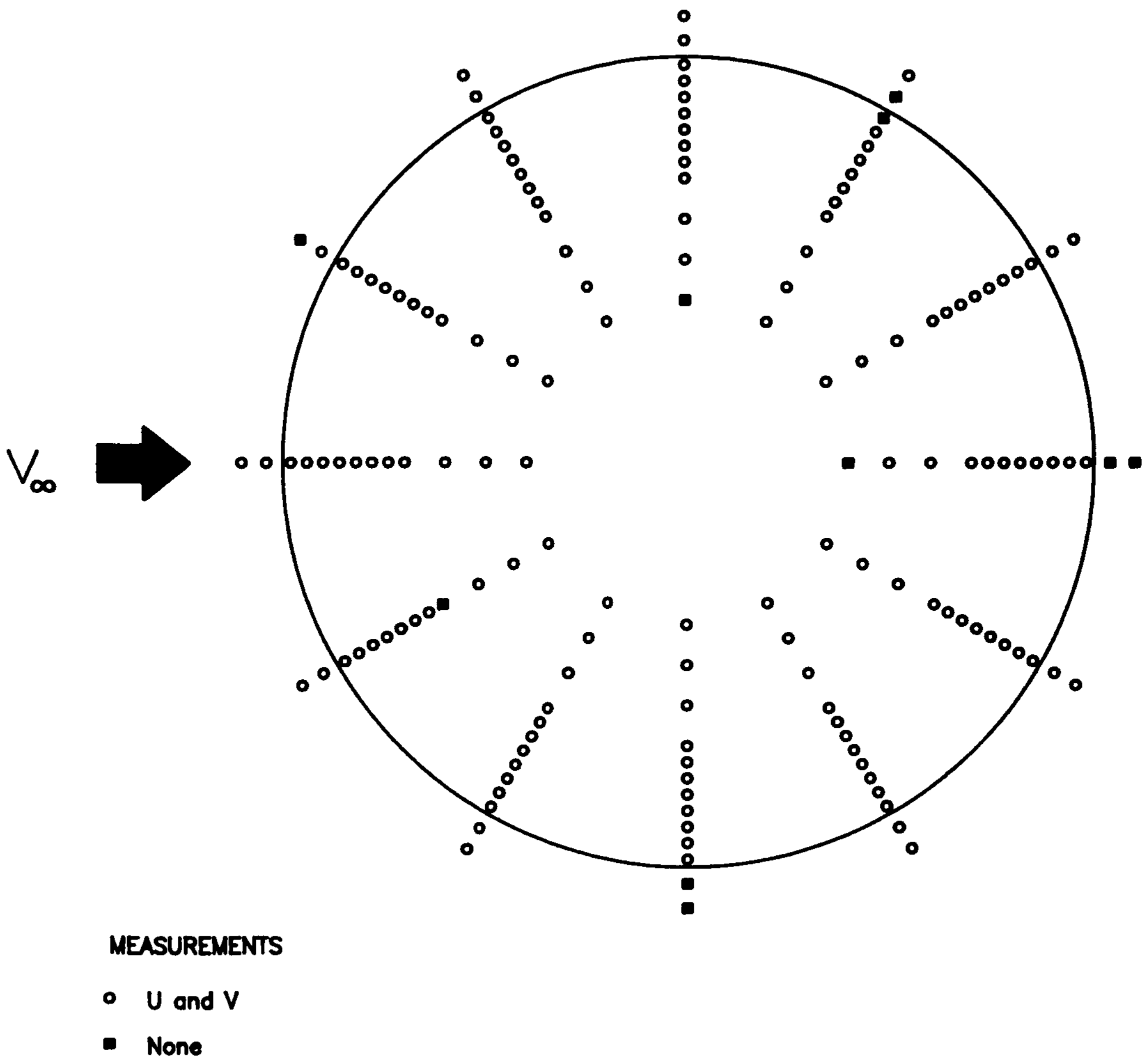

Figure 8.– Locations of velocity measurements, 3.0 inches above rotor tip path plane.

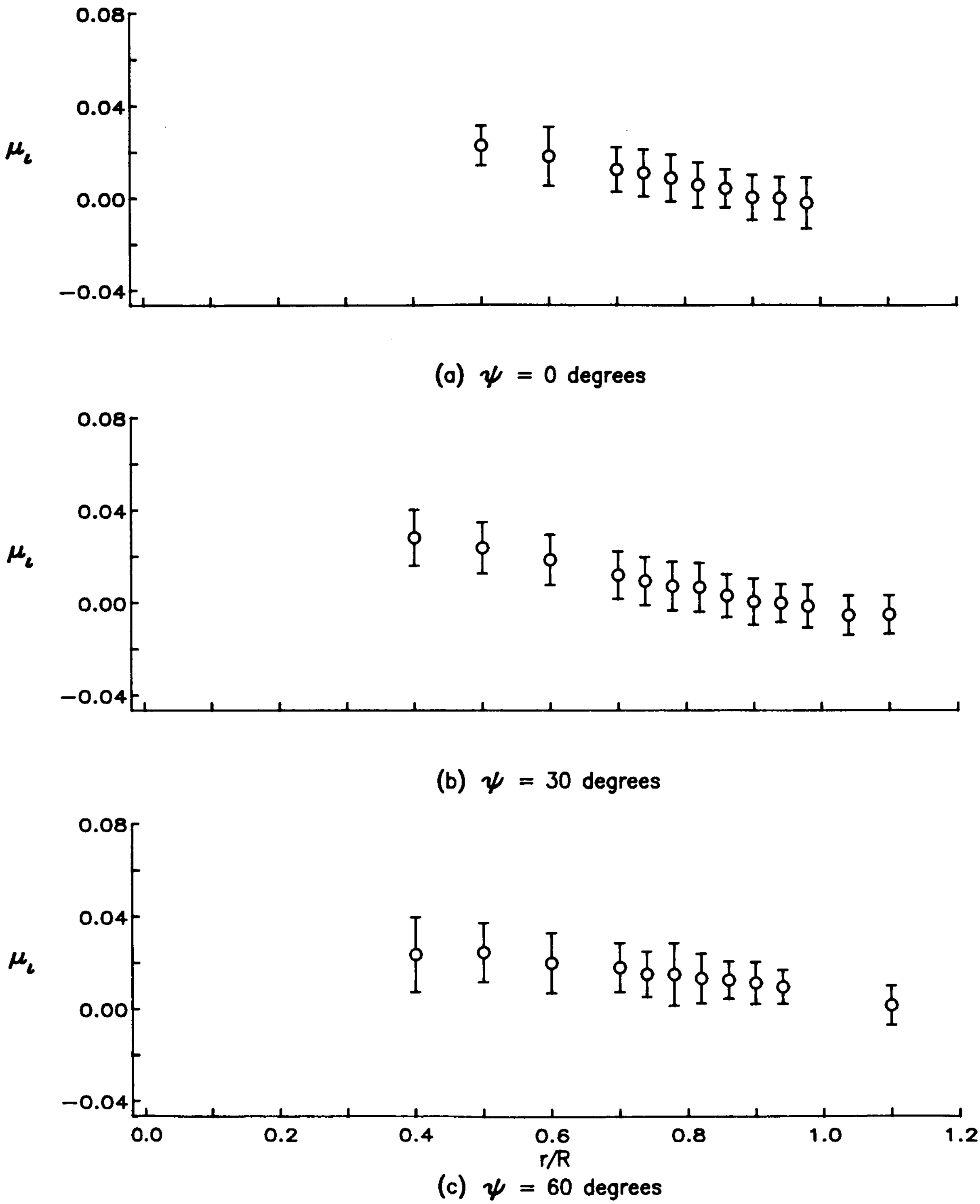

Figure 9.– Radial distribution of mean induced inflow ratio (μ_i).

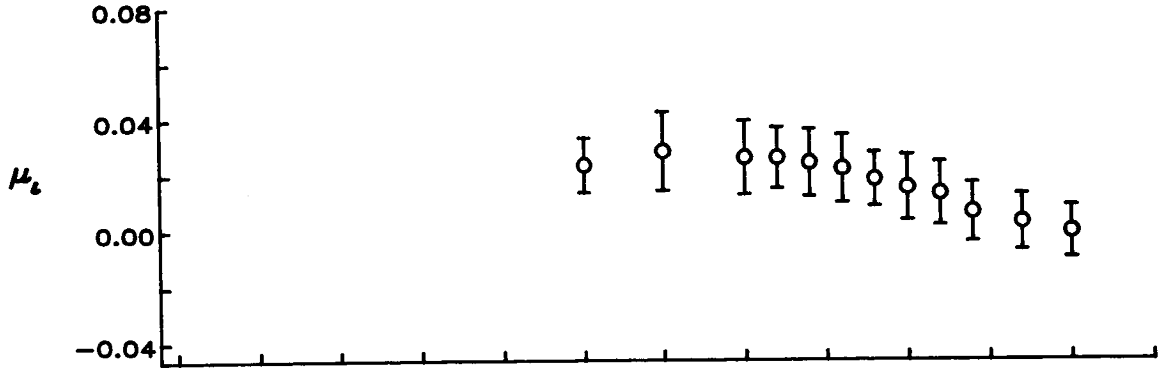

(d) ψ = 90 degrees

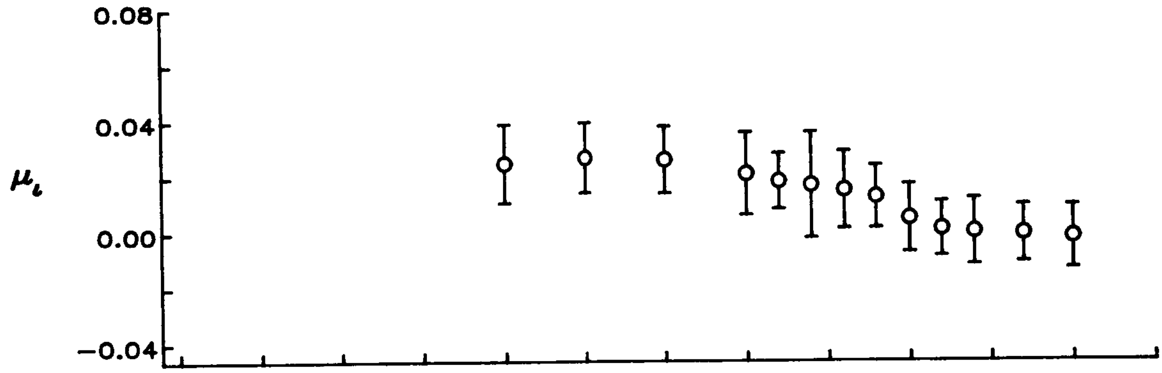

(e) ψ = 120 degrees

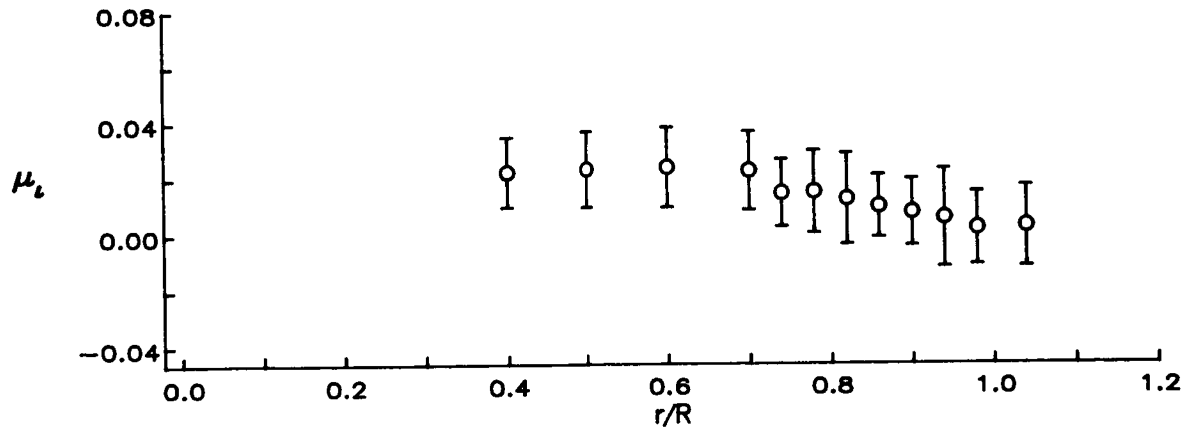

(f) ψ = 150 degrees

Figure 9.– Continued.

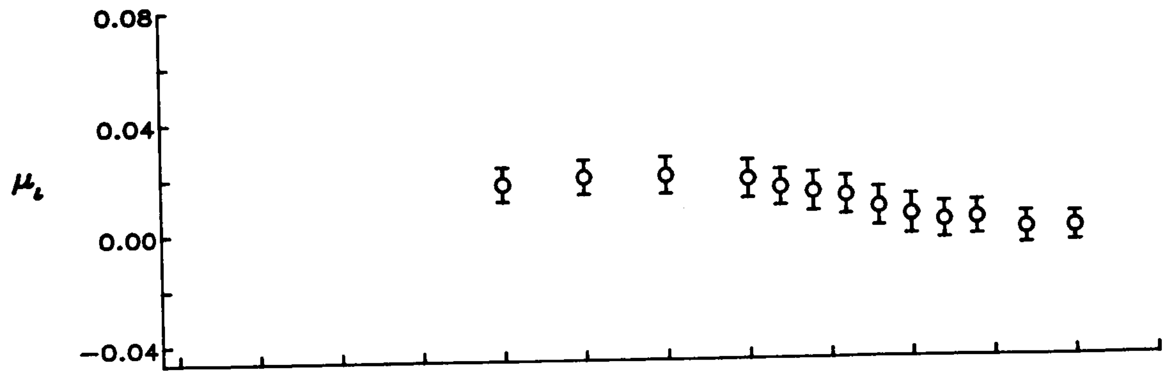

(g) ψ = 180 degrees

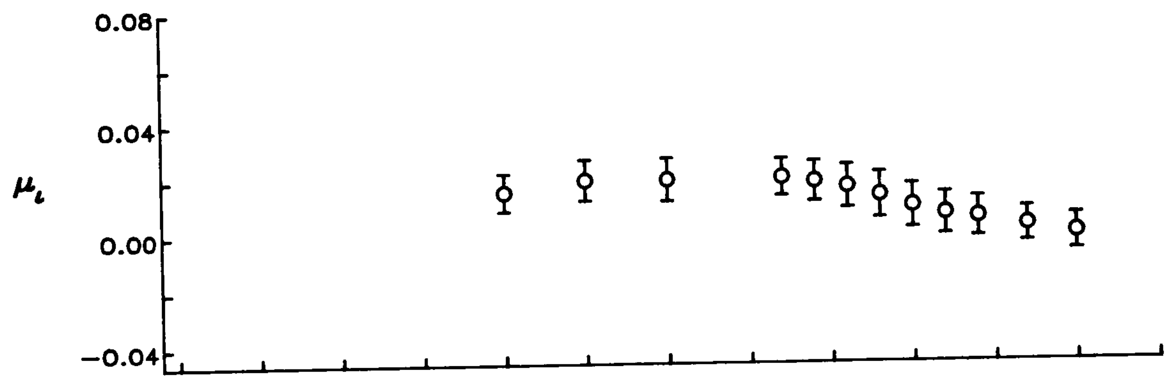

(h) ψ = 210 degrees

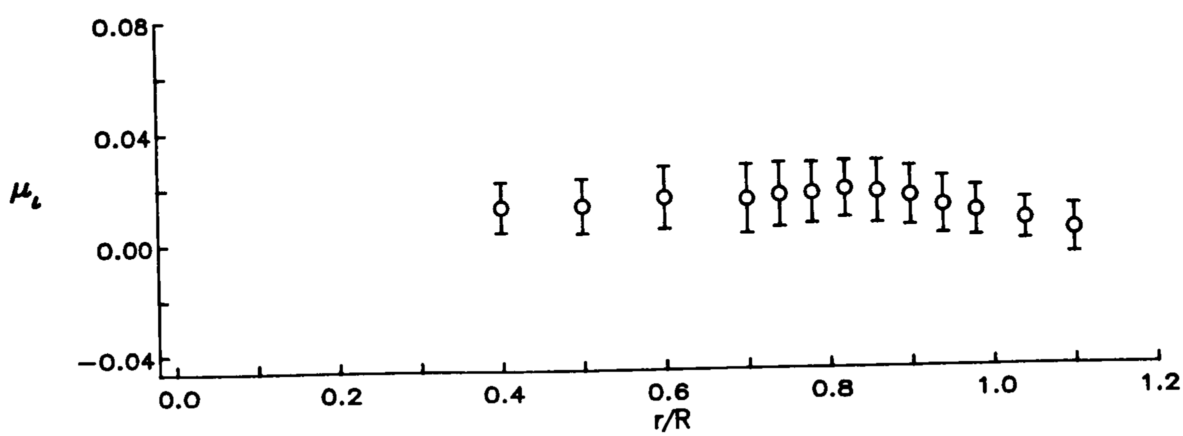

(i) ψ = 240 degrees

Figure 9.– Continued.

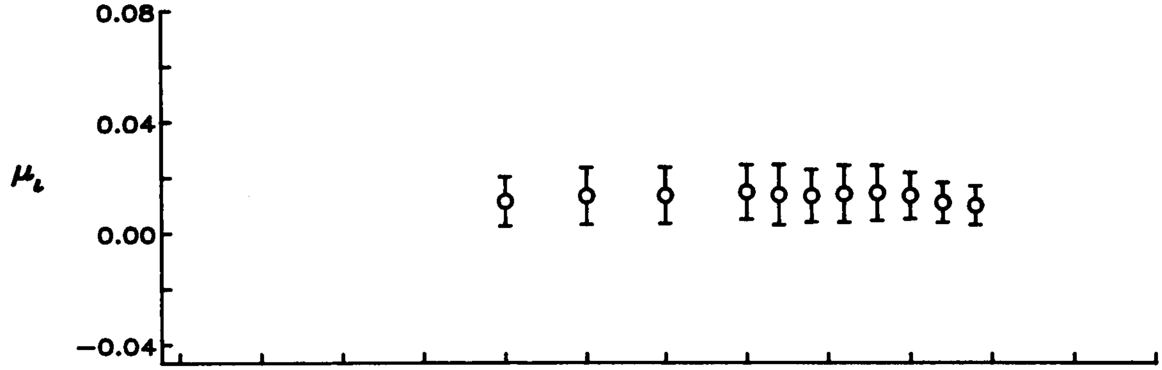

(j) ψ = 270 degrees

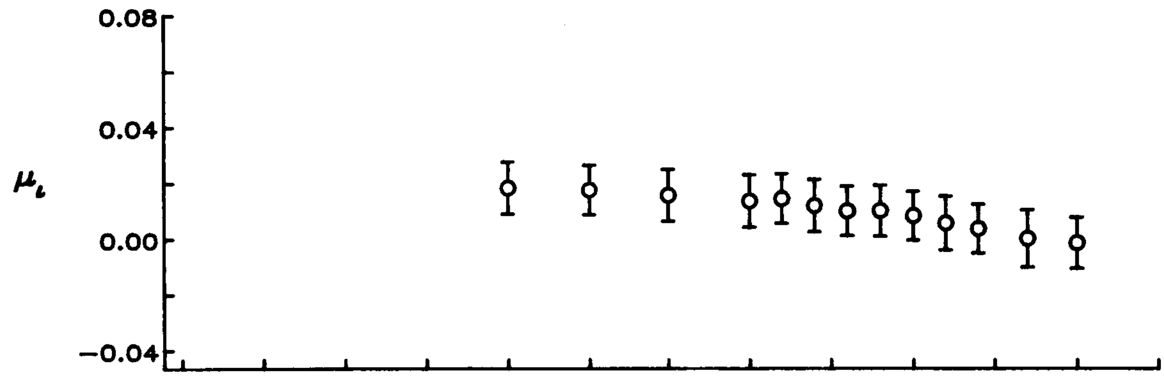

(k) ψ = 300 degrees.

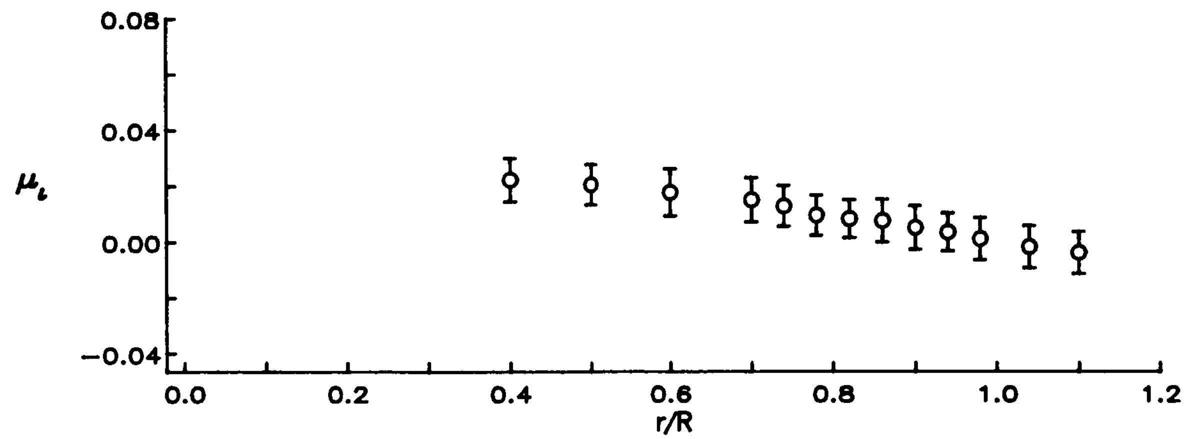

(l) ψ = 330 degrees

Figure 9.– Concluded.

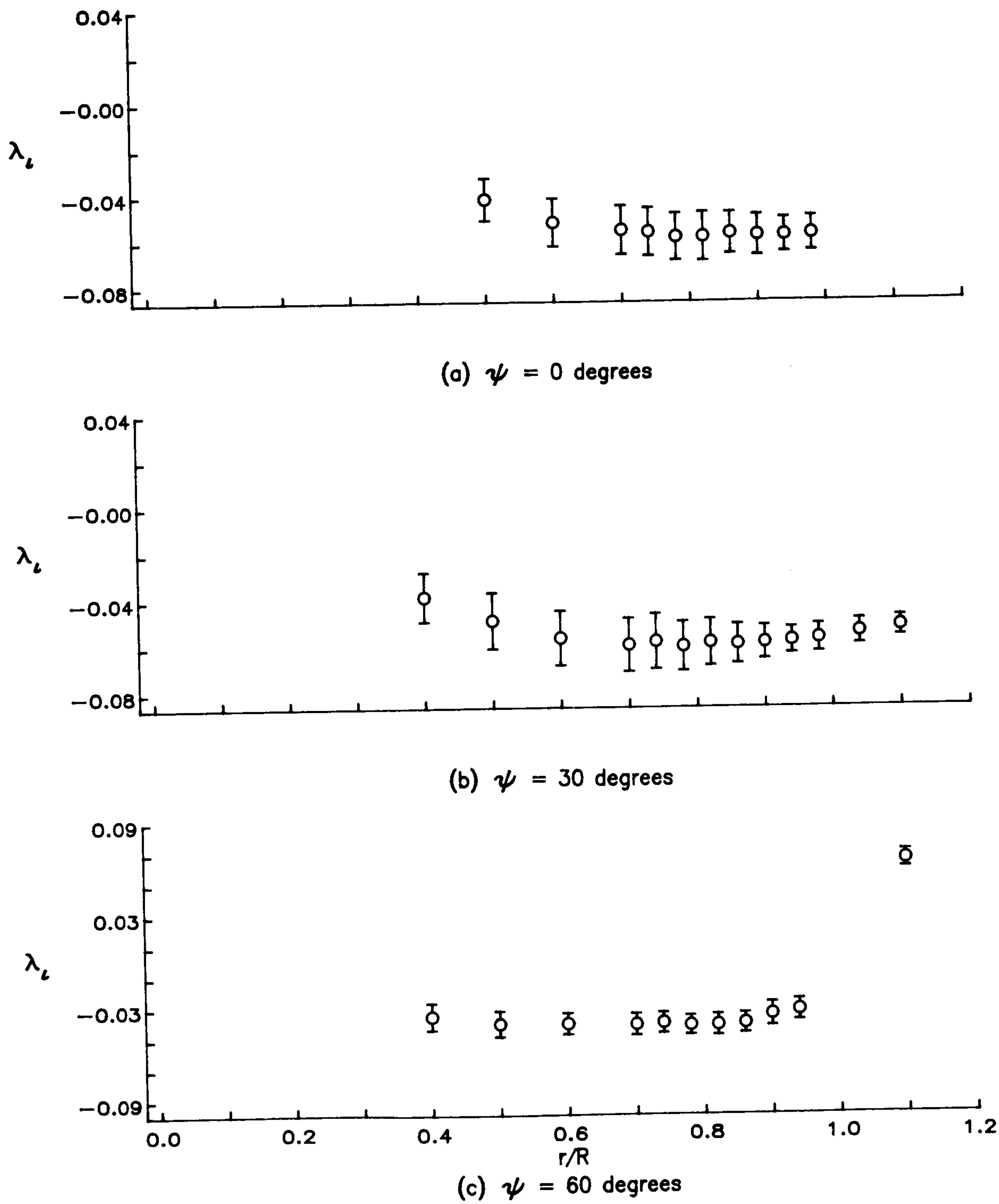

Figure 10.– Radial distribution of mean induced inflow ratio (λ_i).

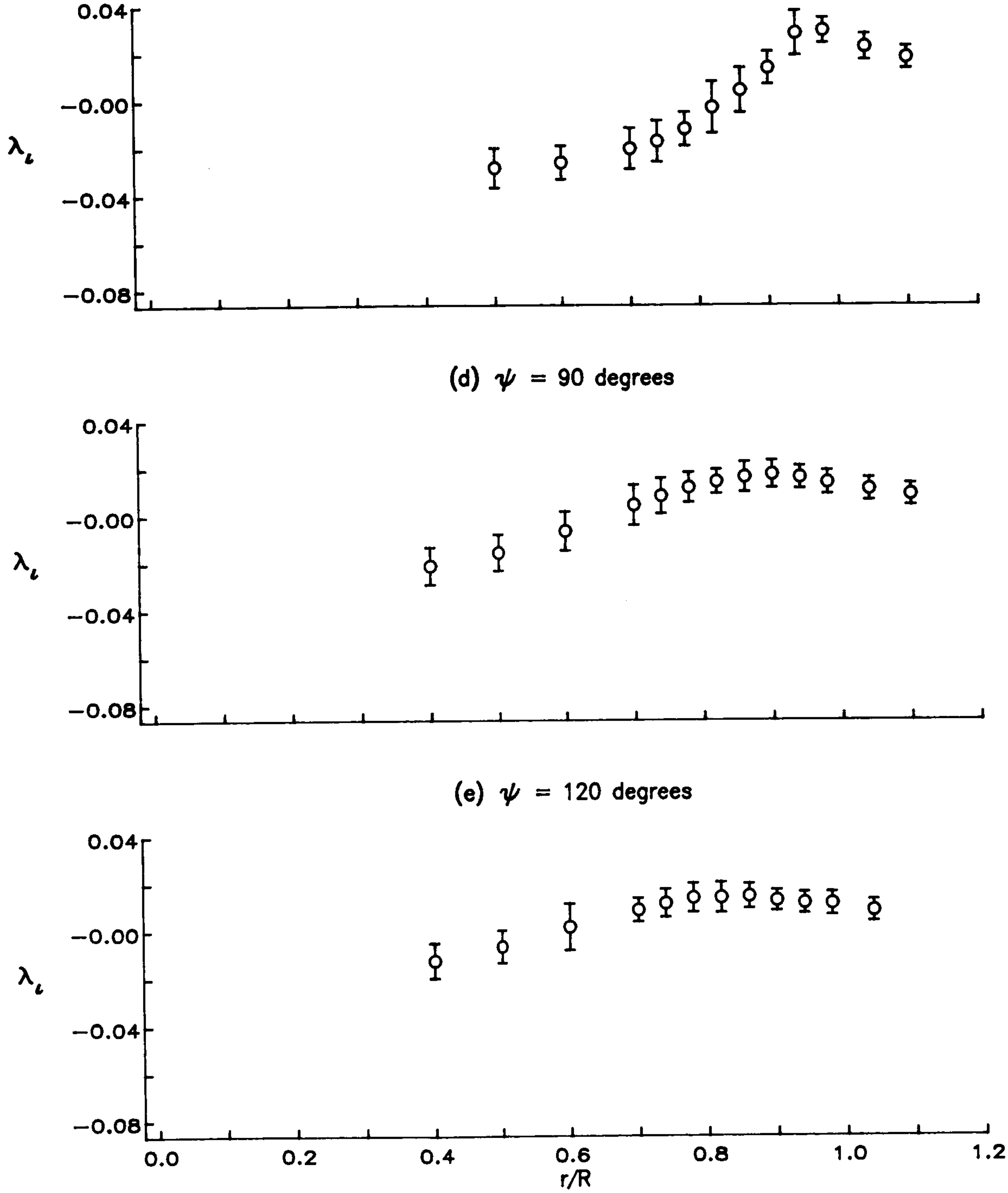

(d) ψ = 90 degrees

(e) ψ = 120 degrees

(f) ψ = 150 degrees

Figure 10.– Continued.

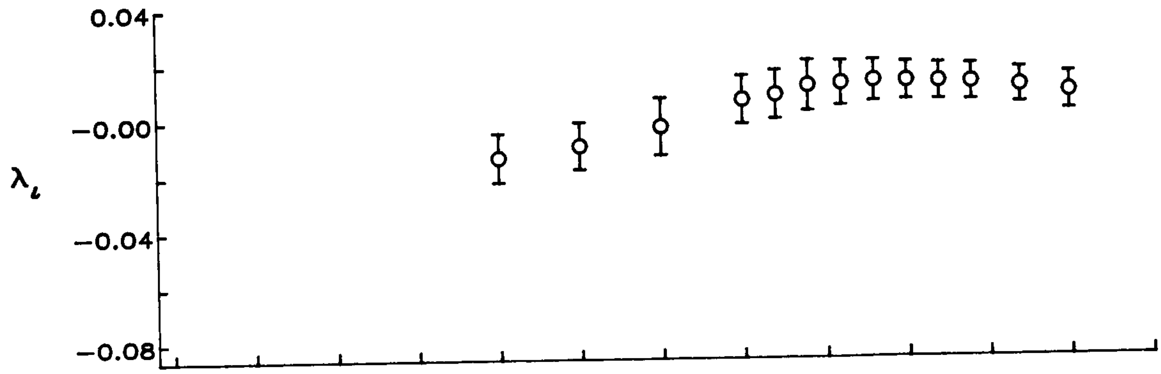

(g) ψ = 180 degrees

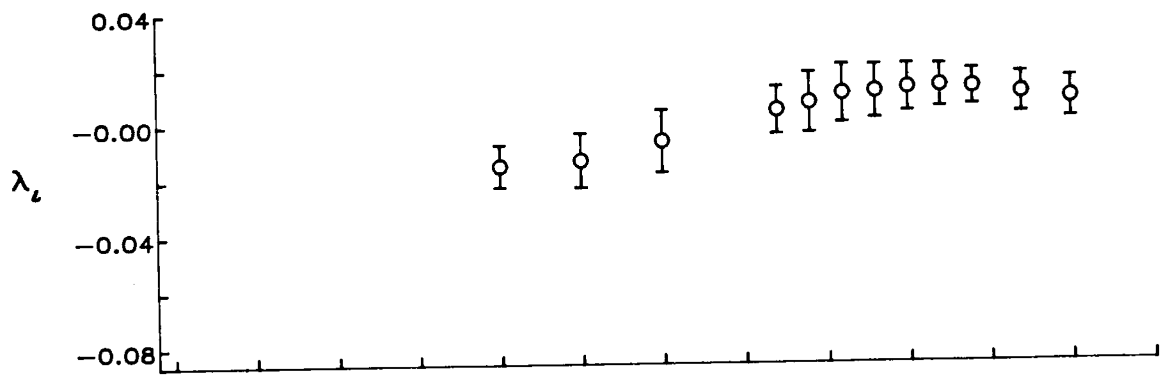

(h) ψ = 210 degrees

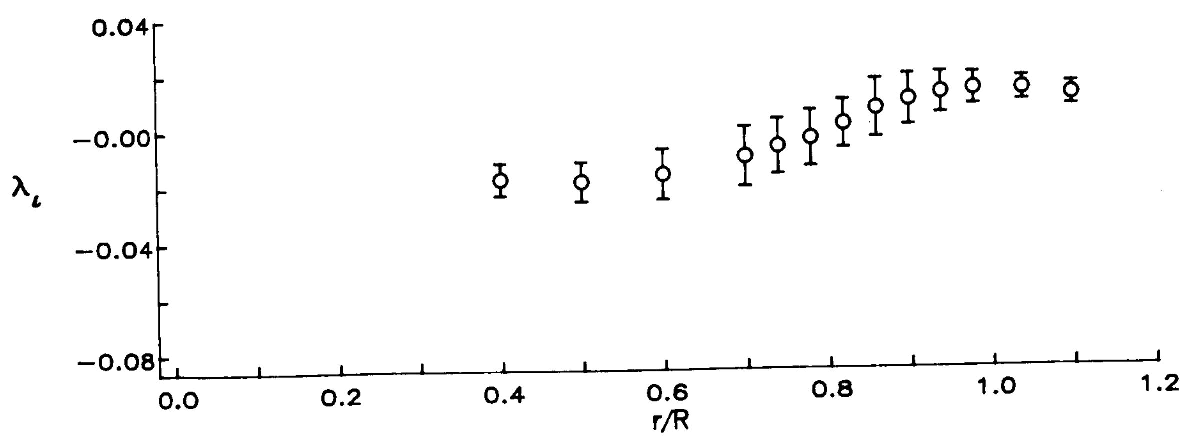

(i) ψ = 240 degrees

Figure 10.– Continued.

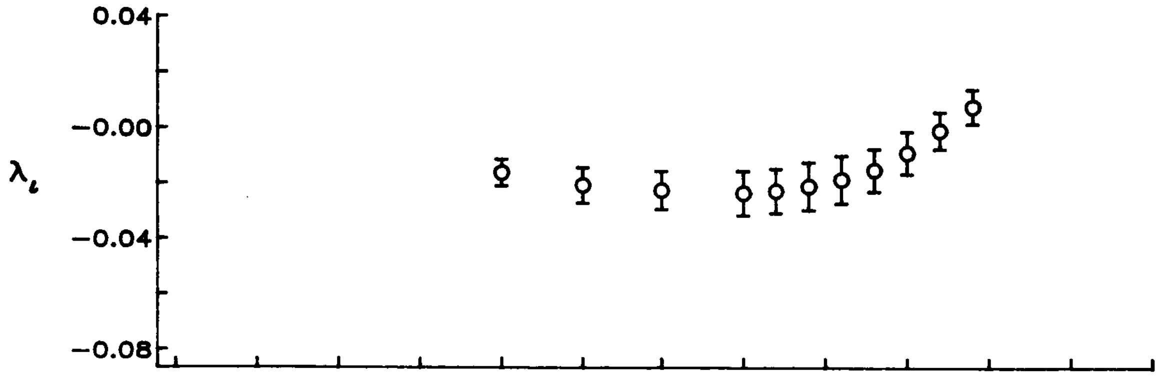

(j) ψ = 270 degrees

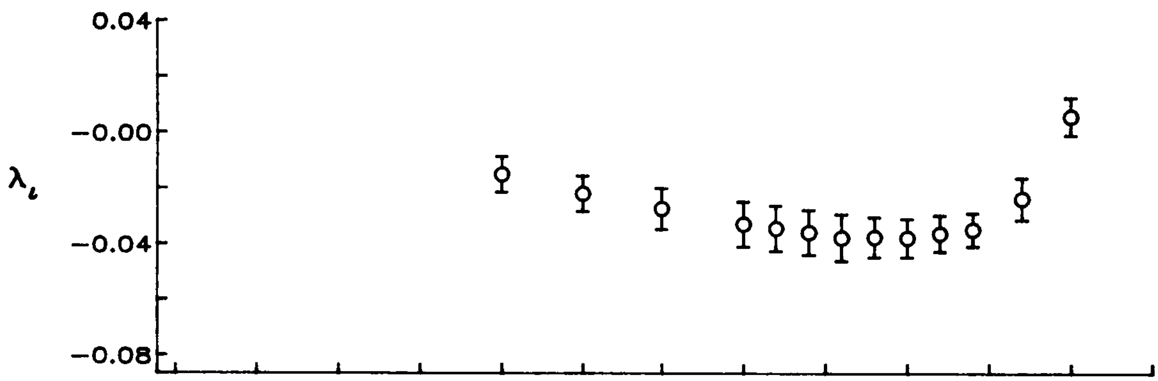

(k) ψ = 300 degrees

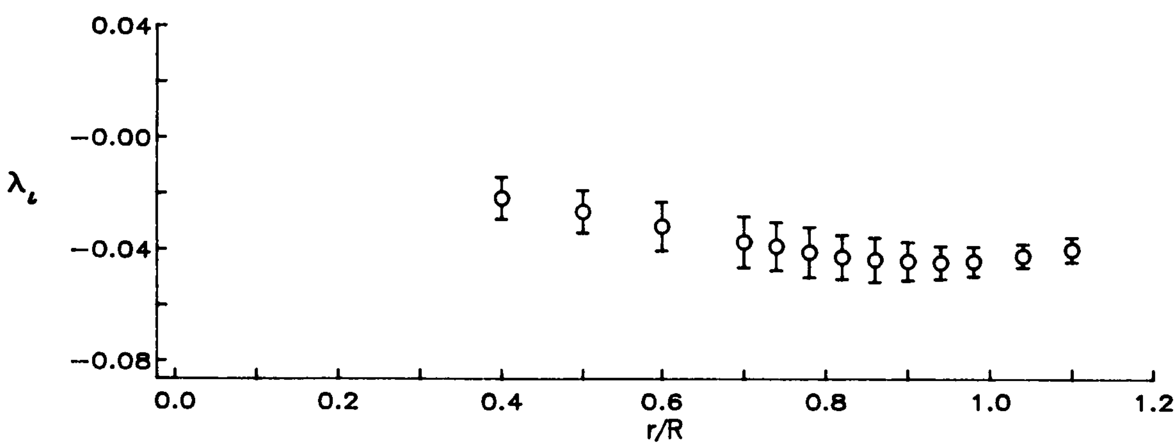

(l) ψ = 330 degrees

Figure 10.– Concluded.

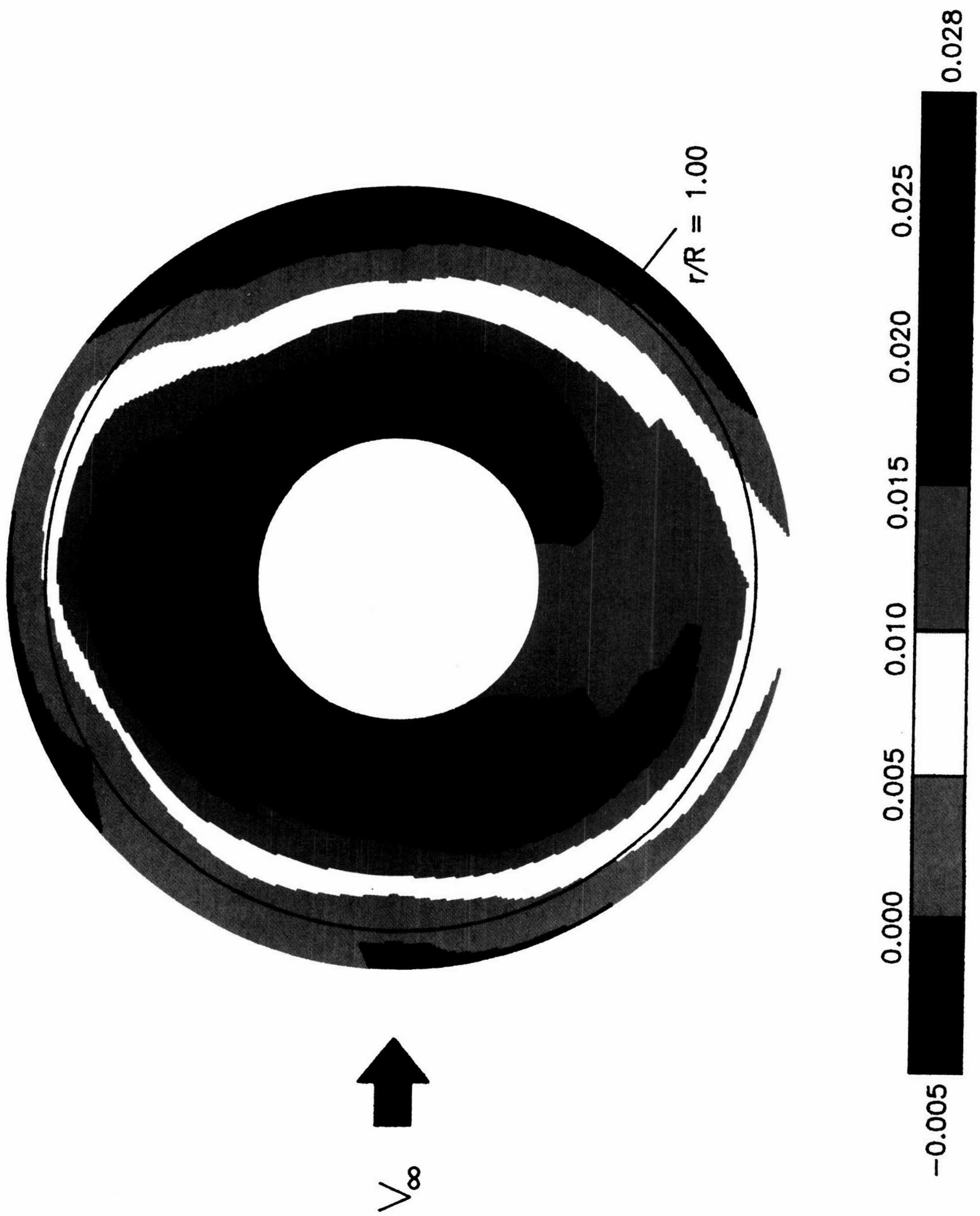

Figure 11.– Contour plot of mean induced inflow ratio (μ_i).

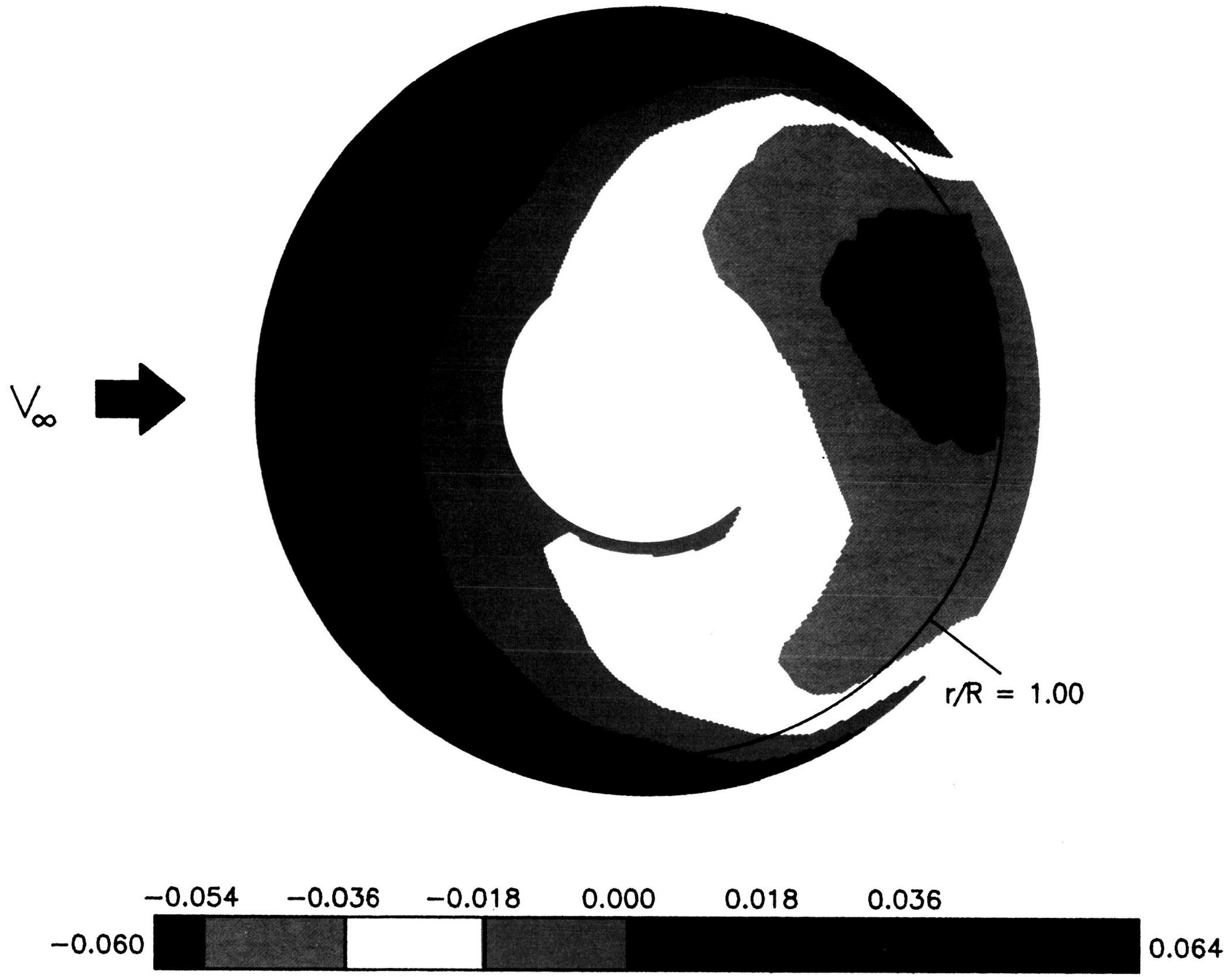

Figure 12.– Contour plot of mean induced inflow ratio (λ_i).

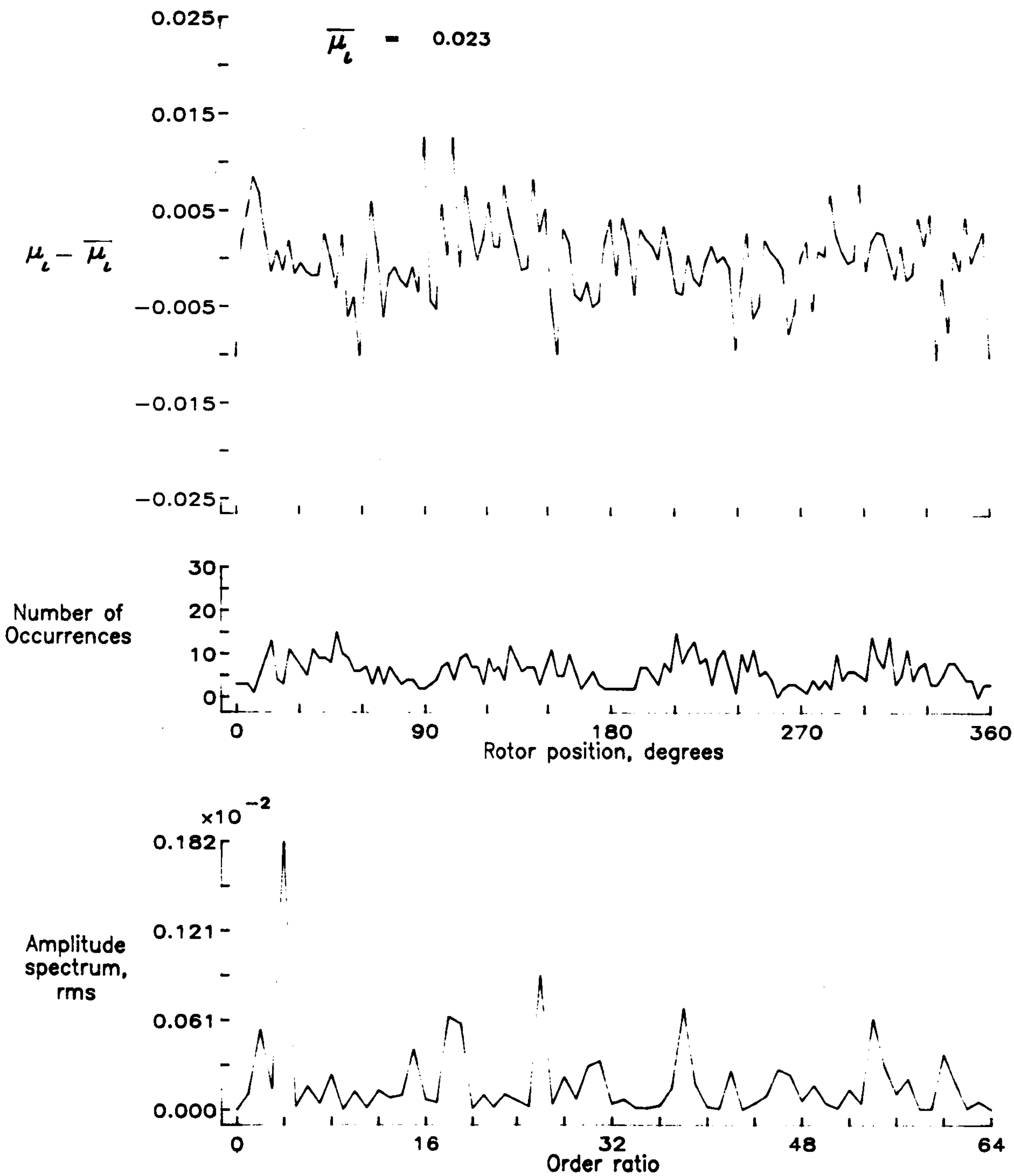

Figure 13.– Induced inflow velocity measured at 0 degrees and r/R of 0.50.

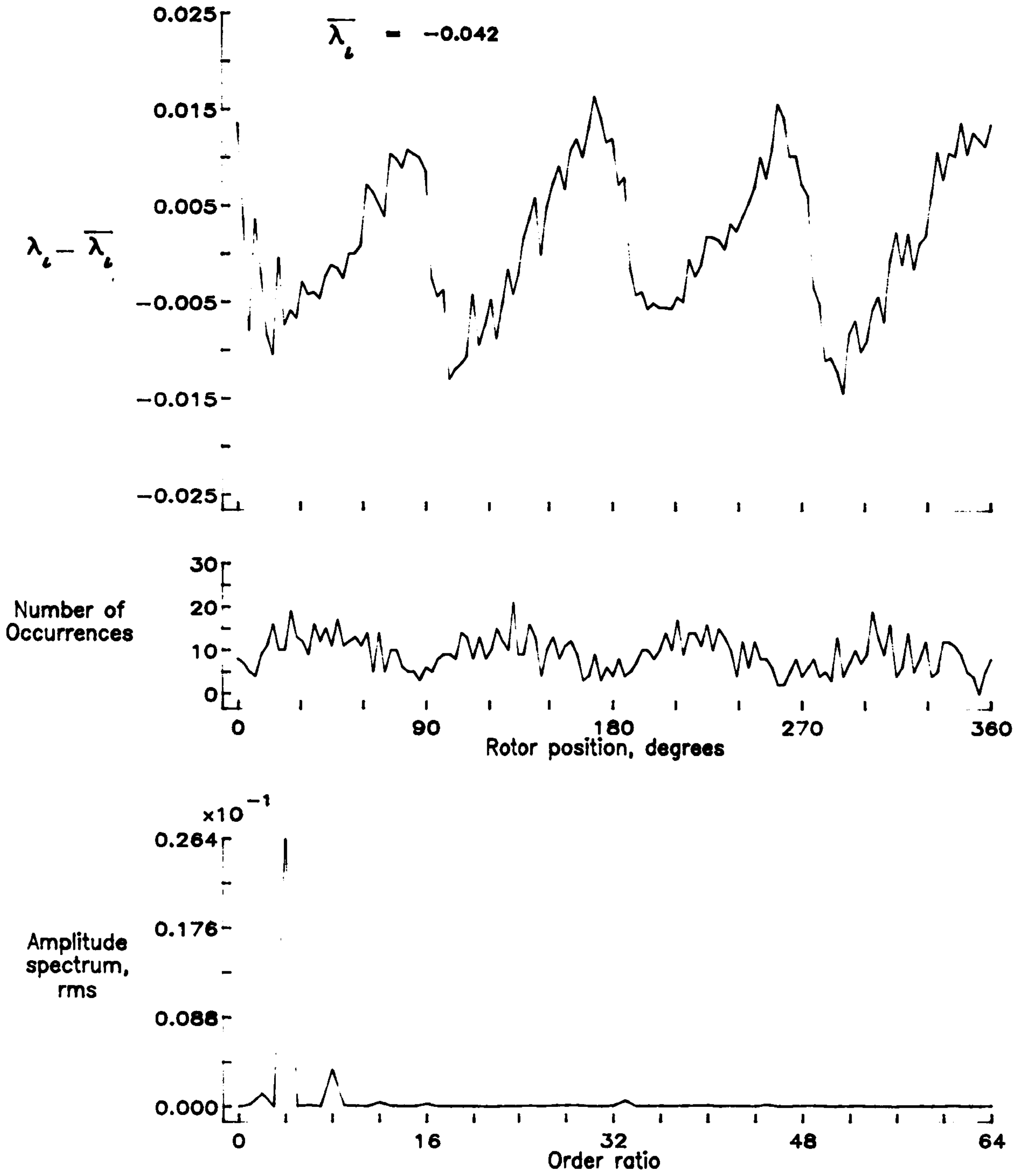

Figure 13.– Concluded.

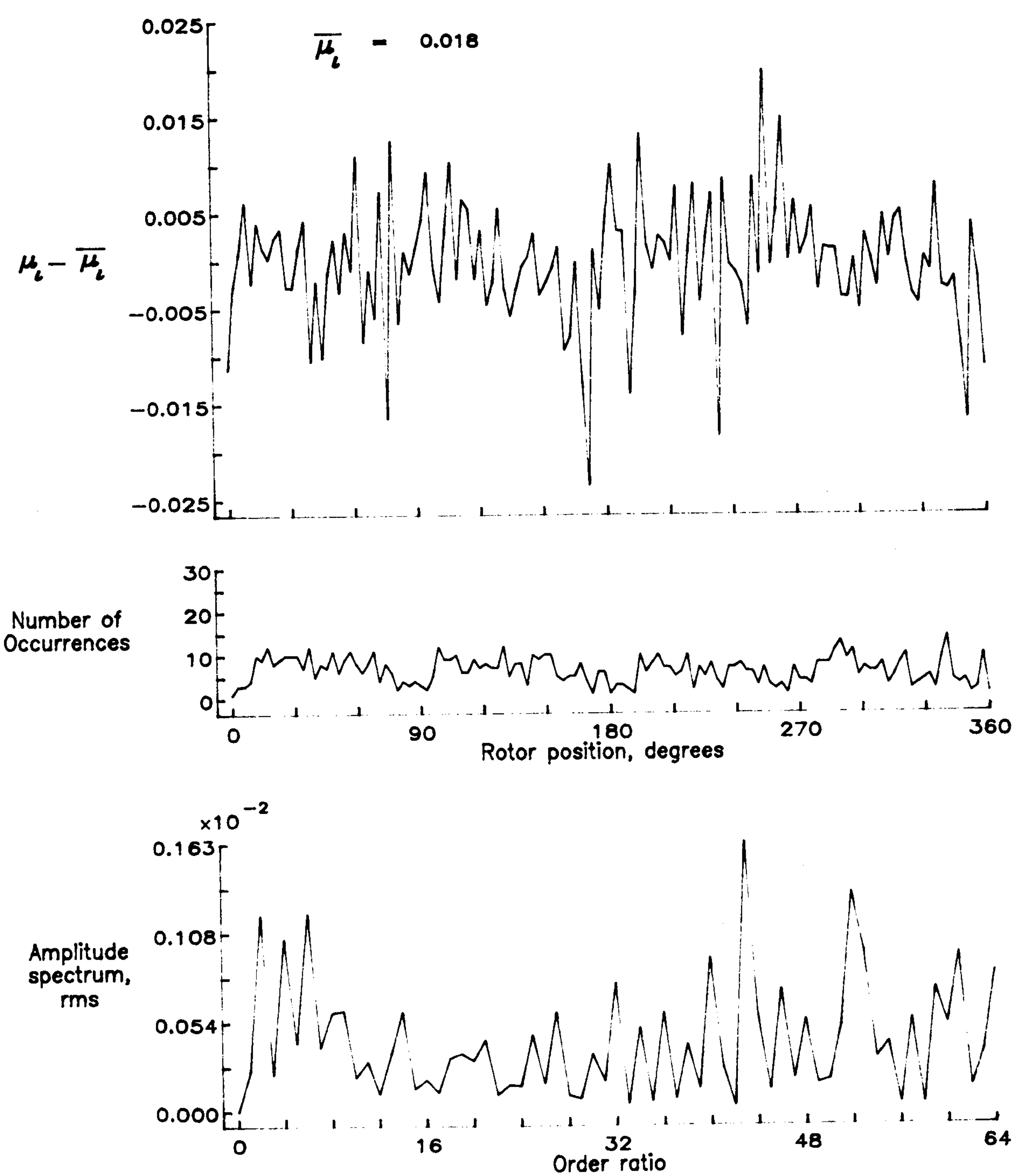

Figure 14.– Induced inflow velocity measured at 0 degrees and r/R of 0.60.

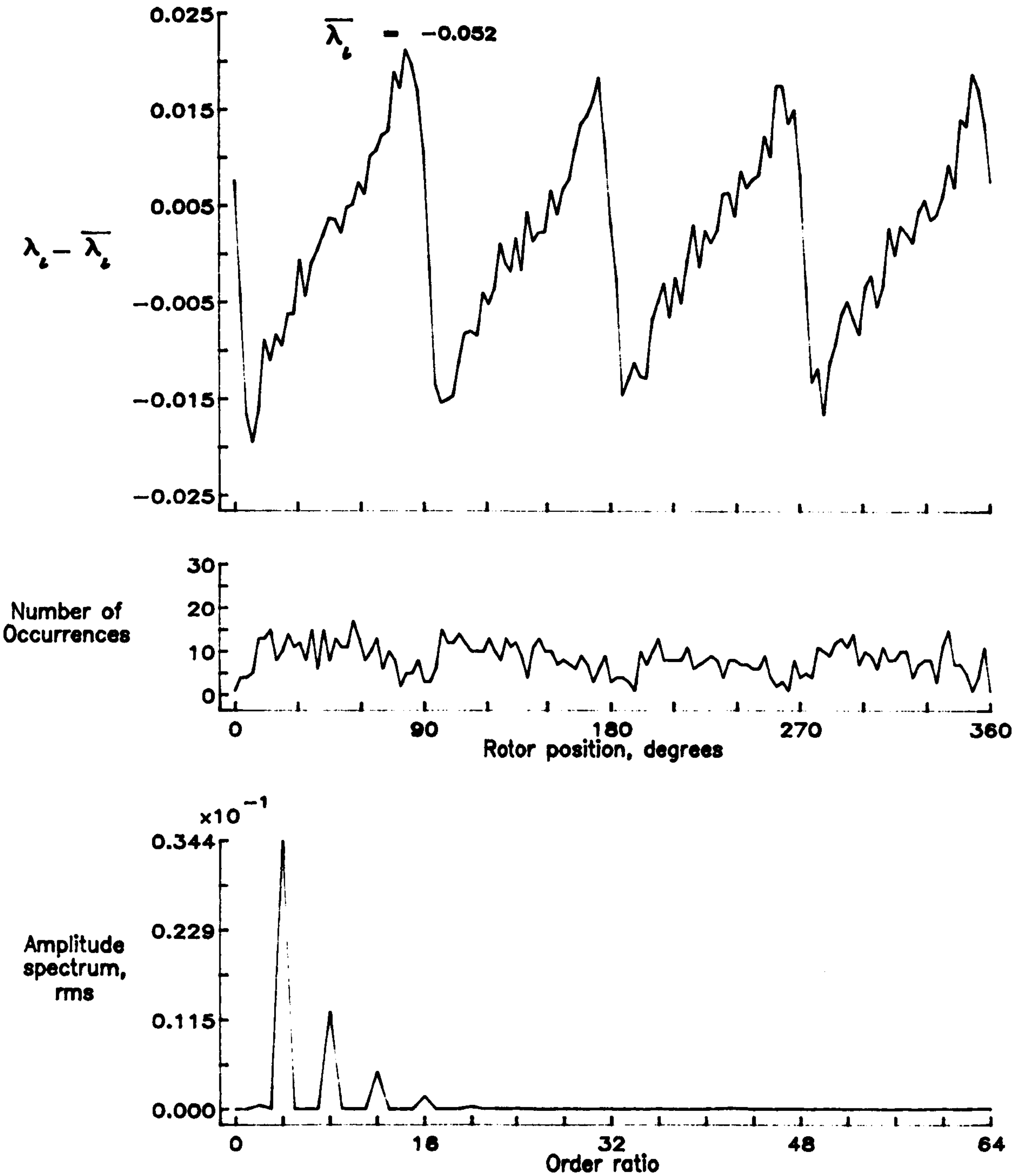

Figure 14.– Concluded.

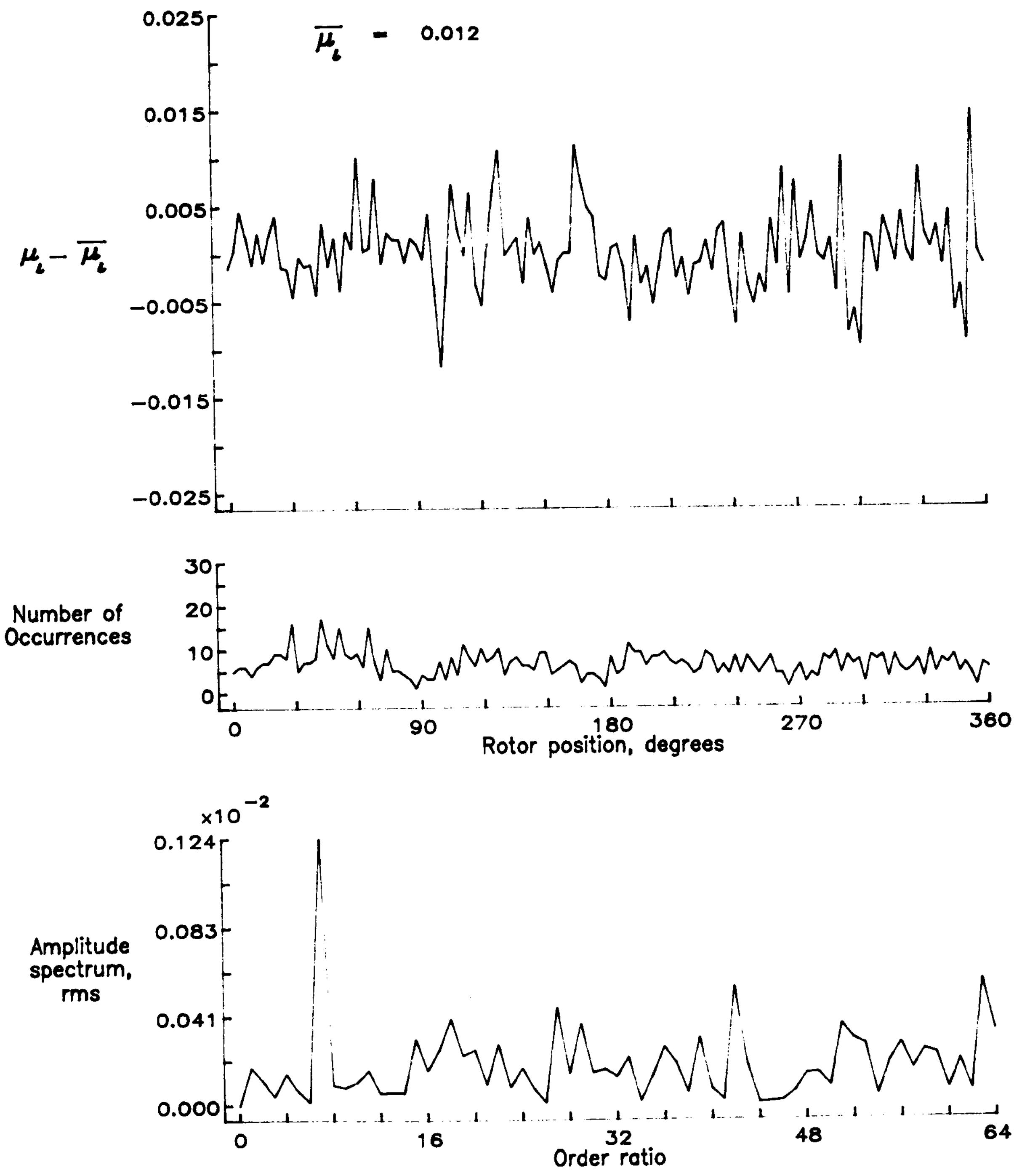

Figure 15.– Induced inflow velocity measured at 0 degrees and r/R of 0.70.

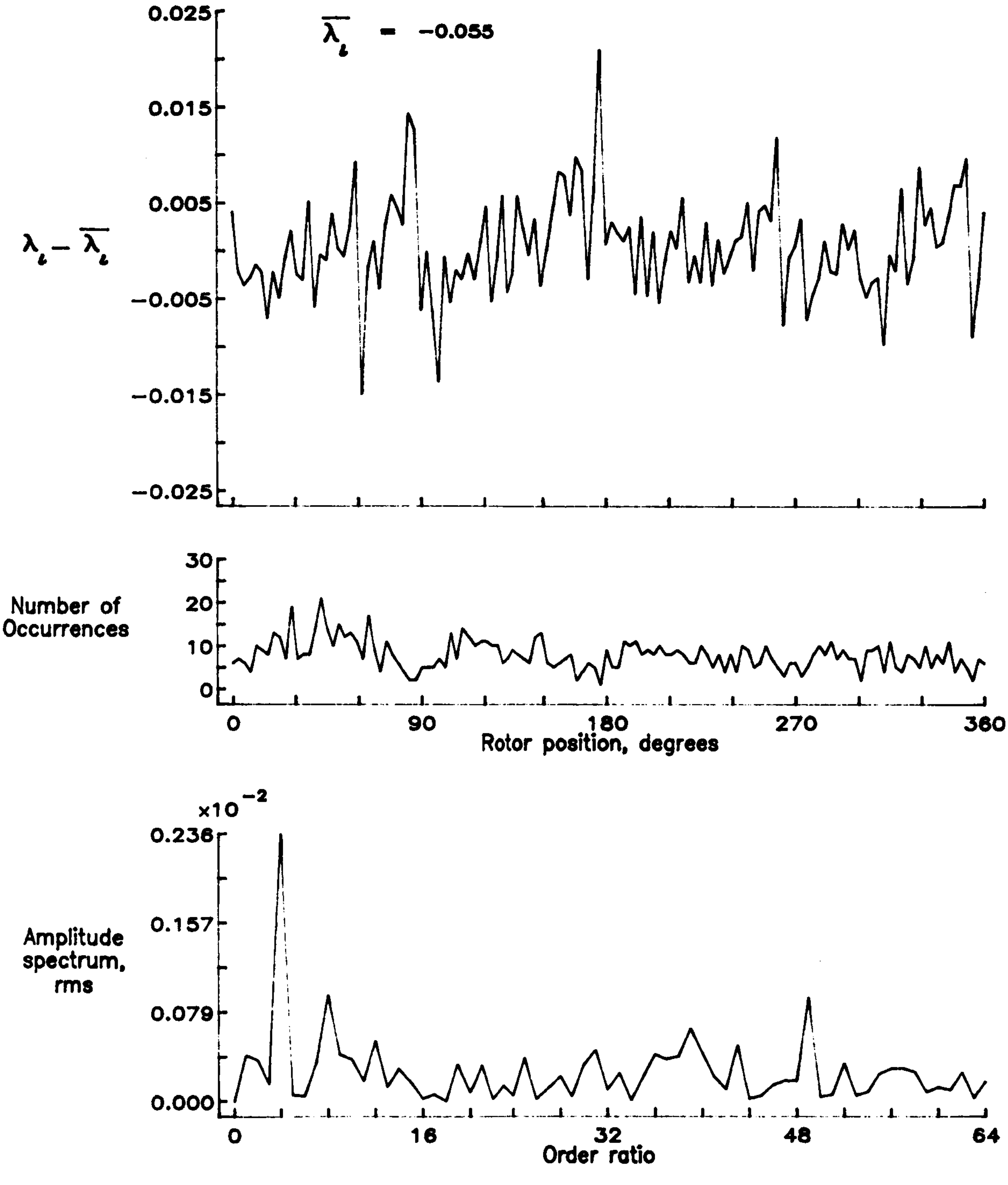

Figure 15.– Concluded.

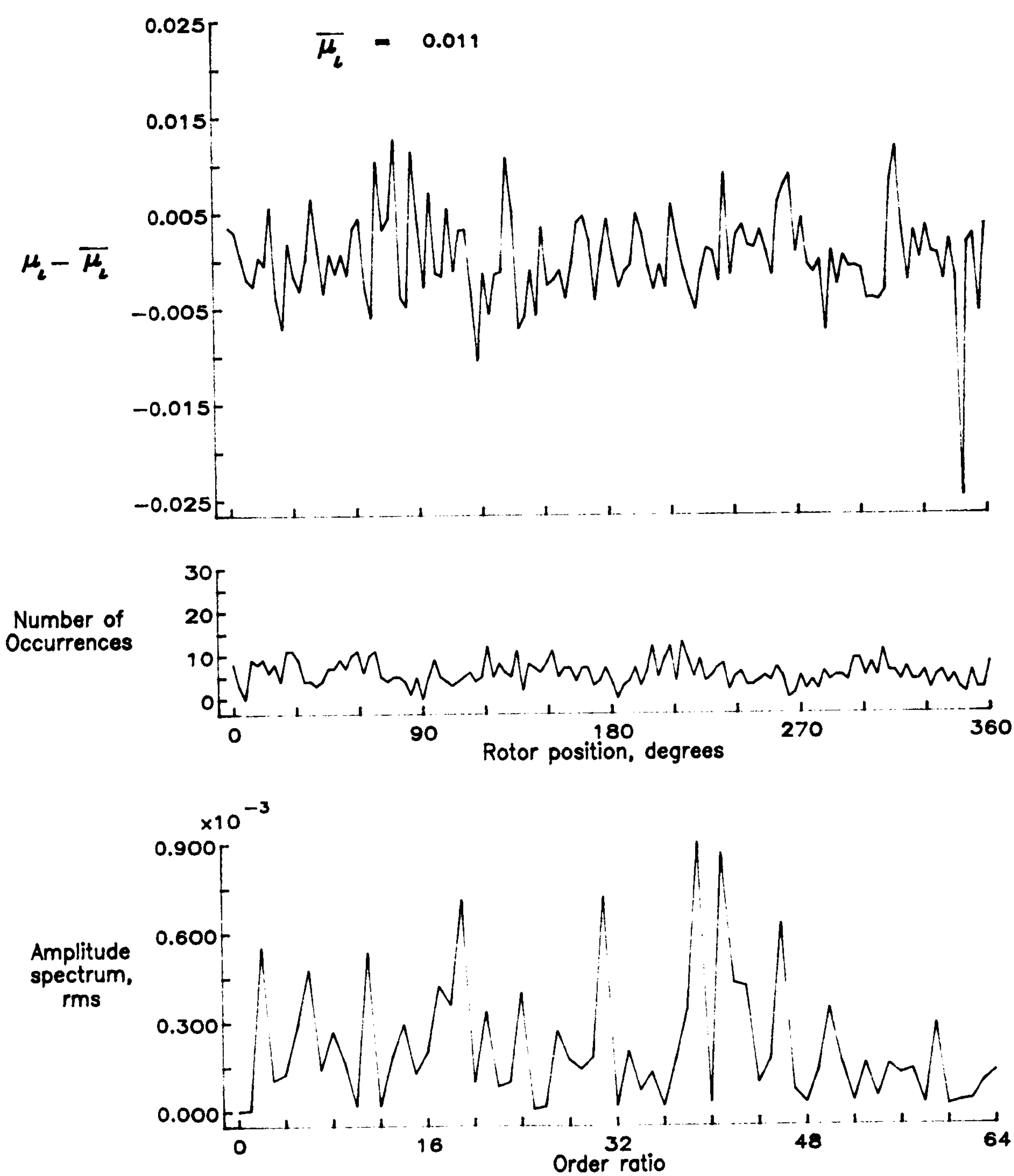

Figure 16.– Induced inflow velocity measured at 0 degrees and r/R of 0.74.

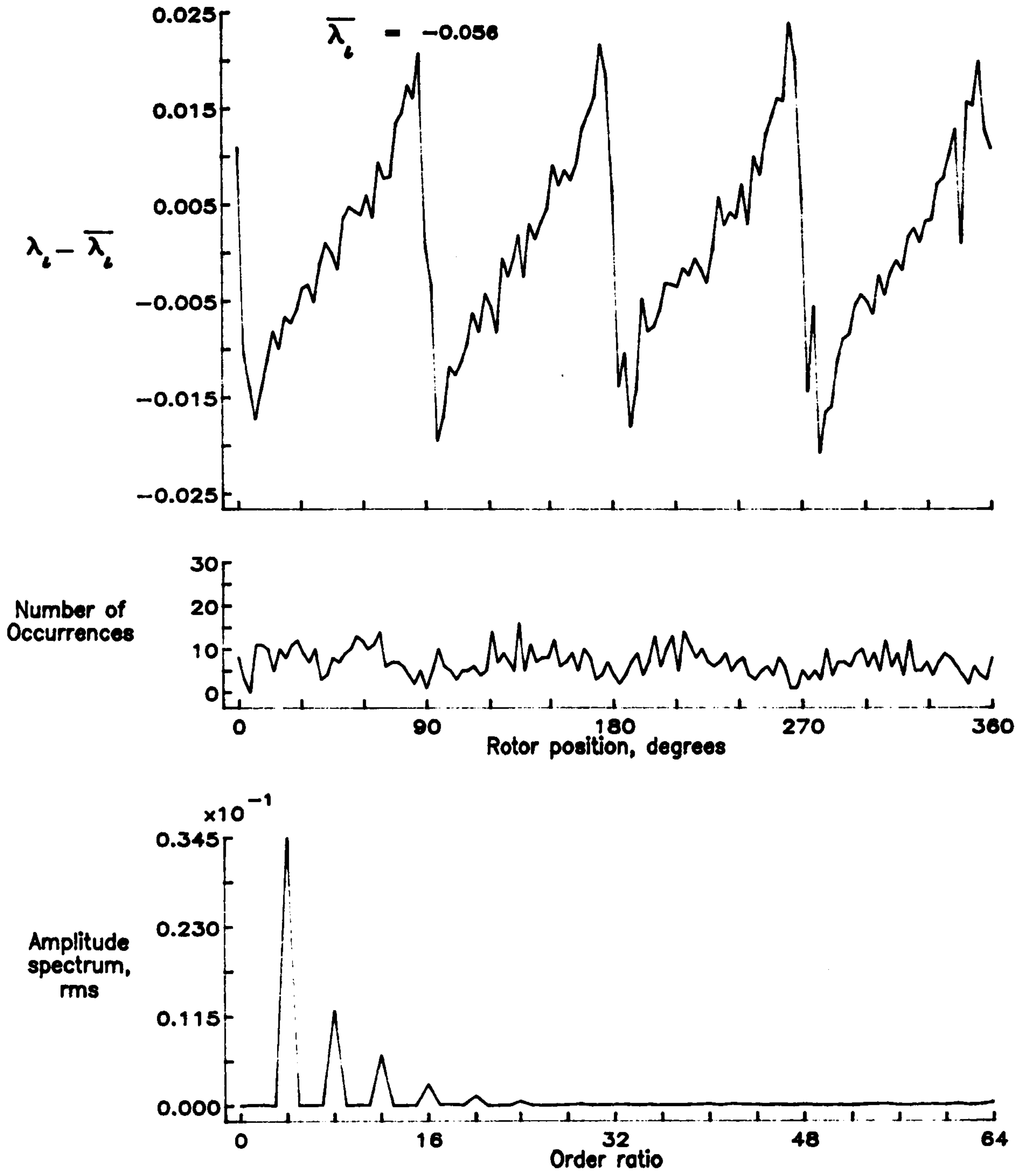

Figure 16.– Concluded.

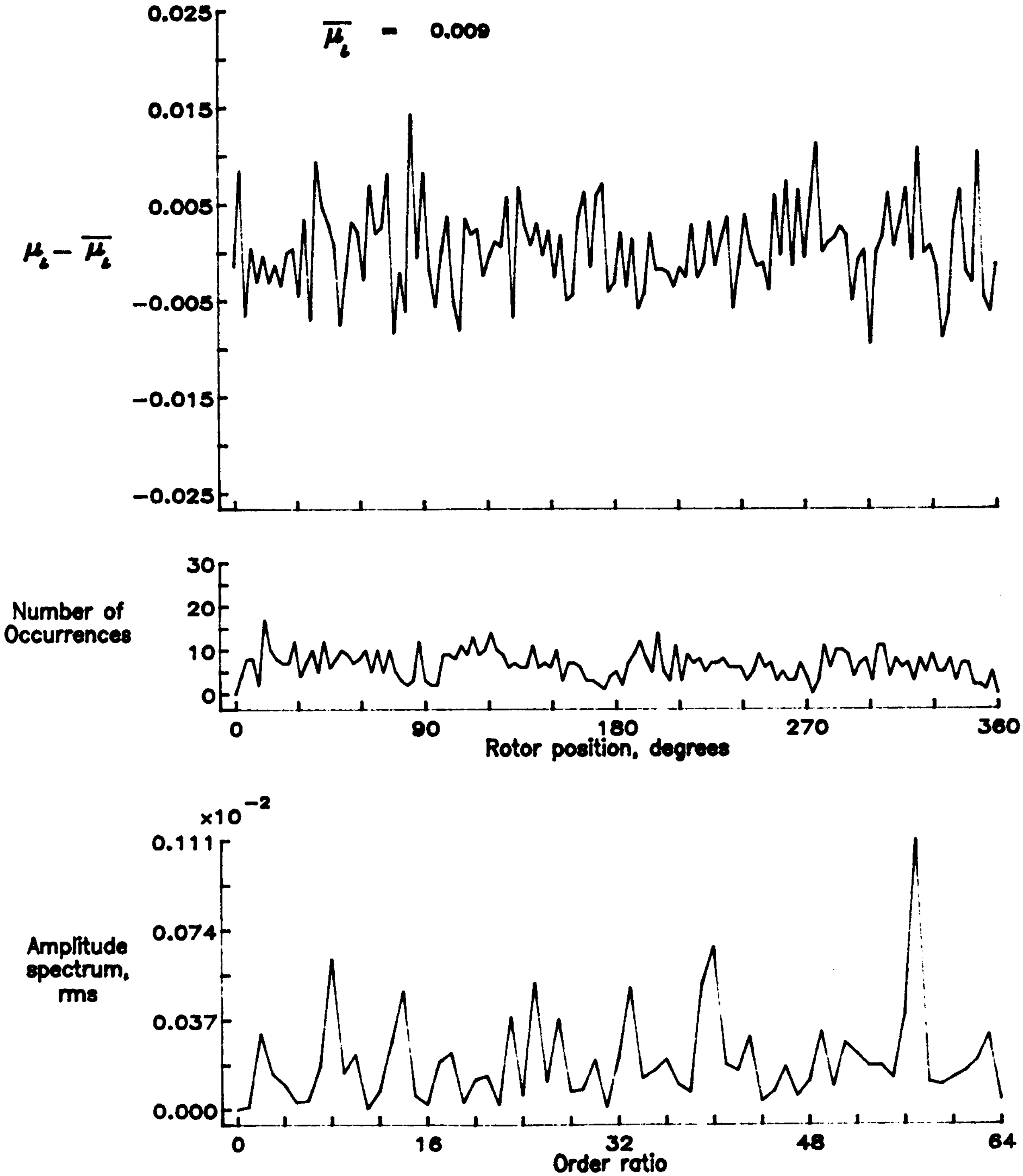

Figure 17.– Induced inflow velocity measured at 0 degrees and r/R of 0.78.

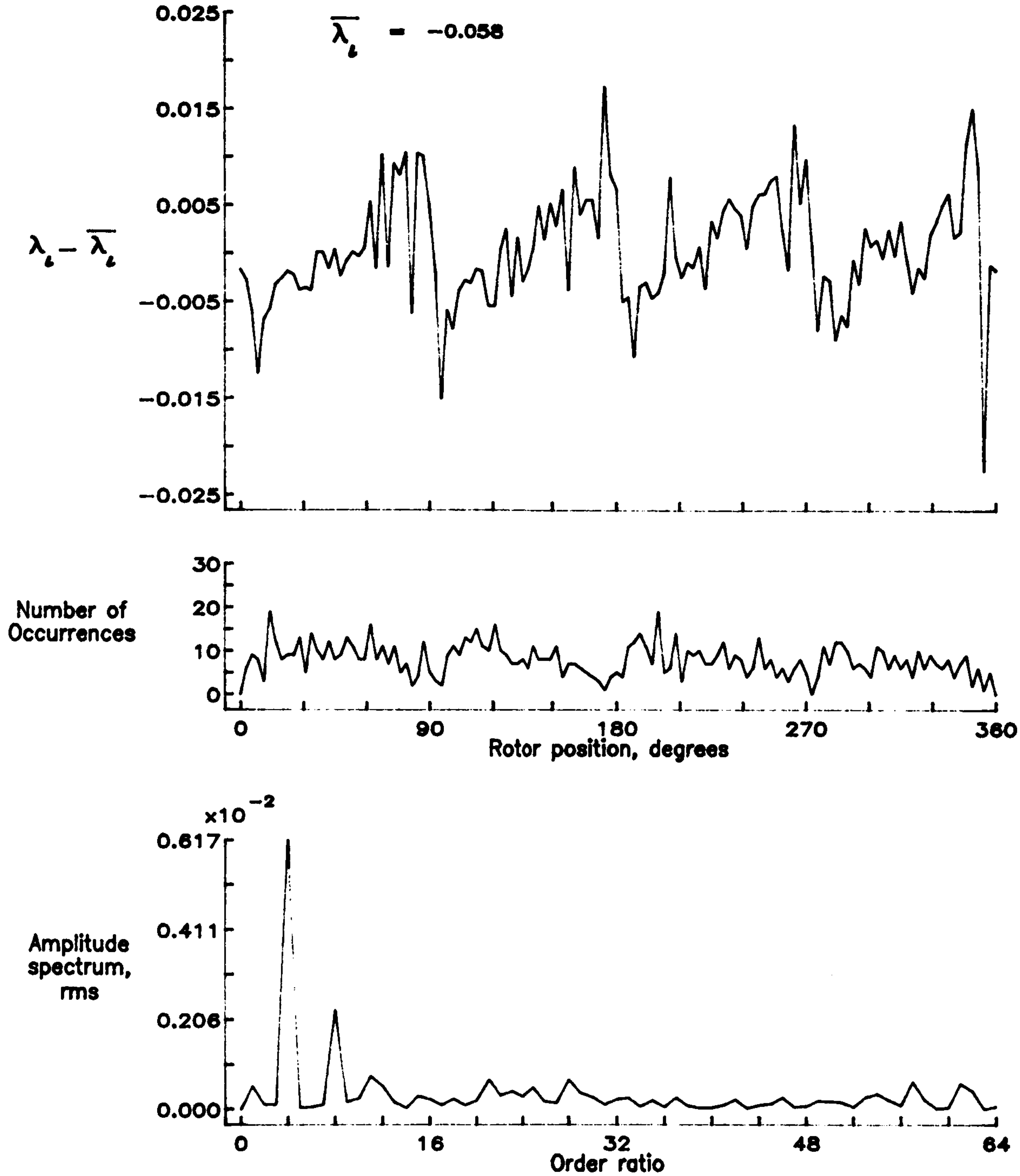

Figure 17.– Concluded.

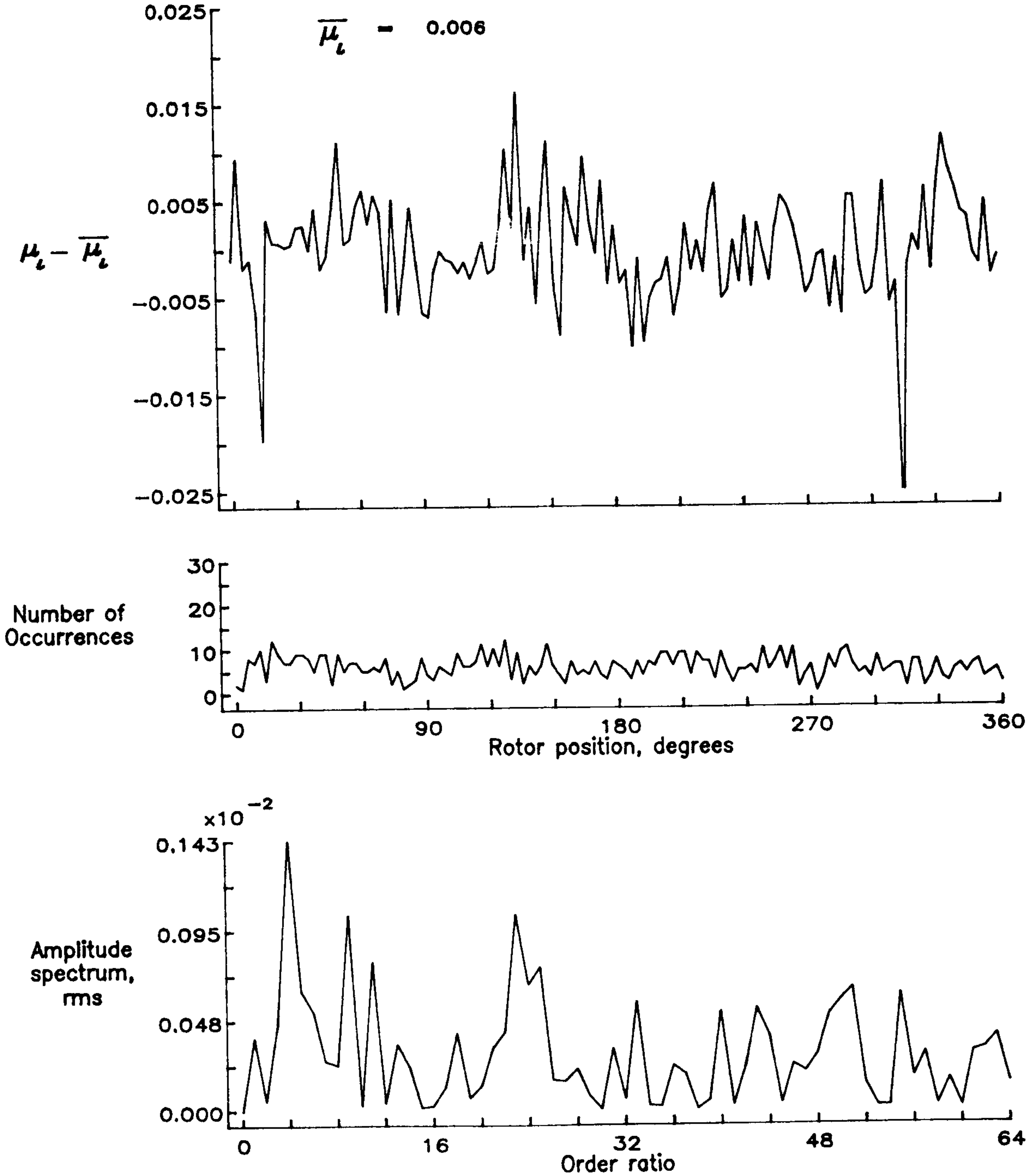

Figure 18.– Induced inflow velocity measured at 0 degrees and r/R of 0.82.

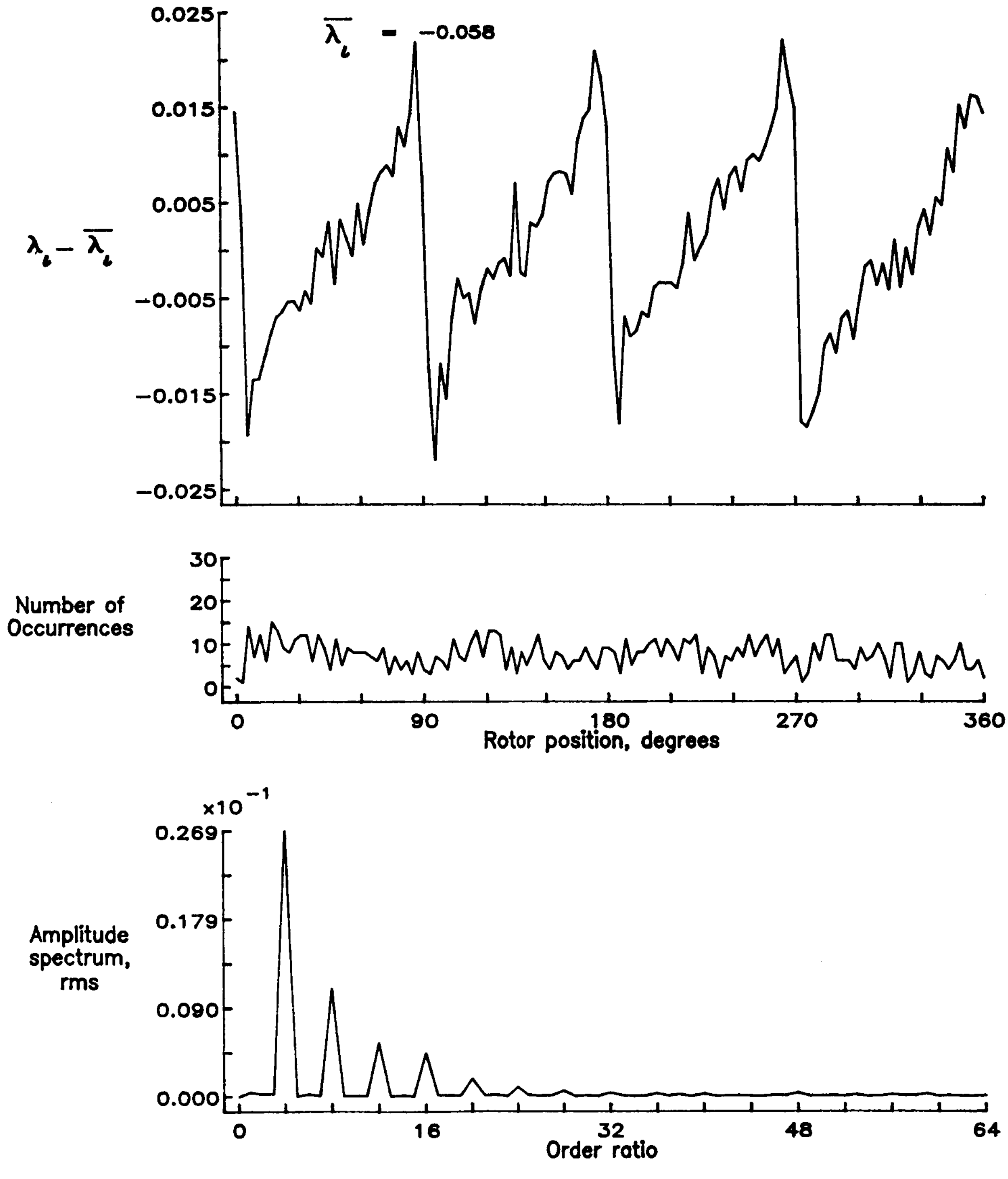

Figure 18.– Concluded.

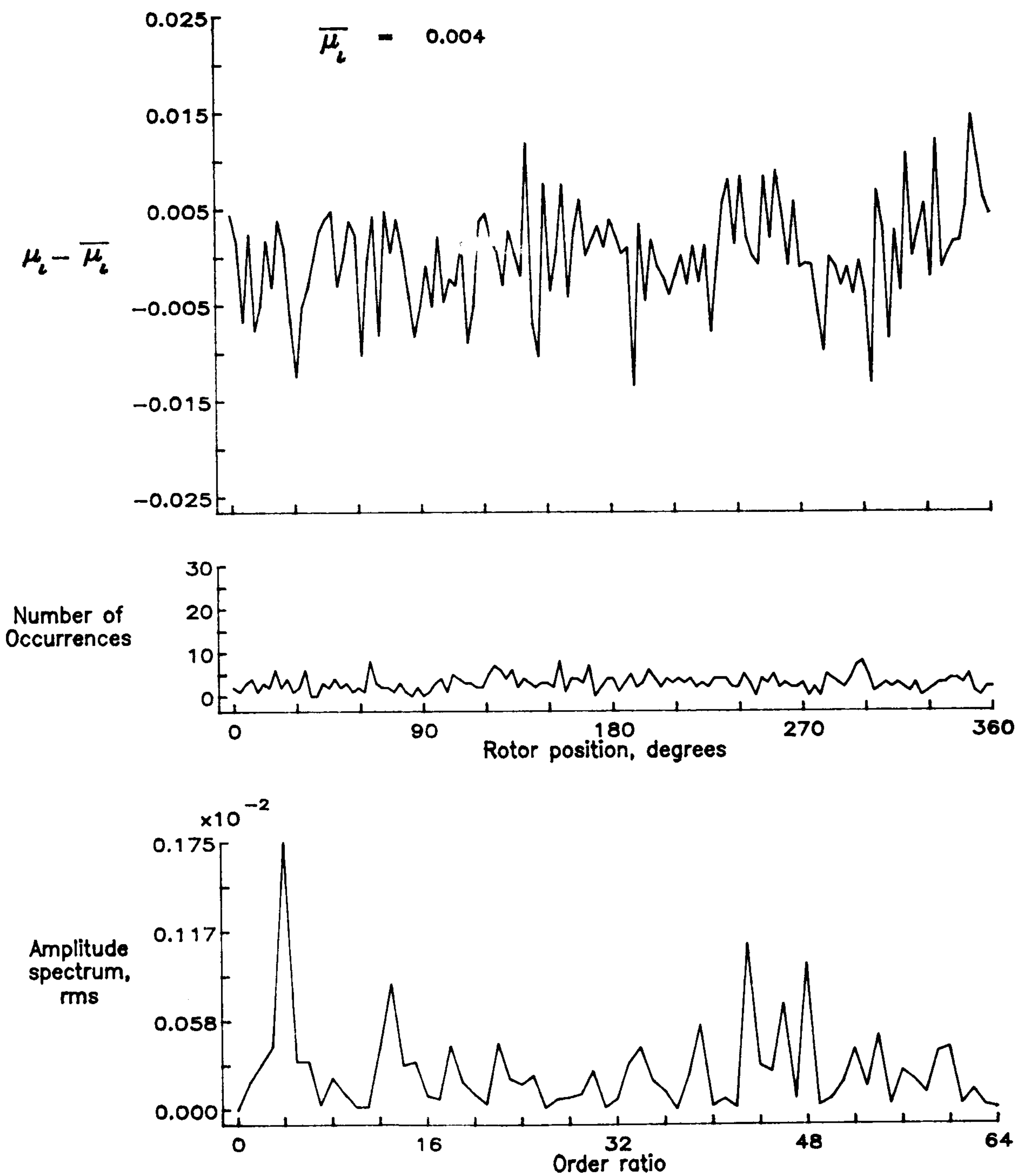

Figure 19.– Induced inflow velocity measured at 0 degrees and r/R of 0.86.

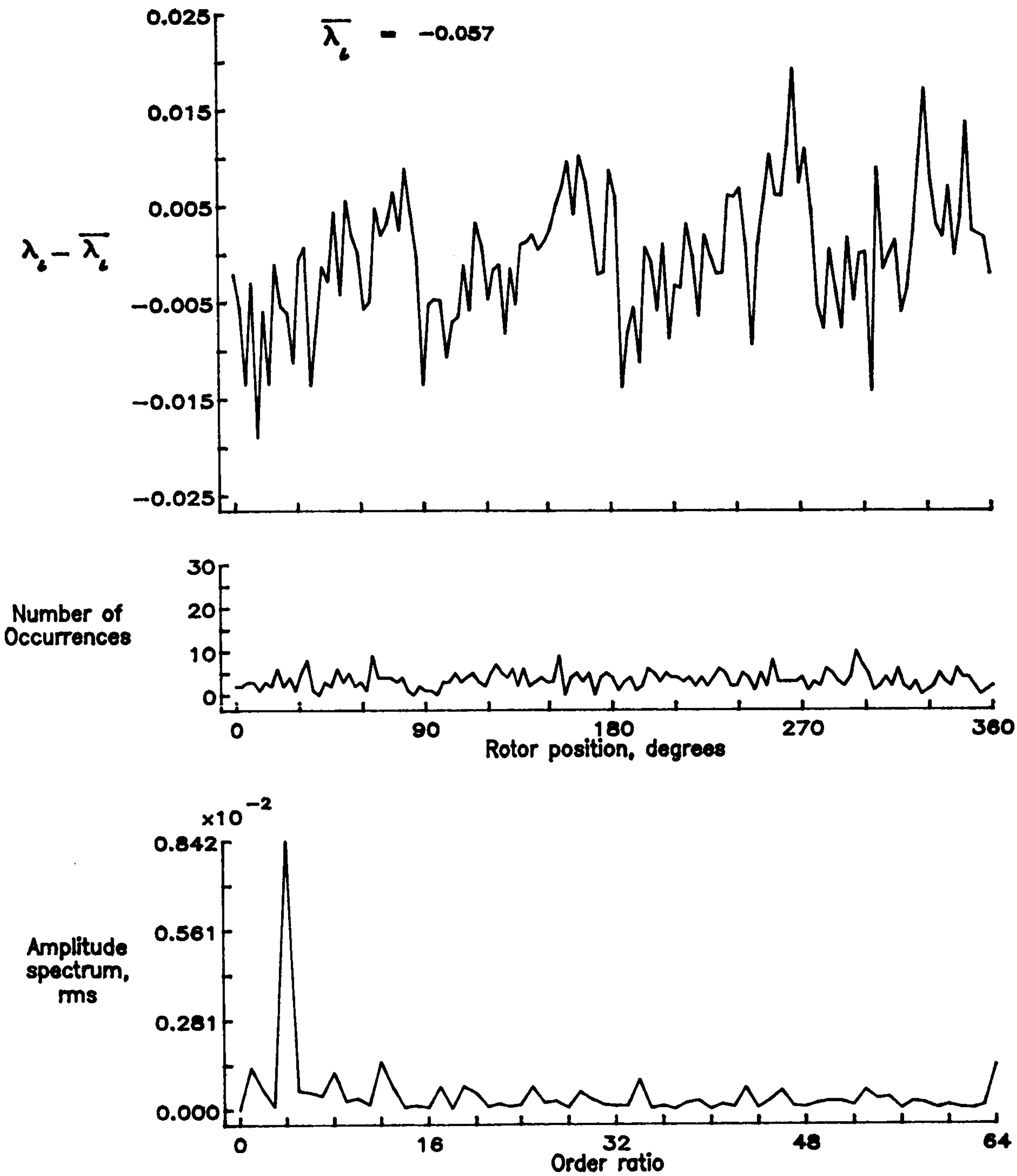

Figure 19.– Concluded.

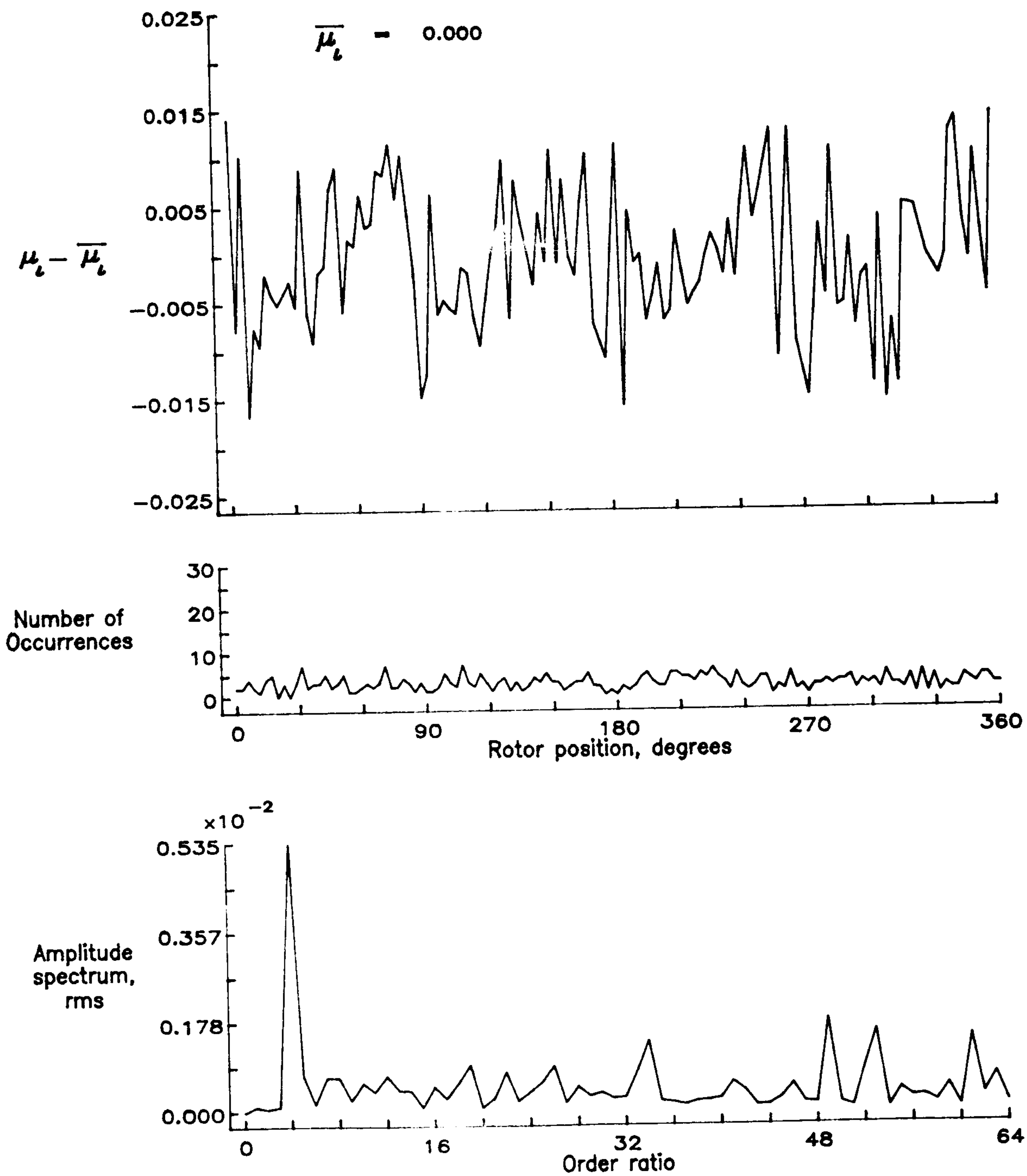

Figure 20.– Induced inflow velocity measured at 0 degrees and r/R of 0.90.

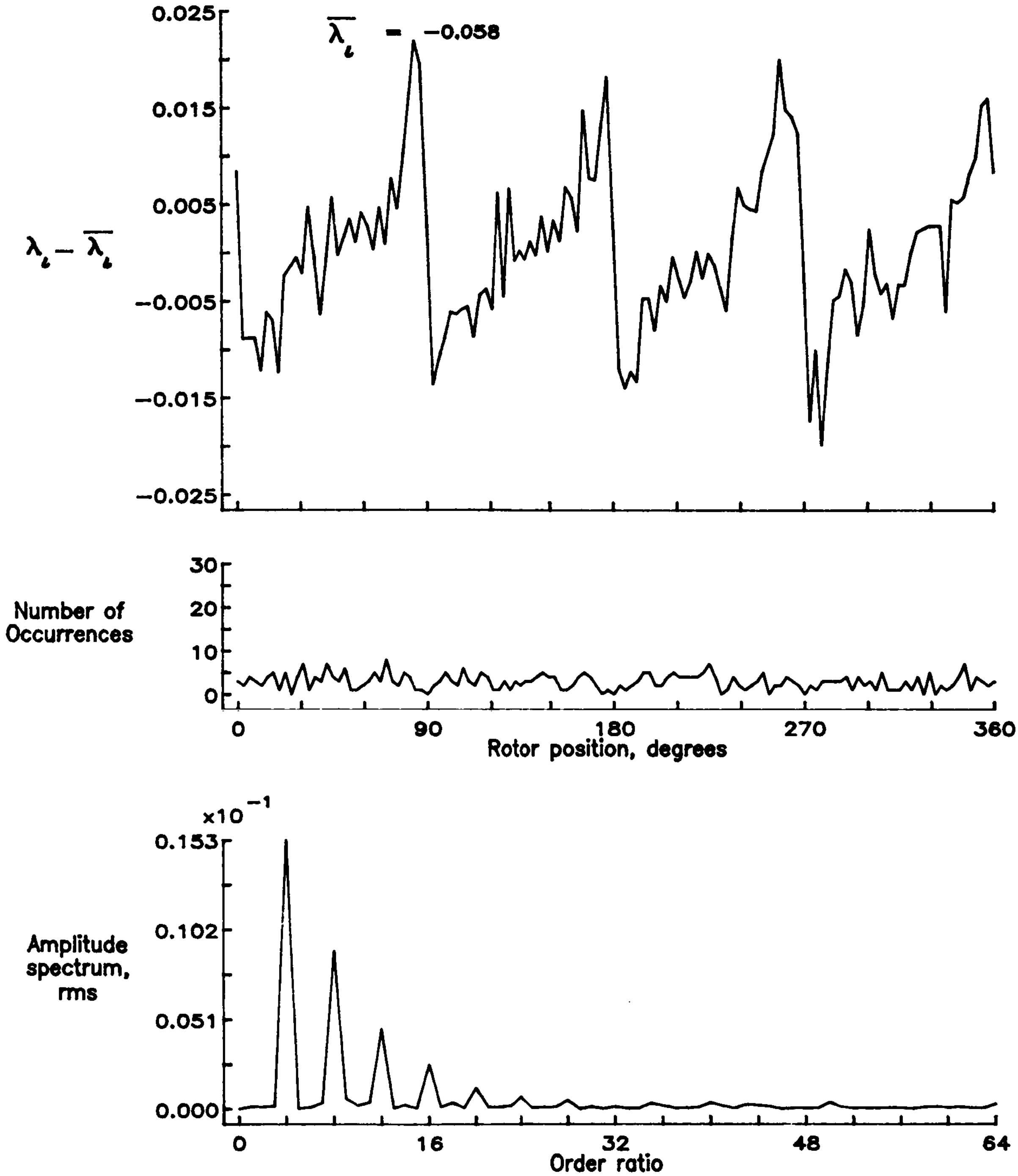

Figure 20.– Concluded.

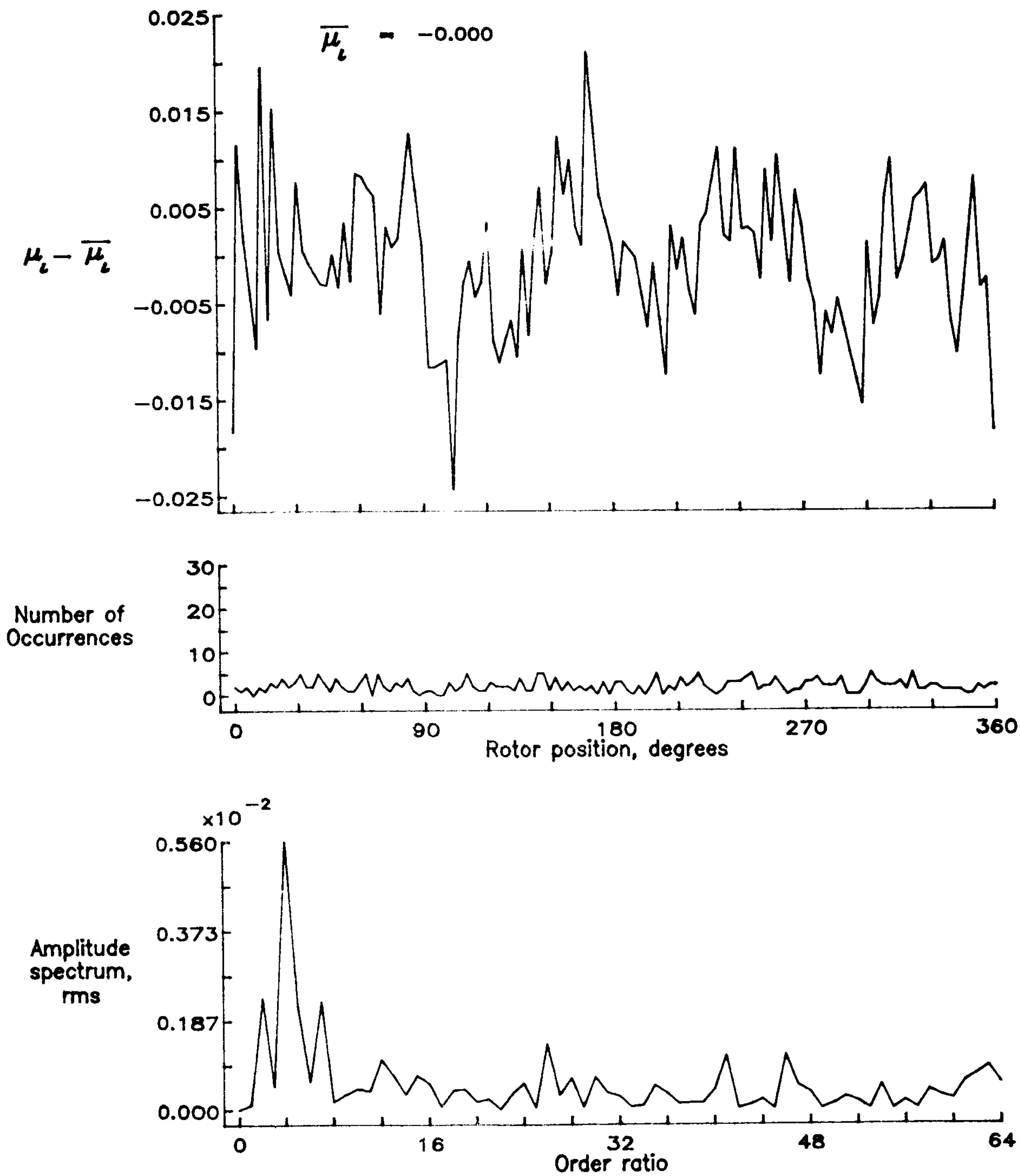

Figure 21.– Induced inflow velocity measured at 0 degrees and r/R of 0.94.

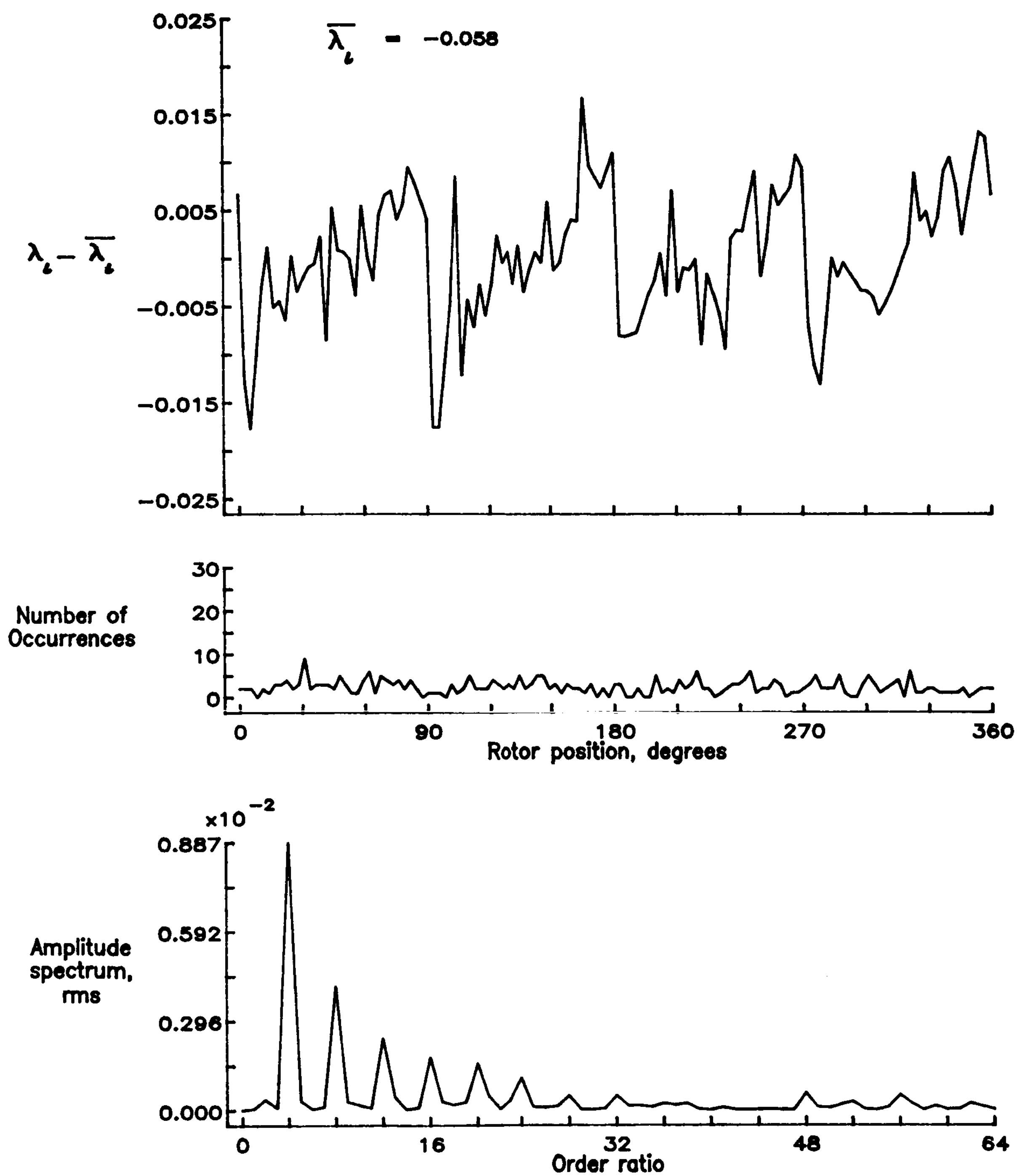

Figure 21.– Concluded.

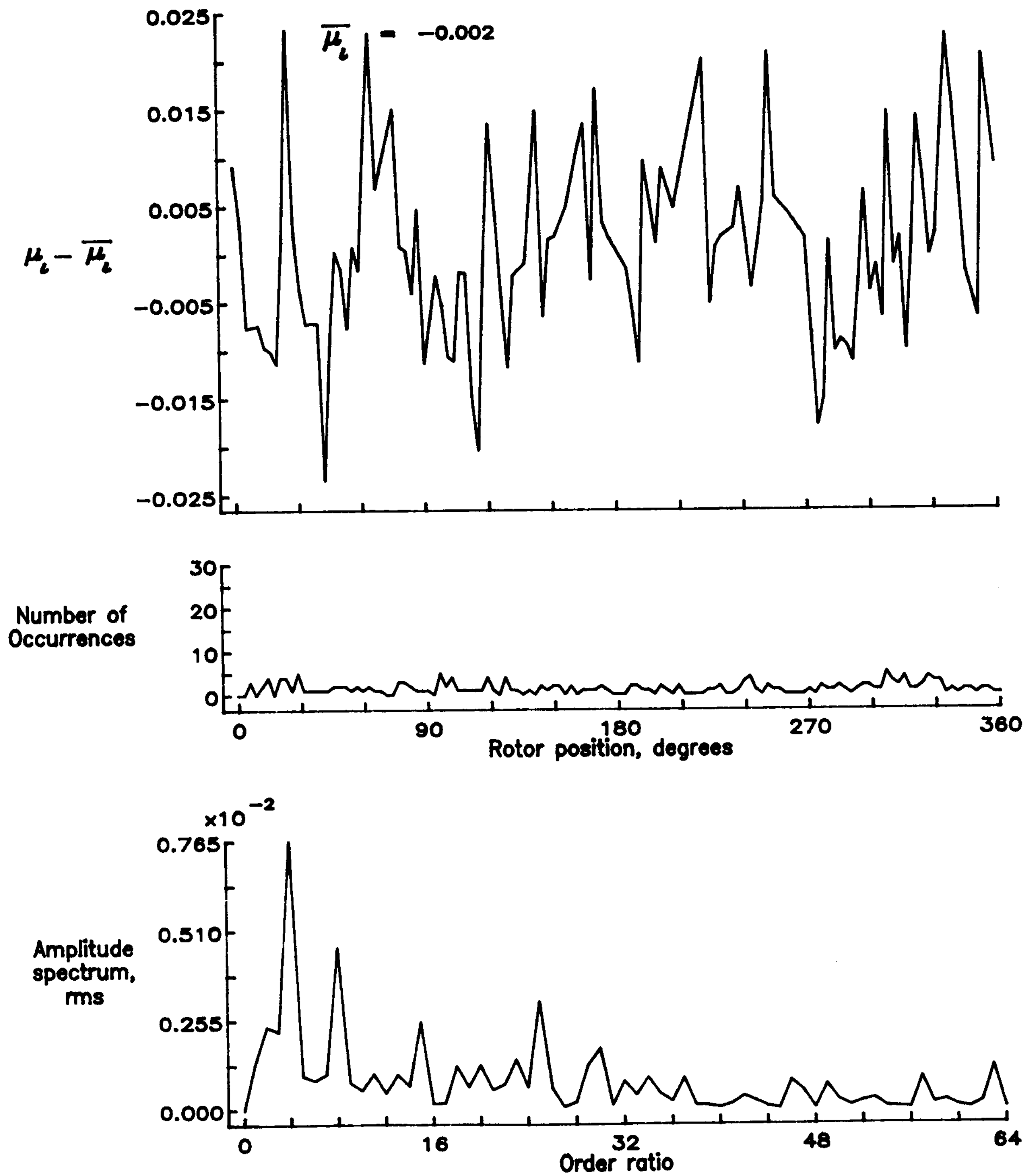

Figure 22.– Induced inflow velocity measured at 0 degrees and r/R of 0.98.

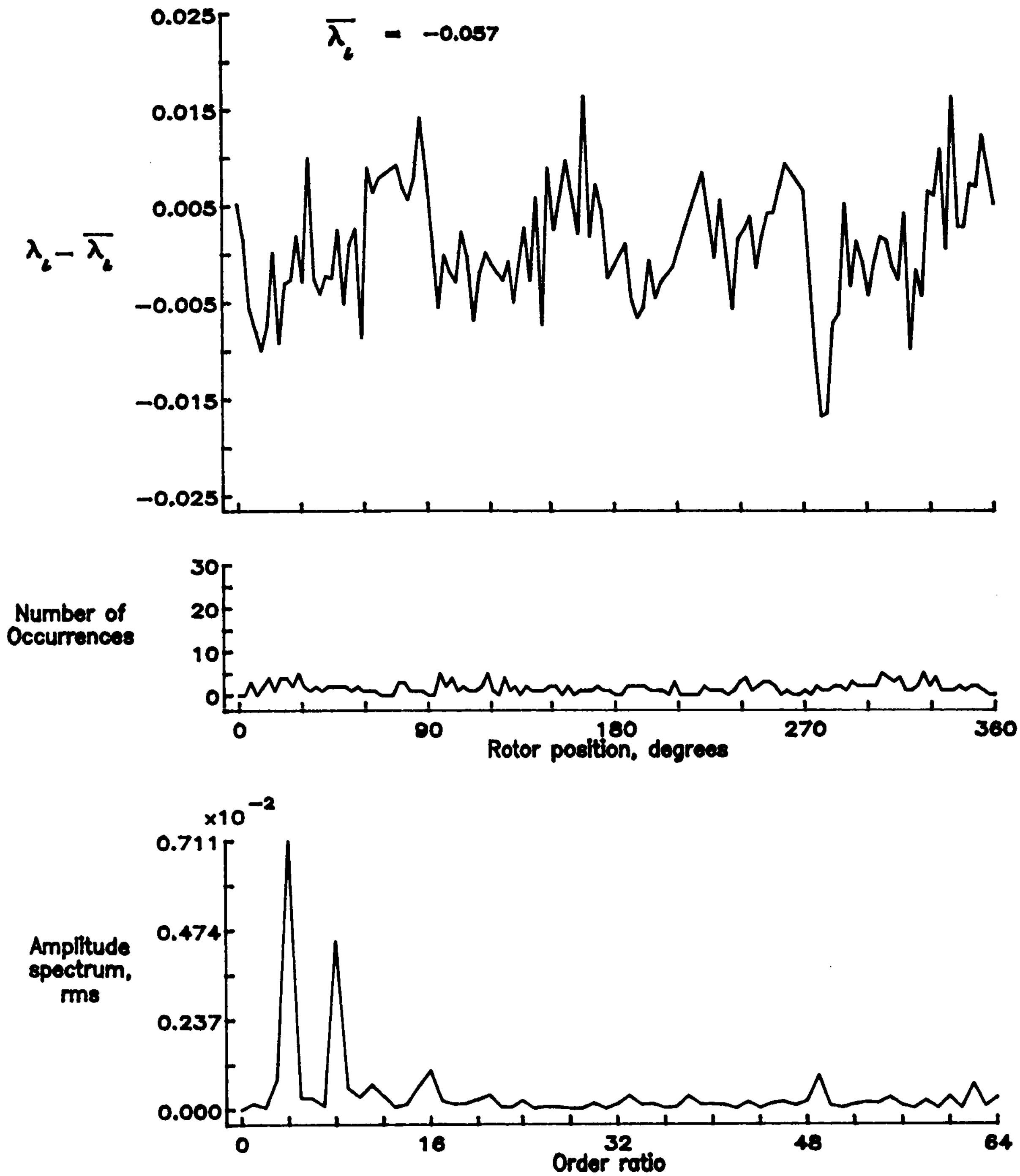

Figure 22.– Concluded.

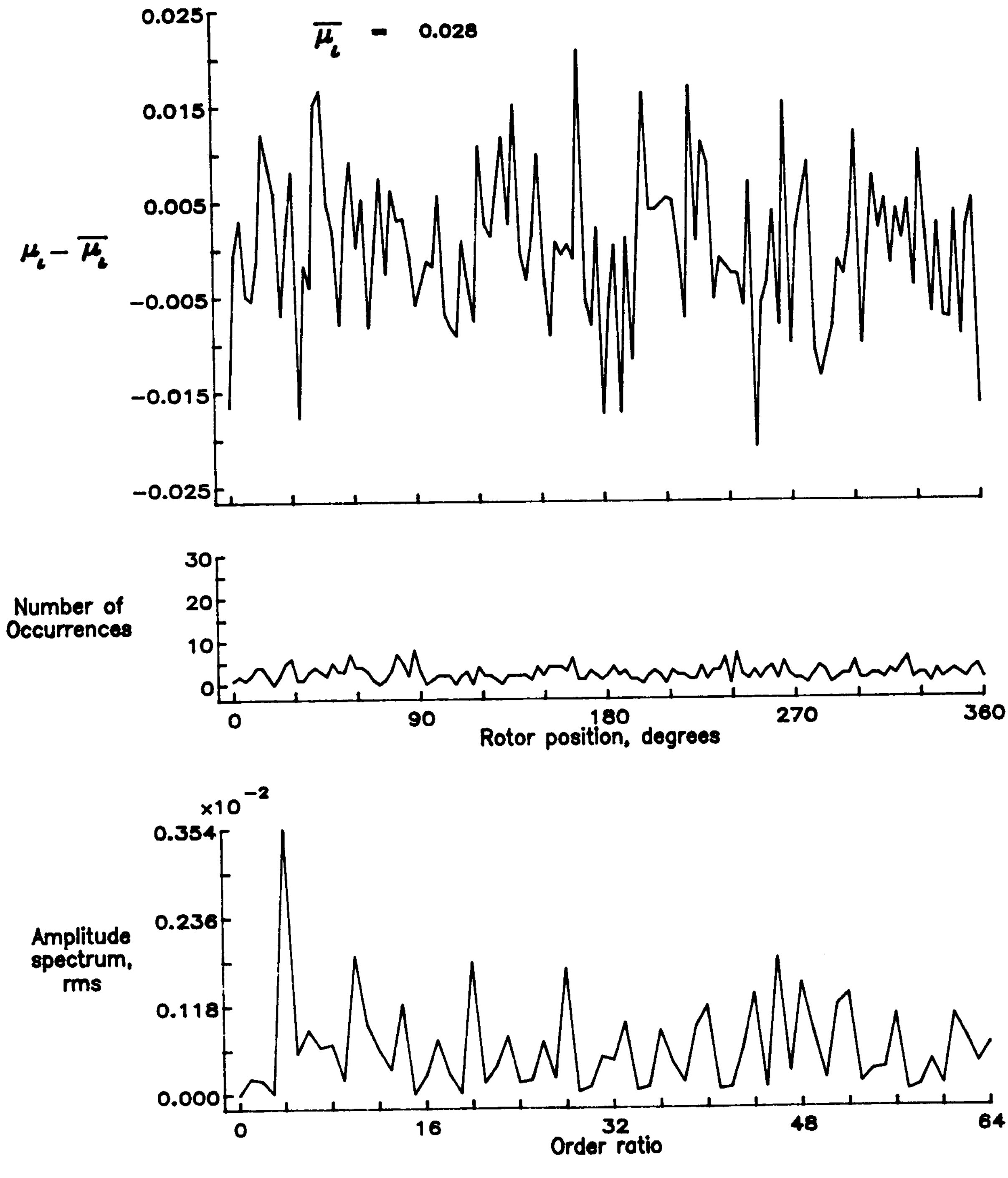

Figure 23.– Induced inflow velocity measured at 30 degrees and r/R of 0.40.

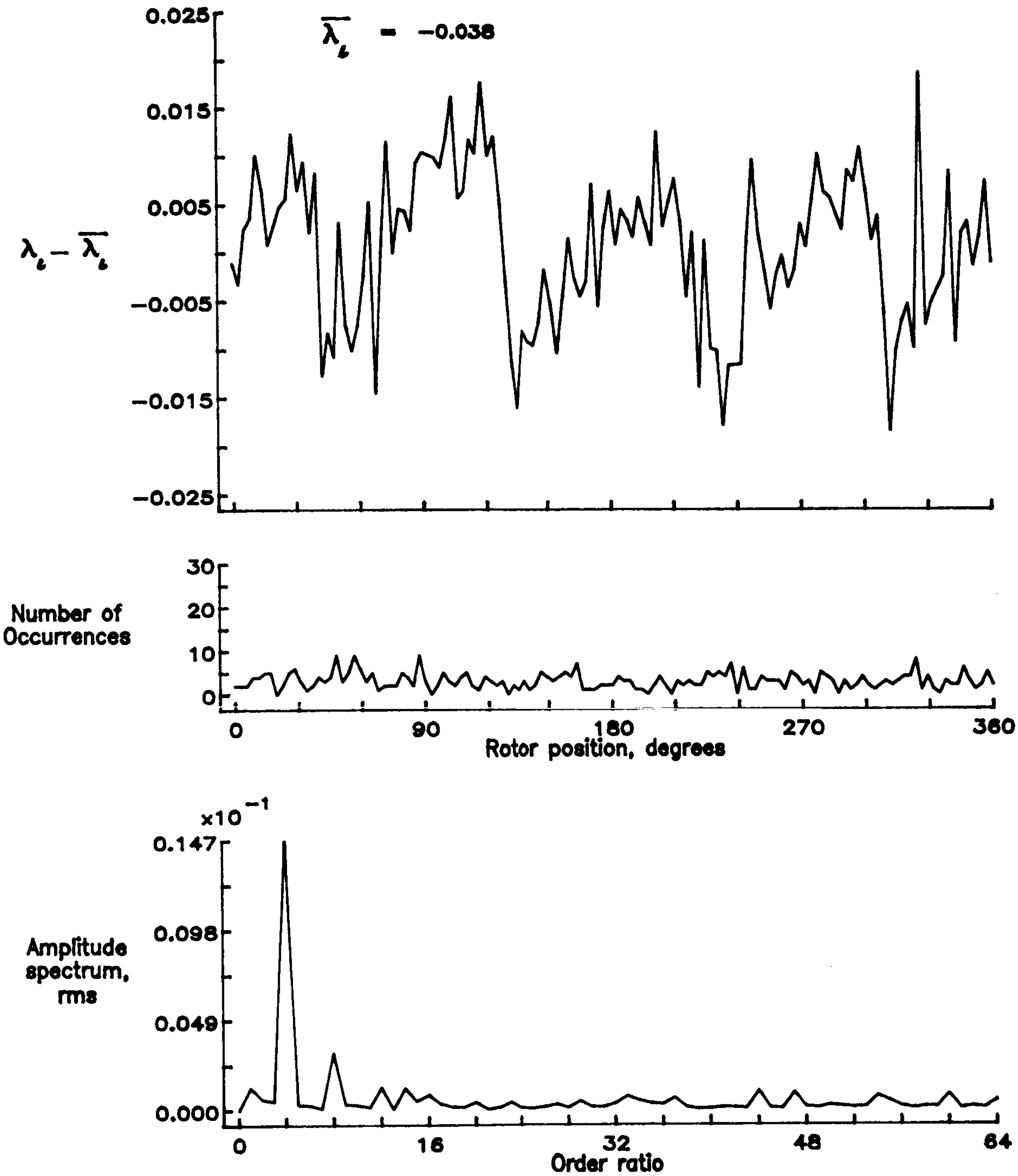

Figure 23.– Concluded.

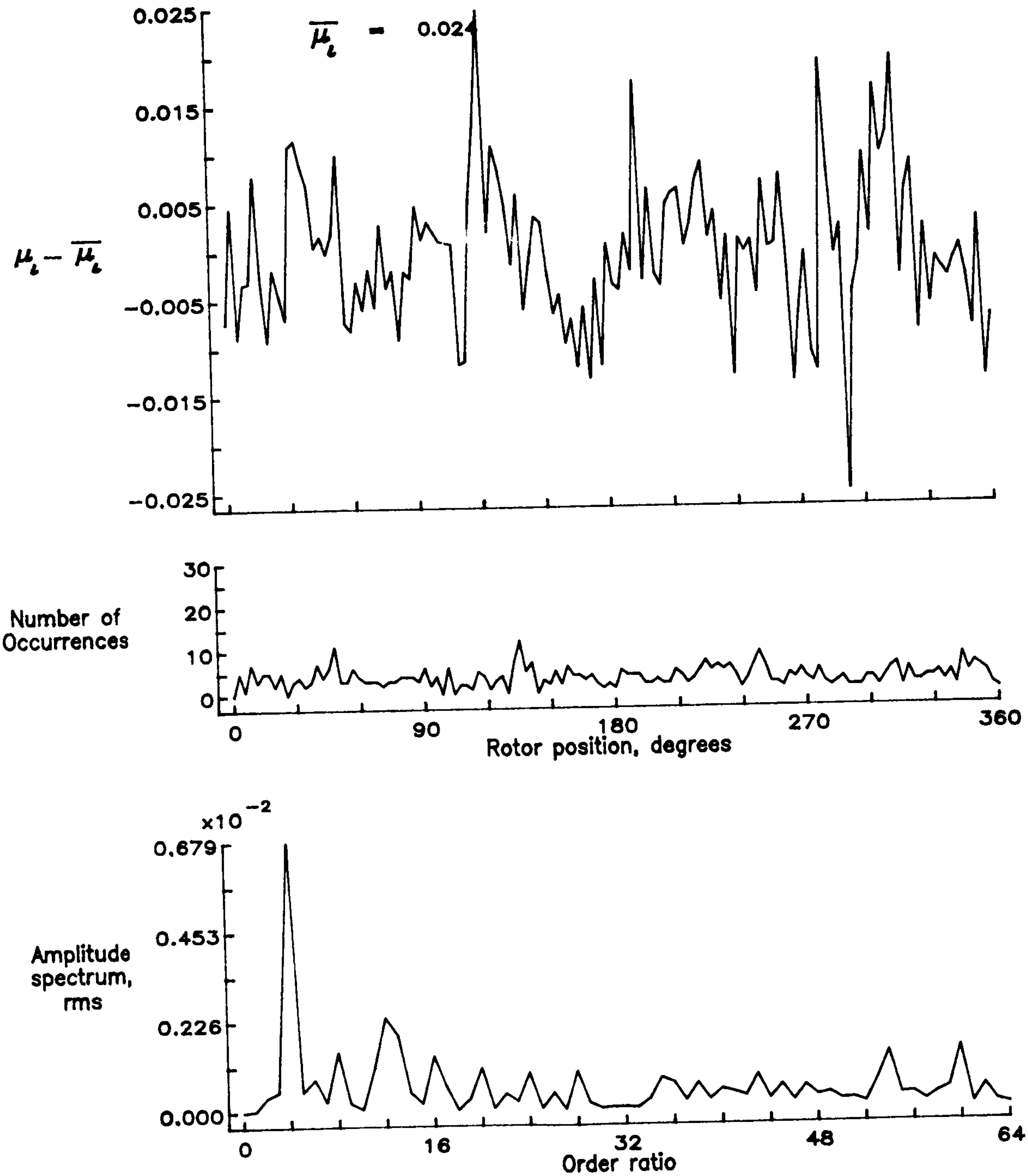

Figure 24.– Induced inflow velocity measured at 30 degrees and r/R of 0.50.

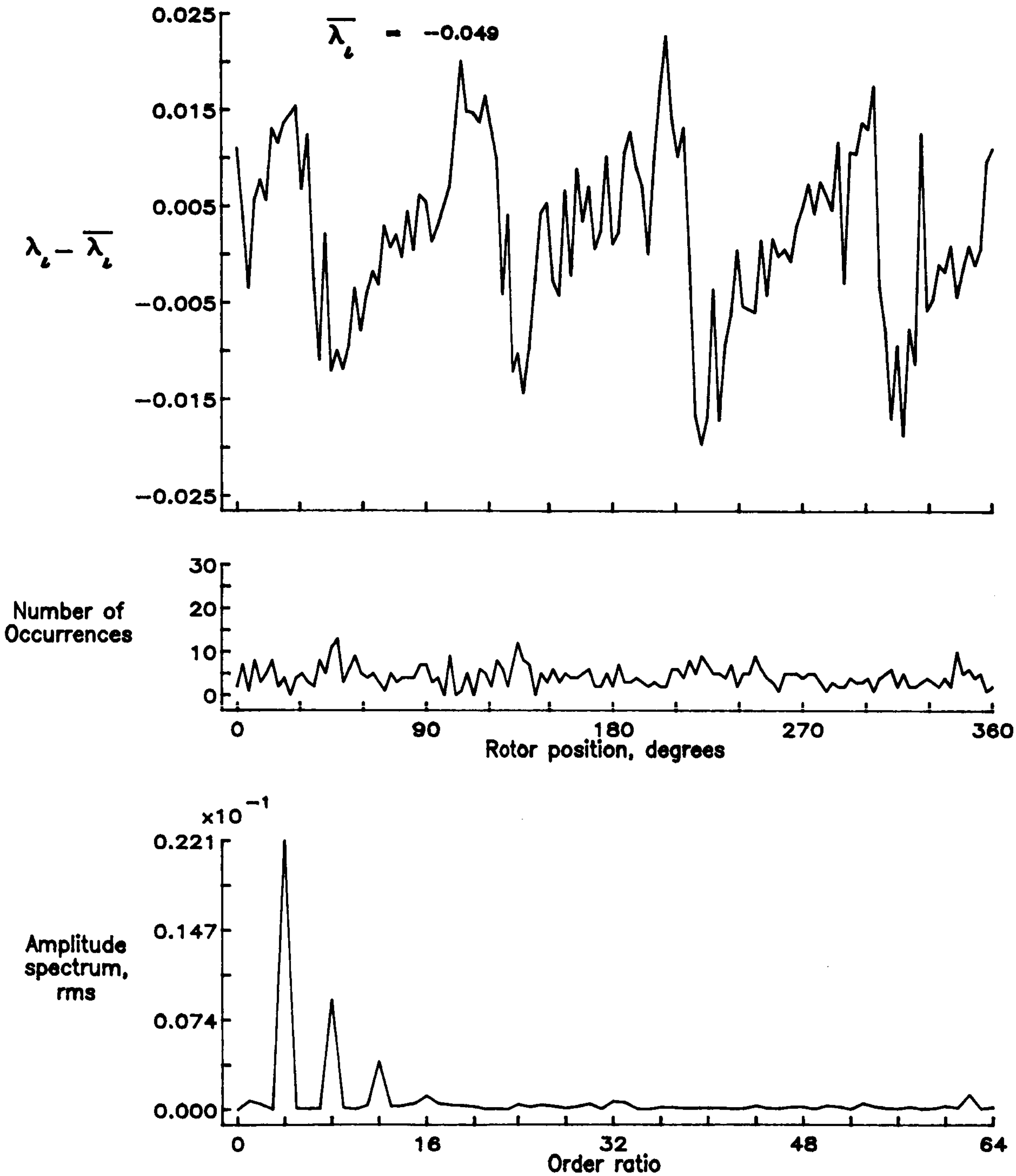

Figure 24.– Concluded.

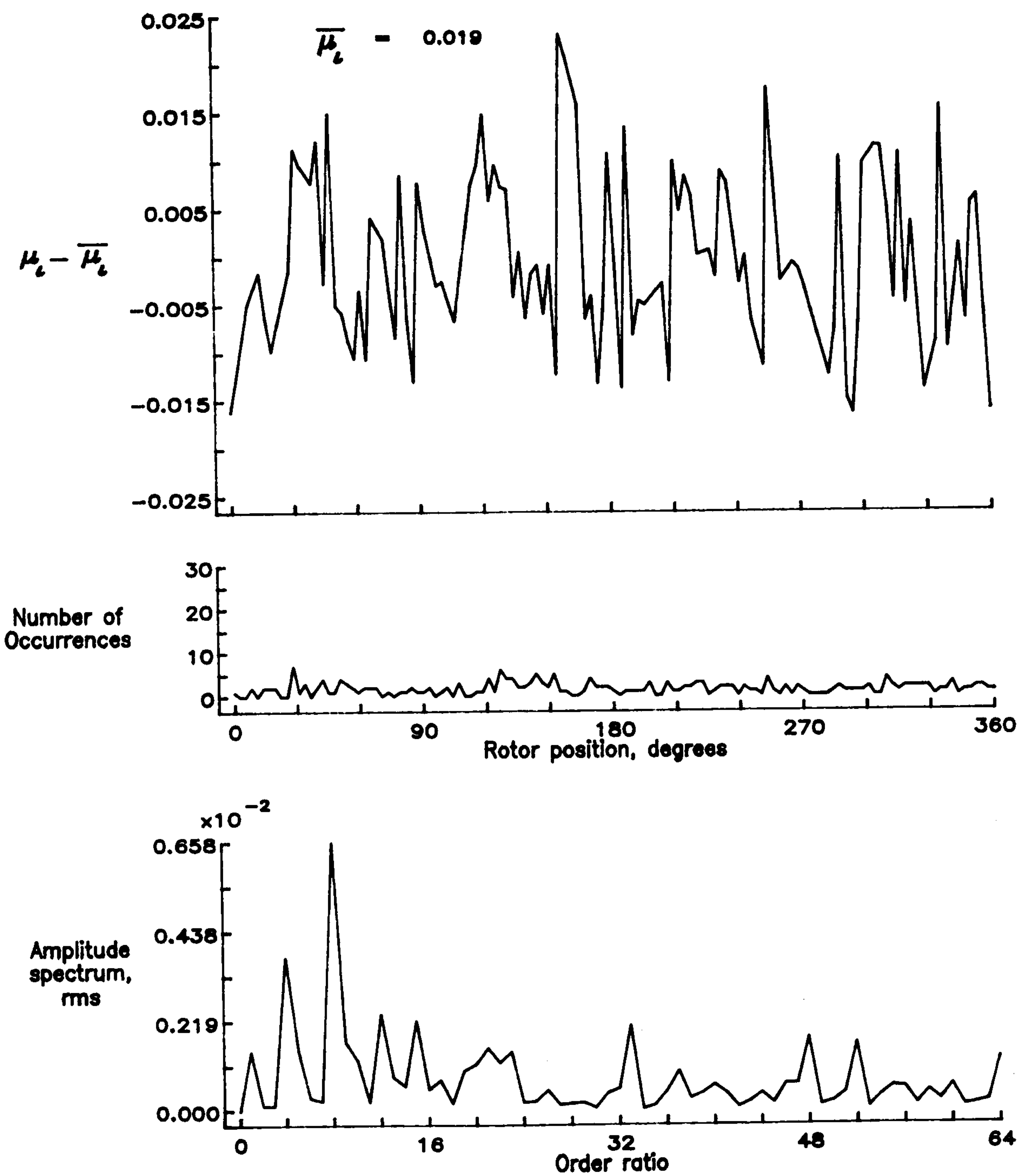

Figure 25.– Induced inflow velocity measured at 30 degrees and r/R of 0.60.

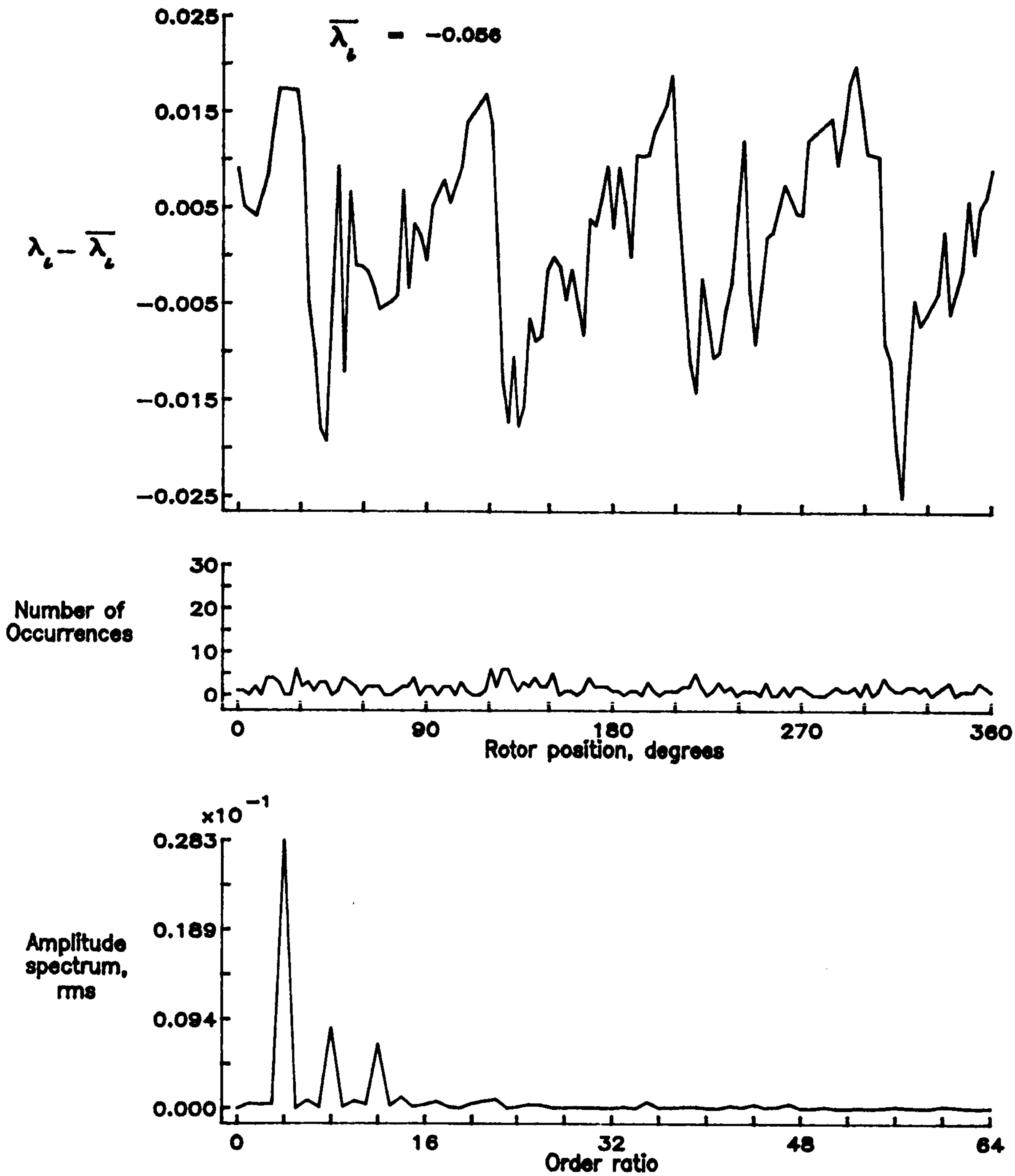

Figure 25.– Concluded.

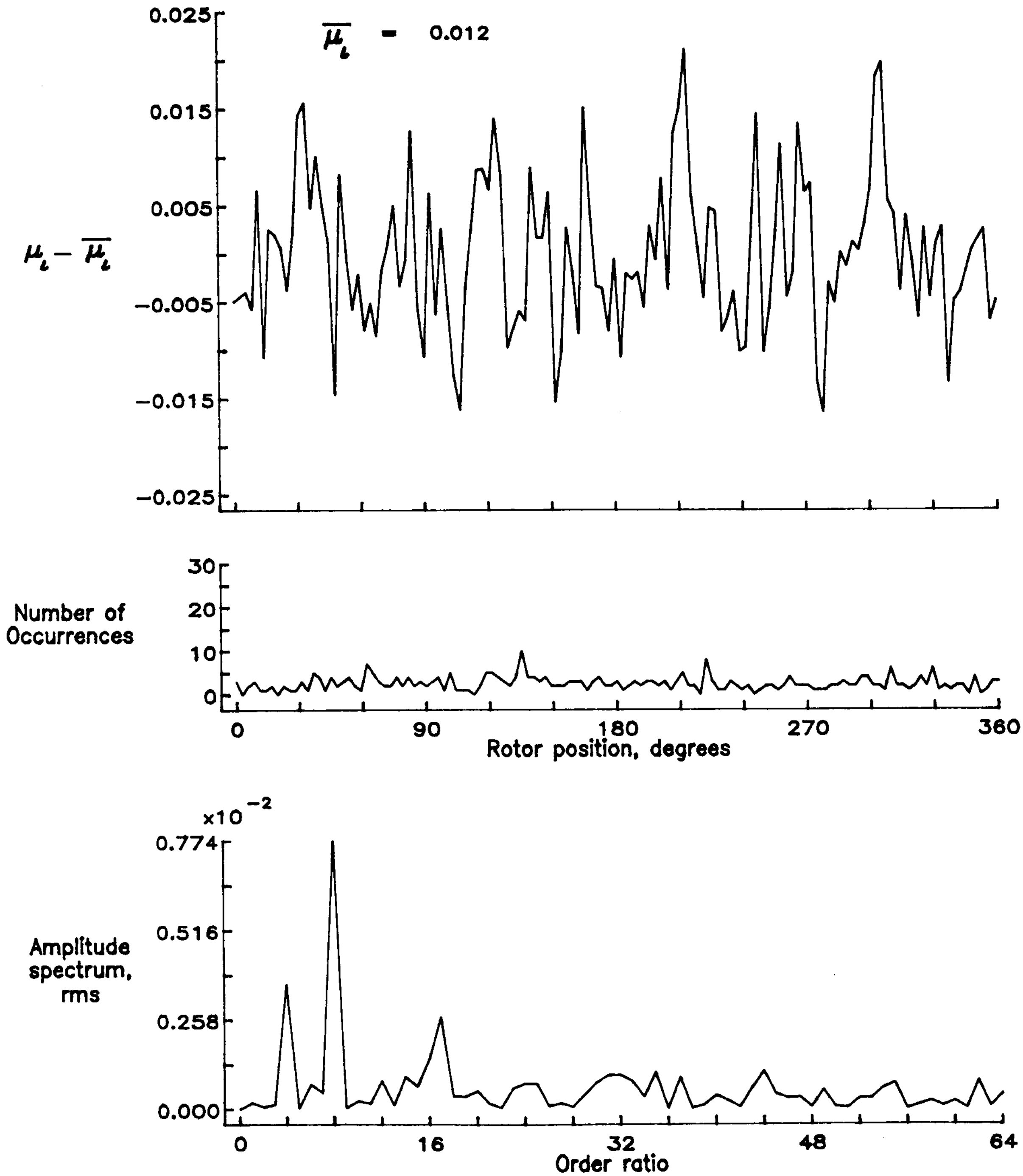

Figure 26.– Induced inflow velocity measured at 30 degrees and r/R of 0.70.

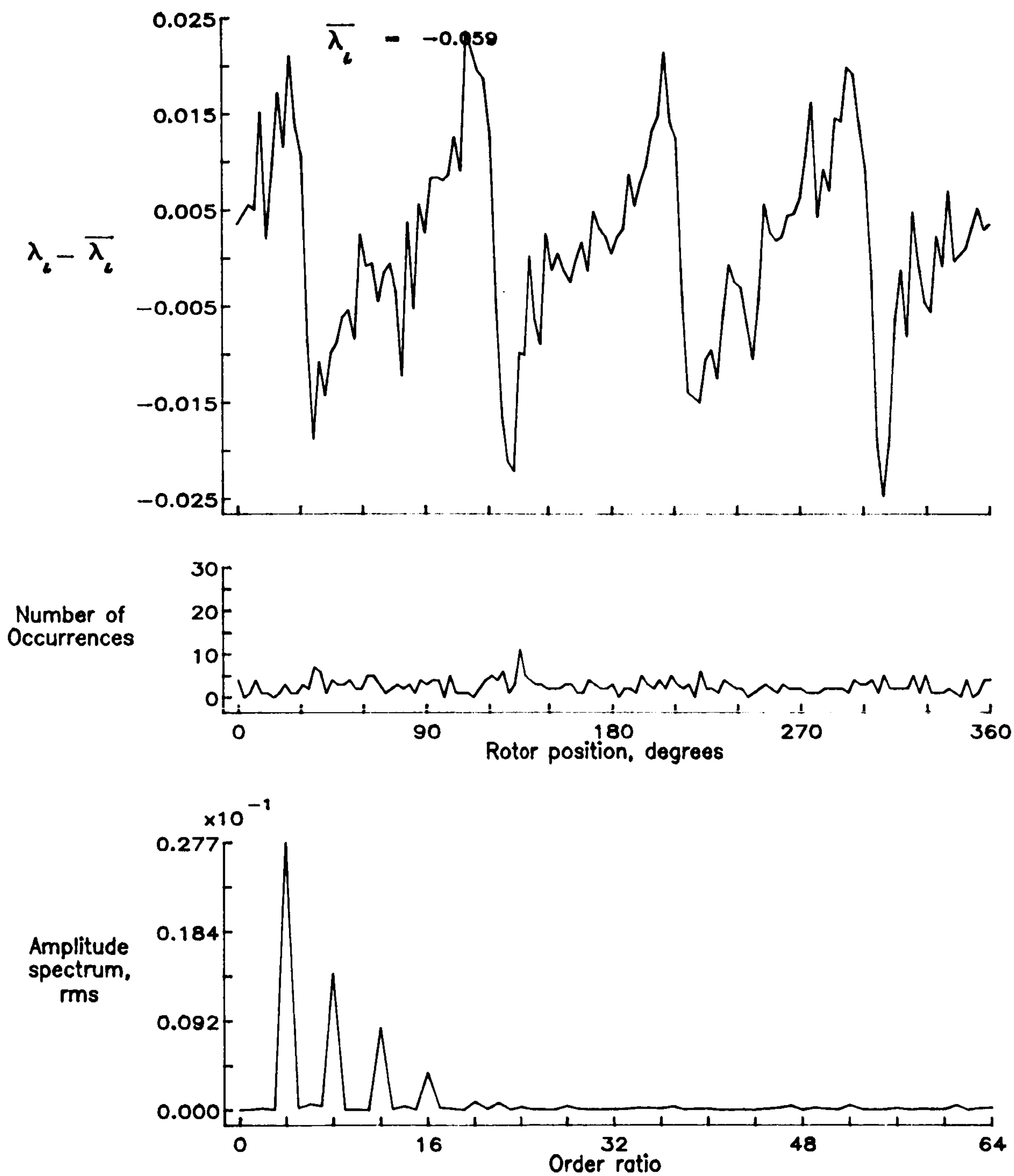

Figure 26.– Concluded.

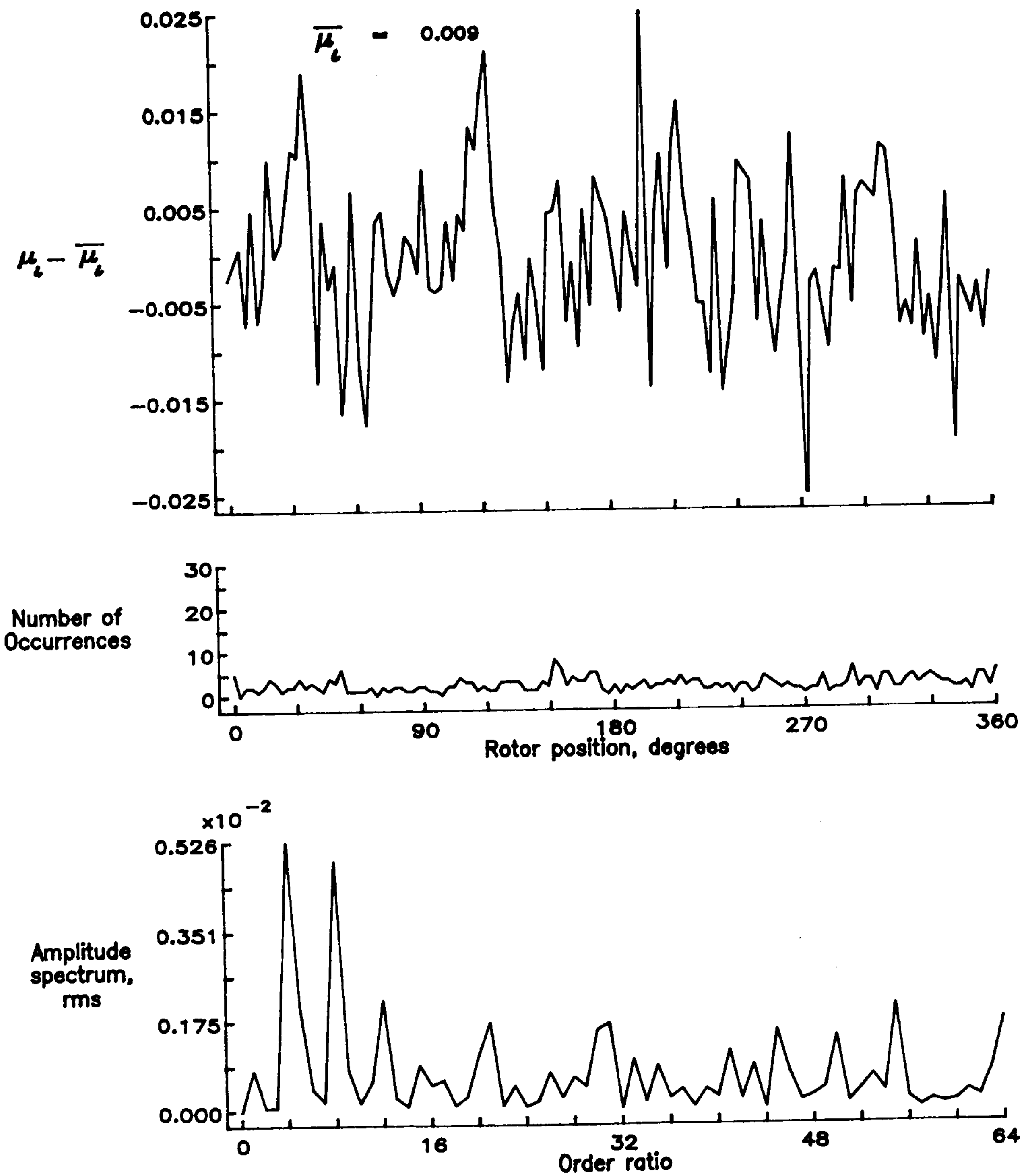

Figure 27.— Induced inflow velocity measured at 30 degrees and r/R of 0.74.

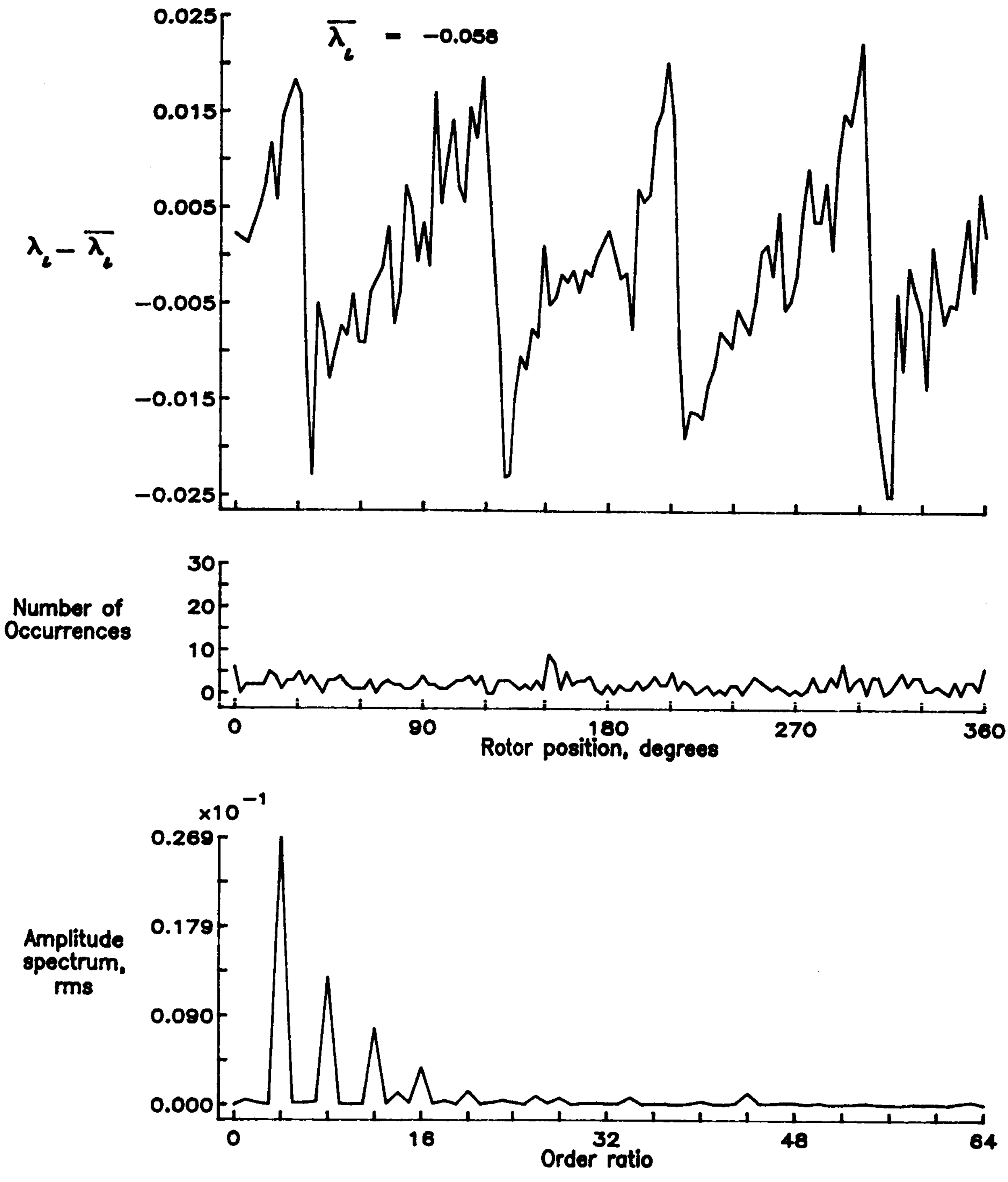

Figure 27.– Concluded.

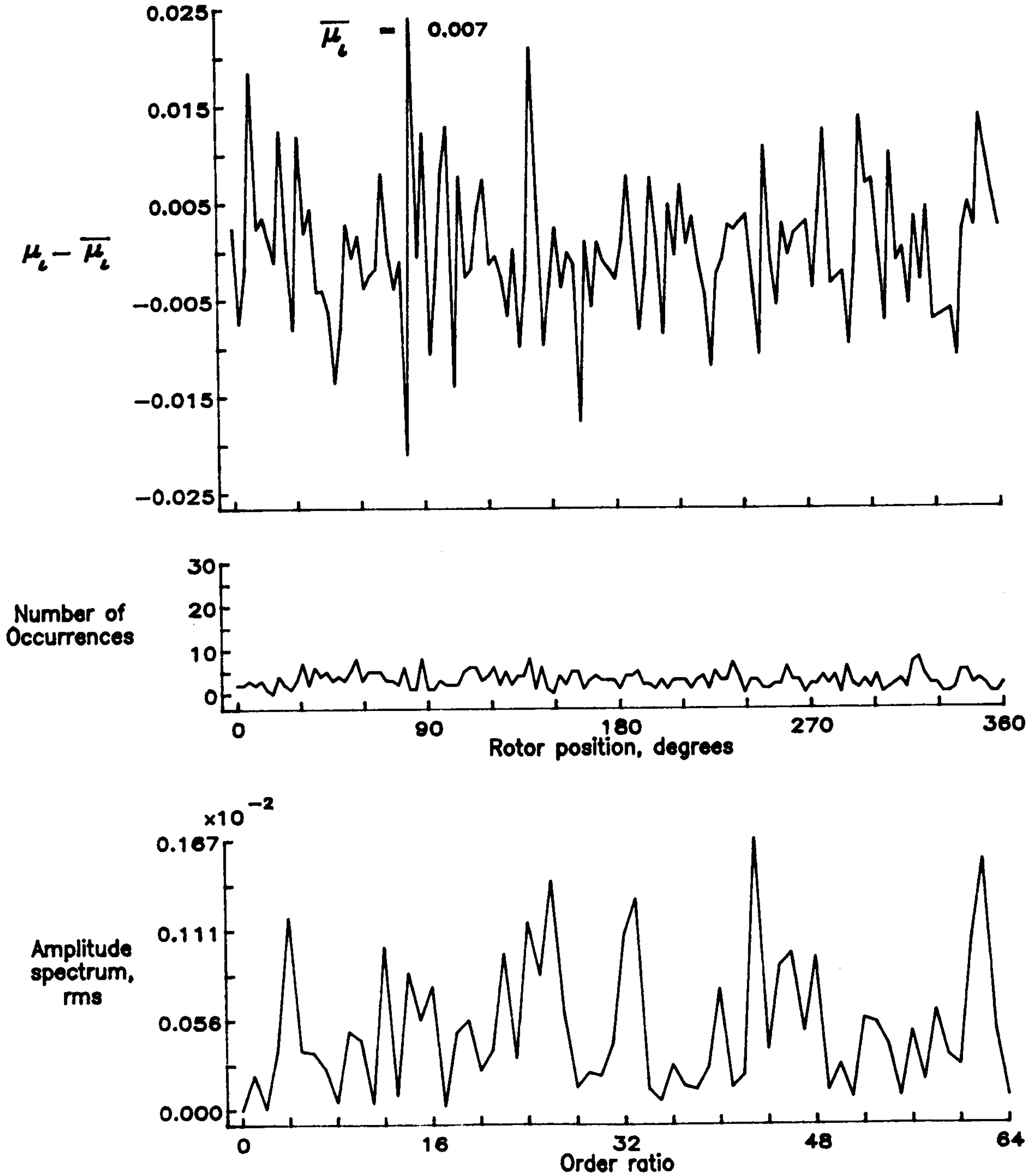

Figure 28.– Induced inflow velocity measured at 30 degrees and r/R of 0.78.

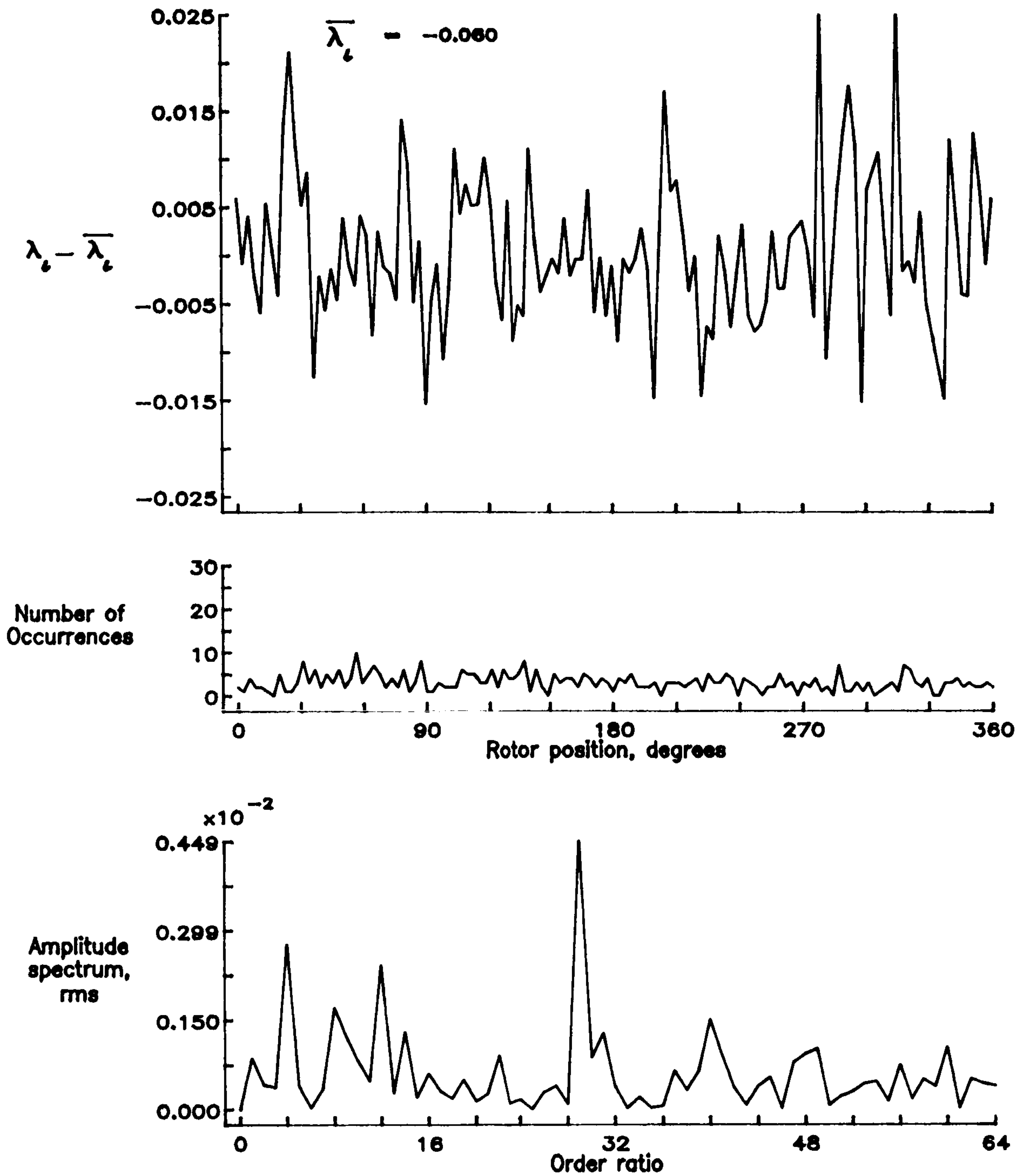

Figure 28.– Concluded.

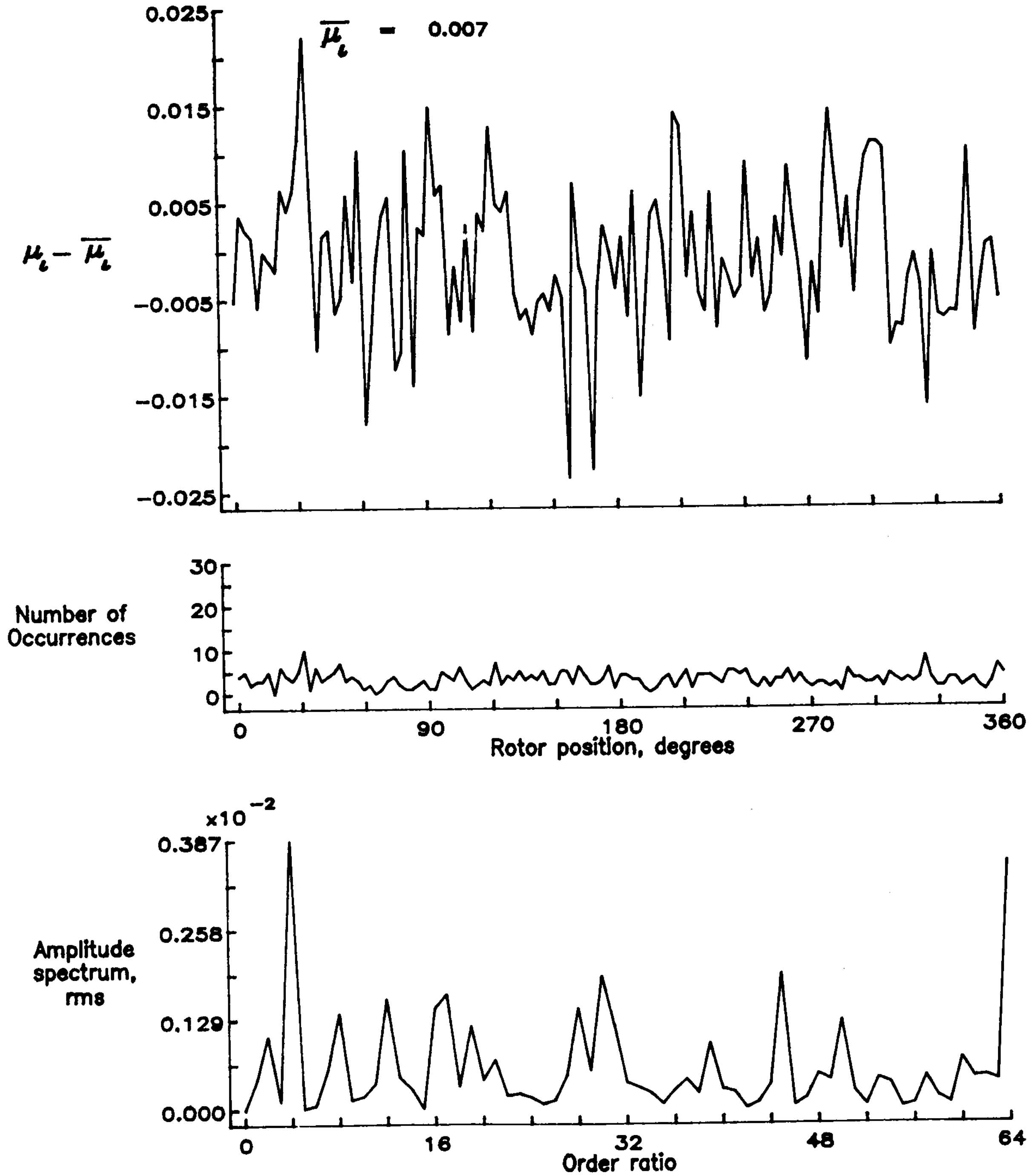

Figure 29.– Induced inflow velocity measured at 30 degrees and r/R of 0.82.

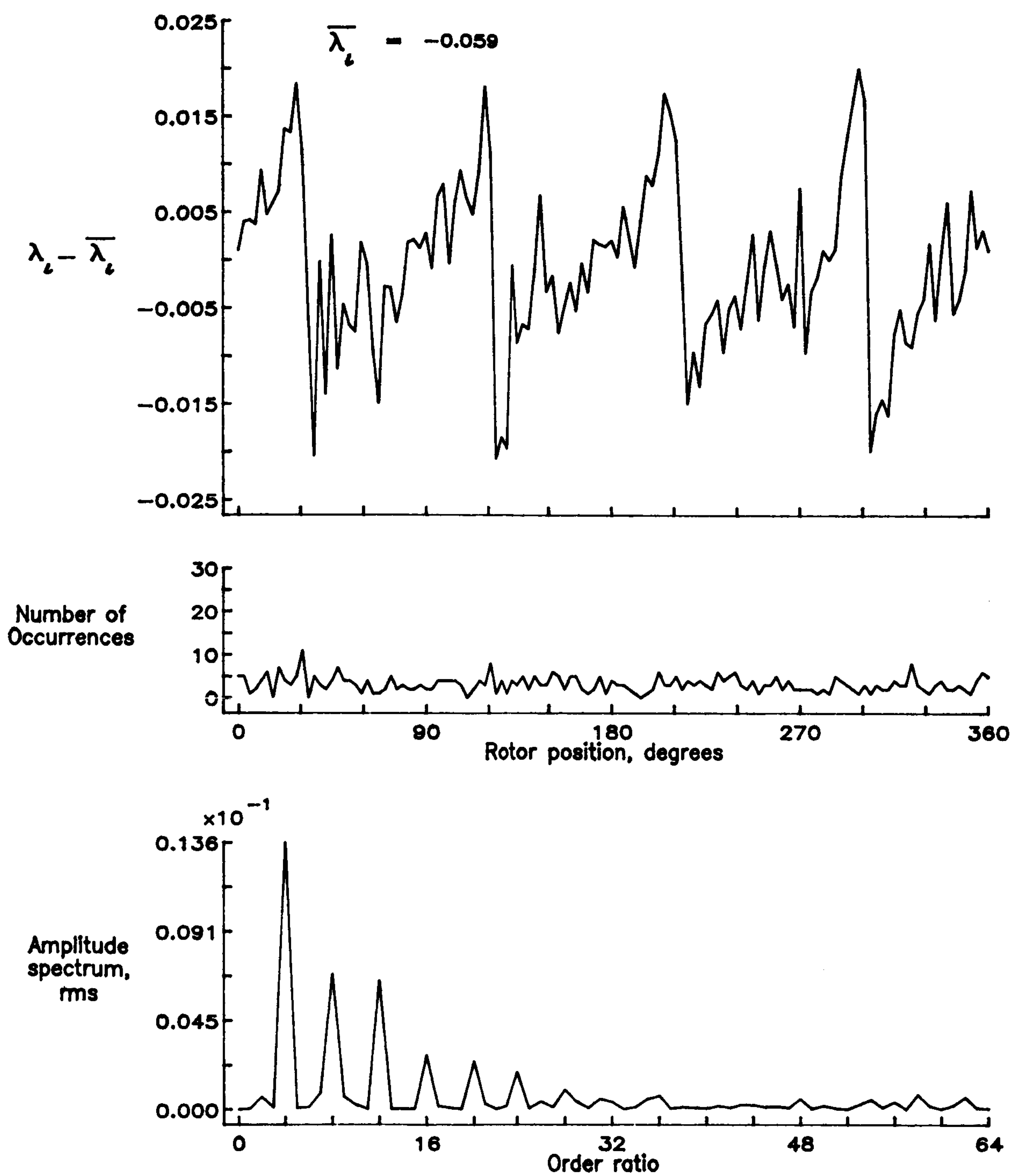

Figure 29.– Concluded.

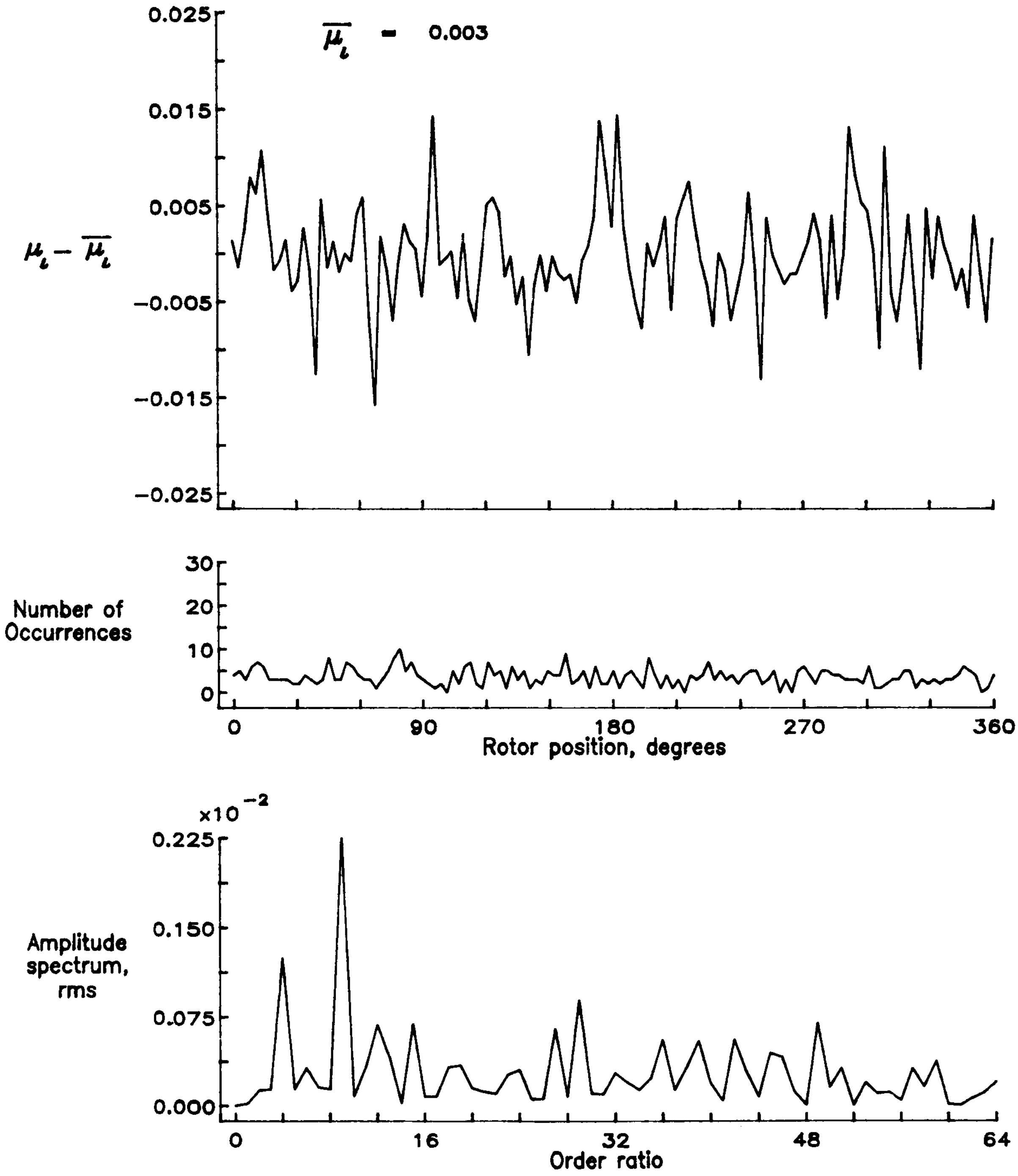

Figure 30.– Induced inflow velocity measured at 30 degrees and r/R of 0.86.

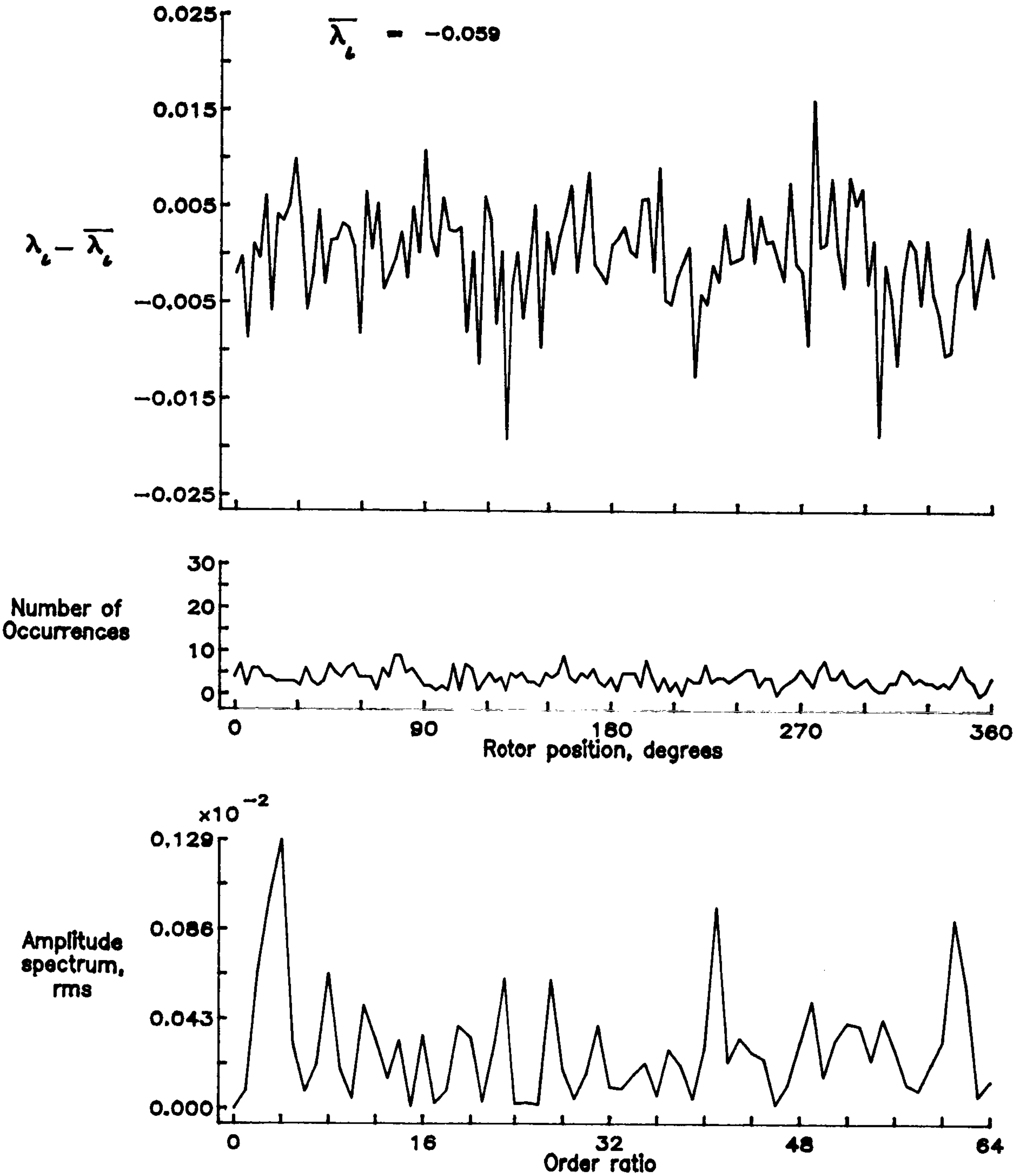

Figure 30.– Concluded.

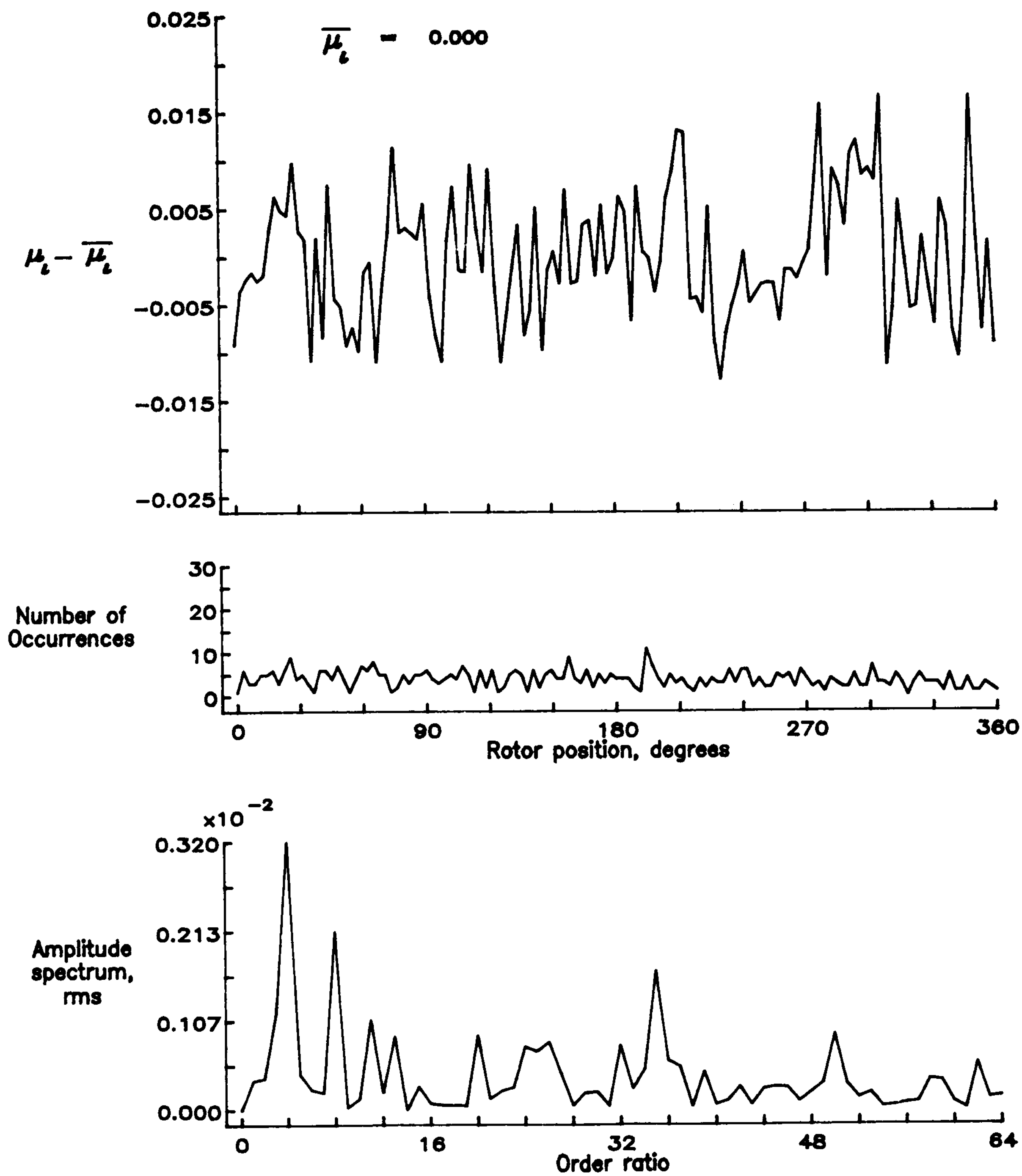

Figure 31.– Induced inflow velocity measured at 30 degrees and r/R of 0.90.

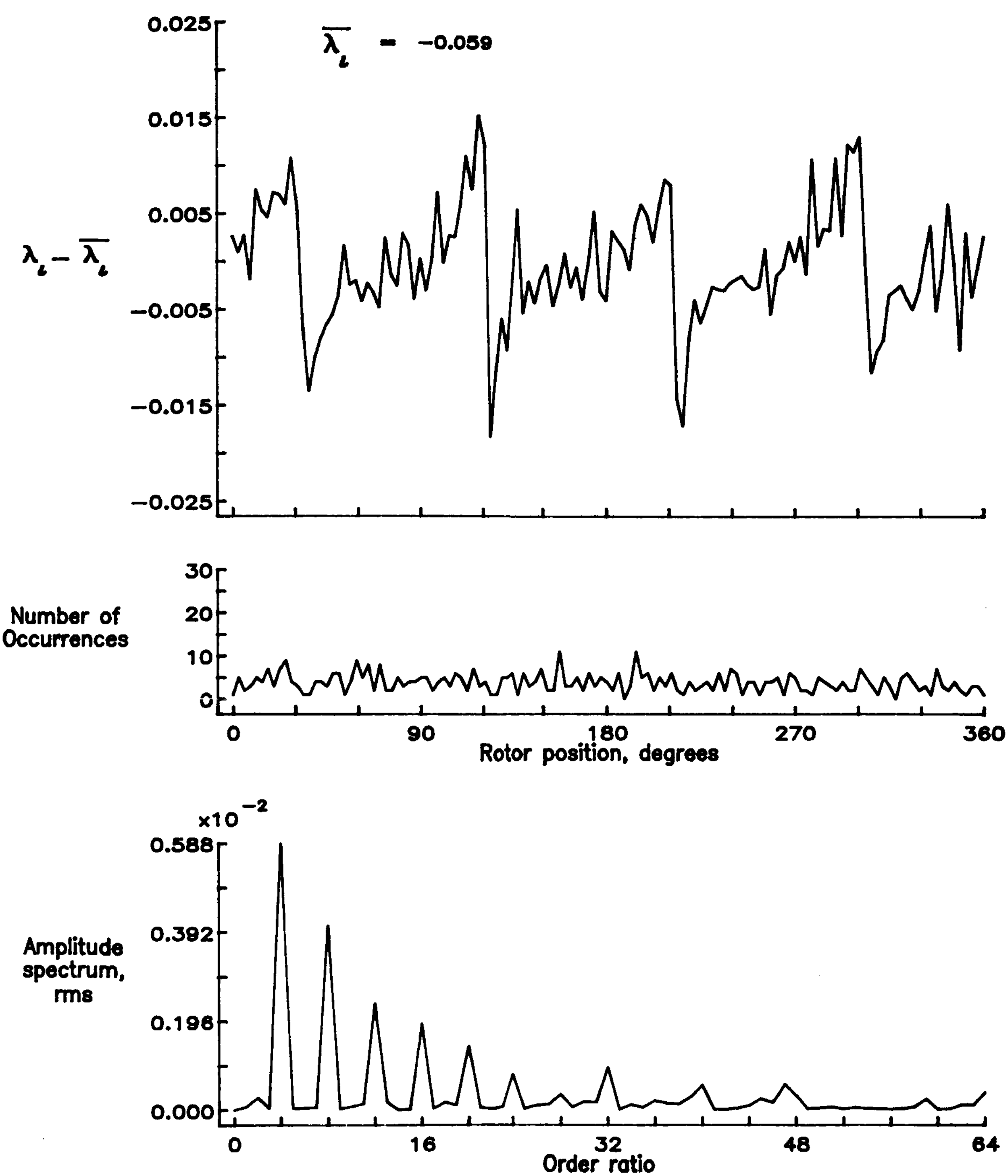

Figure 31.– Concluded.

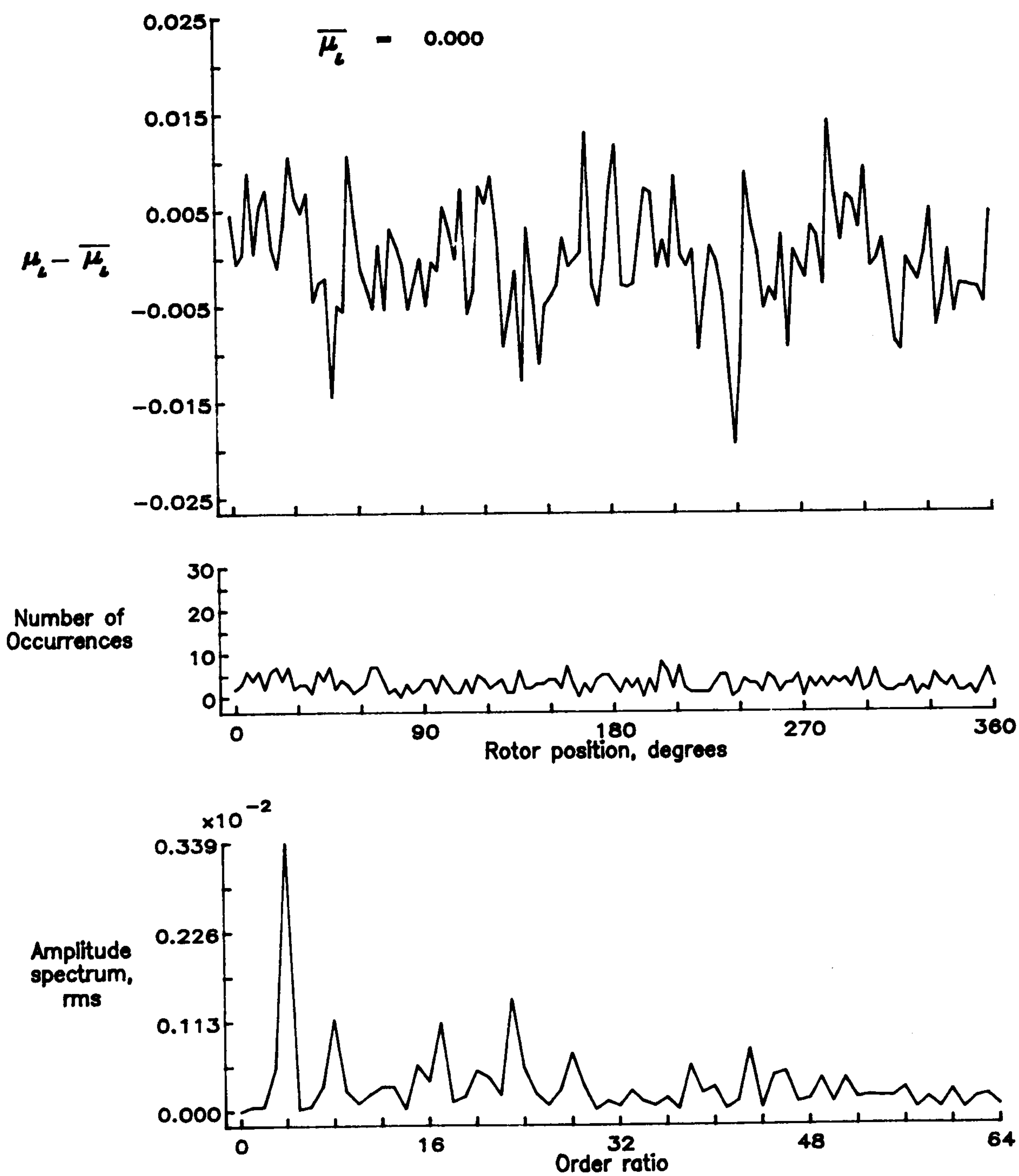

Figure 32.– Induced inflow velocity measured at 30 degrees and r/R of 0.94.

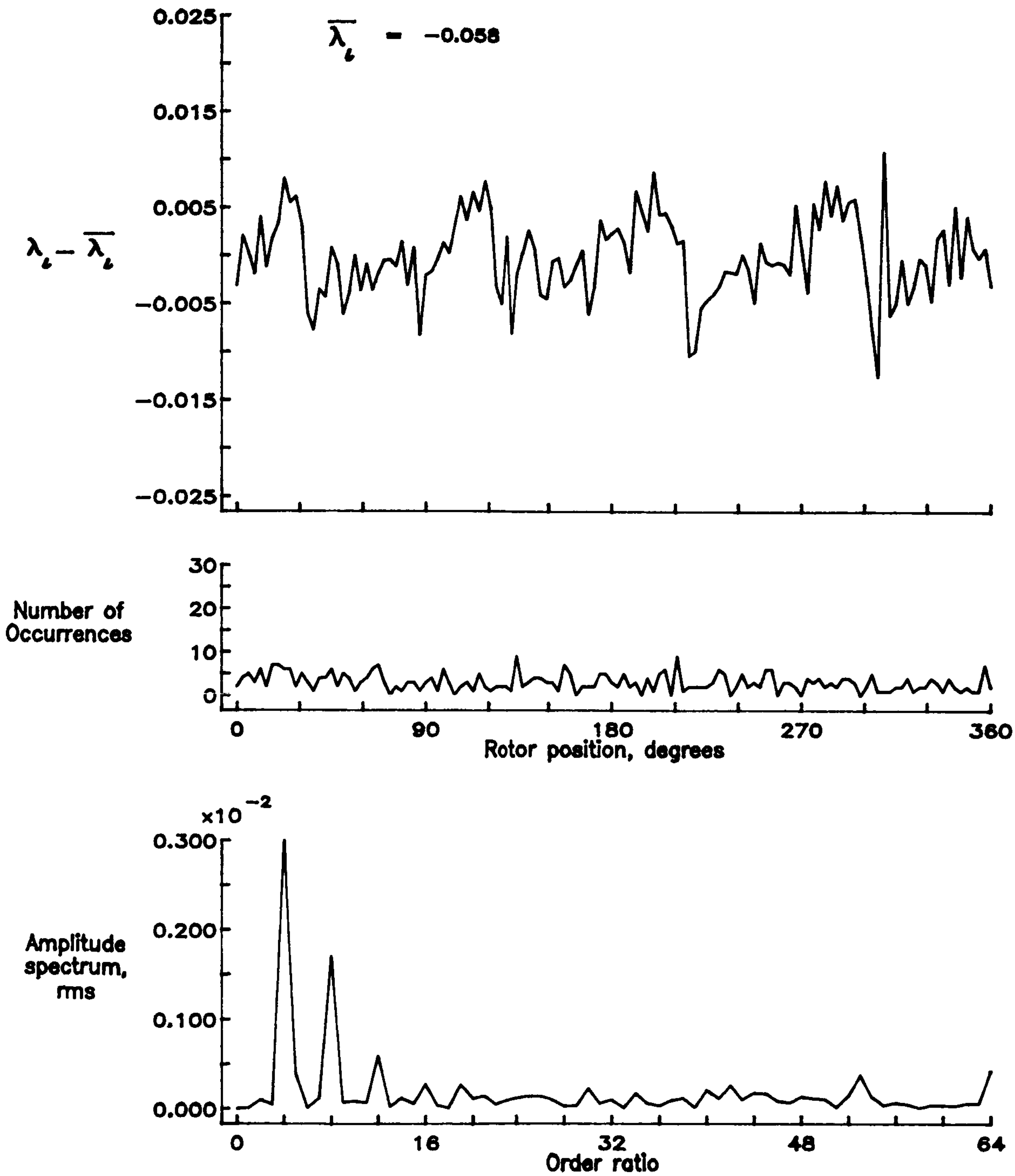

Figure 32.– Concluded.

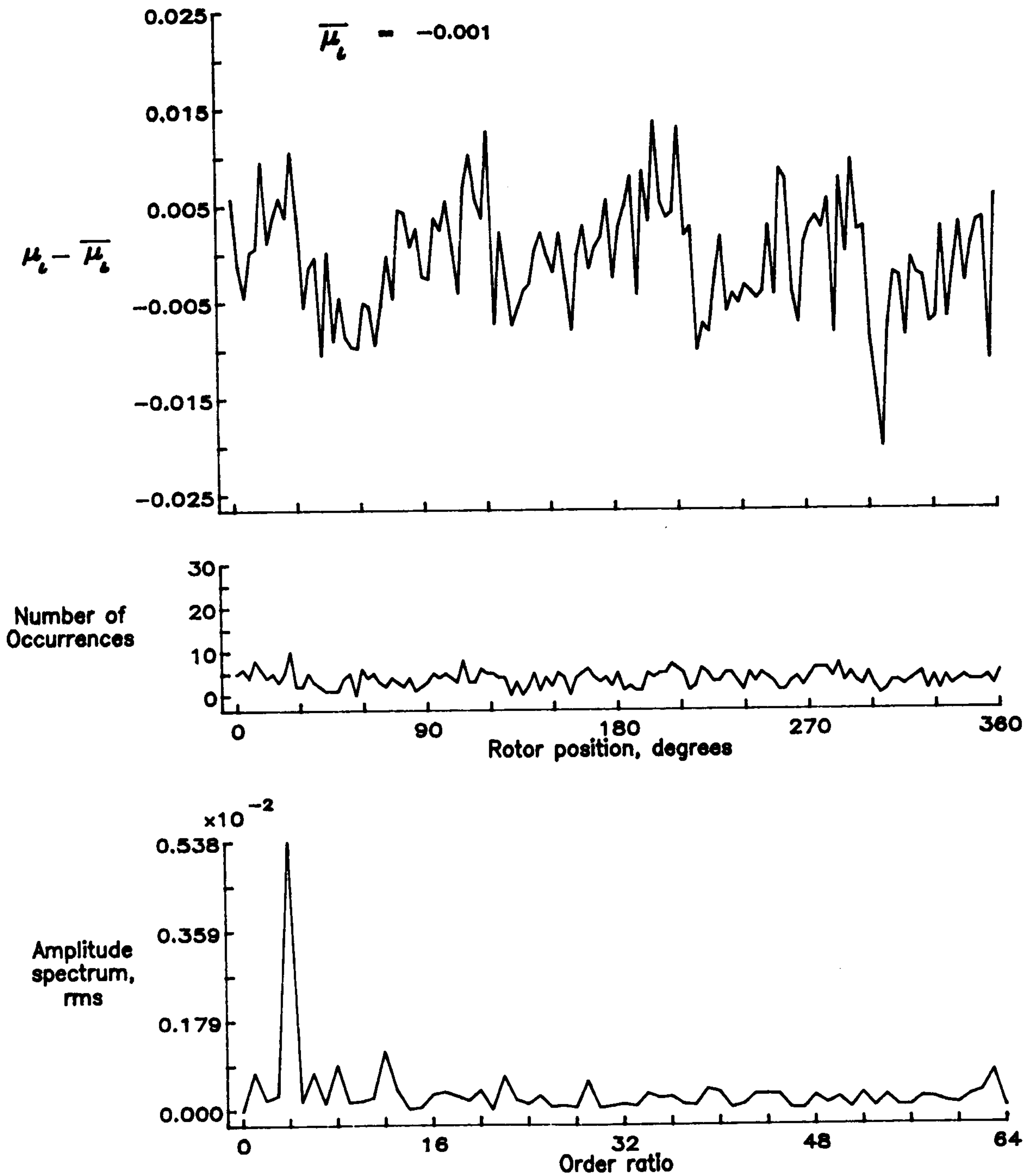

Figure 33.– Induced inflow velocity measured at 30 degrees and r/R of 0.98.

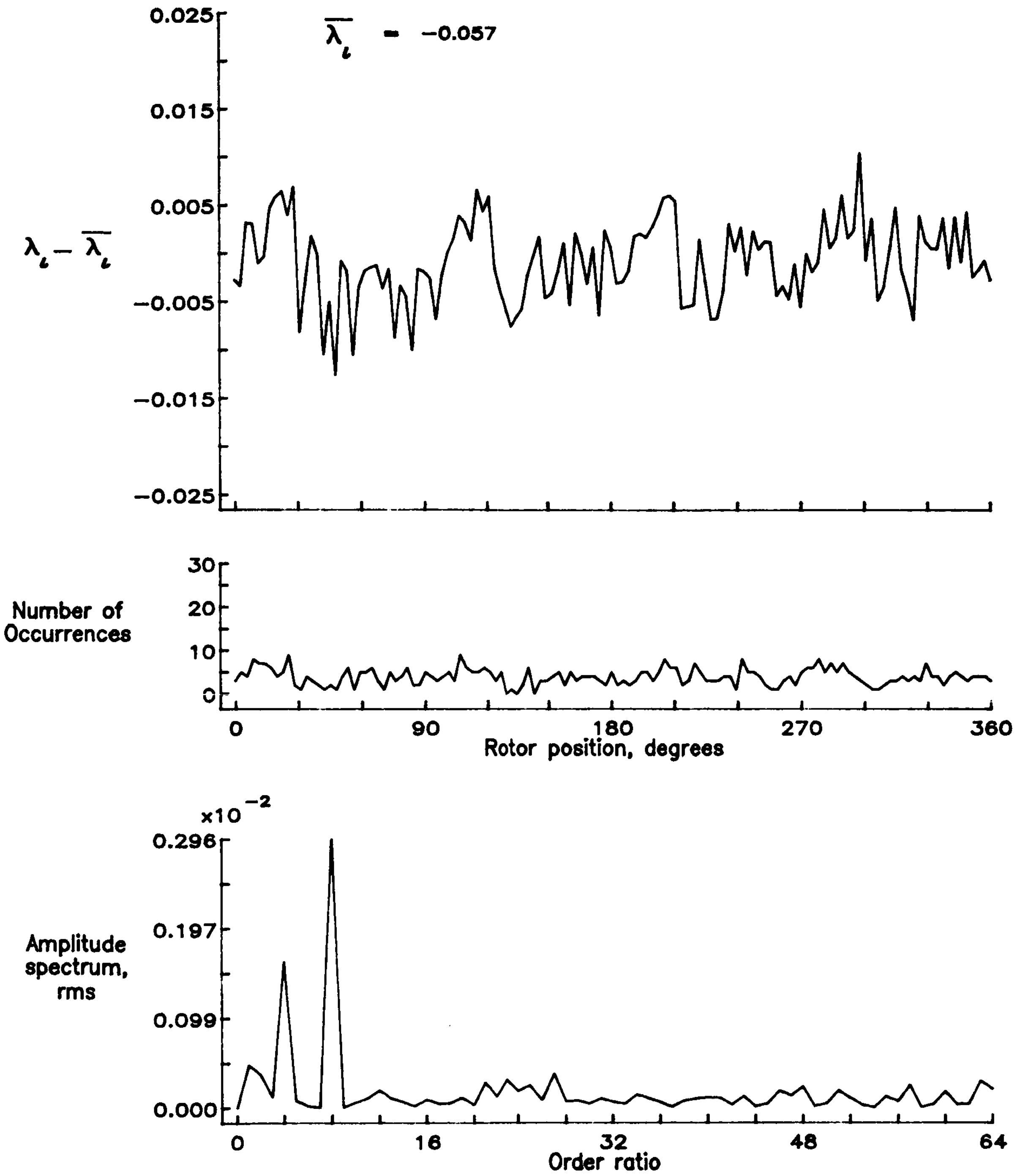

Figure 33.– Concluded.

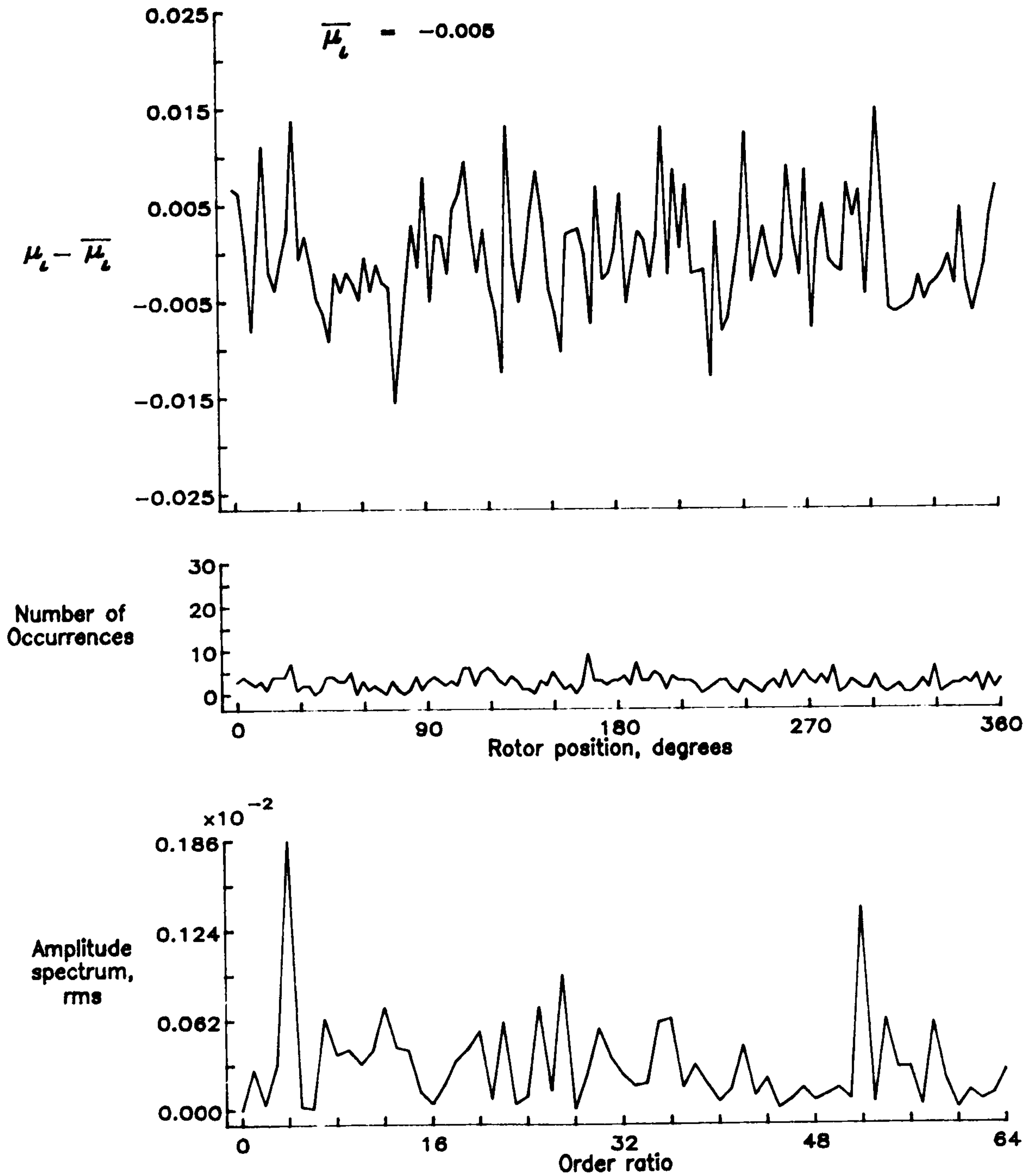

Figure 34.– Induced inflow velocity measured at 30 degrees and r/R of 1.04.

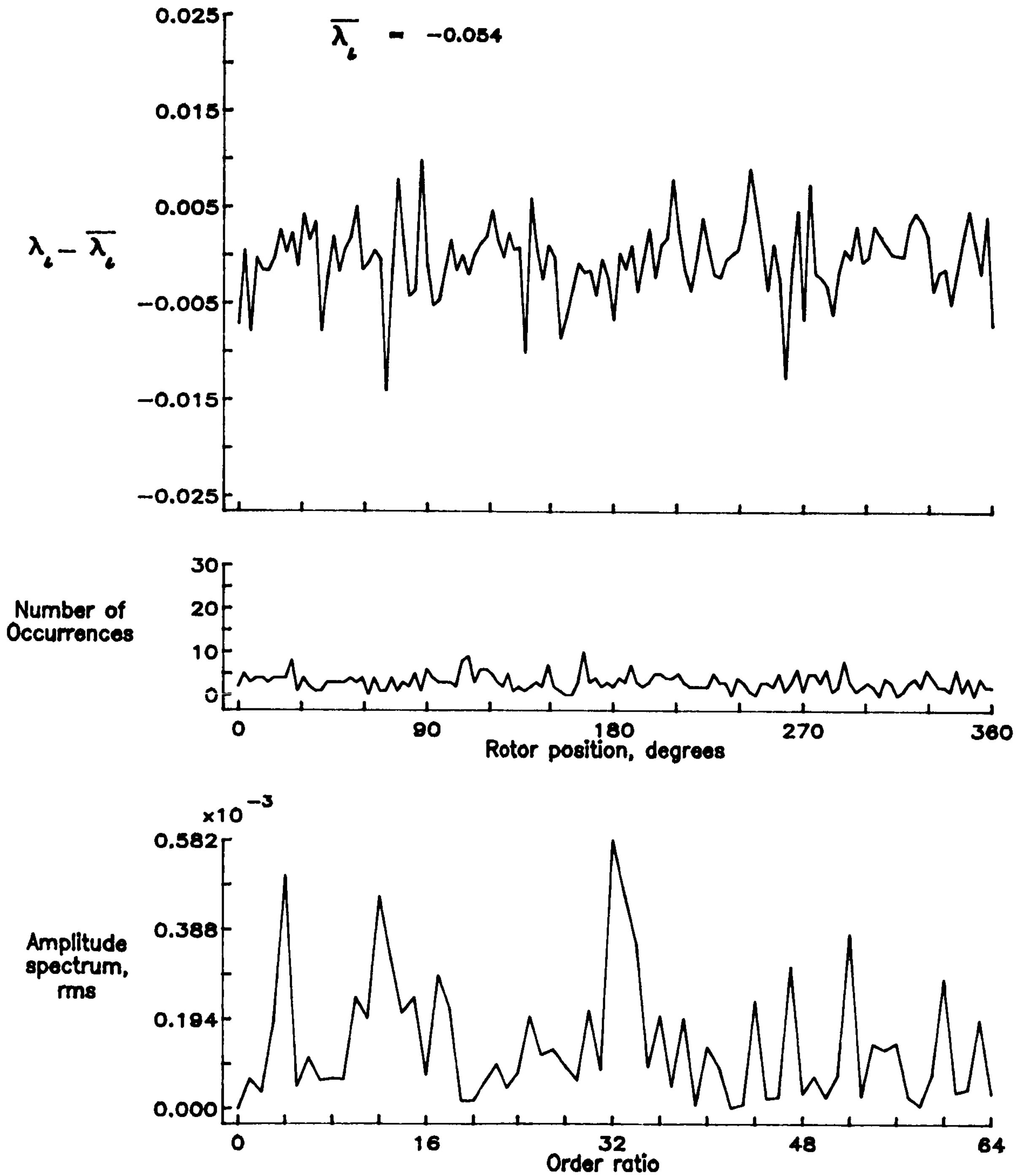

Figure 34.– Concluded.

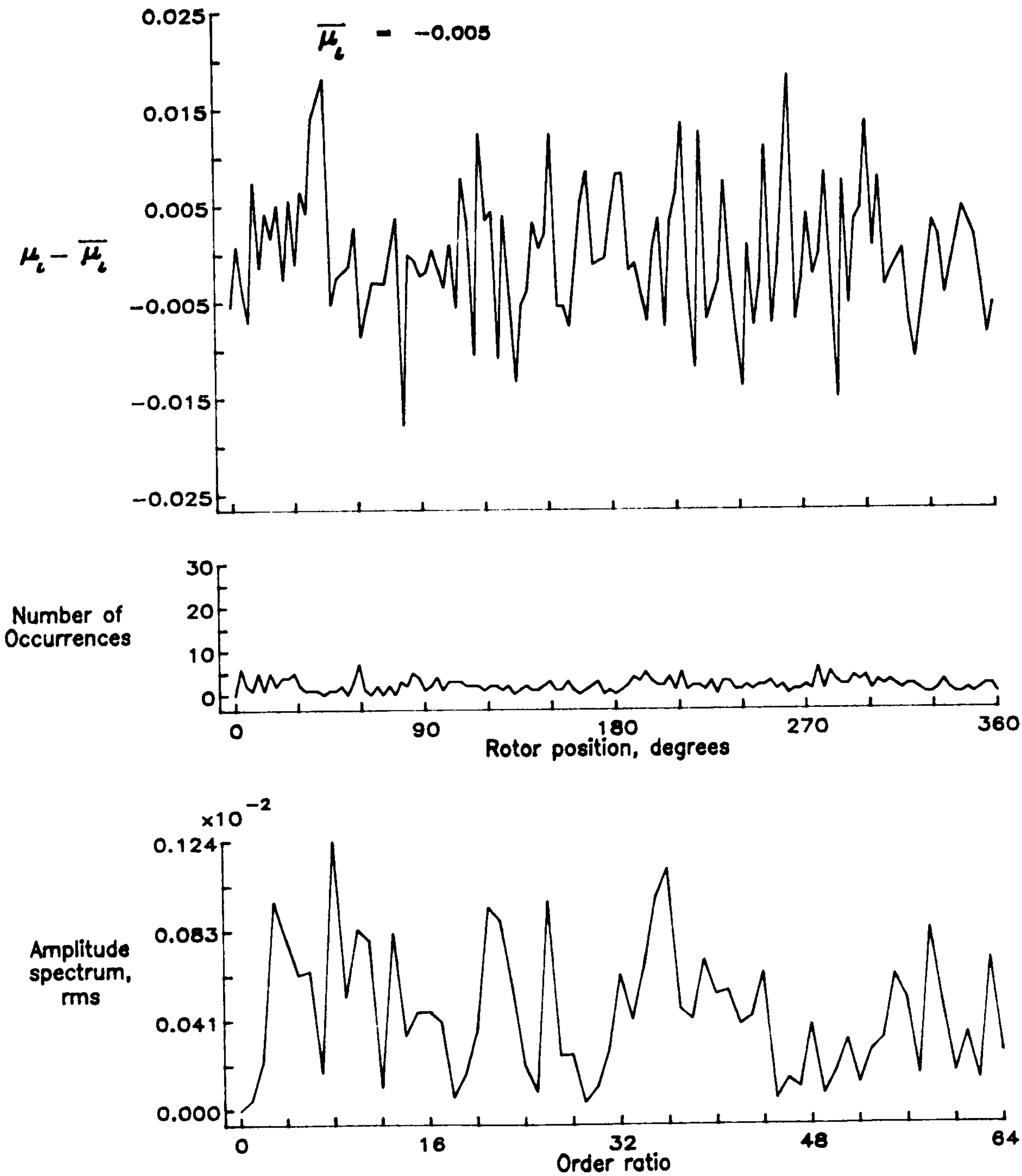

Figure 35.– Induced inflow velocity measured at 30 degrees and r/R of 1.10.

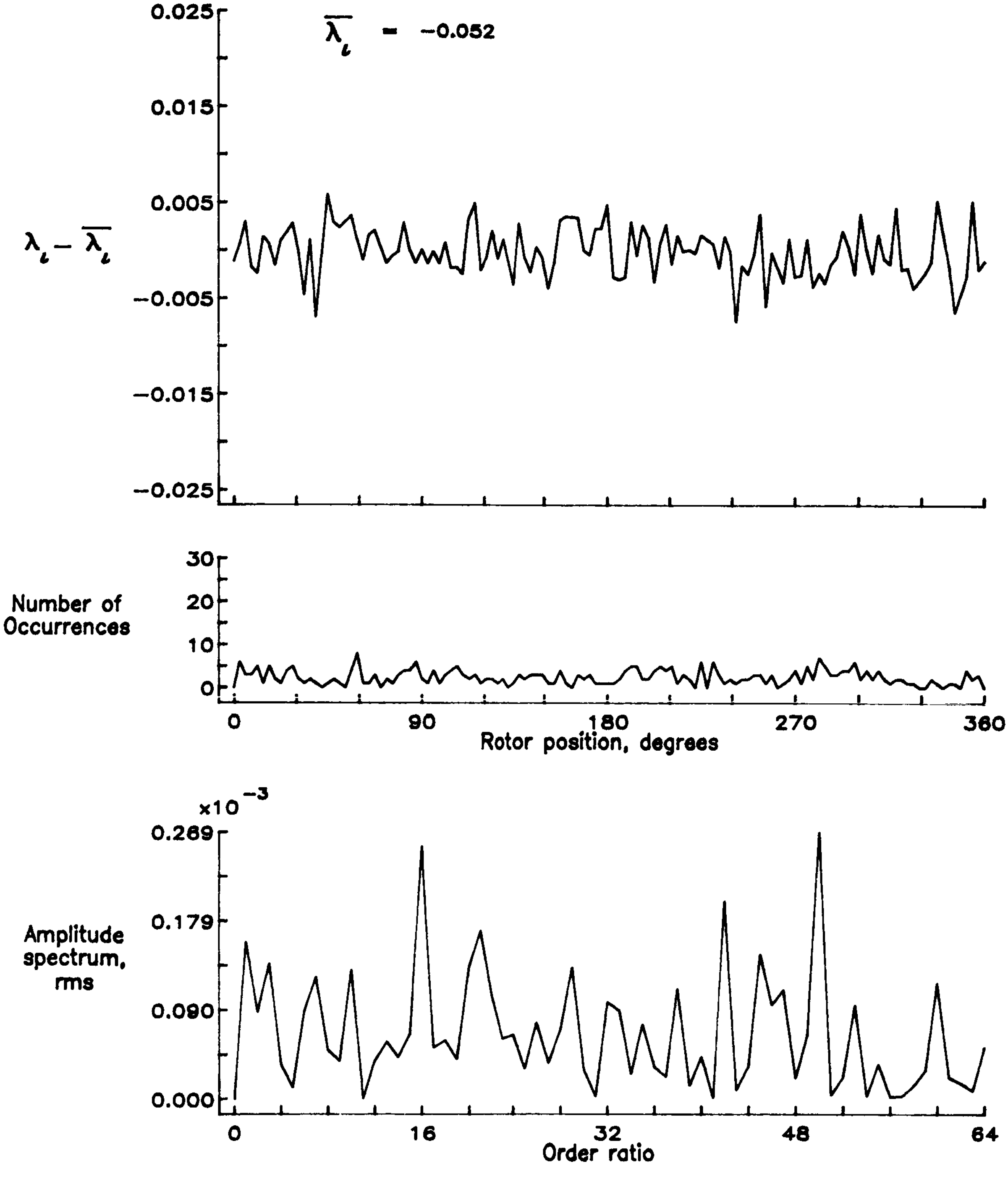

Figure 35.– Concluded.

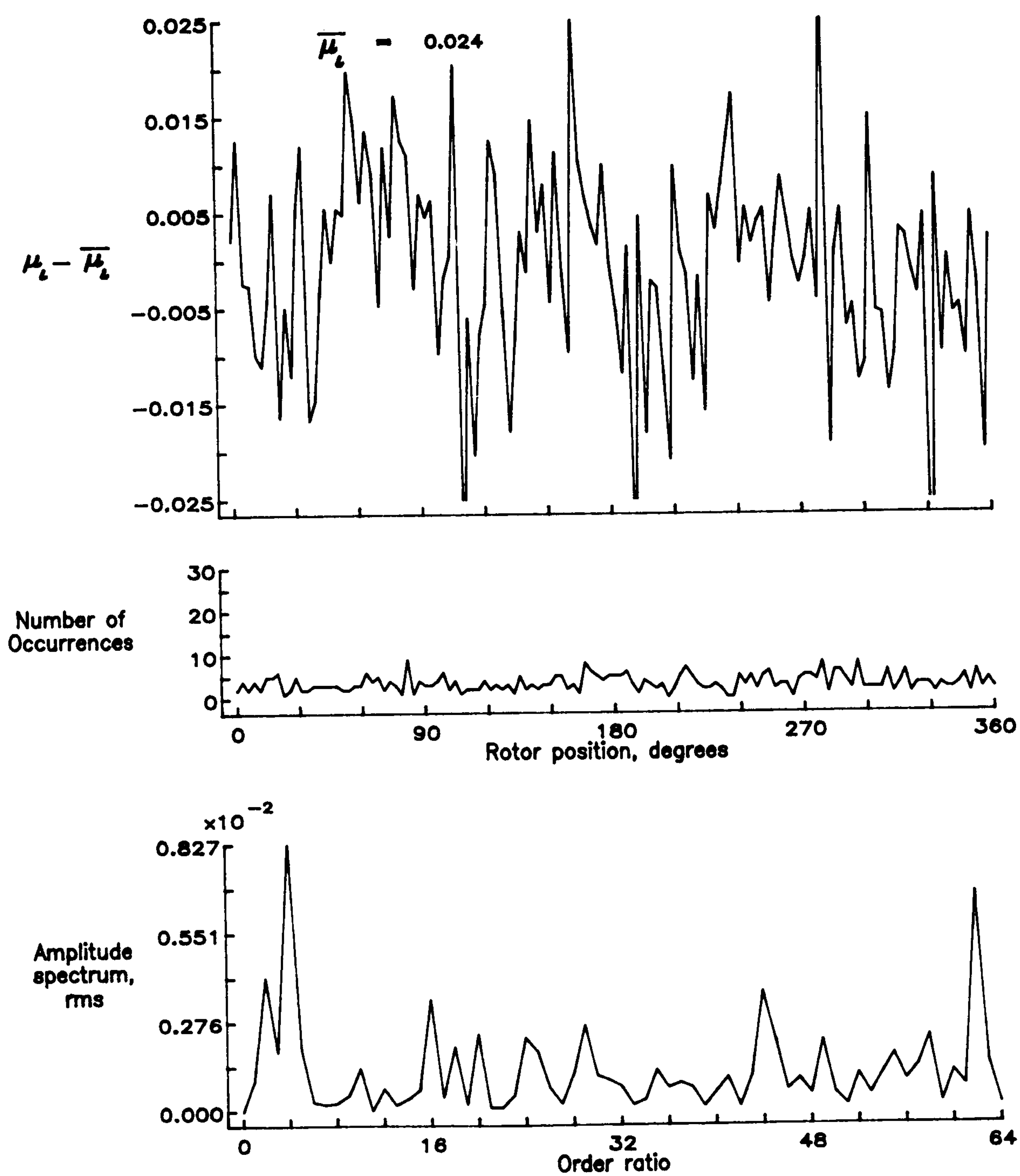

Figure 36.– Induced inflow velocity measured at 60 degrees and r/R of 0.40.

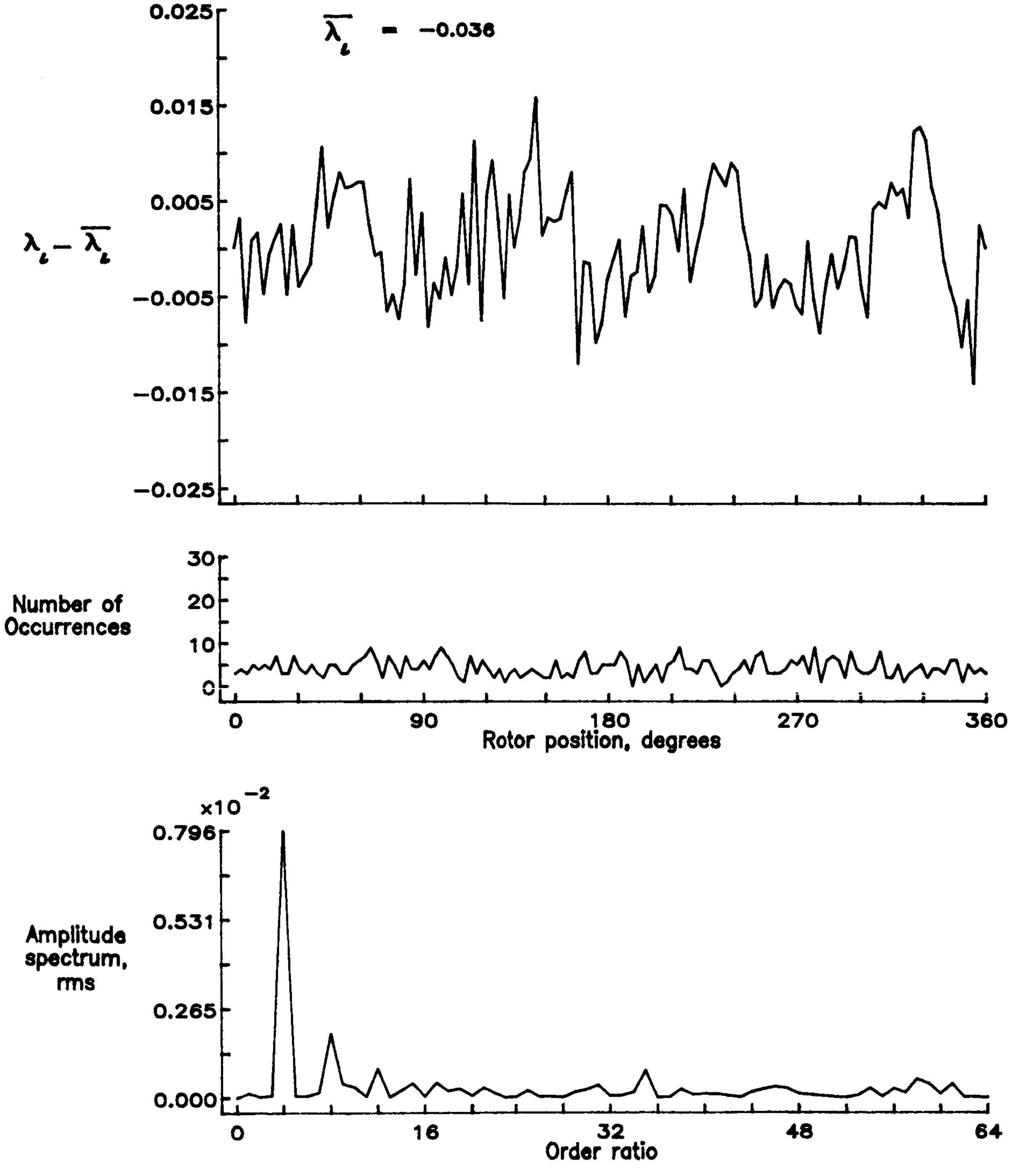

Figure 36.– Concluded.

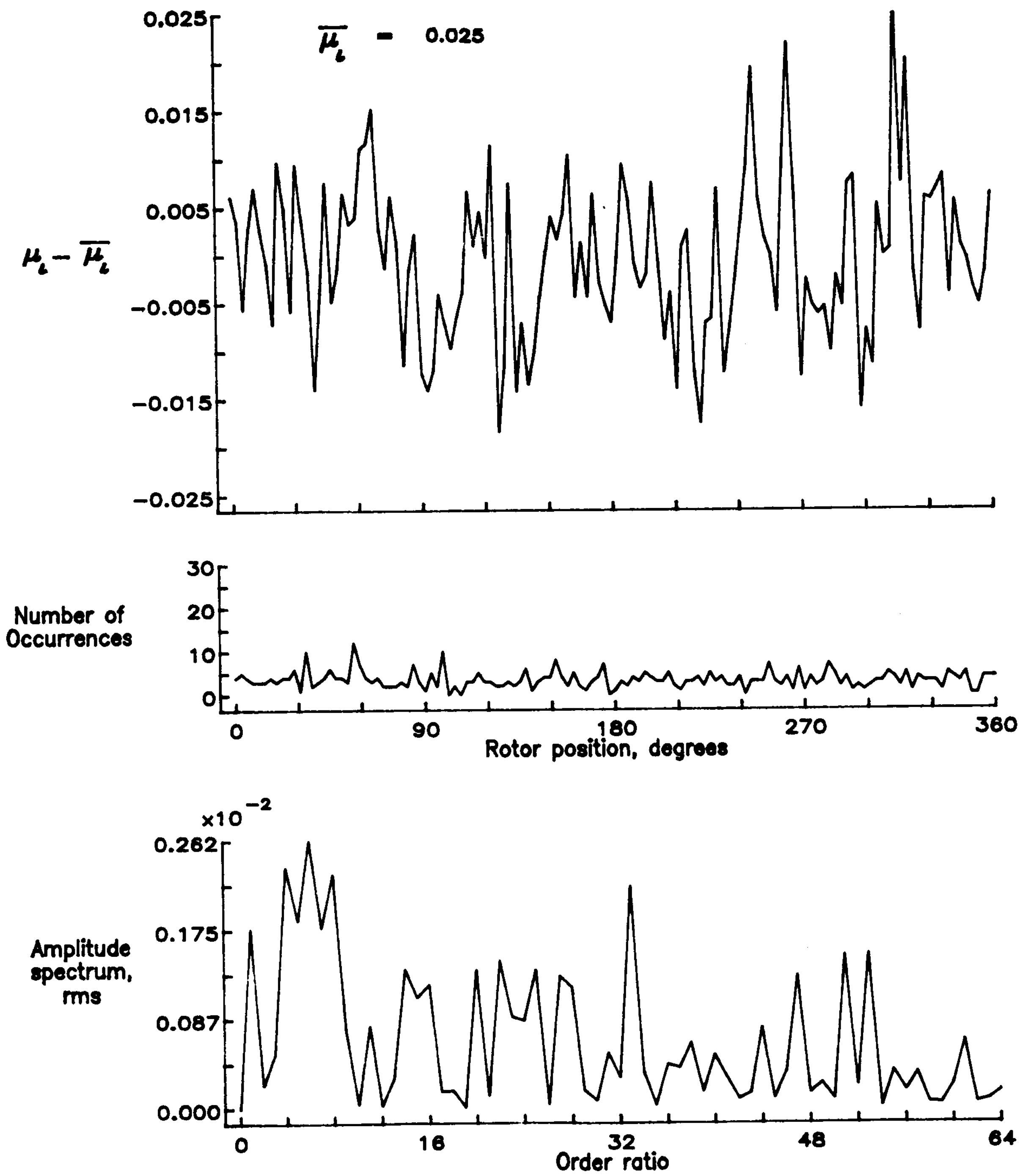

Figure 37.– Induced inflow velocity measured at 60 degrees and r/R of 0.50.

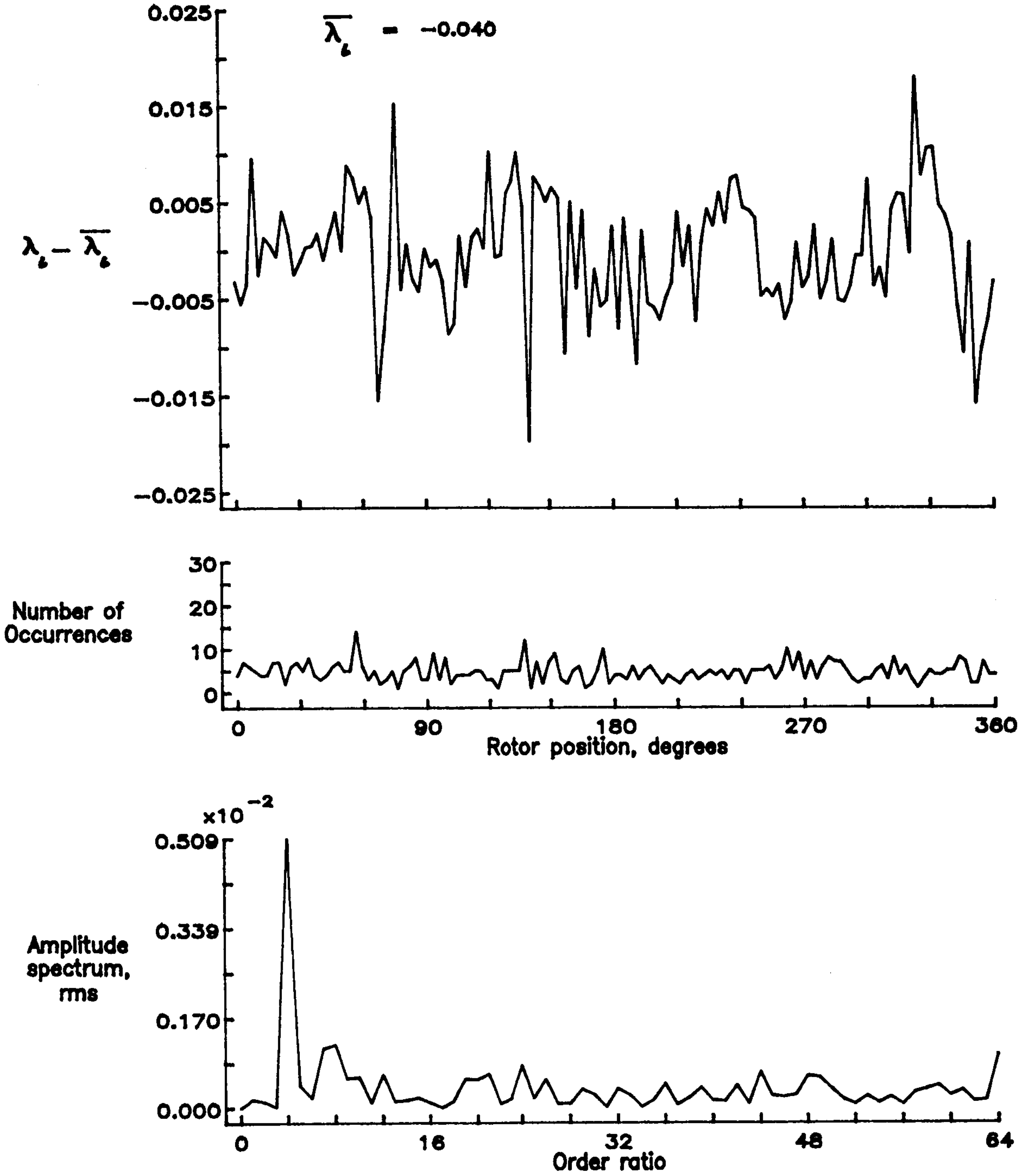

Figure 37.– Concluded.

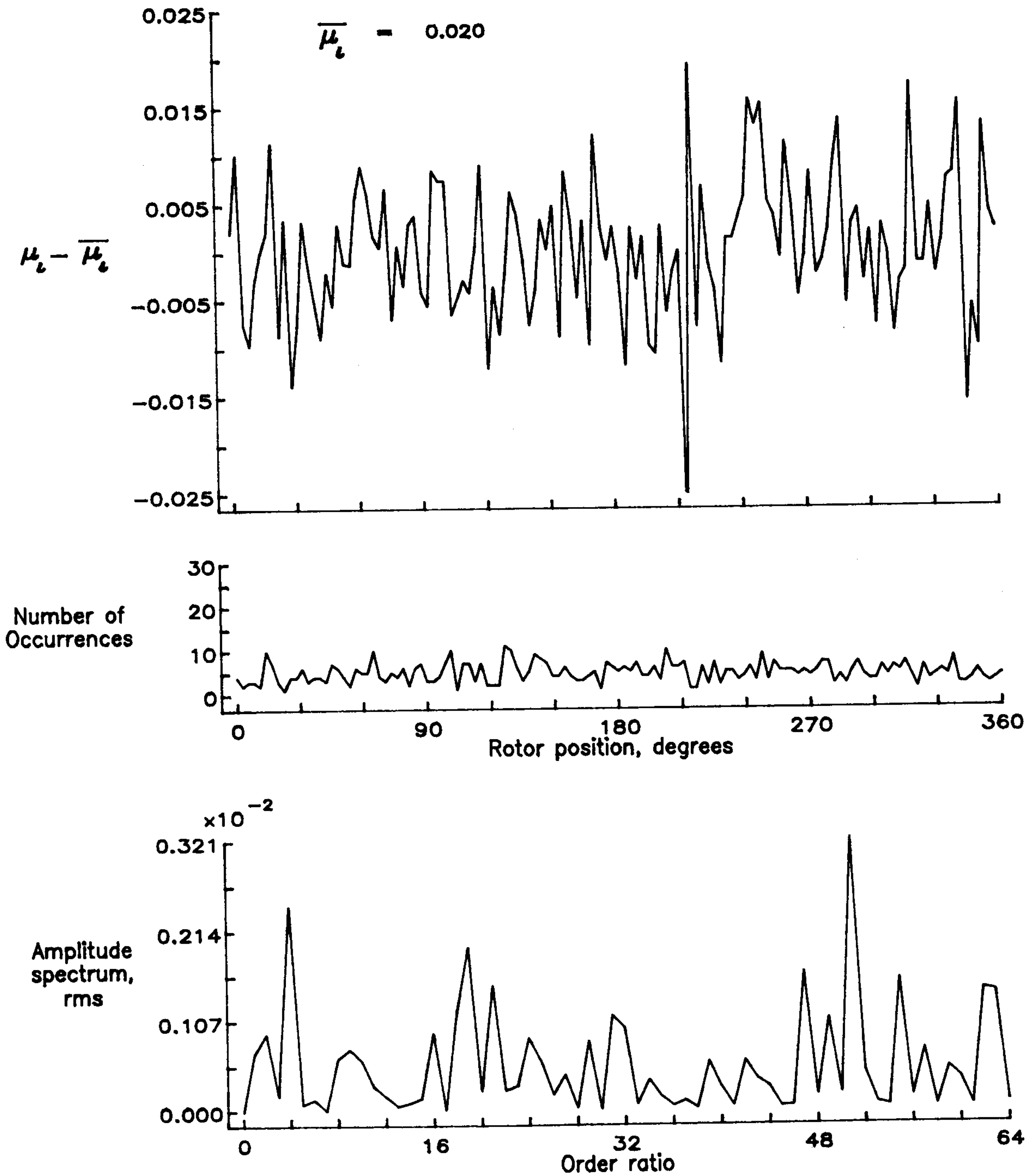

Figure 38.– Induced inflow velocity measured at 60 degrees and r/R of 0.60.

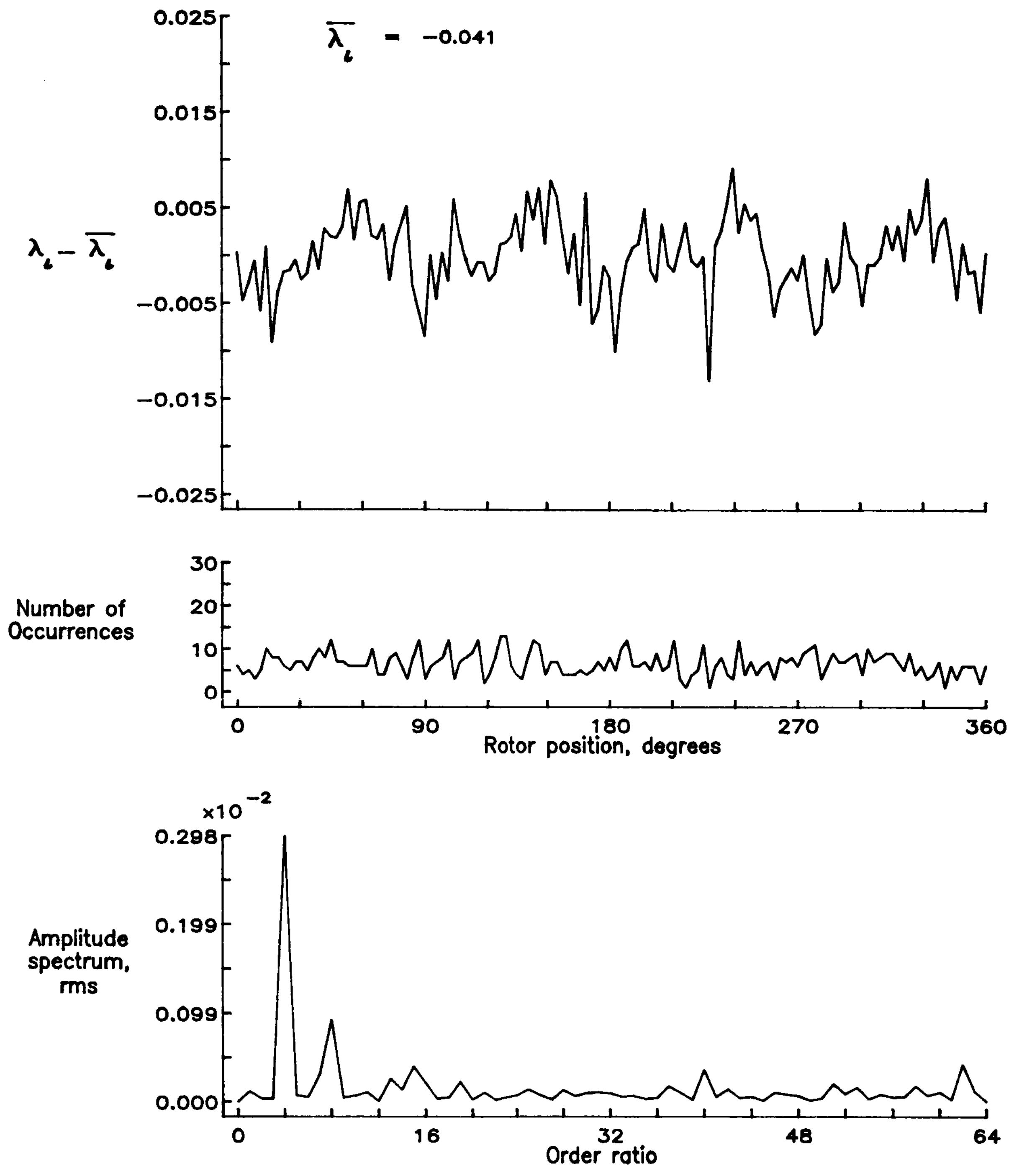

Figure 38.– Concluded.

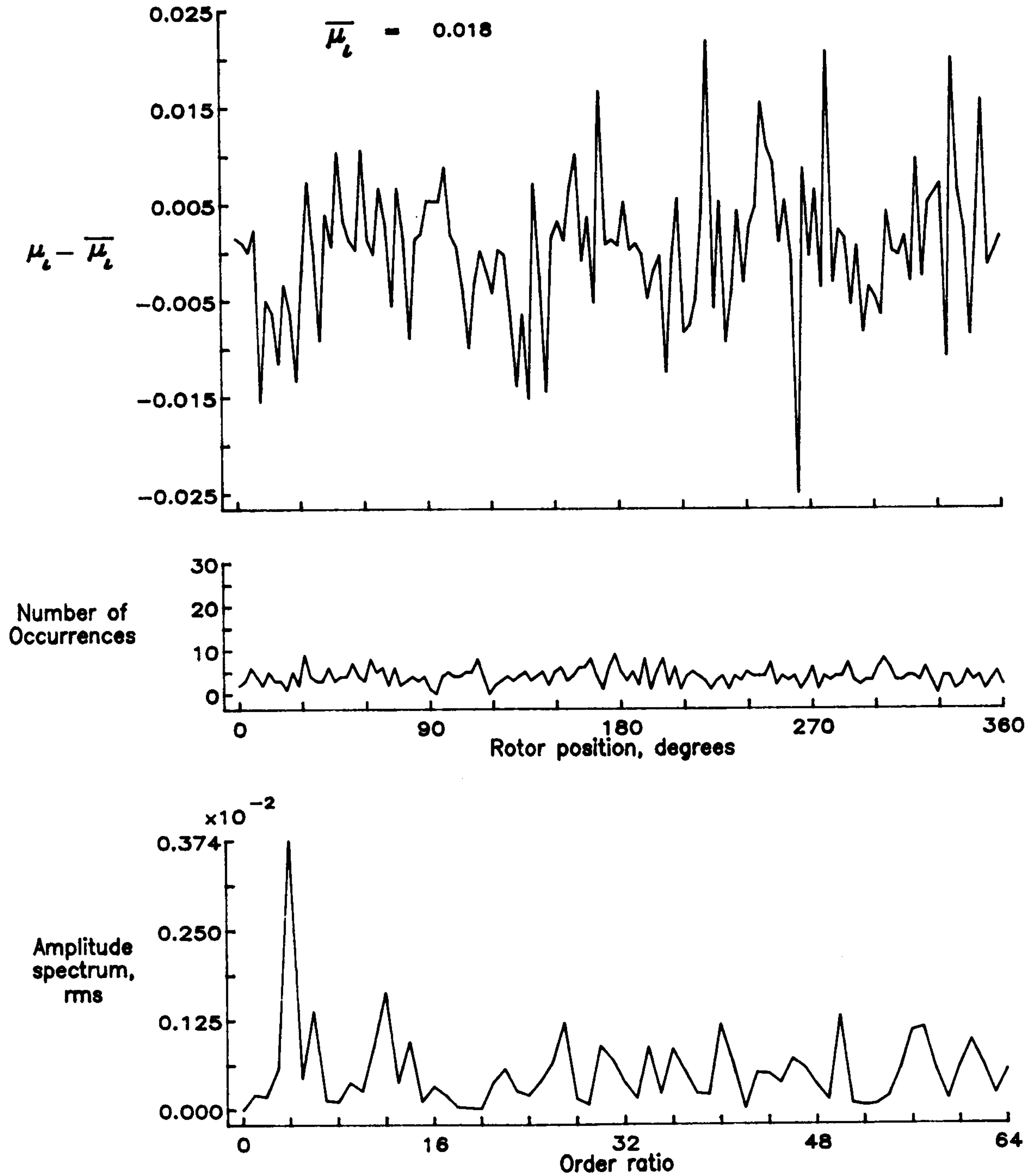

Figure 39.— Induced inflow velocity measured at 60 degrees and r/R of 0.70.

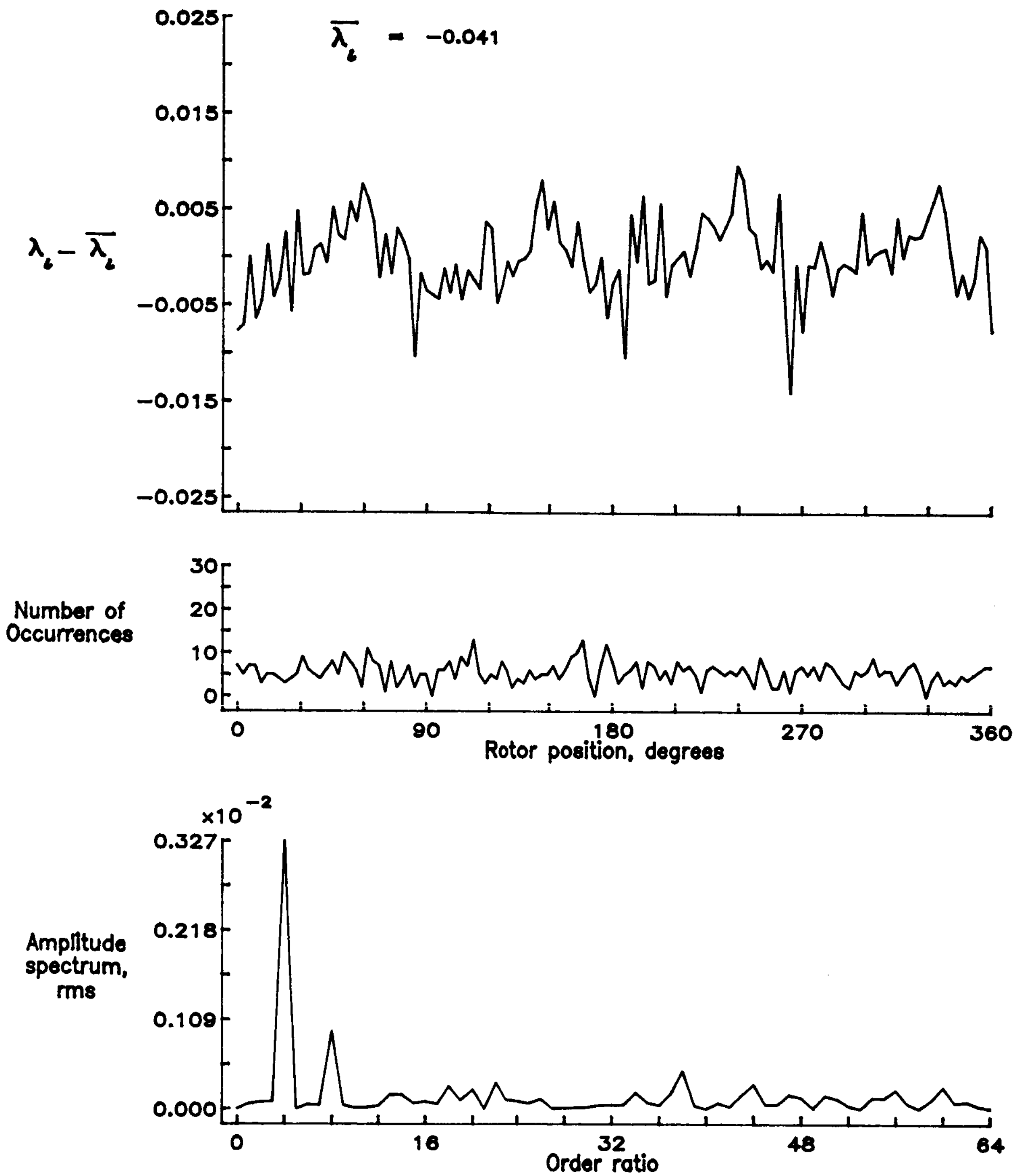

Figure 39.– Concluded.

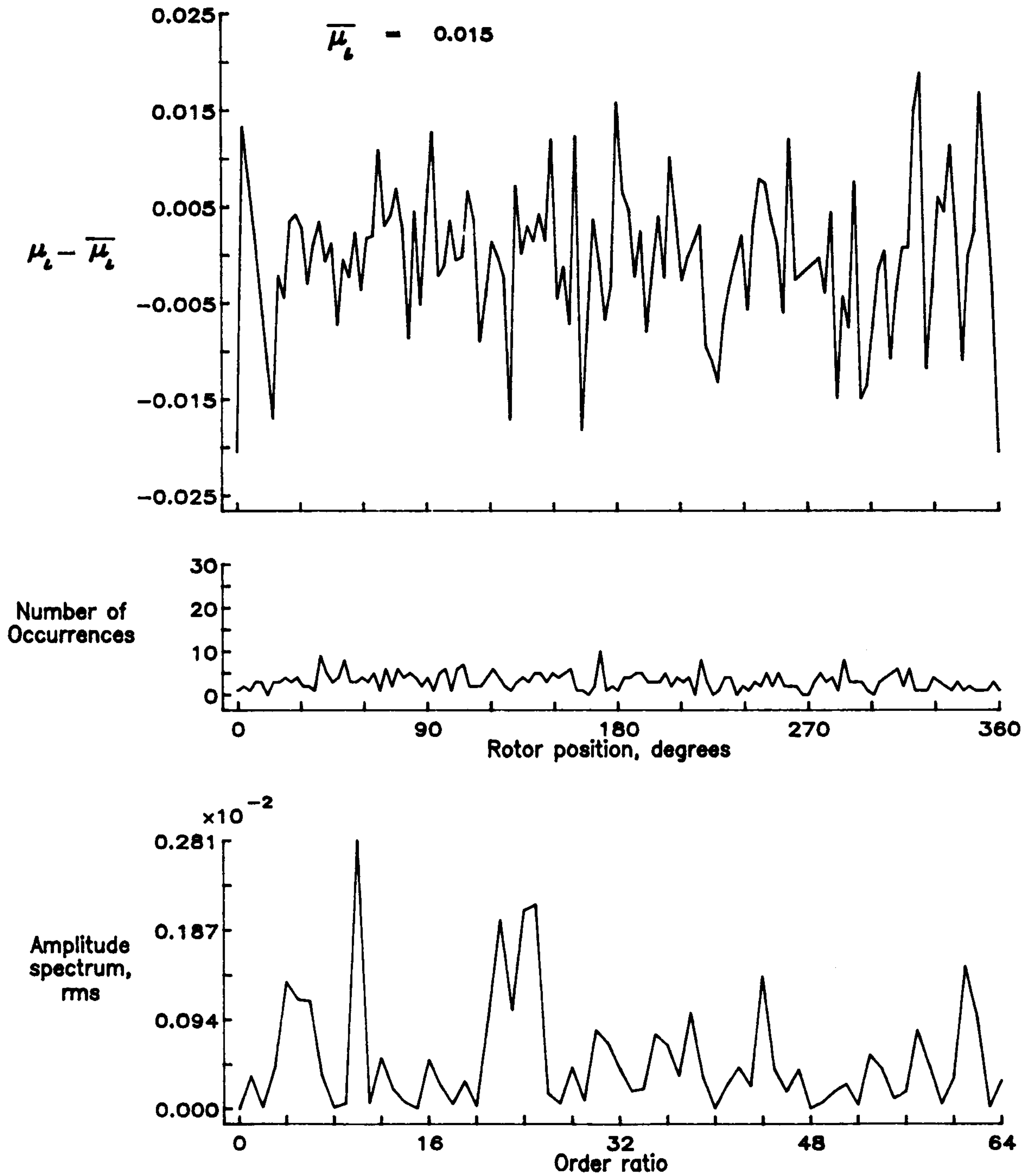

Figure 40.– Induced inflow velocity measured at 60 degrees and r/R of 0.74.

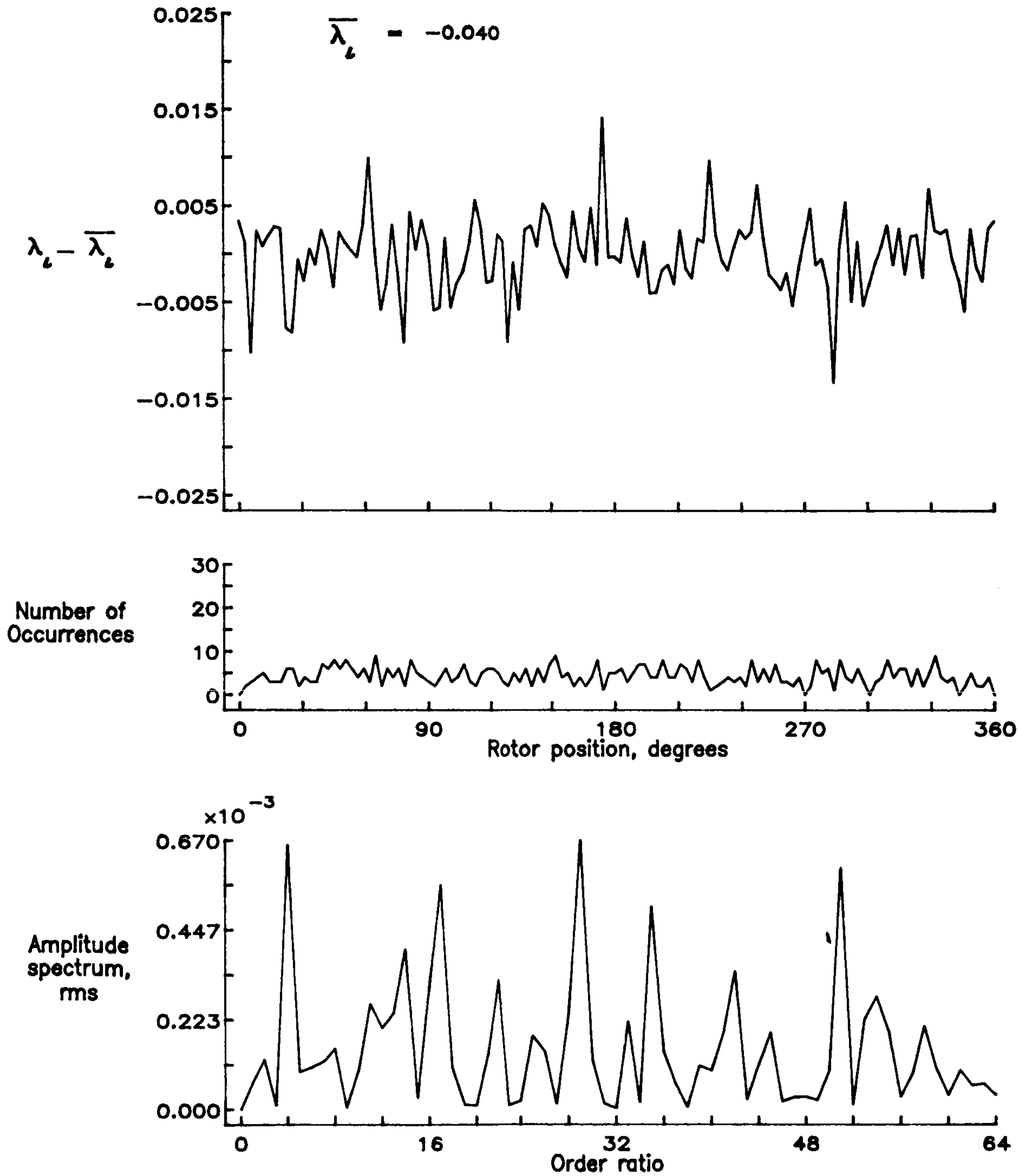

Figure 40.– Concluded.

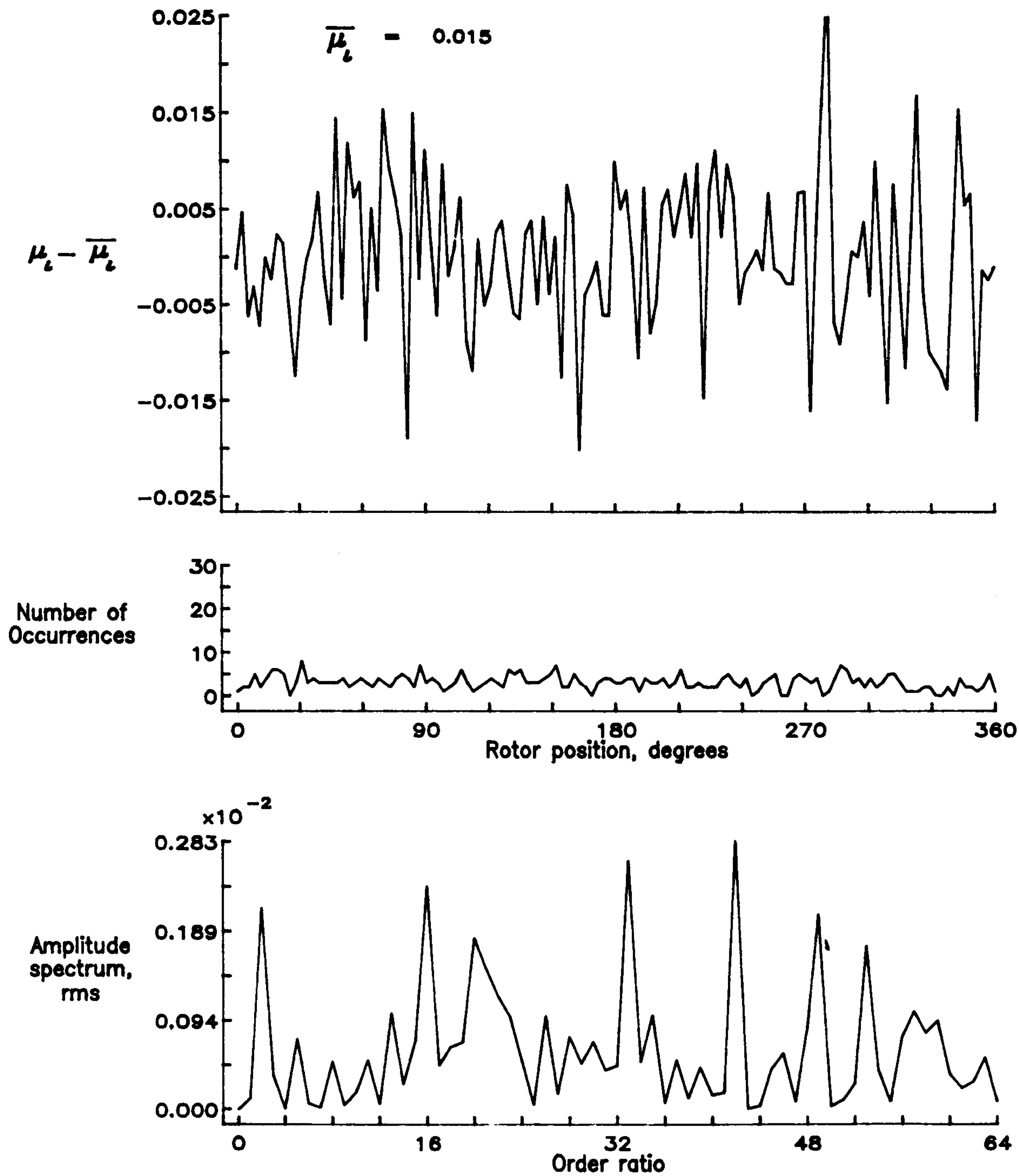

Figure 41.– Induced inflow velocity measured at 60 degrees and r/R of 0.78.

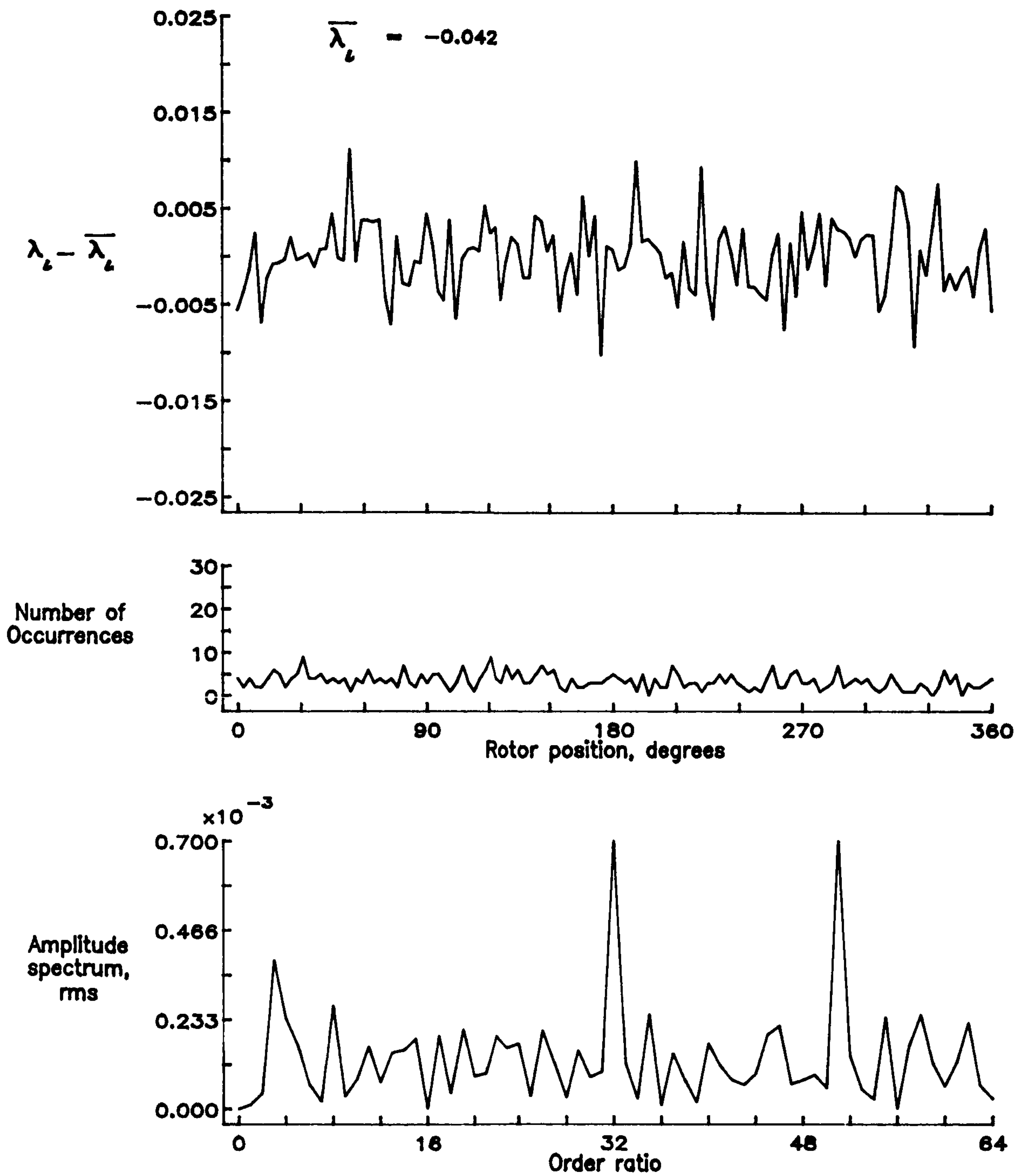

Figure 41.– Concluded.

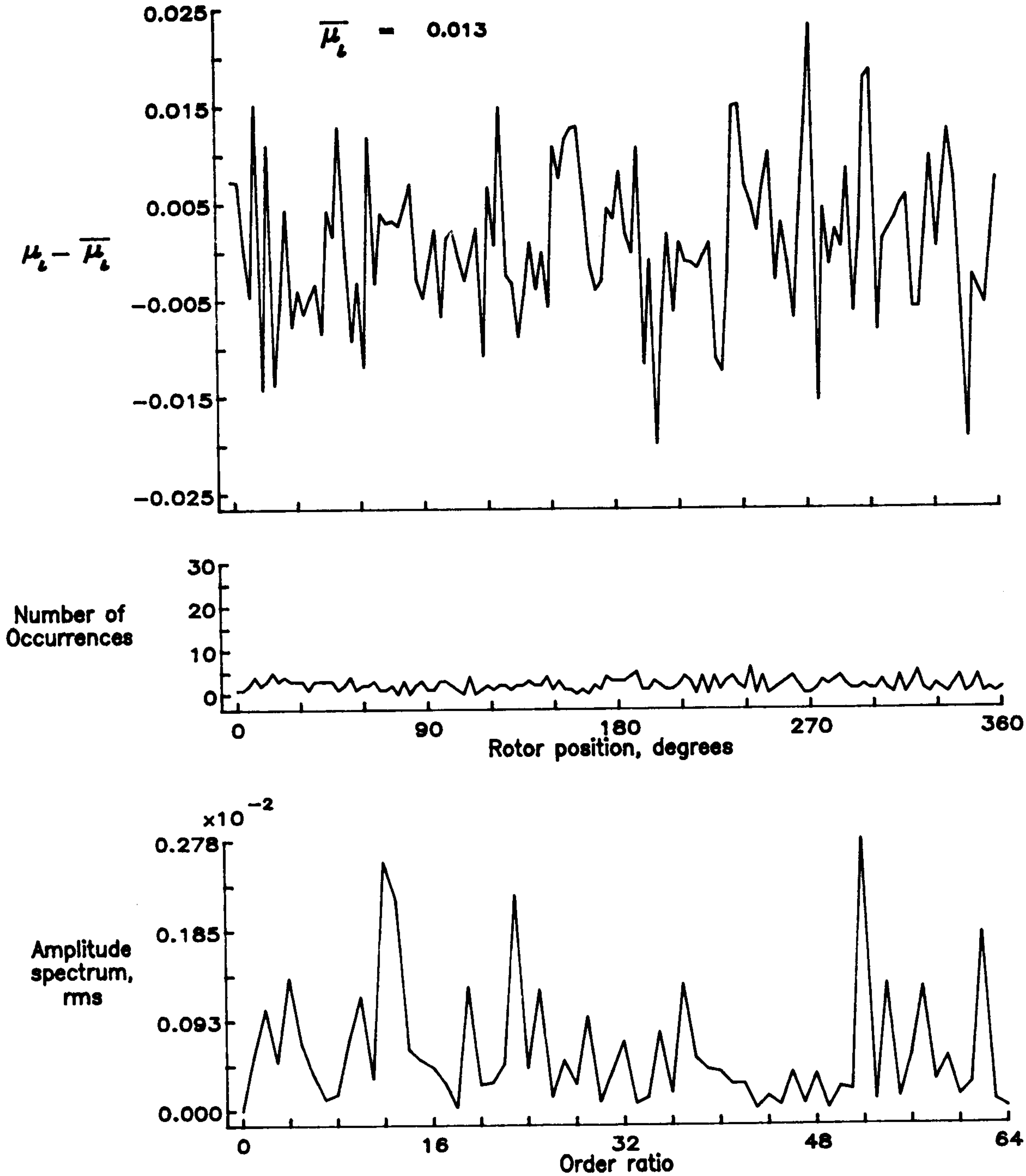

Figure 42.– Induced inflow velocity measured at 60 degrees and r/R of 0.82.

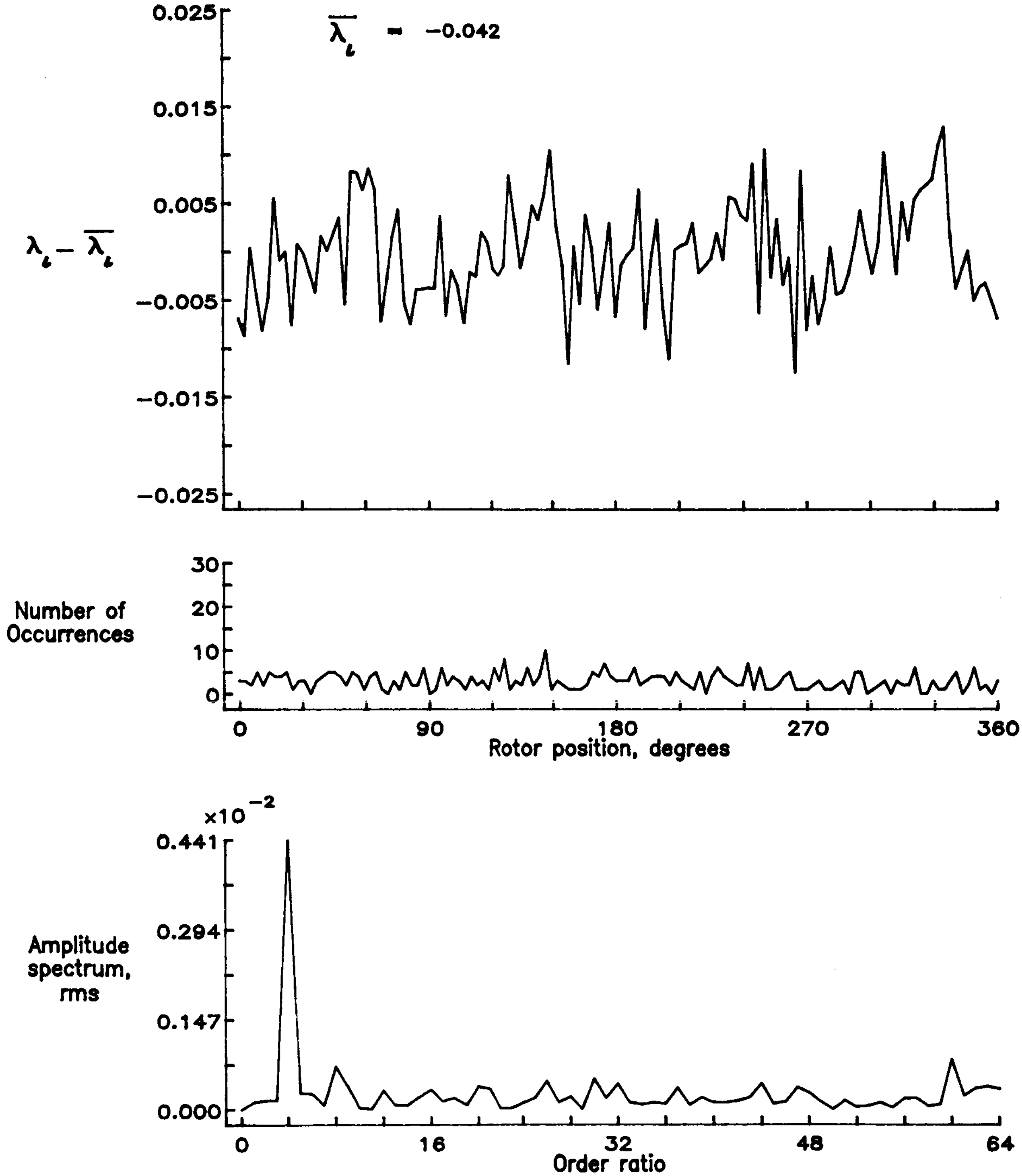

Figure 42.– Concluded.

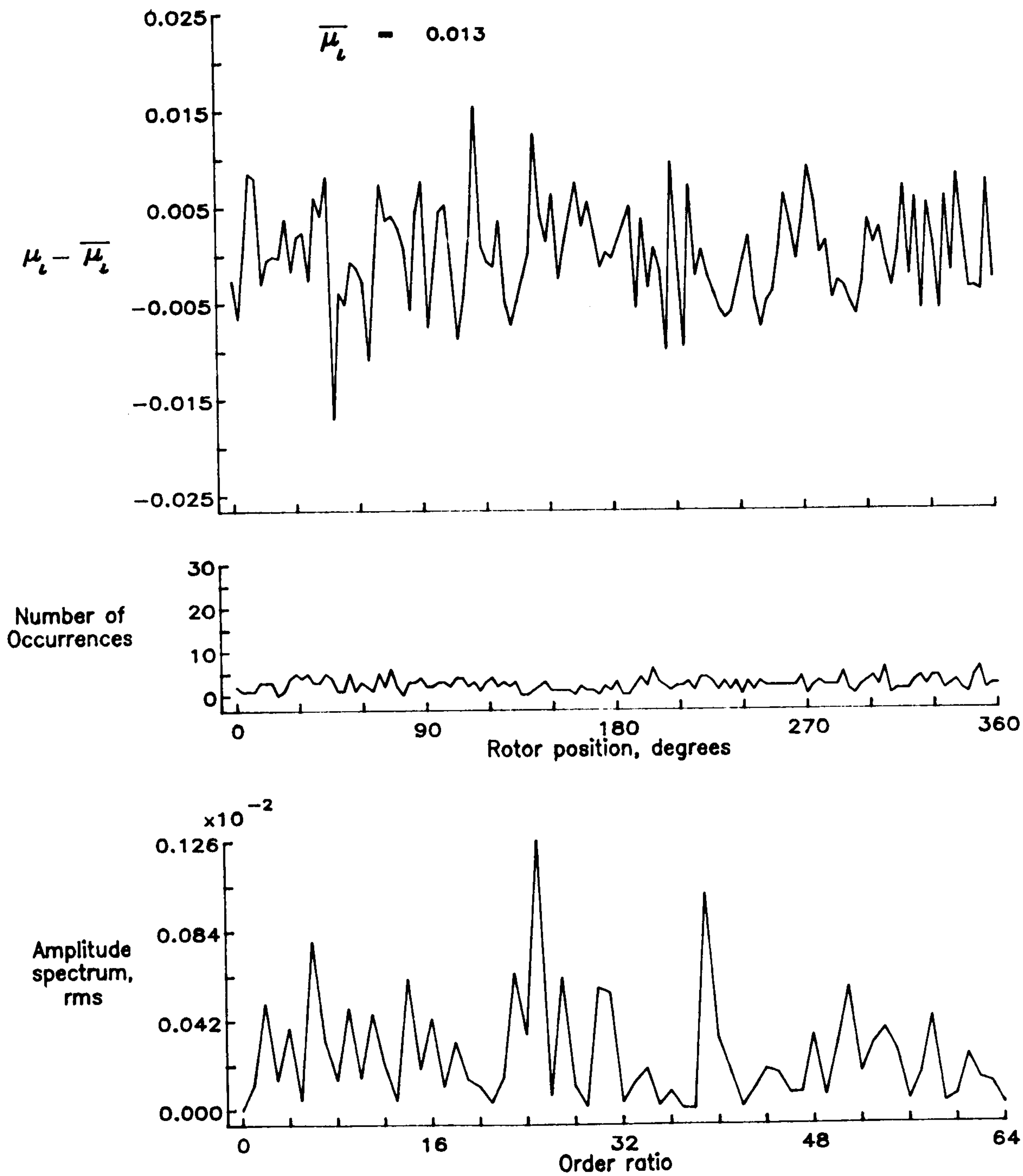

Figure 43.– Induced inflow velocity measured at 60 degrees and r/R of 0.86.

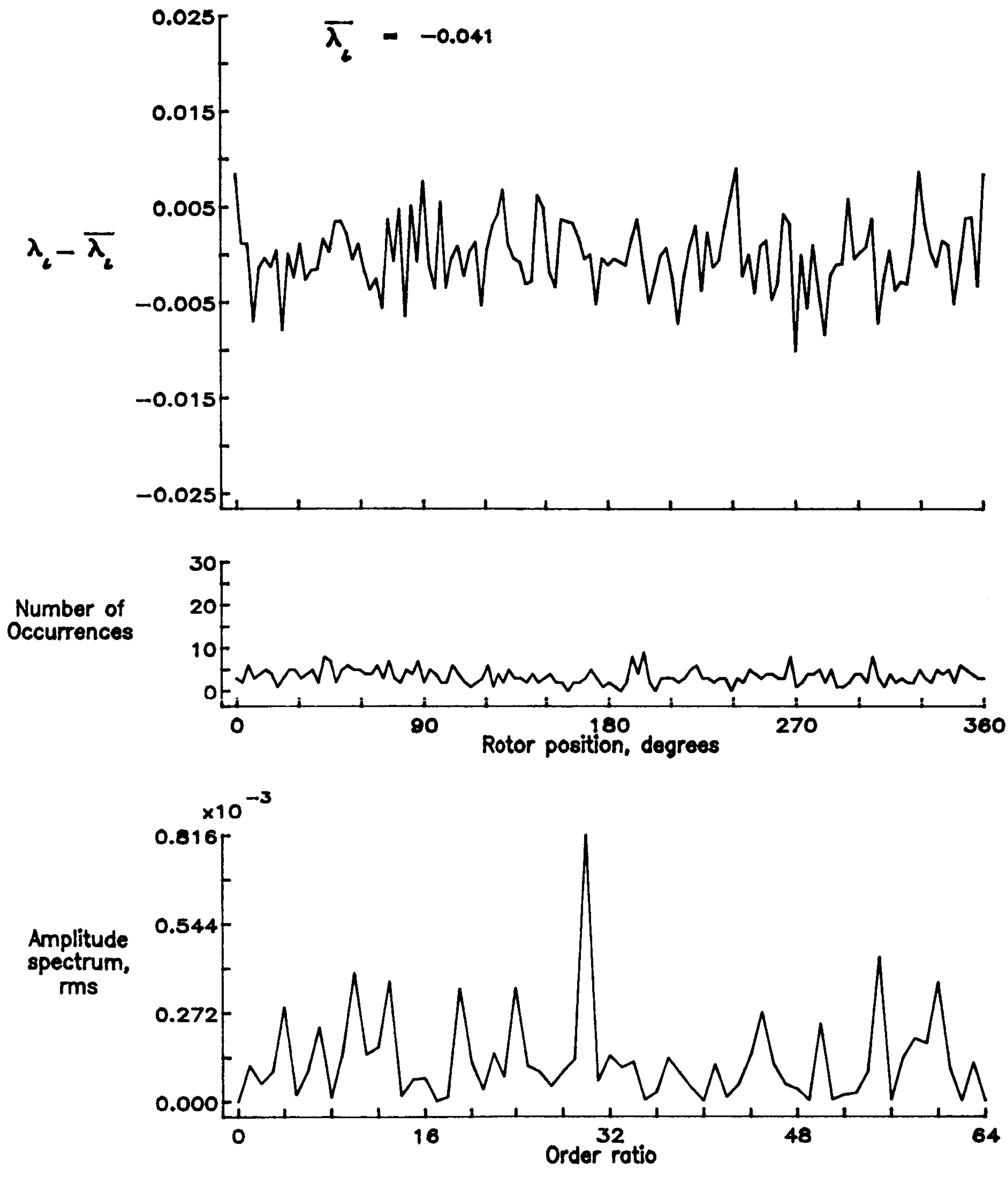

Figure 43.– Concluded.

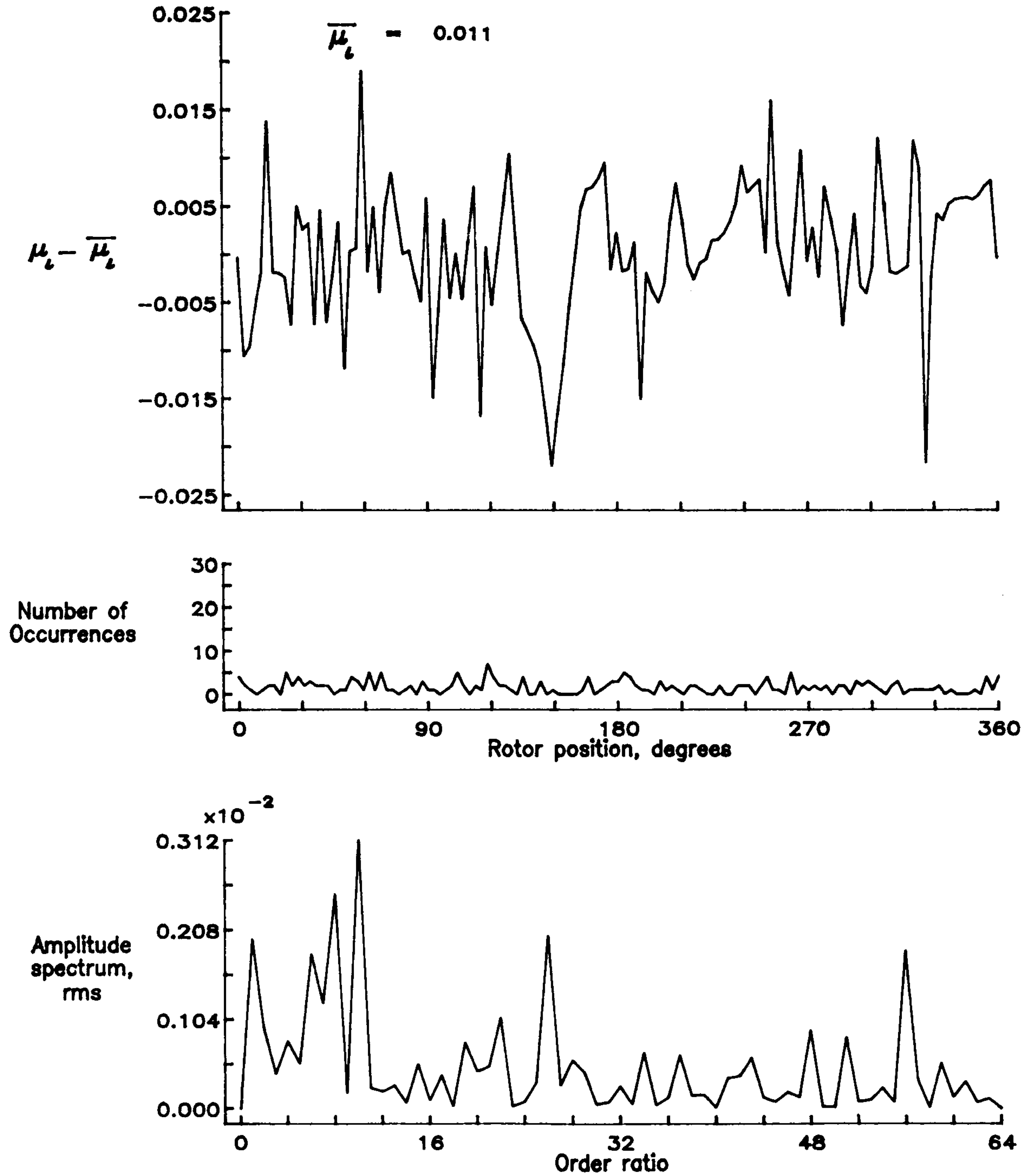

Figure 44.– Induced inflow velocity measured at 60 degrees and r/R of 0.90.

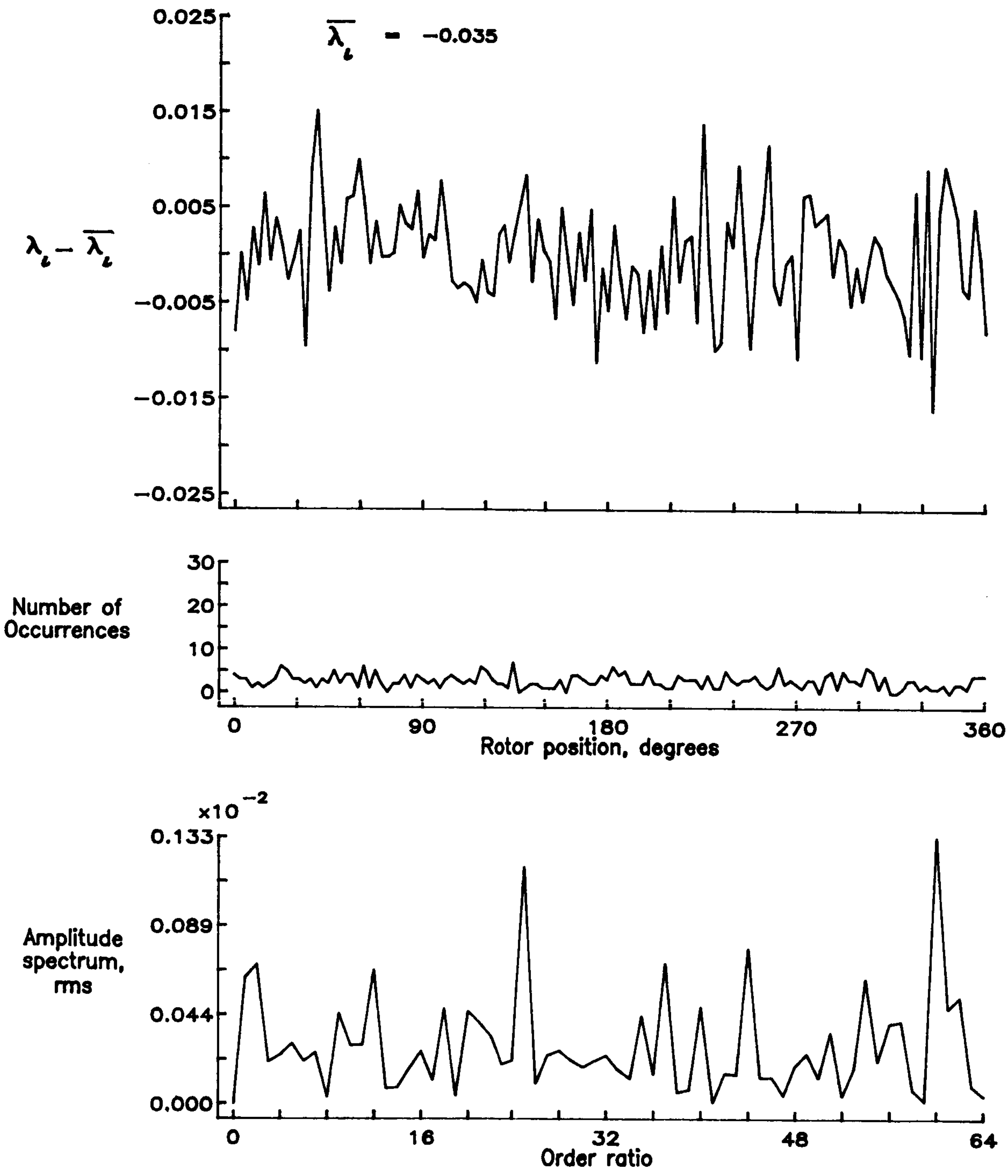

Figure 44.– Concluded.

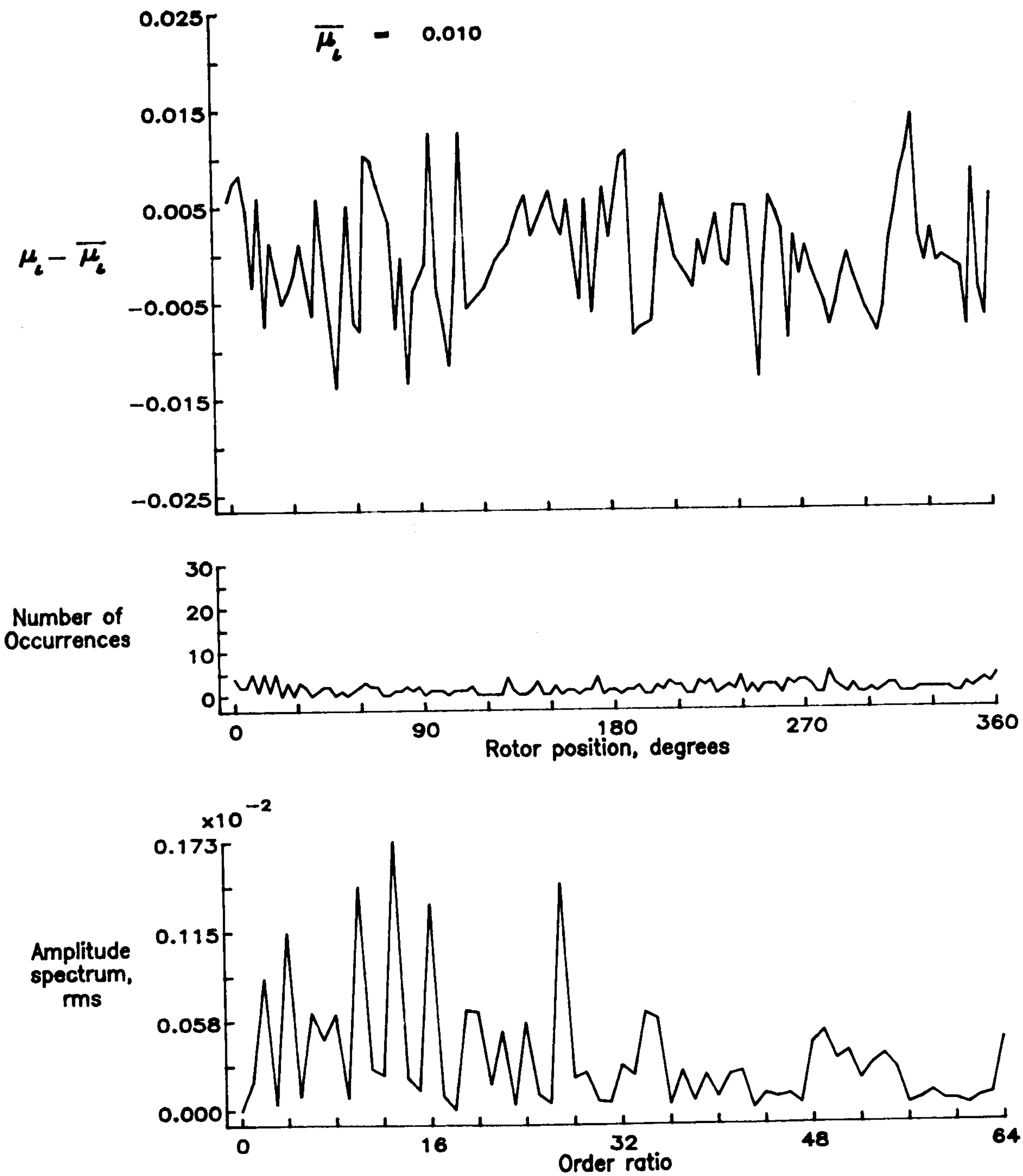

Figure 45.– Induced inflow velocity measured at 60 degrees and r/R of 0.94.

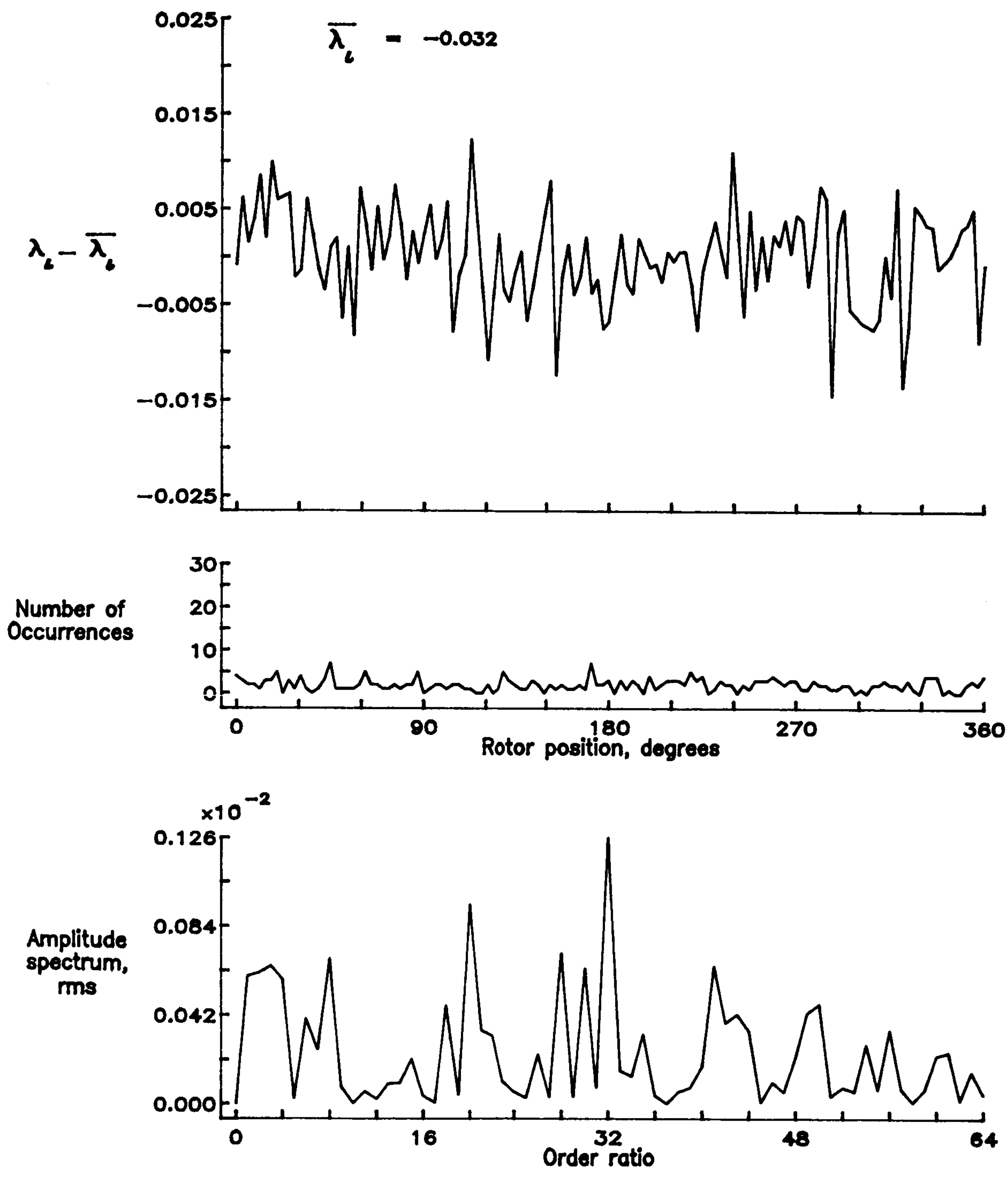

Figure 45.– Concluded.

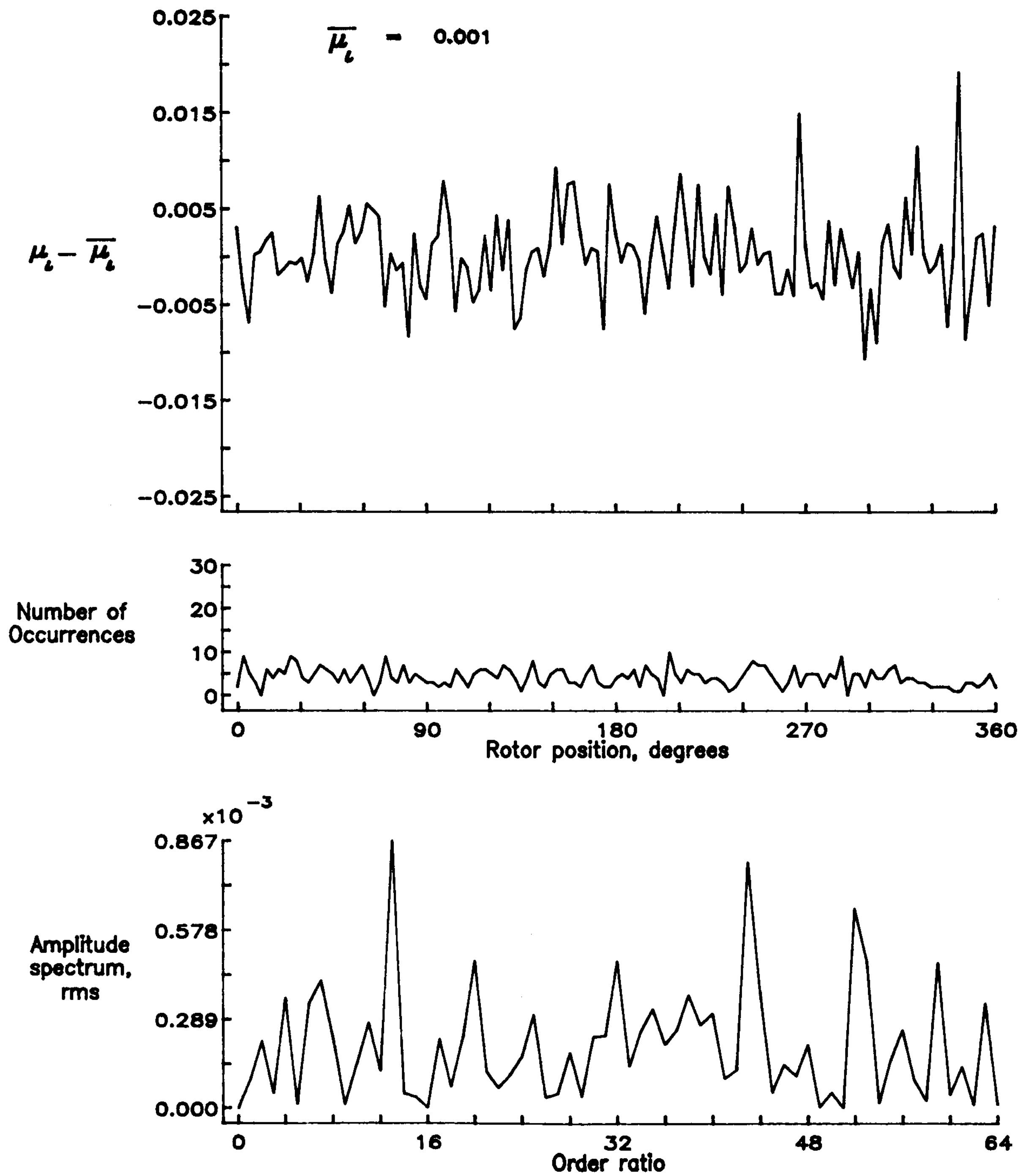

Figure 46.– Induced inflow velocity measured at 60 degrees and r/R of 1.10.

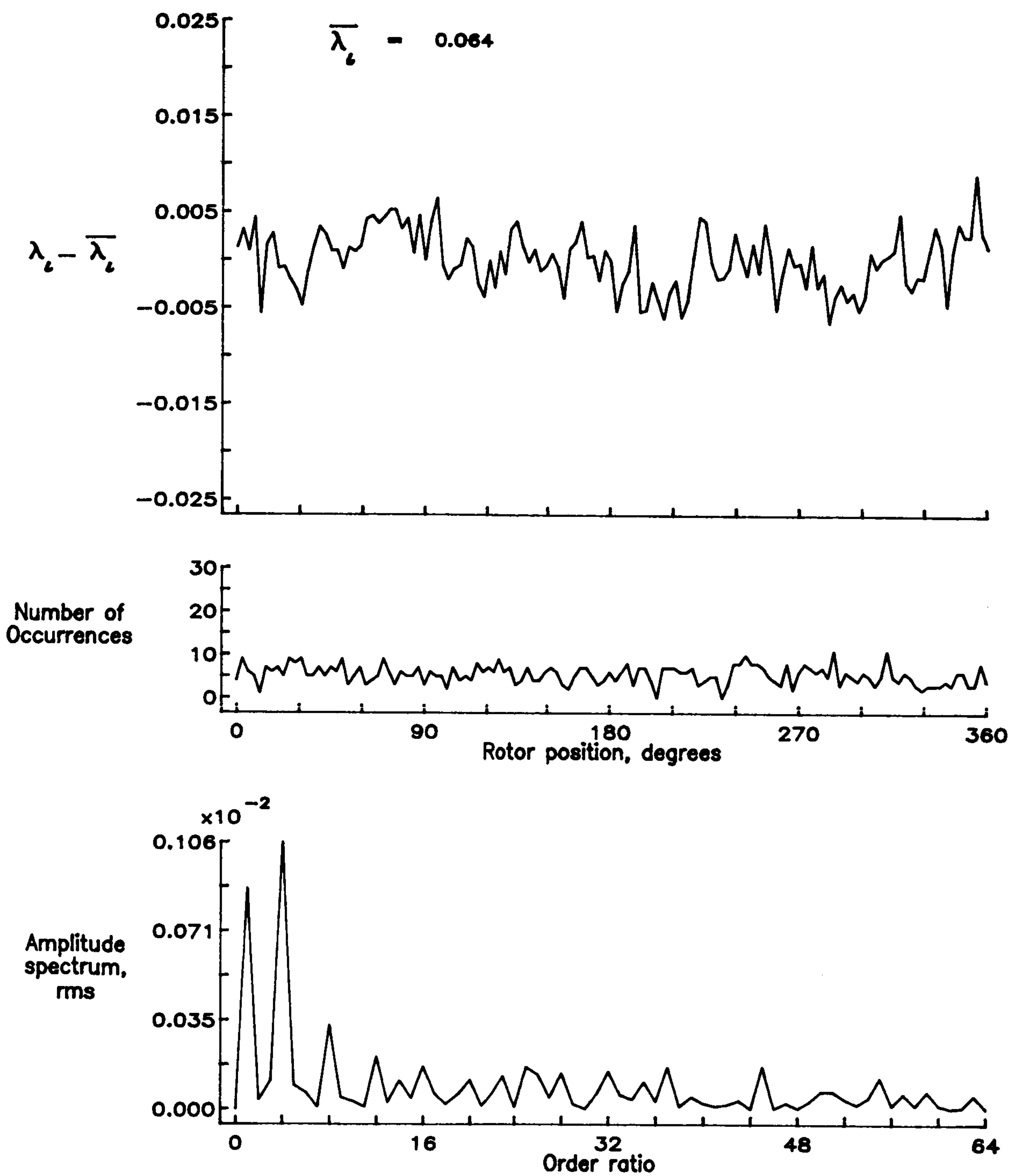

Figure 46.– Concluded.

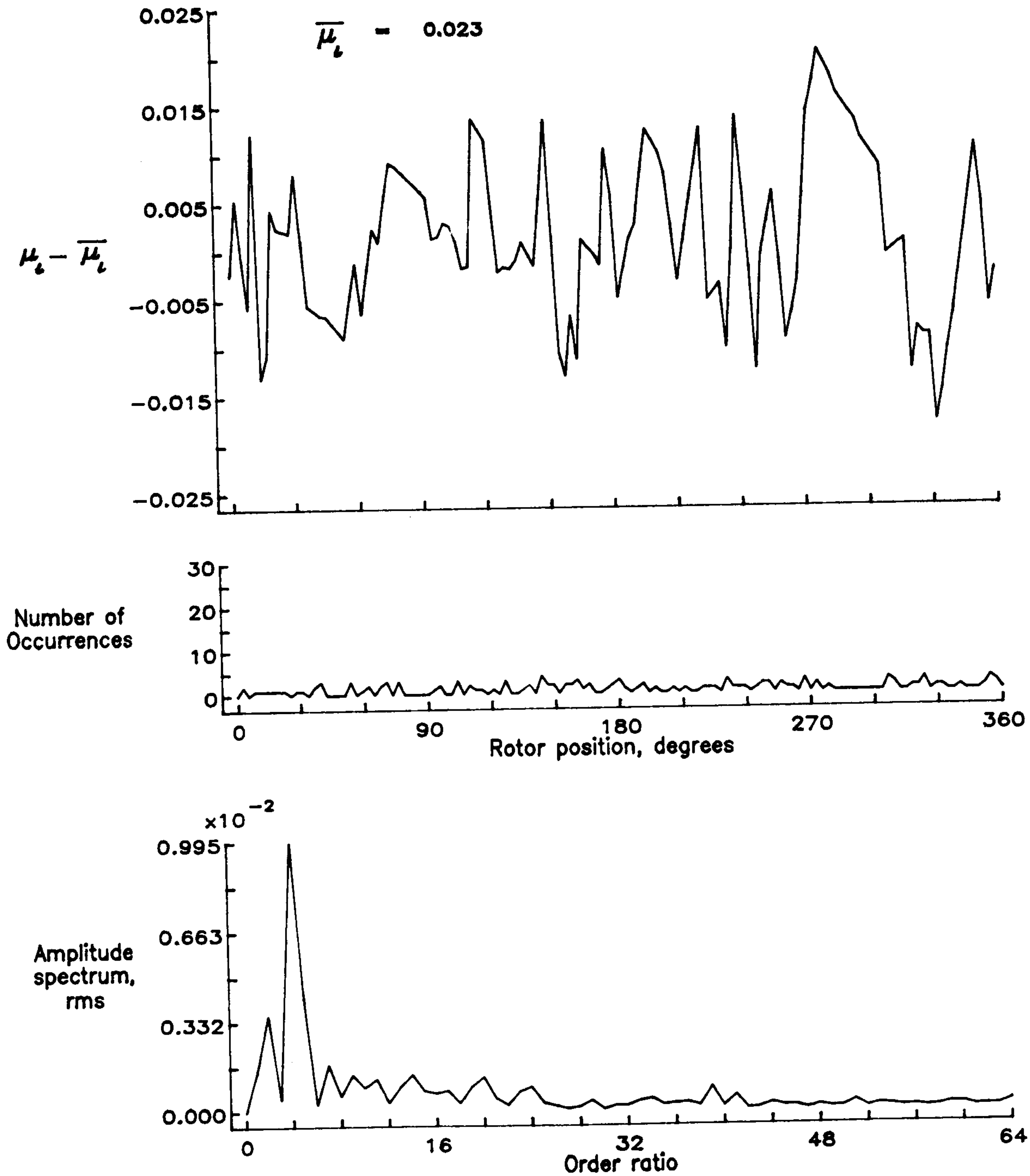

Figure 47.– Induced inflow velocity measured at 90 degrees and r/R of 0.50.

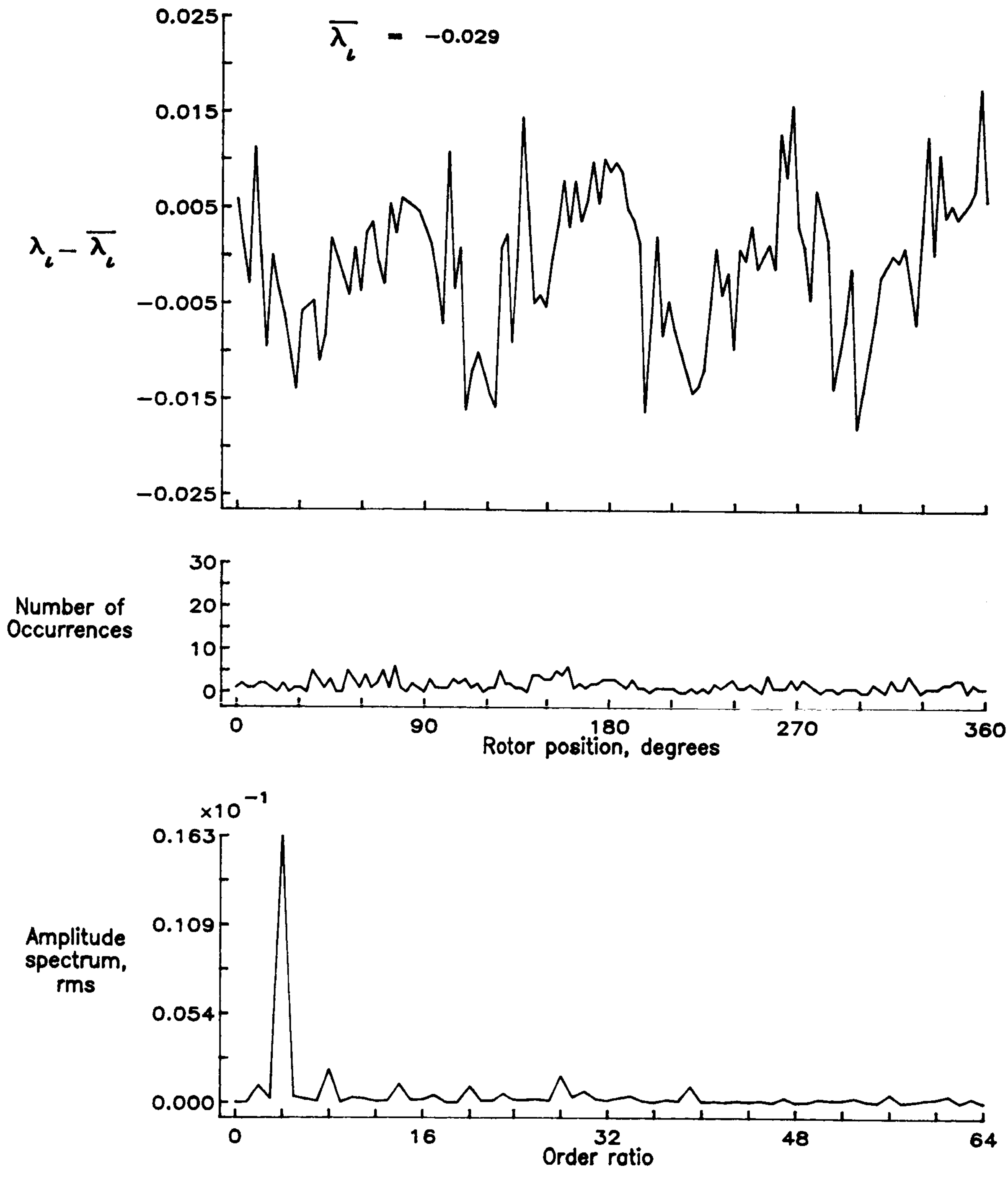

Figure 47.– Concluded.

C-2

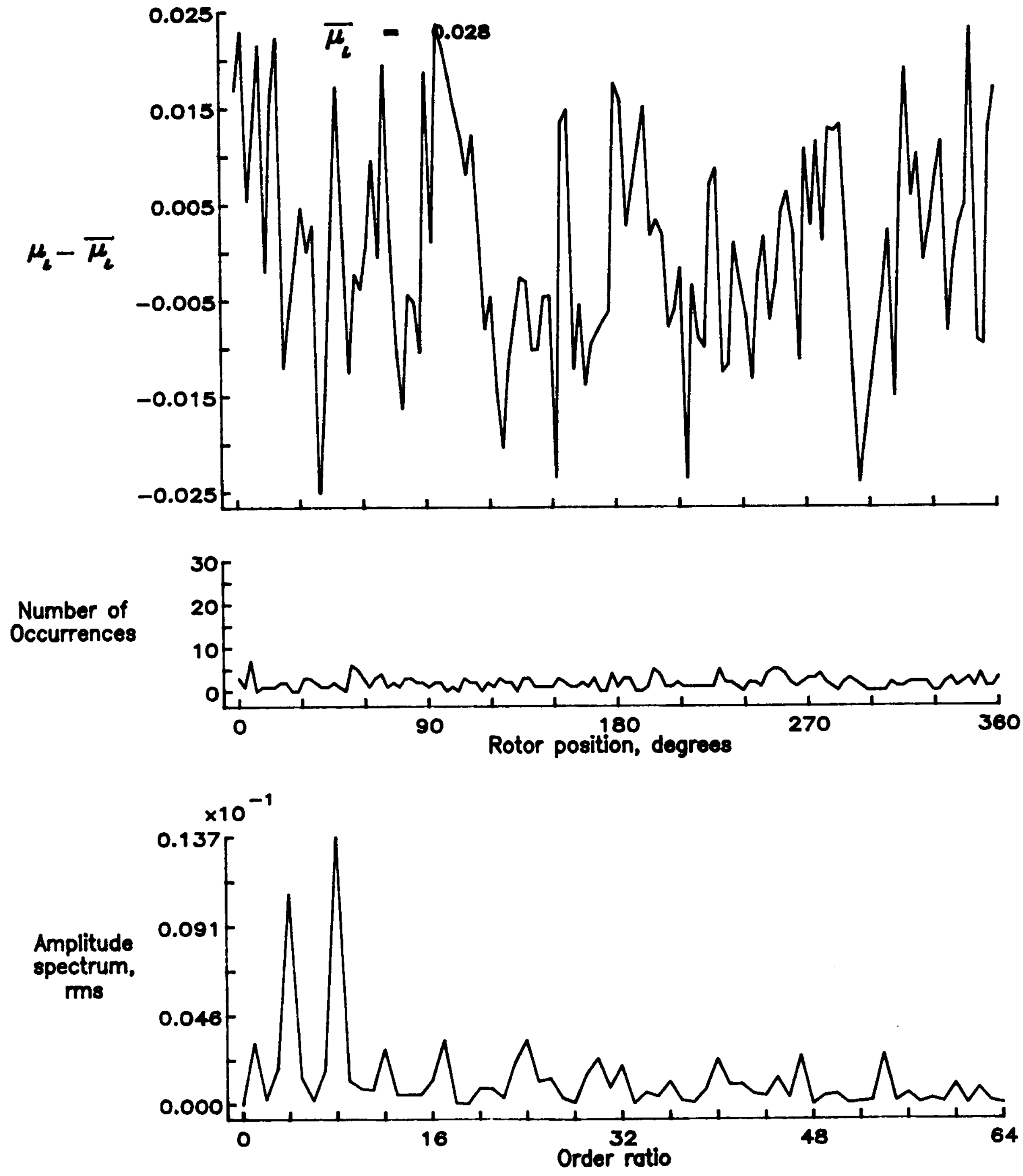

Figure 48.– Induced inflow velocity measured at 90 degrees and r/R of 0.60.

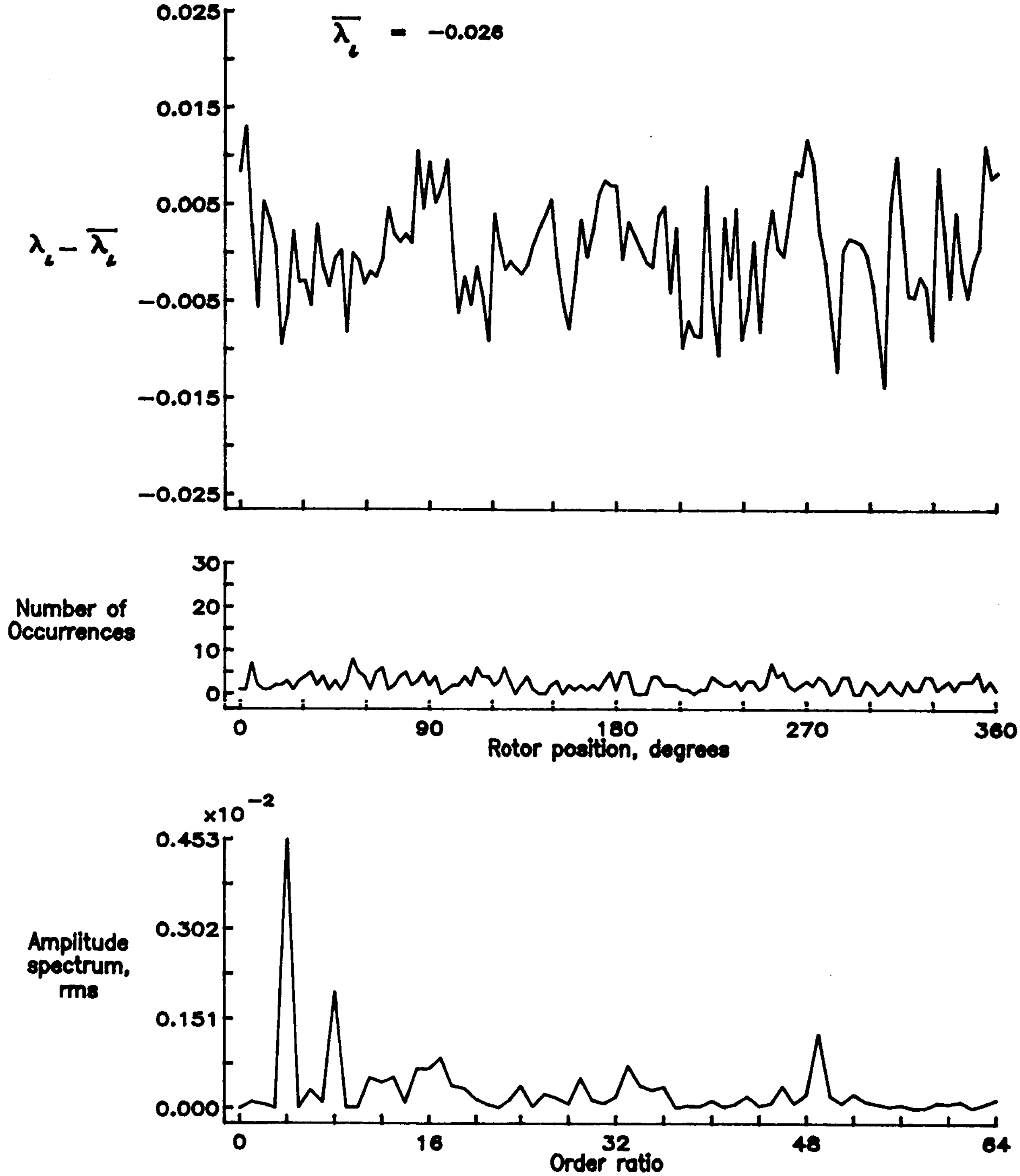

Figure 48.– Concluded.

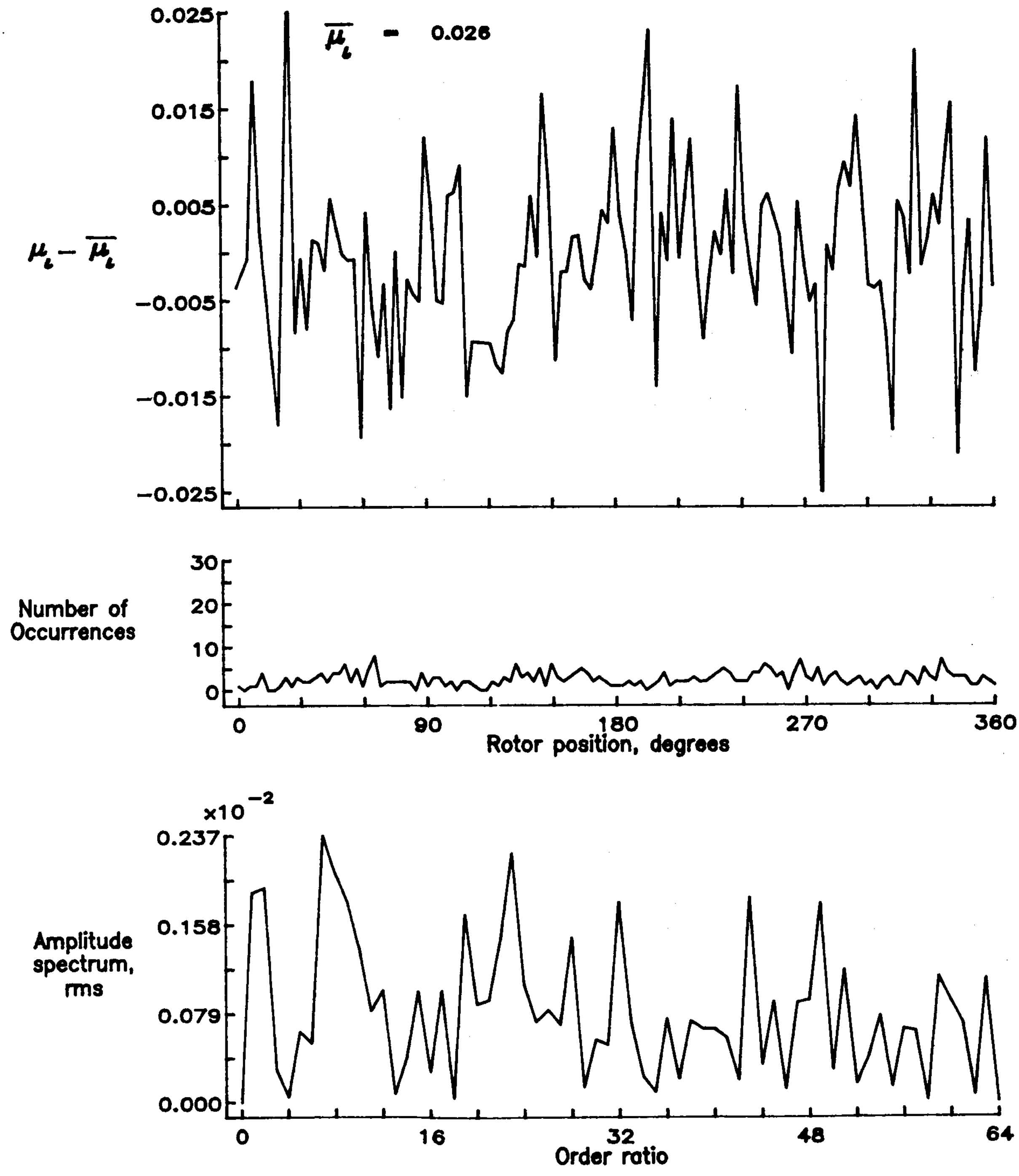

Figure 49.– Induced inflow velocity measured at 90 degrees and r/R of 0.70.

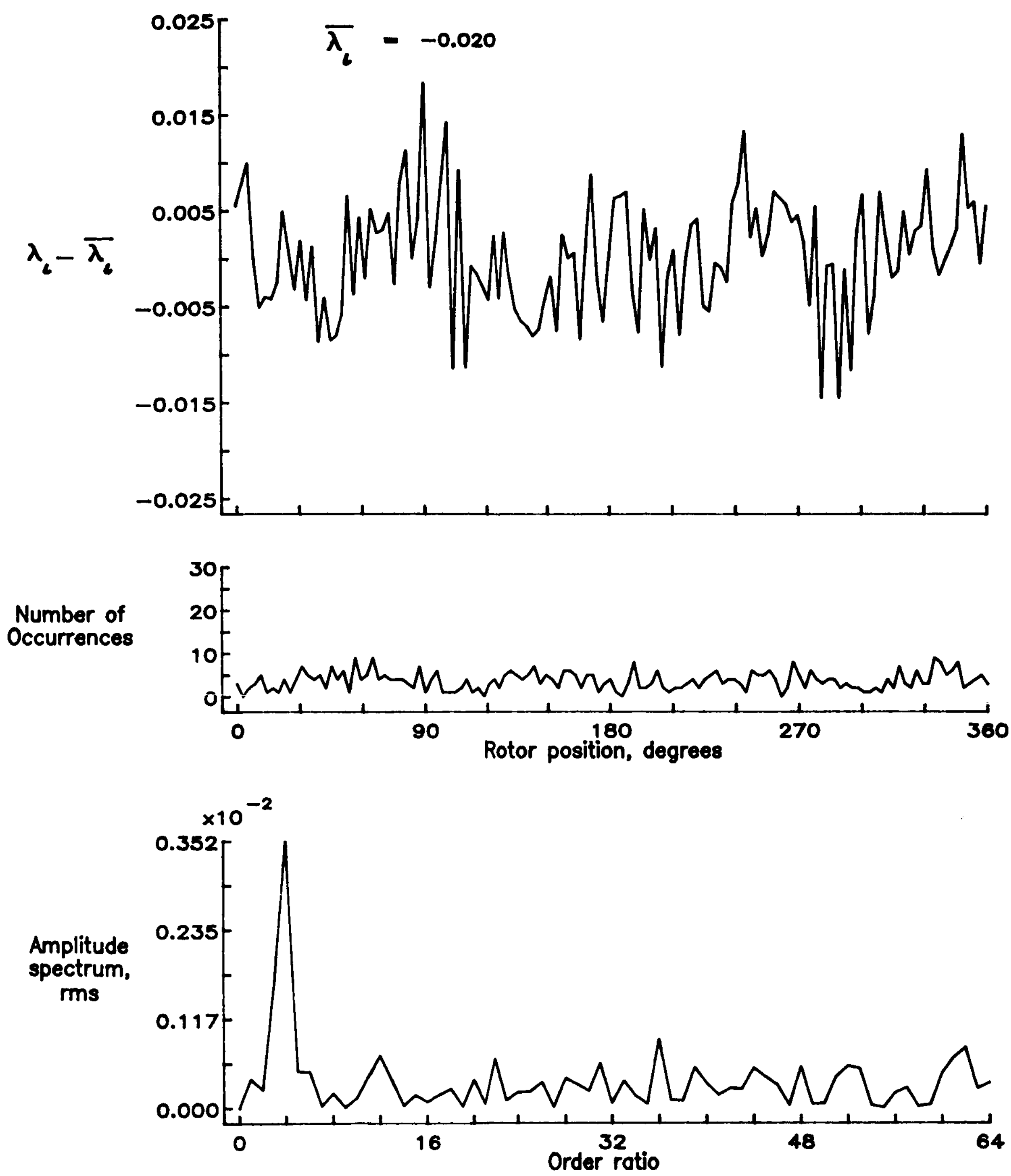

Figure 49.– Concluded.

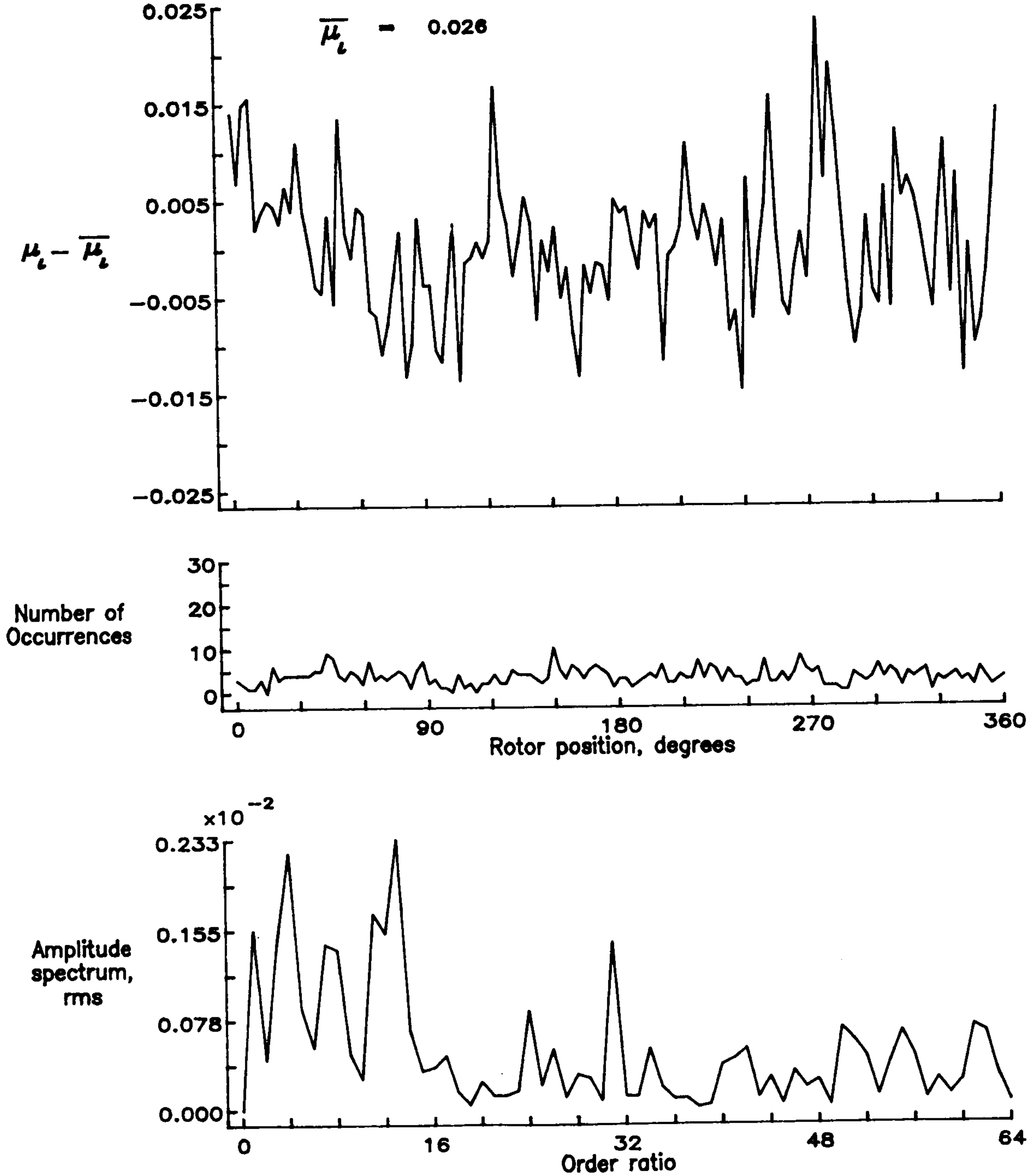

Figure 50.— Induced inflow velocity measured at 90 degrees and r/R of 0.74.

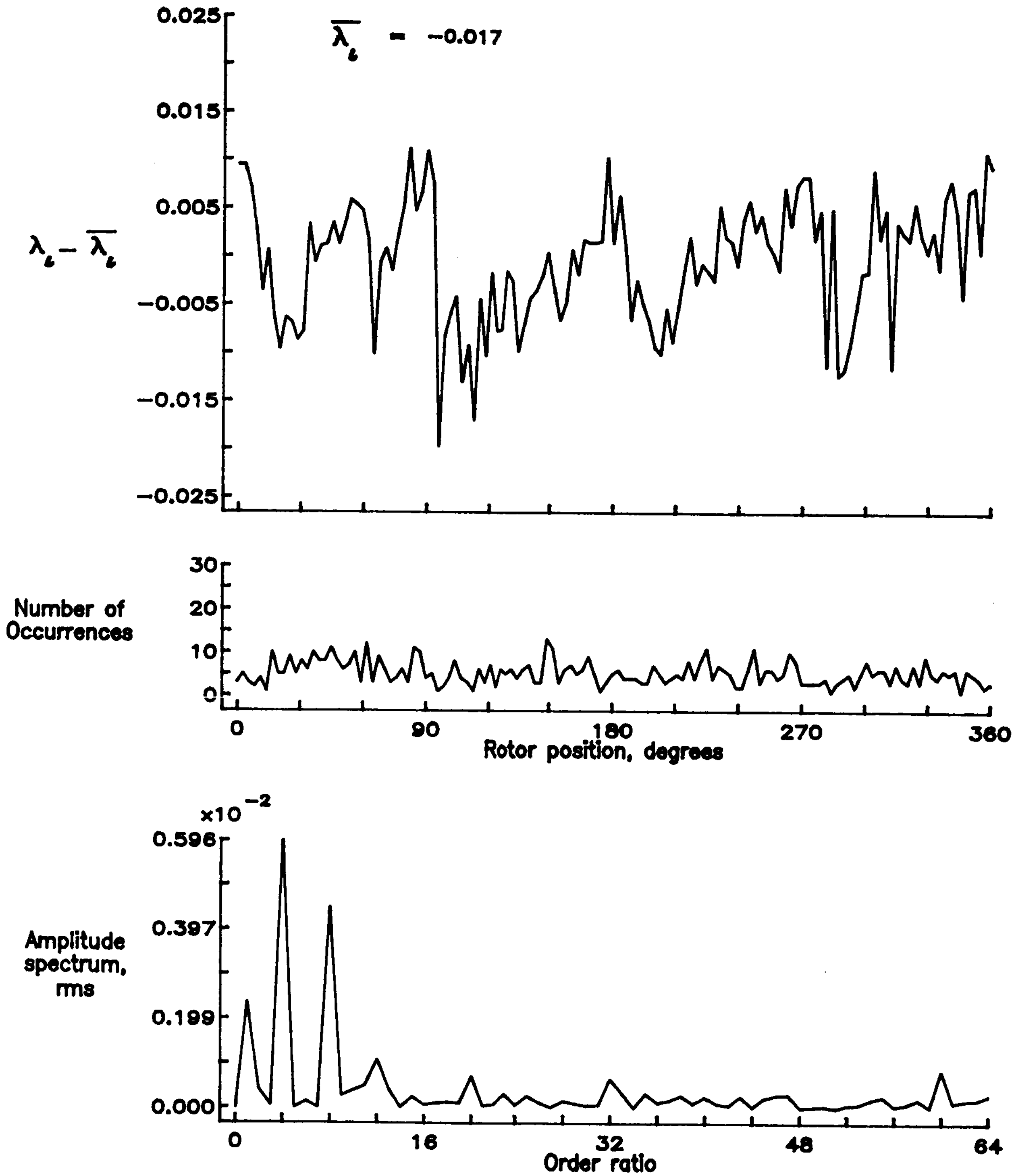

Figure 50.– Concluded.

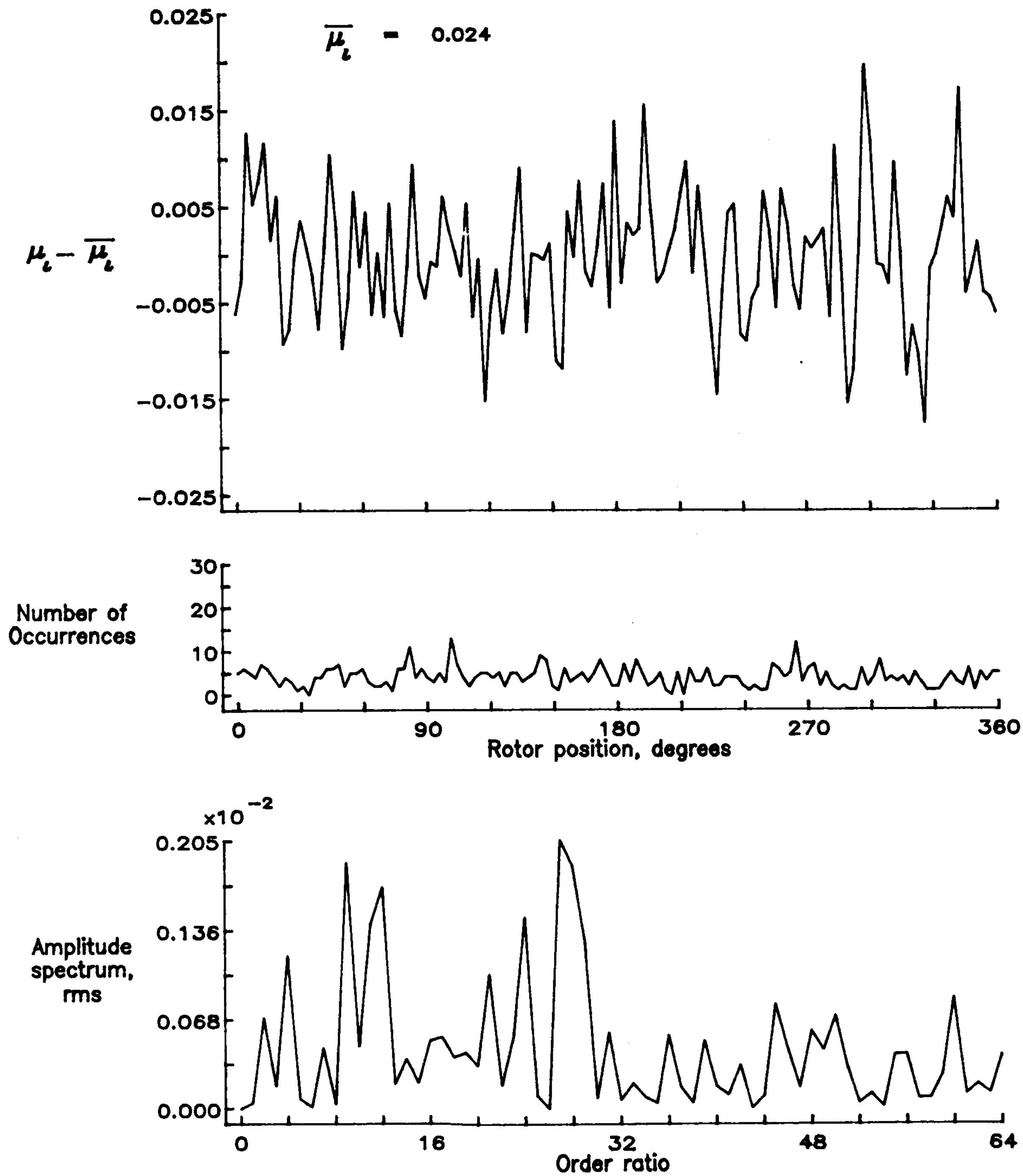

Figure 51.– Induced inflow velocity measured at 90 degrees and r/R of 0.78.

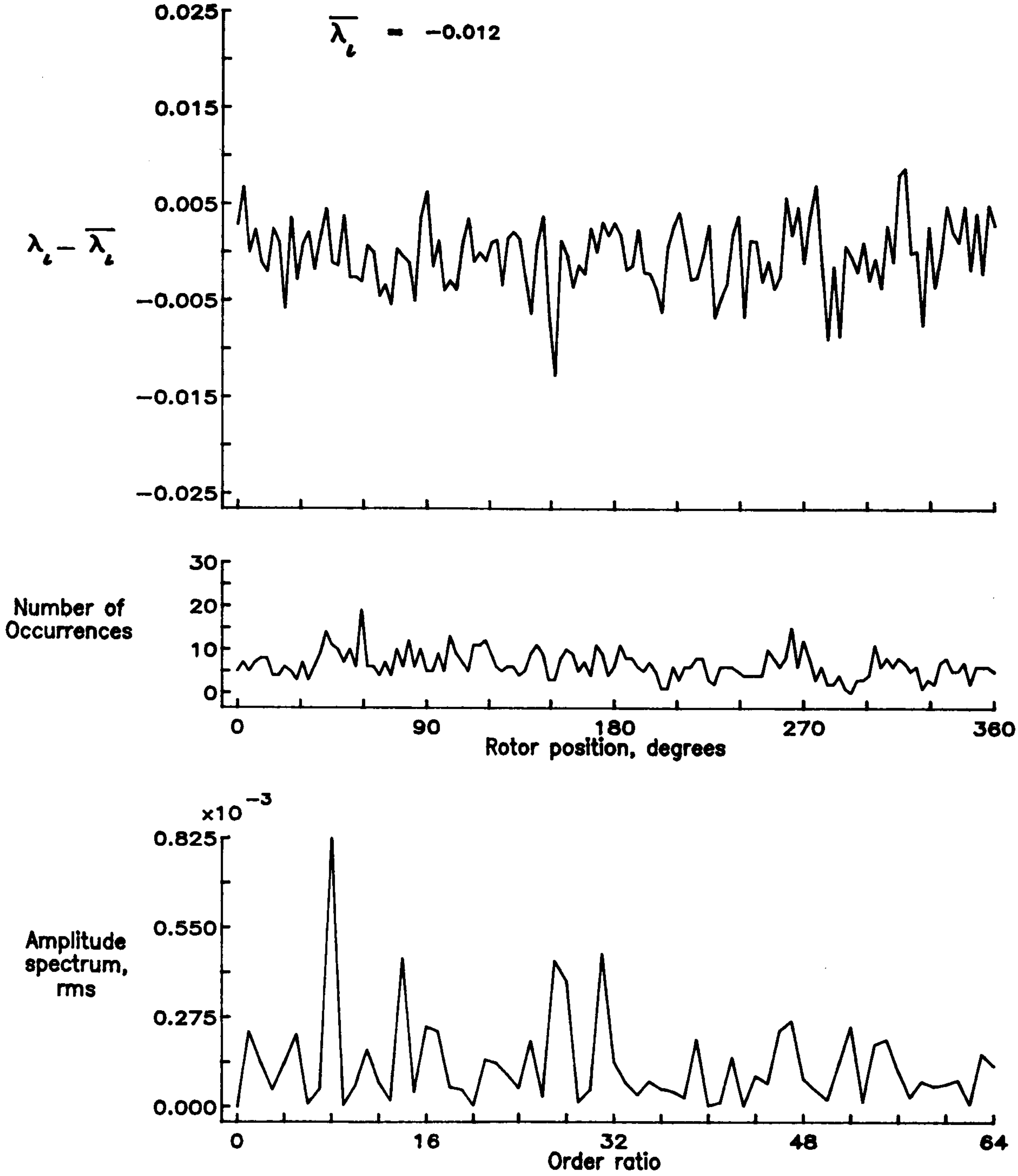

Figure 51.– Concluded.

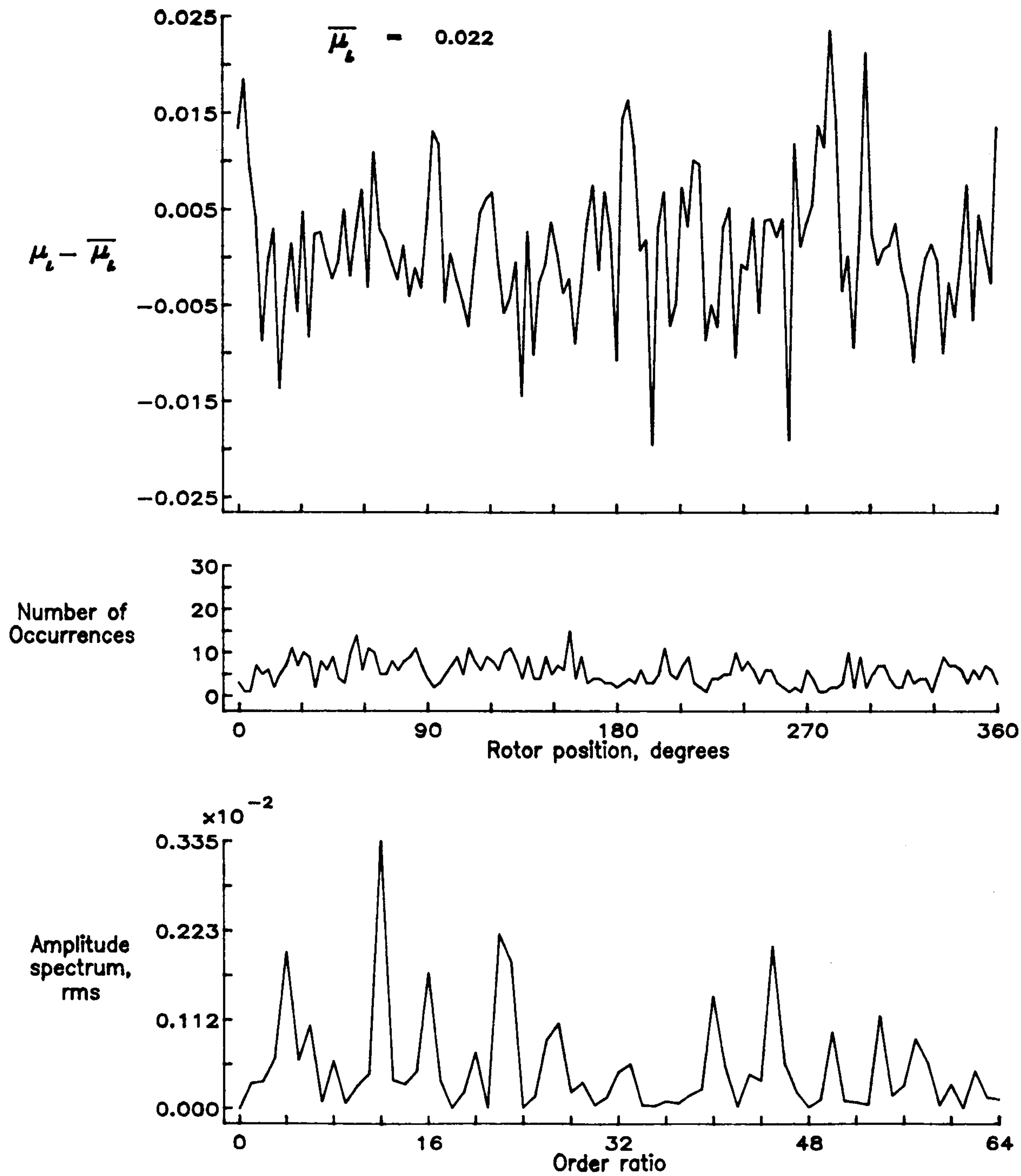

Figure 52.– Induced inflow velocity measured at 90 degrees and r/R of 0.82.

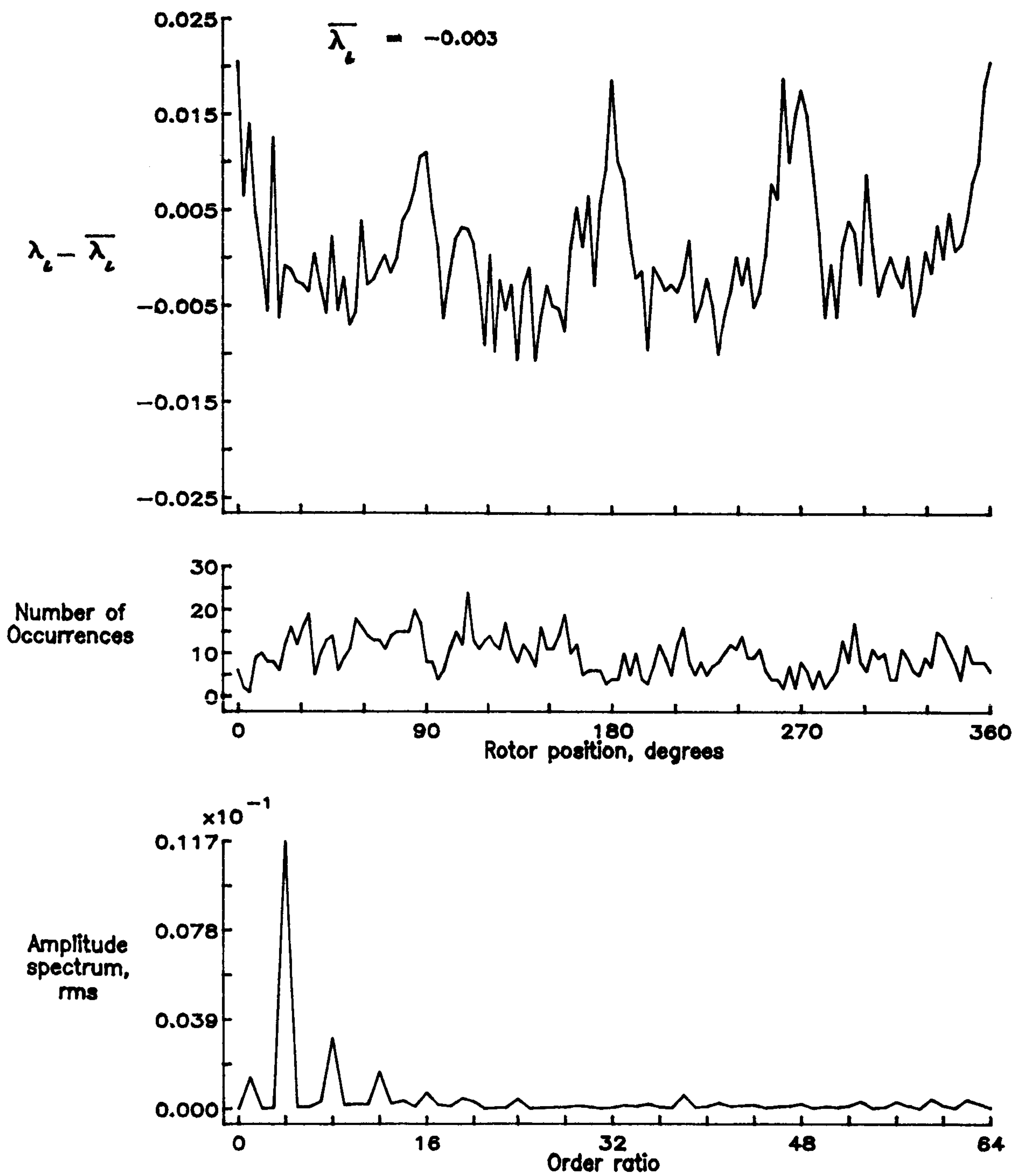

Figure 52.– Concluded.

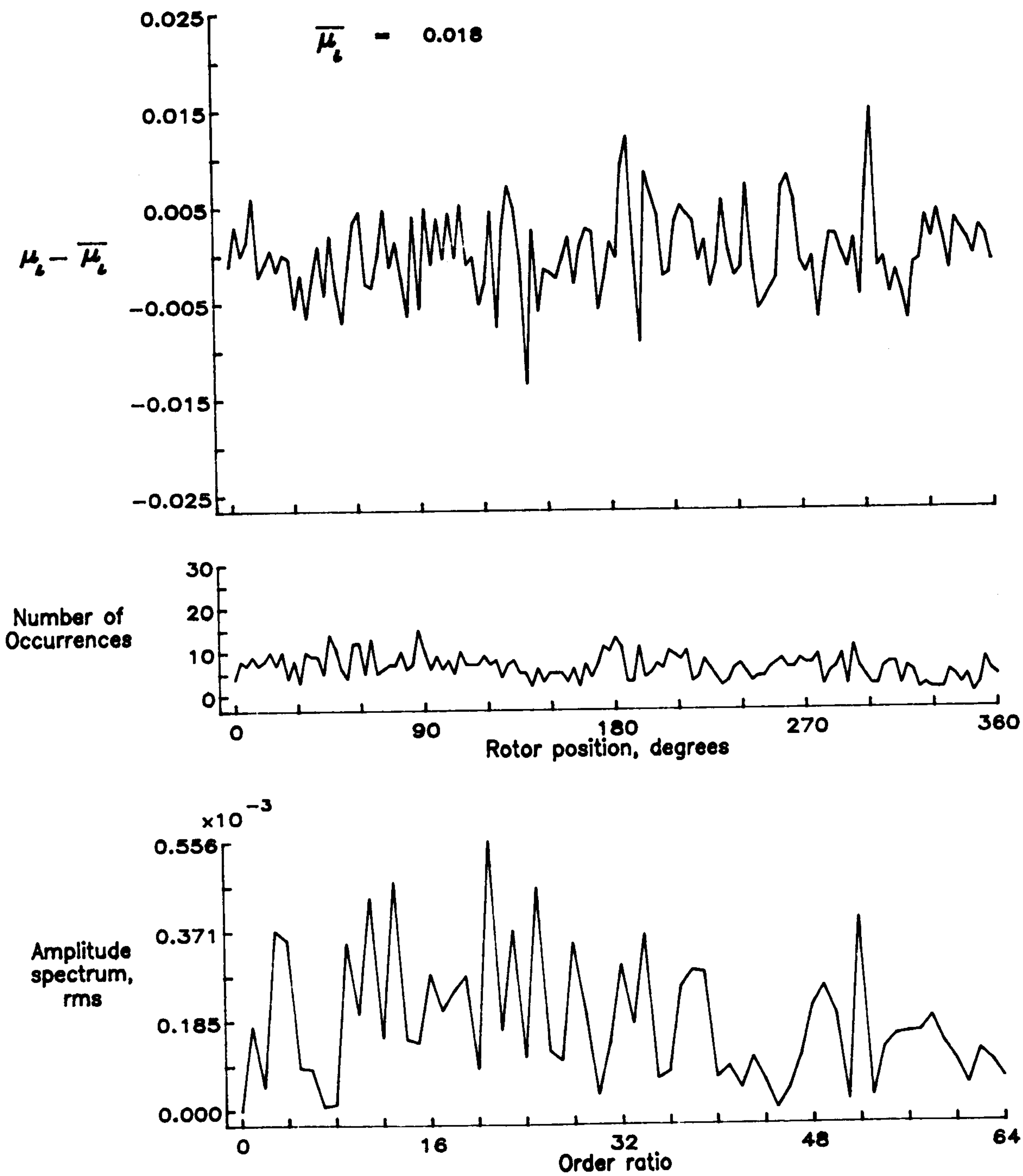

Figure 53.– Induced inflow velocity measured at 90 degrees and r/R of 0.86.

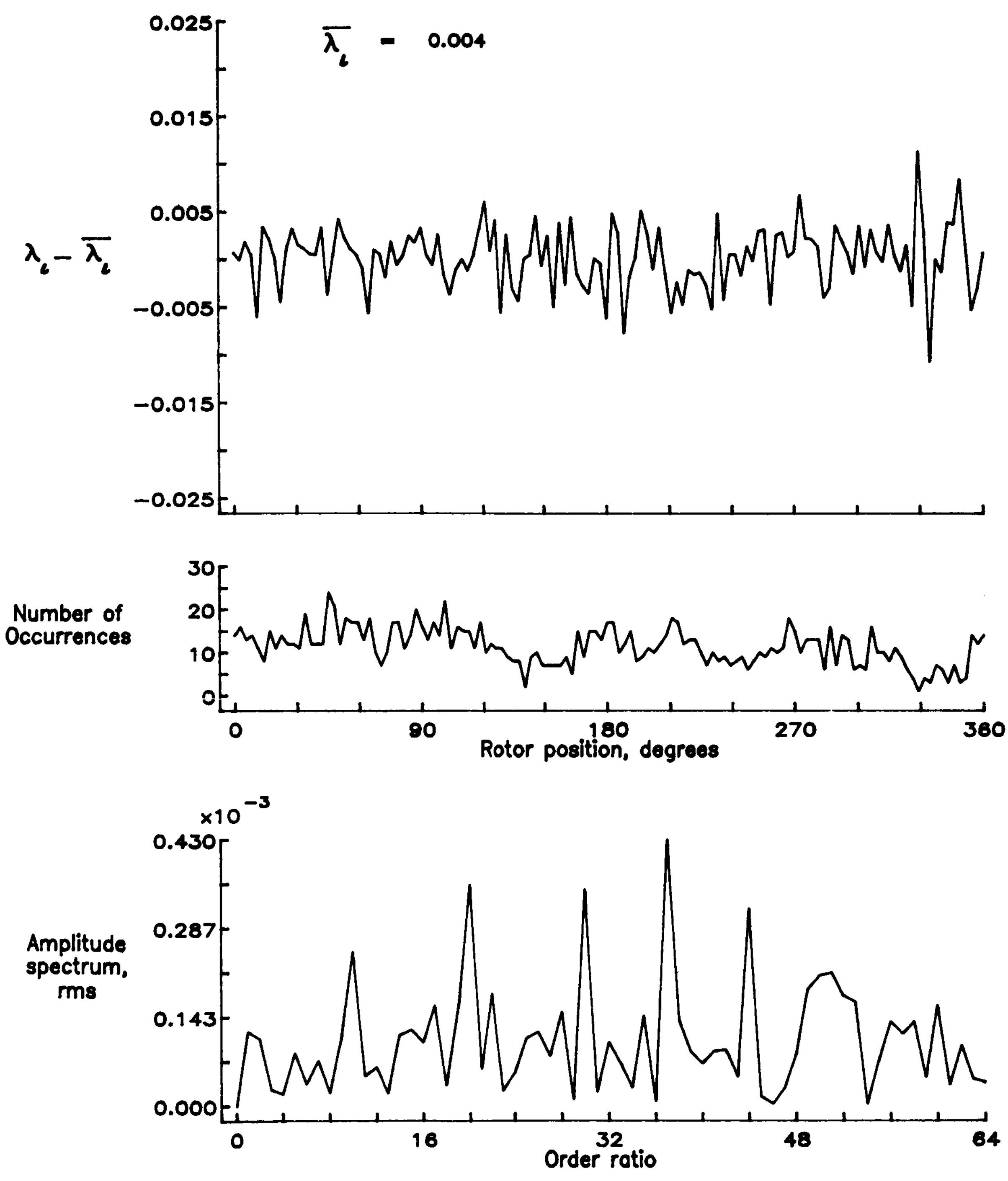

Figure 53.– Concluded.

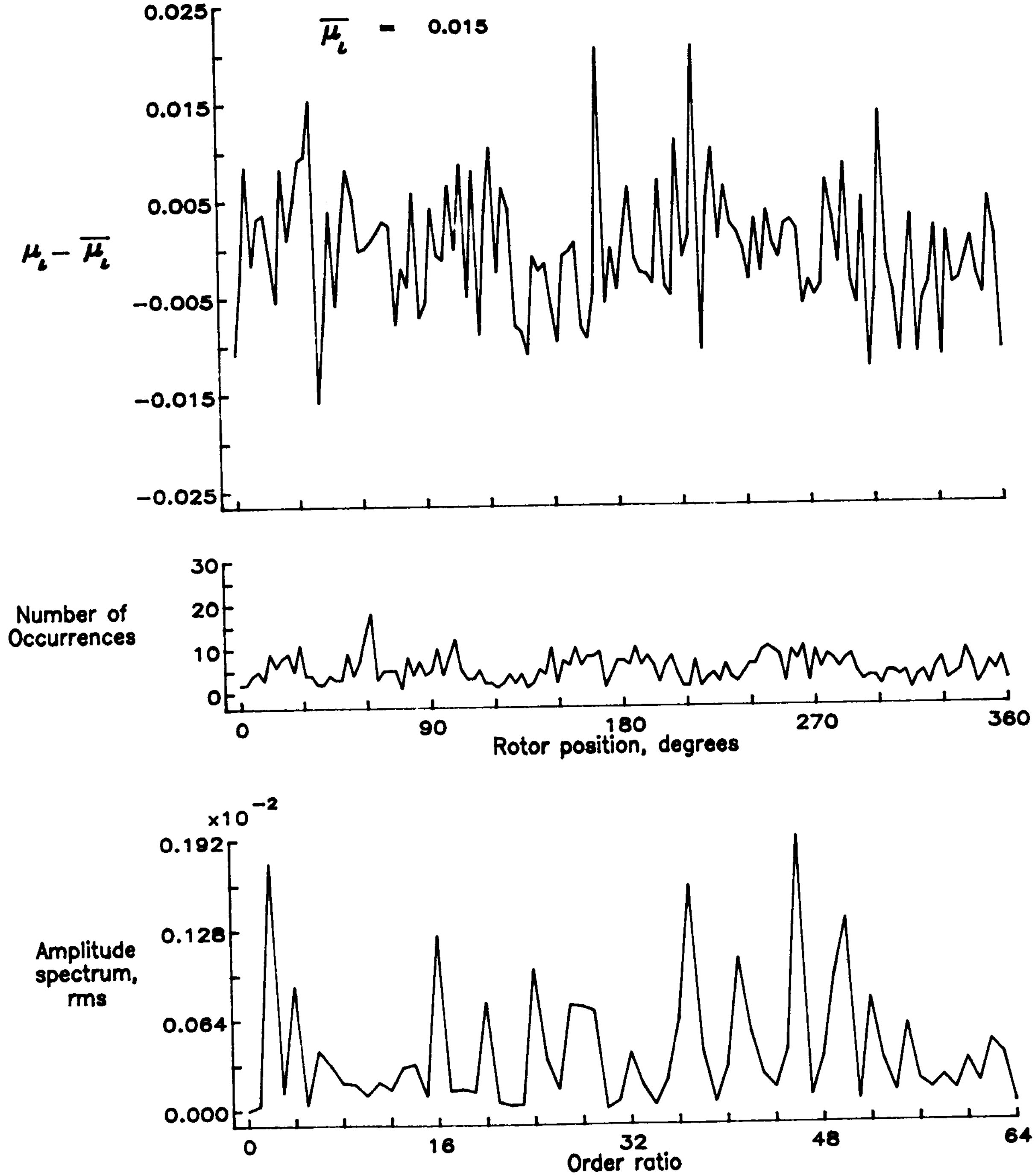

Figure 54.– Induced inflow velocity measured at 90 degrees and r/R of 0.90.

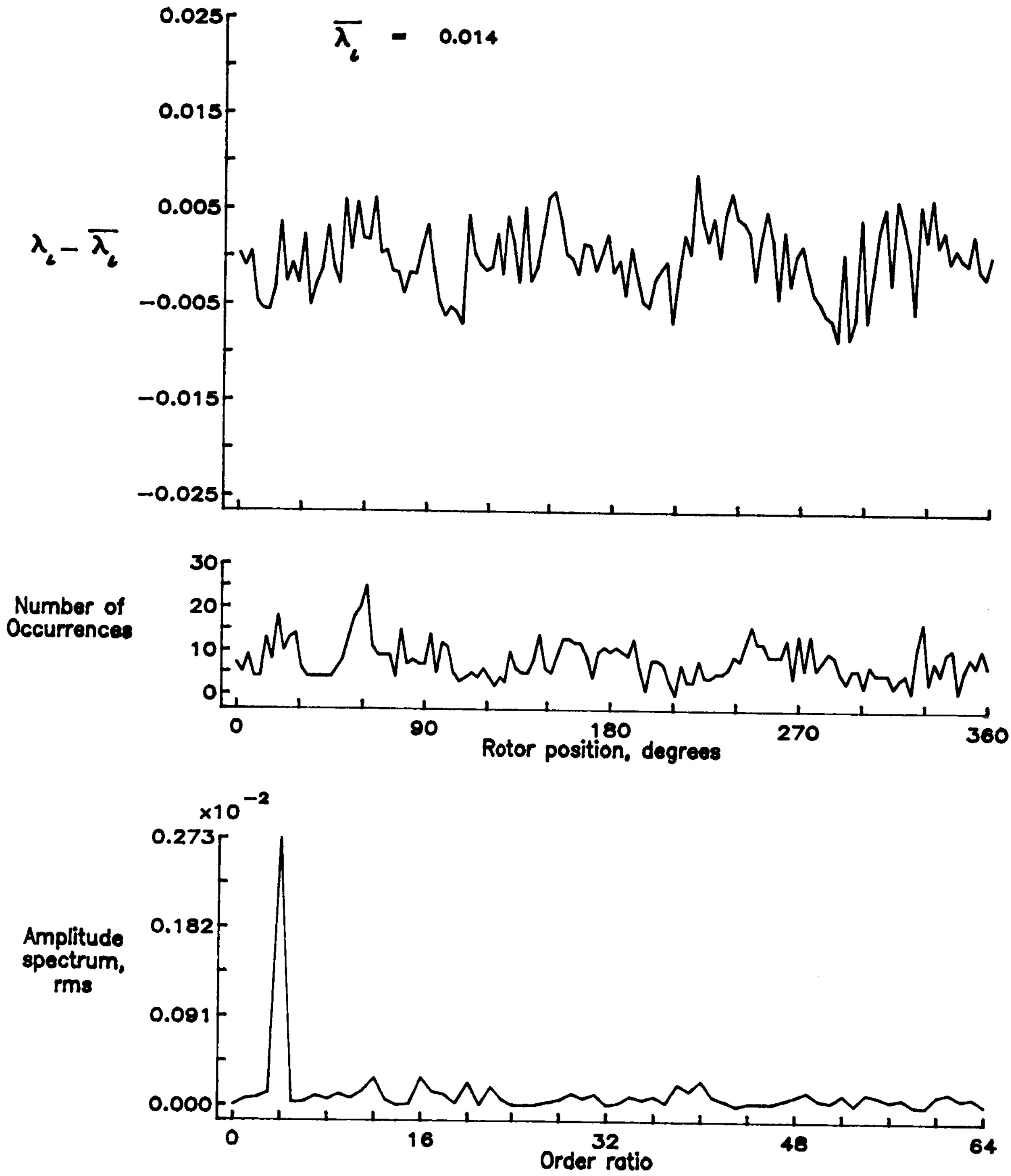

Figure 54.– Concluded.

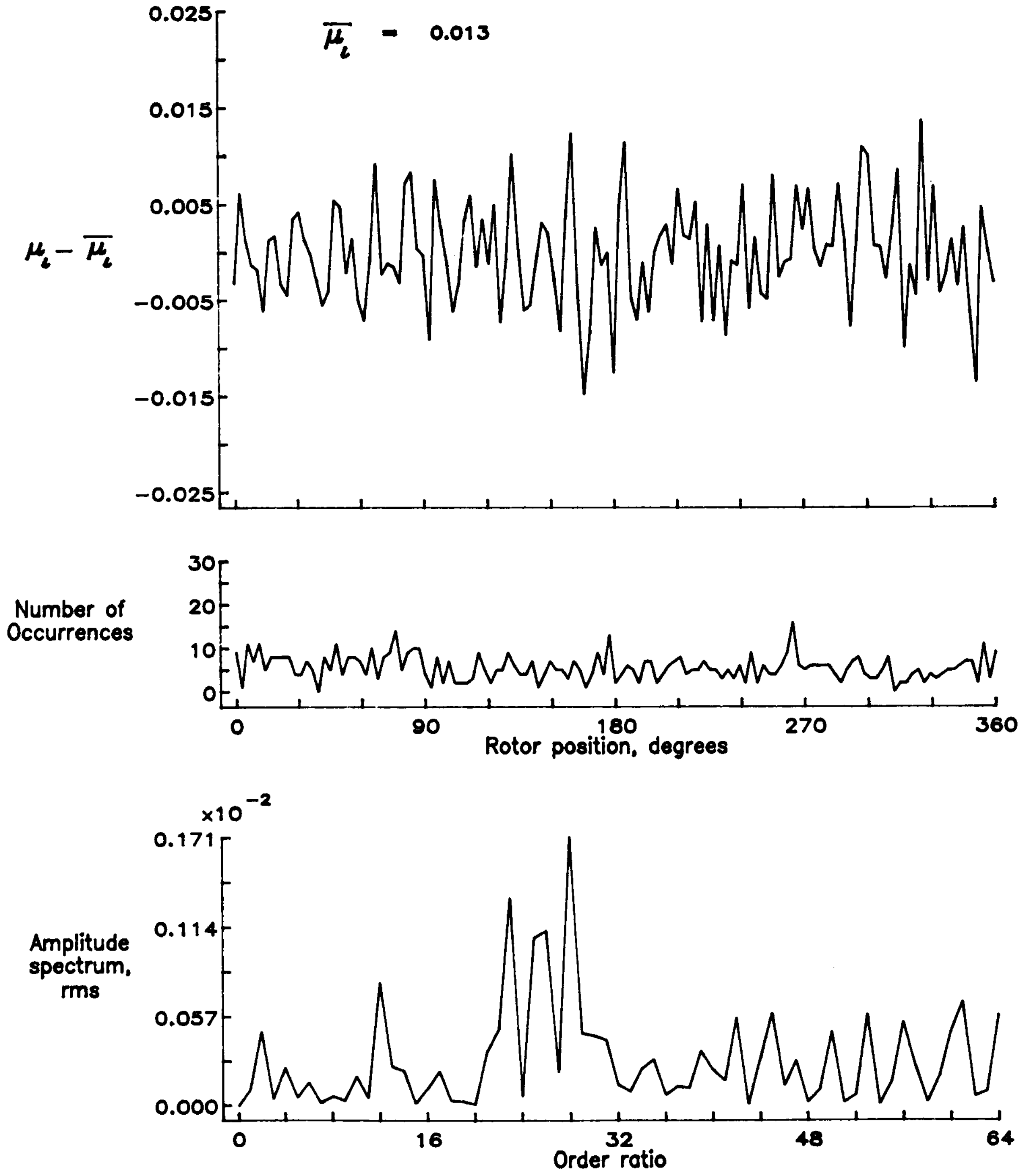

Figure 55.— Induced inflow velocity measured at 90 degrees and r/R of 0.94.

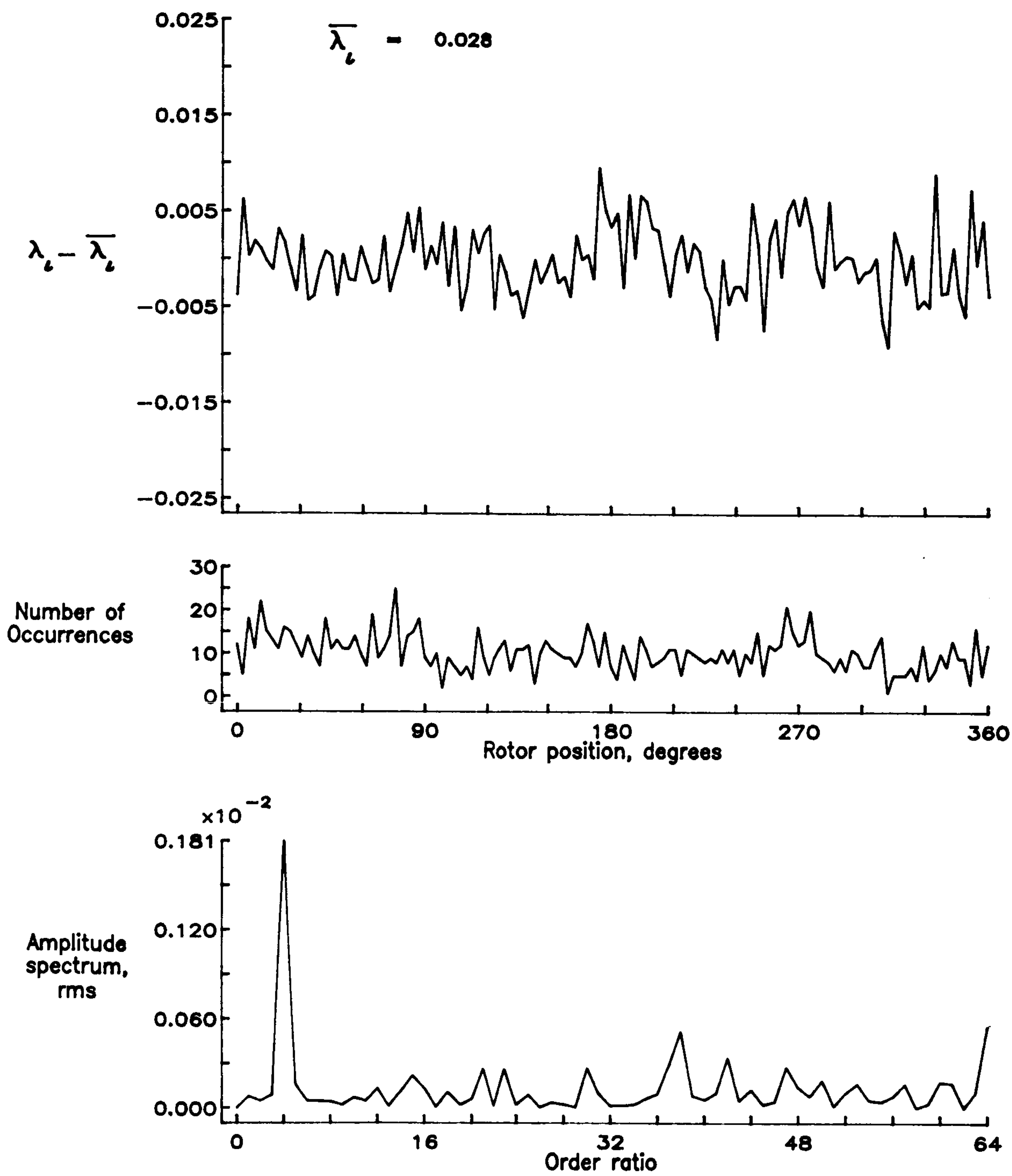

Figure 55.– Concluded.

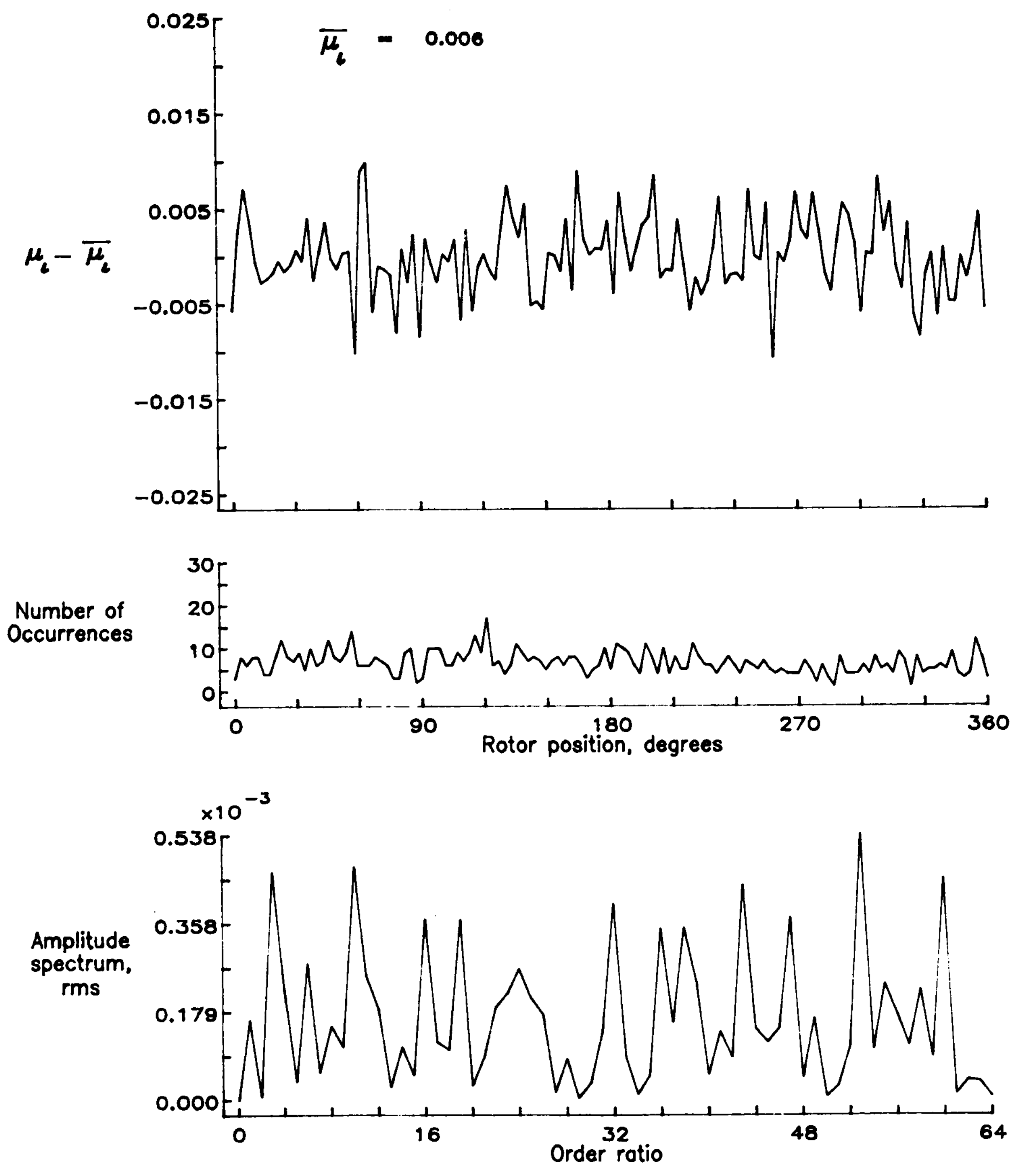

Figure 56.– Induced inflow velocity measured at 90 degrees and r/R of 0.98.

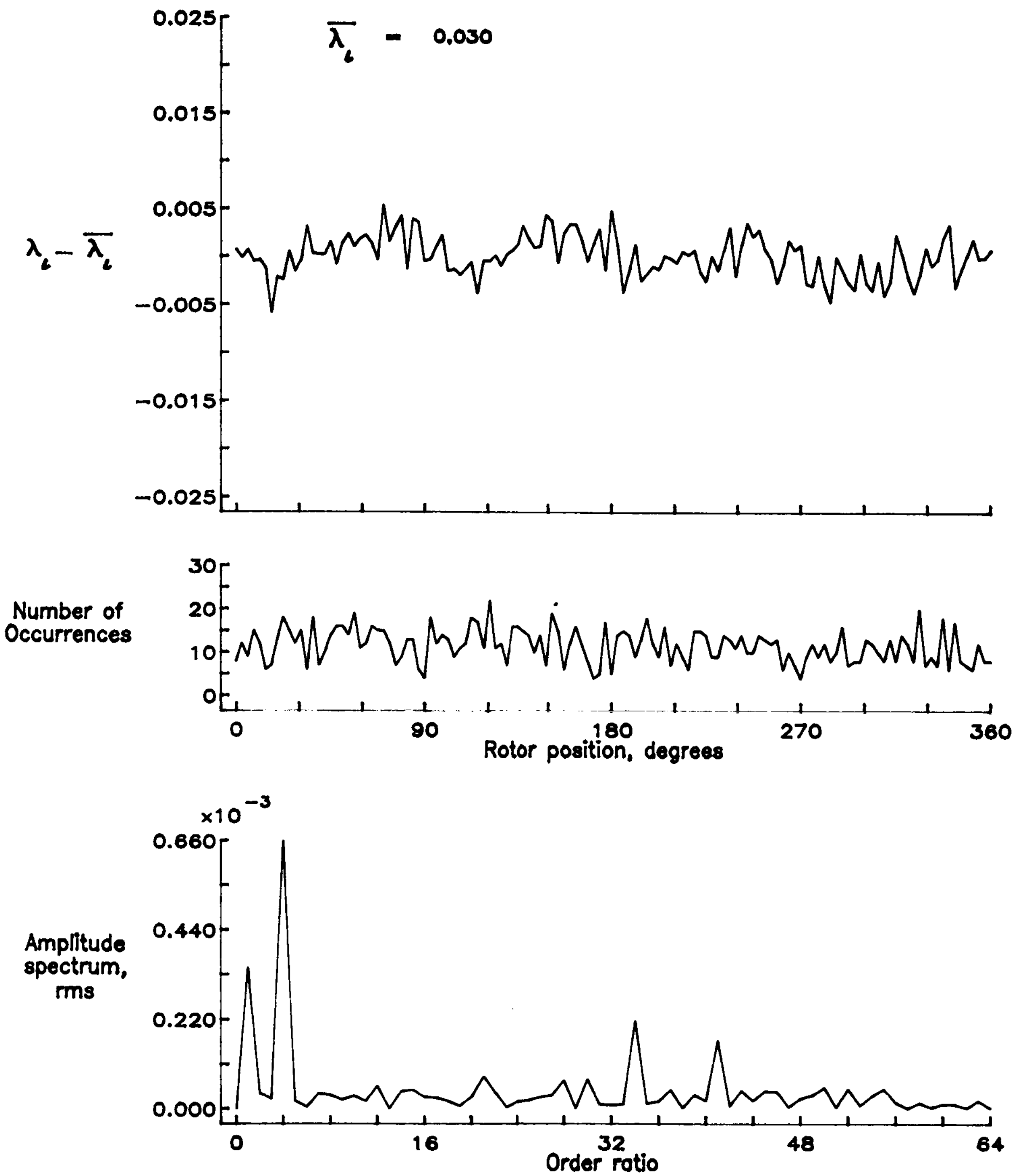

Figure 56.– Concluded.

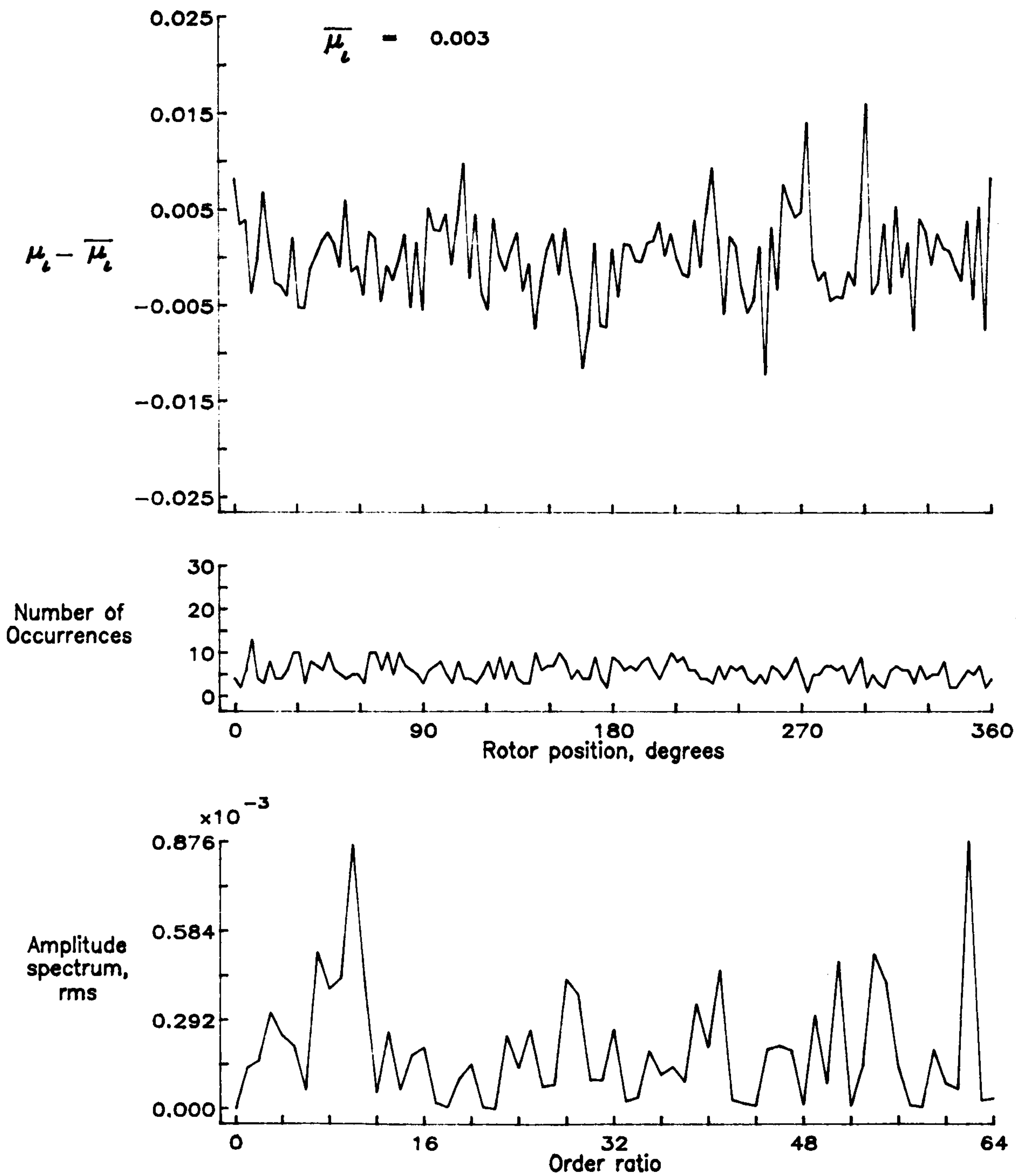

Figure 57.– Induced inflow velocity measured at 90 degrees and r/R of 1.04.

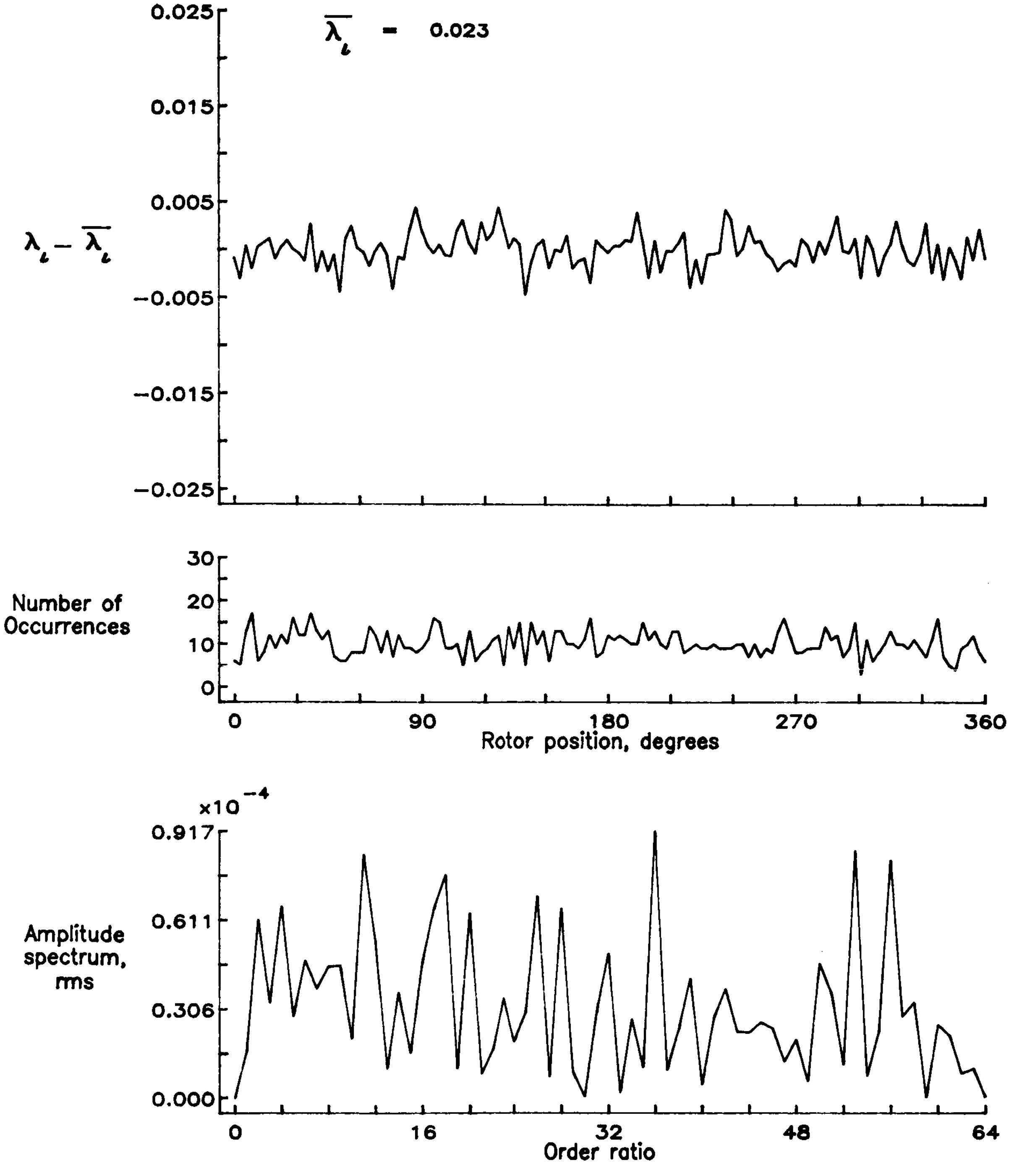

Figure 57.– Concluded.

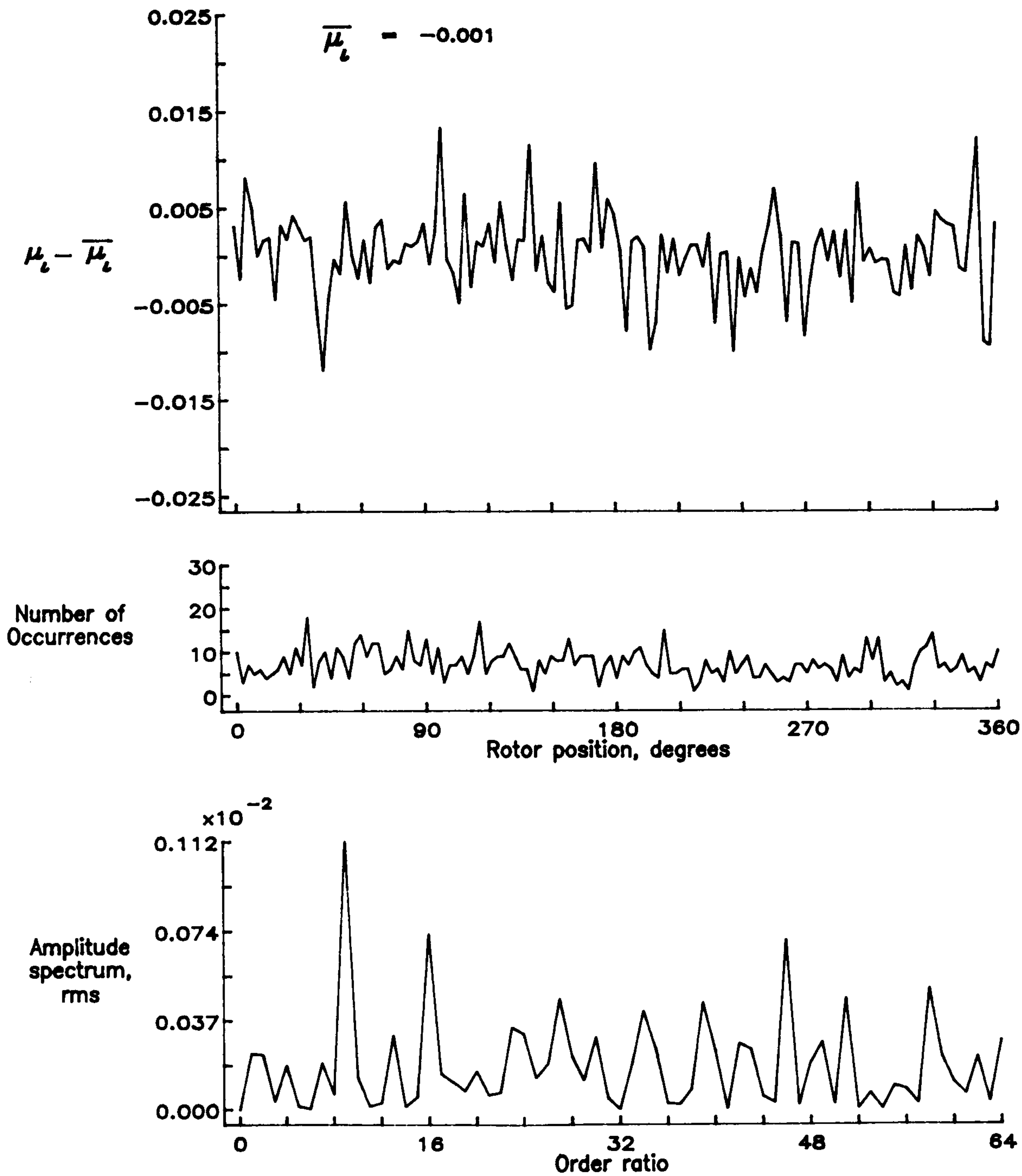

Figure 58.— Induced inflow velocity measured at 90 degrees and r/R of 1.10.

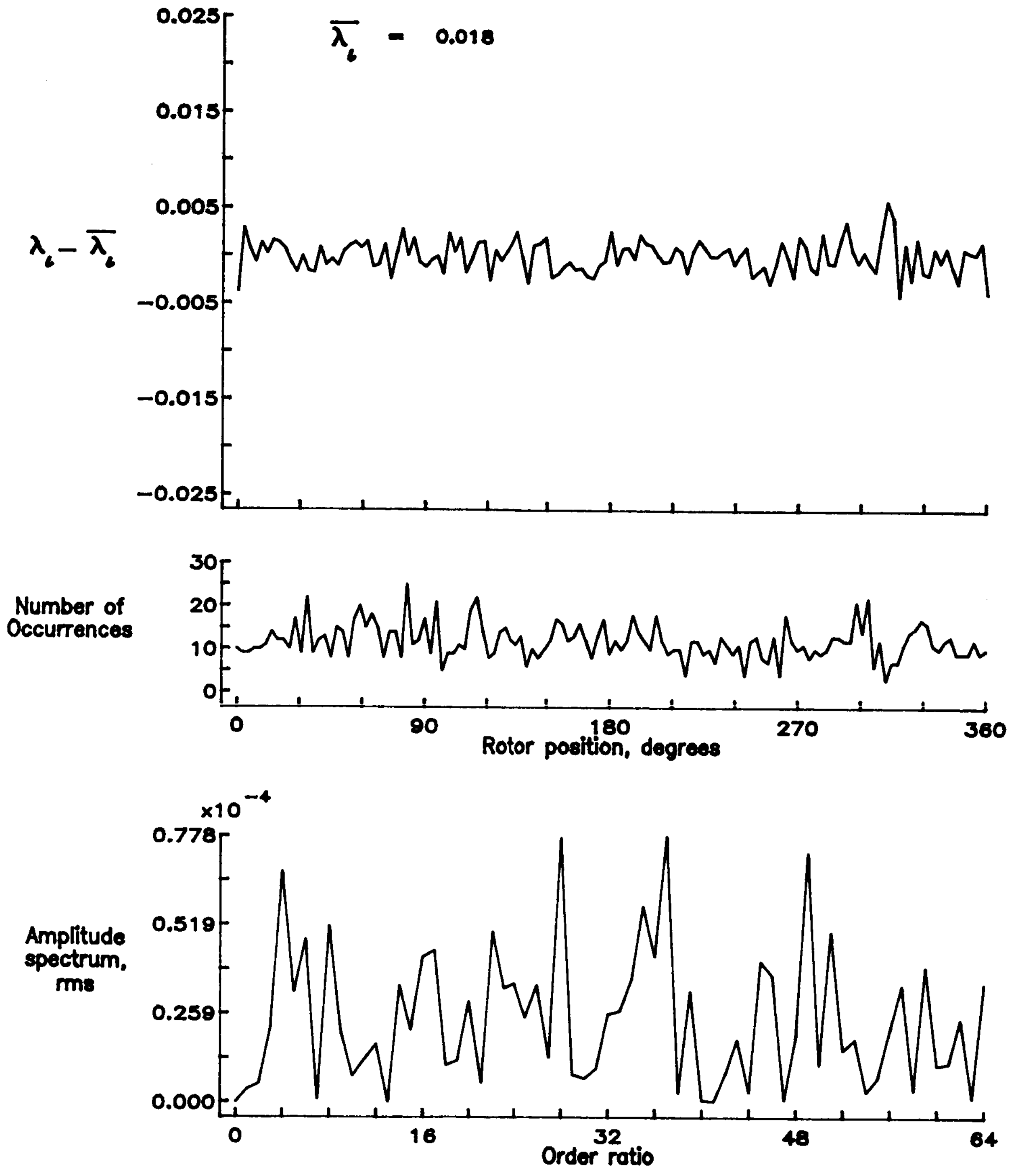

Figure 58.– Concluded.

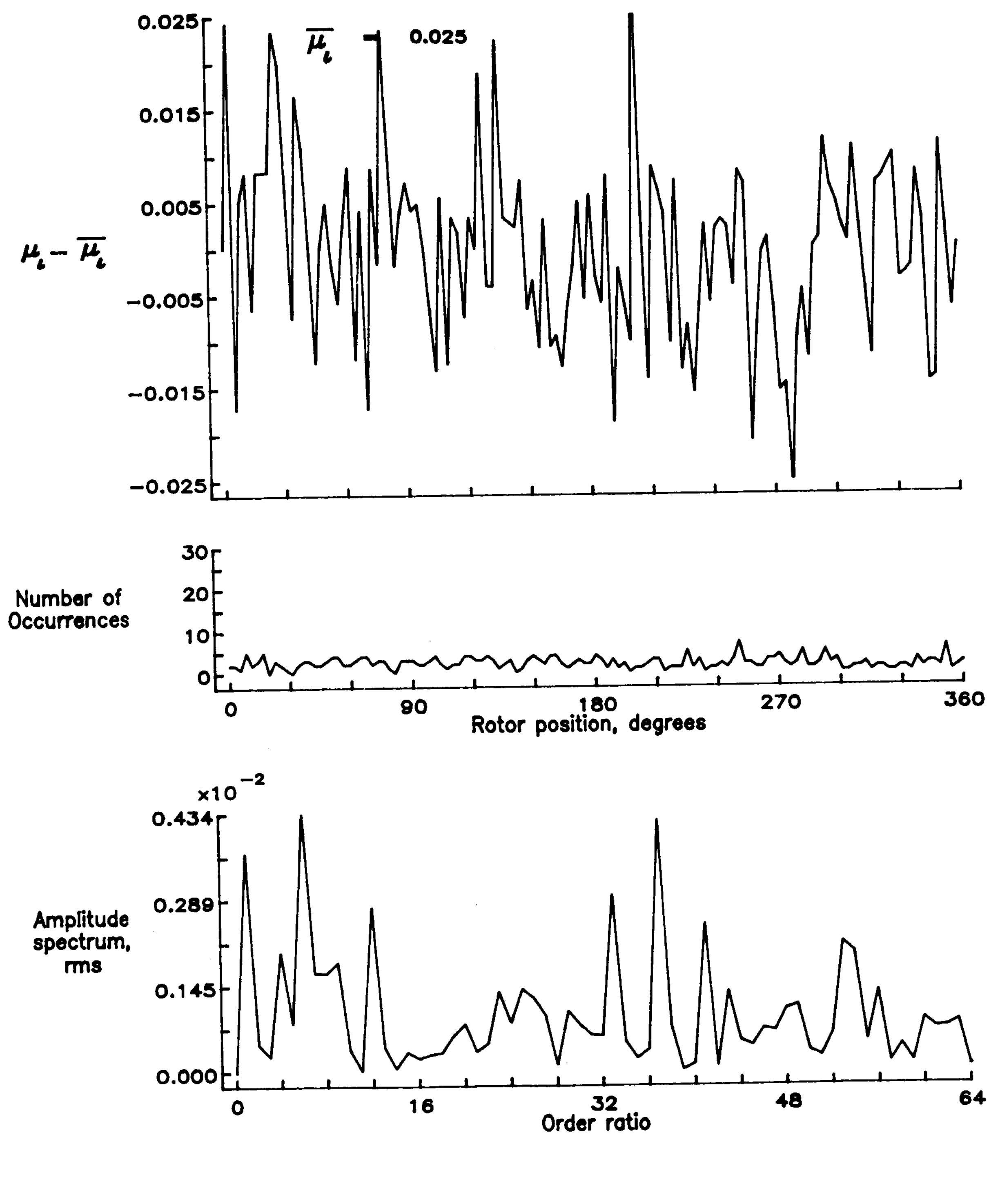

Figure 59.– Induced inflow velocity measured at 120 degrees and r/R of 0.40.

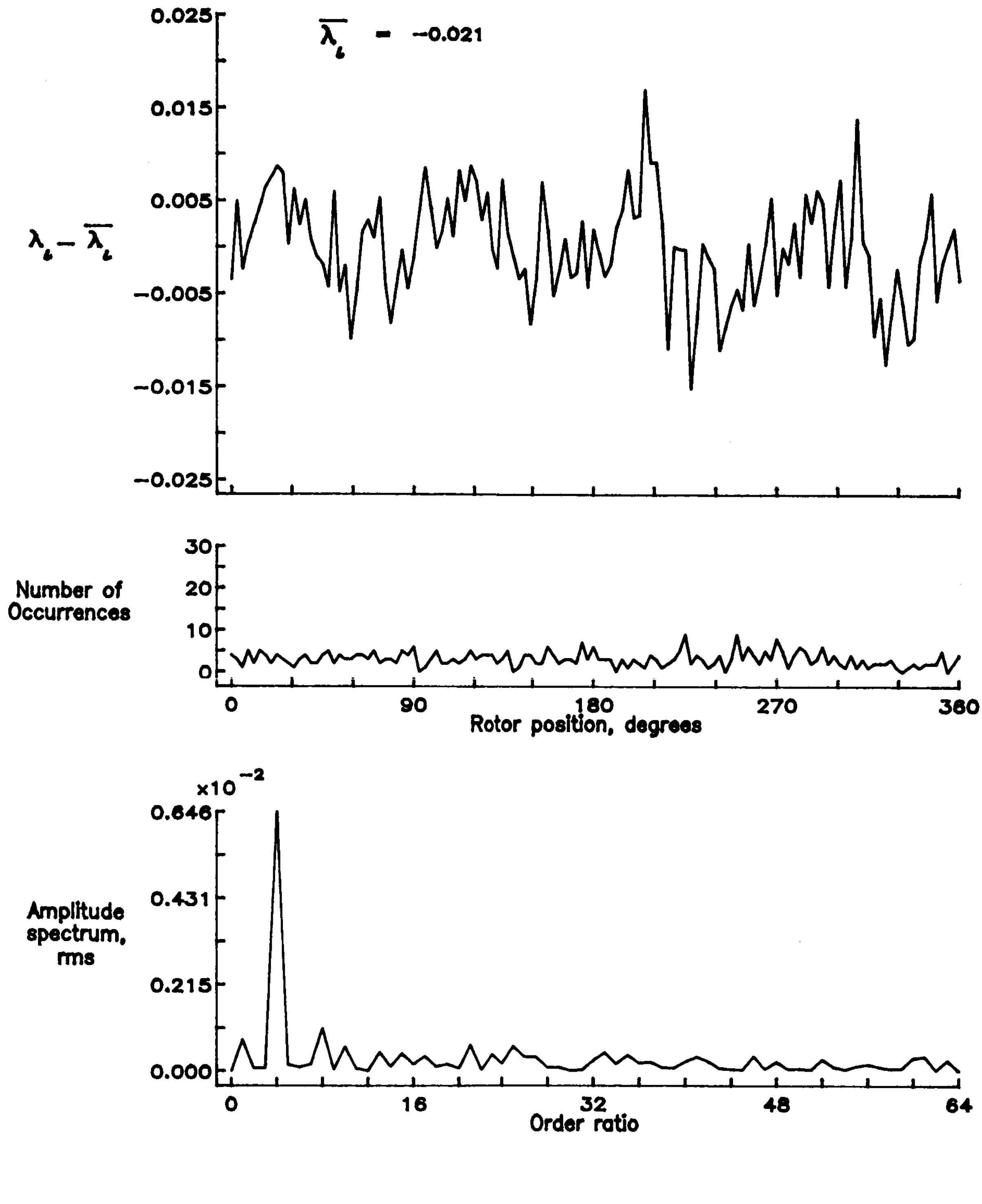

Figure 59.– Concluded.

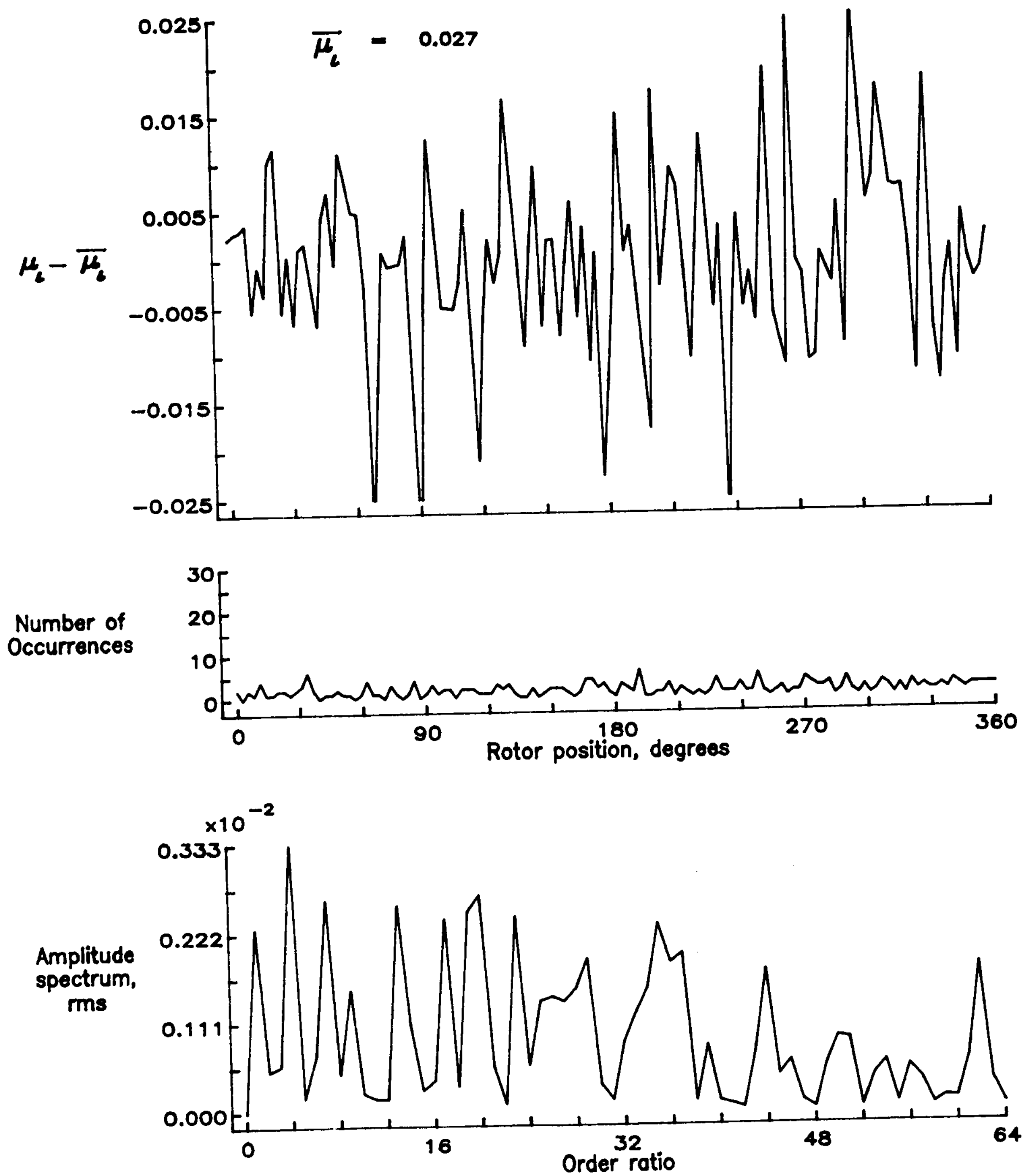

Figure 60.– Induced inflow velocity measured at 120 degrees and r/R of 0.50.

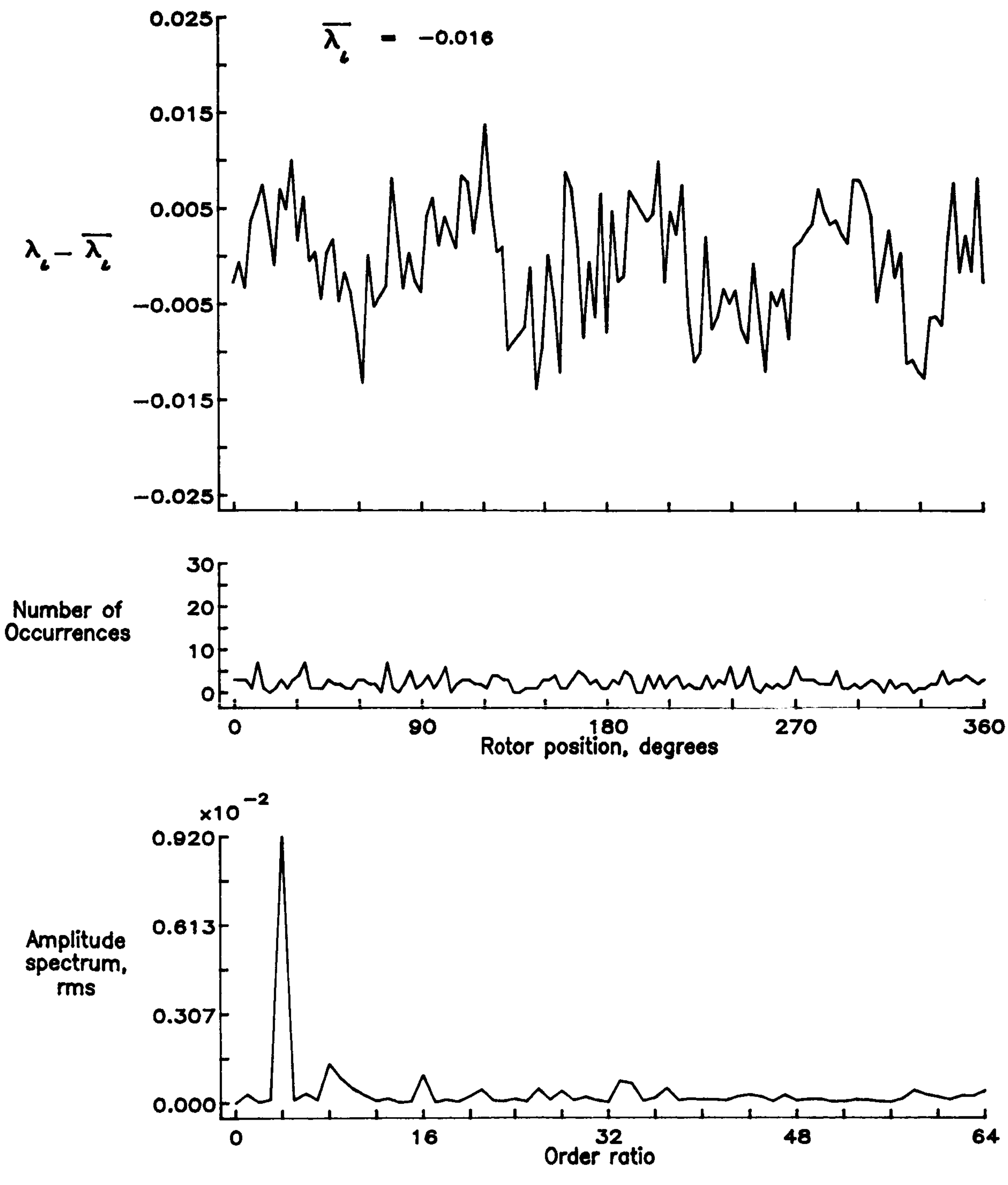

Figure 60.– Concluded.

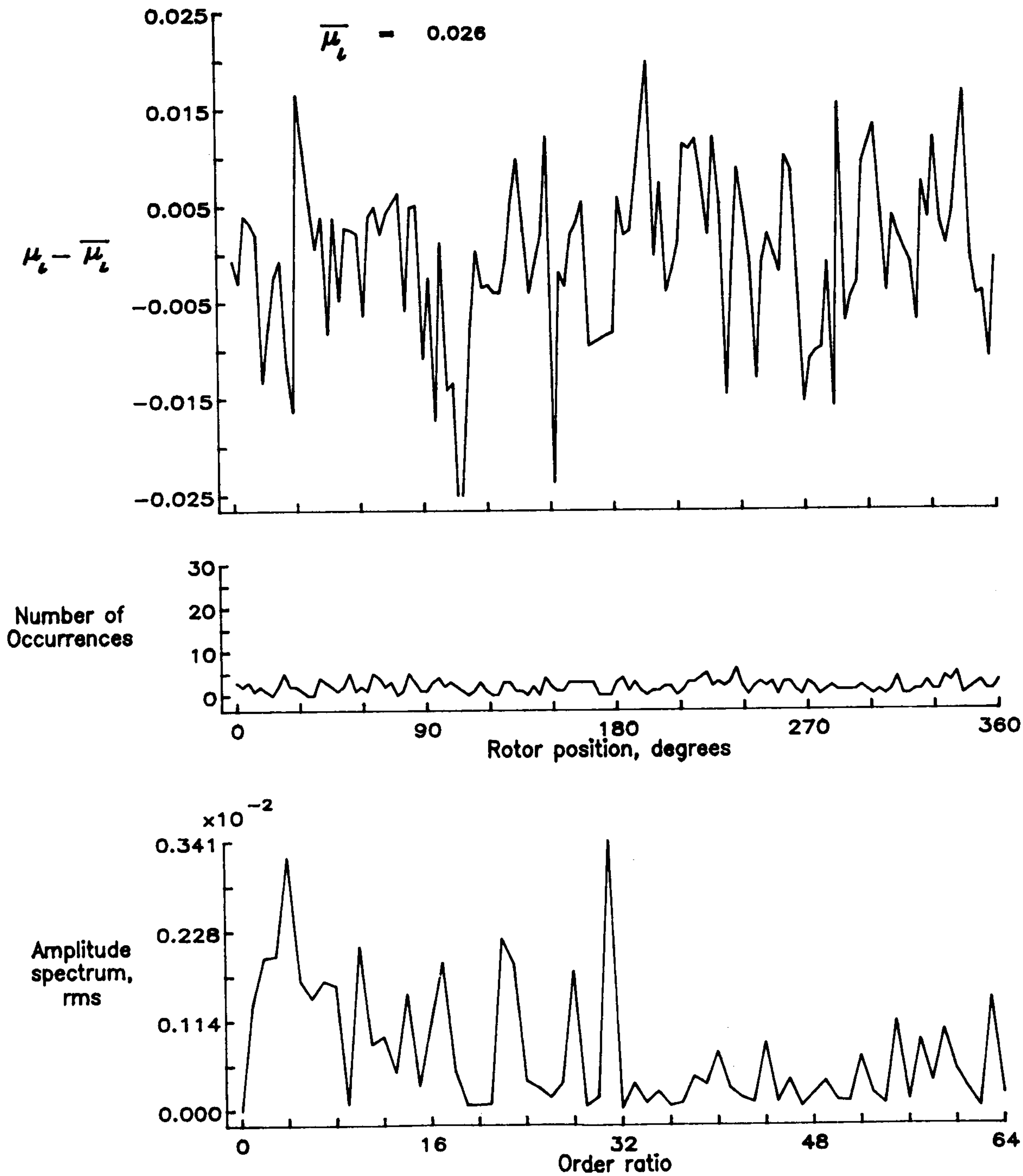

Figure 61.– Induced inflow velocity measured at 120 degrees and r/R of 0.60.

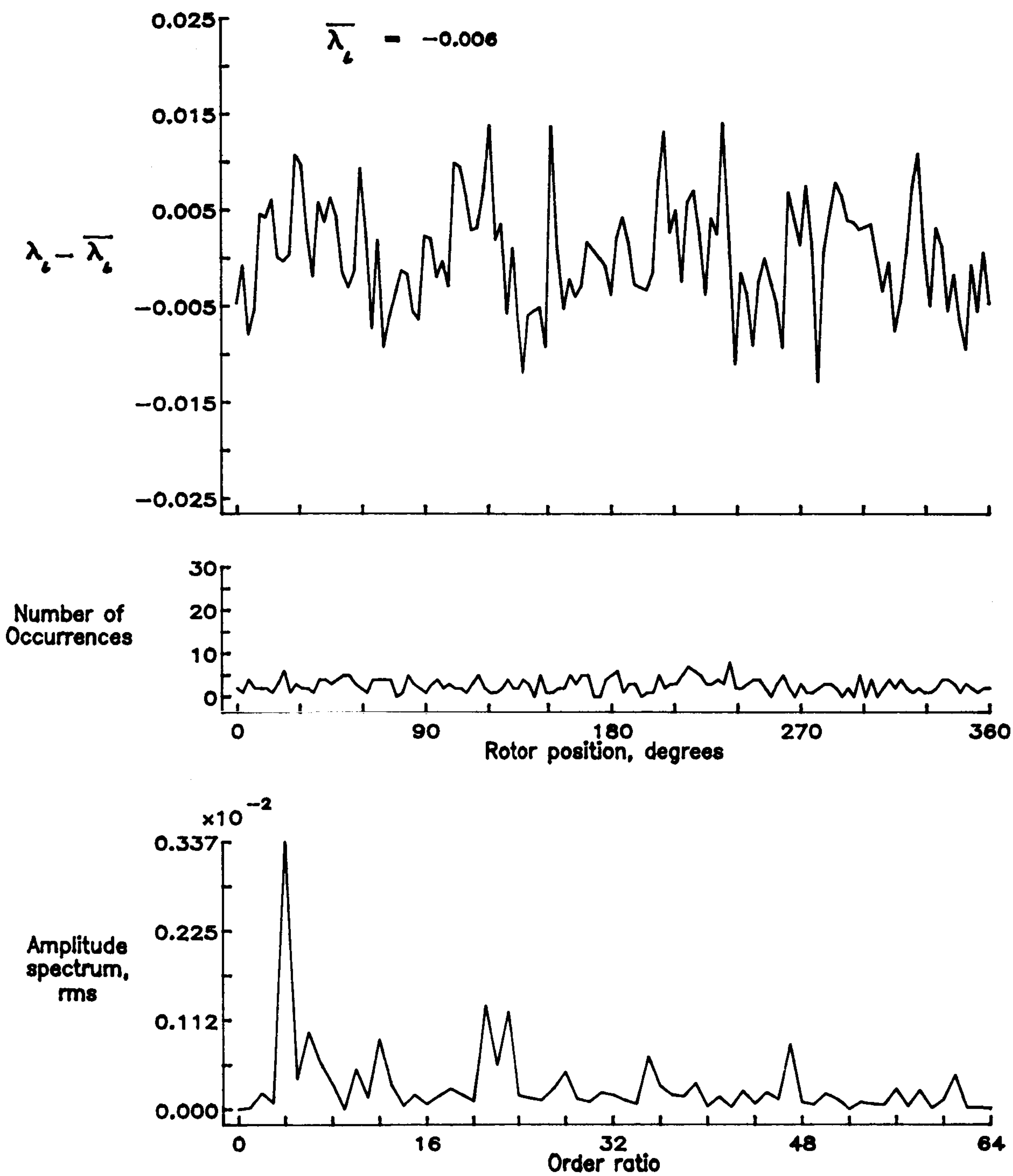

Figure 61.– Concluded.

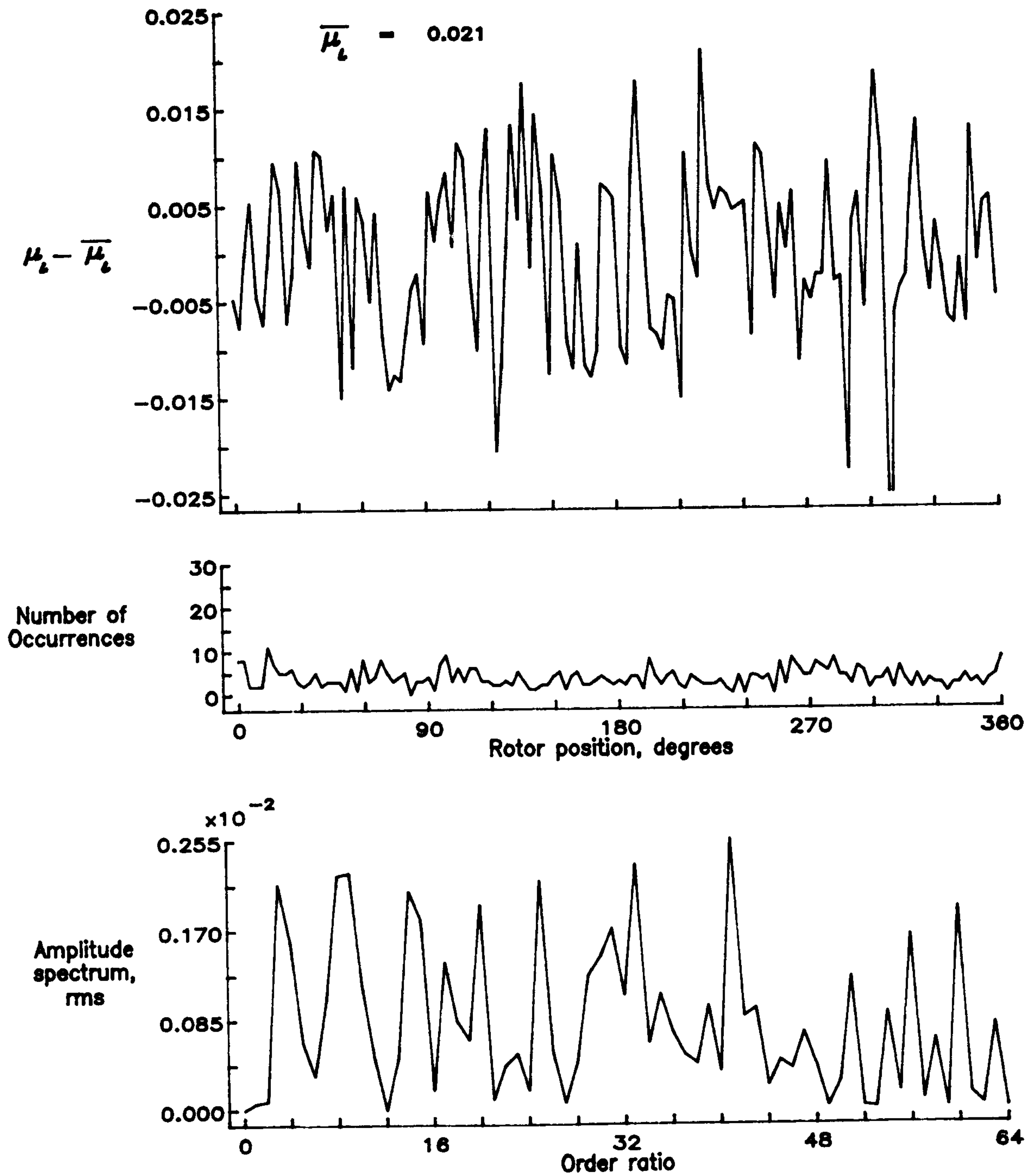

Figure 62.– Induced inflow velocity measured at 120 degrees and r/R of 0.70.

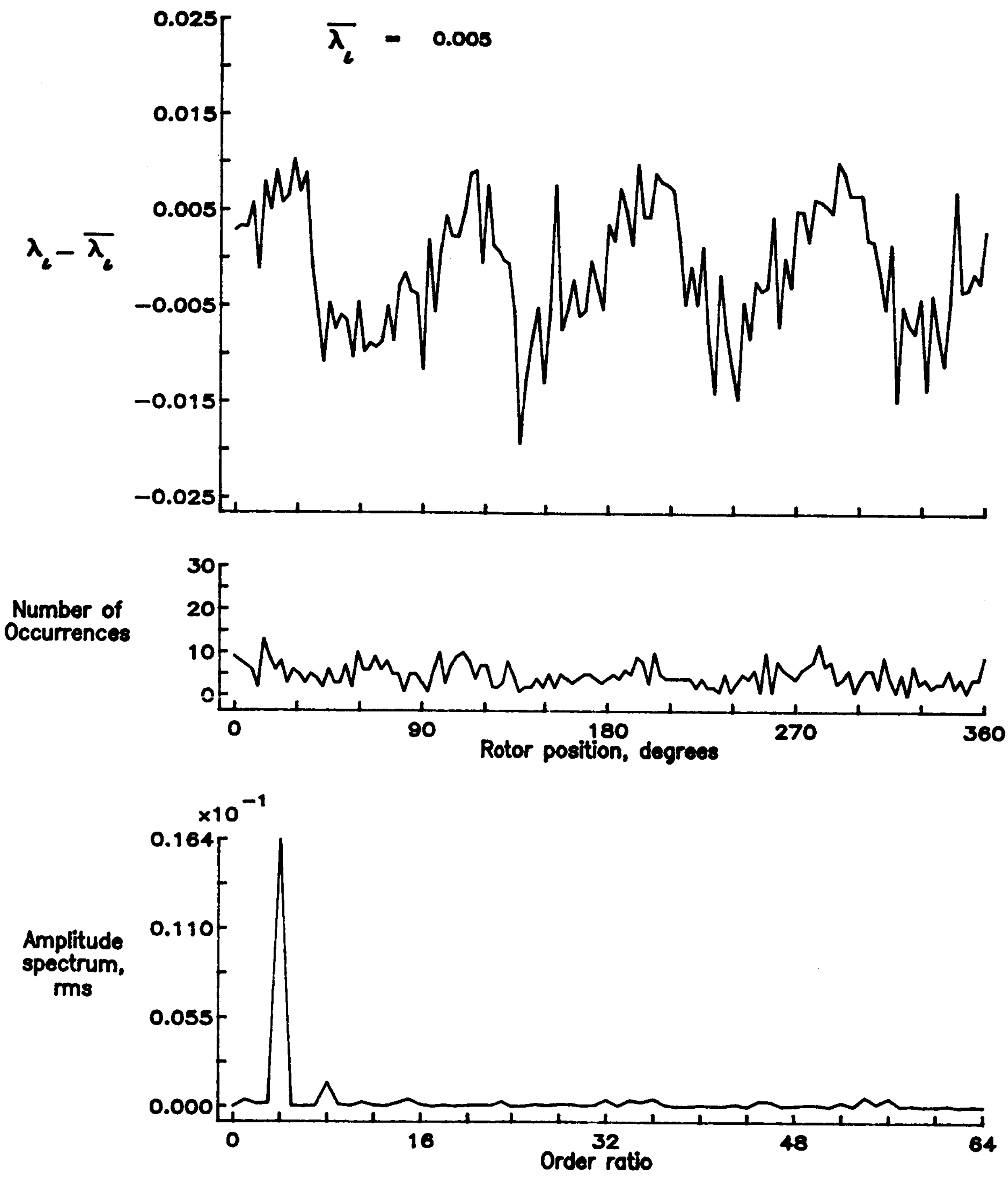

Figure 62.– Concluded.

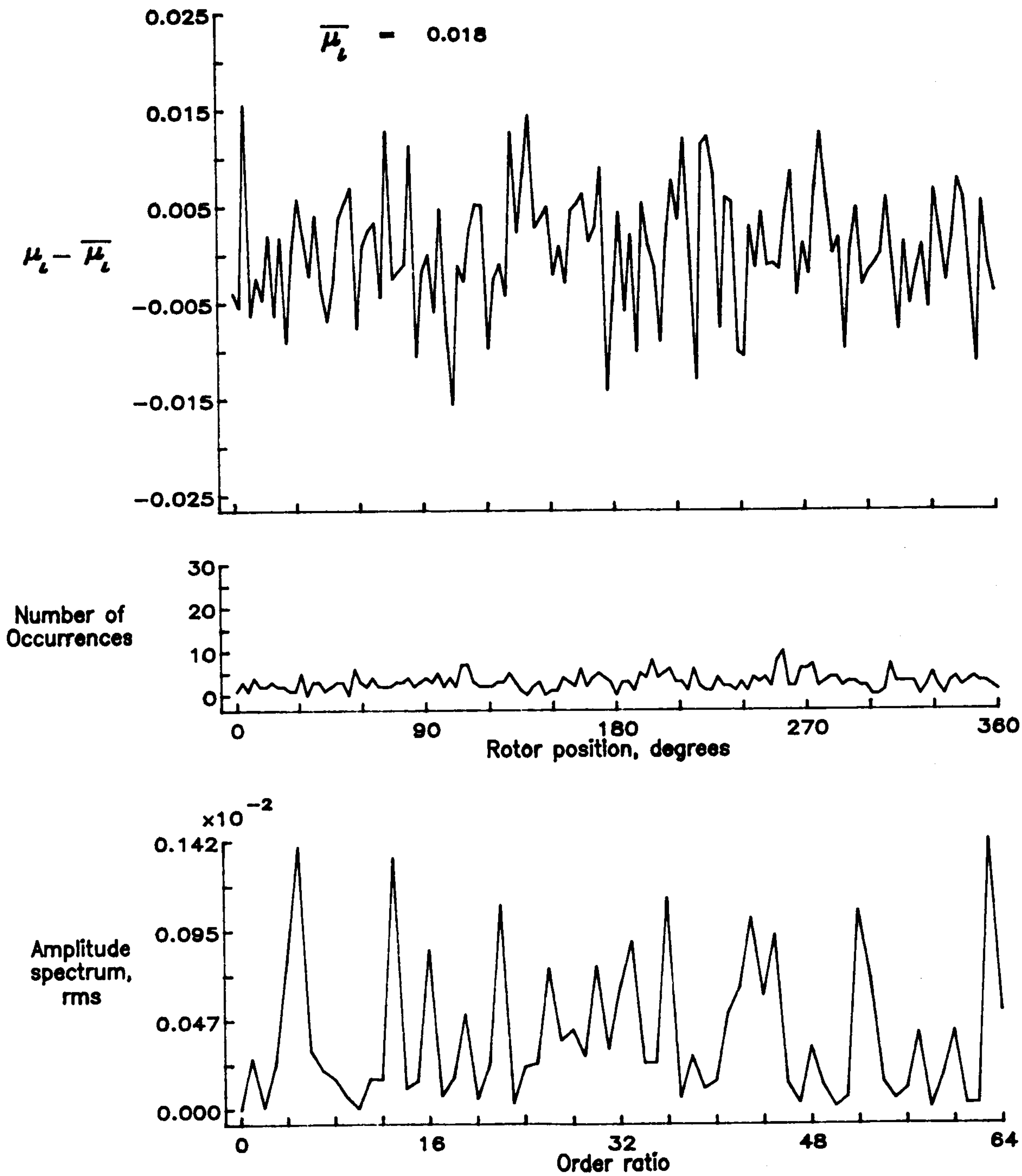

Figure 63.– Induced inflow velocity measured at 120 degrees and r/R of 0.74.

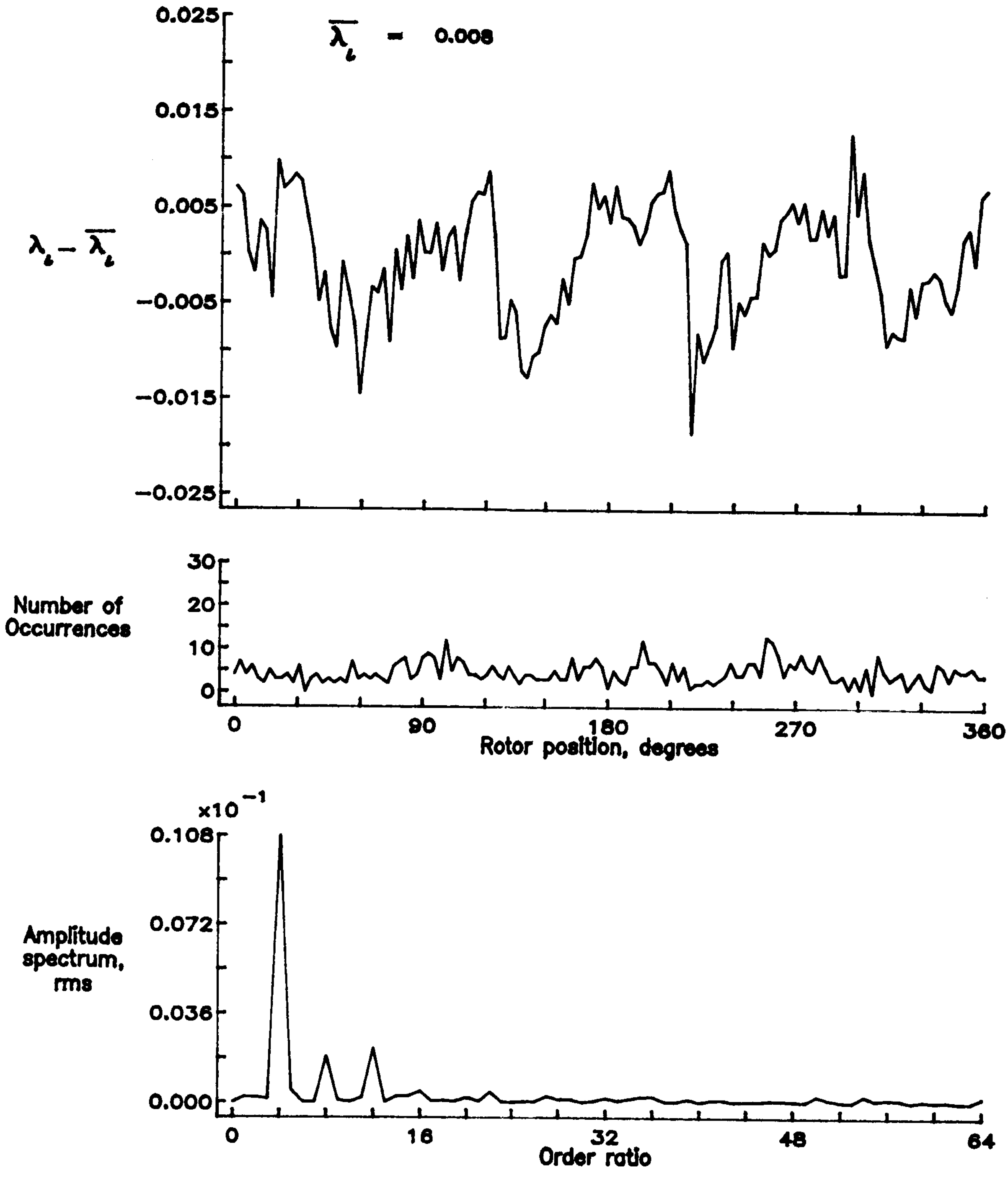

Figure 63.– Concluded.

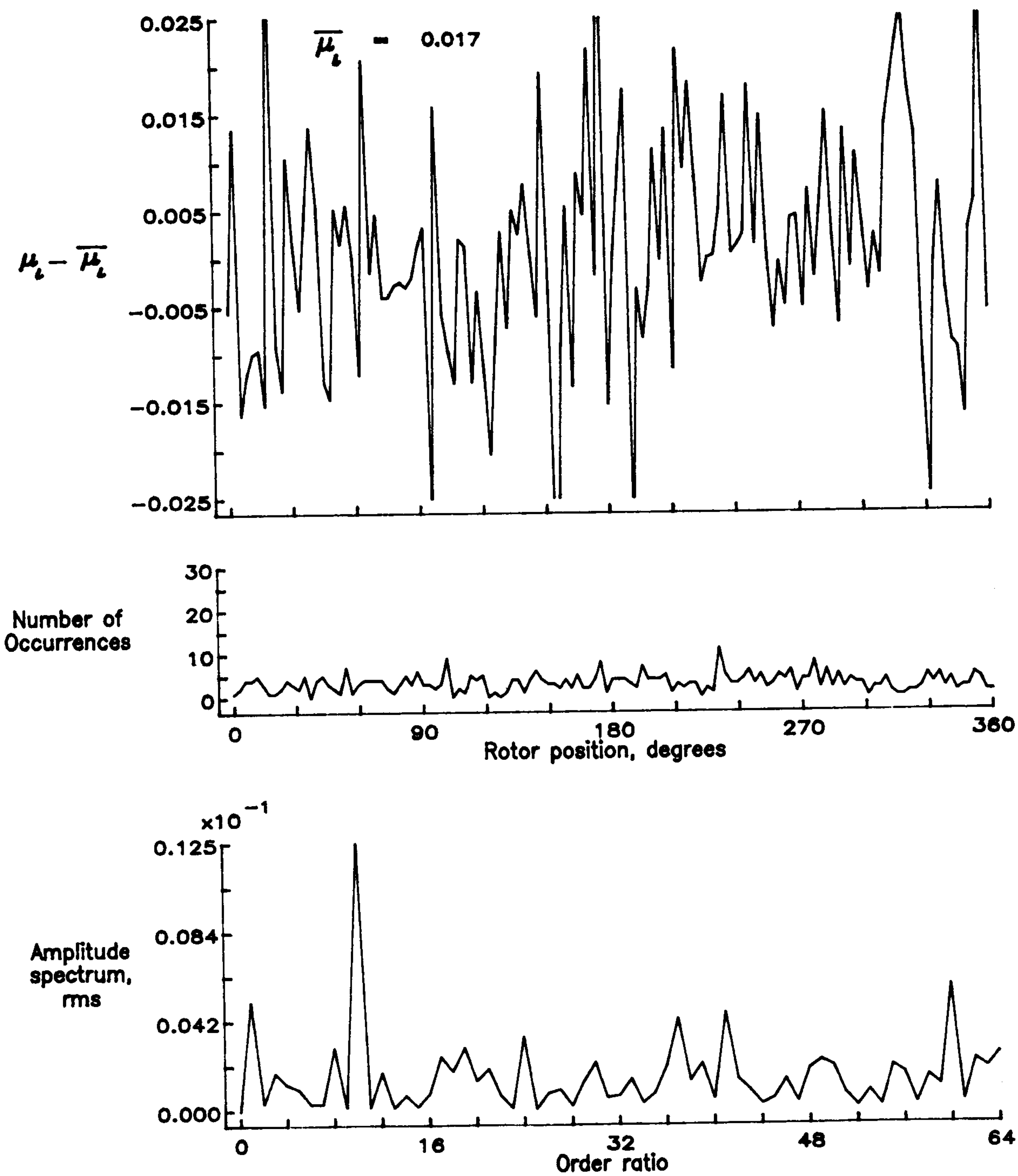

Figure 64.– Induced inflow velocity measured at 120 degrees and r/R of 0.78.

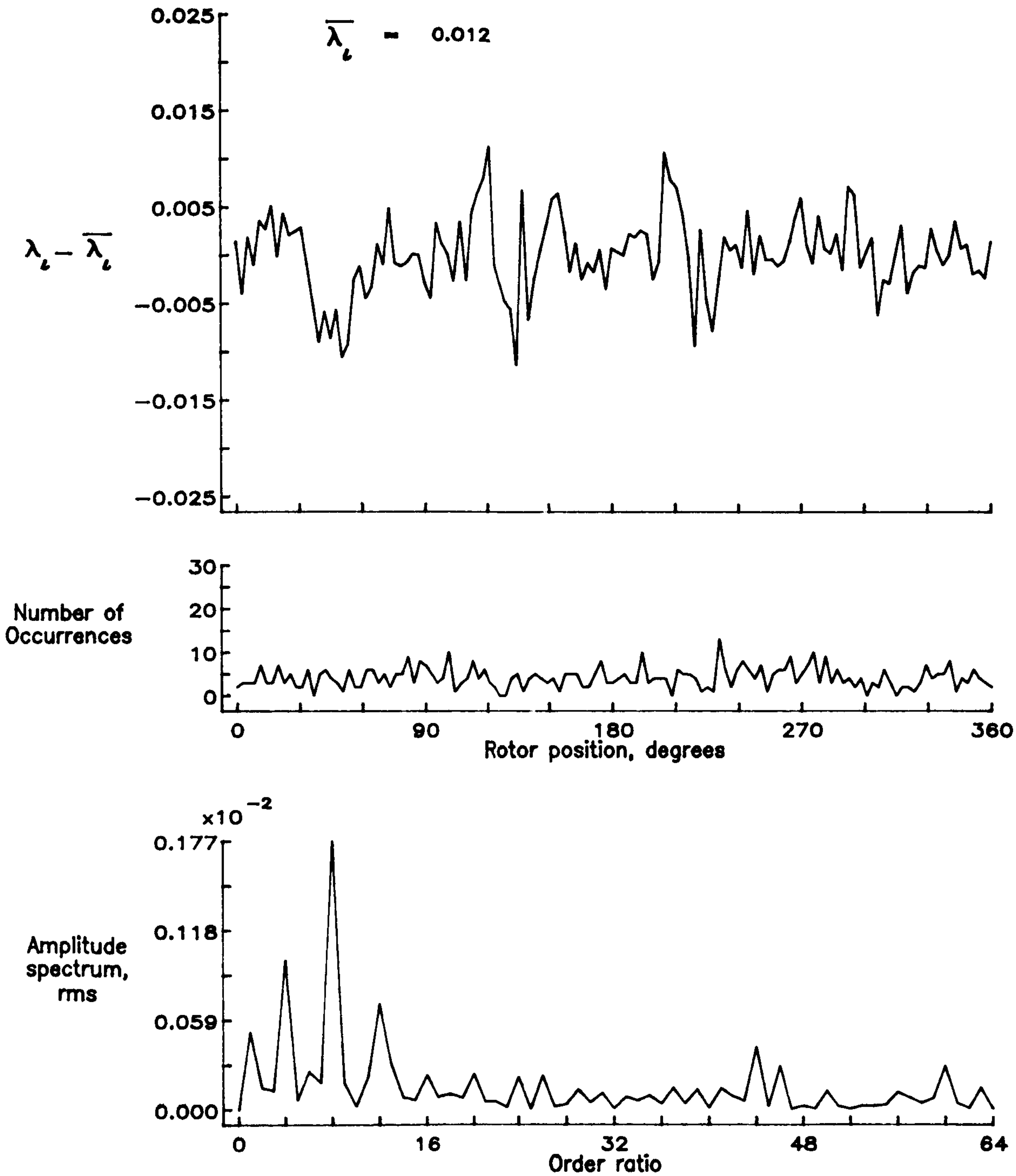

Figure 64.– Concluded.

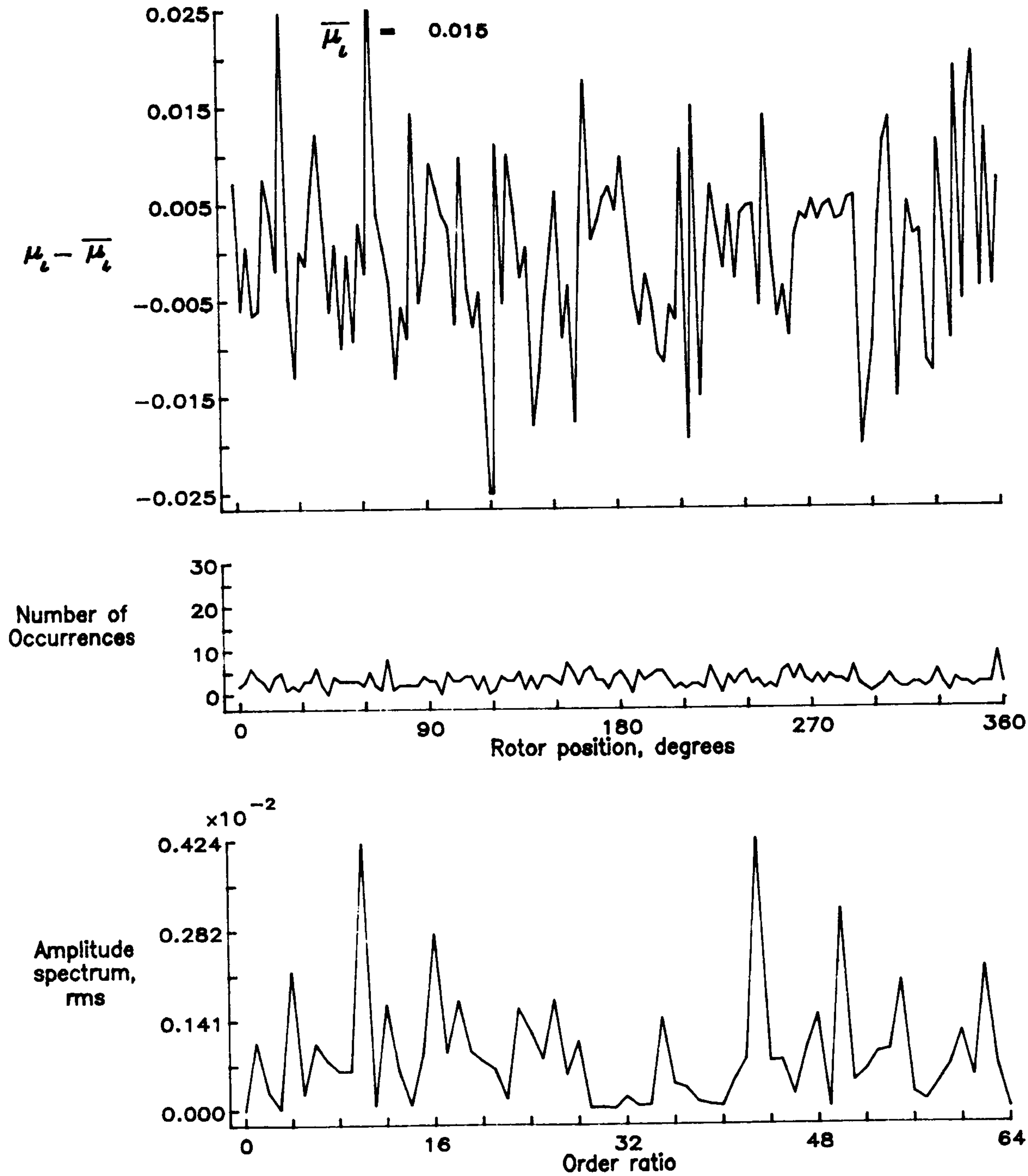

Figure 65.– Induced inflow velocity measured at 120 degrees and r/R of 0.82.

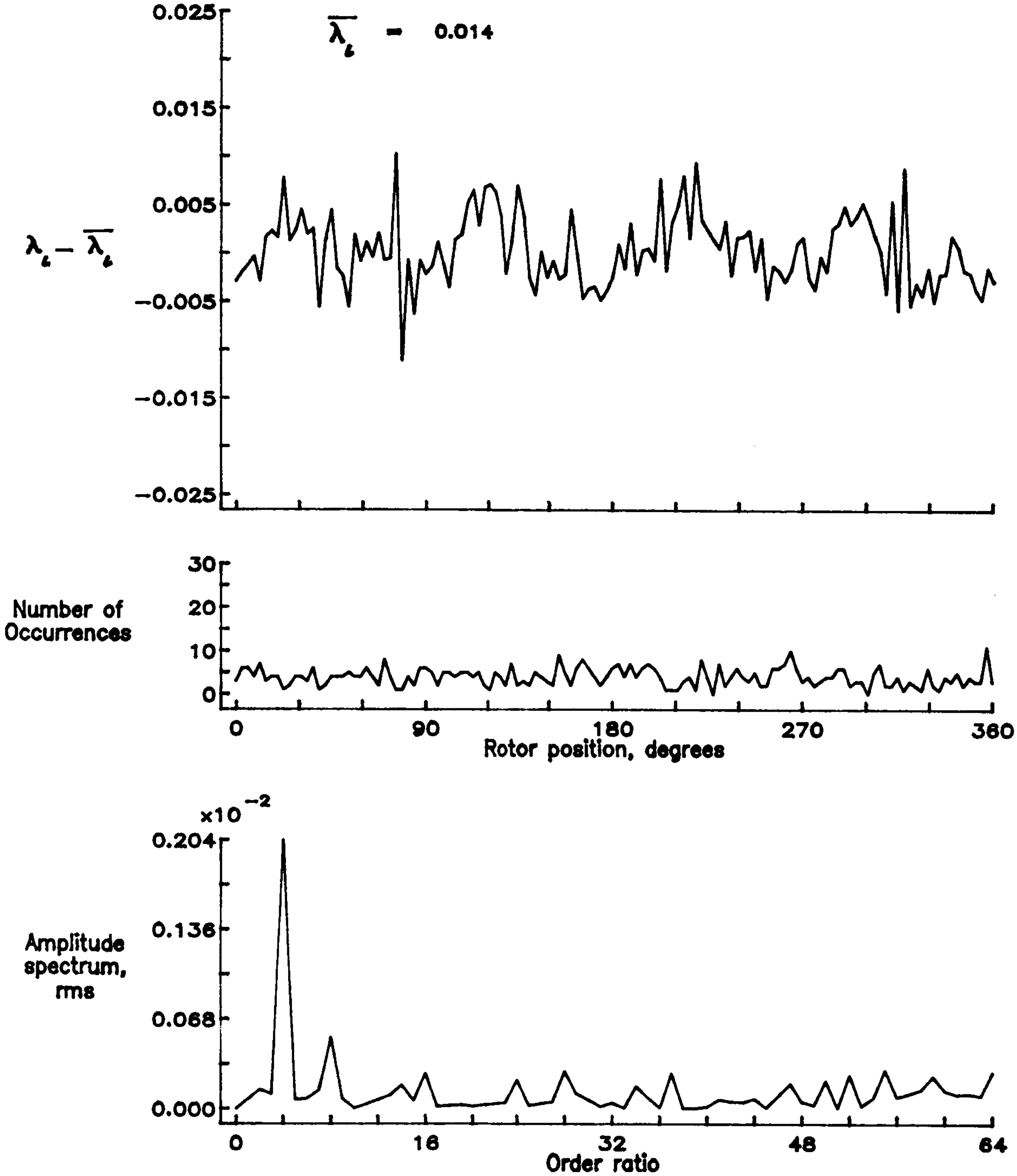

Figure 65.– Concluded.

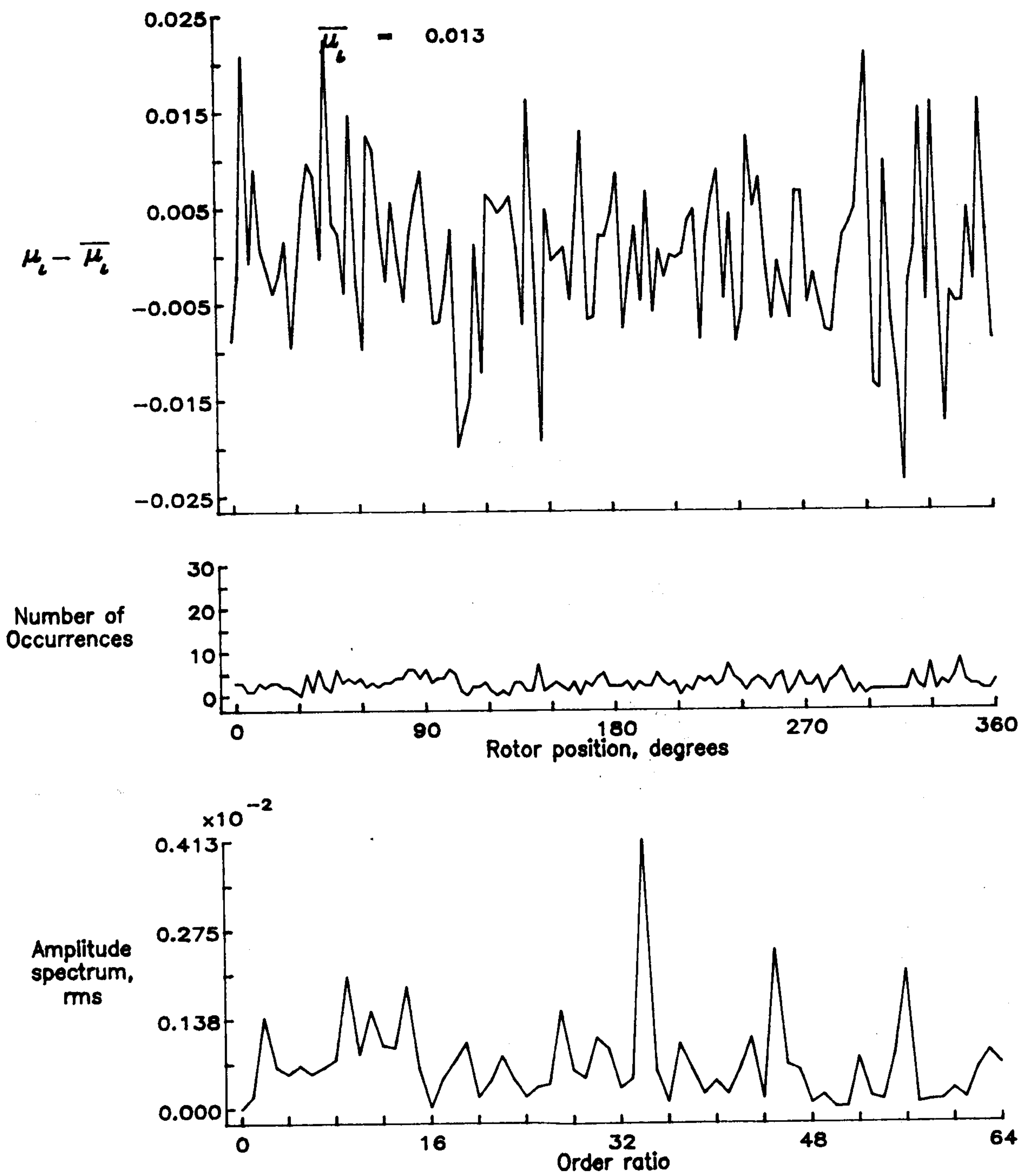

Figure 66.– Induced inflow velocity measured at 120 degrees and r/R of 0.86.

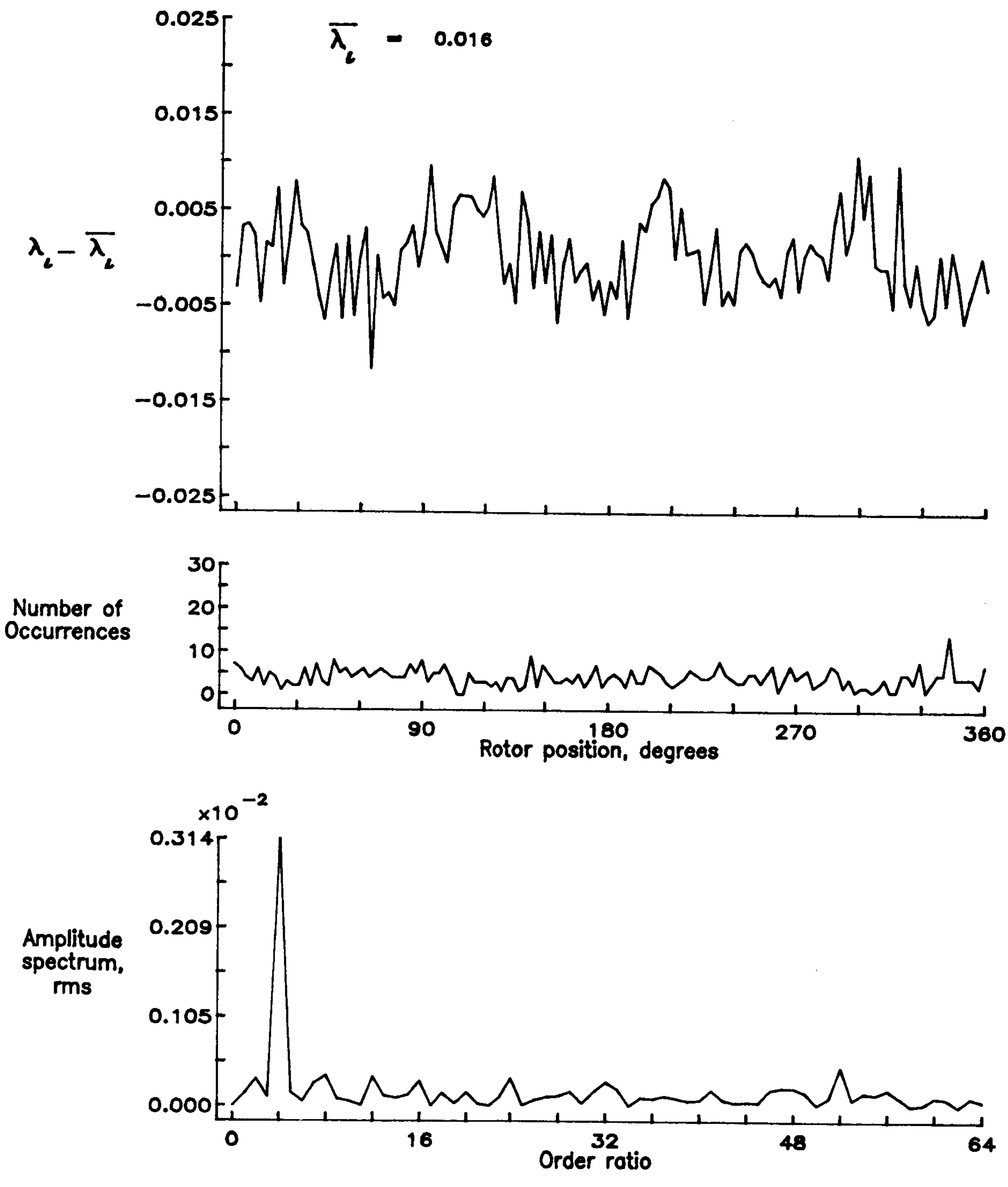

Figure 66.– Concluded.

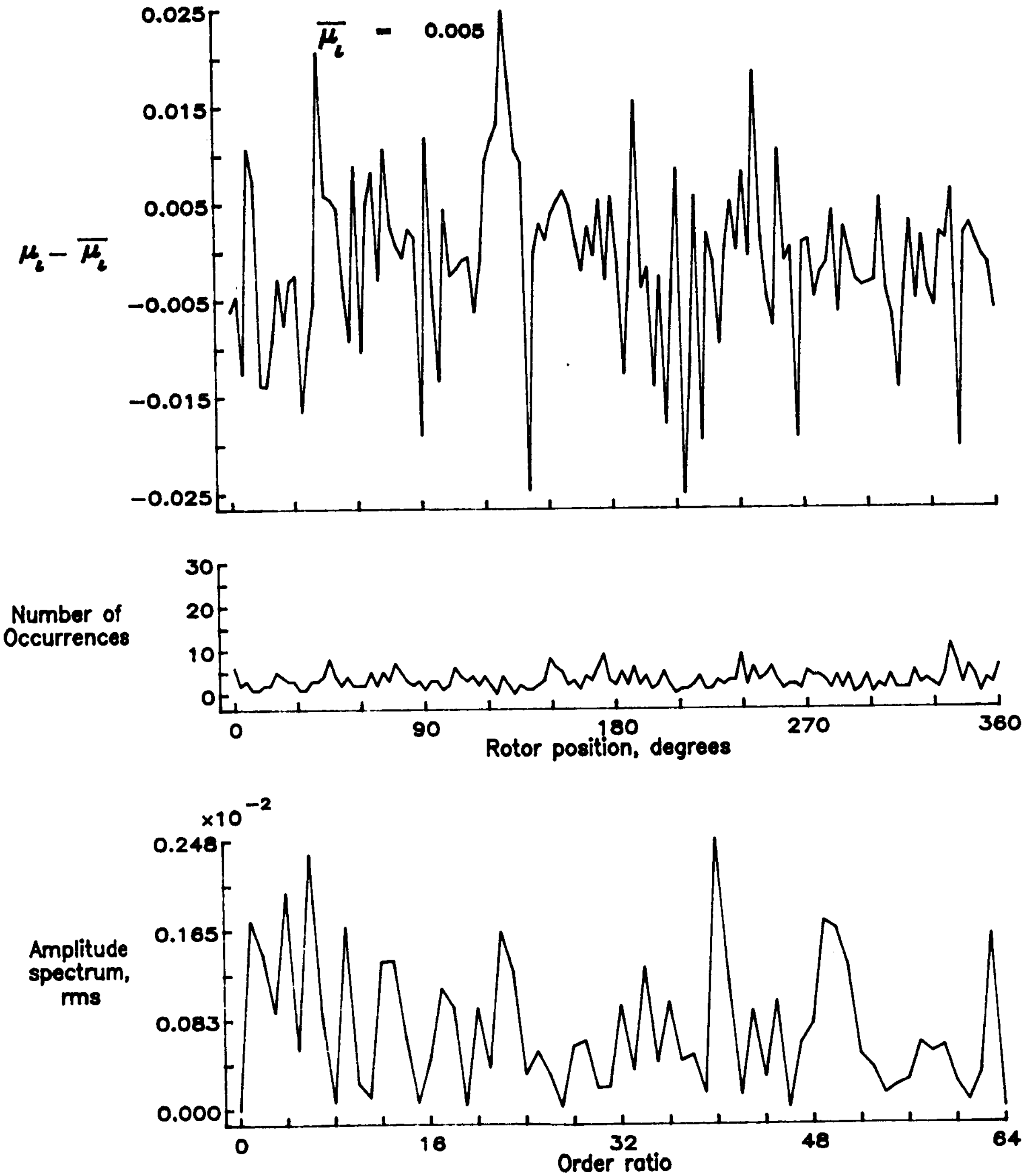

Figure 67.— Induced inflow velocity measured at 120 degrees and r/R of 0.90.

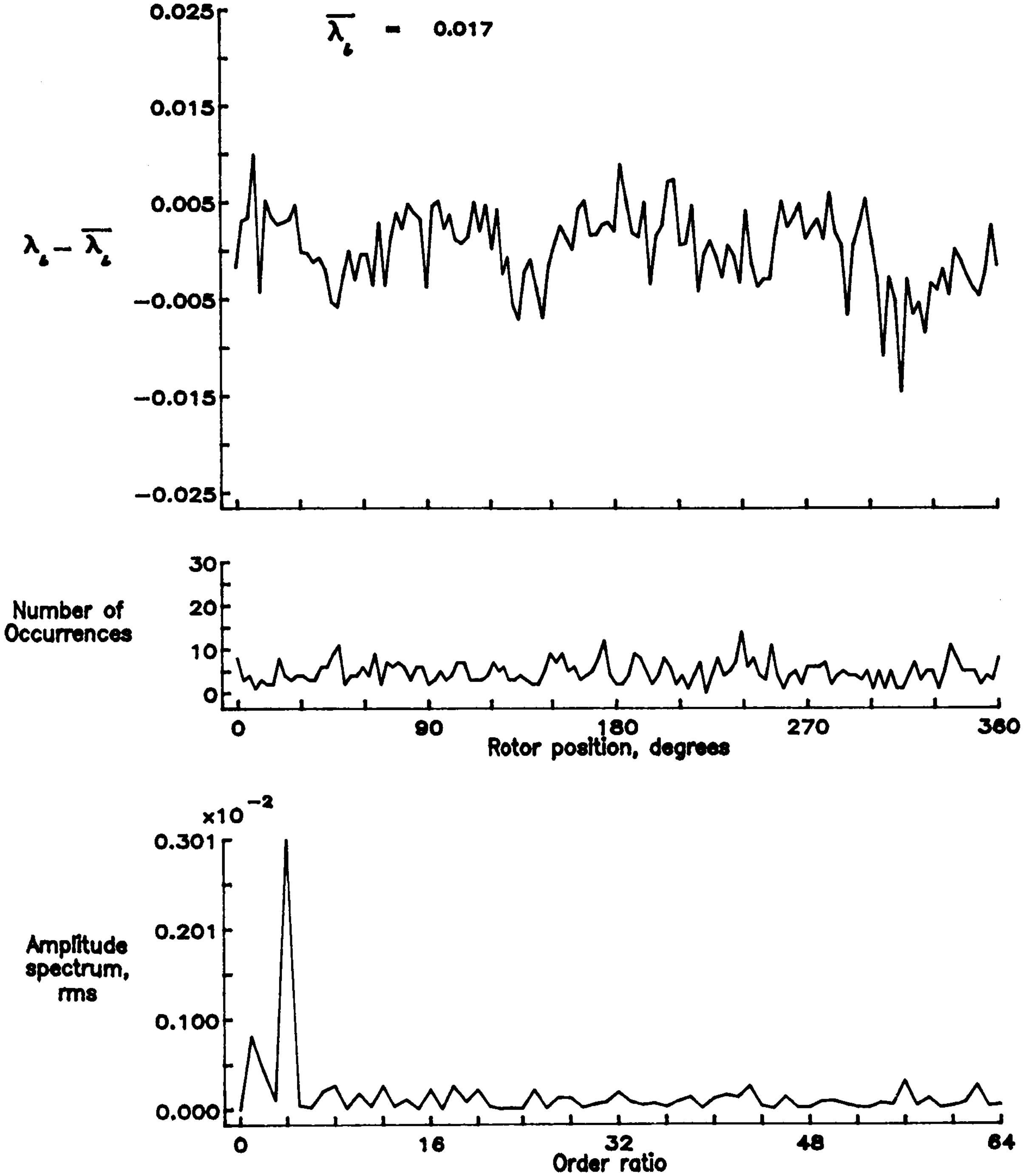

Figure 67.- Concluded.

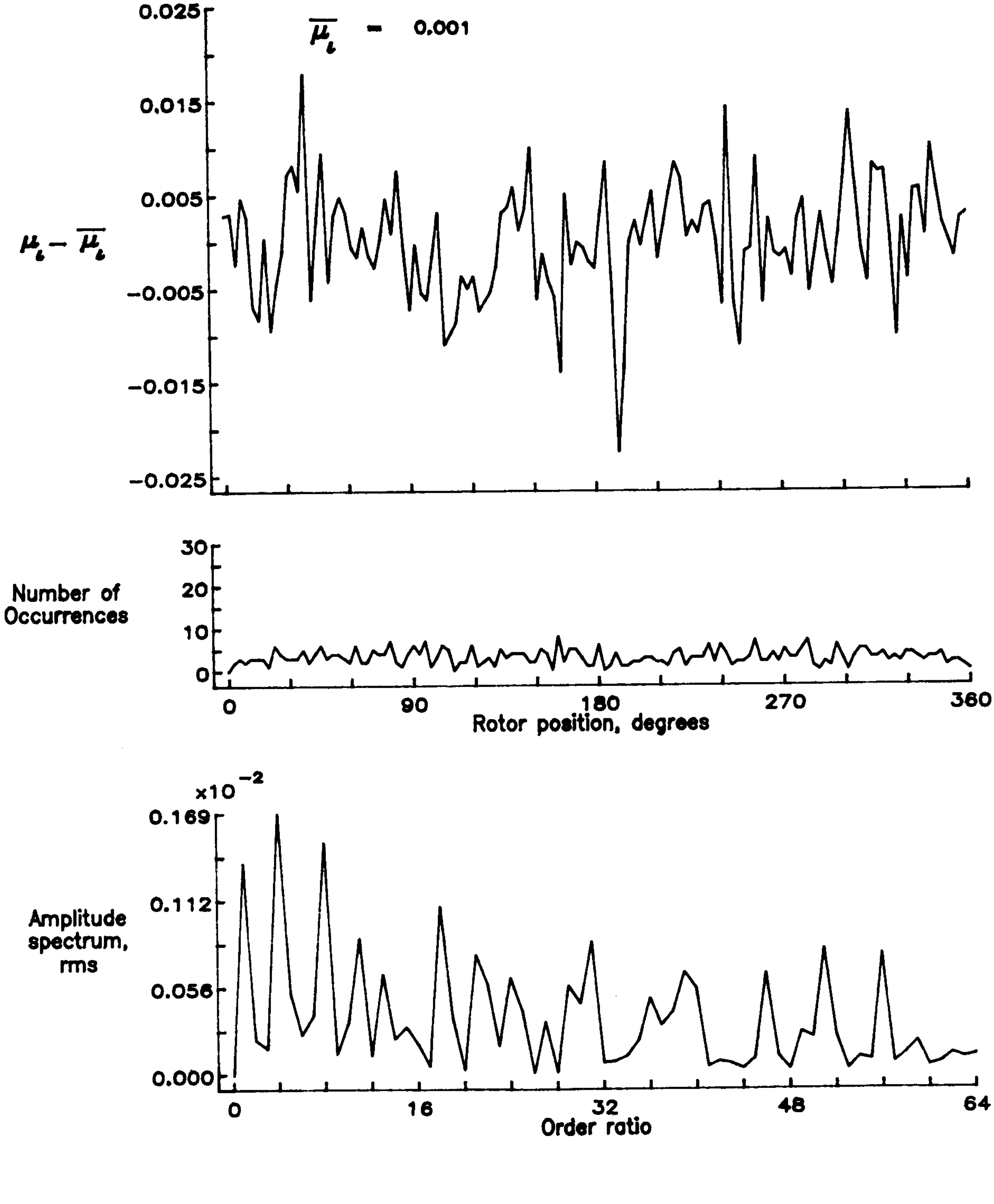

Figure 68.– Induced inflow velocity measured at 120 degrees and r/R of 0.94.

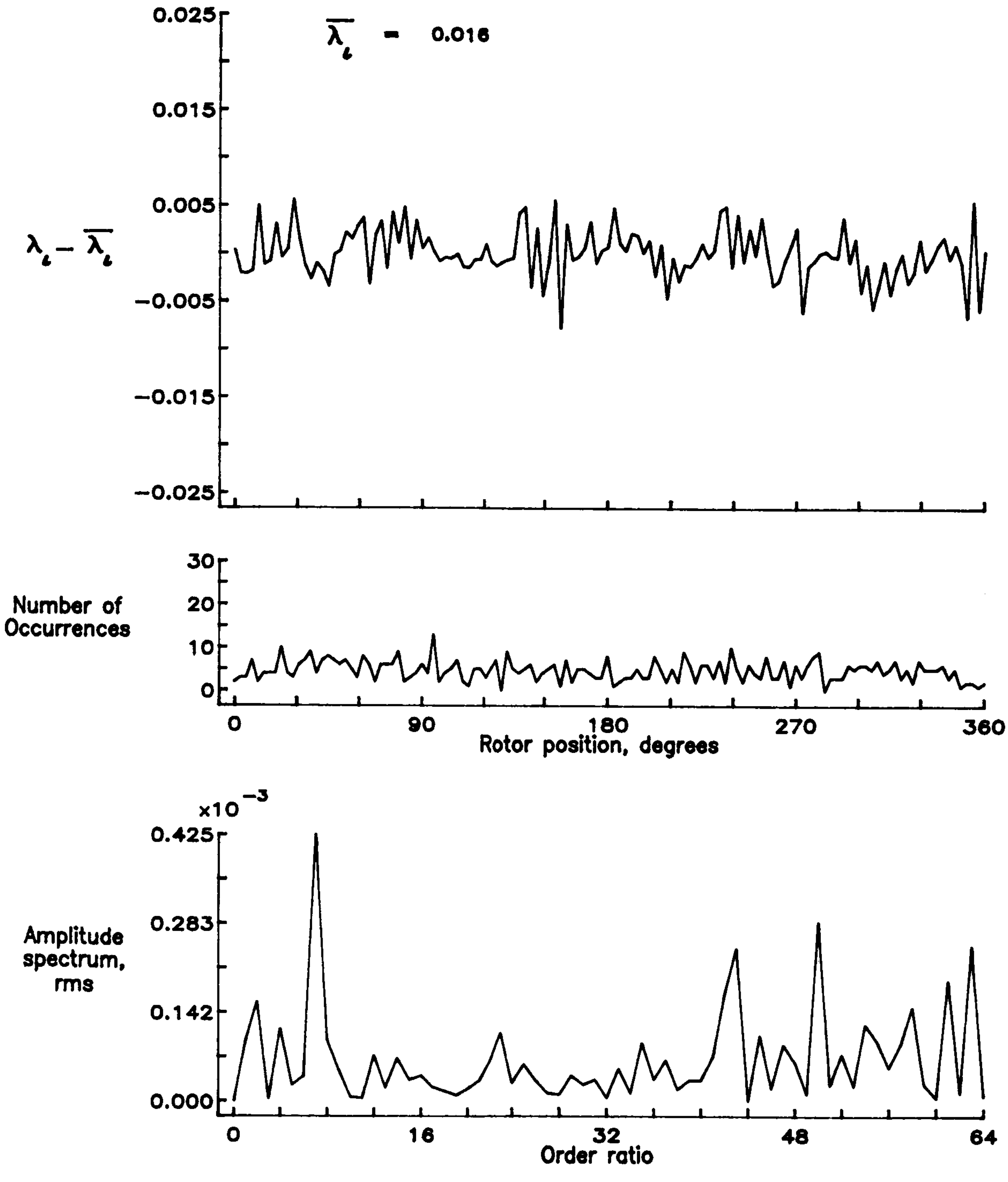

Figure 68.– Concluded.

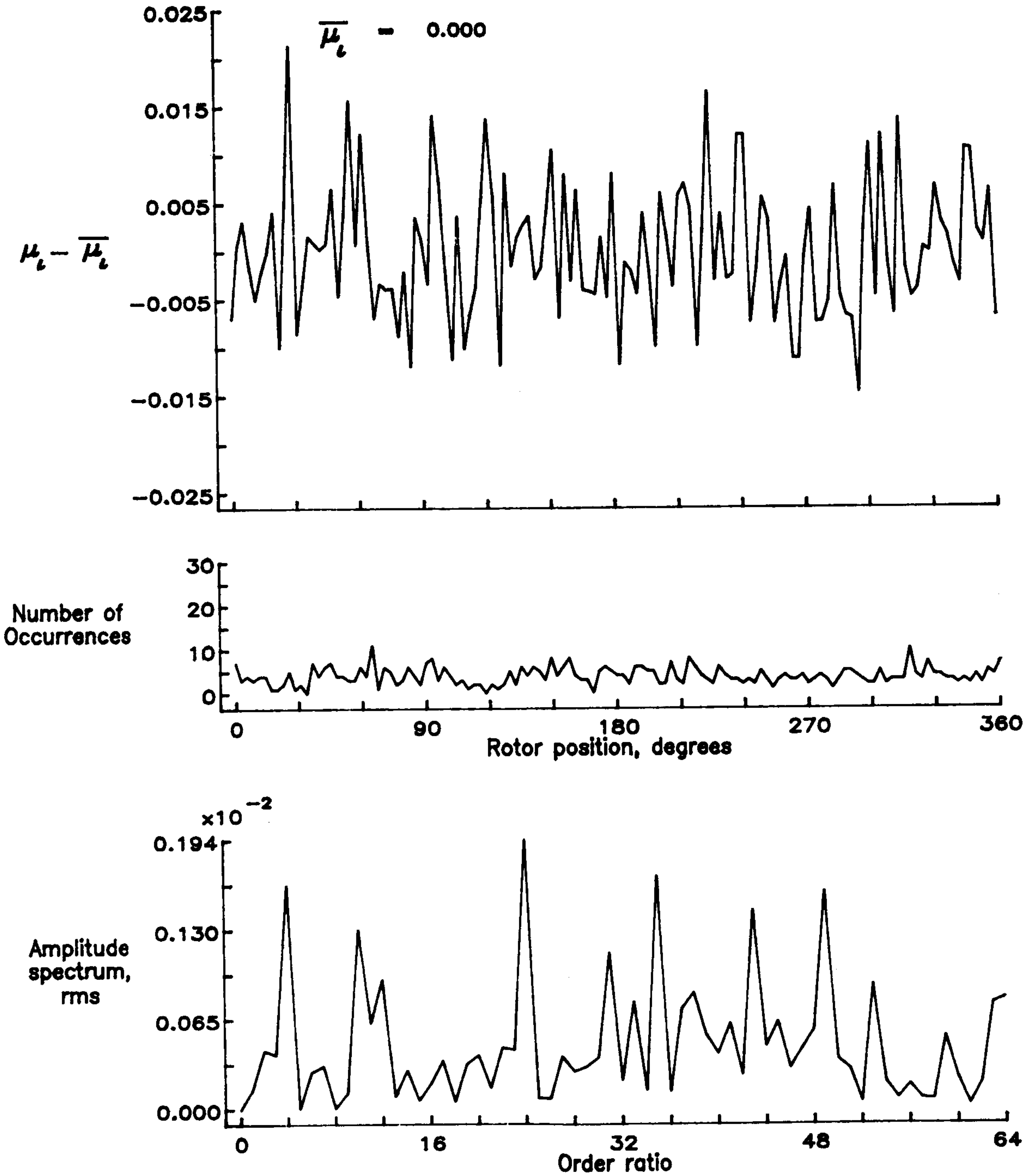

Figure 69.– Induced inflow velocity measured at 120 degrees and r/R of 0.98.

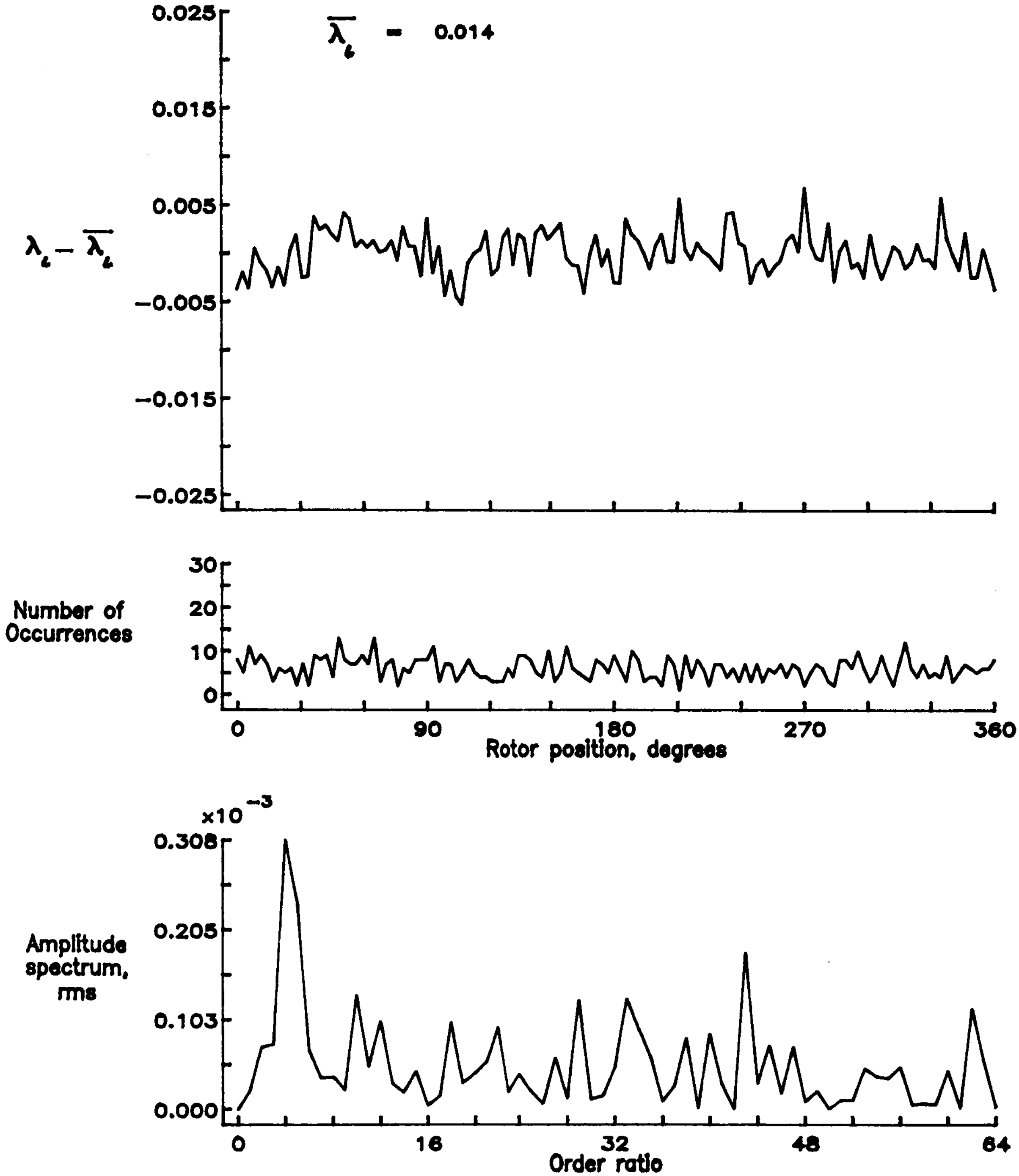

Figure 69.– Concluded.

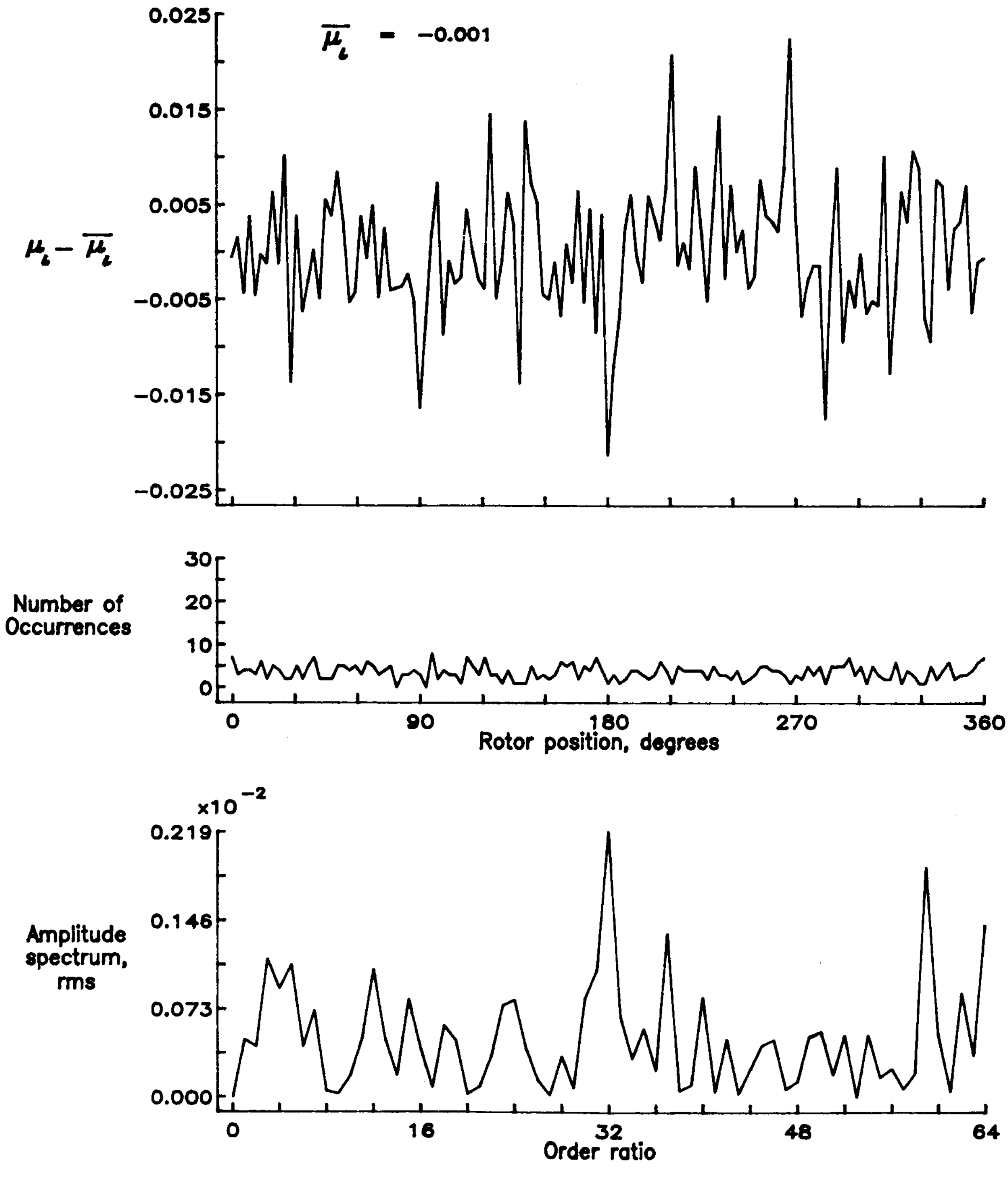

Figure 70.– Induced inflow velocity measured at 120 degrees and r/R of 1.04.

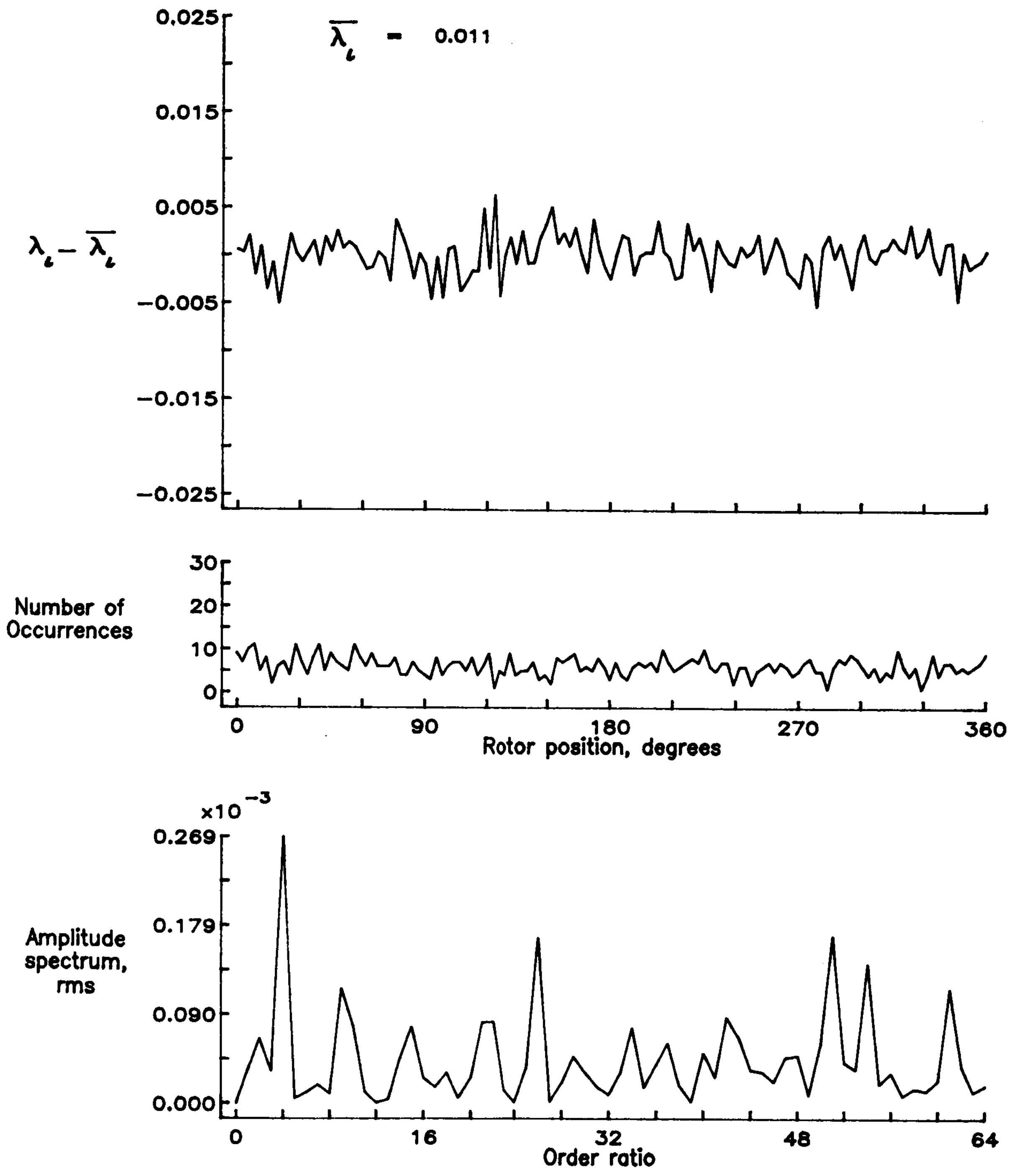

Figure 70.– Concluded.

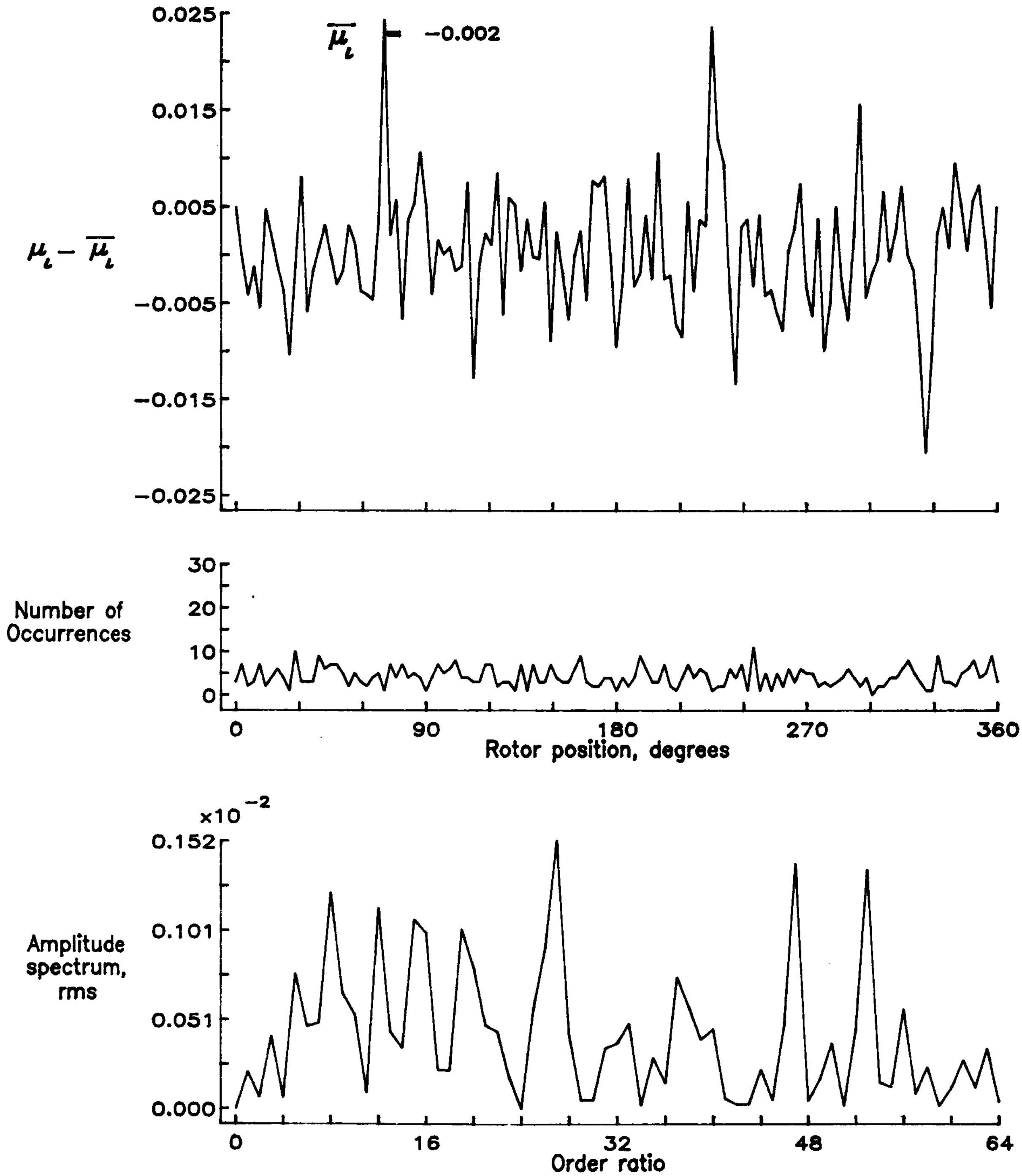

Figure 71.– Induced inflow velocity measured at 120 degrees and r/R of 1.10.

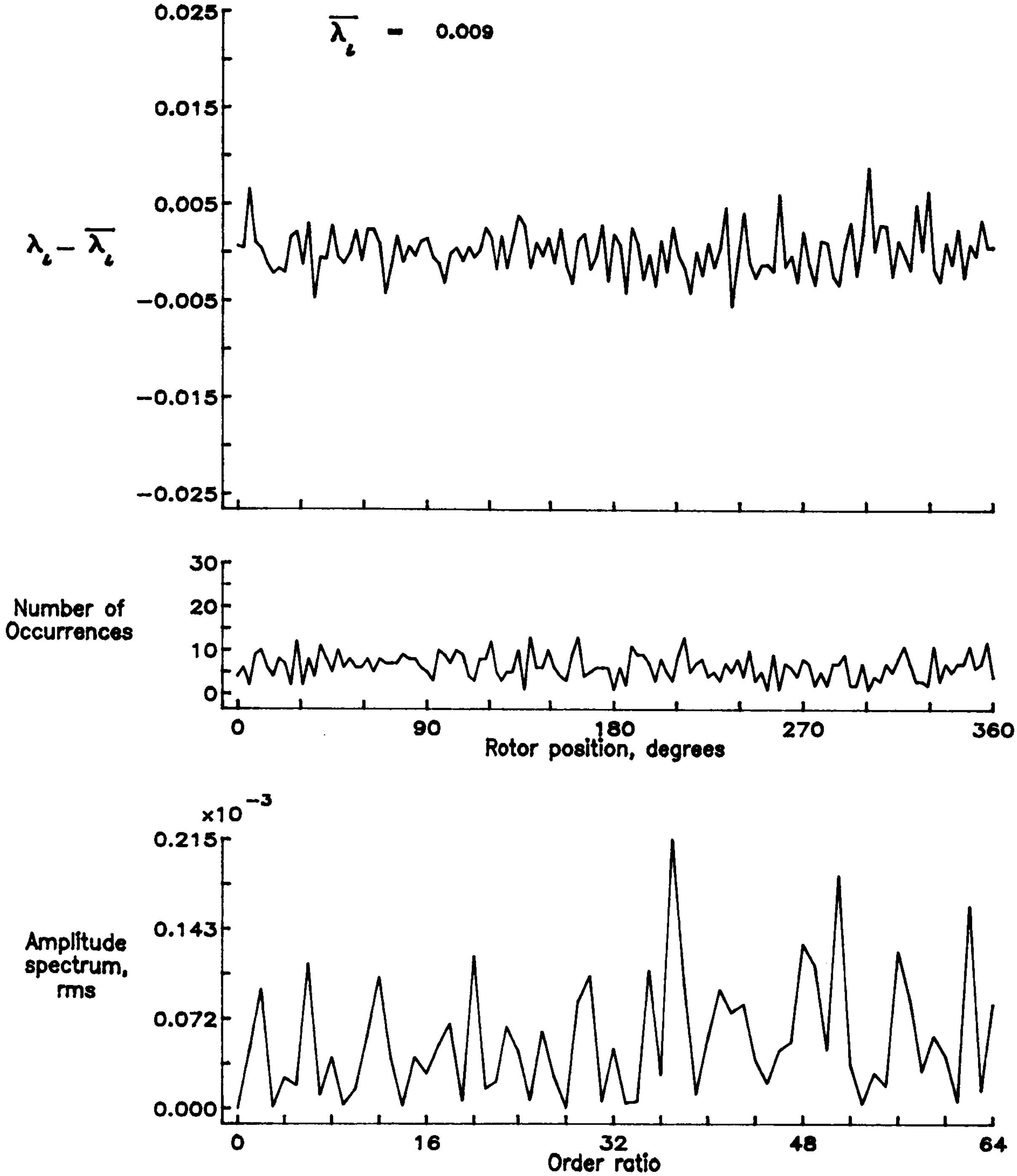

Figure 71.– Concluded.

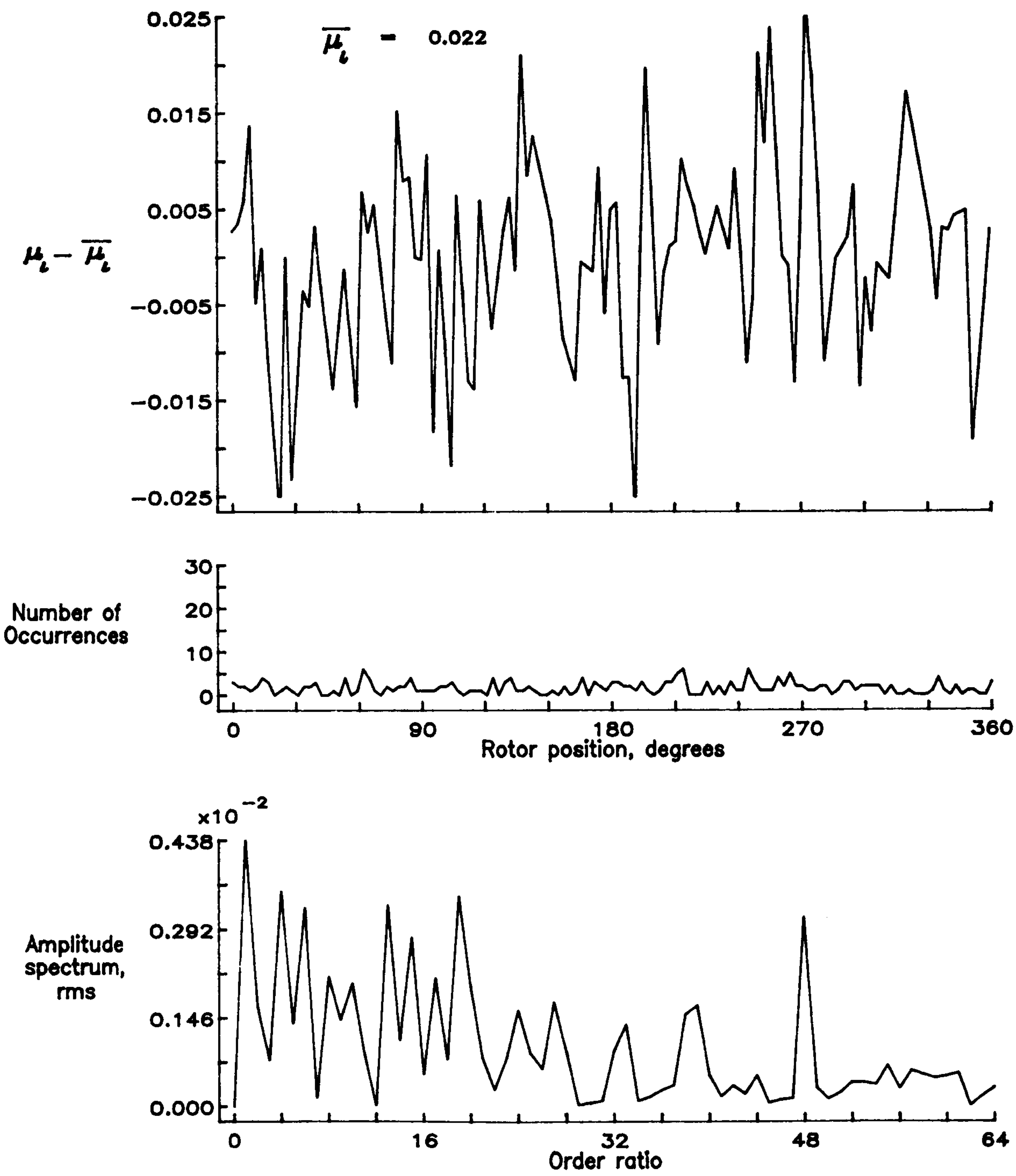

Figure 72.– Induced inflow velocity measured at 150 degrees and r/R of 0.40.

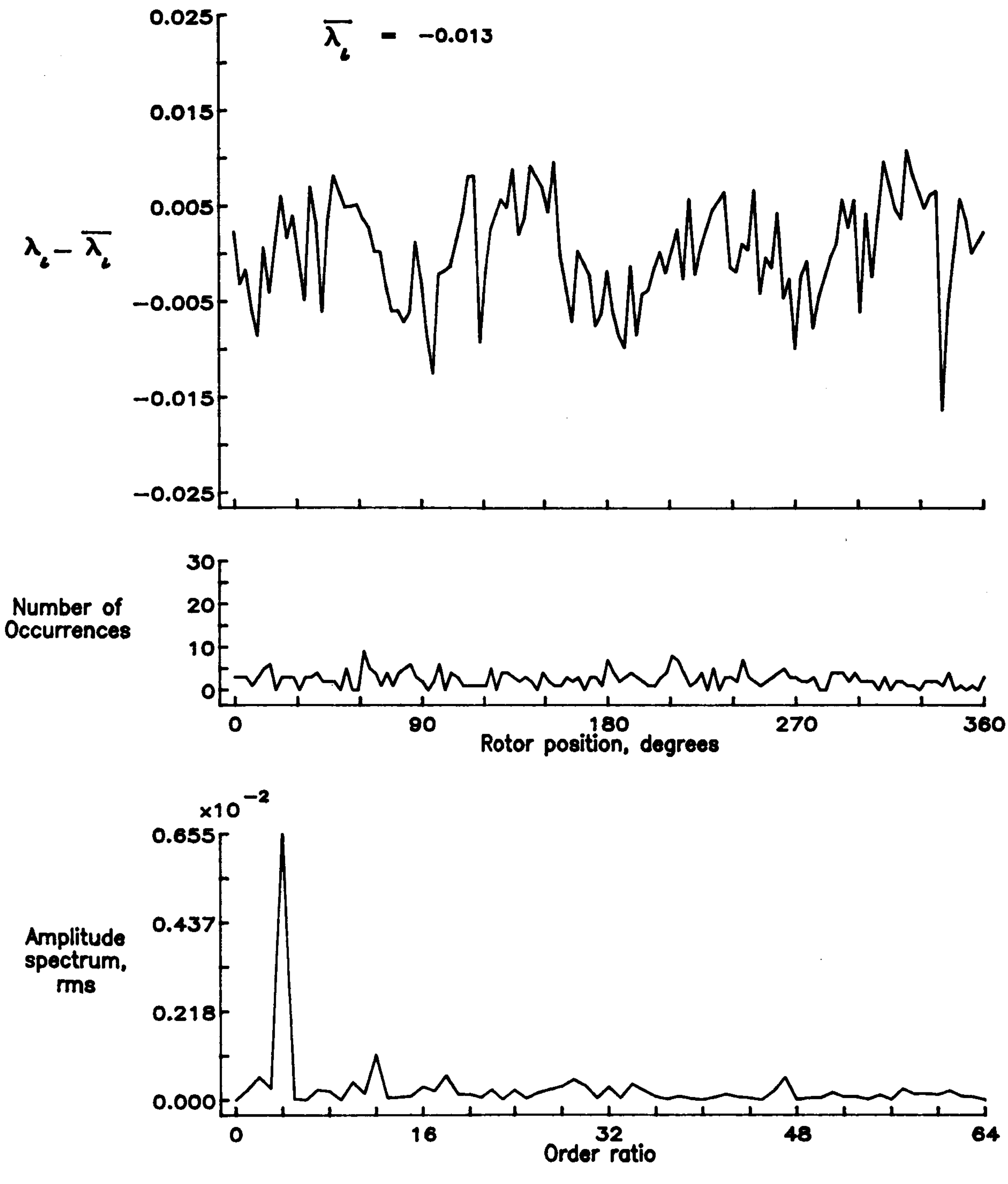

Figure 72.– Concluded.

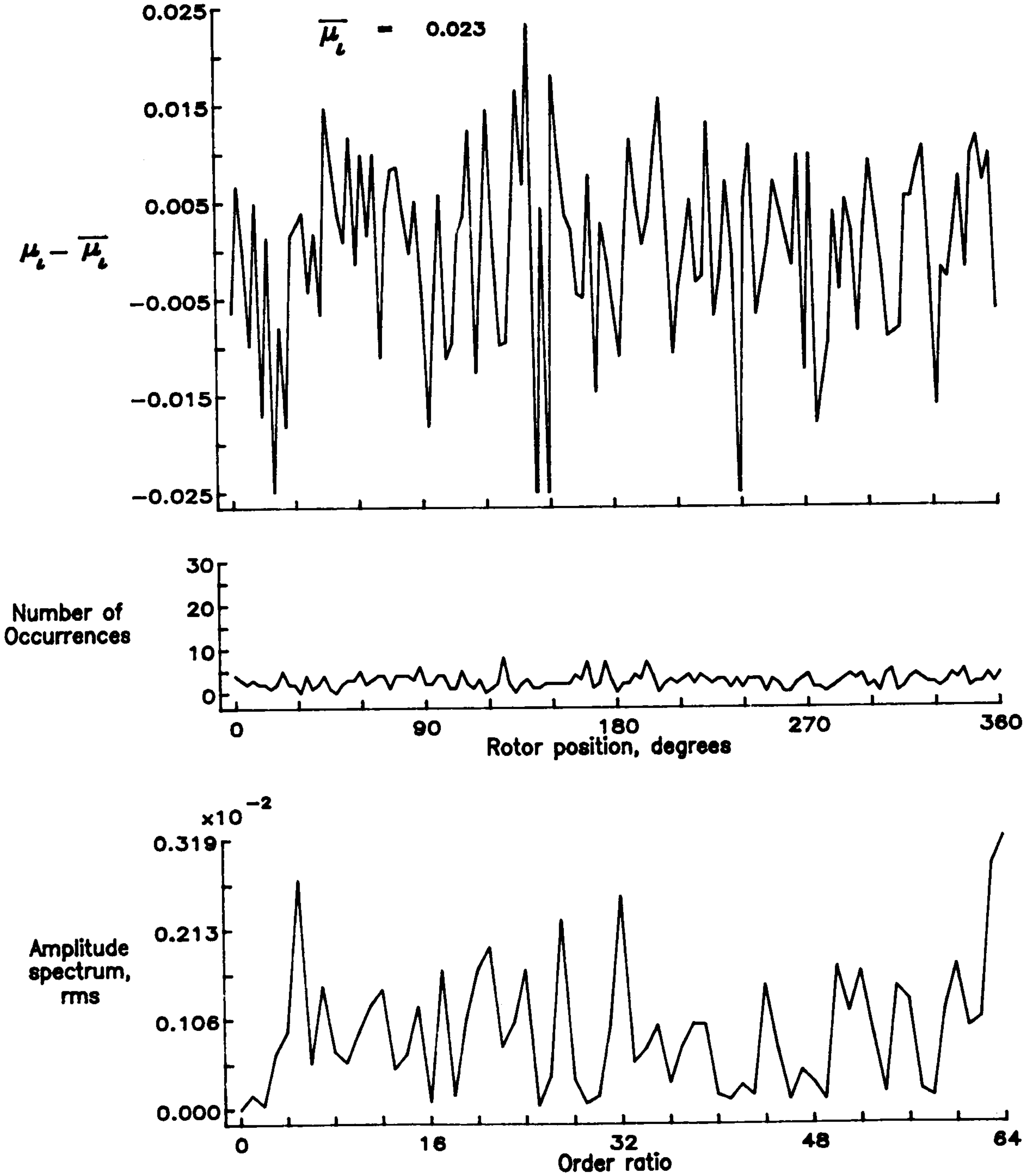

Figure 73.– Induced inflow velocity measured at 150 degrees and r/R of 0.50.

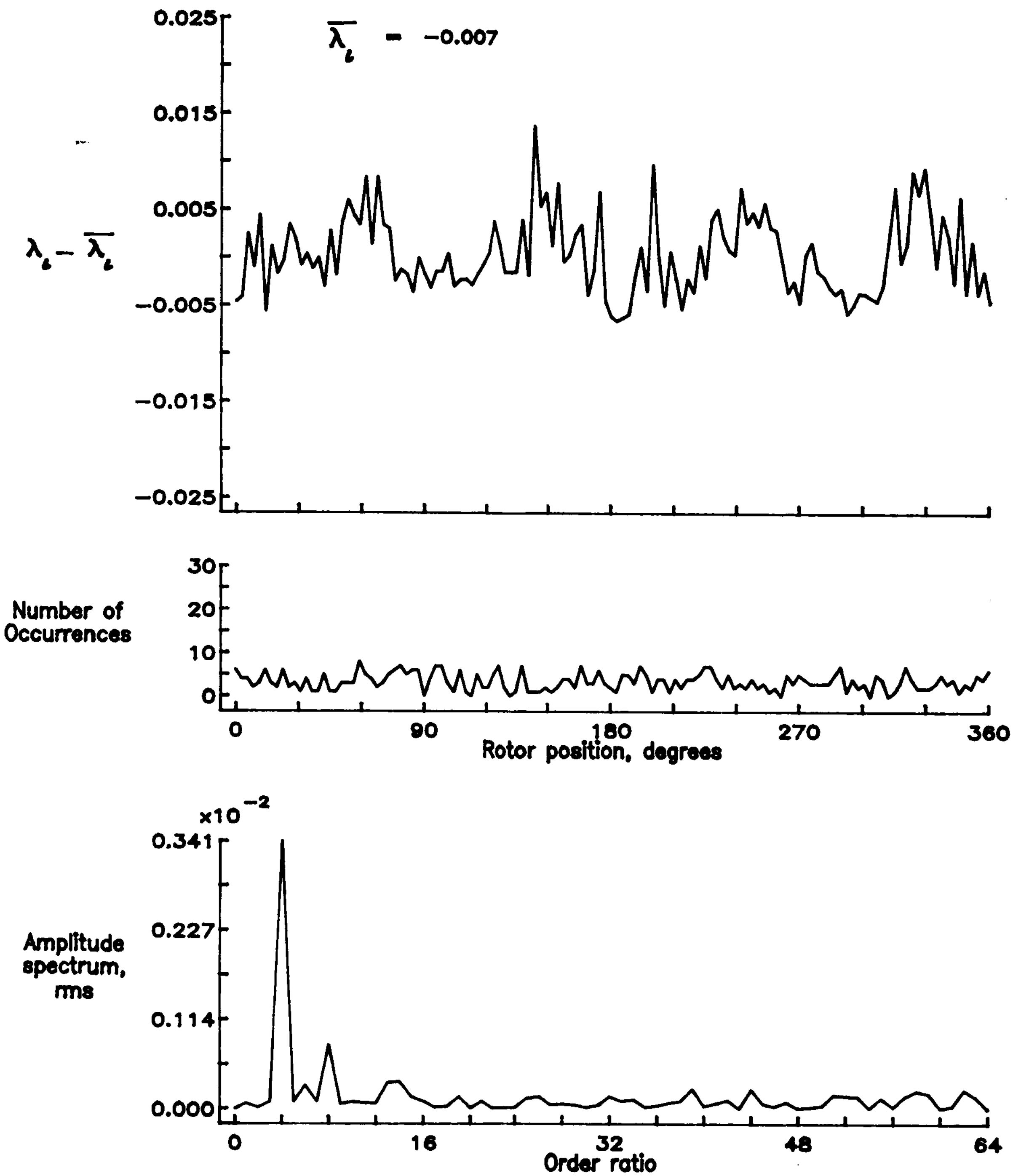

Figure 73.– Concluded.

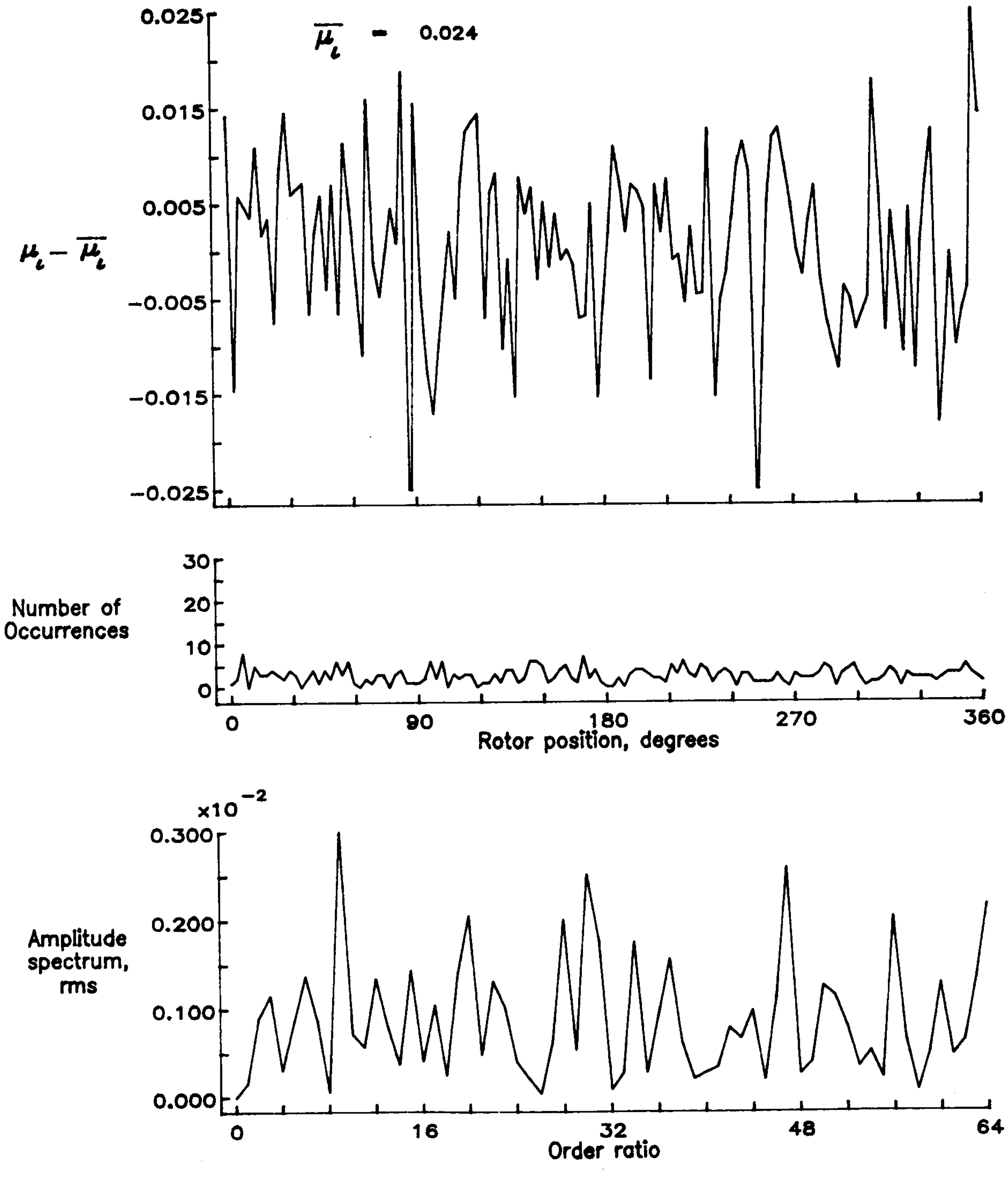

Figure 74.– Induced inflow velocity measured at 150 degrees and r/R of 0.60.

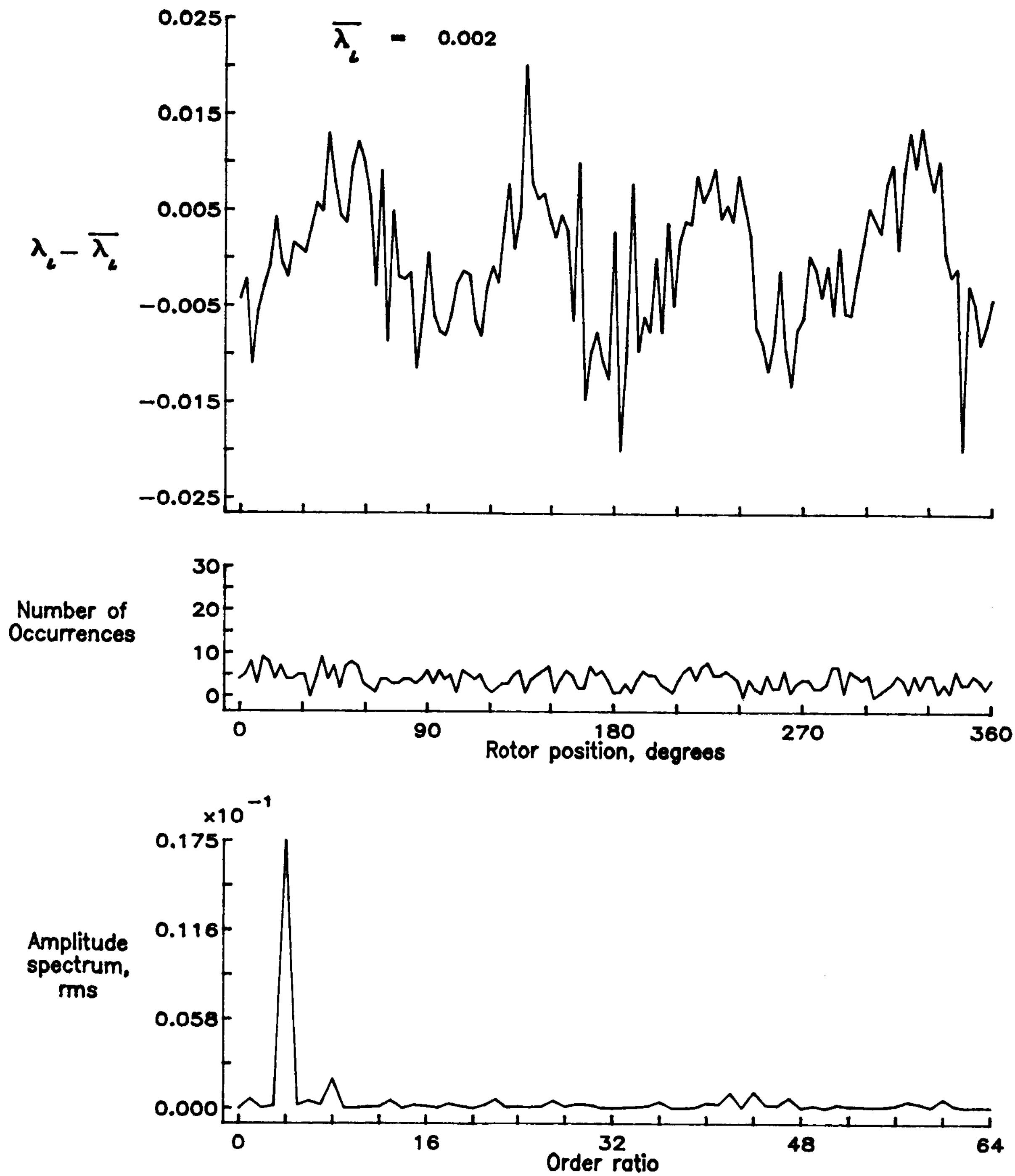

Figure 74.– Concluded.

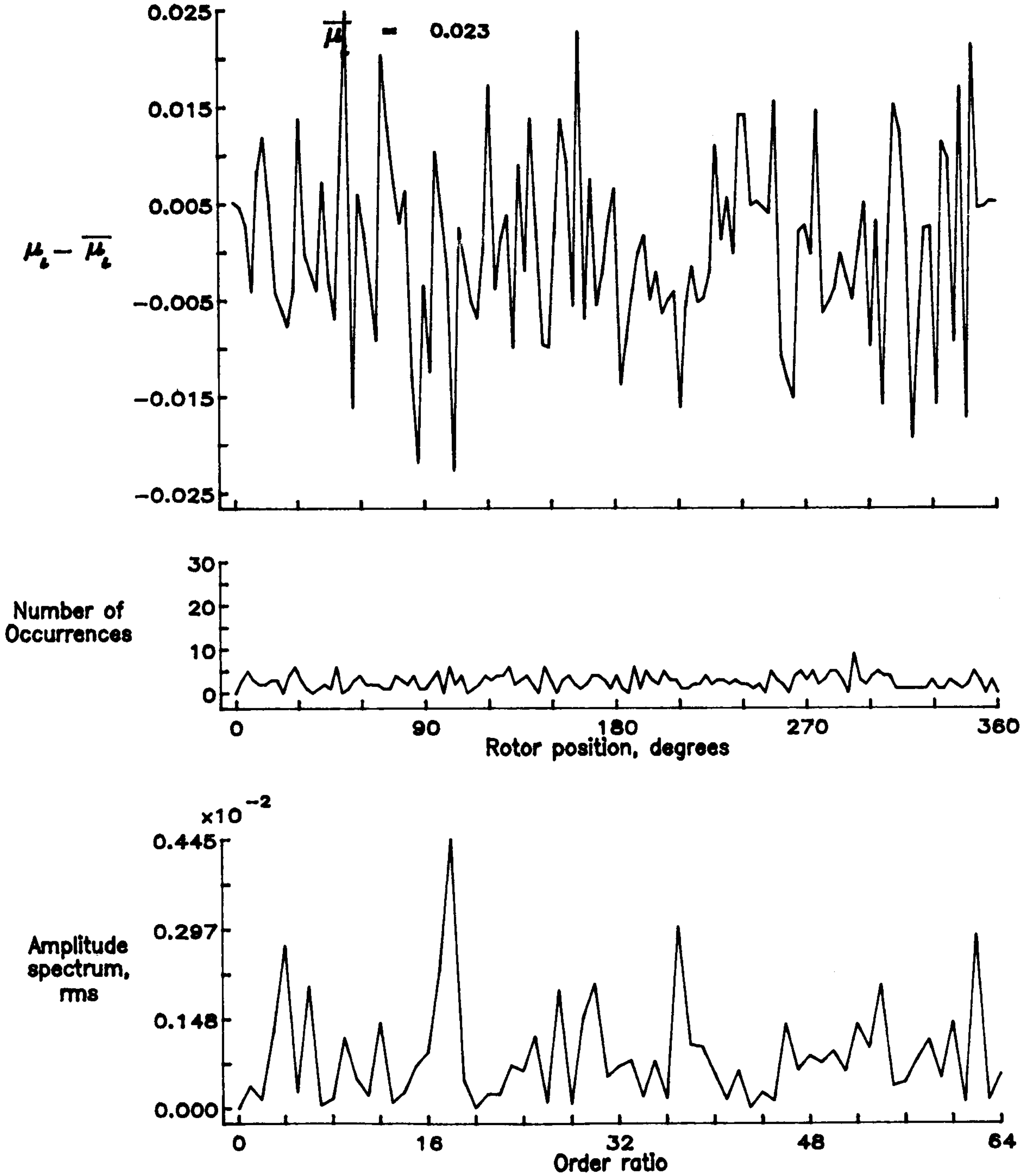

Figure 75.– Induced inflow velocity measured at 150 degrees and r/R of 0.70.

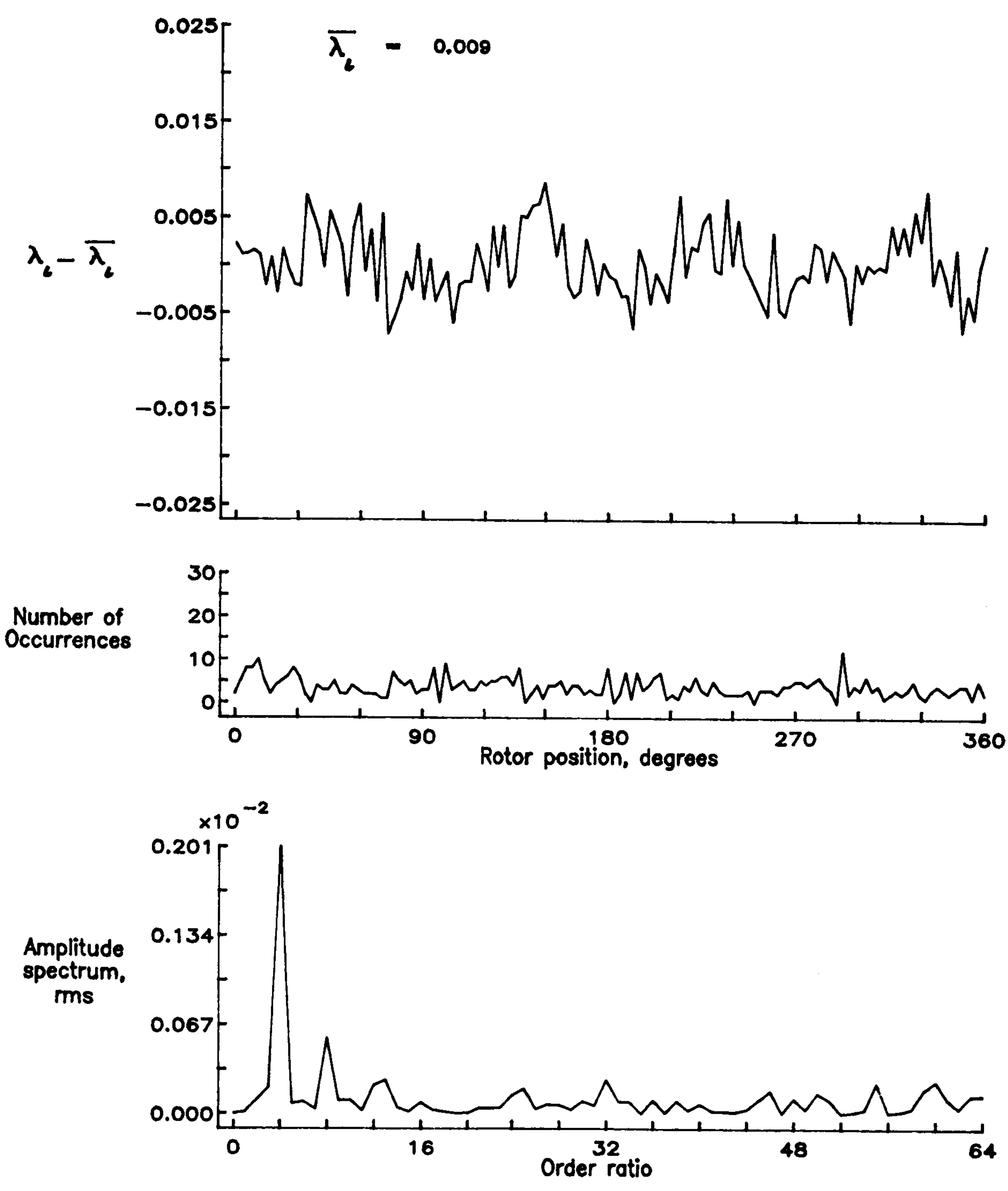

Figure 75.– Concluded.

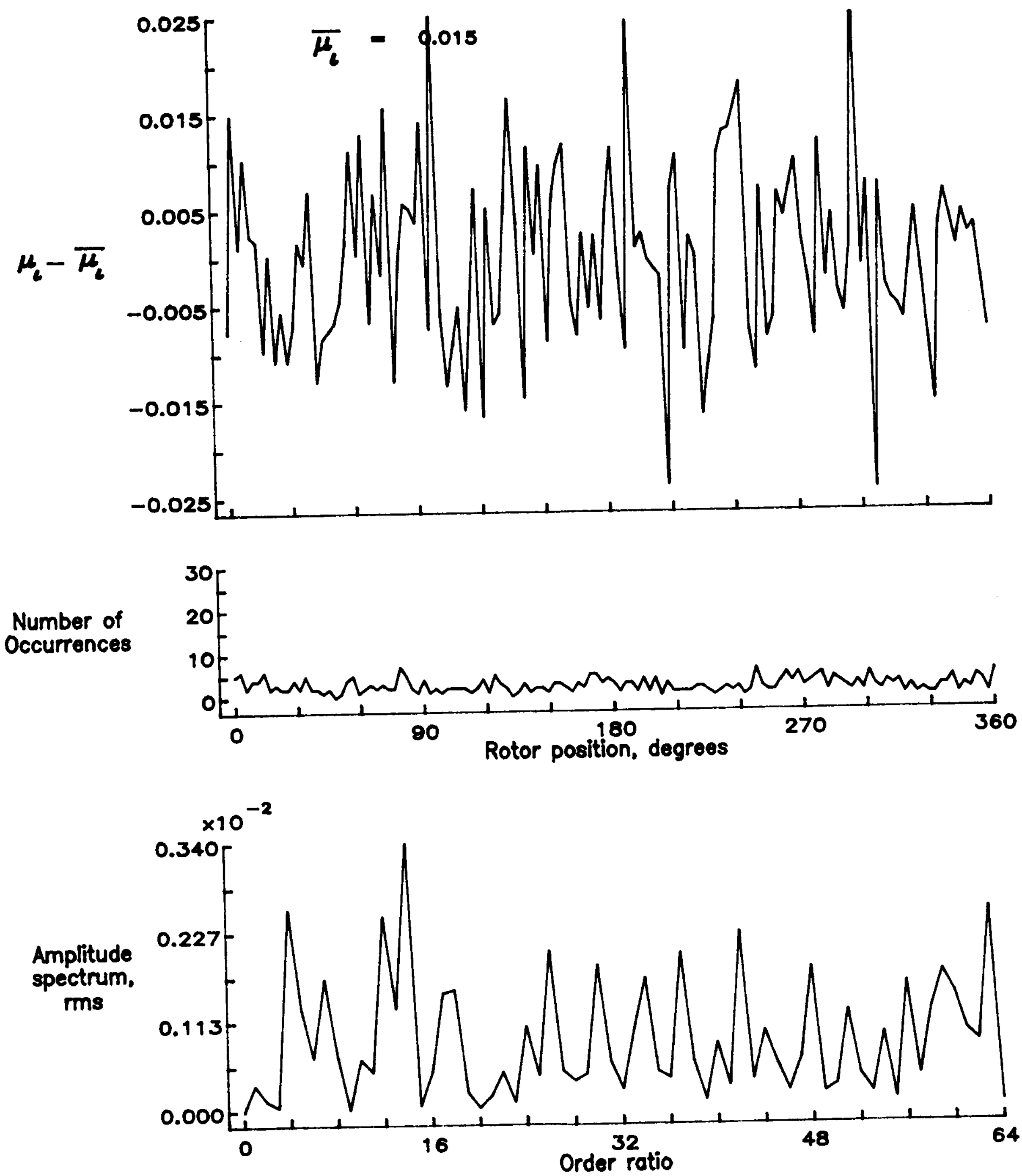

Figure 76.– Induced inflow velocity measured at 150 degrees and r/R of 0.74.

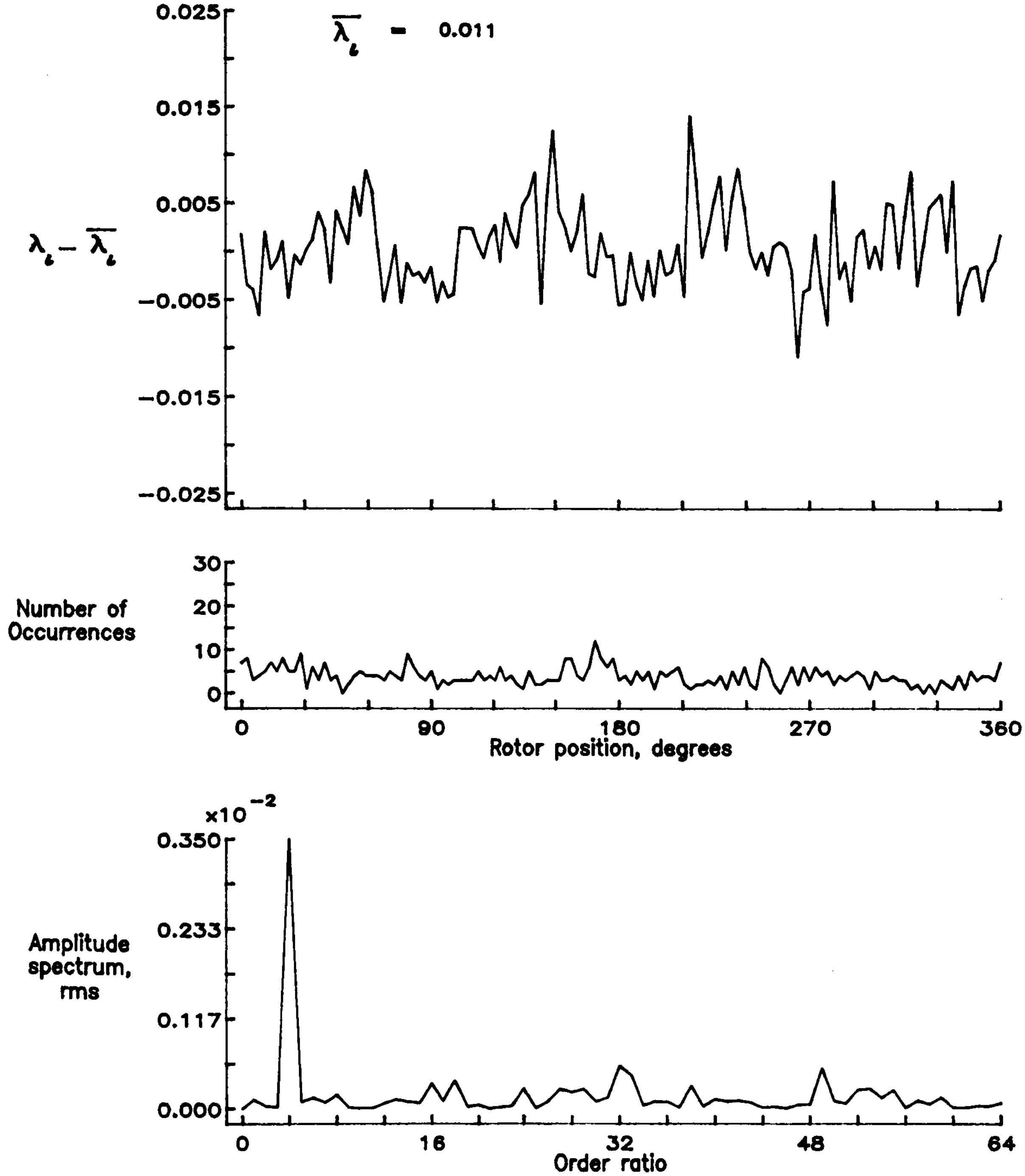

Figure 76.– Concluded.

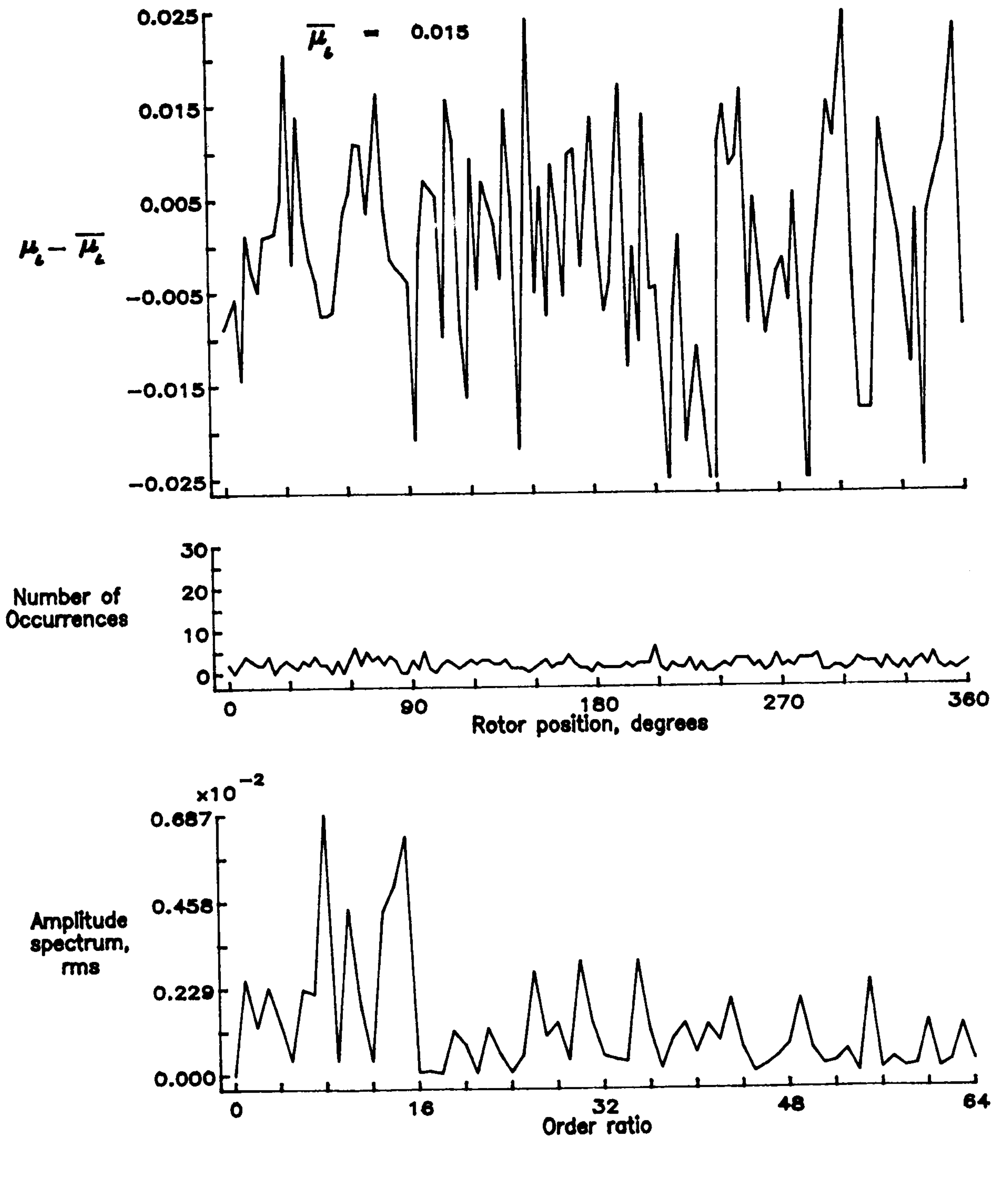

Figure 77.– Induced inflow velocity measured at 150 degrees and r/R of 0.78.

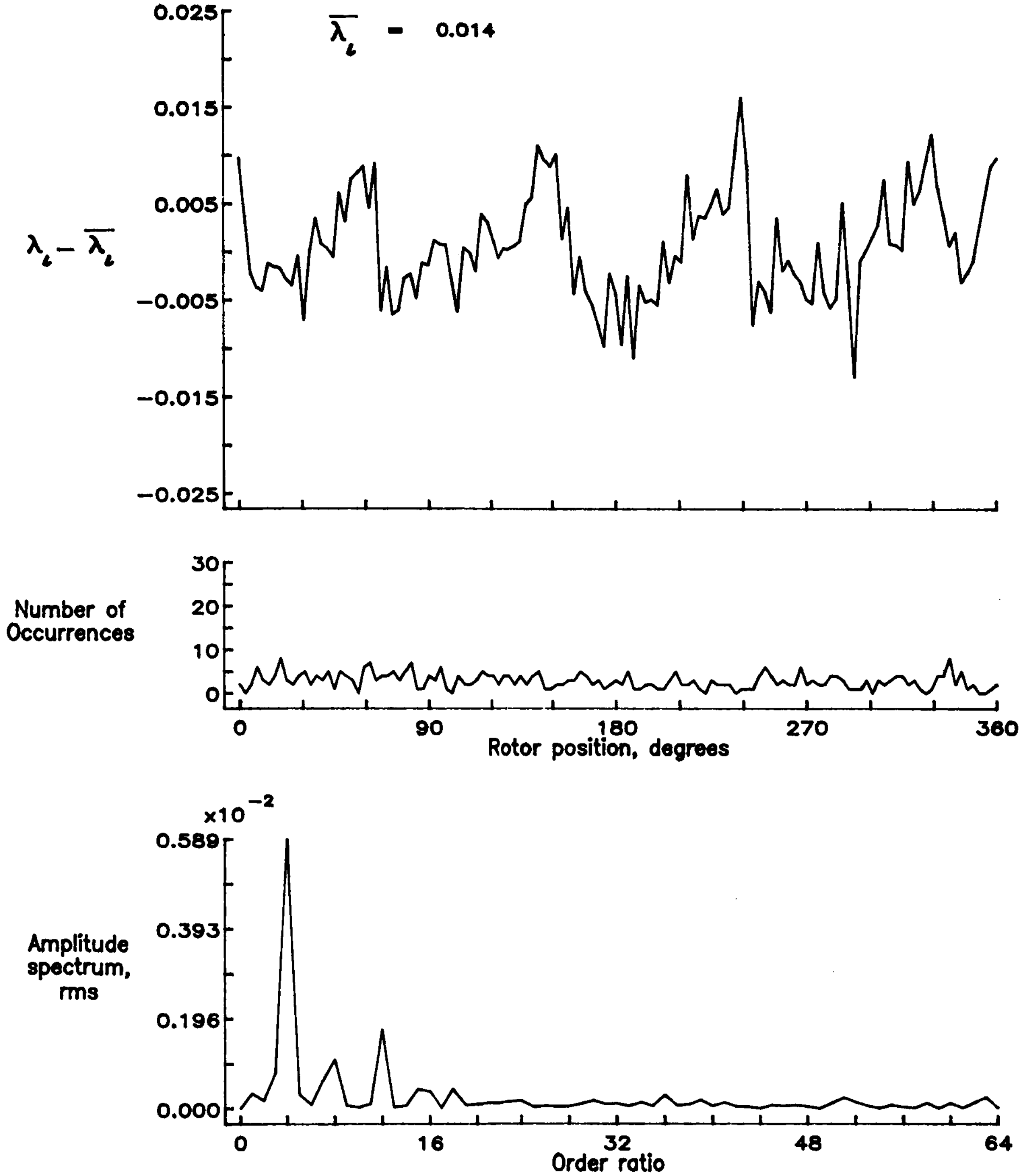

Figure 77.– Concluded.

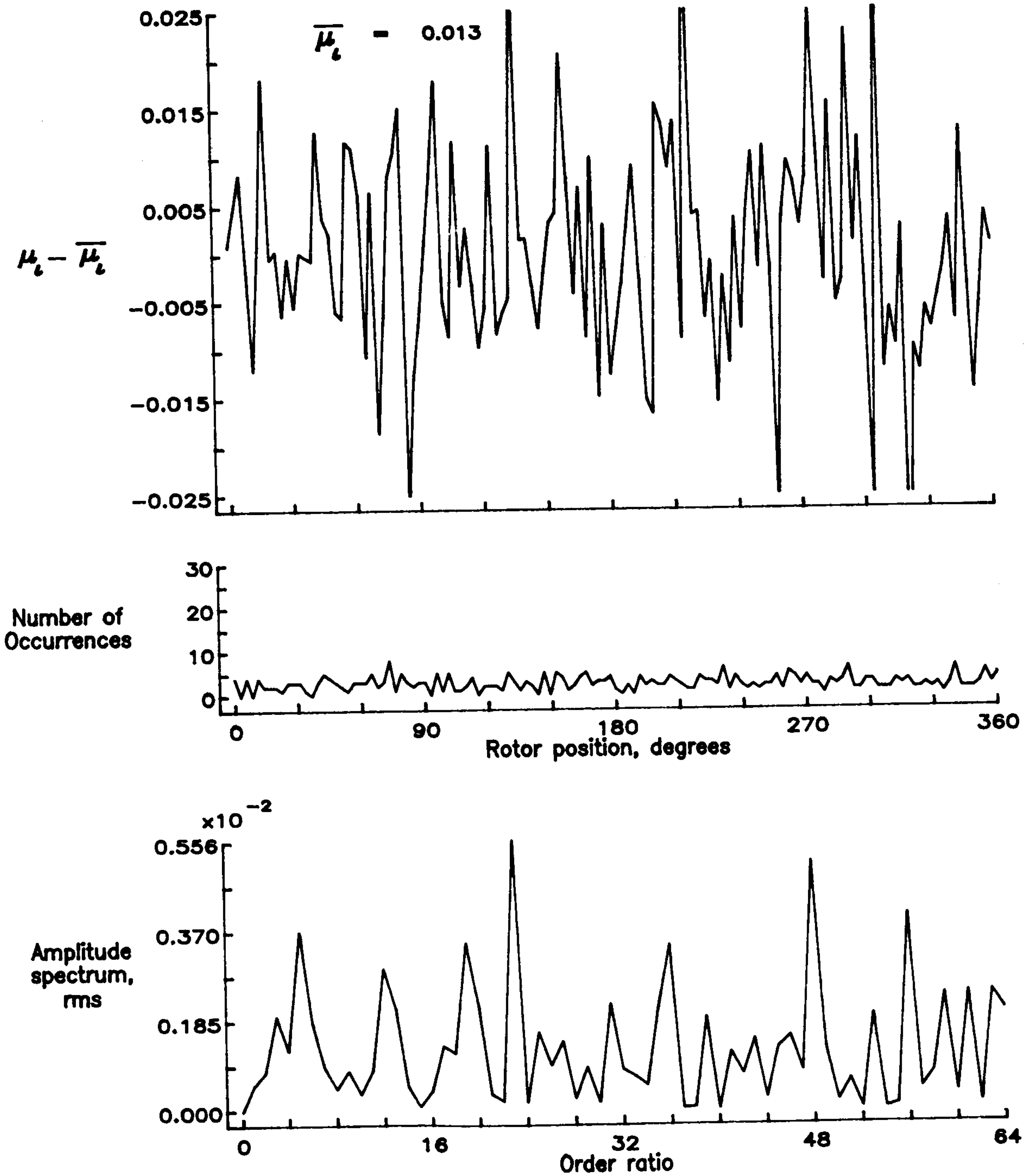

Figure 78.– Induced inflow velocity measured at 150 degrees and r/R of 0.82.

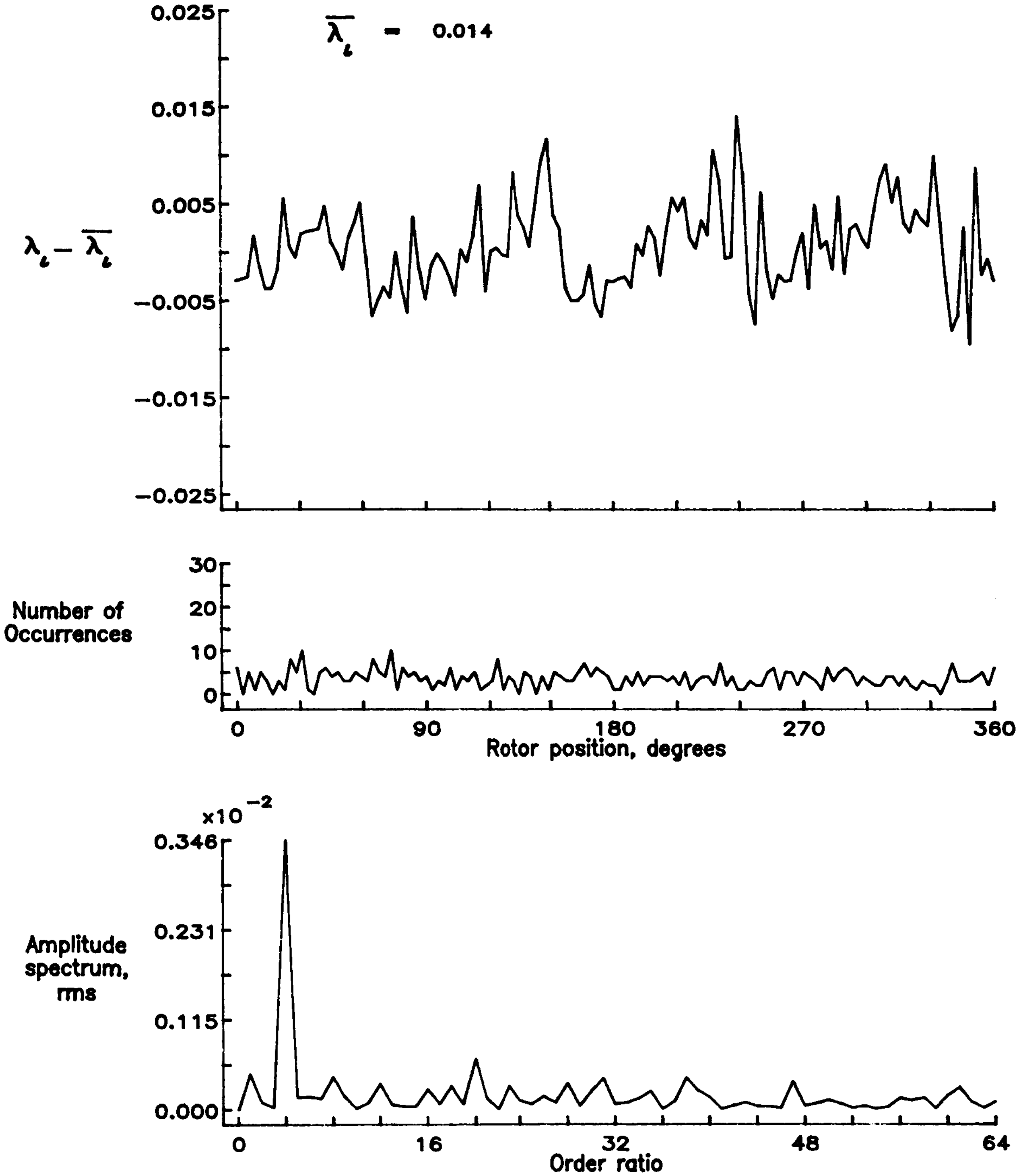

Figure 78.– Concluded.

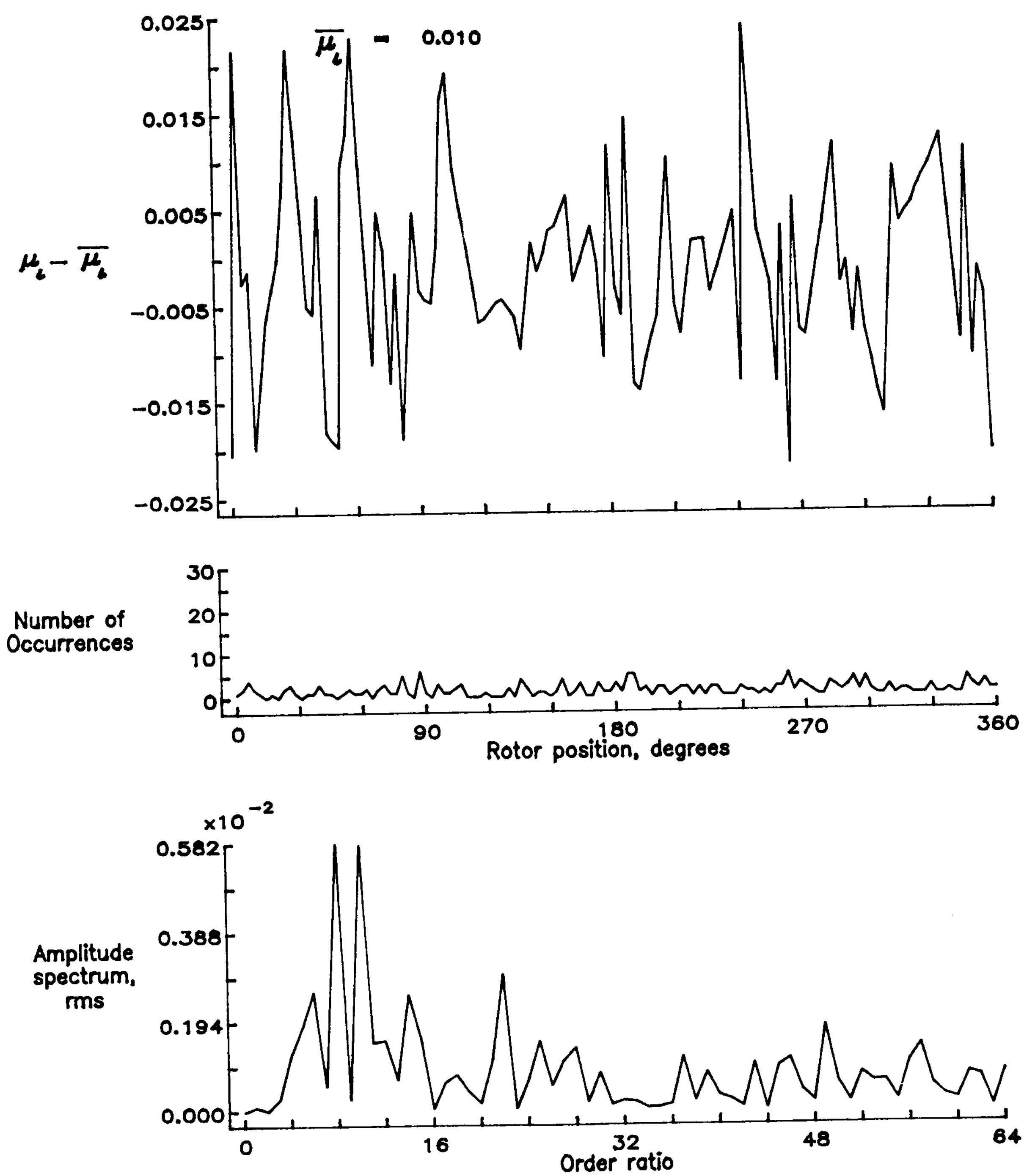

Figure 79.– Induced inflow velocity measured at 150 degrees and r/R of 0.86.

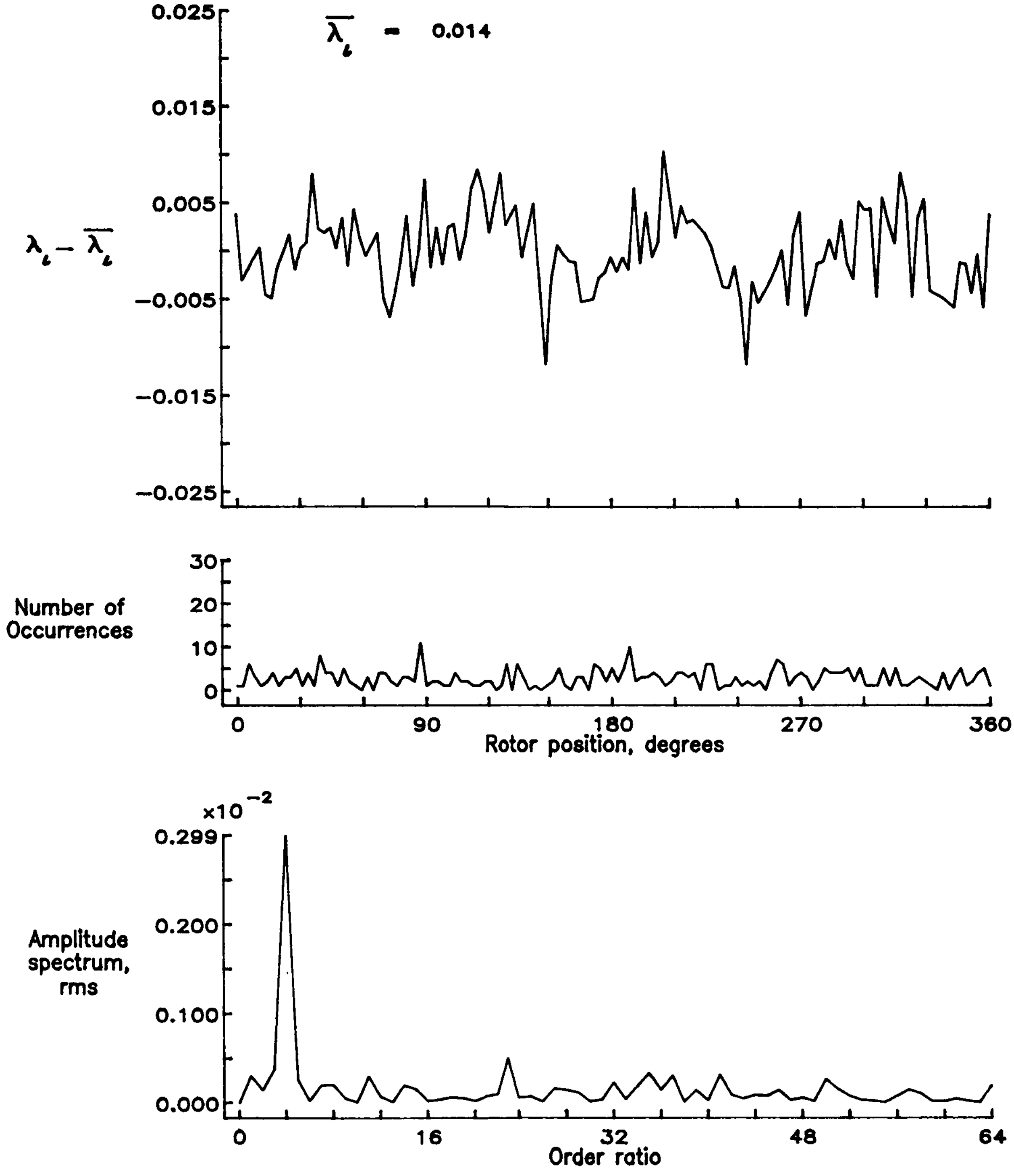

Figure 79.– Concluded.

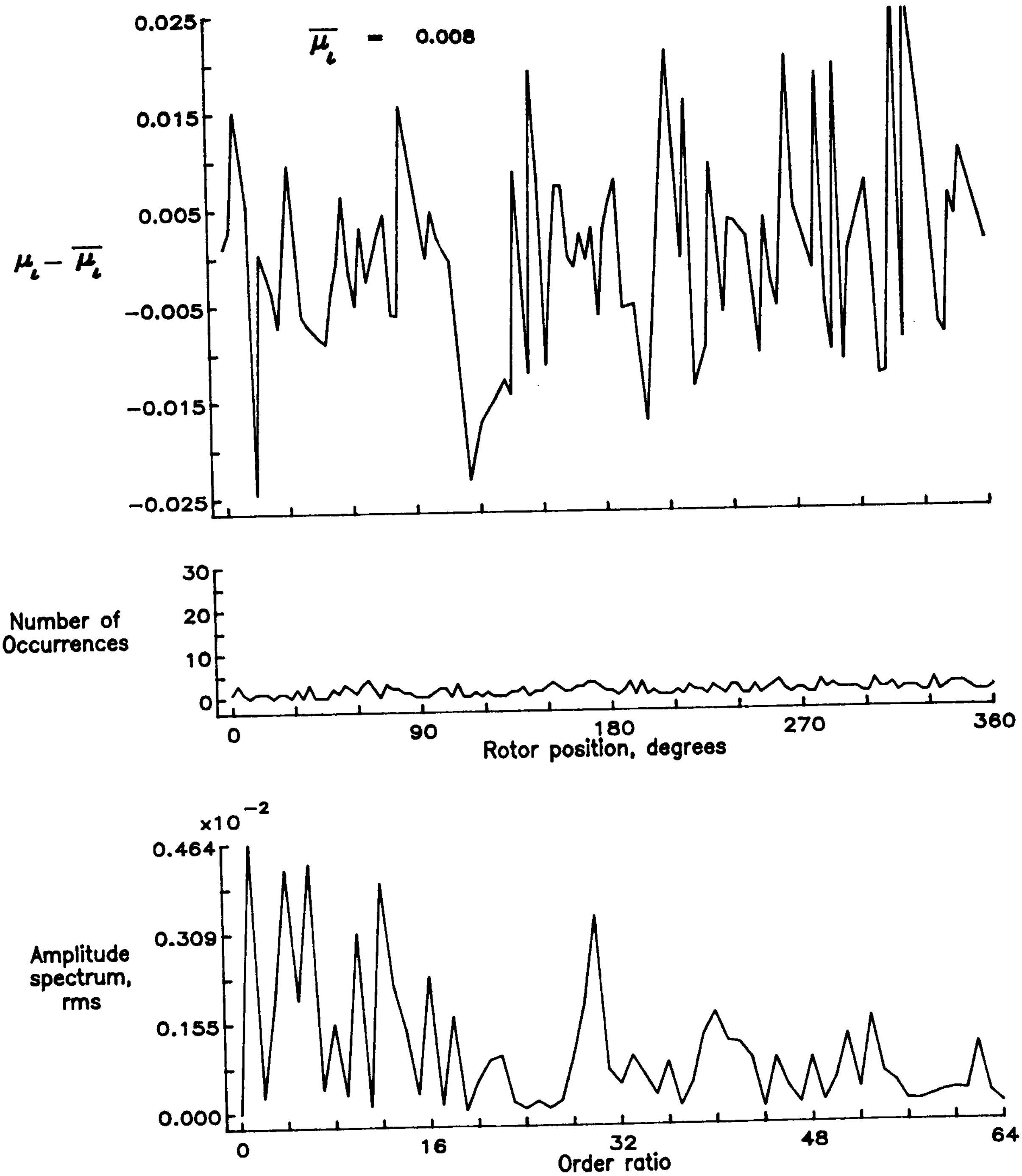

Figure 80.– Induced inflow velocity measured at 150 degrees and r/R of 0.90.

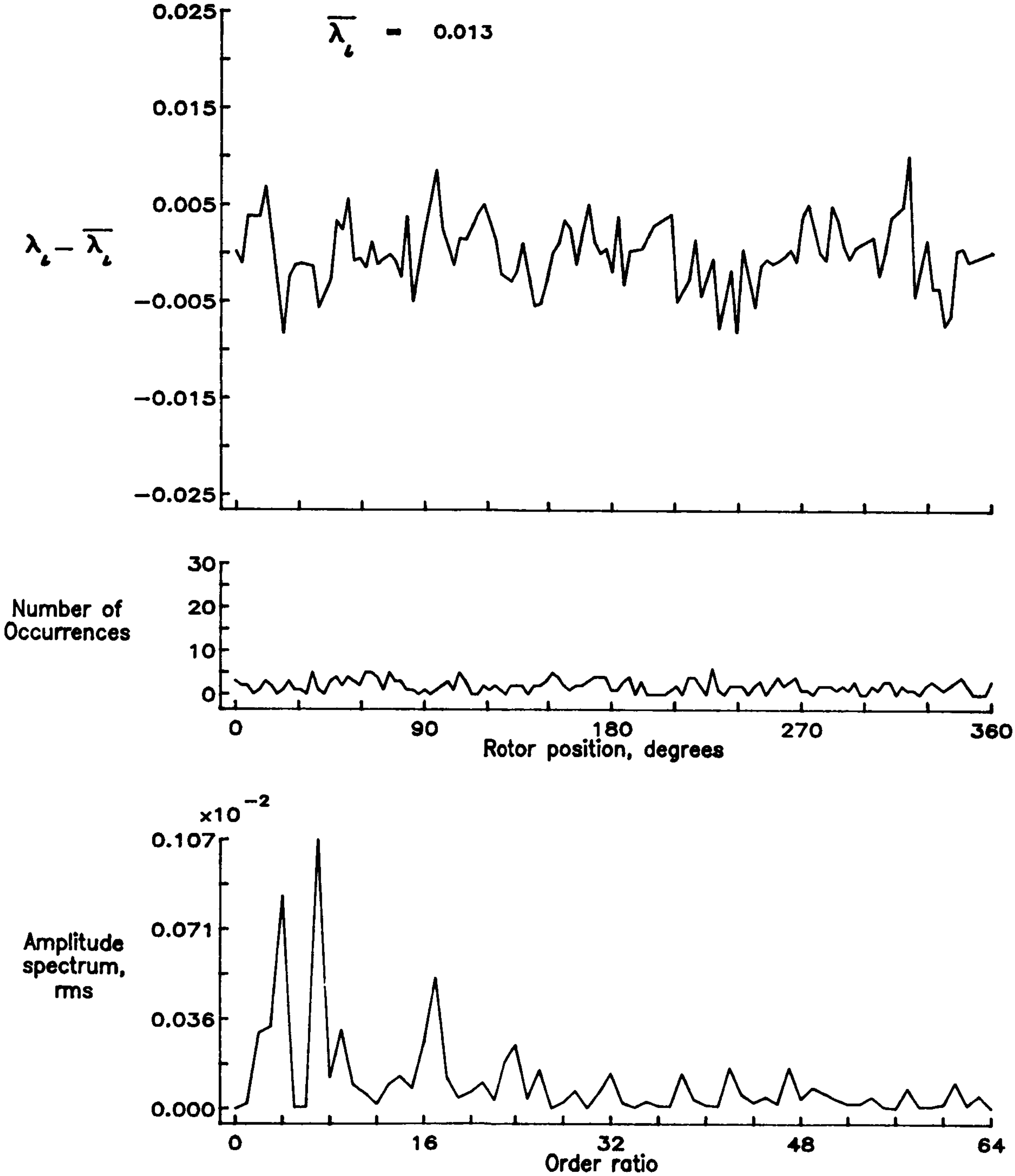

Figure 80.– Concluded.

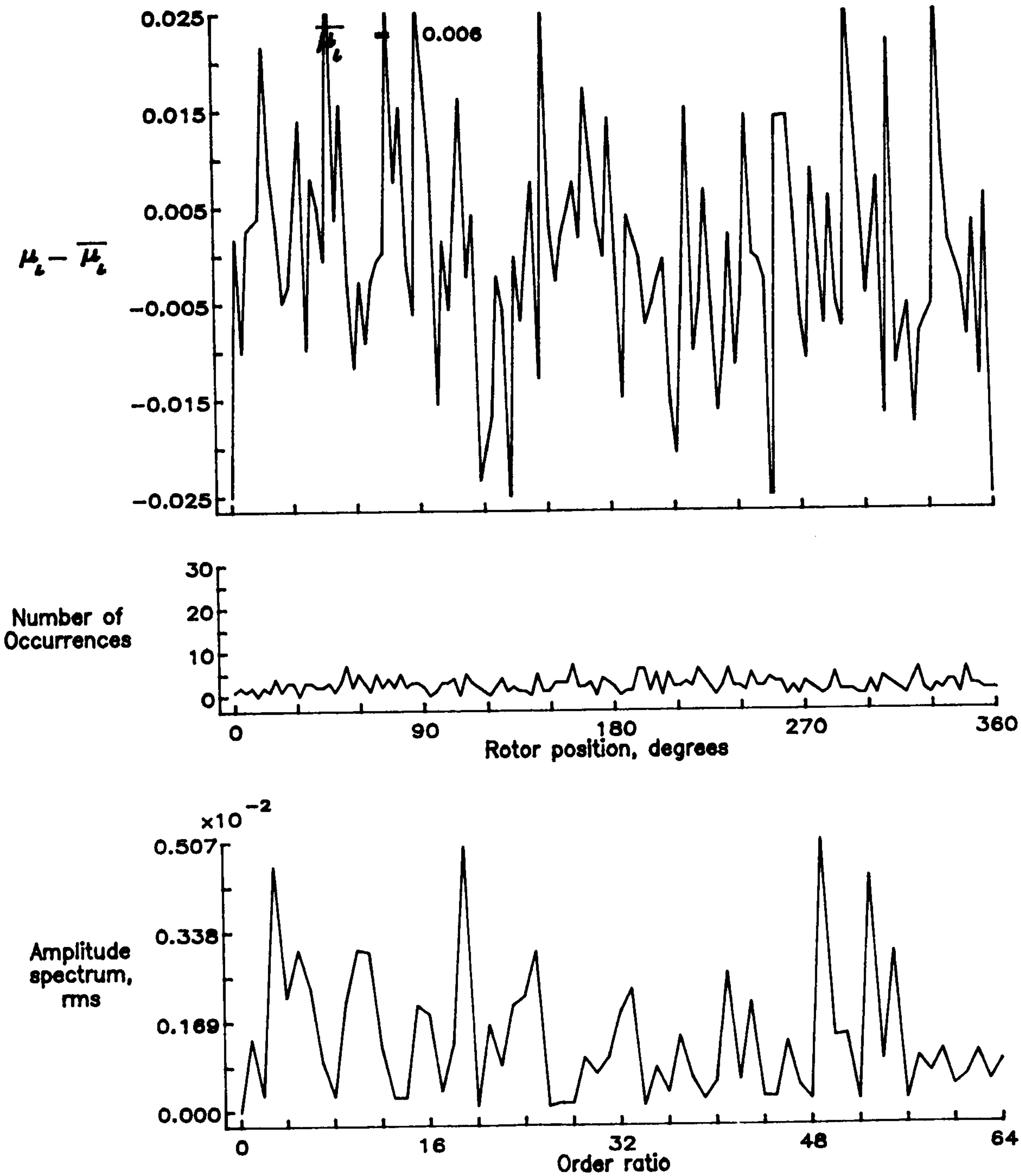

Figure 81.– Induced inflow velocity measured at 150 degrees and r/R of 0.94.

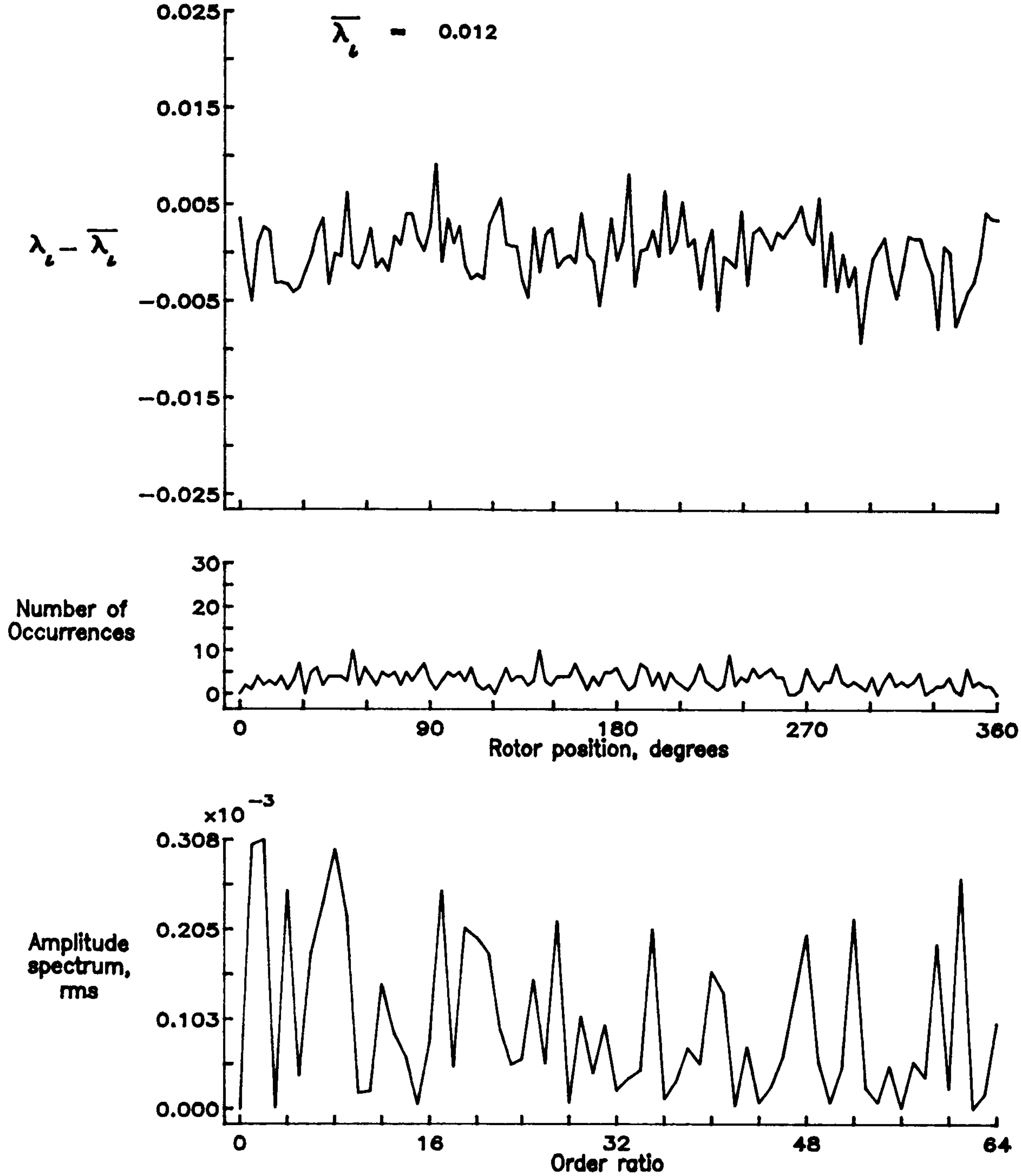

Figure 81.– Concluded.

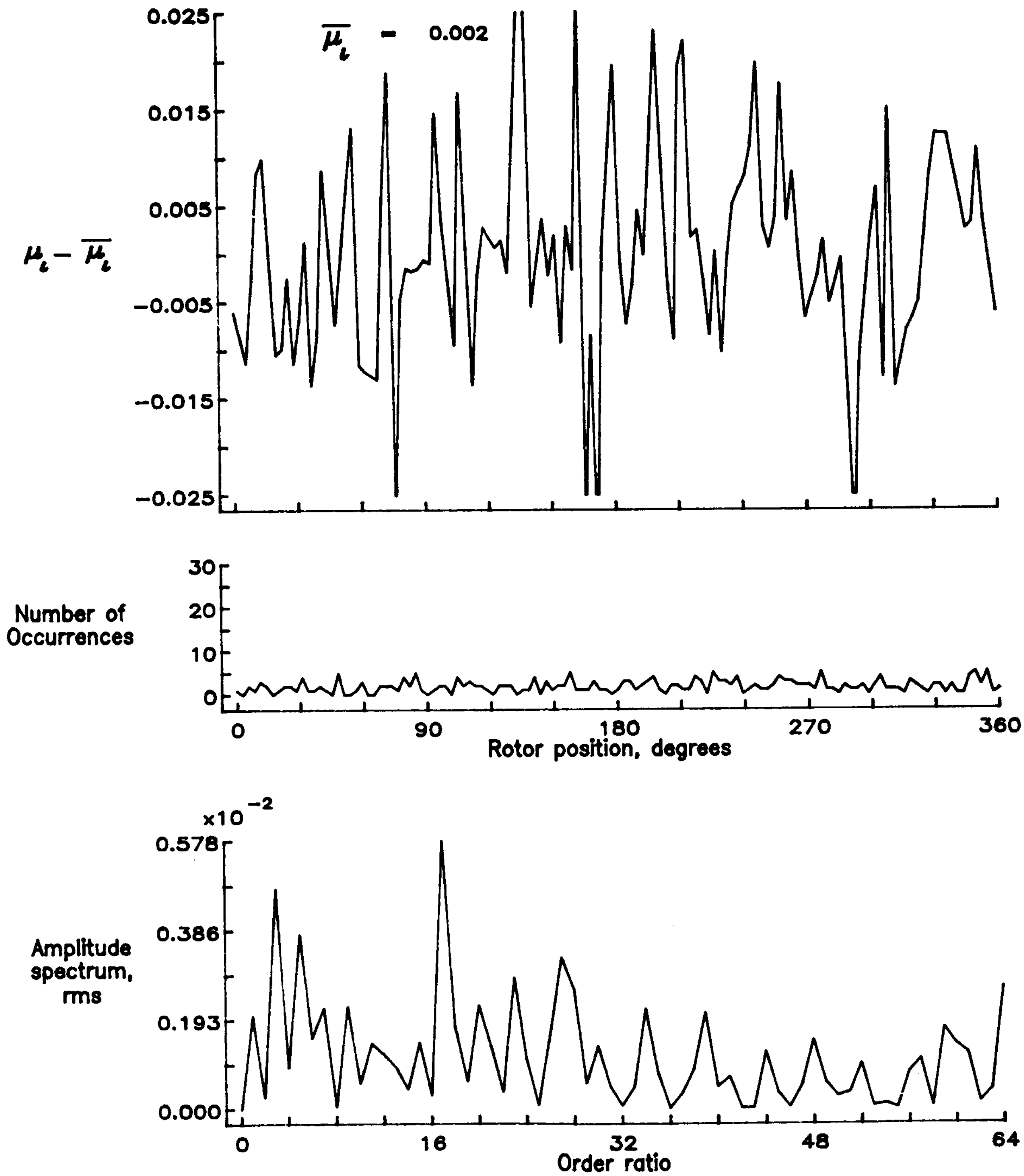

Figure 82.– Induced inflow velocity measured at 150 degrees and r/R of 0.98.

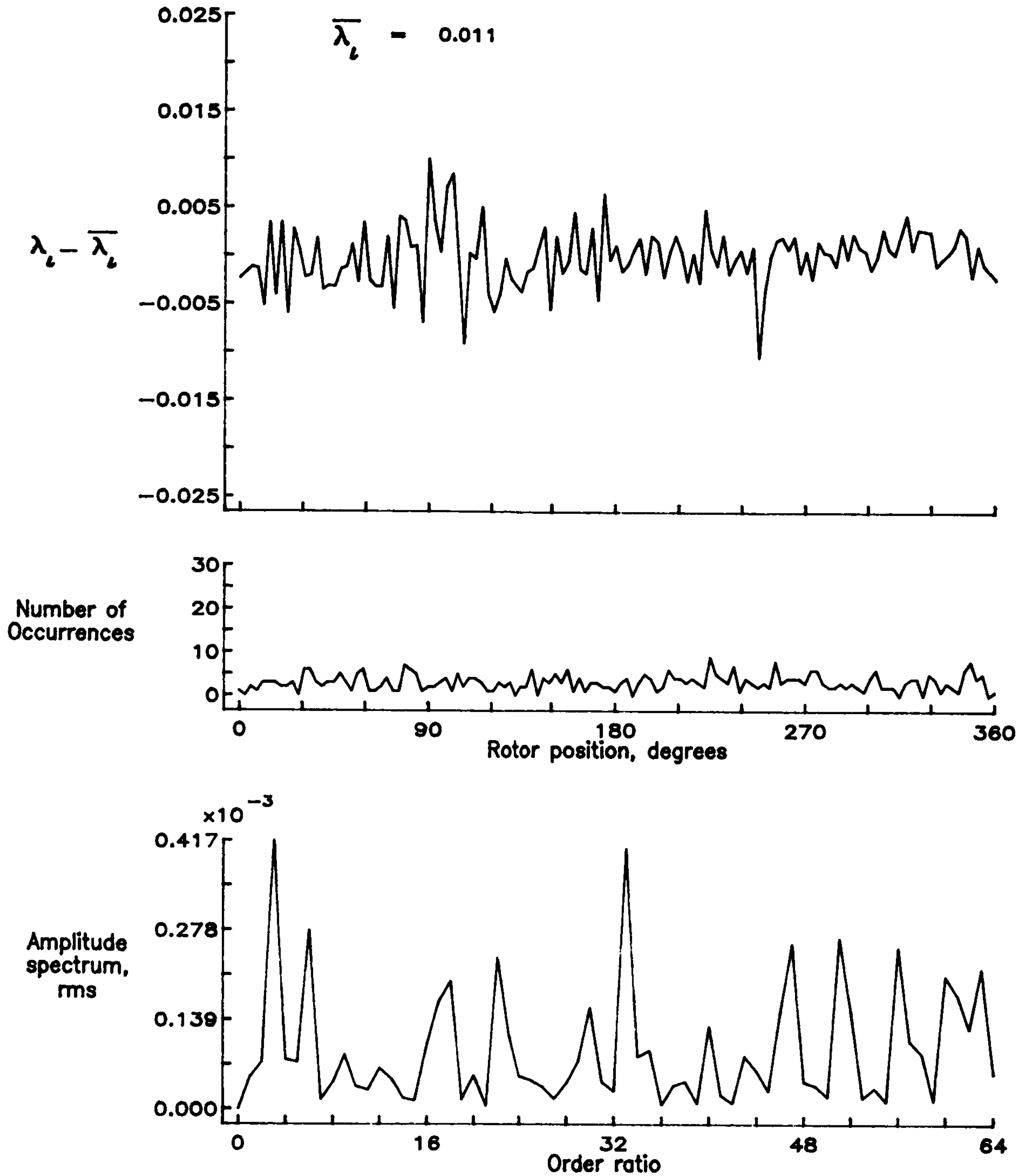

Figure 82.– Concluded.

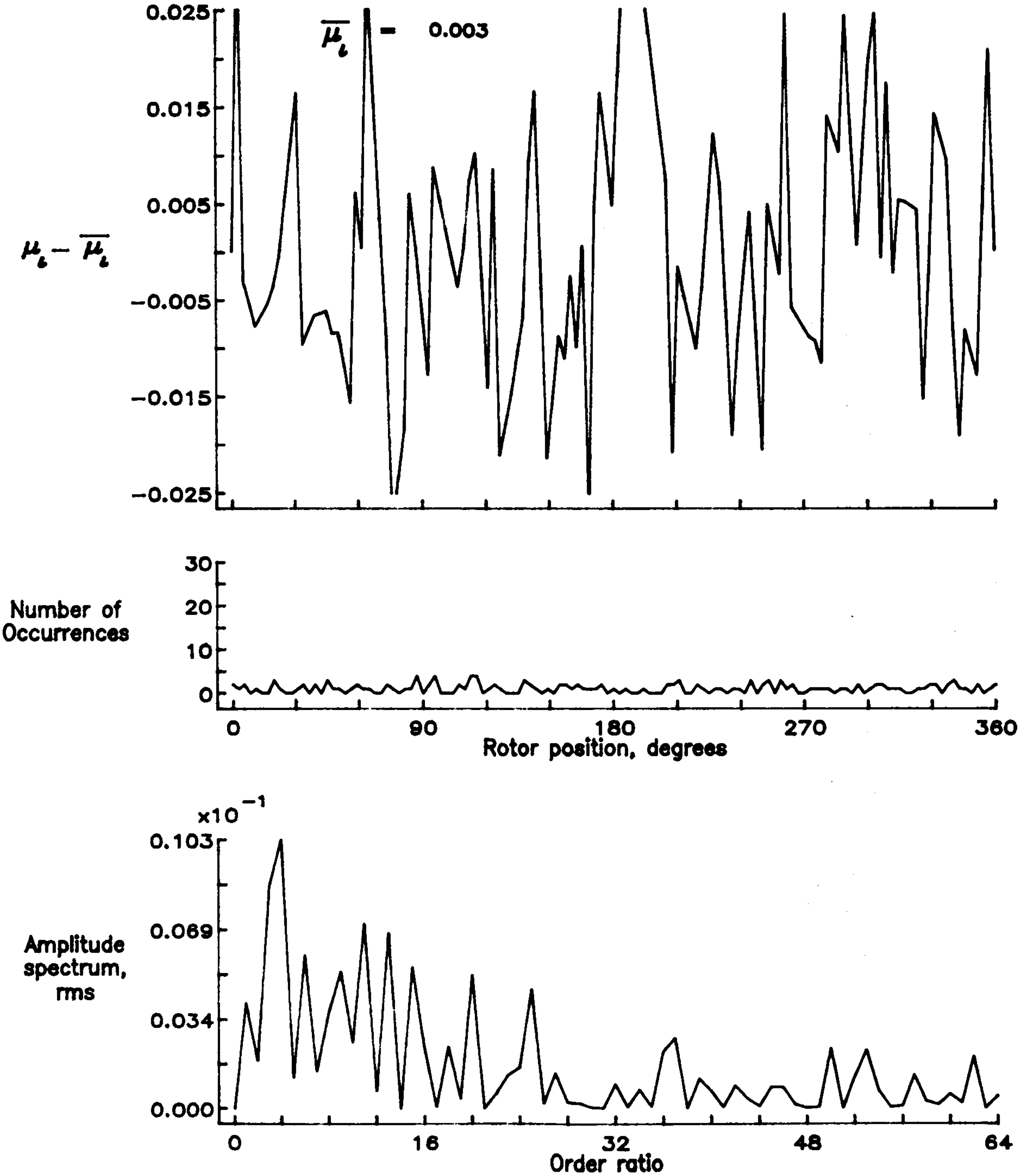

Figure 83.– Induced inflow velocity measured at 150 degrees and r/R of 1.04.

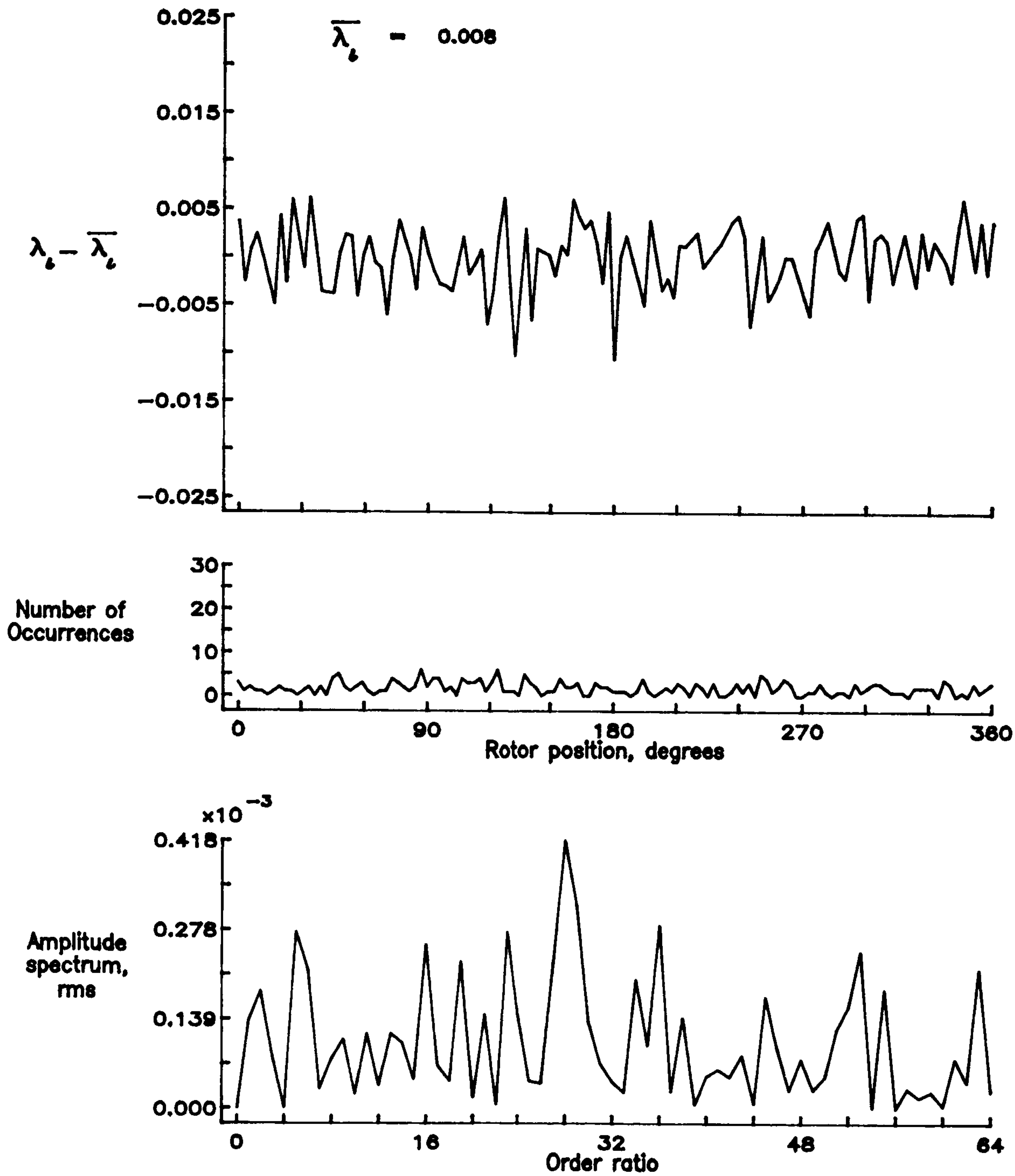

Figure 83.— Concluded.

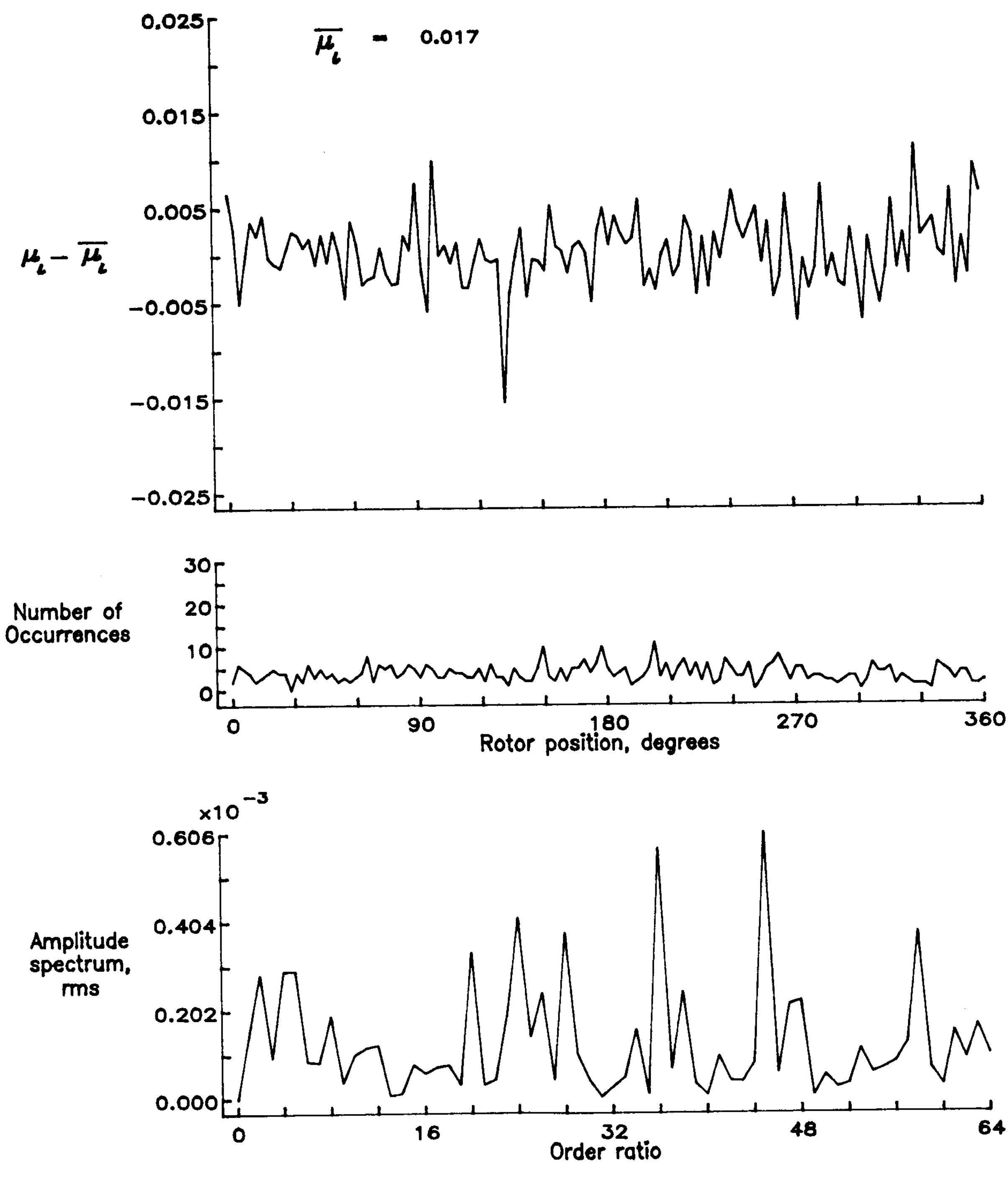

Figure 84.– Induced inflow velocity measured at 180 degrees and r/R of 0.40.

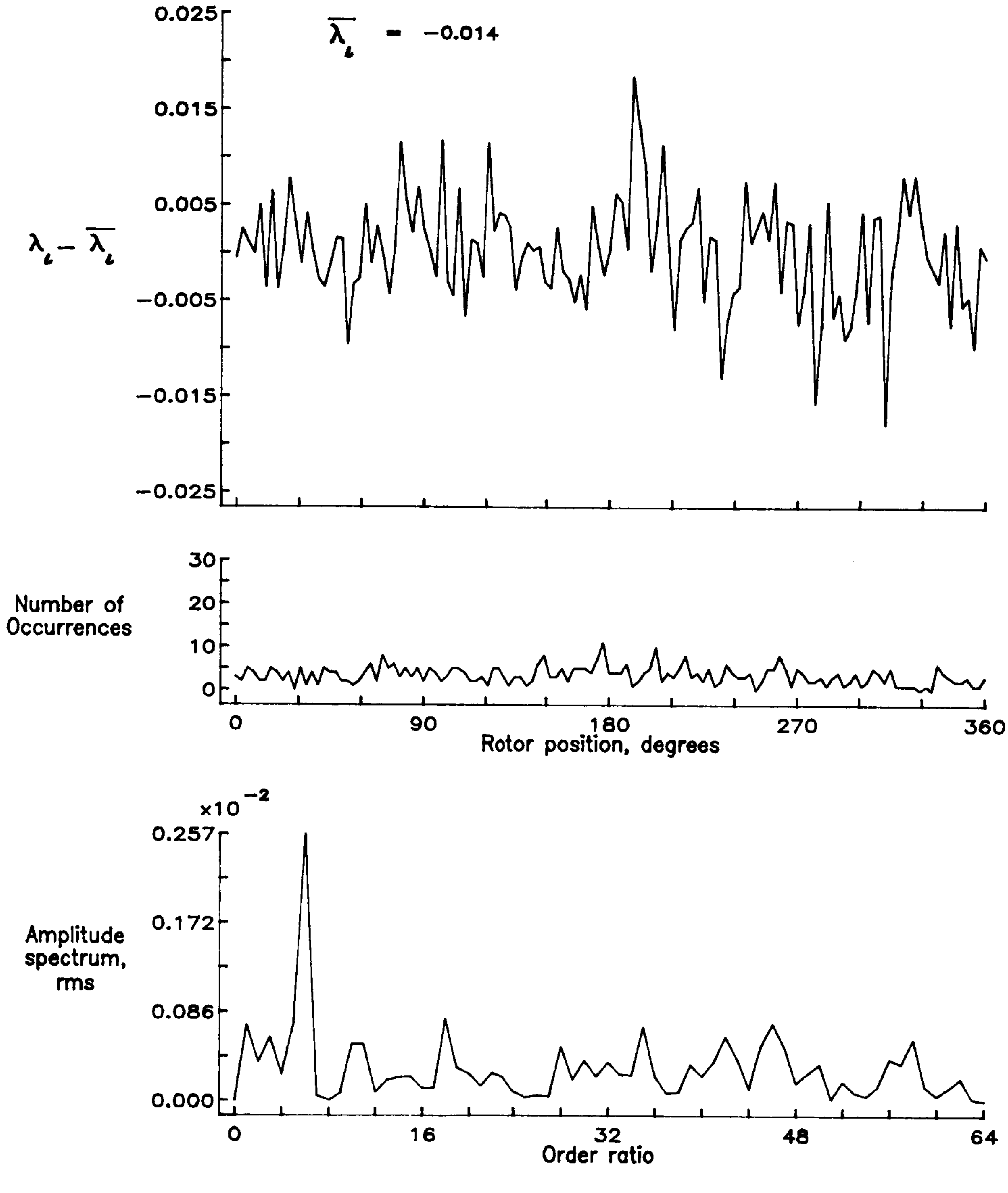

Figure 84.– Concluded.

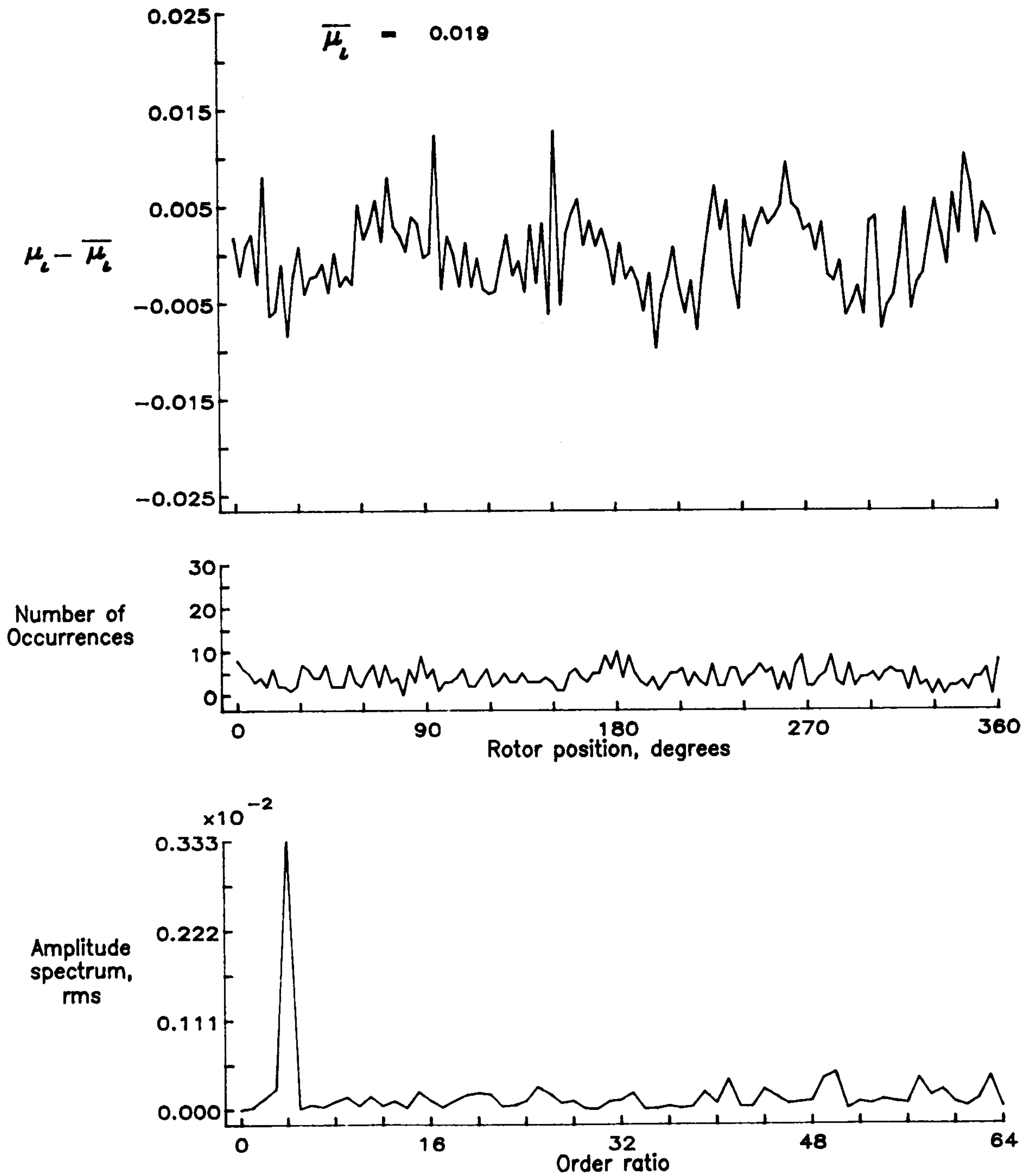

Figure 85.— Induced inflow velocity measured at 180 degrees and r/R of 0.50.

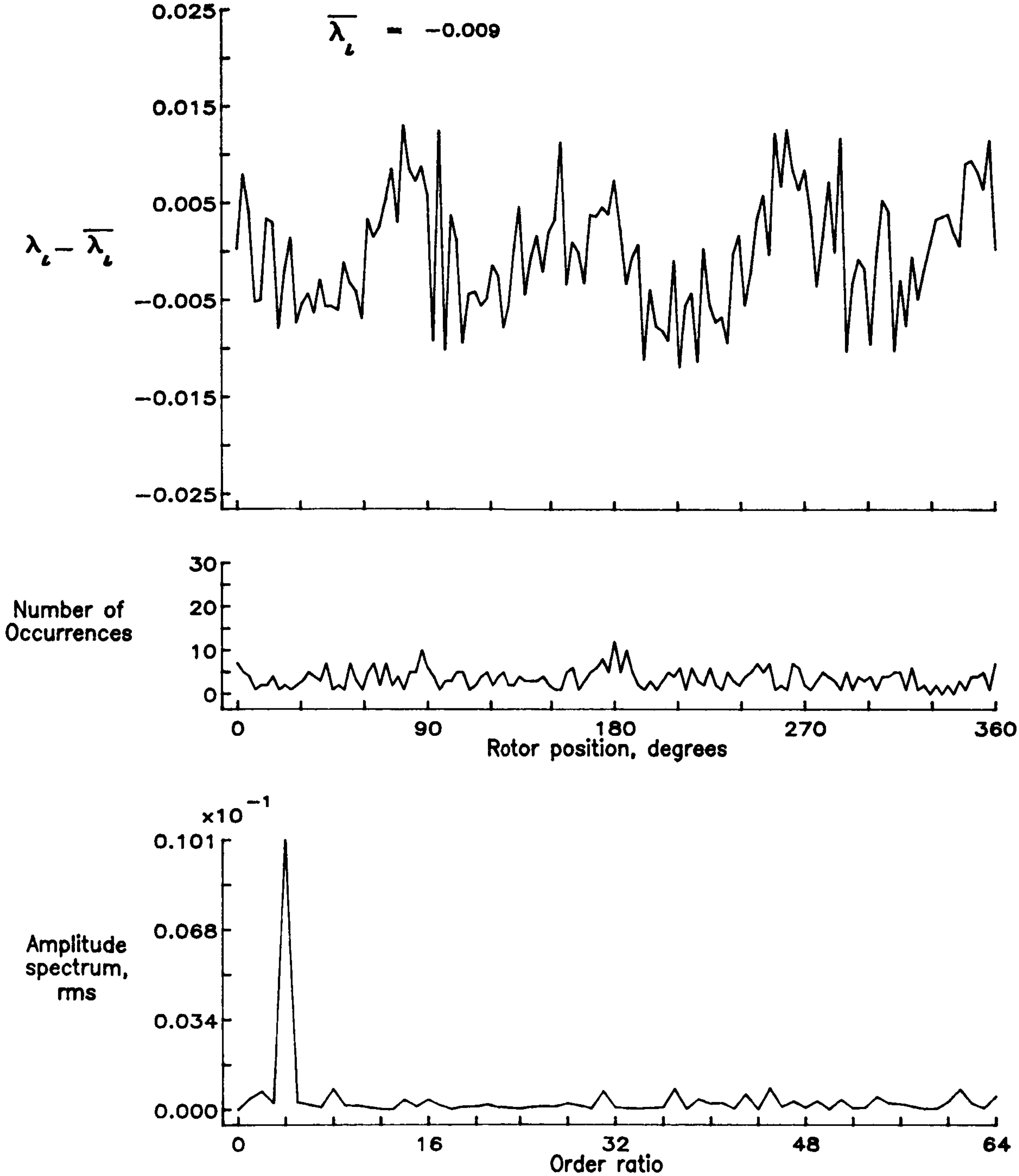

Figure 85.– Concluded.

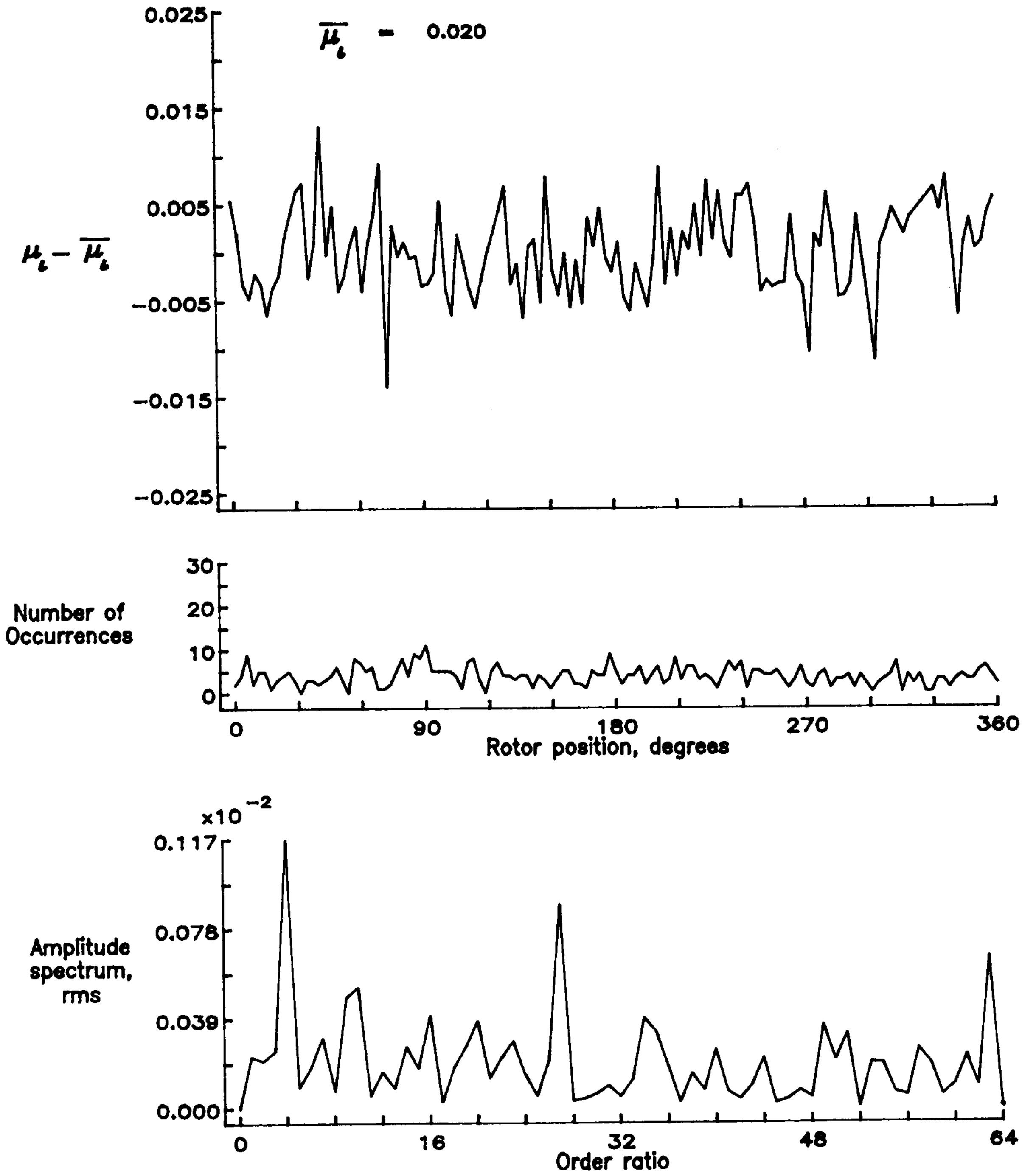

Figure 86.– Induced inflow velocity measured at 180 degrees and r/R of 0.60.

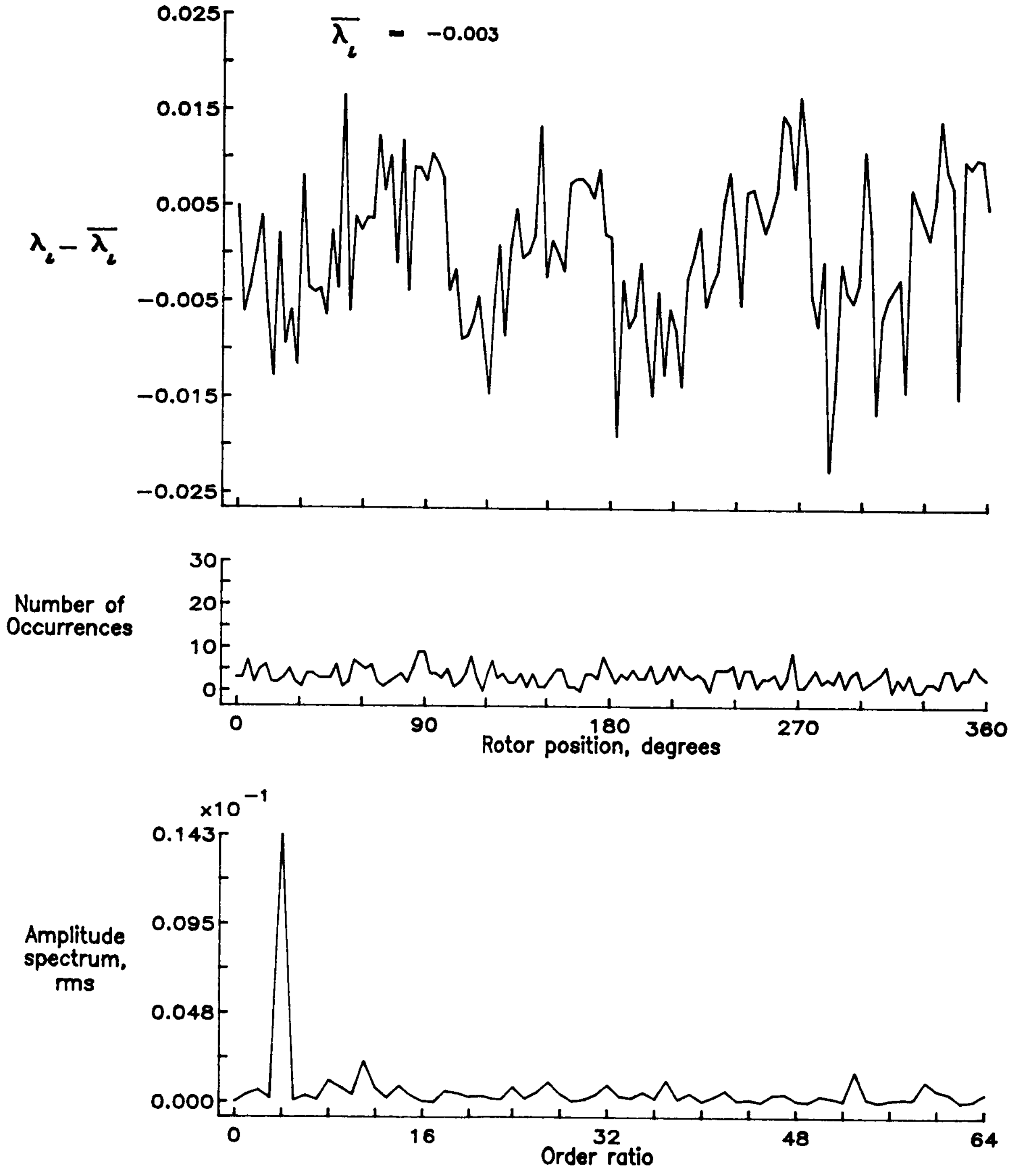

Figure 86.- Concluded.

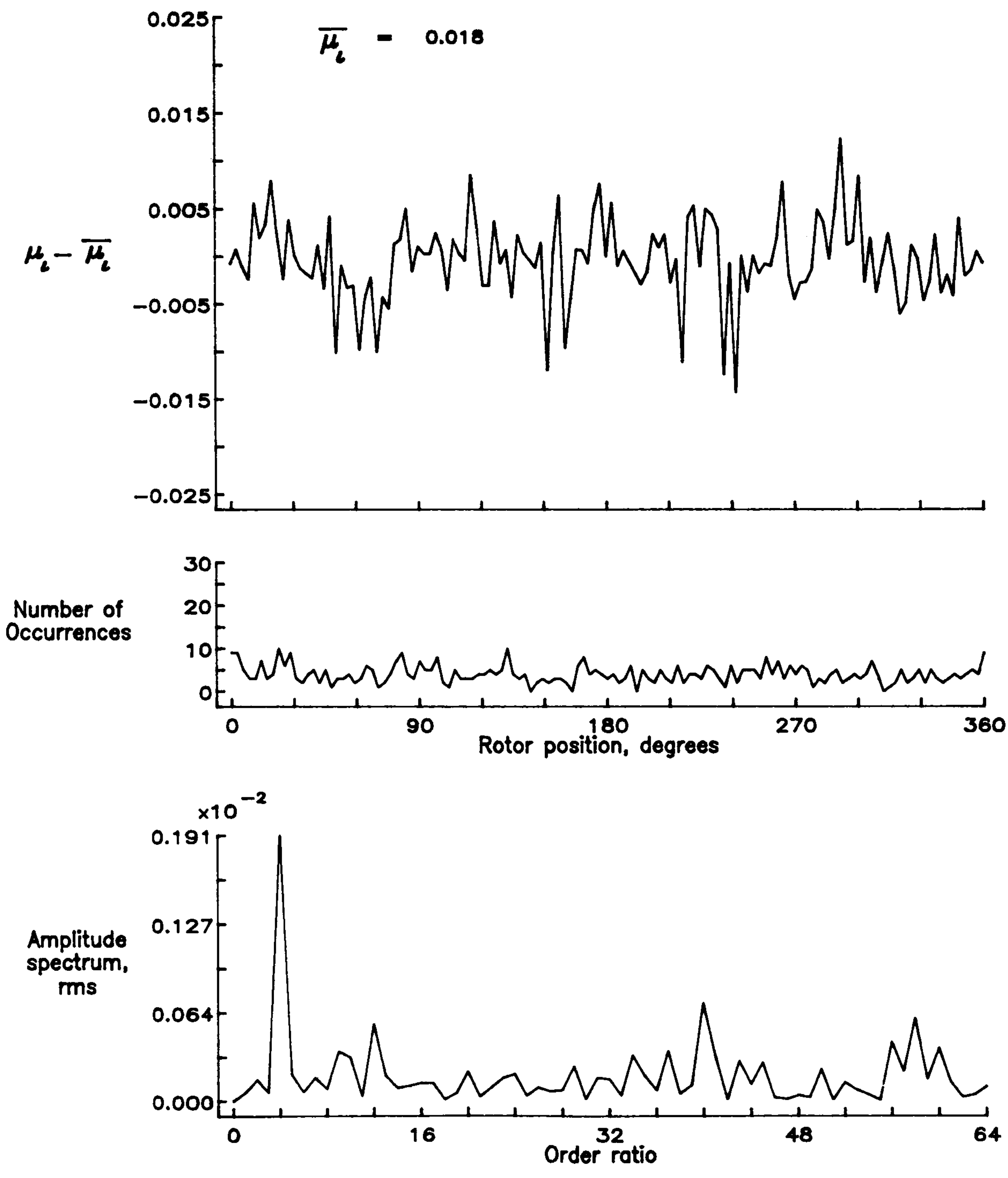

Figure 87.– Induced inflow velocity measured at 180 degrees and r/R of 0.70.

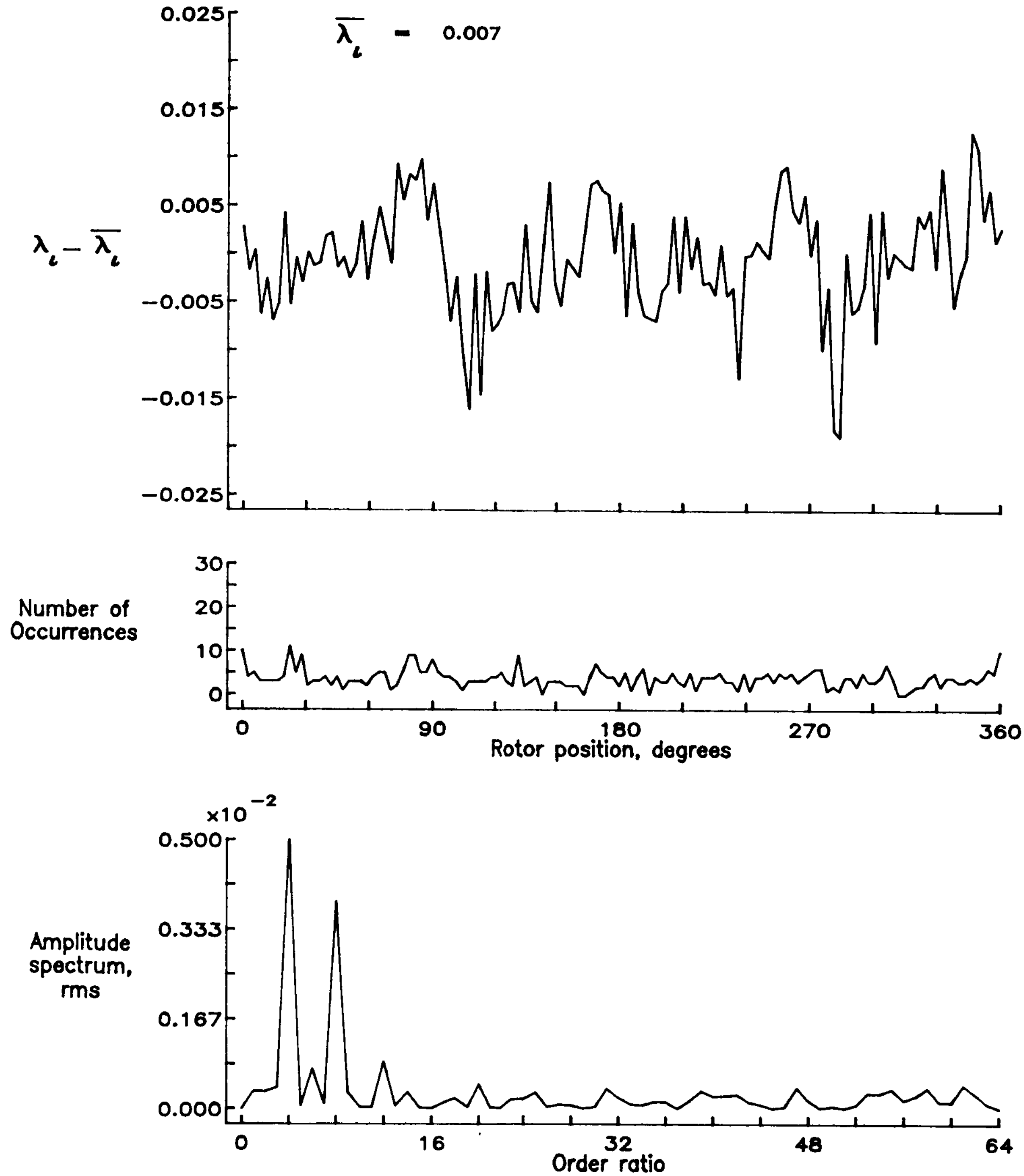

Figure 87.– Concluded.

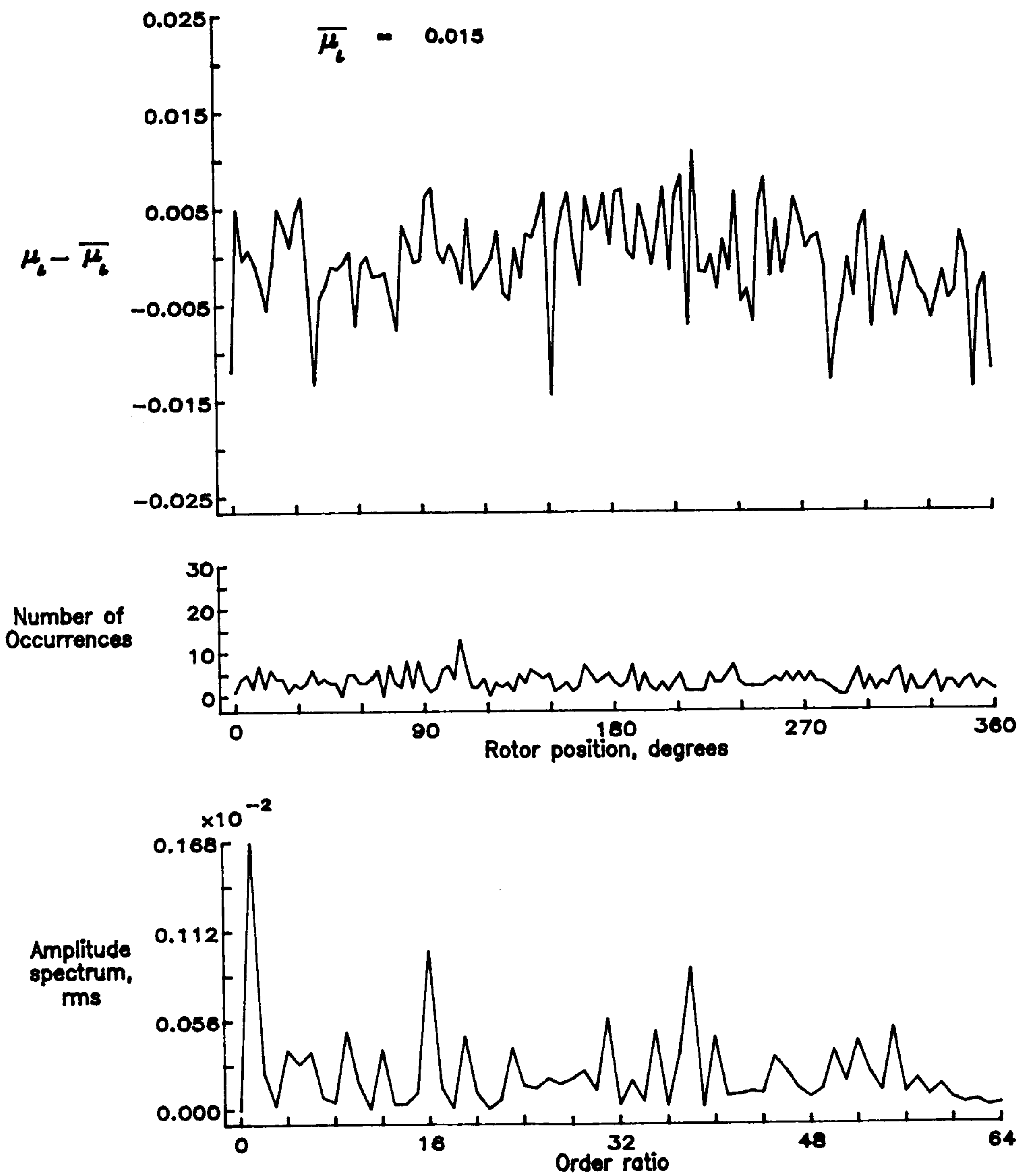

Figure 88.– Induced inflow velocity measured at 180 degrees and r/R of 0.74.

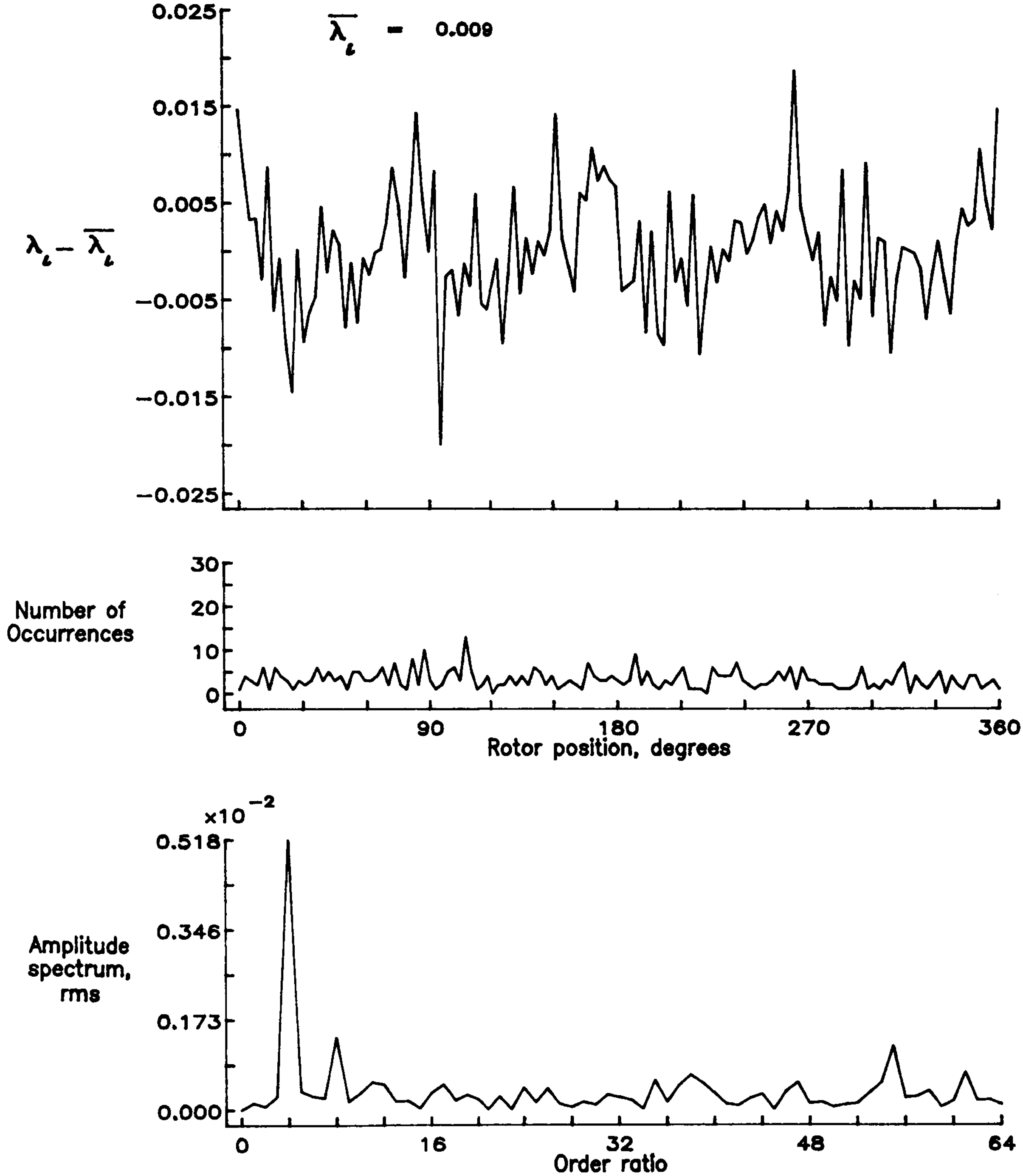

Figure 88.— Concluded.

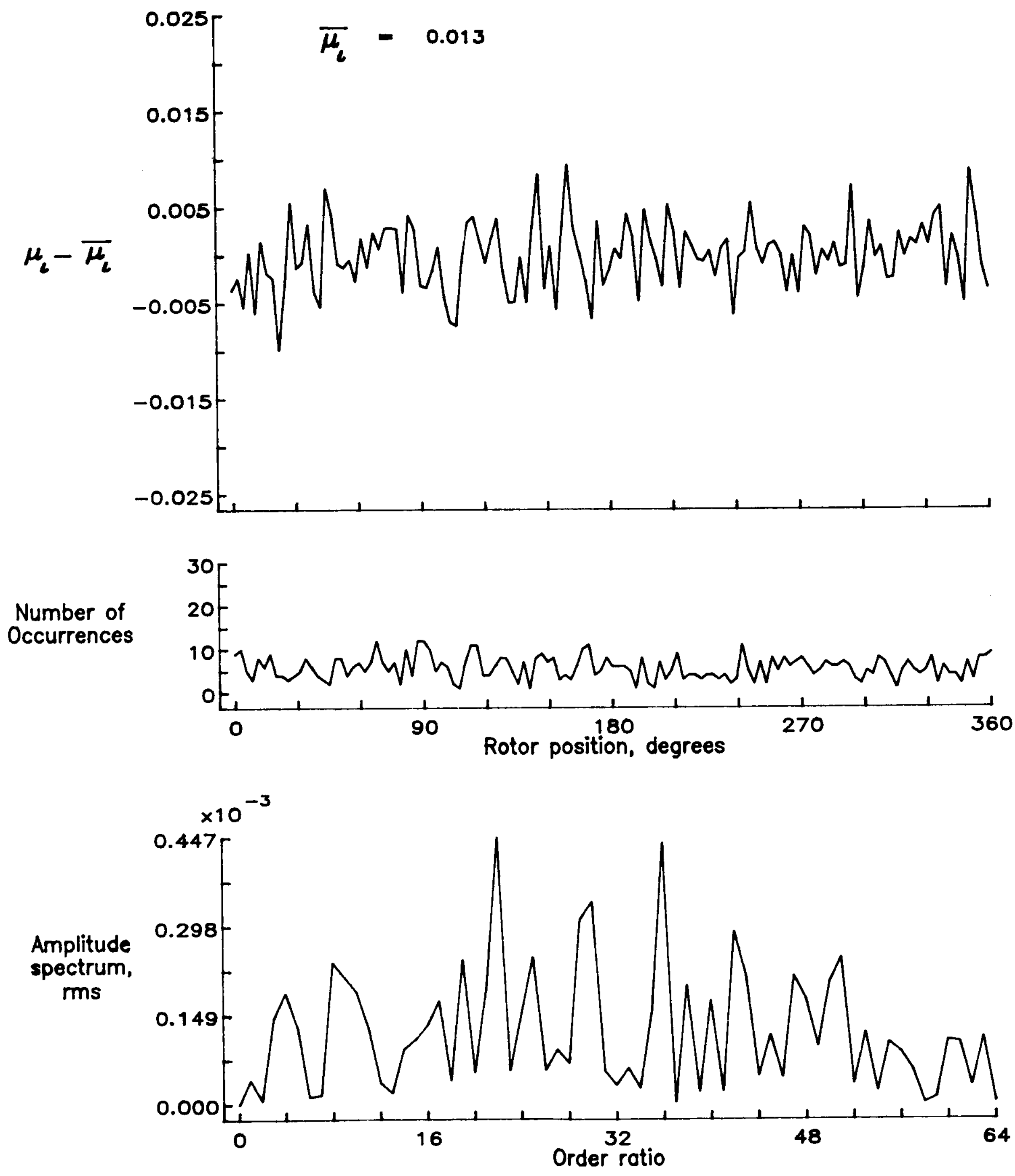

Figure 89.– Induced inflow velocity measured at 180 degrees and r/R of 0.78.

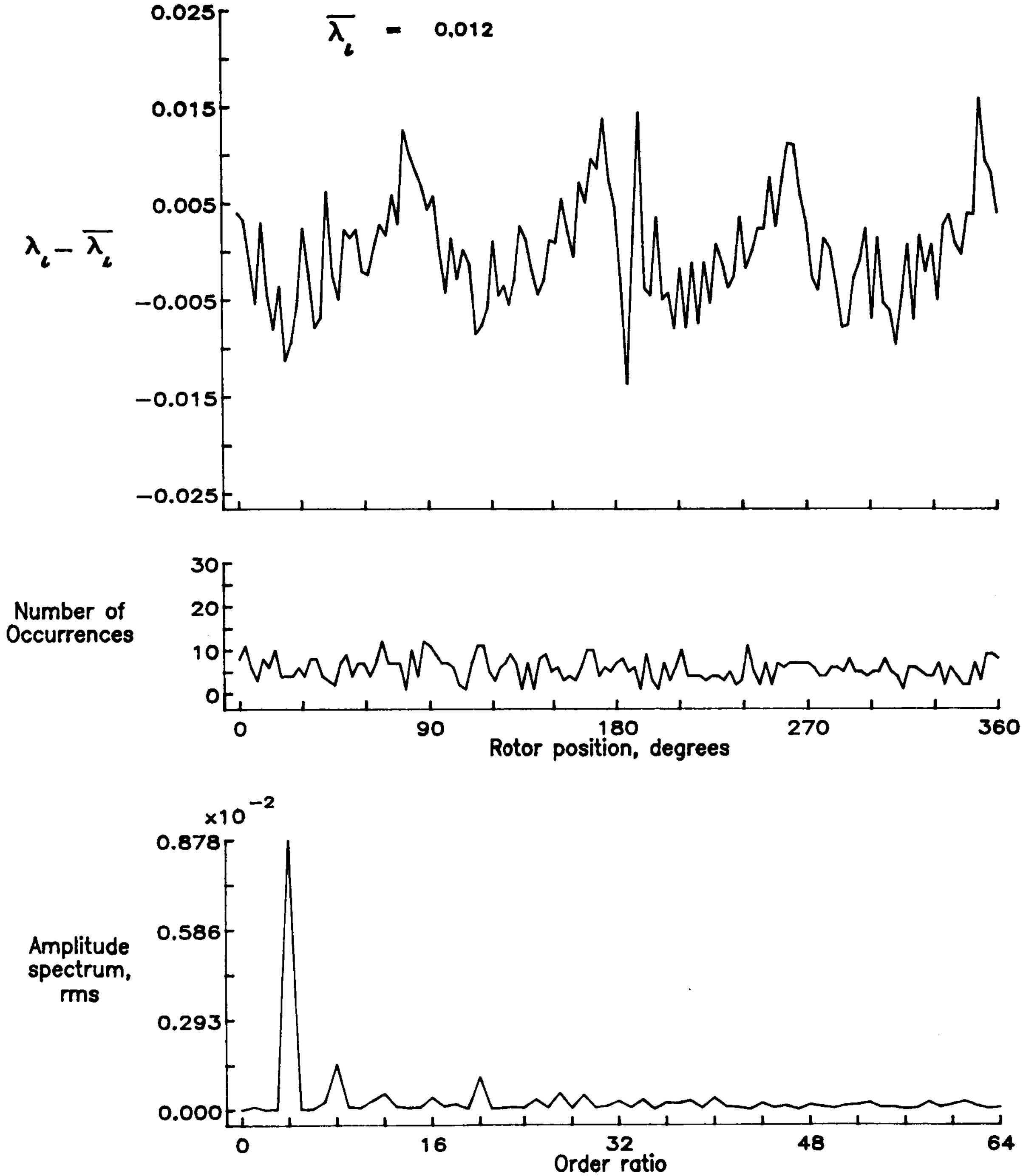

Figure 89.– Concluded.

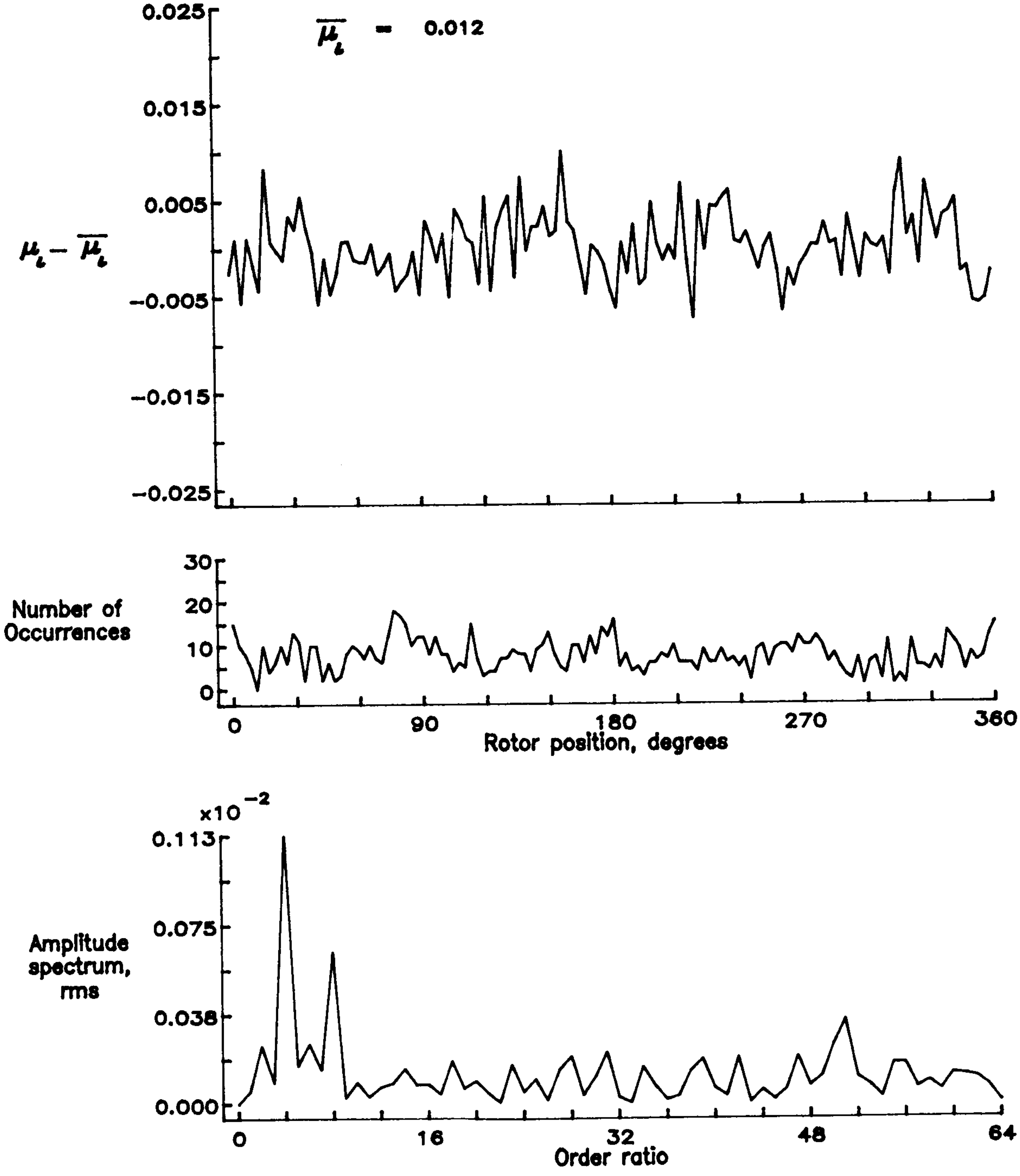

Figure 90.– Induced inflow velocity measured at 180 degrees and r/R of 0.82.

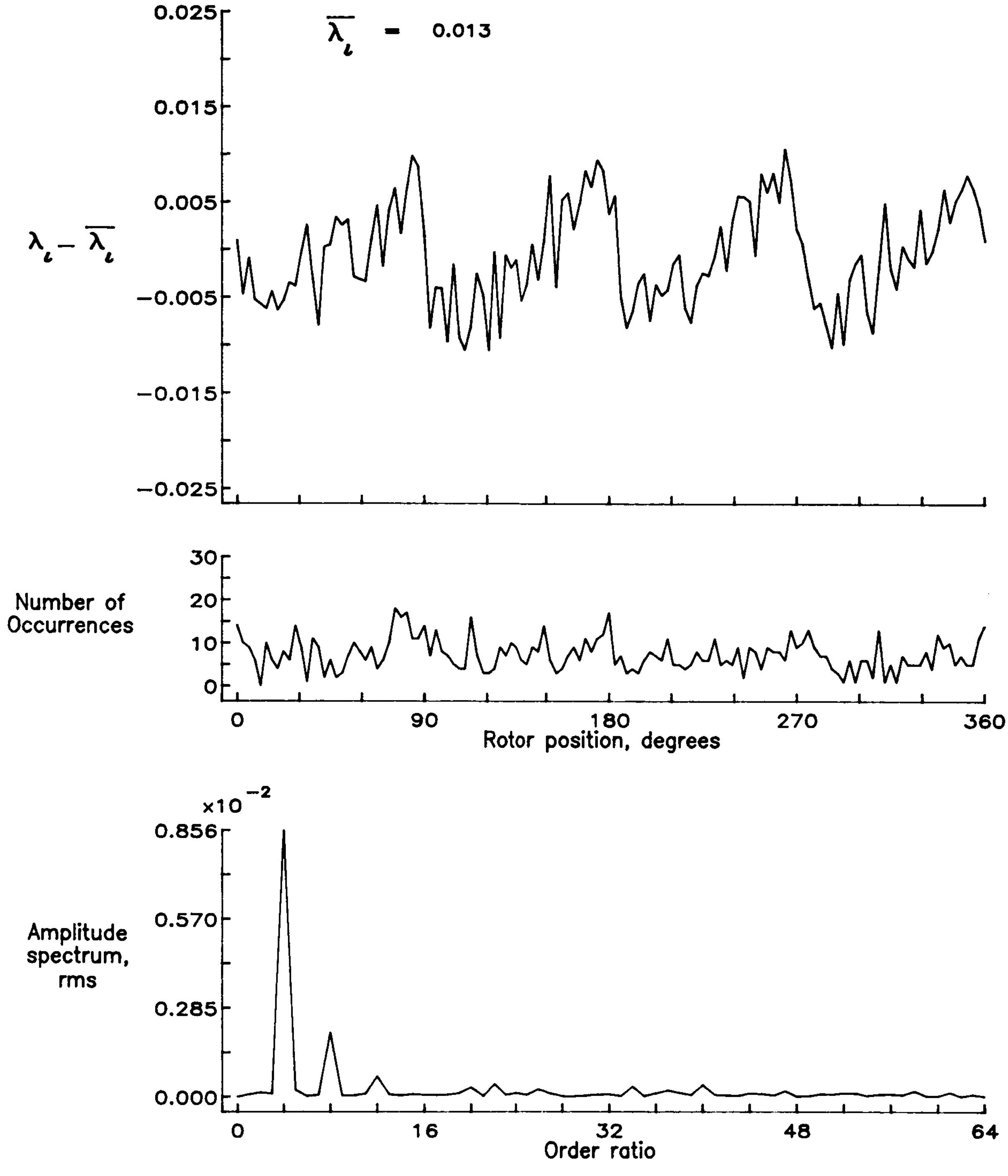

Figure 90.– Concluded.

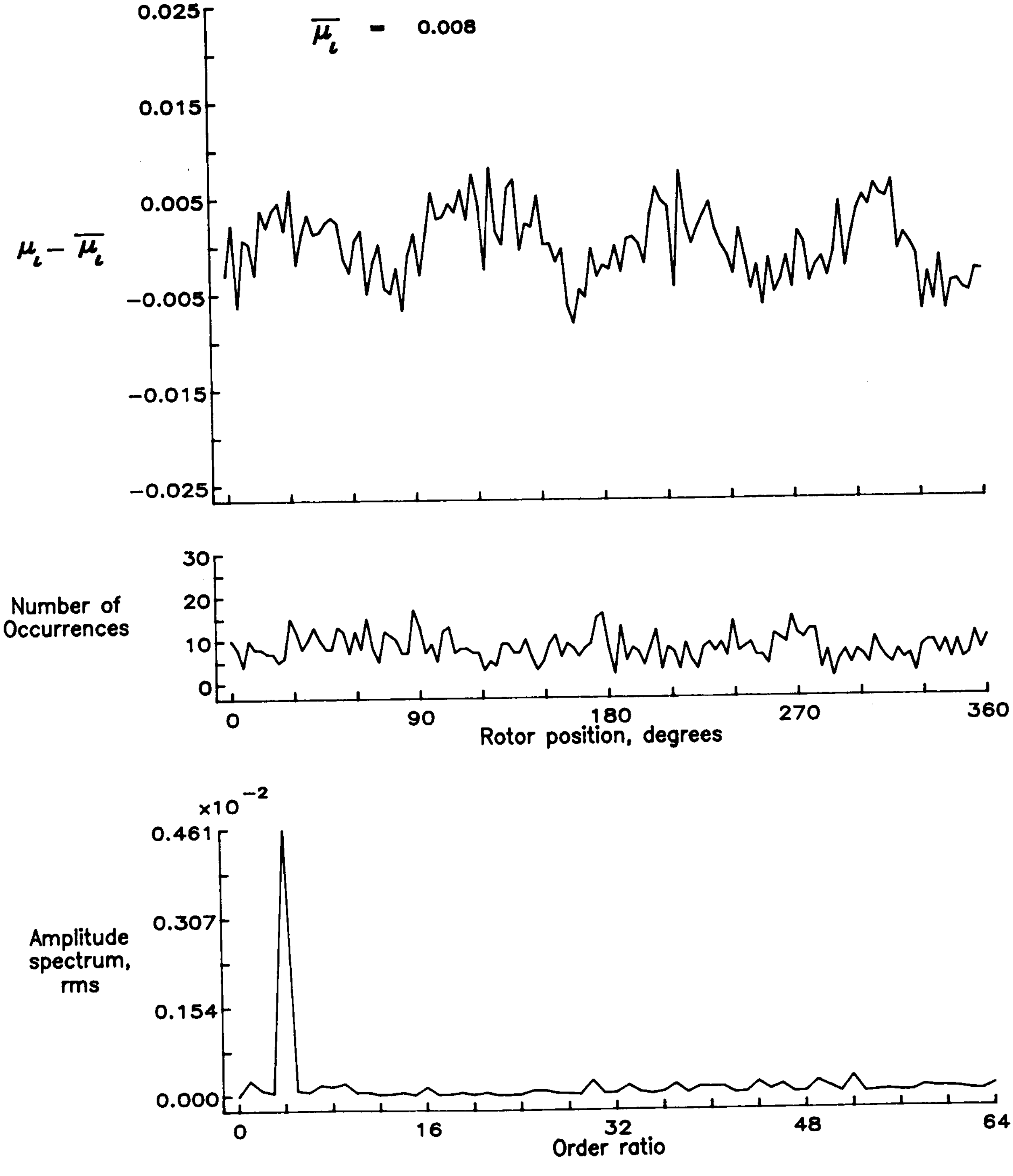

Figure 91.– Induced inflow velocity measured at 180 degrees and r/R of 0.86.

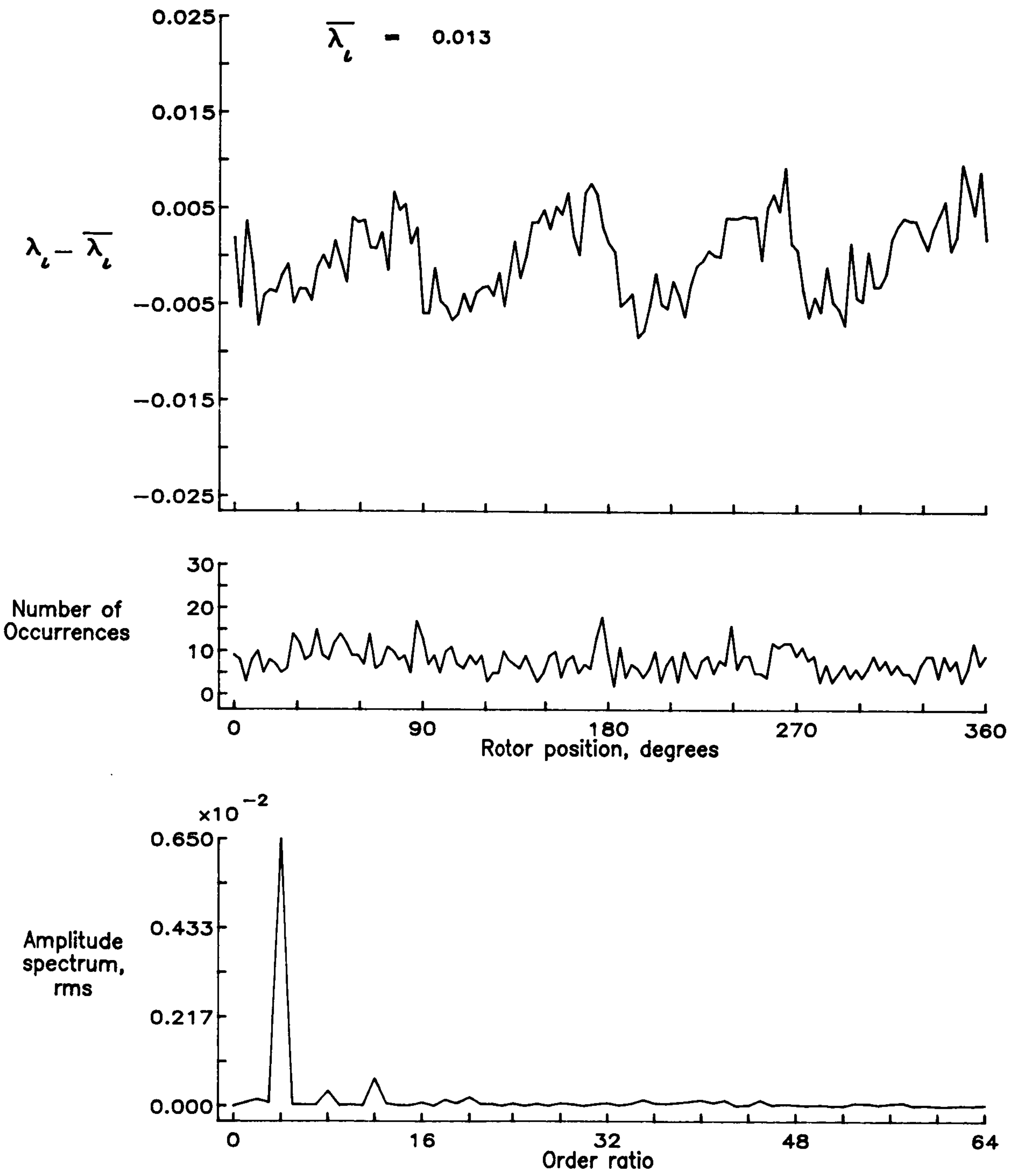

Figure 91.– Concluded.

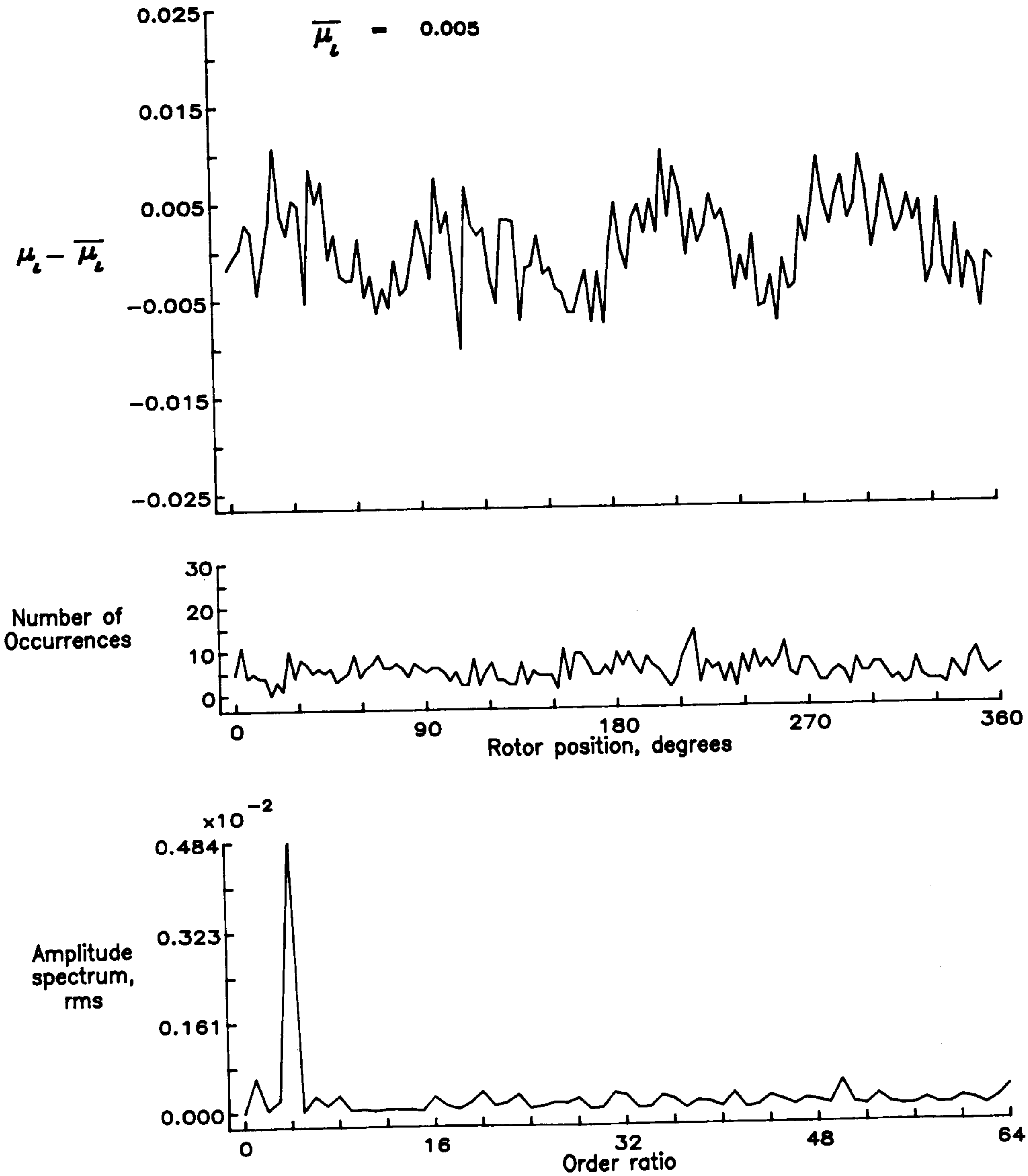

Figure 92.– Induced inflow velocity measured at 180 degrees and r/R of 0.90.

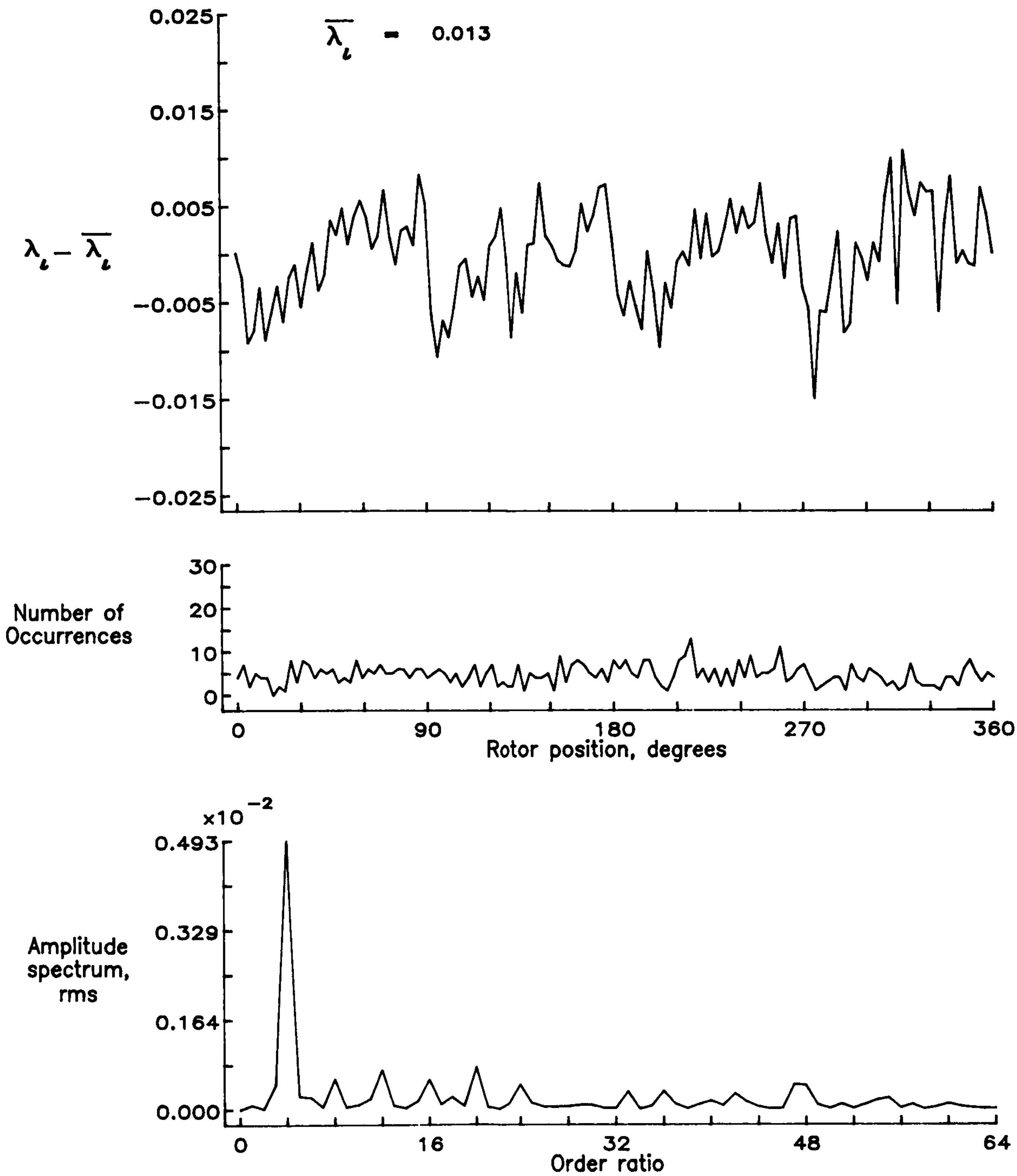

Figure 92.– Concluded.

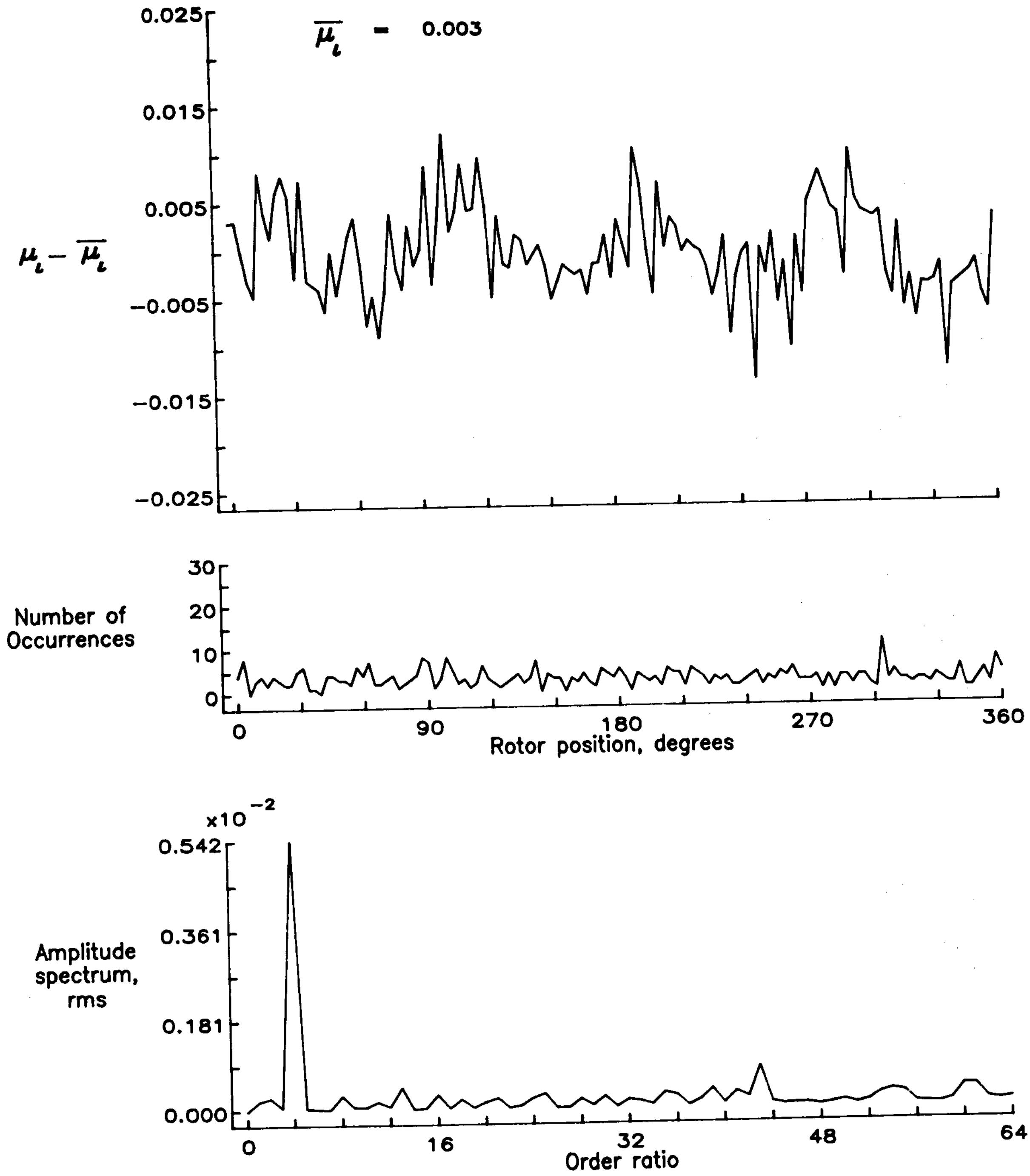

Figure 93.– Induced inflow velocity measured at 180 degrees and r/R of 0.94.

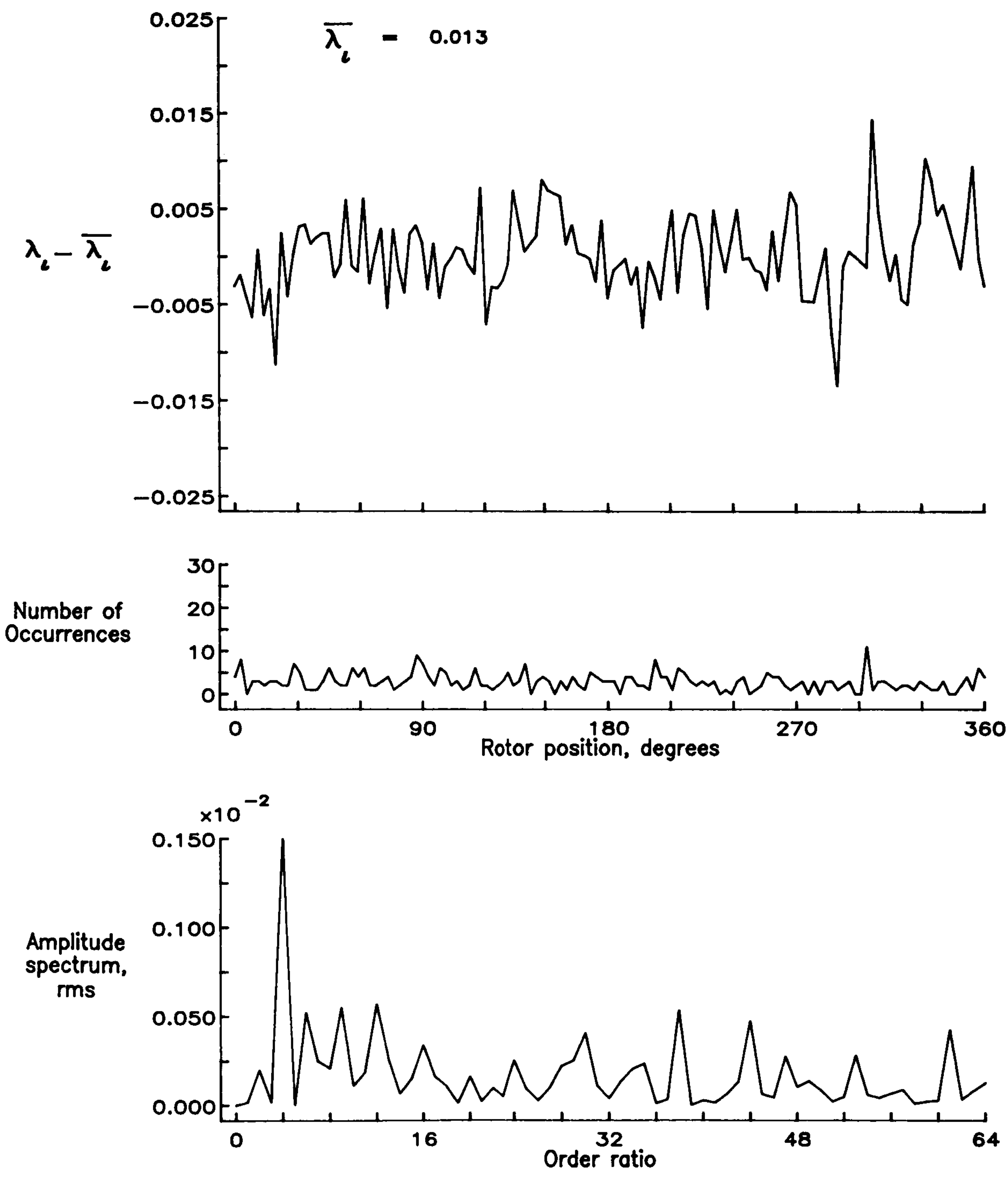

Figure 93.– Concluded.

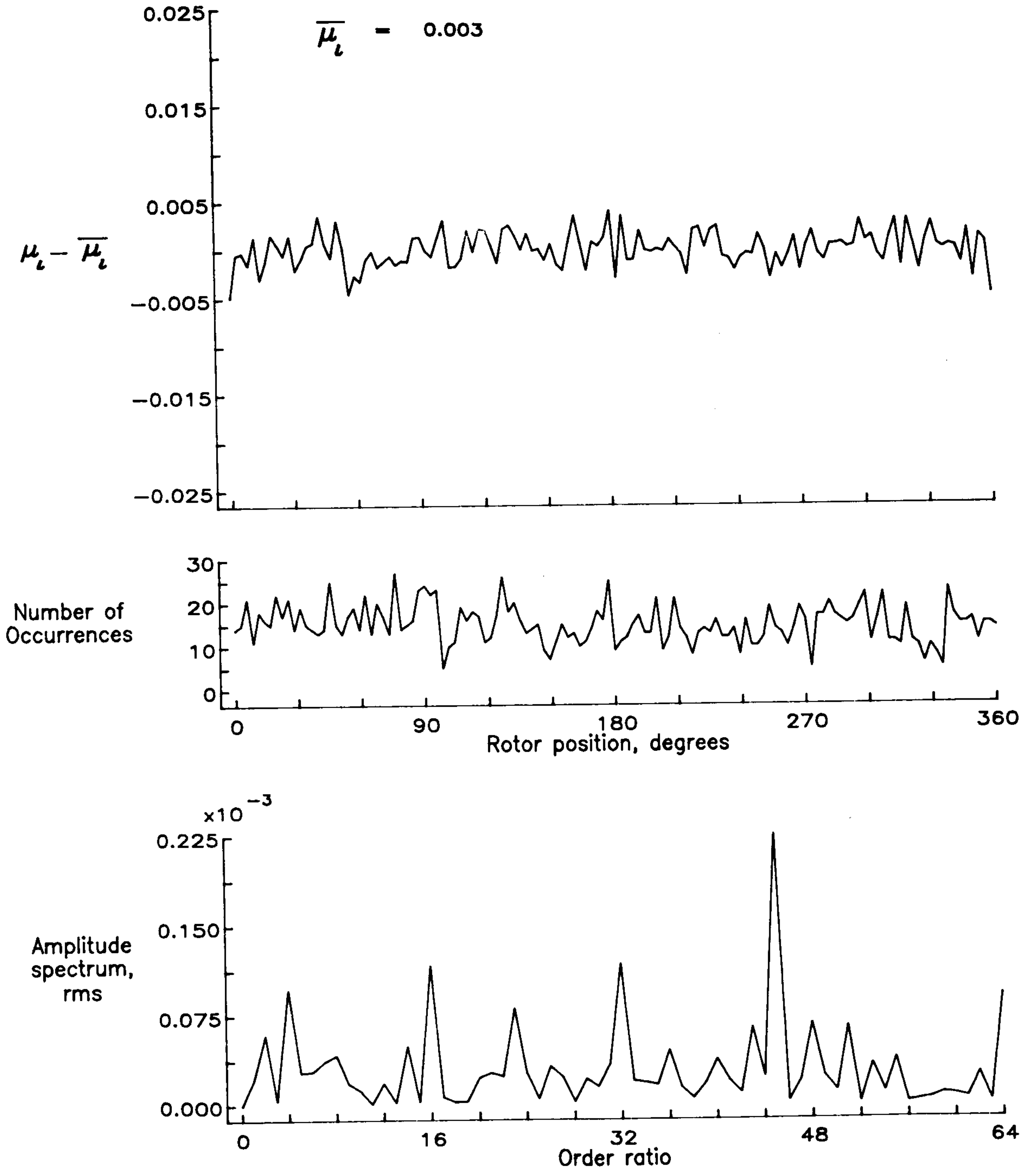

Figure 94.– Induced inflow velocity measured at 180 degrees and r/R of 0.98.

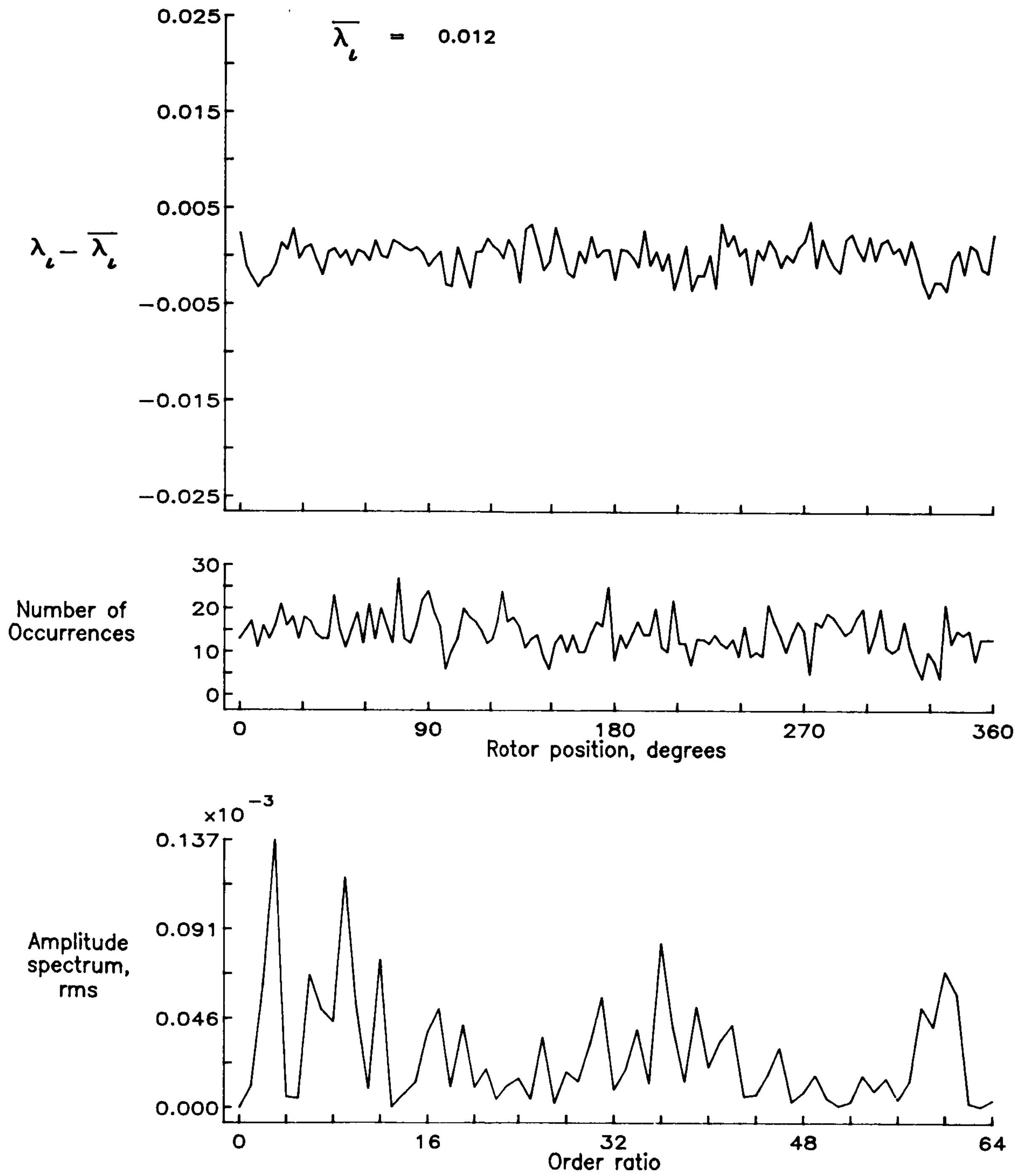

Figure 94.– Concluded.

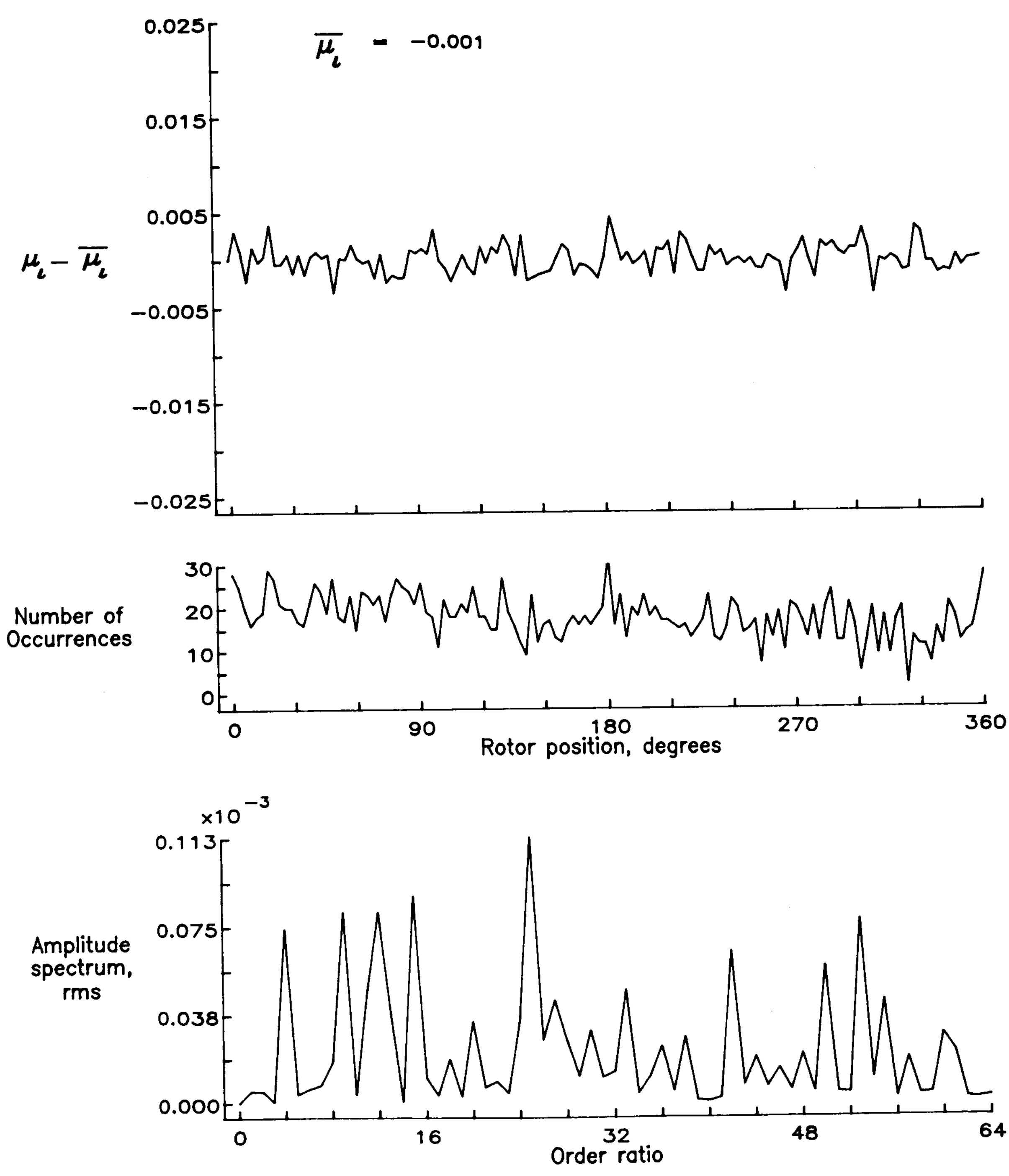

Figure 95.– Induced inflow velocity measured at 180 degrees and r/R of 1.04.

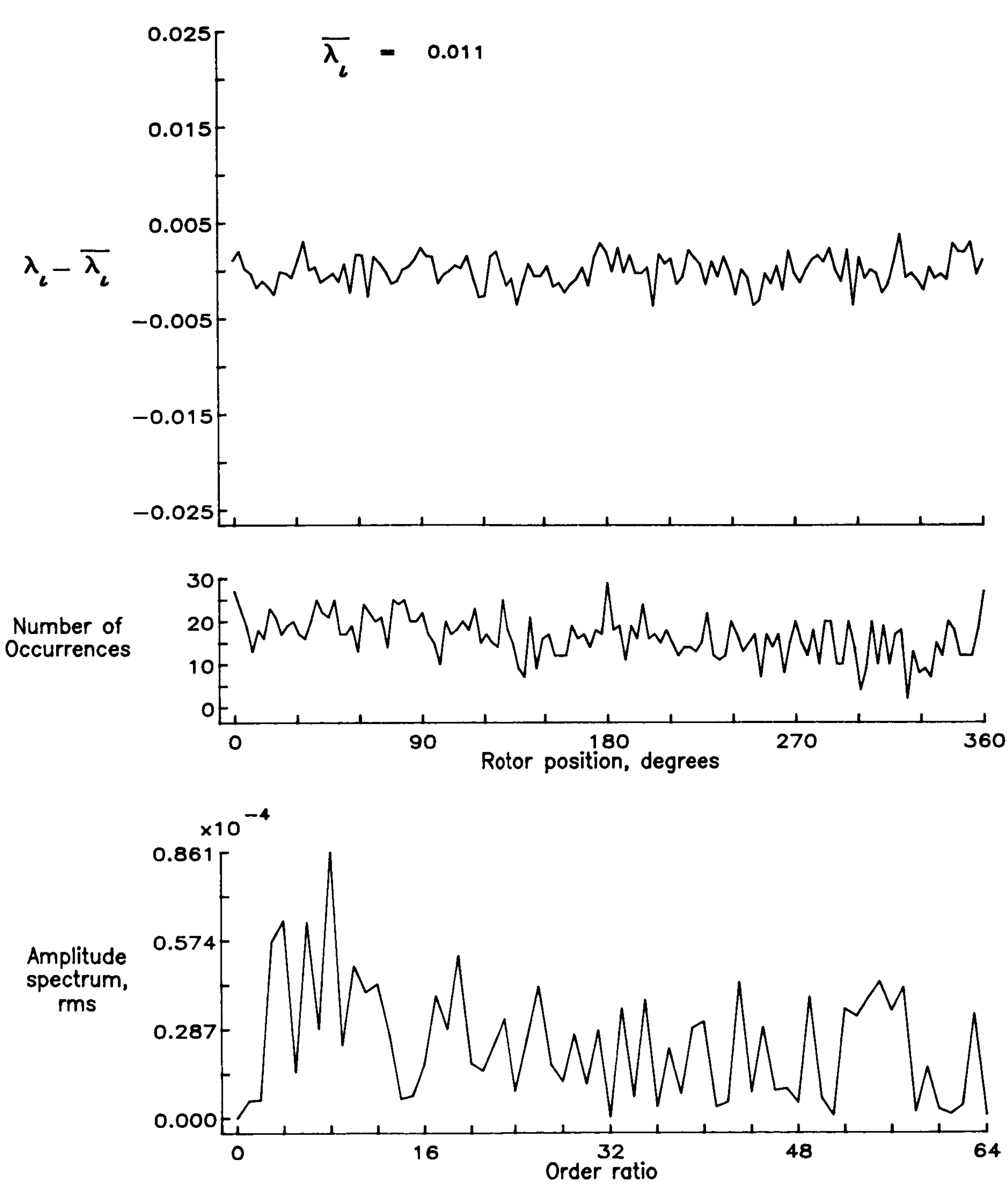

Figure 95.– Concluded.

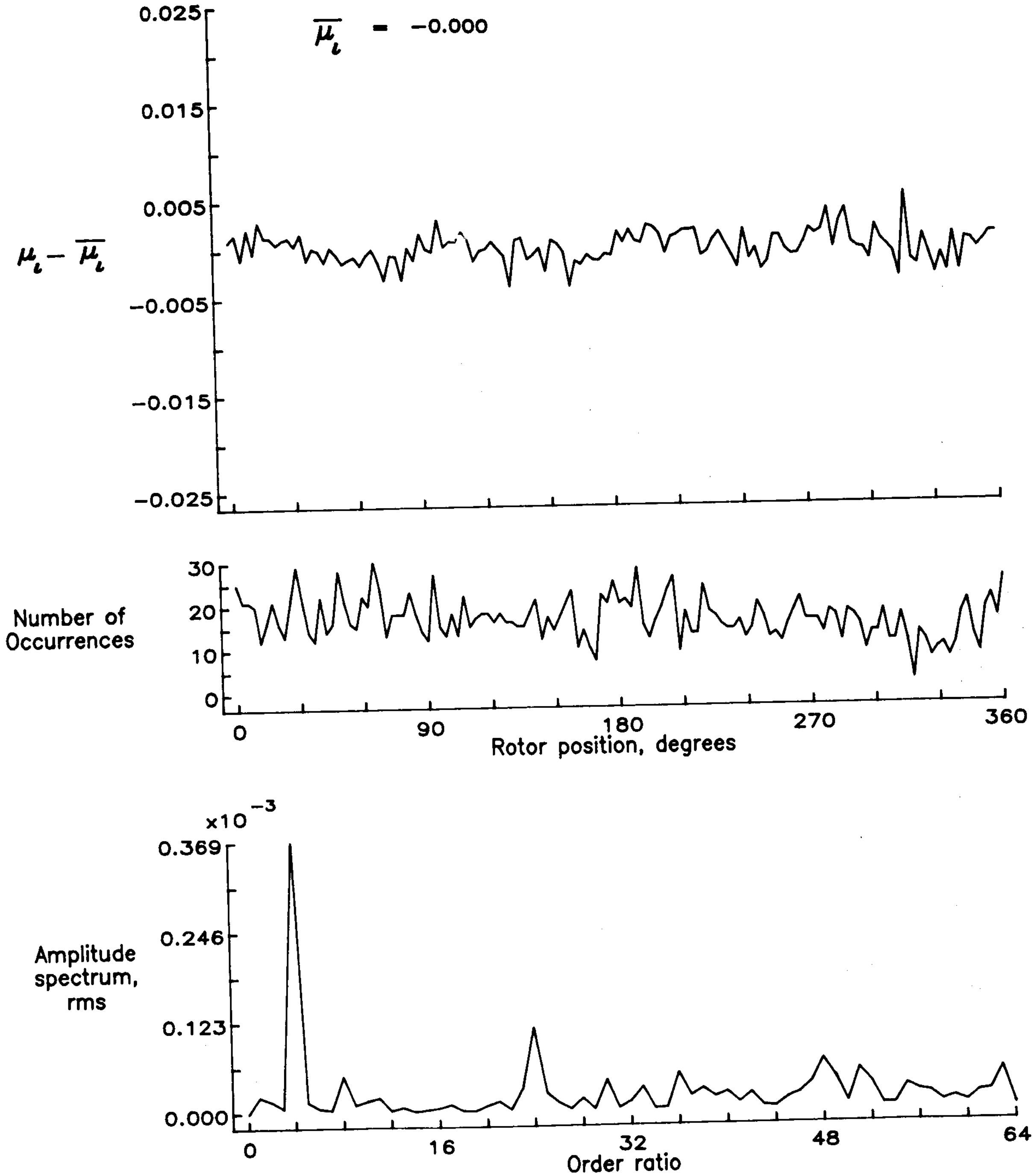

Figure 96.– Induced inflow velocity measured at 180 degrees and r/R of 1.10.

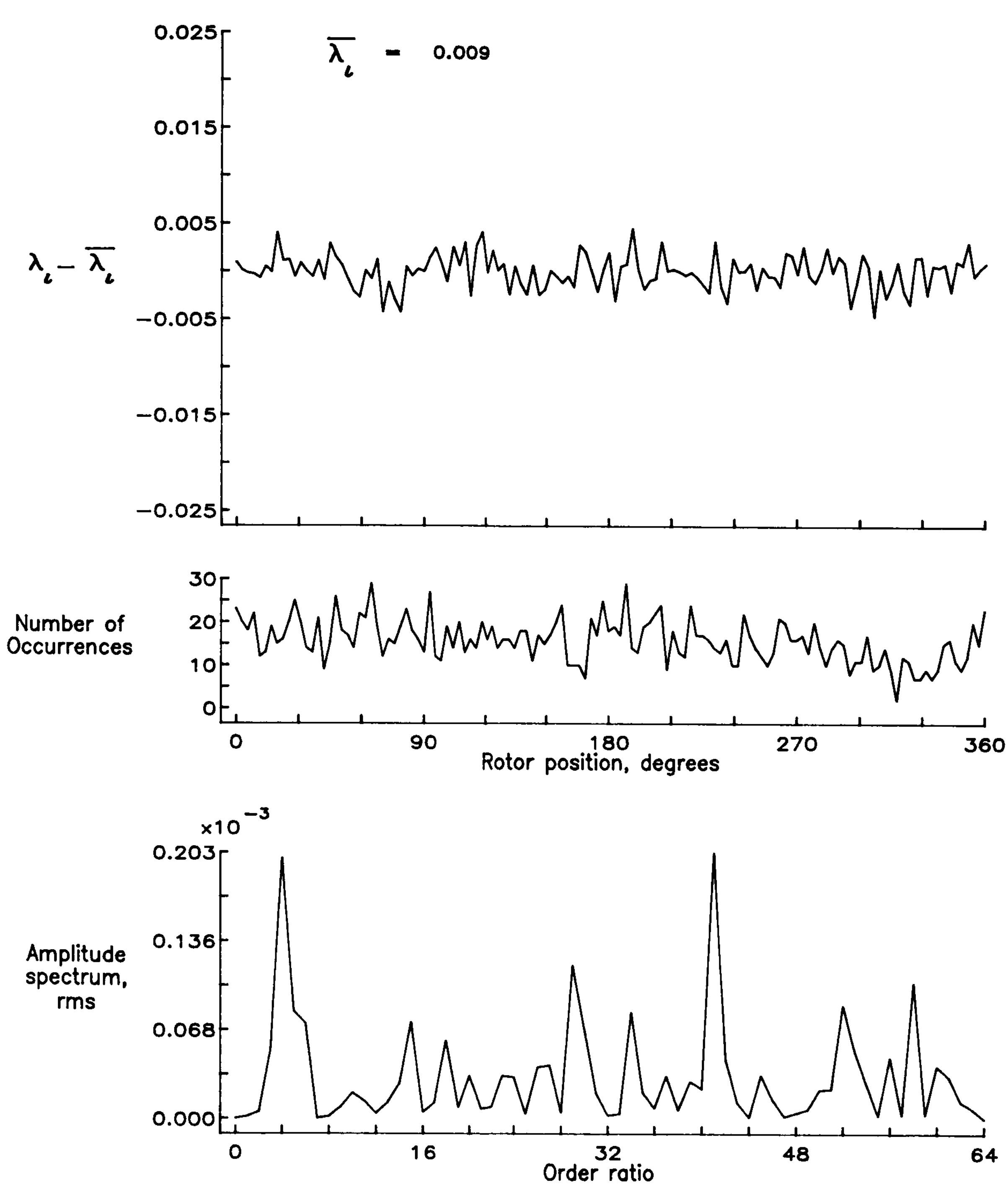

Figure 96.– Concluded.

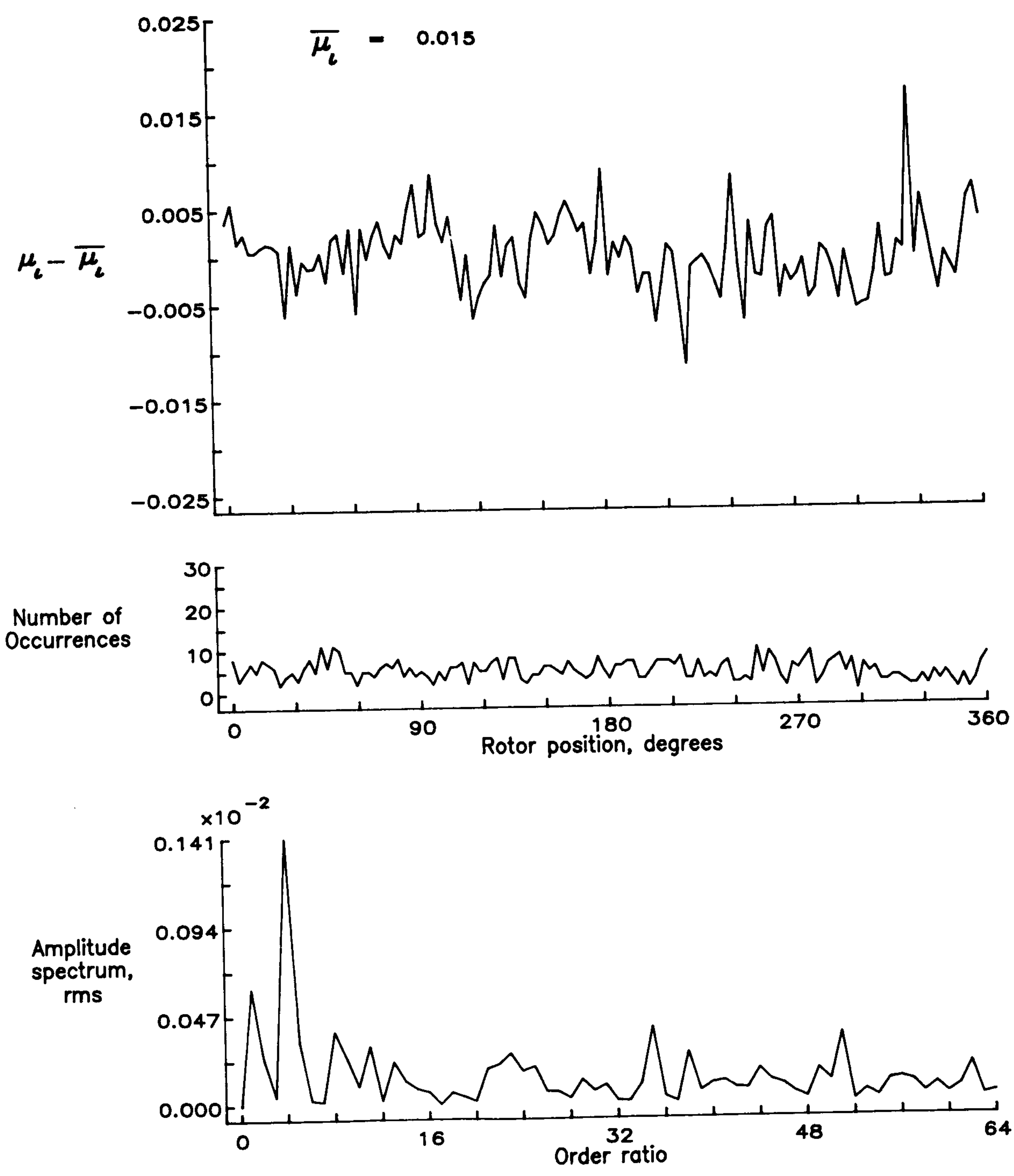

Figure 97.– Induced inflow velocity measured at 210 degrees and r/R of 0.40.

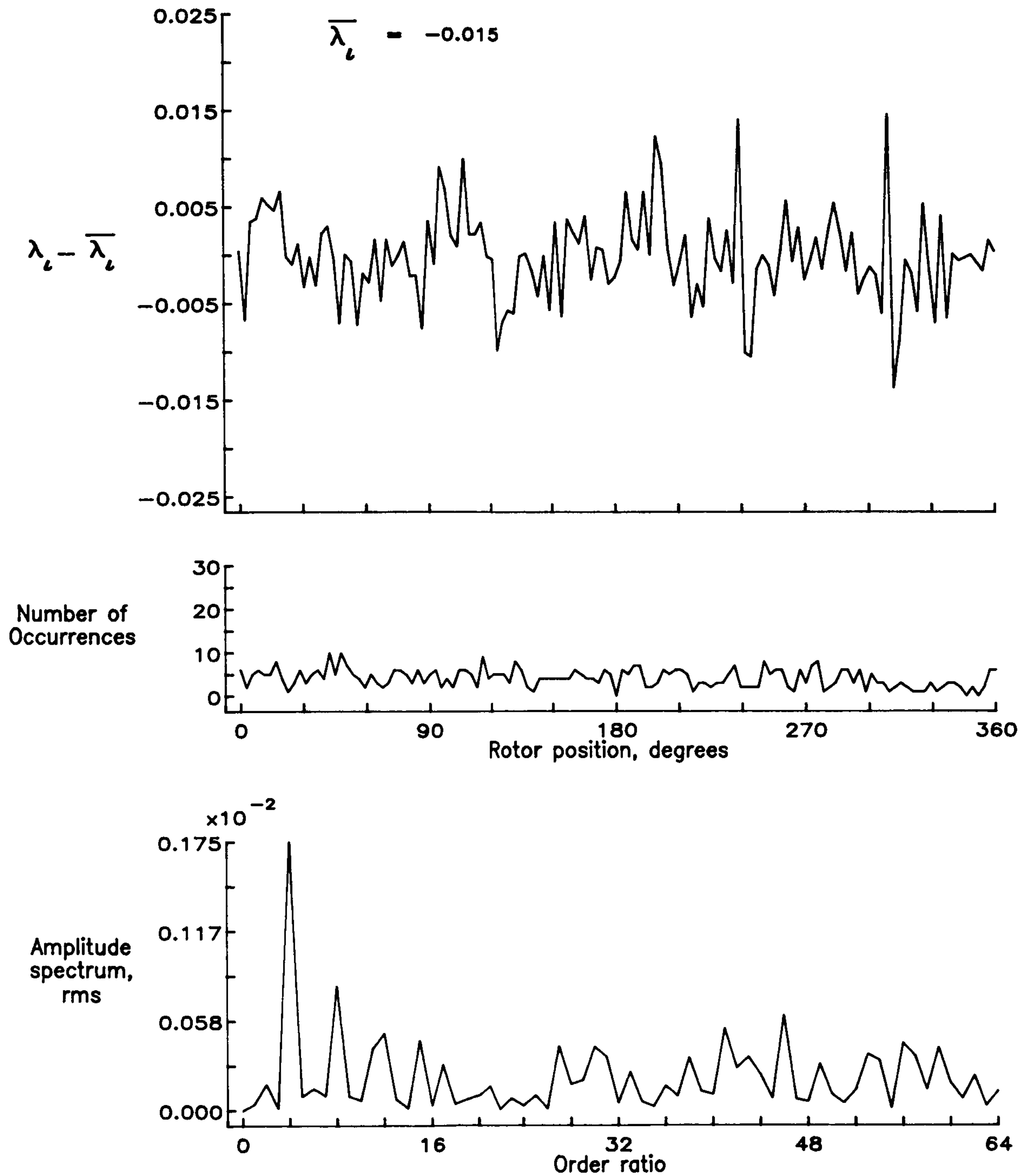

Figure 97.– Concluded.

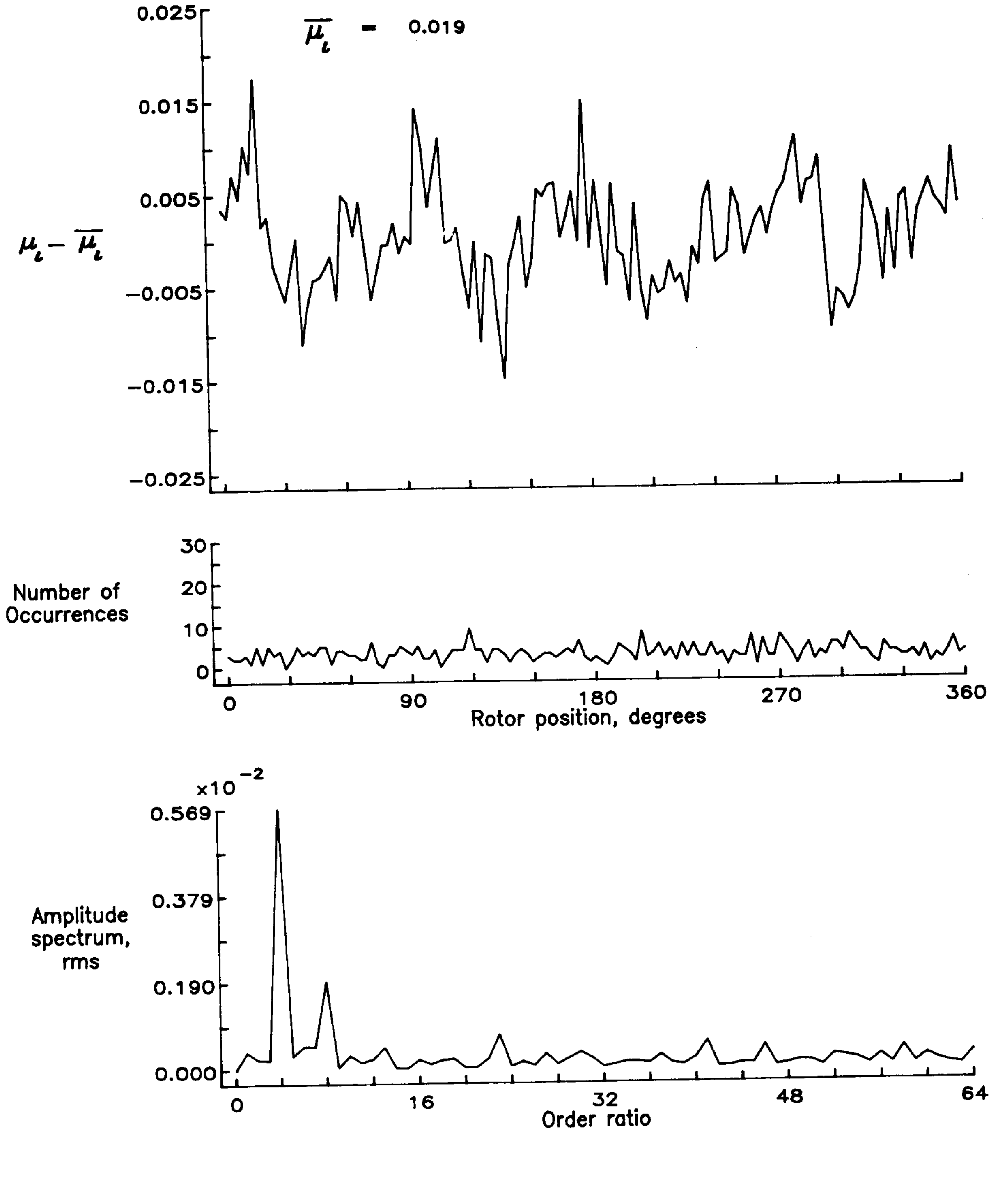

Figure 98.– Induced inflow velocity measured at 210 degrees and r/R of 0.50.

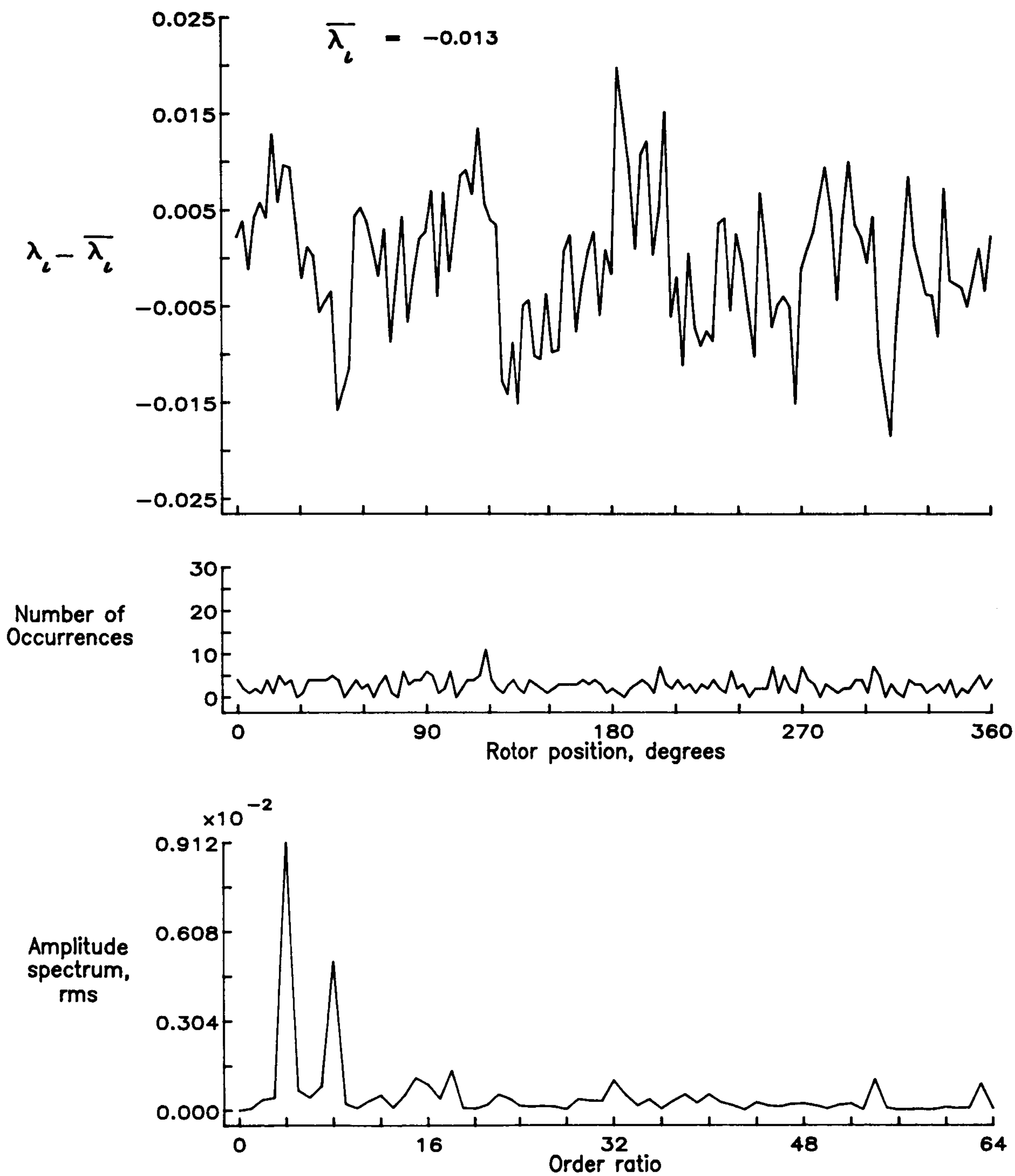

Figure 98.– Concluded.

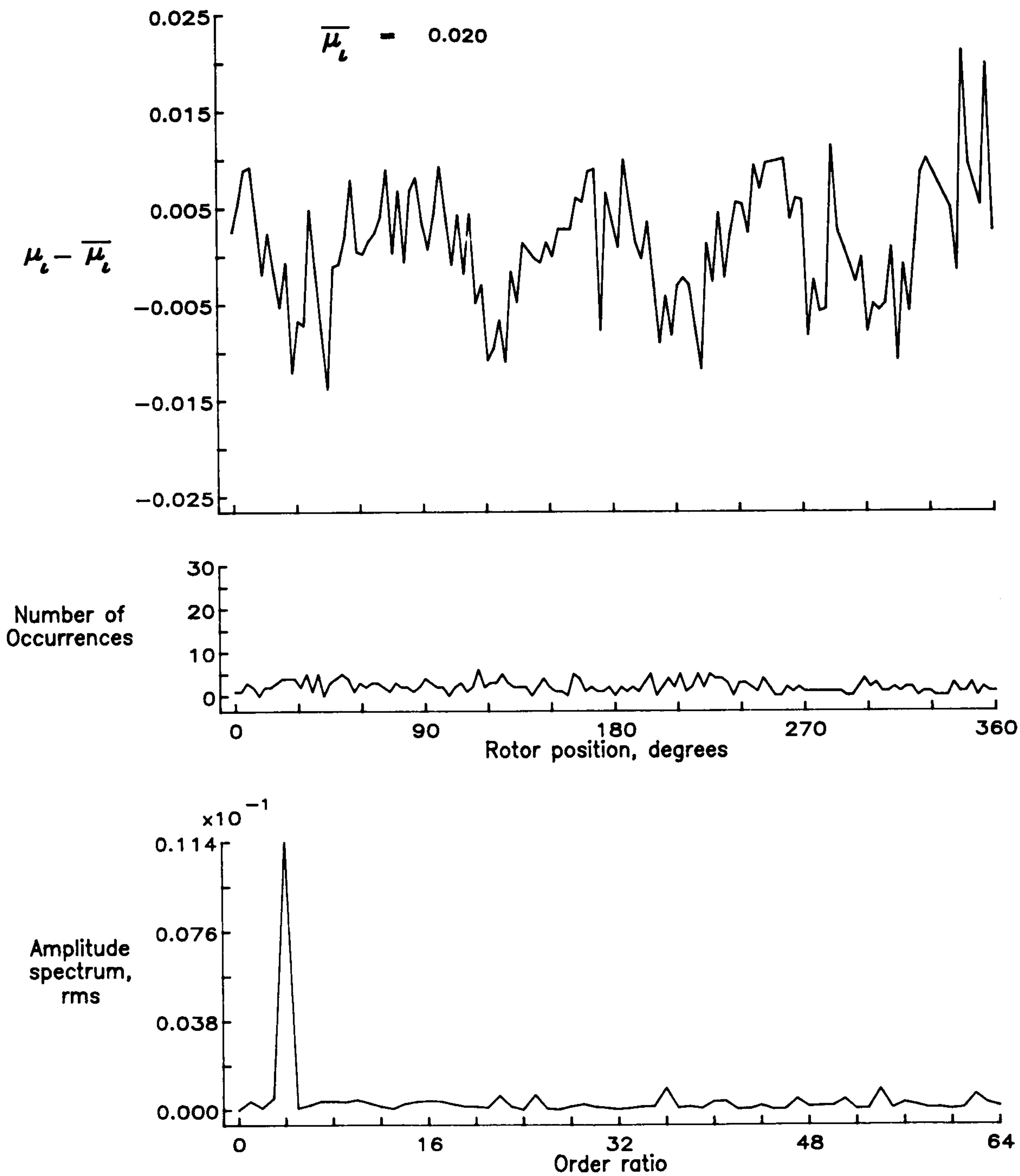

Figure 99.– Induced inflow velocity measured at 210 degrees and r/R of 0.60.

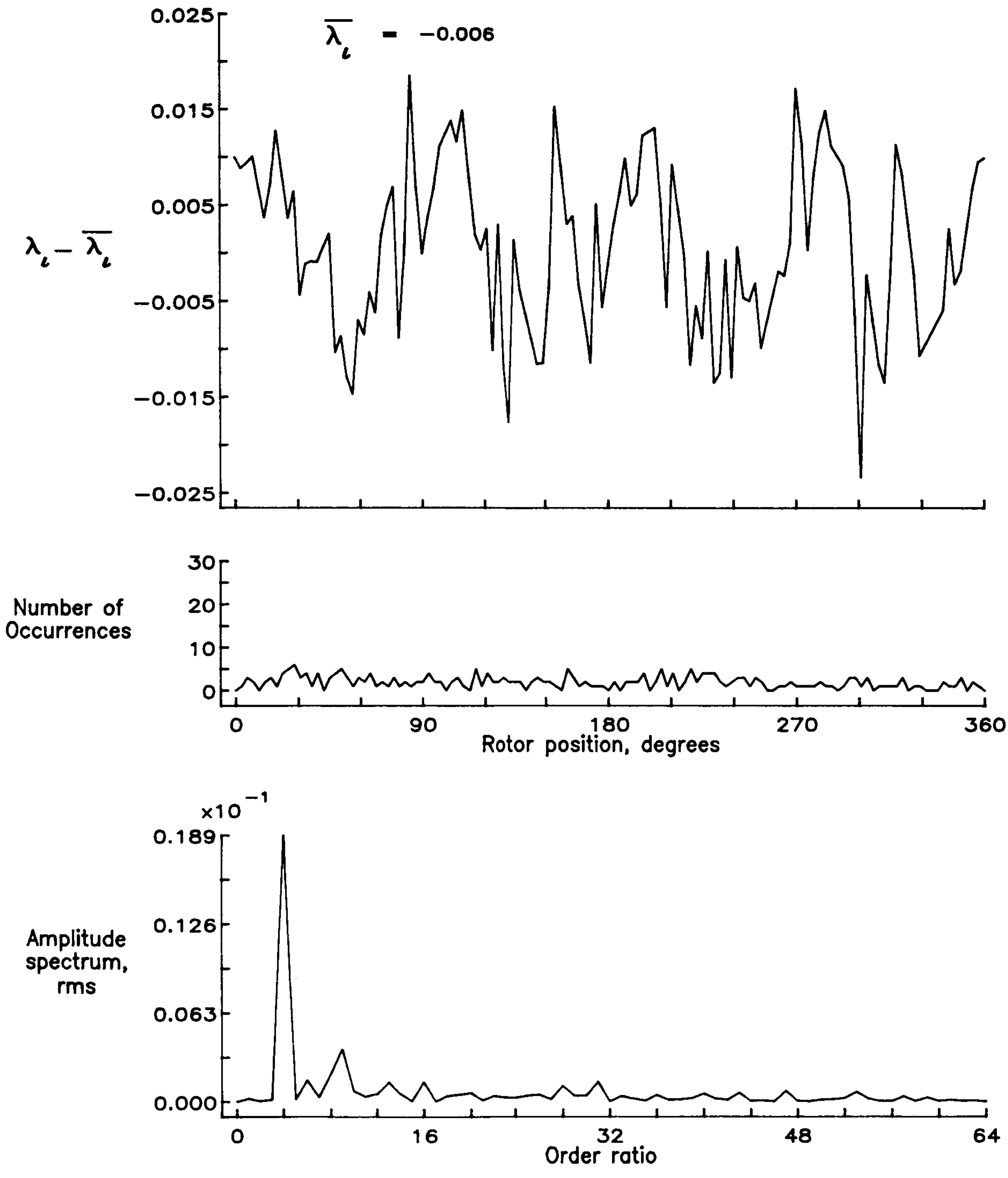

Figure 99.– Concluded.

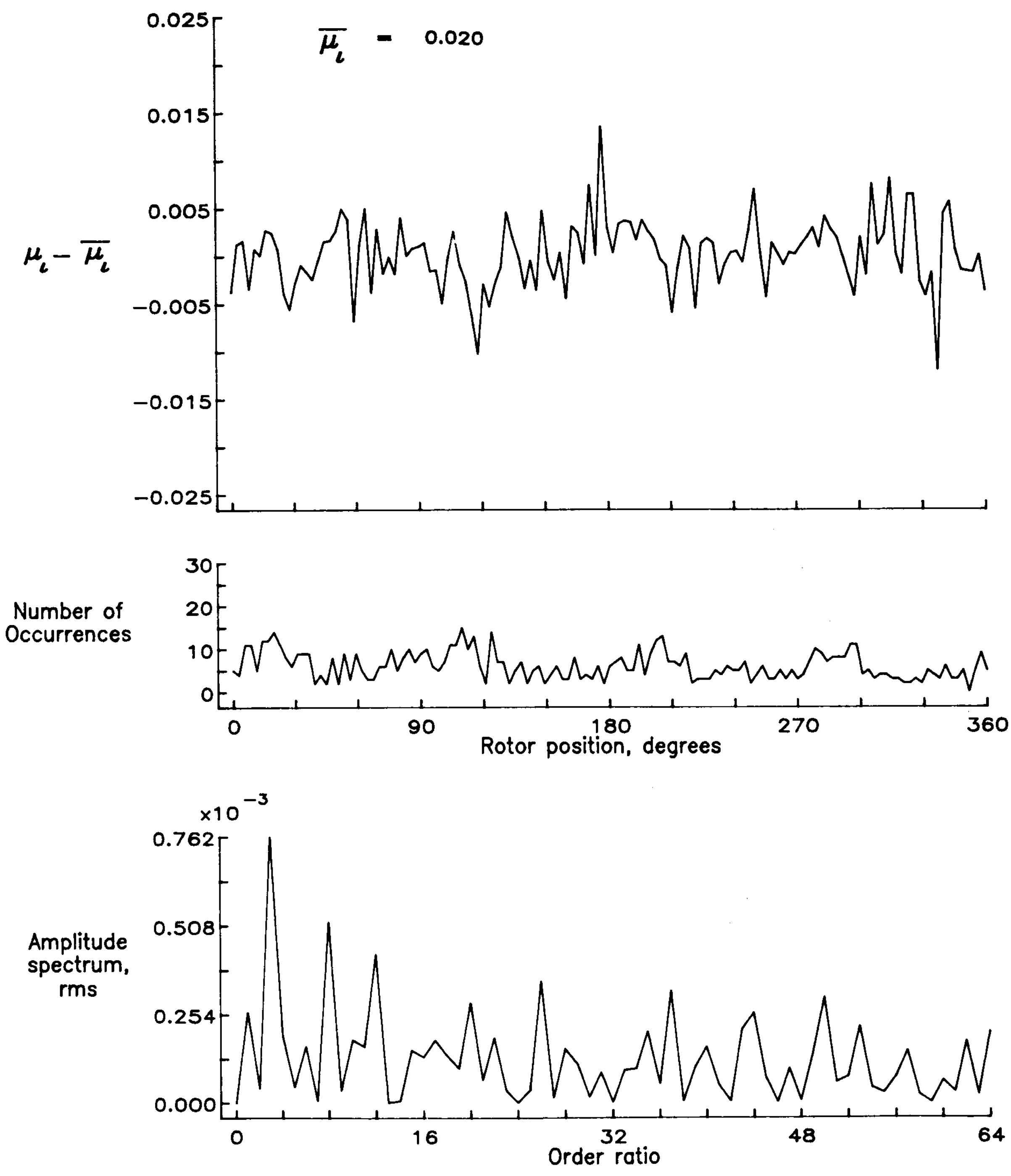

Figure 100.– Induced inflow velocity measured at 210 degrees and r/R of 0.74.

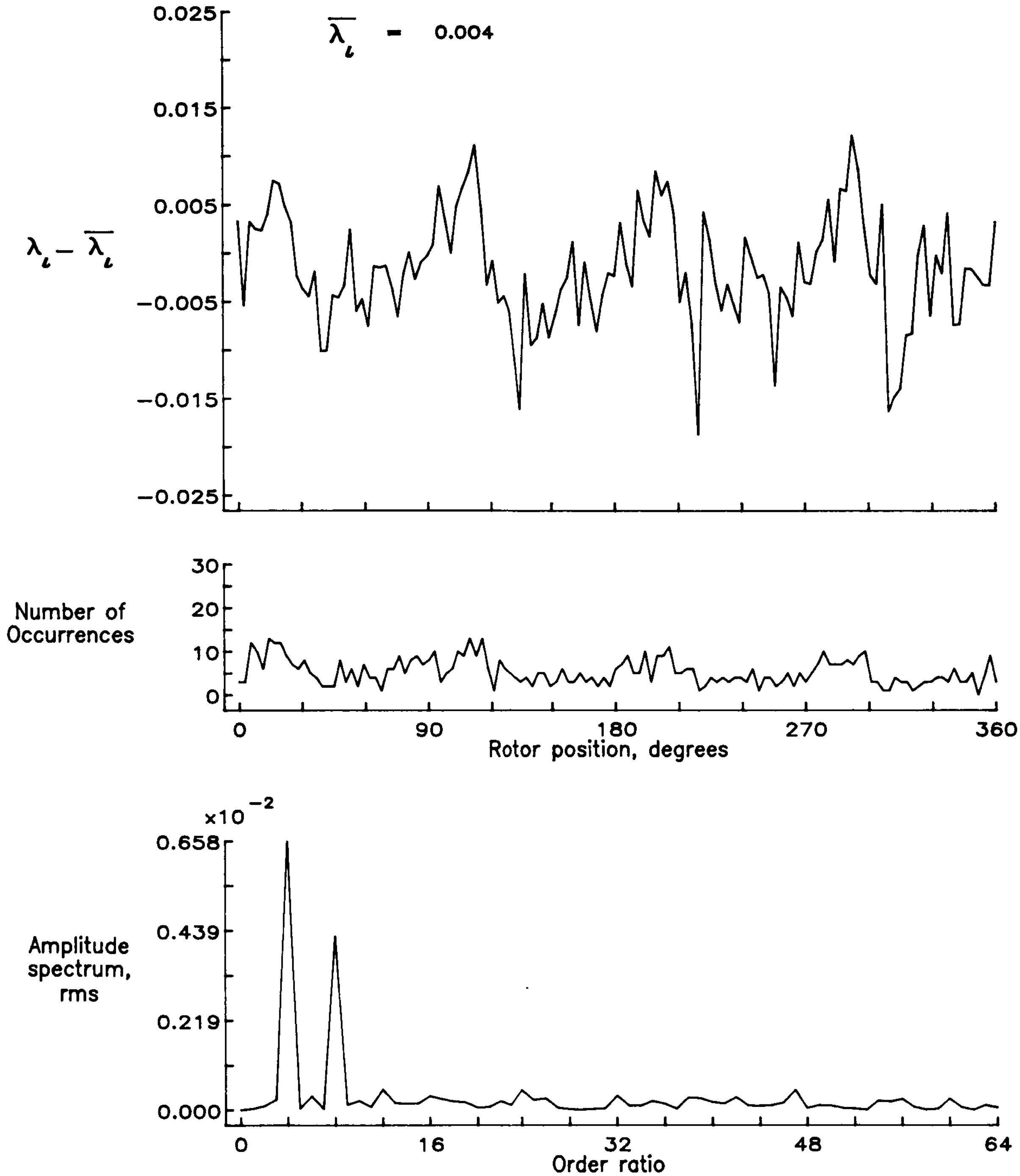

Figure 100.– Concluded.

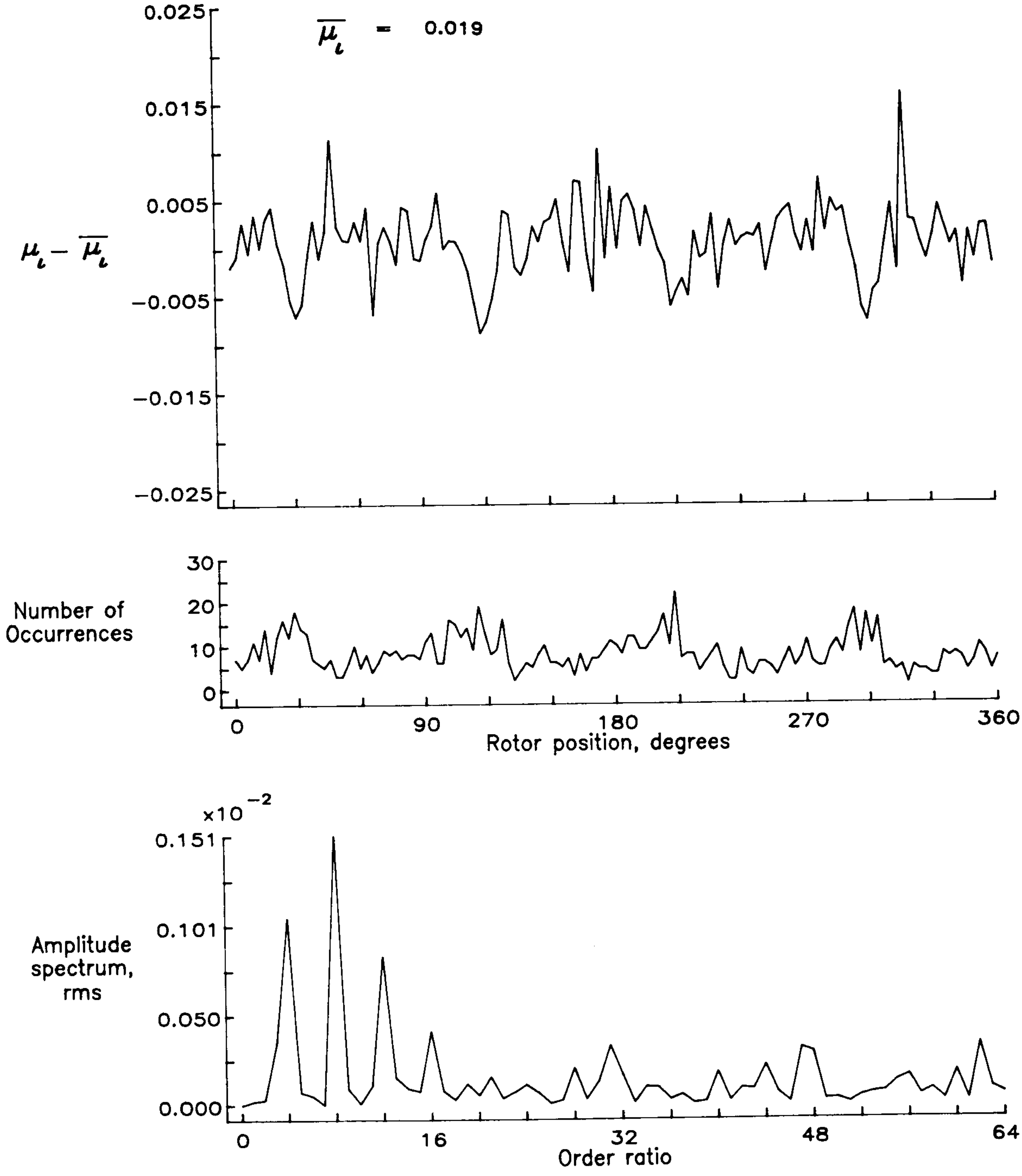

Figure 101.– Induced inflow velocity measured at 210 degrees and r/R of 0.78.

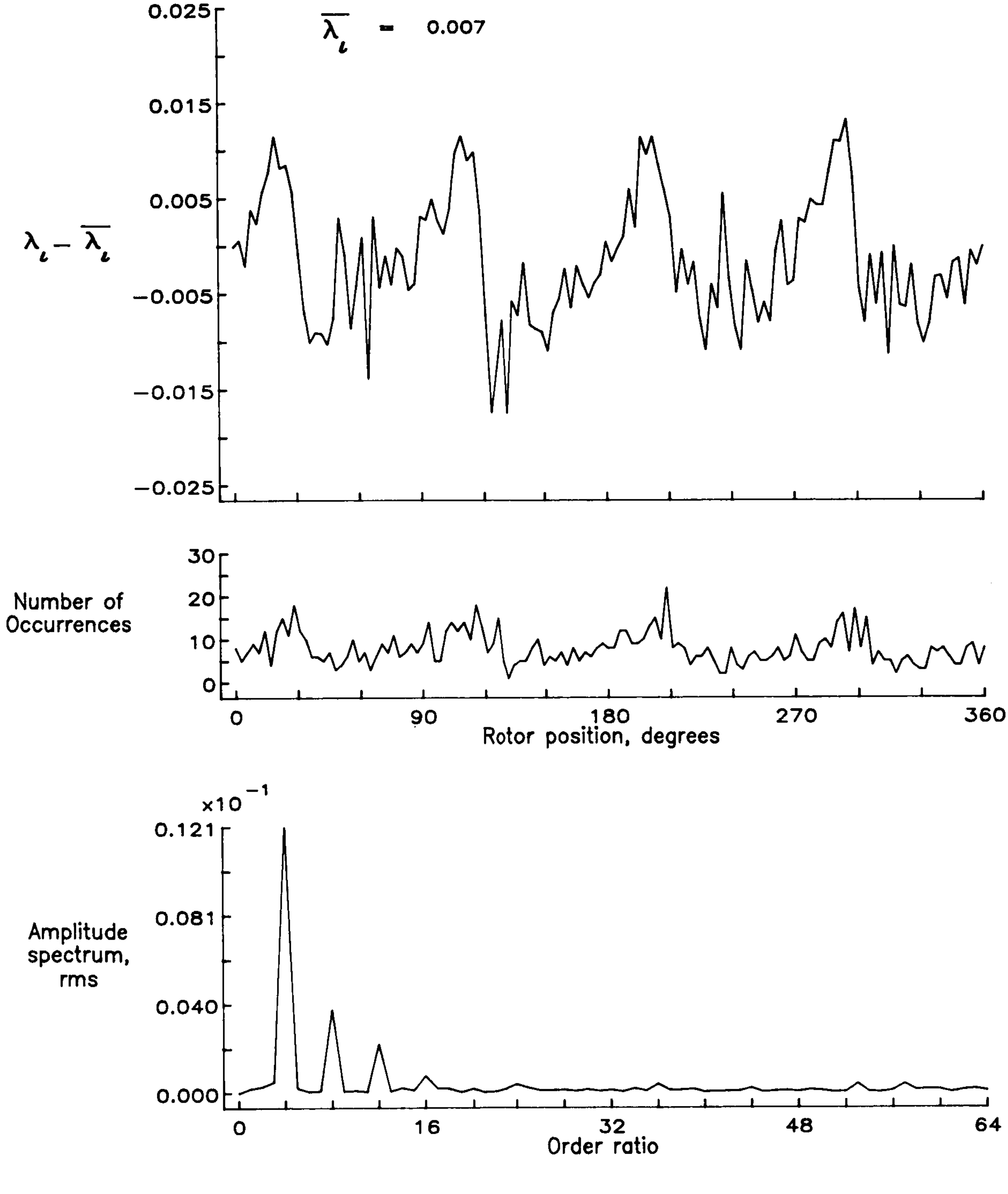

Figure 101.– Concluded.

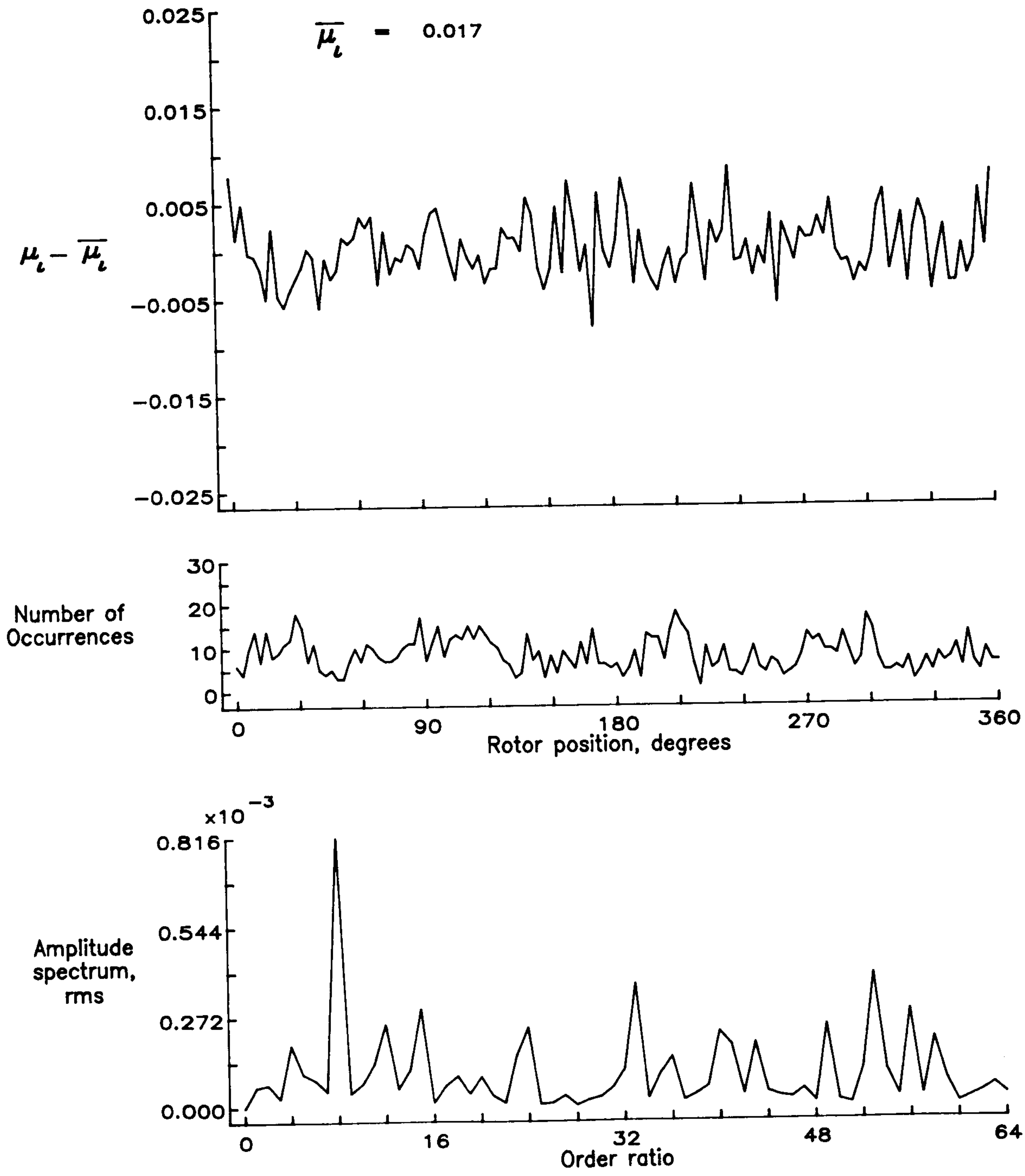

Figure 102.– Induced inflow velocity measured at 210 degrees and r/R of 0.82.

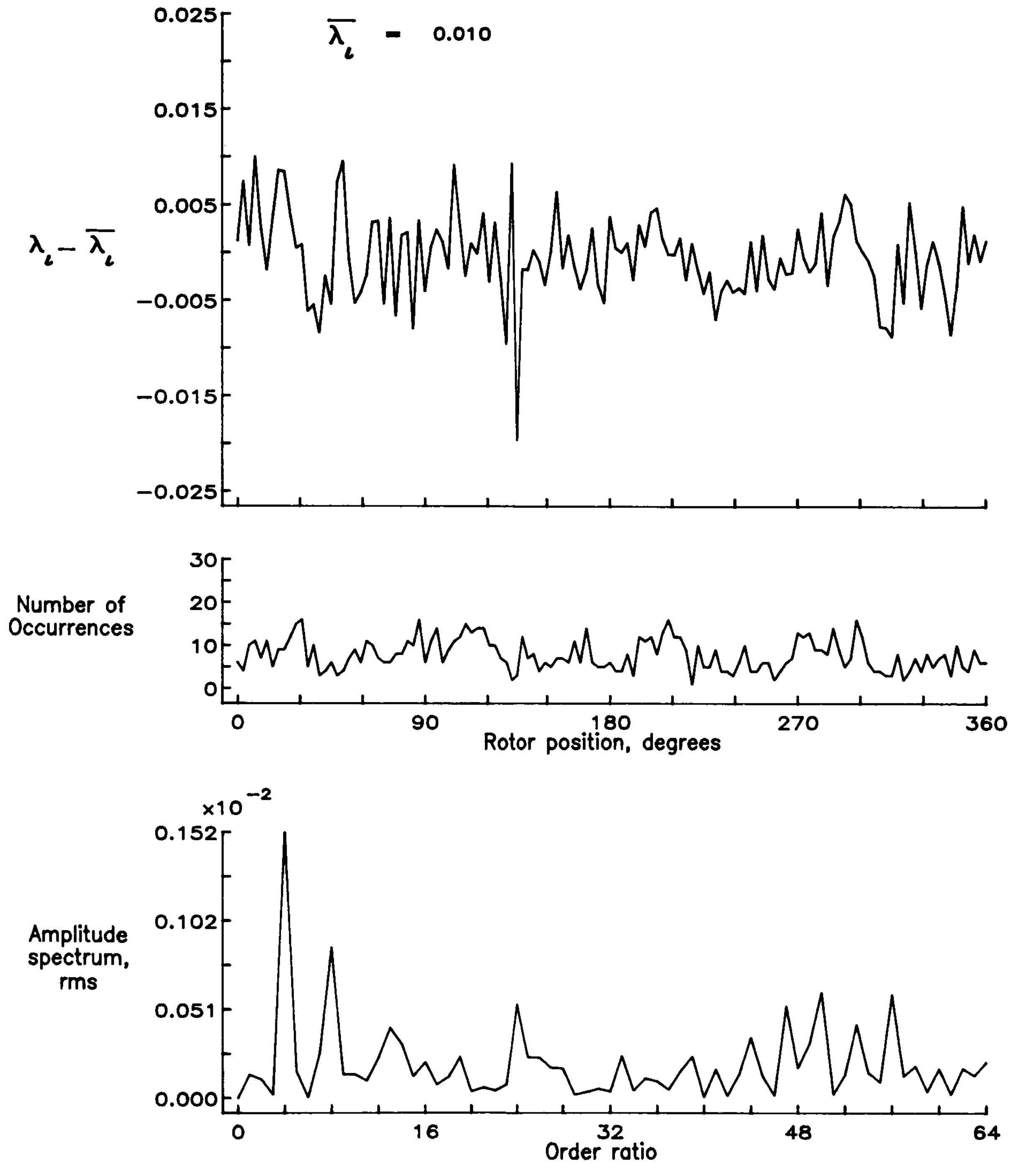

Figure 102.– Concluded.

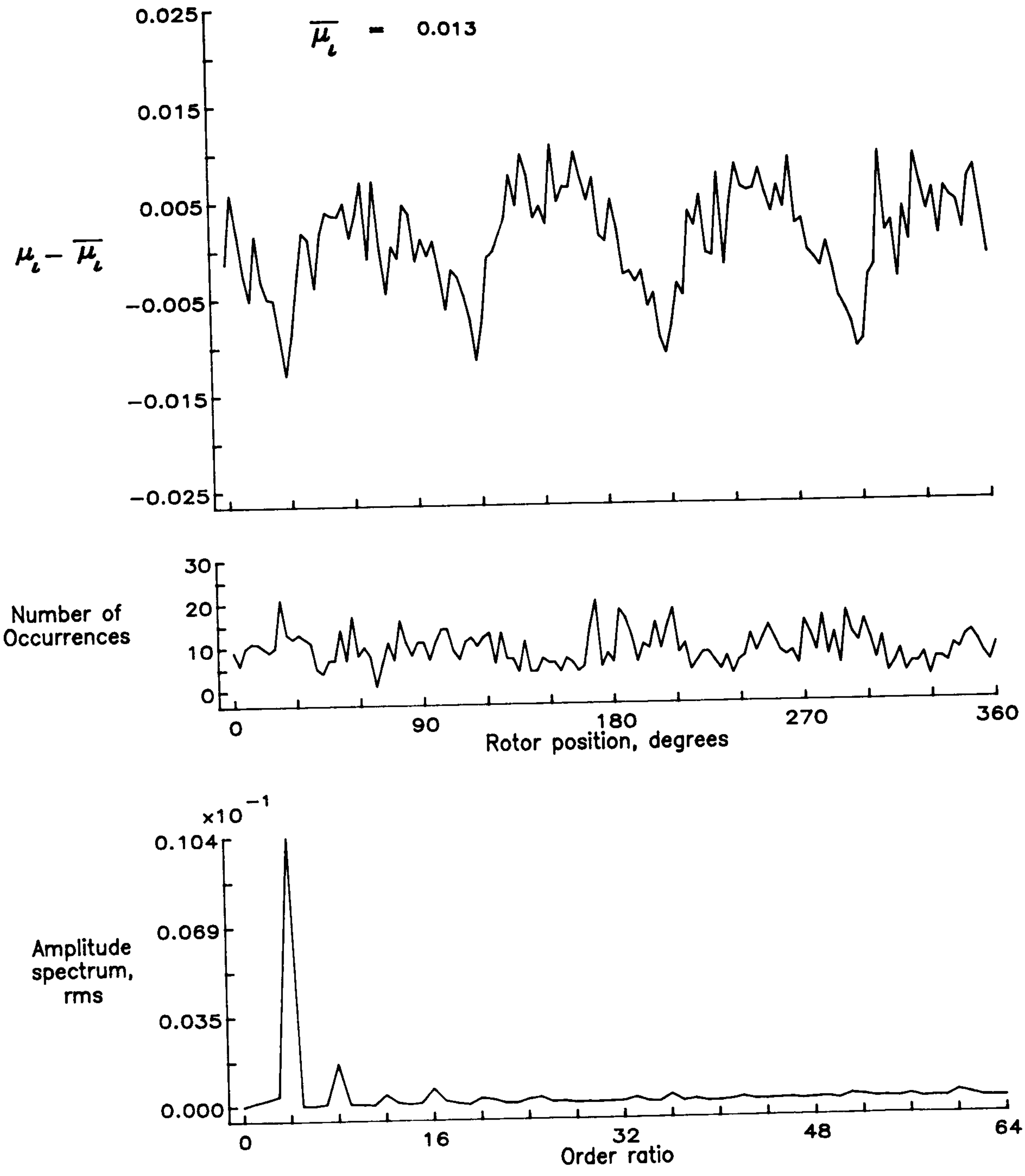

Figure 103.– Induced inflow velocity measured at 210 degrees and r/R of 0.86.

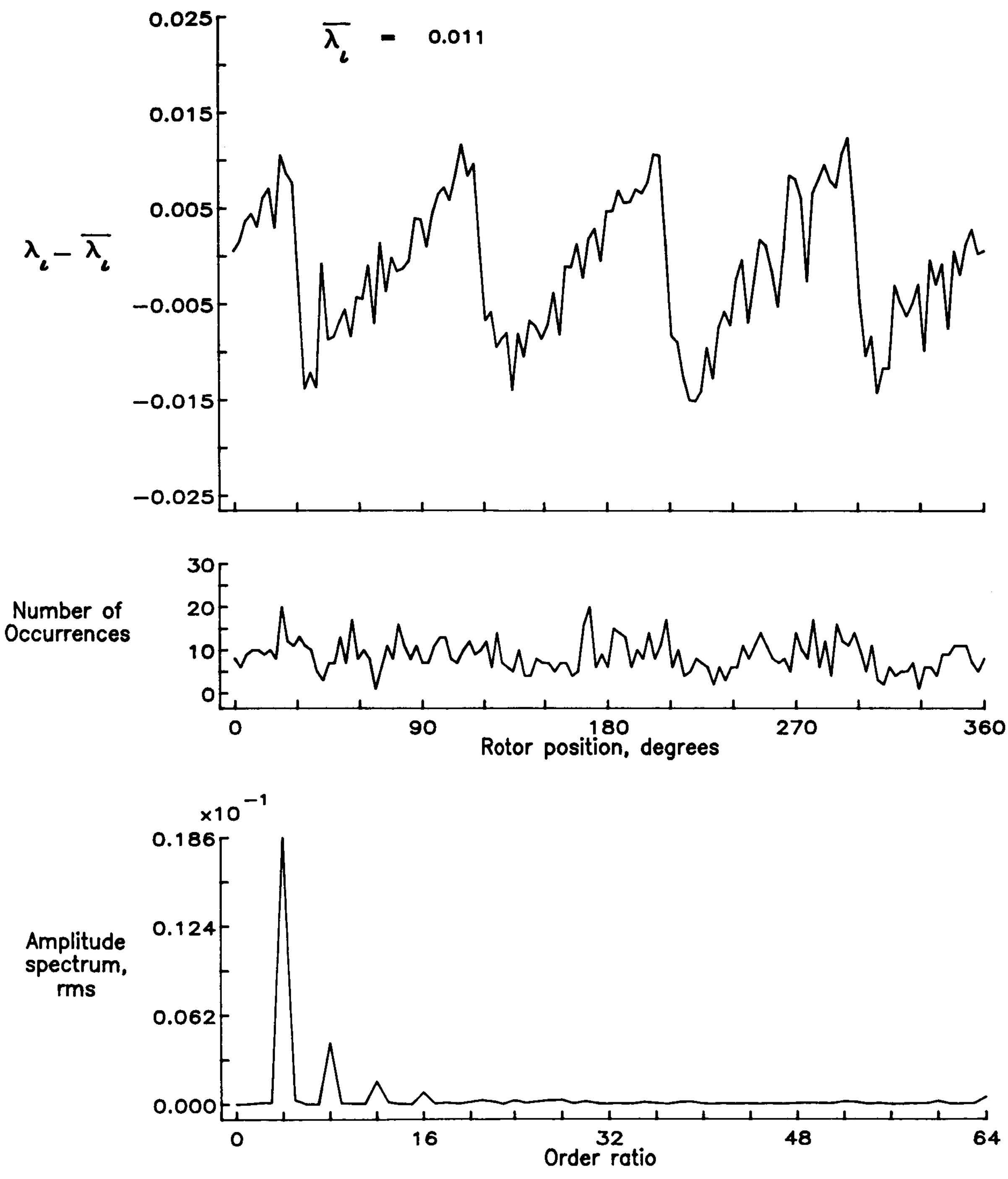

Figure 103.– Concluded.

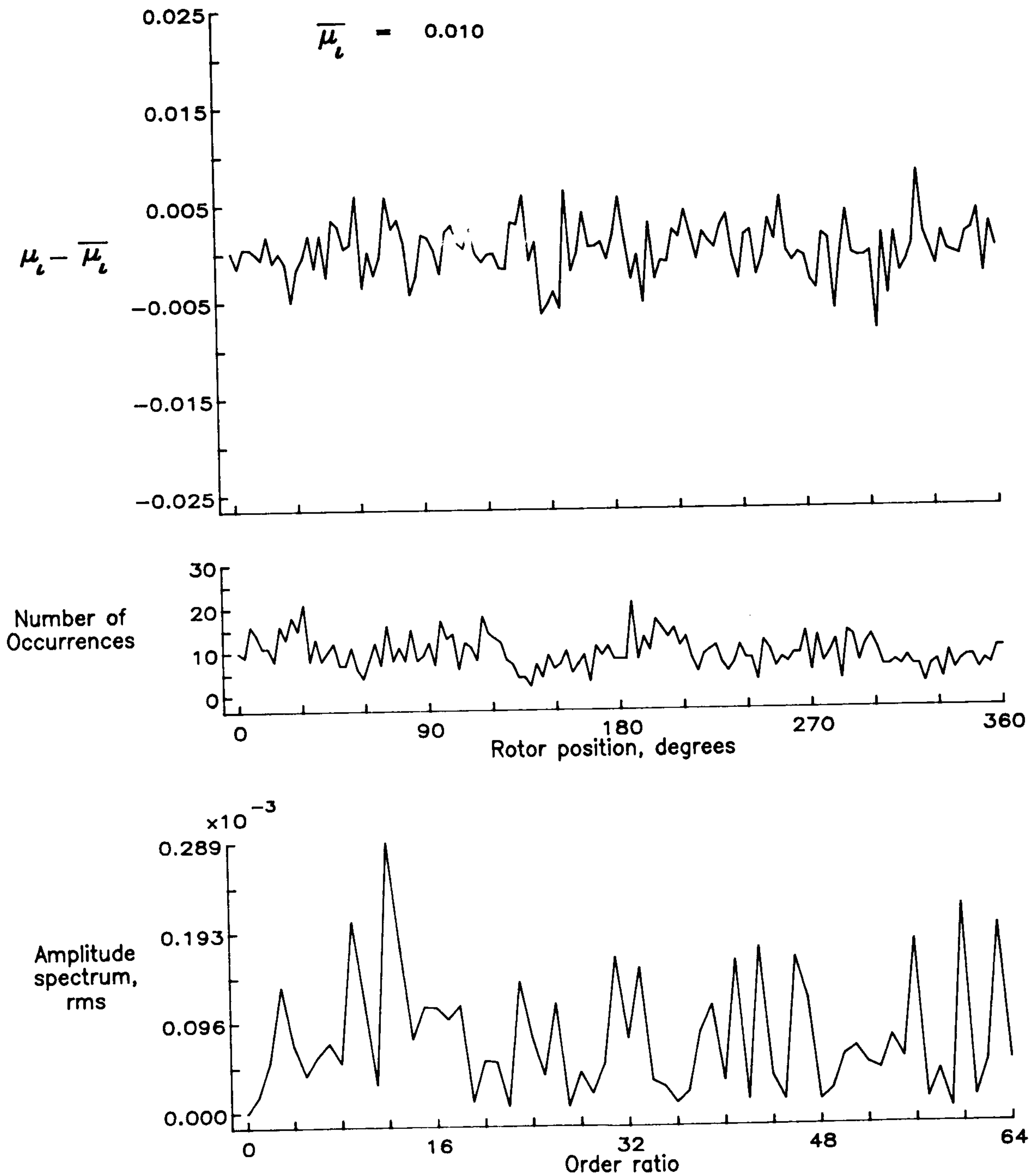

Figure 104.– Induced inflow velocity measured at 210 degrees and r/R of 0.90.

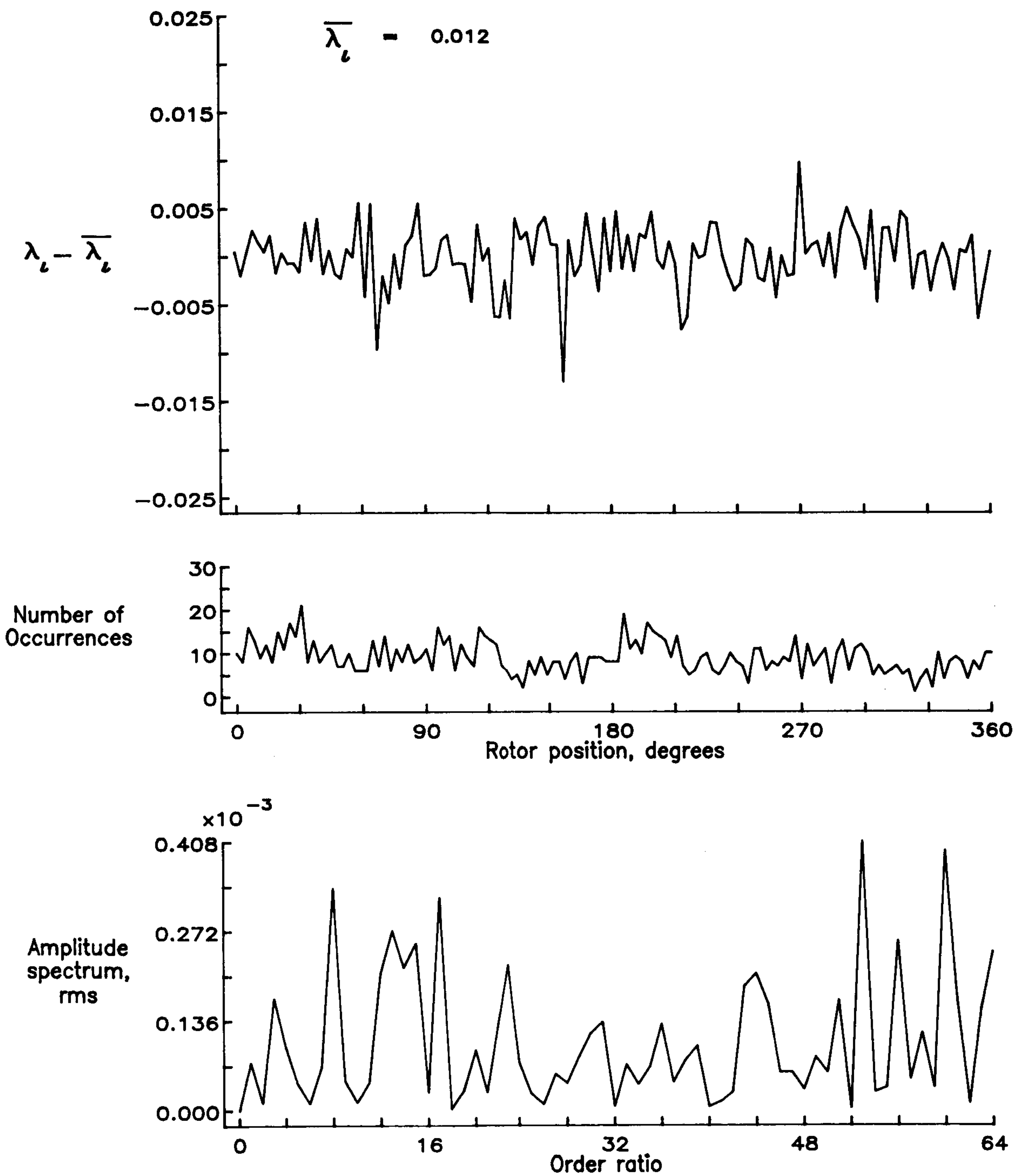

Figure 104.– Concluded.

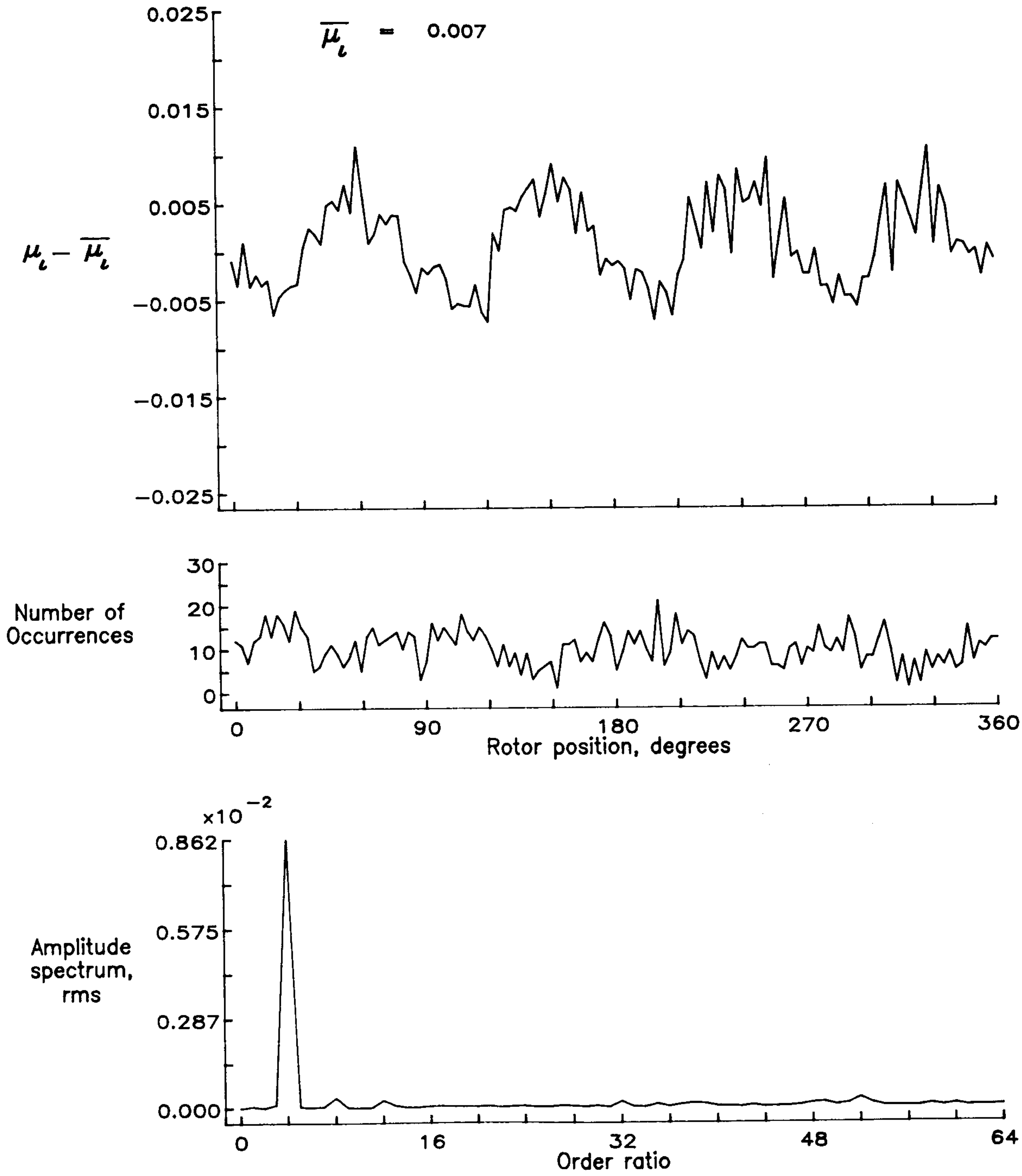

Figure 105.– Induced inflow velocity measured at 210 degrees and r/R of 0.94.

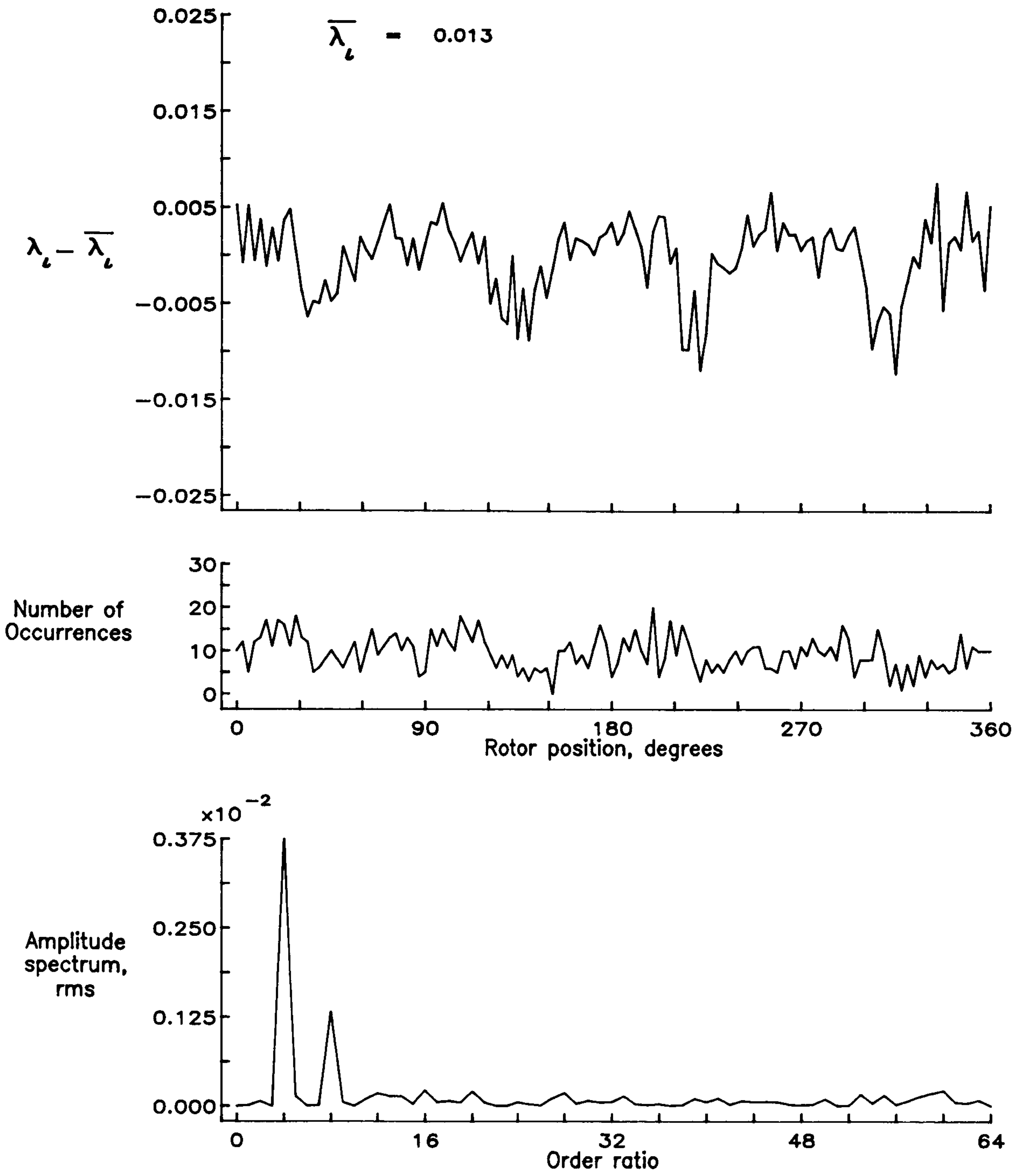

Figure 105.– Concluded.

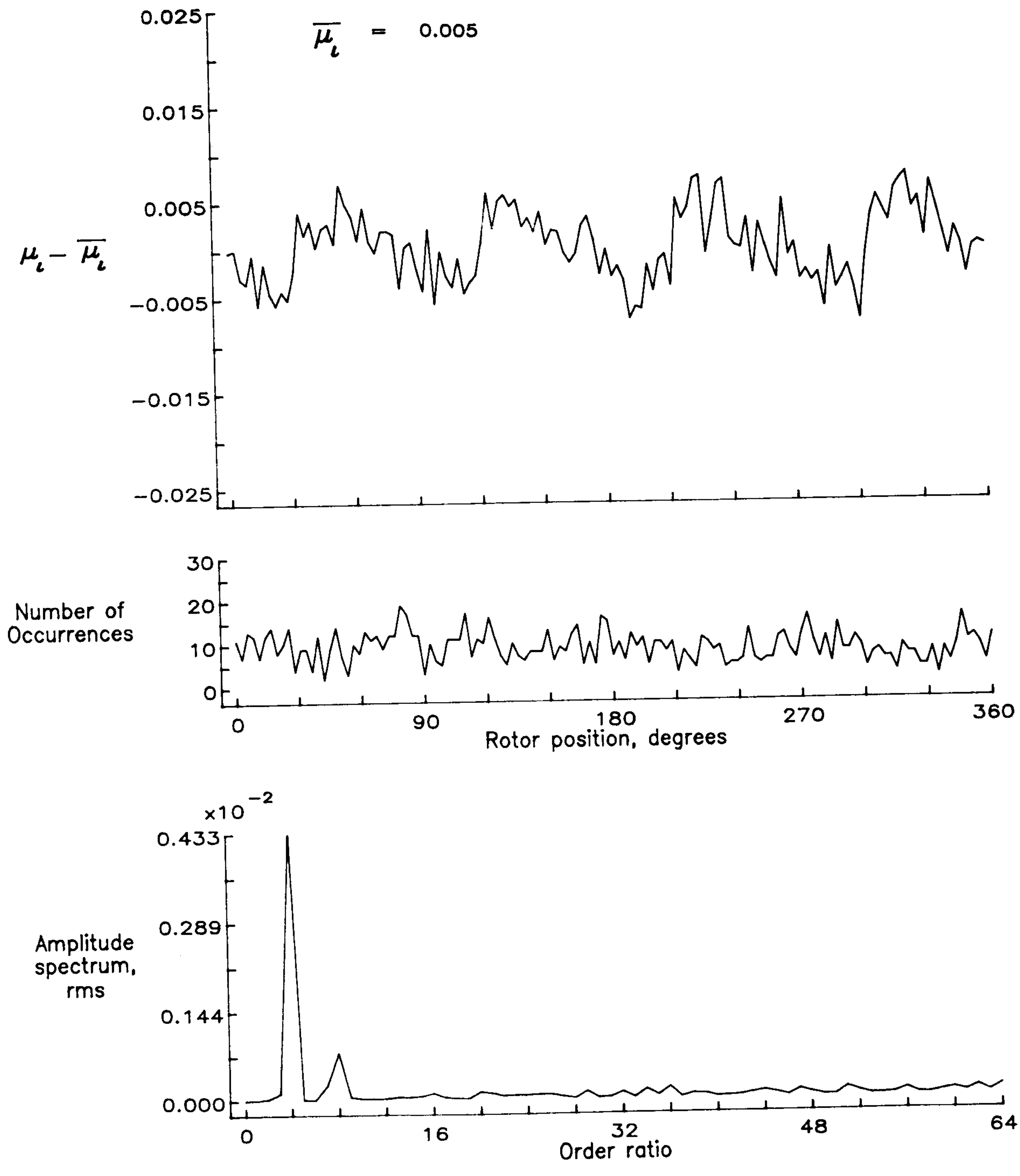

Figure 106.— Induced inflow velocity measured at 210 degrees and r/R of 0.98.

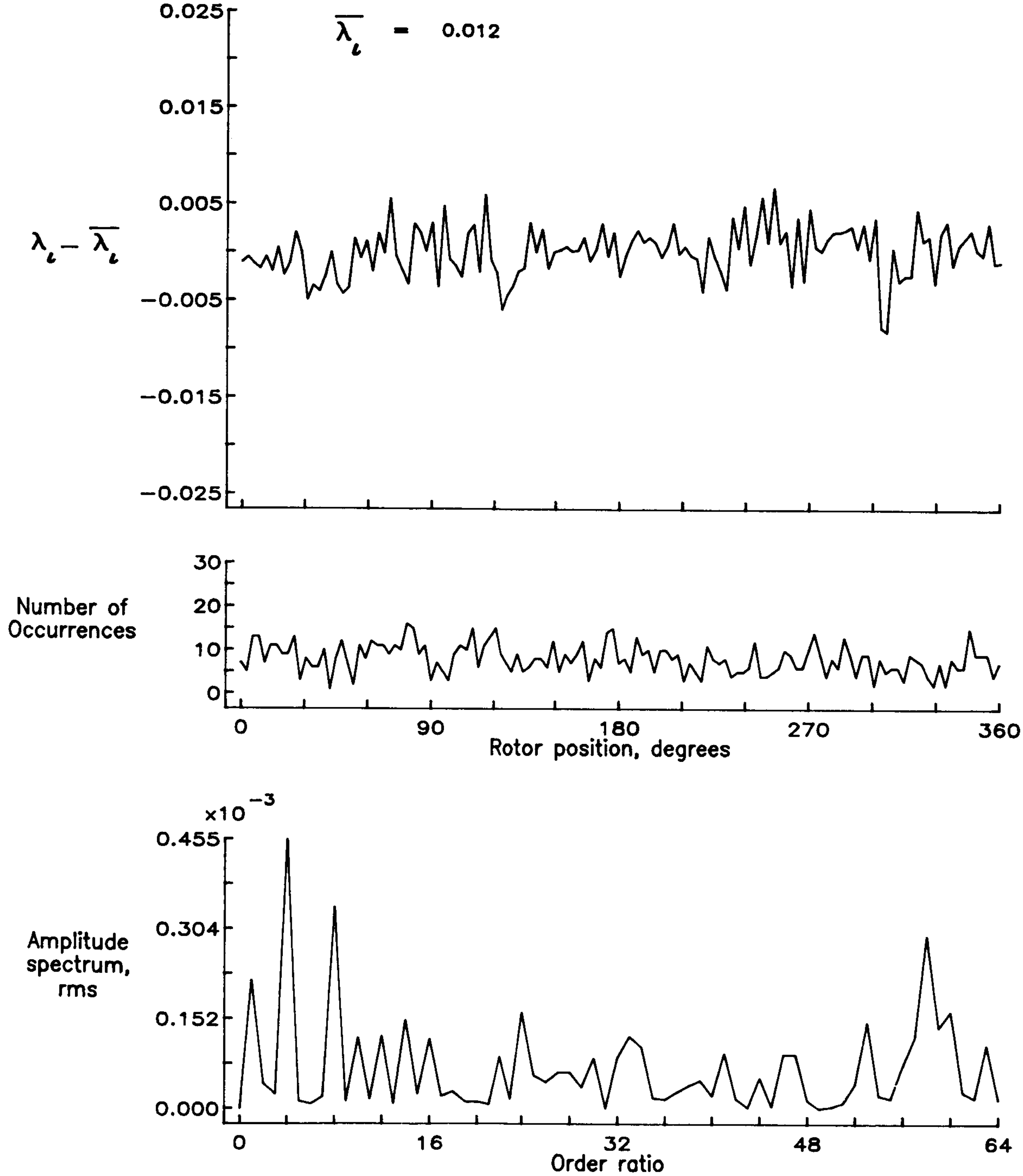

Figure 106.– Concluded.

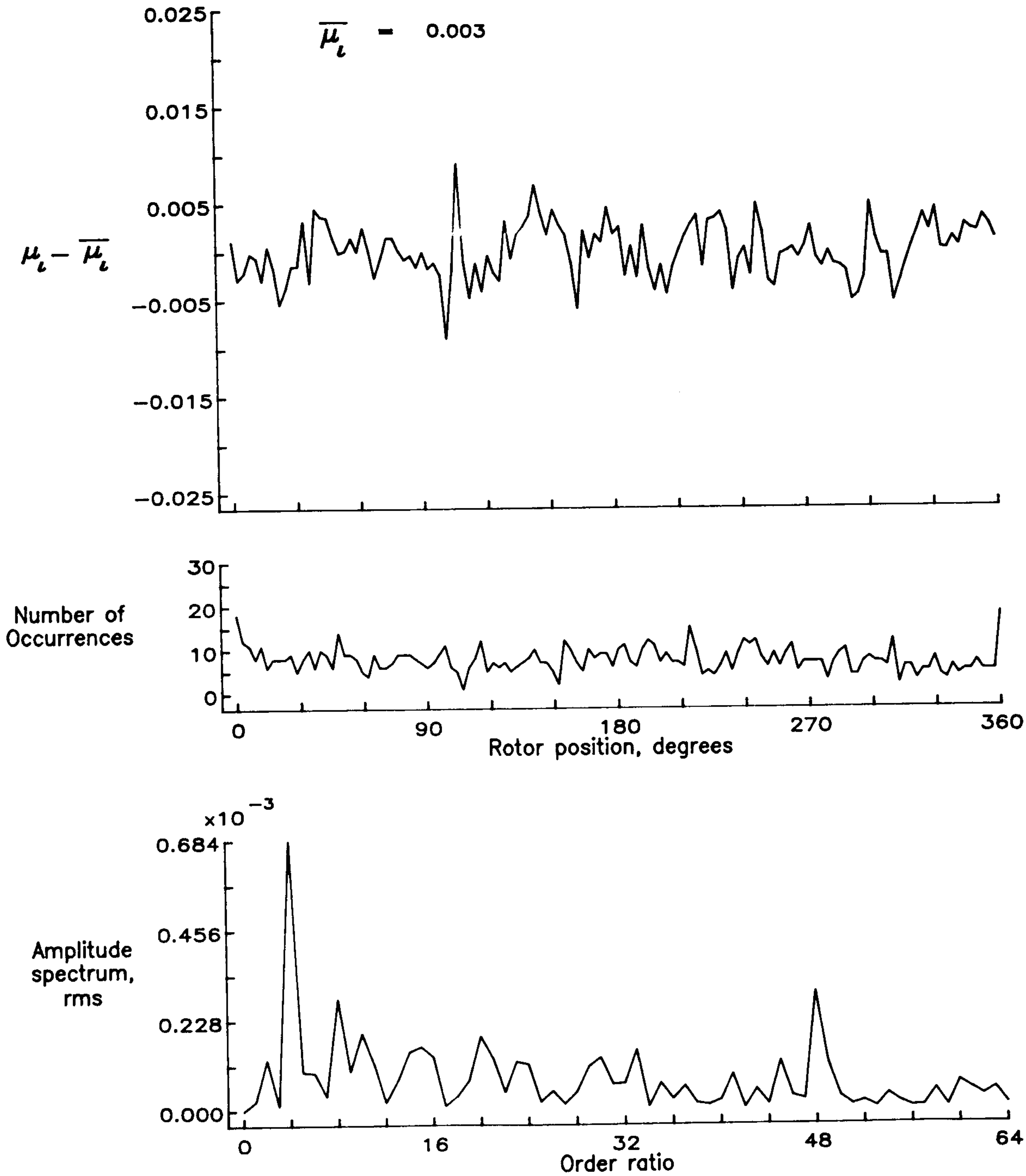

Figure 107.– Induced inflow velocity measured at 210 degrees and r/R of 1.04.

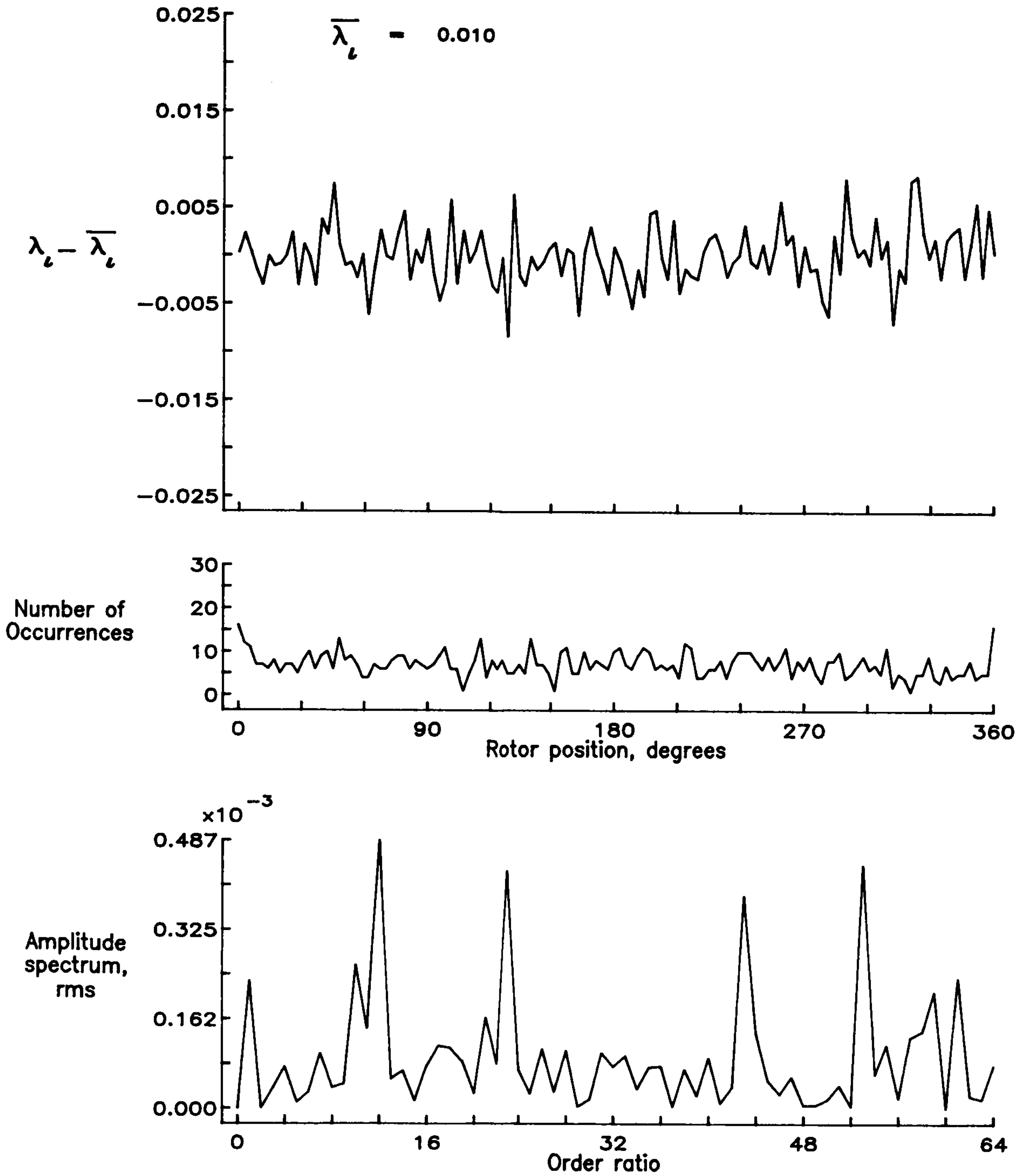

Figure 107.– Concluded.

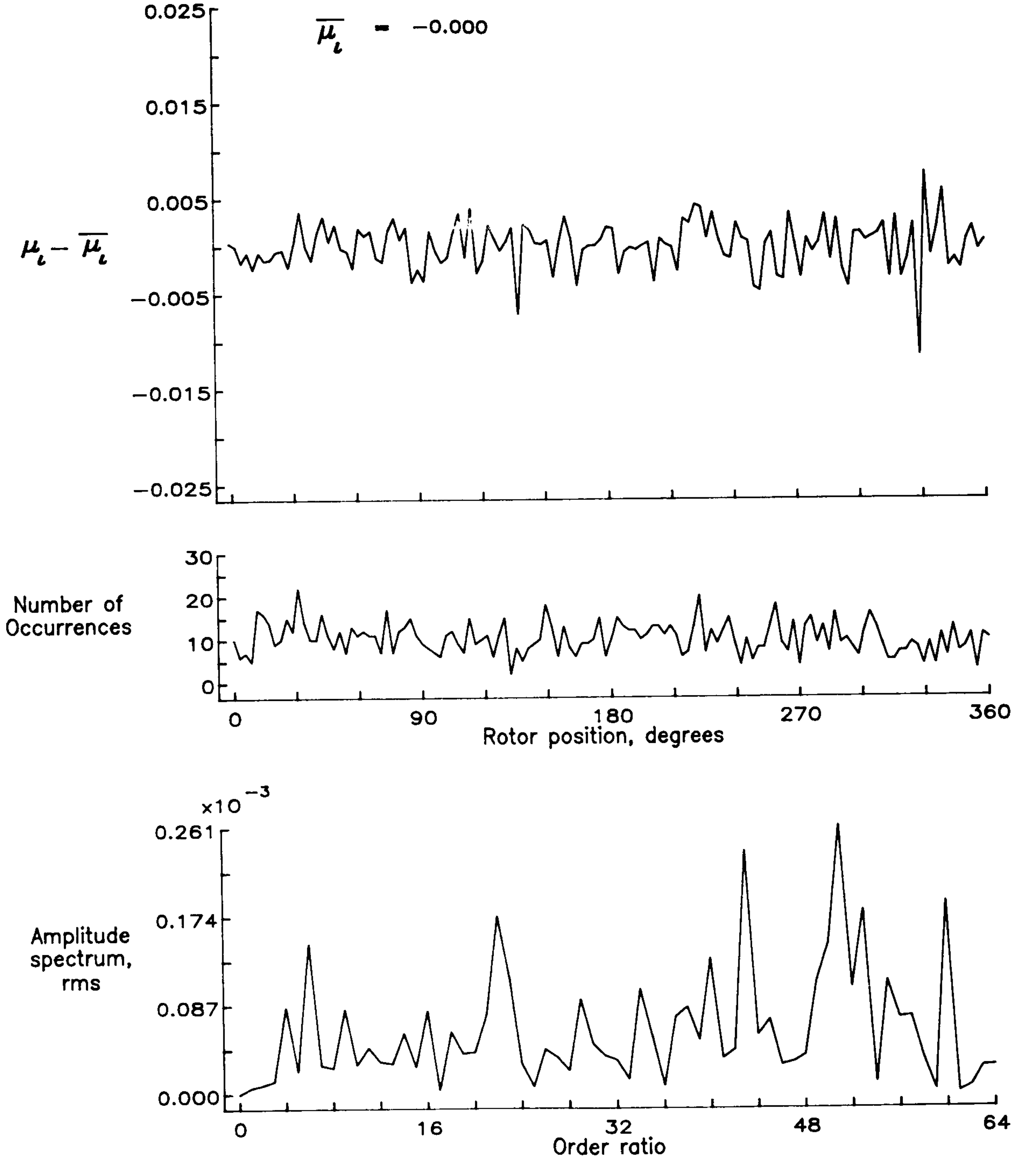

Figure 108.– Induced inflow velocity measured at 210 degrees and r/R of 1.10.

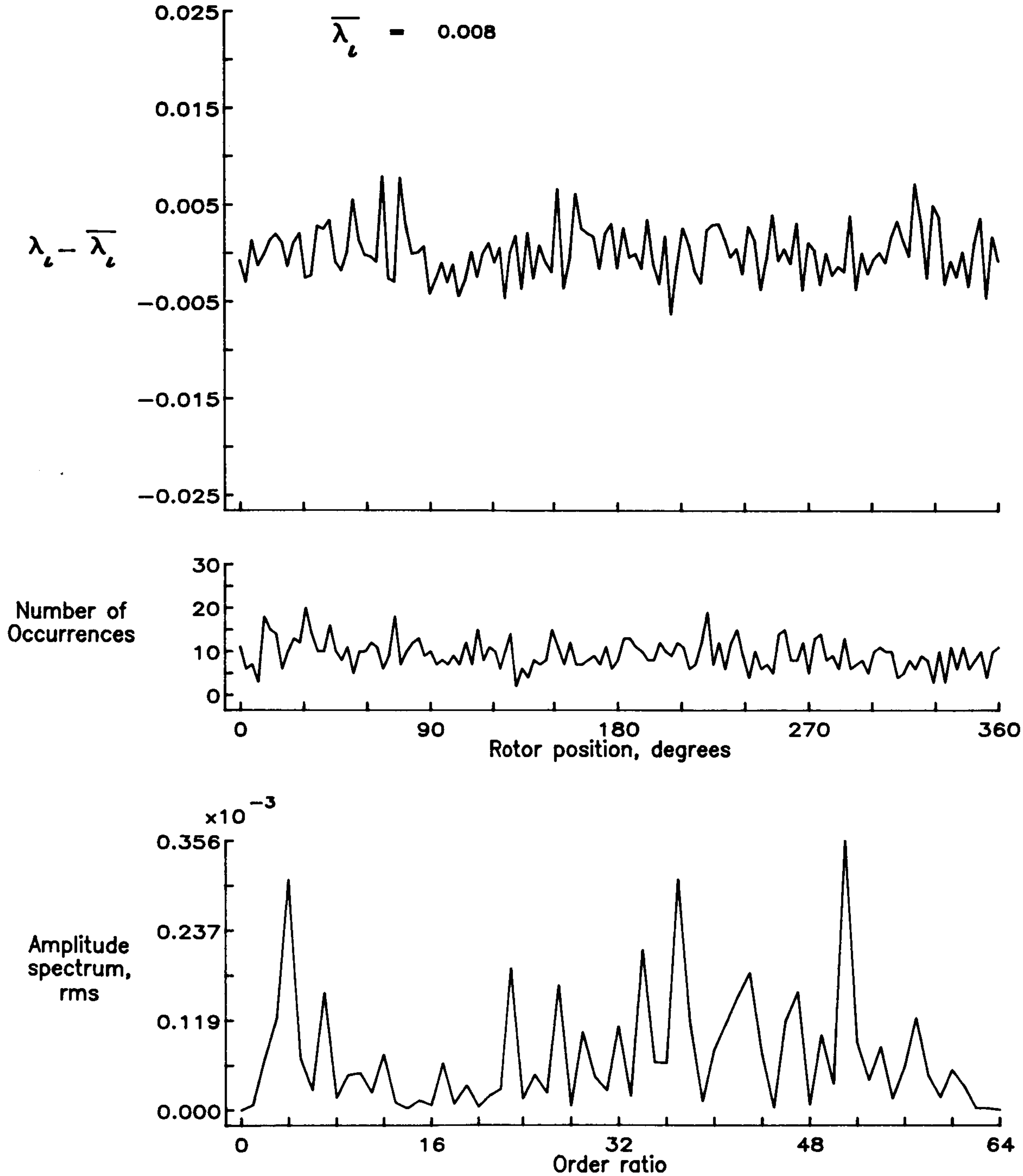

Figure 108.– Concluded.

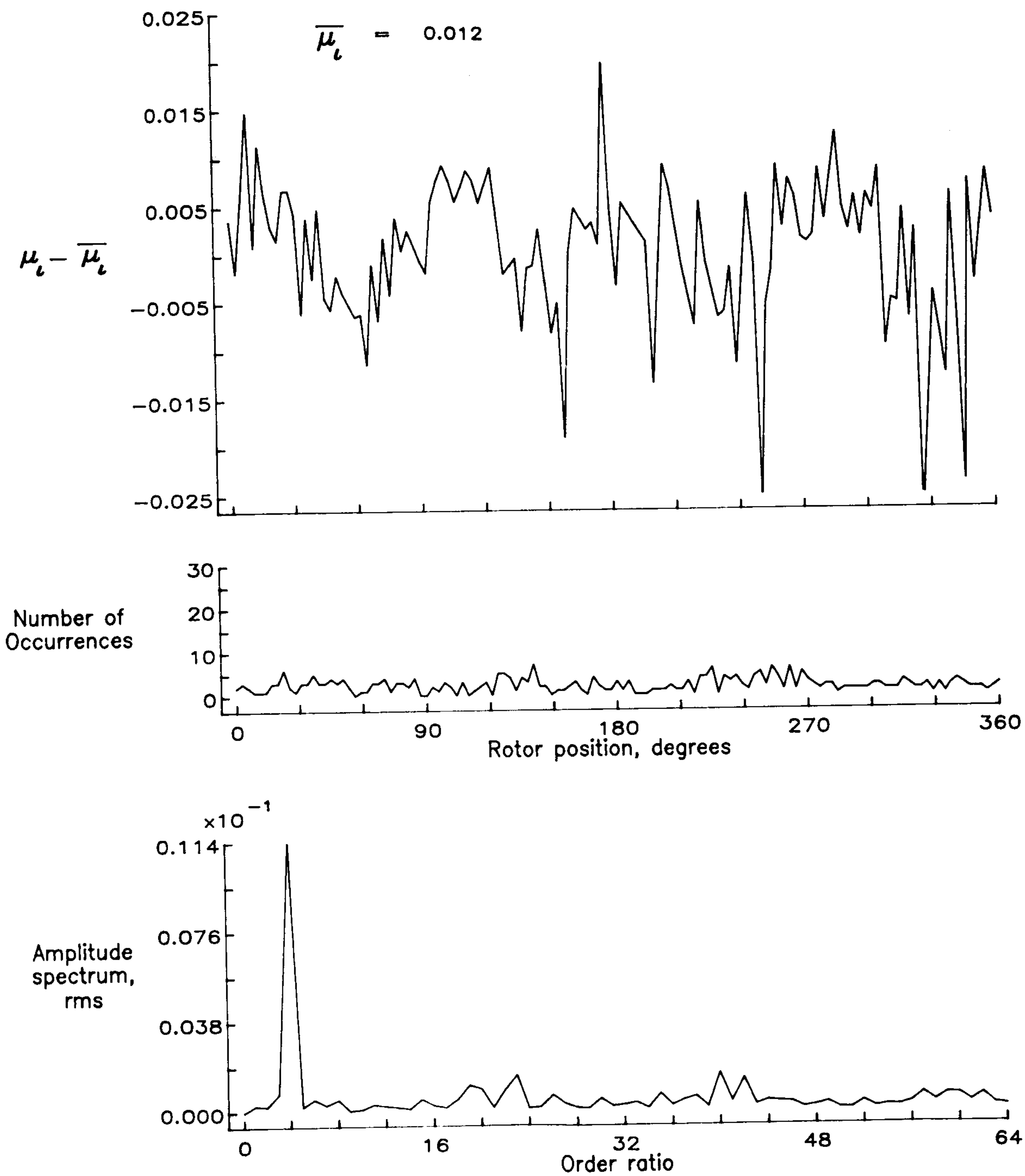

Figure 109.– Induced inflow velocity measured at 240 degrees and r/R of 0.40.

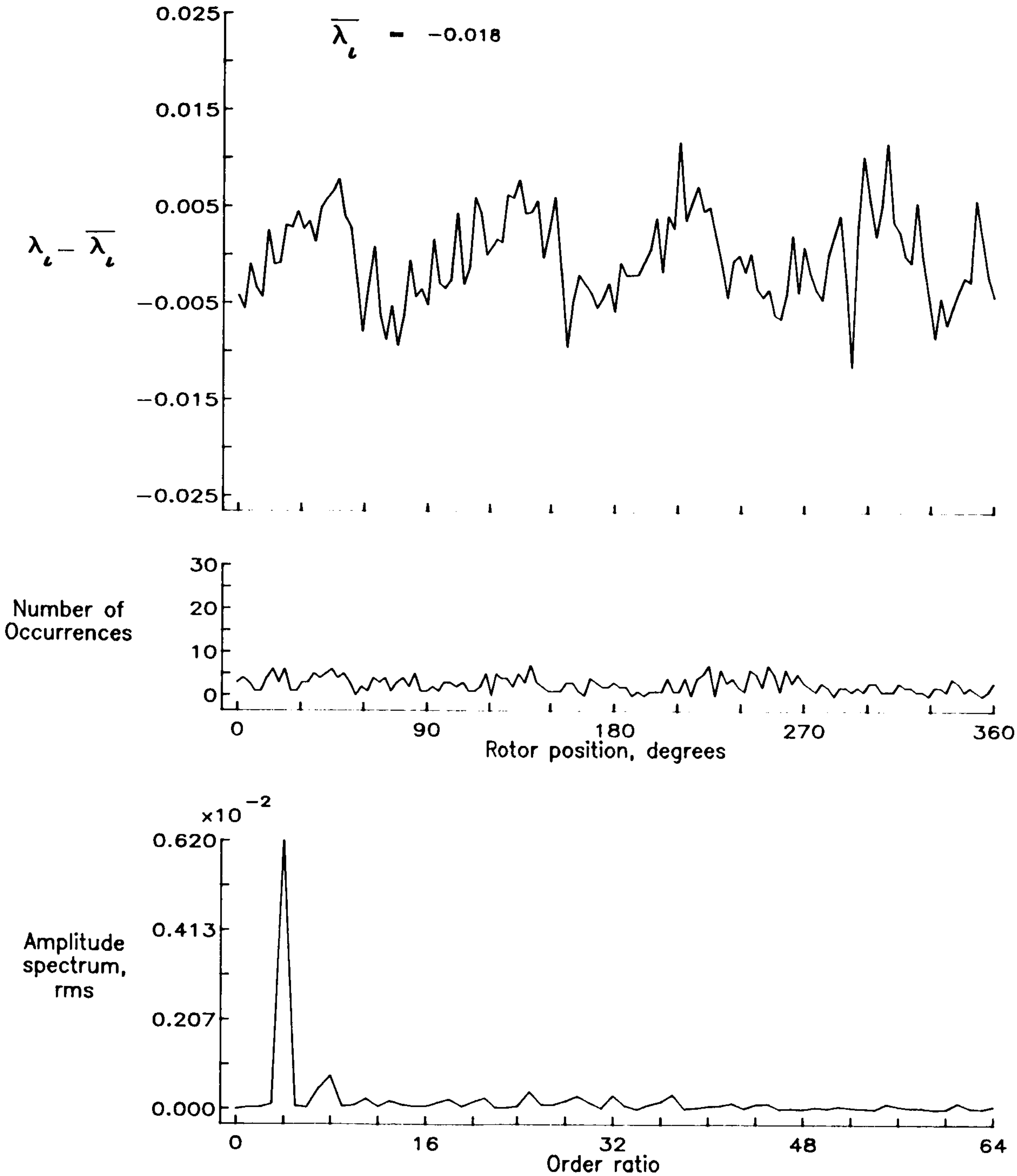

Figure 109.– Concluded.

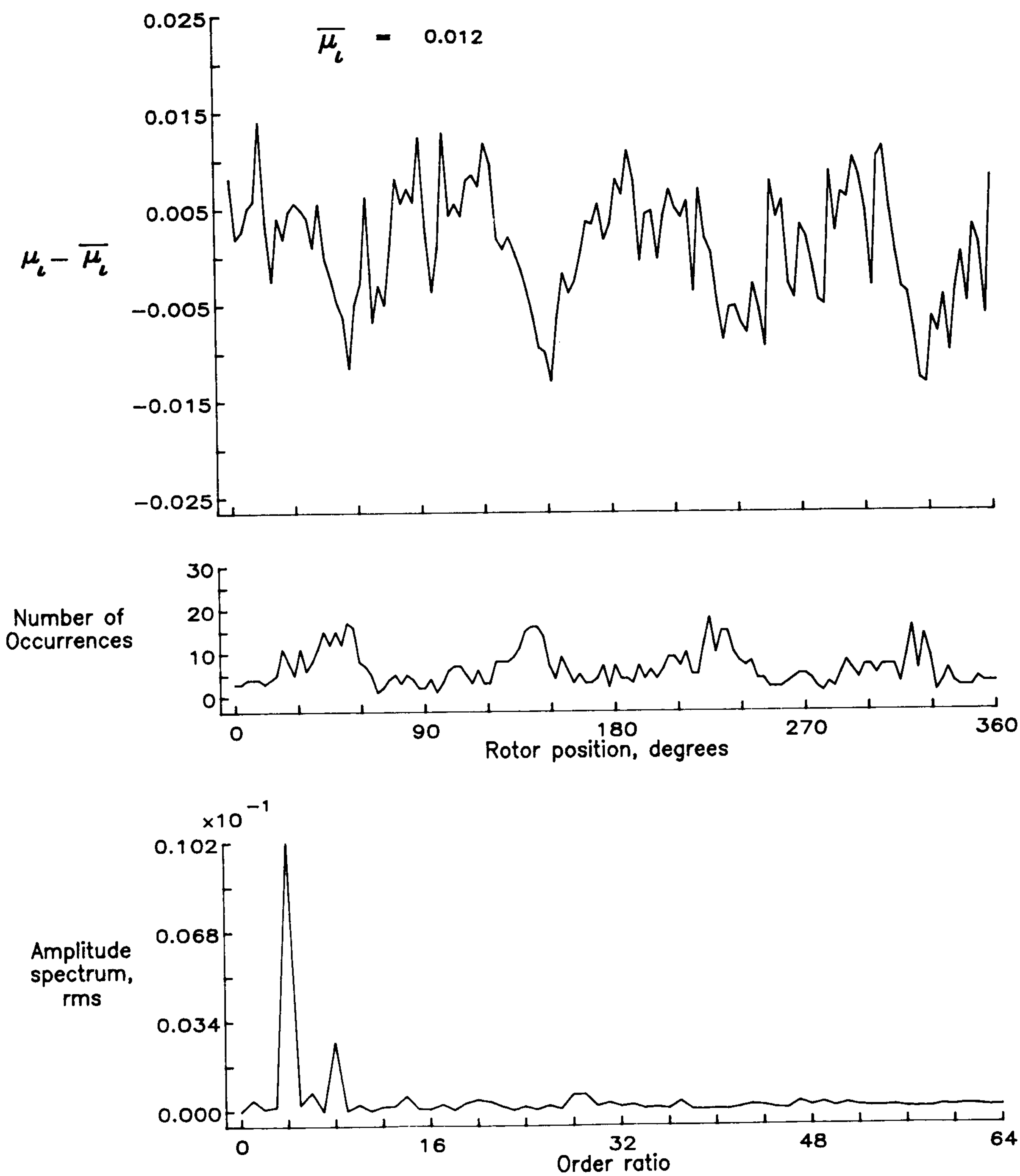

Figure 110.– Induced inflow velocity measured at 240 degrees and r/R of 0.50.

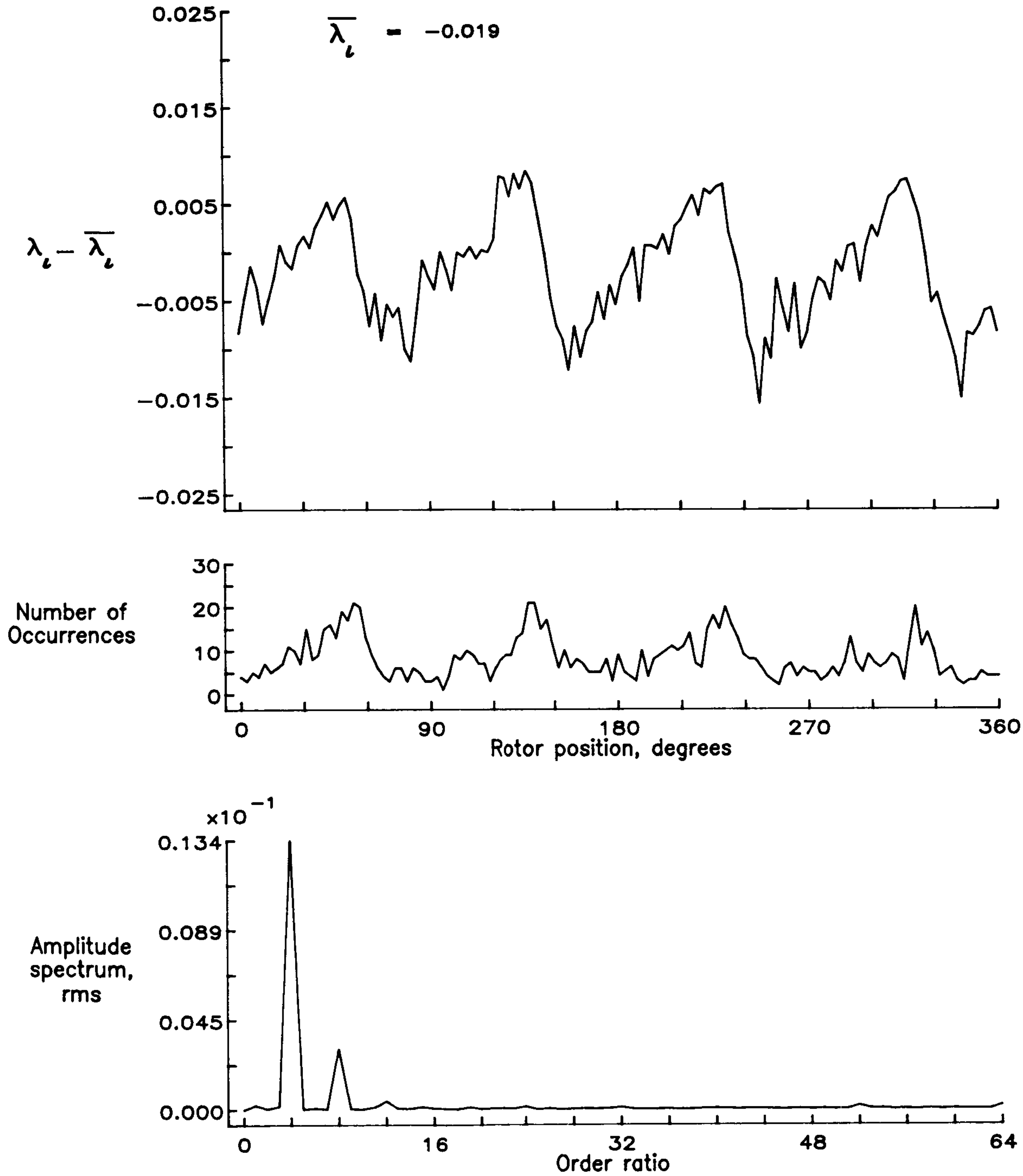

Figure 110.– Concluded.

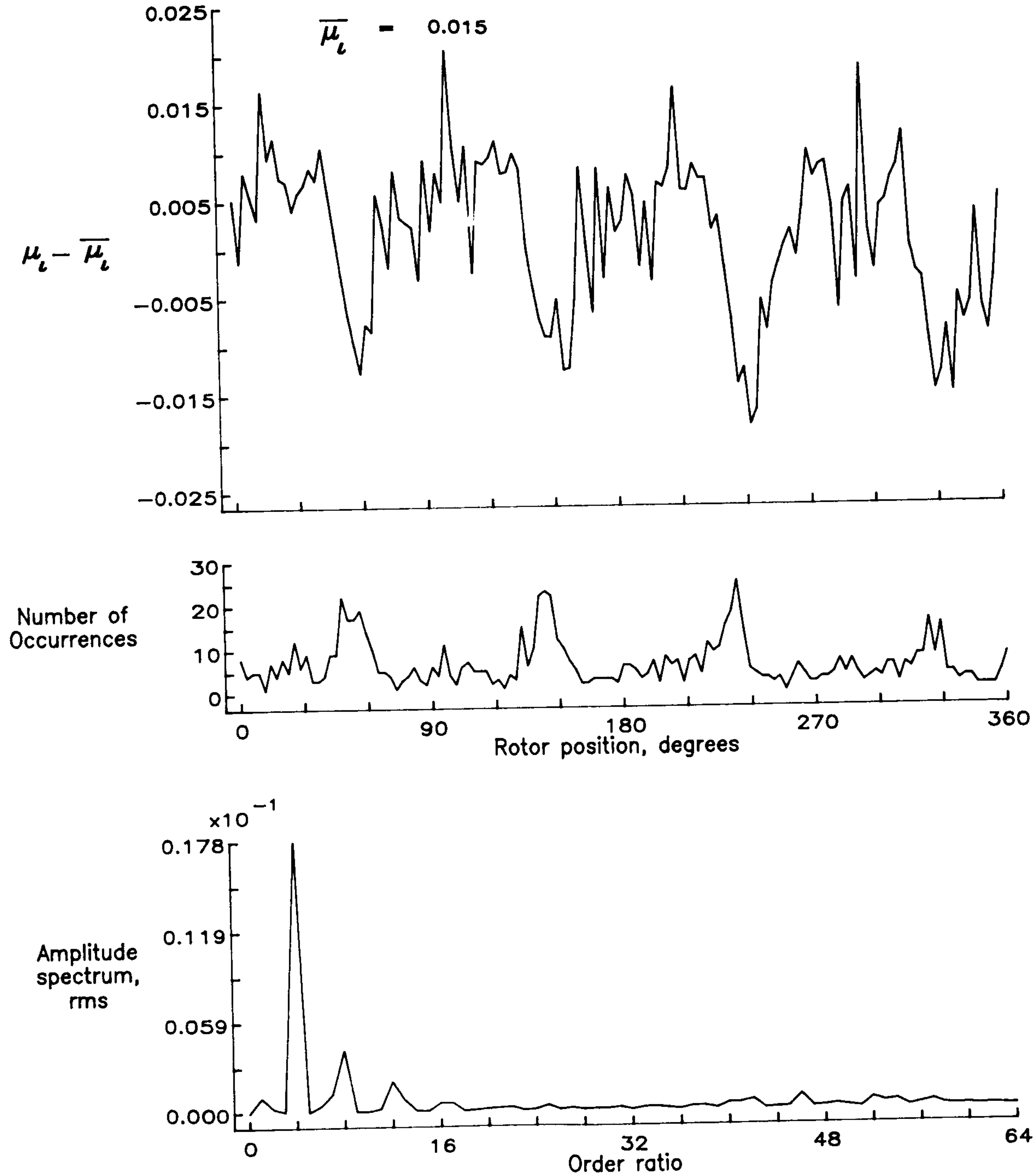

Figure 111.– Induced inflow velocity measured at 240 degrees and r/R of 0.60.

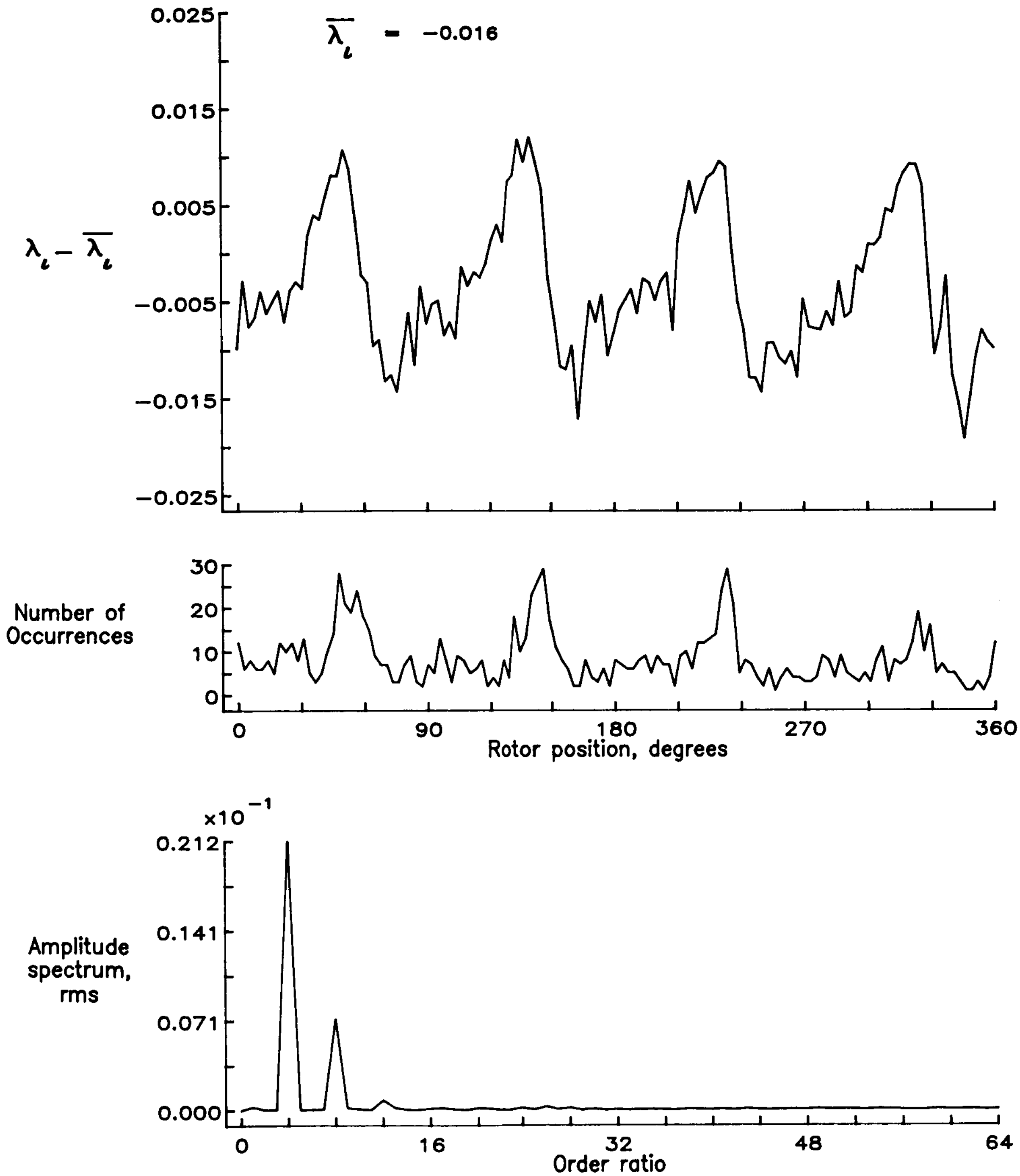

Figure 111.– Concluded.

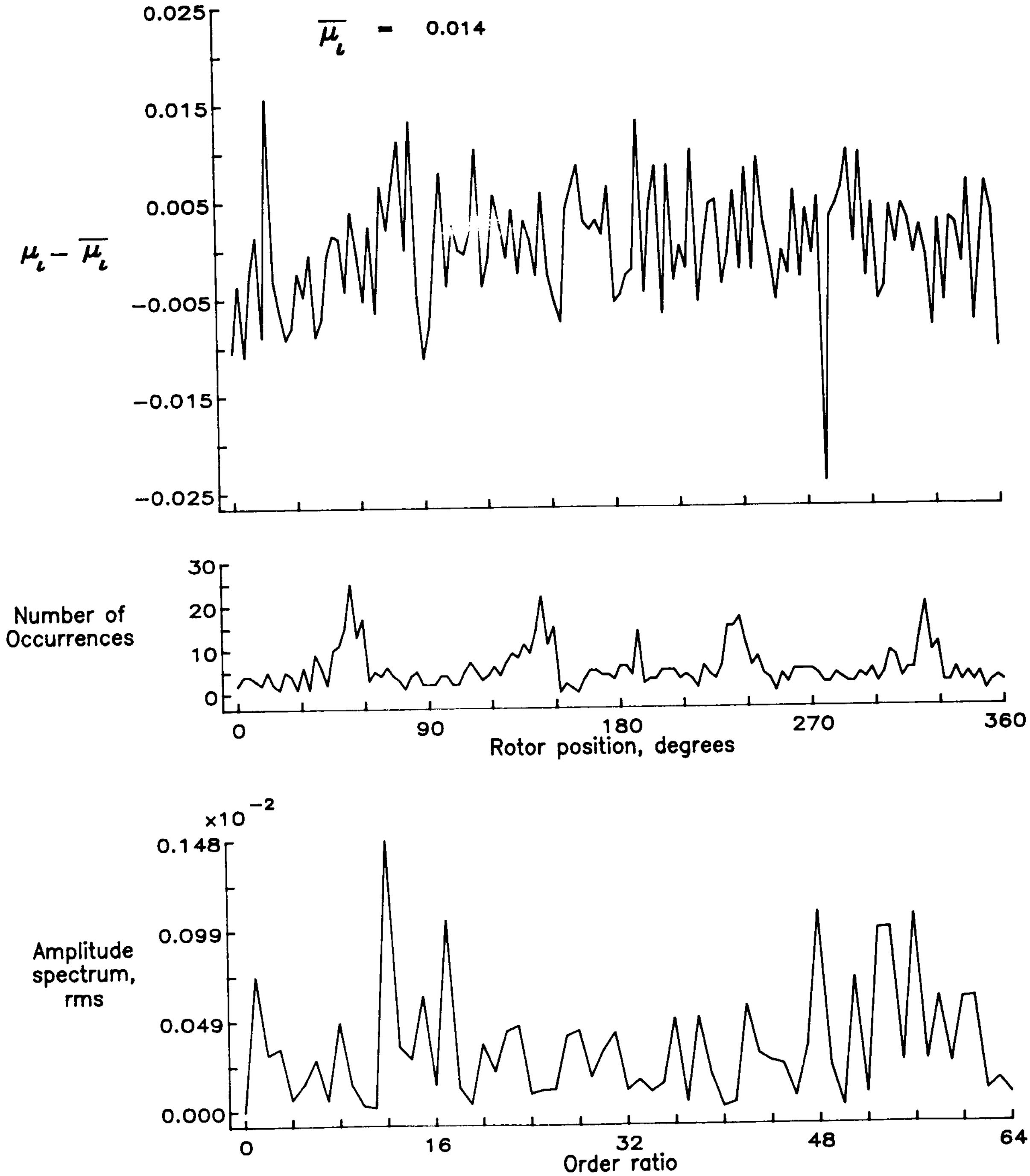

Figure 112.– Induced inflow velocity measured at 240 degrees and r/R of 0.70.

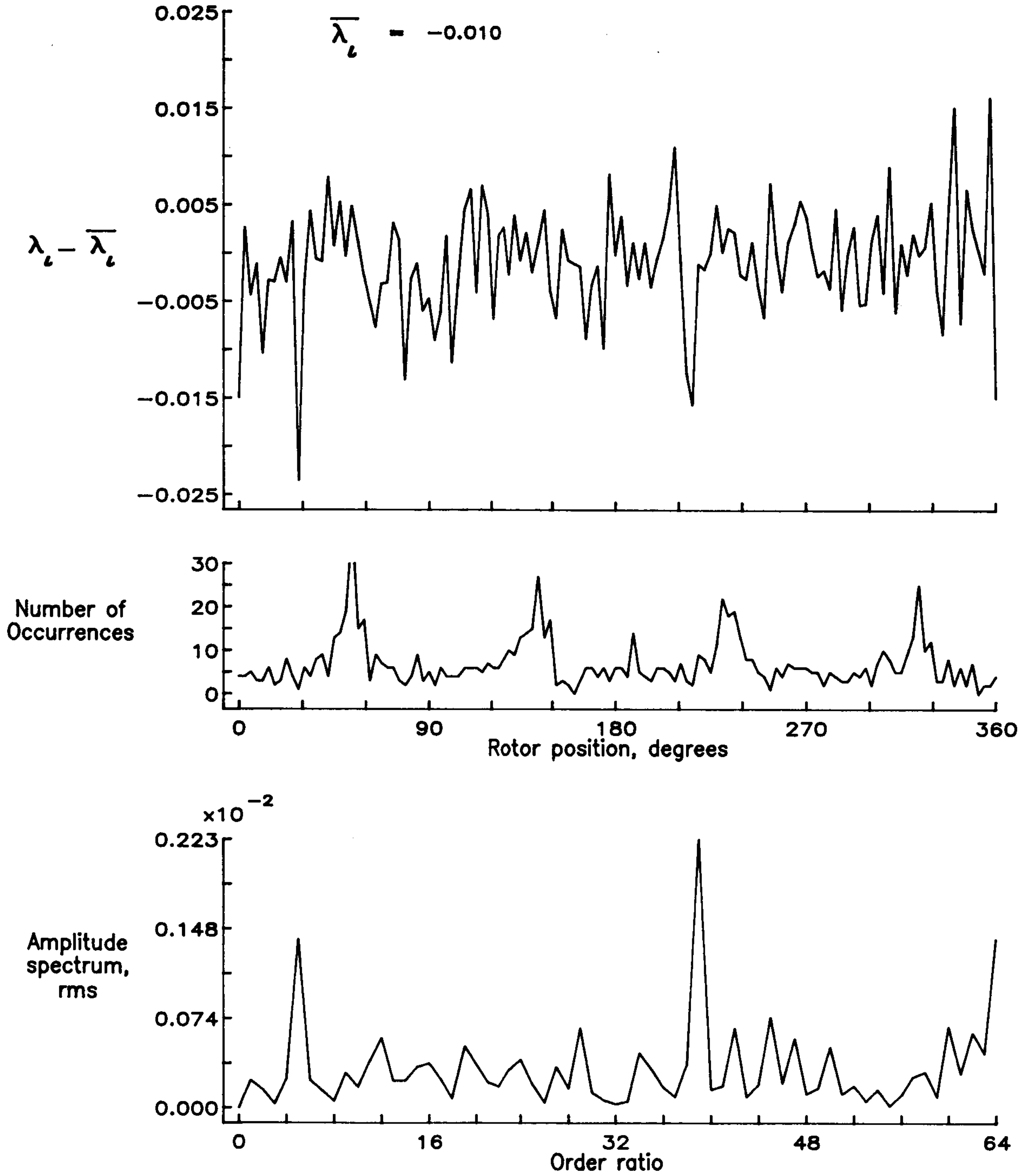

Figure 112.– Concluded.

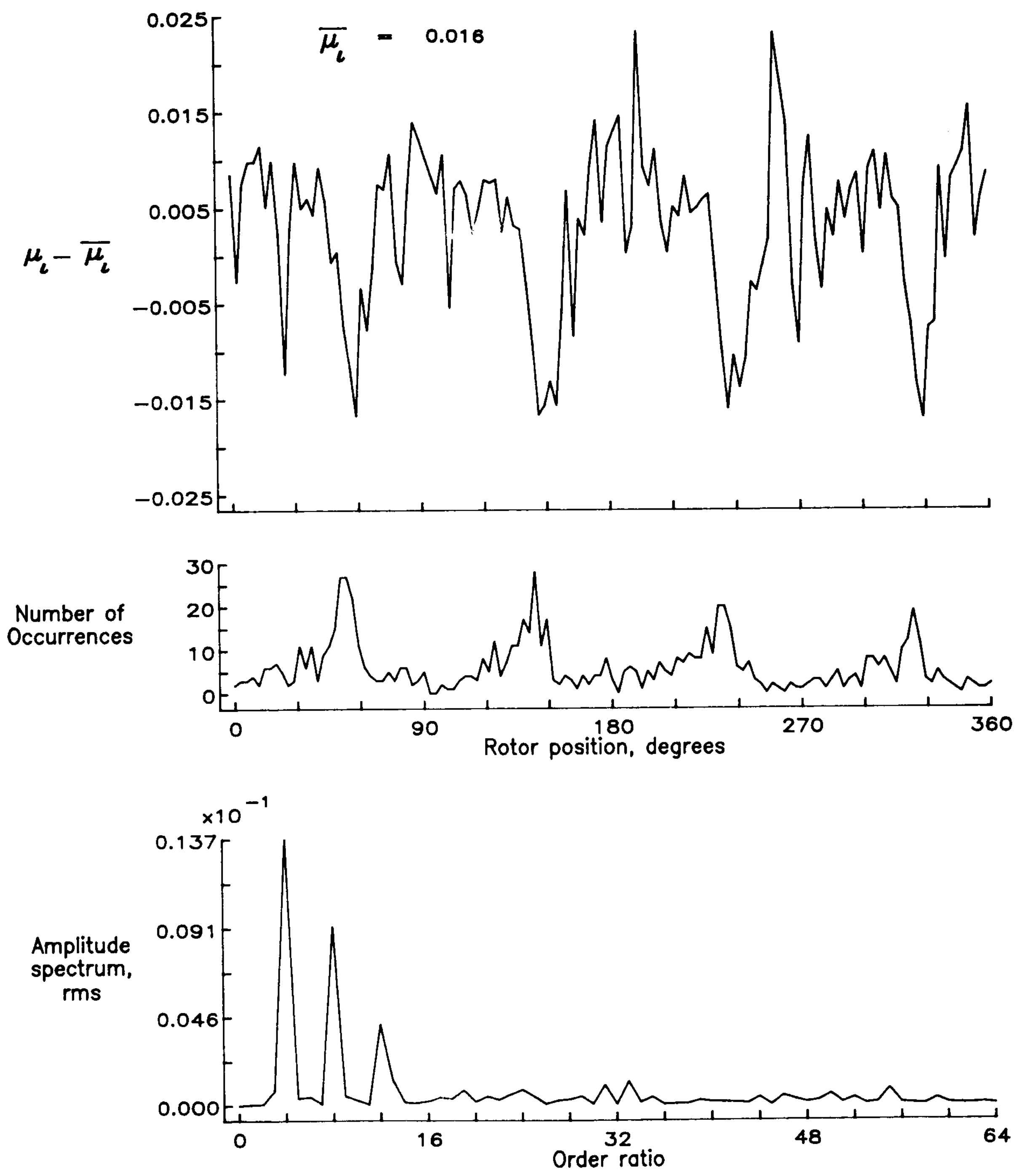

Figure 113.– Induced inflow velocity measured at 240 degrees and r/R of 0.74.

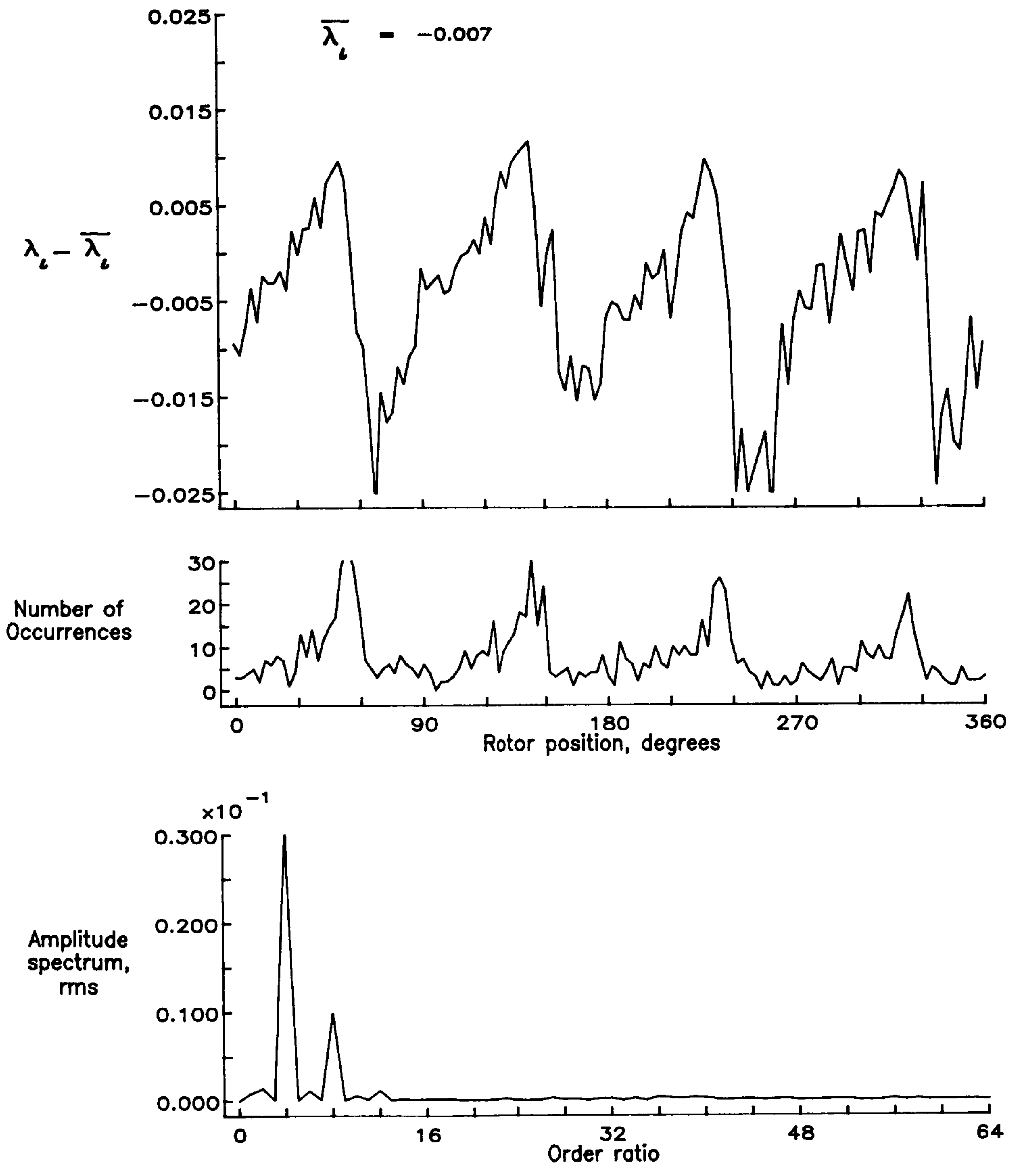

Figure 113.– Concluded.

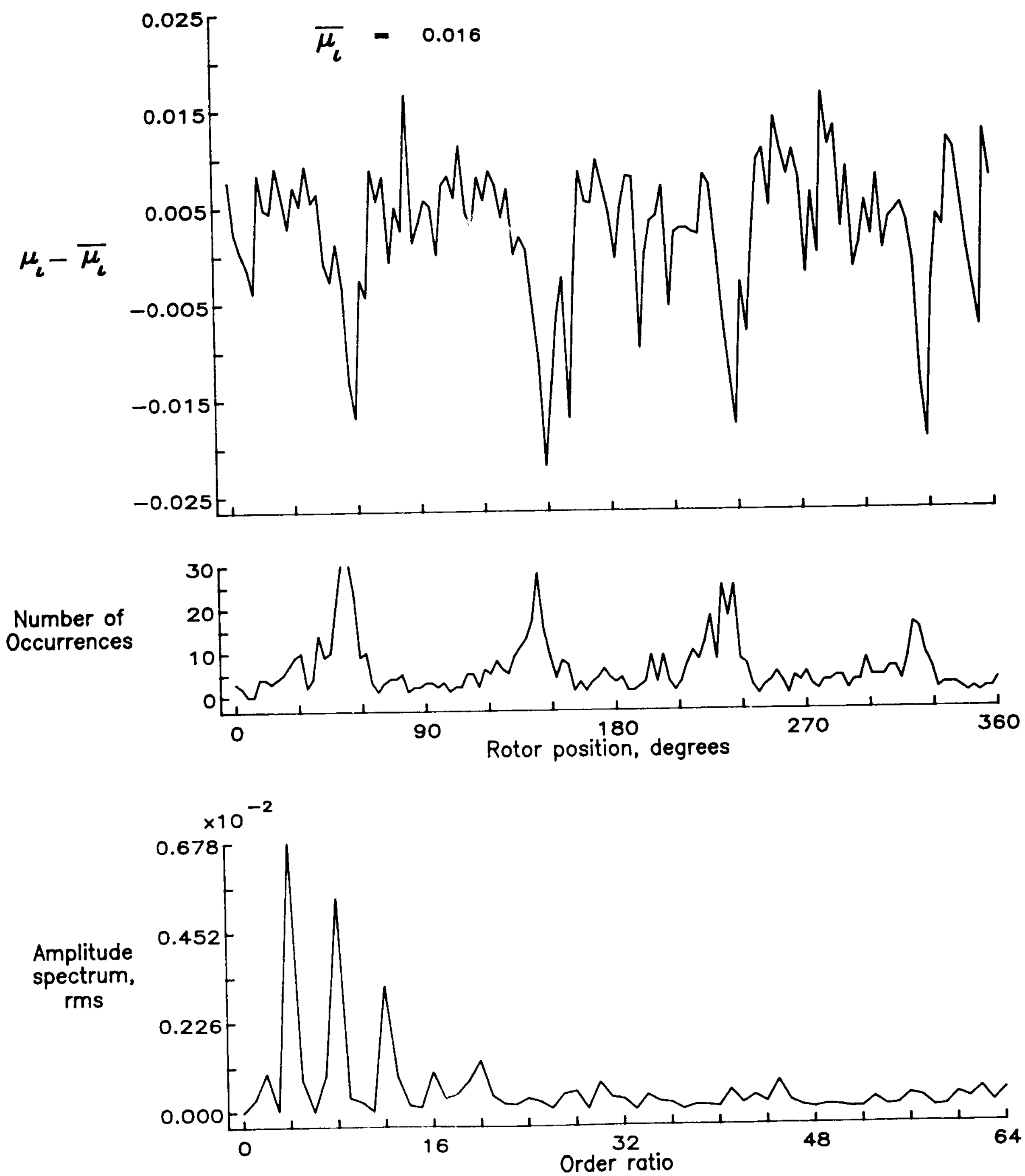

Figure 114.– Induced inflow velocity measured at 240 degrees and r/R of 0.78.

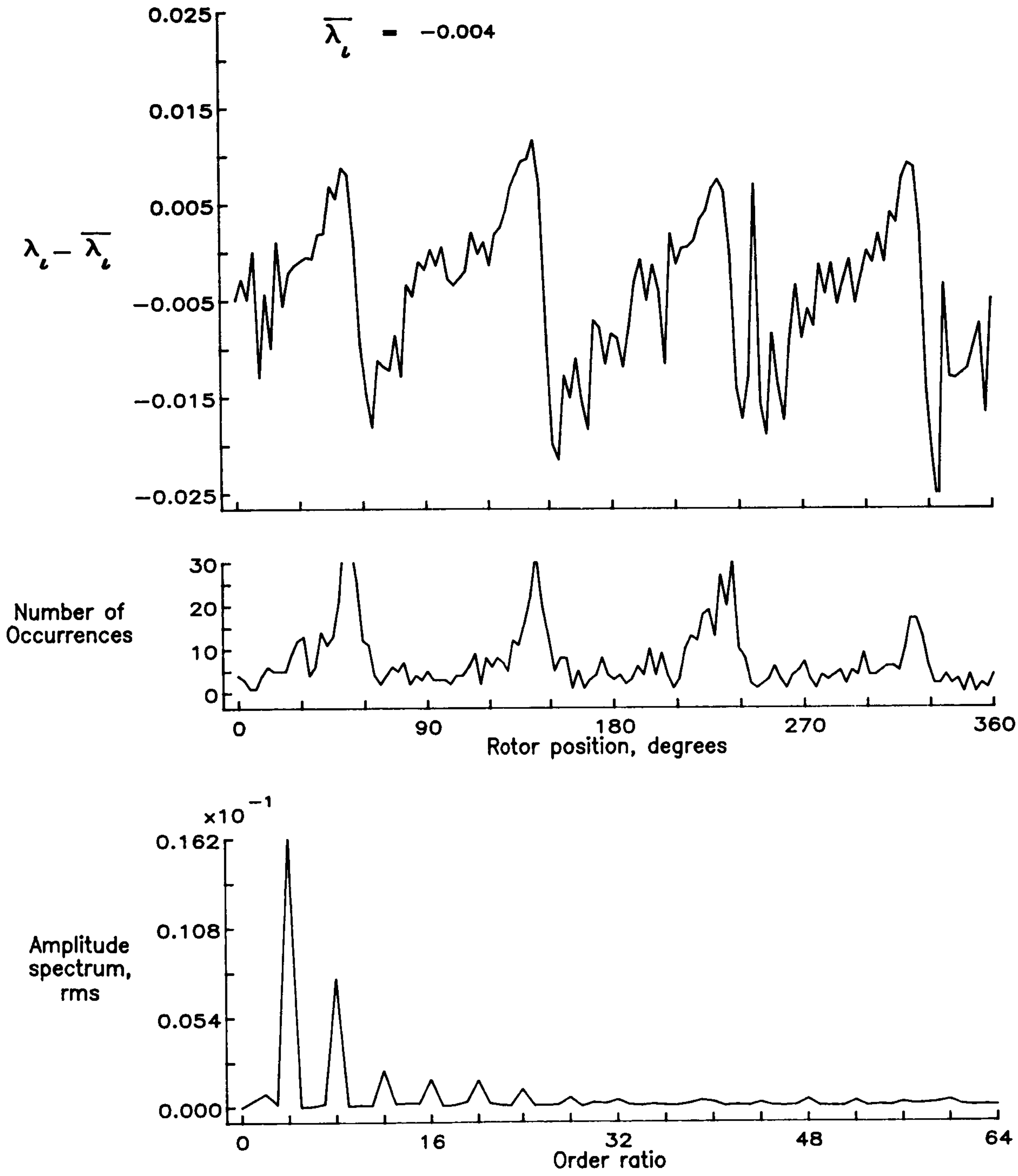

Figure 114.– Concluded.

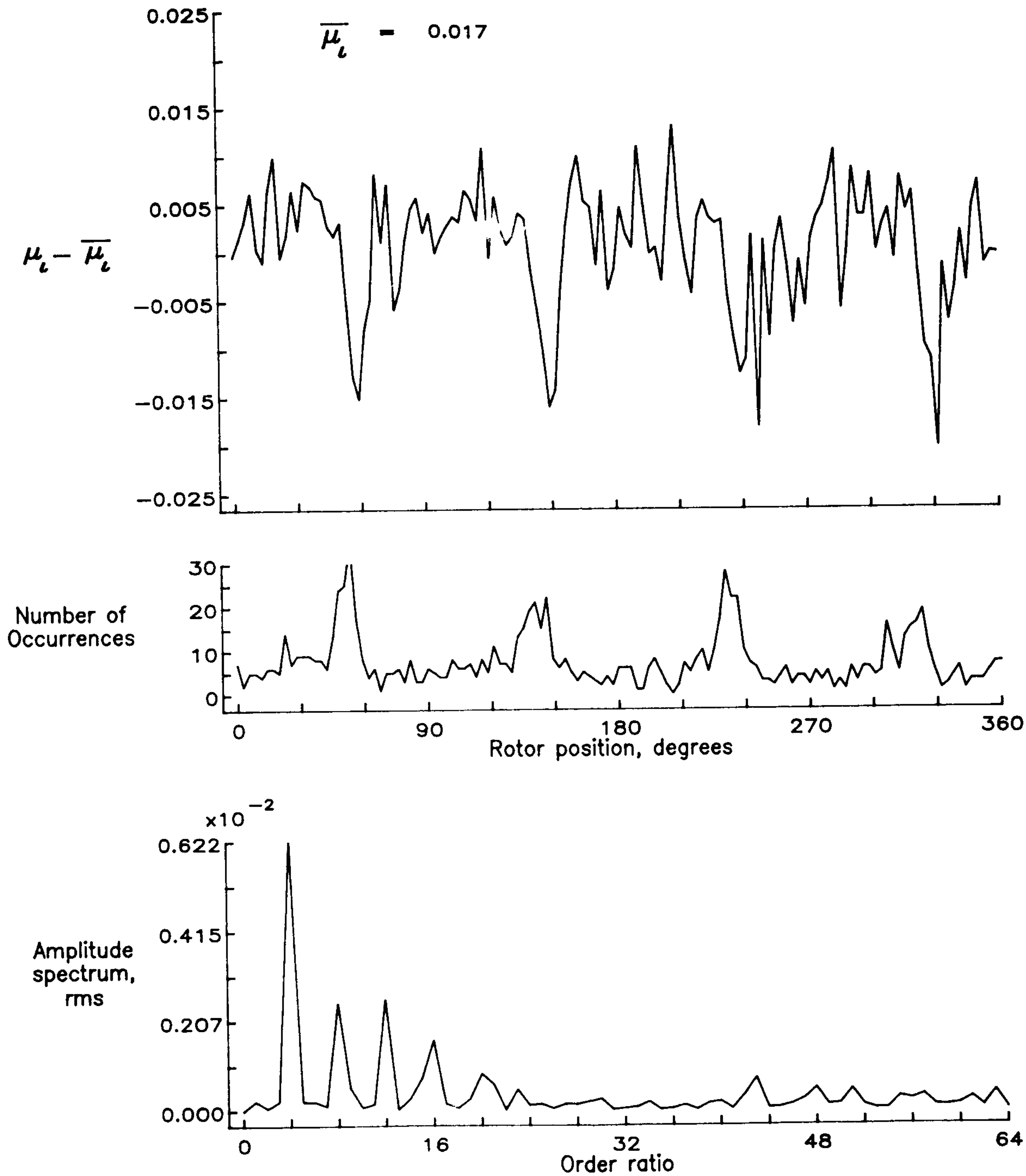

Figure 115.– Induced inflow velocity measured at 240 degrees and r/R of 0.82.

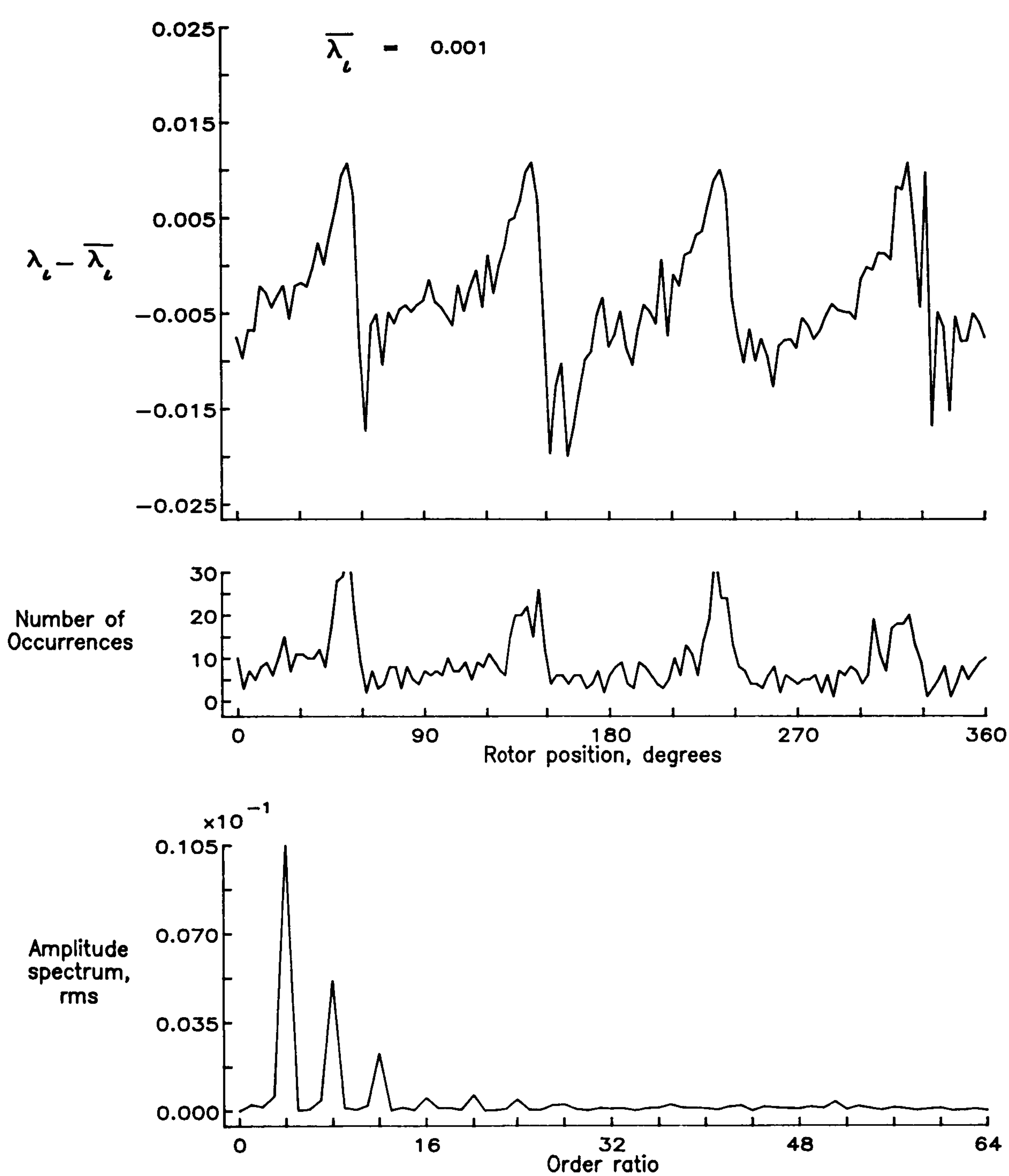

Figure 115.– Concluded.

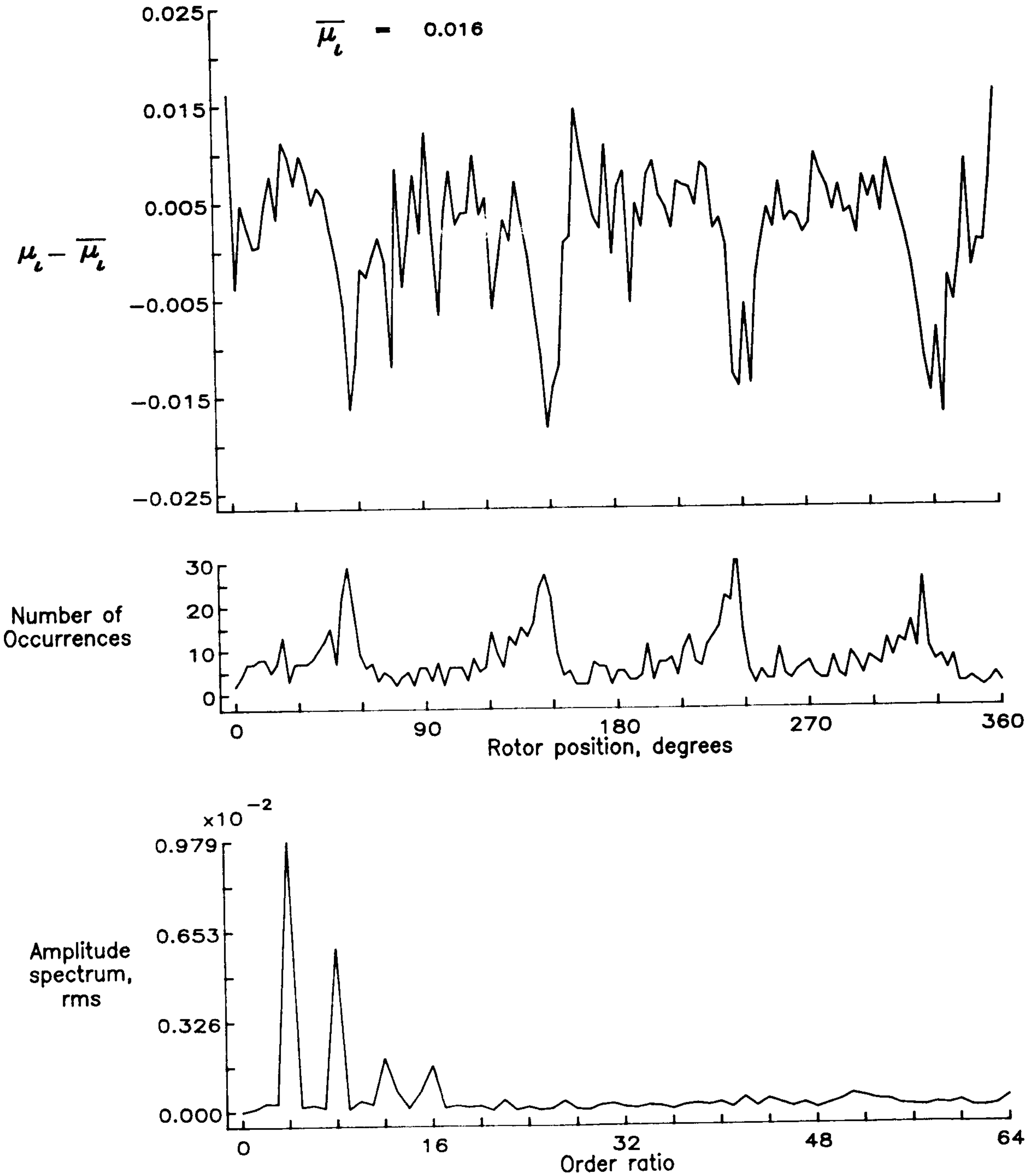

Figure 116.– Induced inflow velocity measured at 240 degrees and r/R of 0.86.

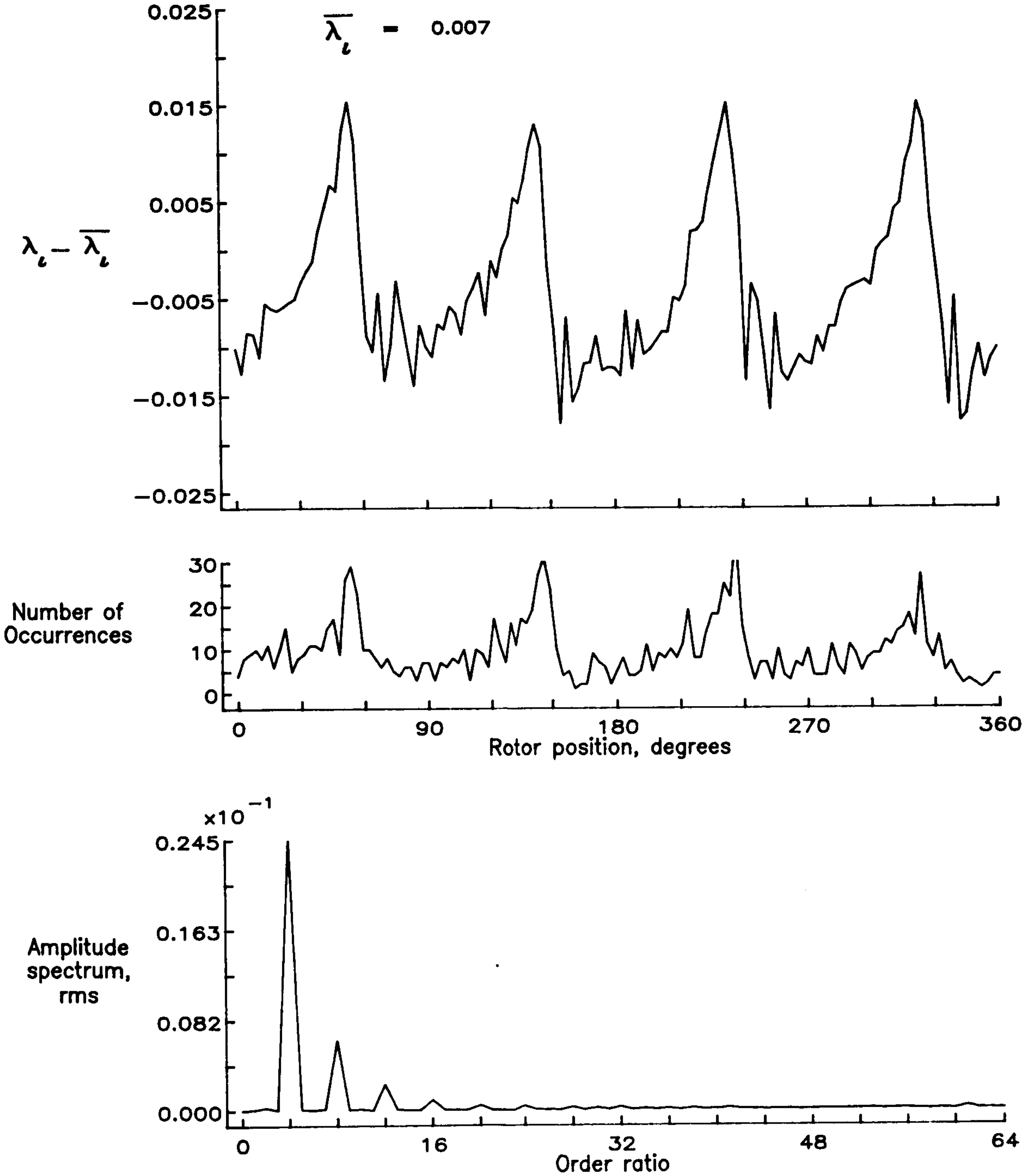

Figure 116.– Concluded.

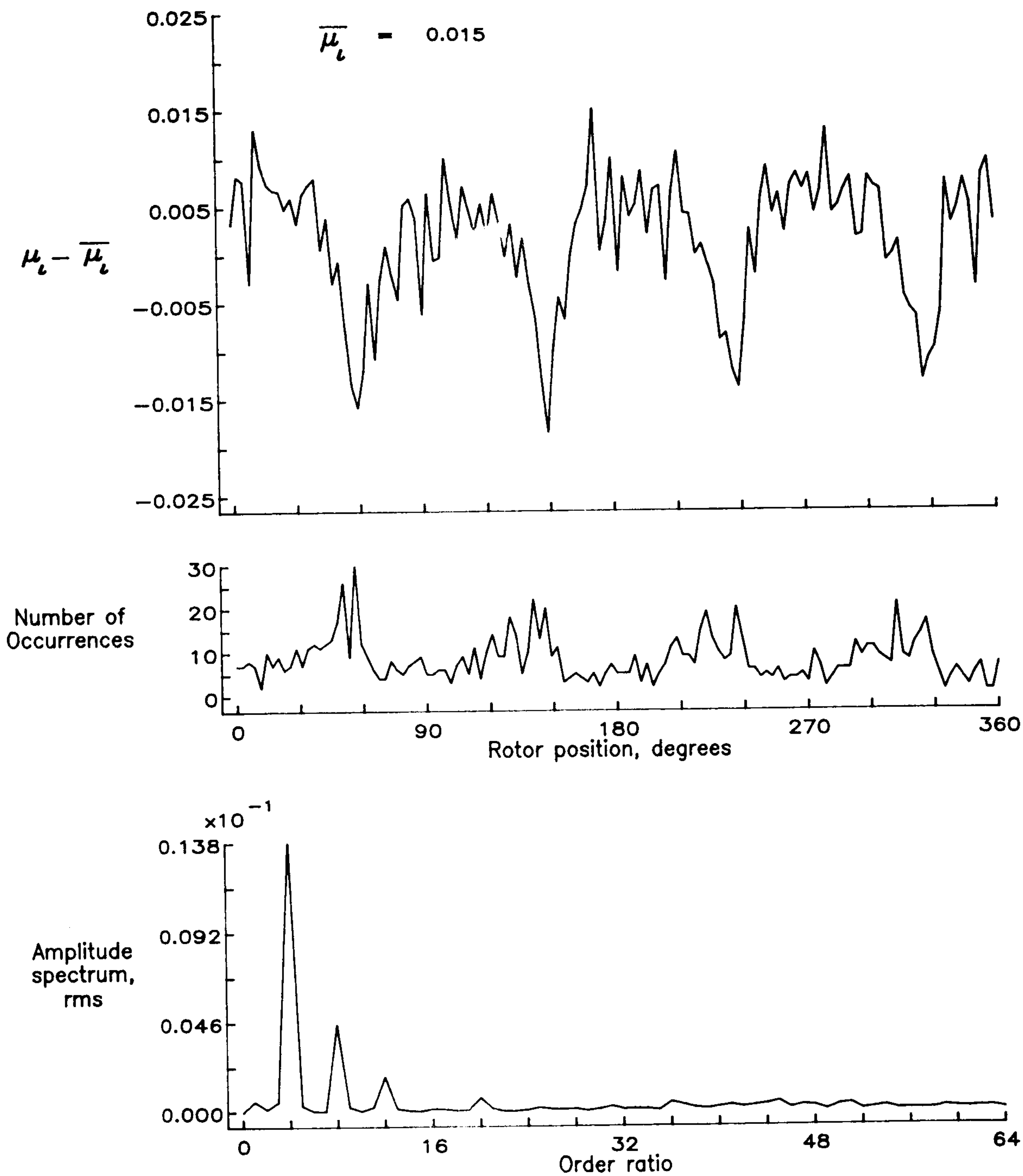

Figure 117.– Induced inflow velocity measured at 240 degrees and r/R of 0.90.

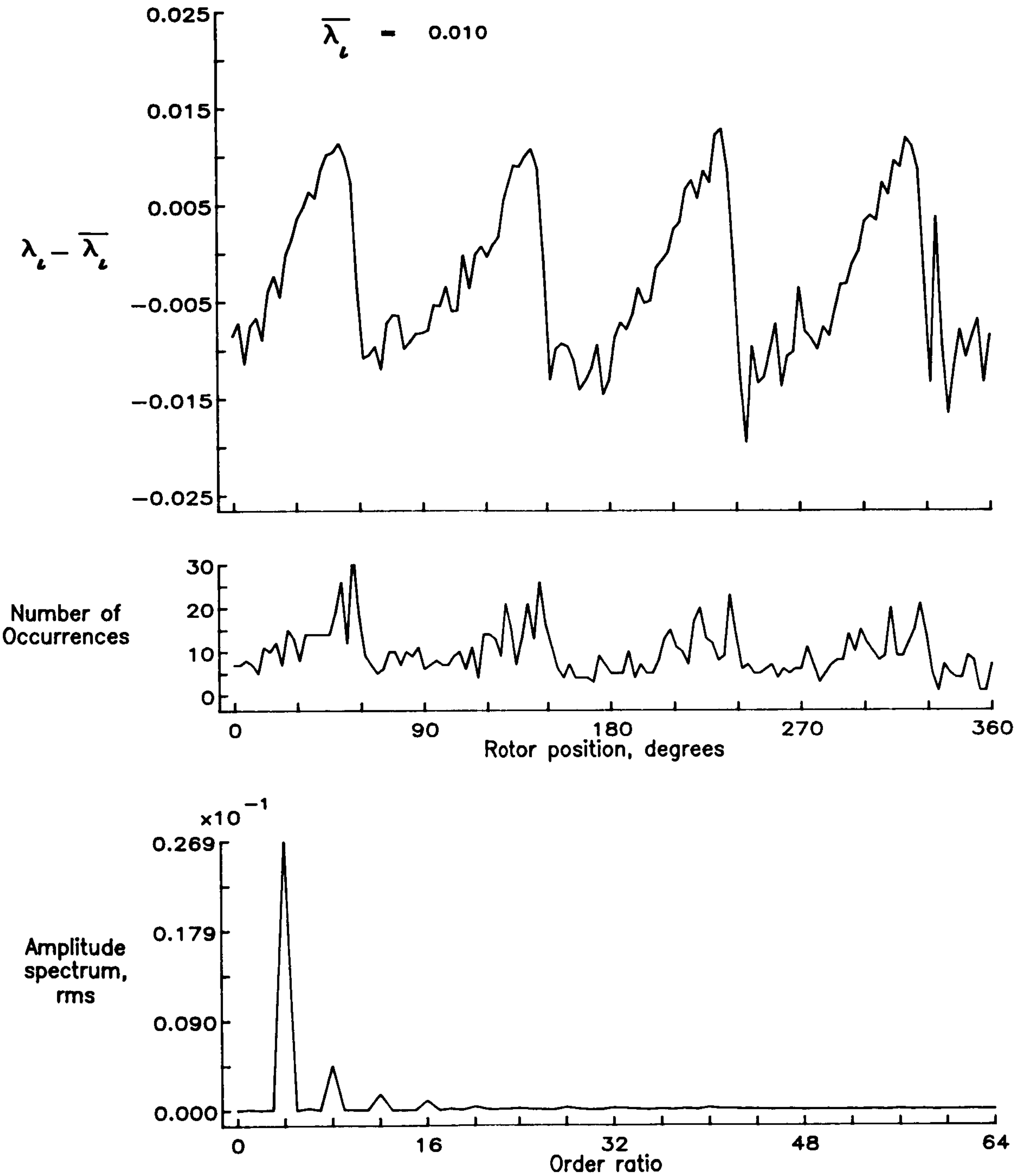

Figure 117.– Concluded.

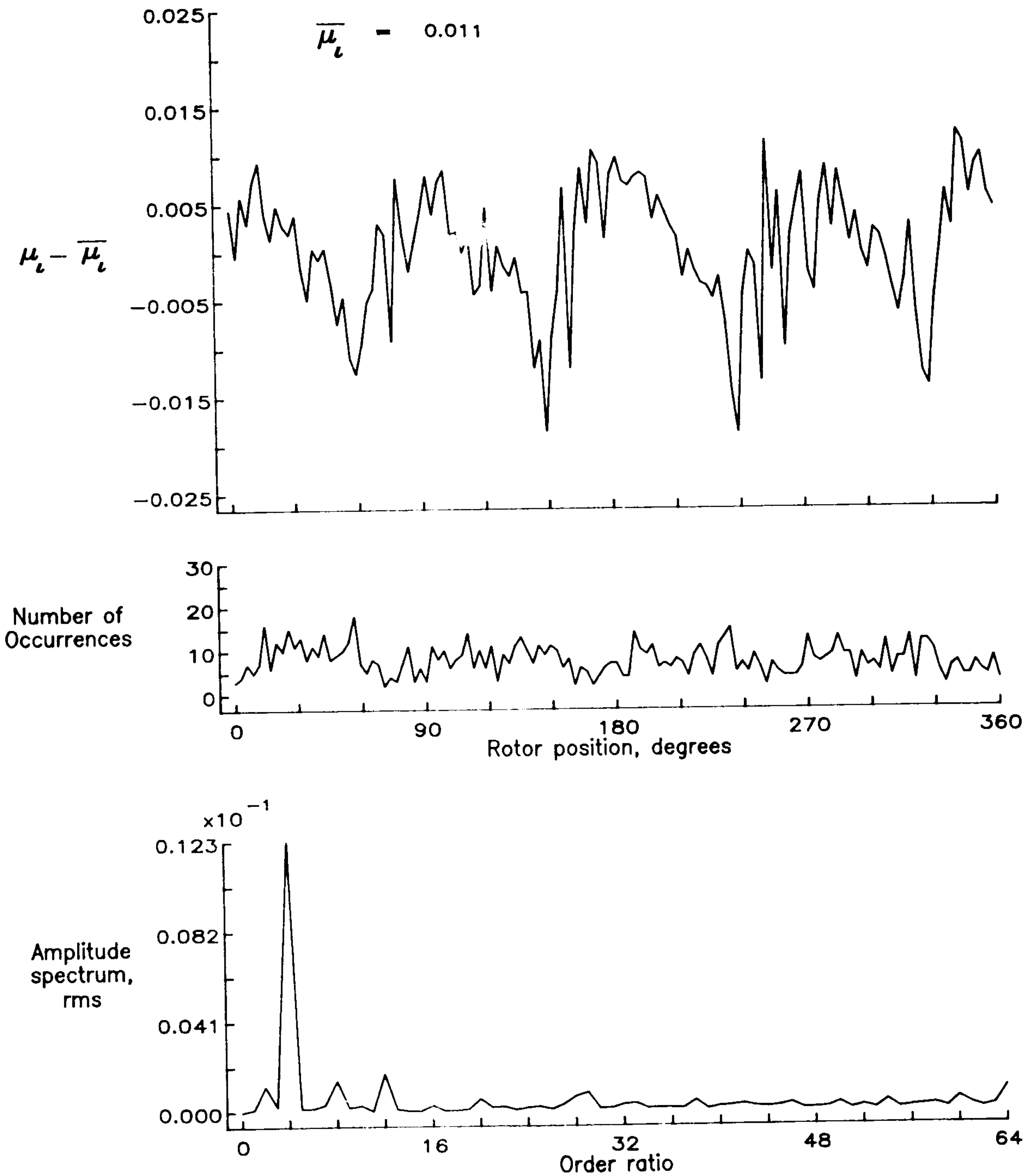

Figure 118.– Induced inflow velocity measured at 240 degrees and r/R of 0.94.

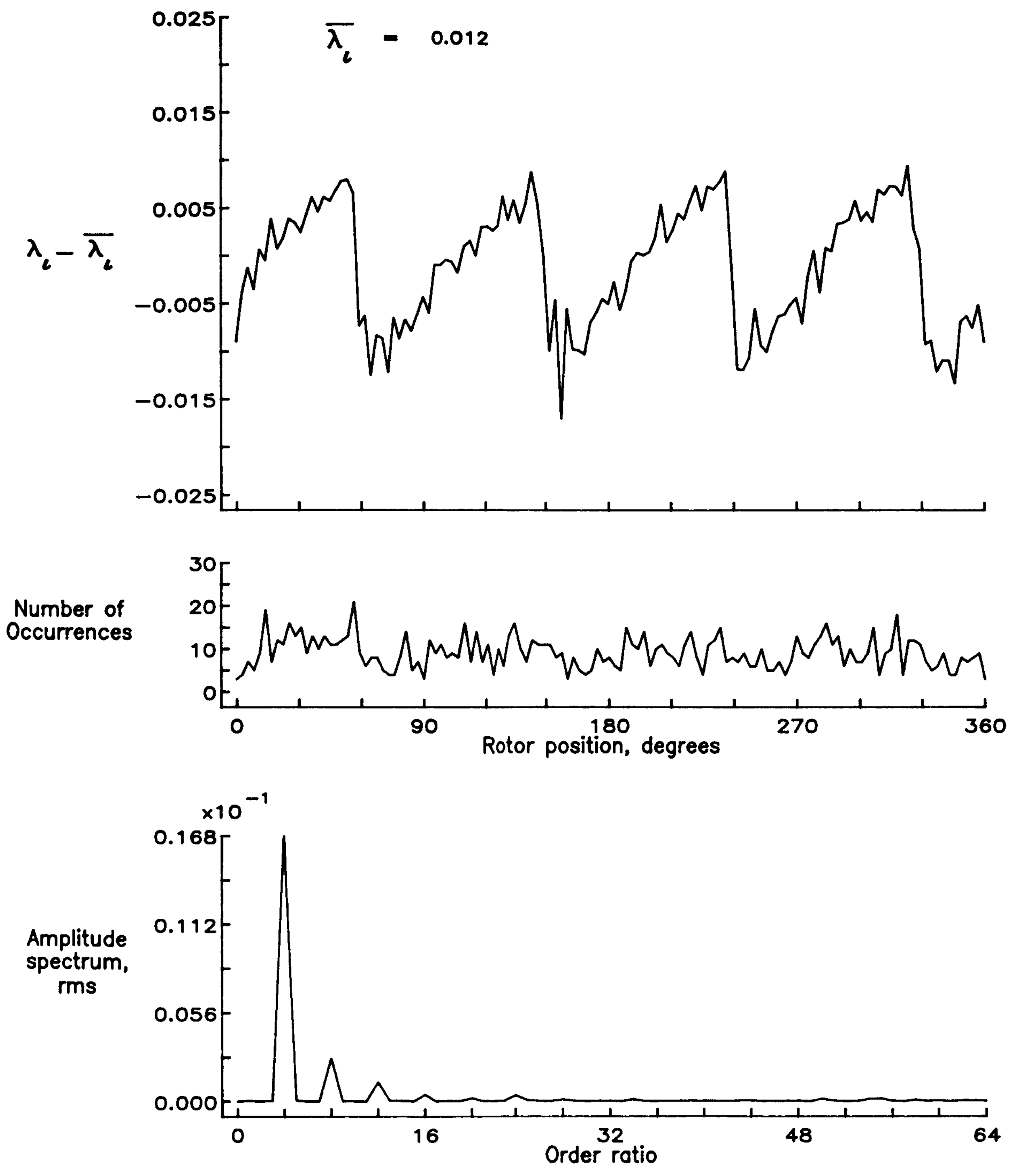

Figure 118.– Concluded.

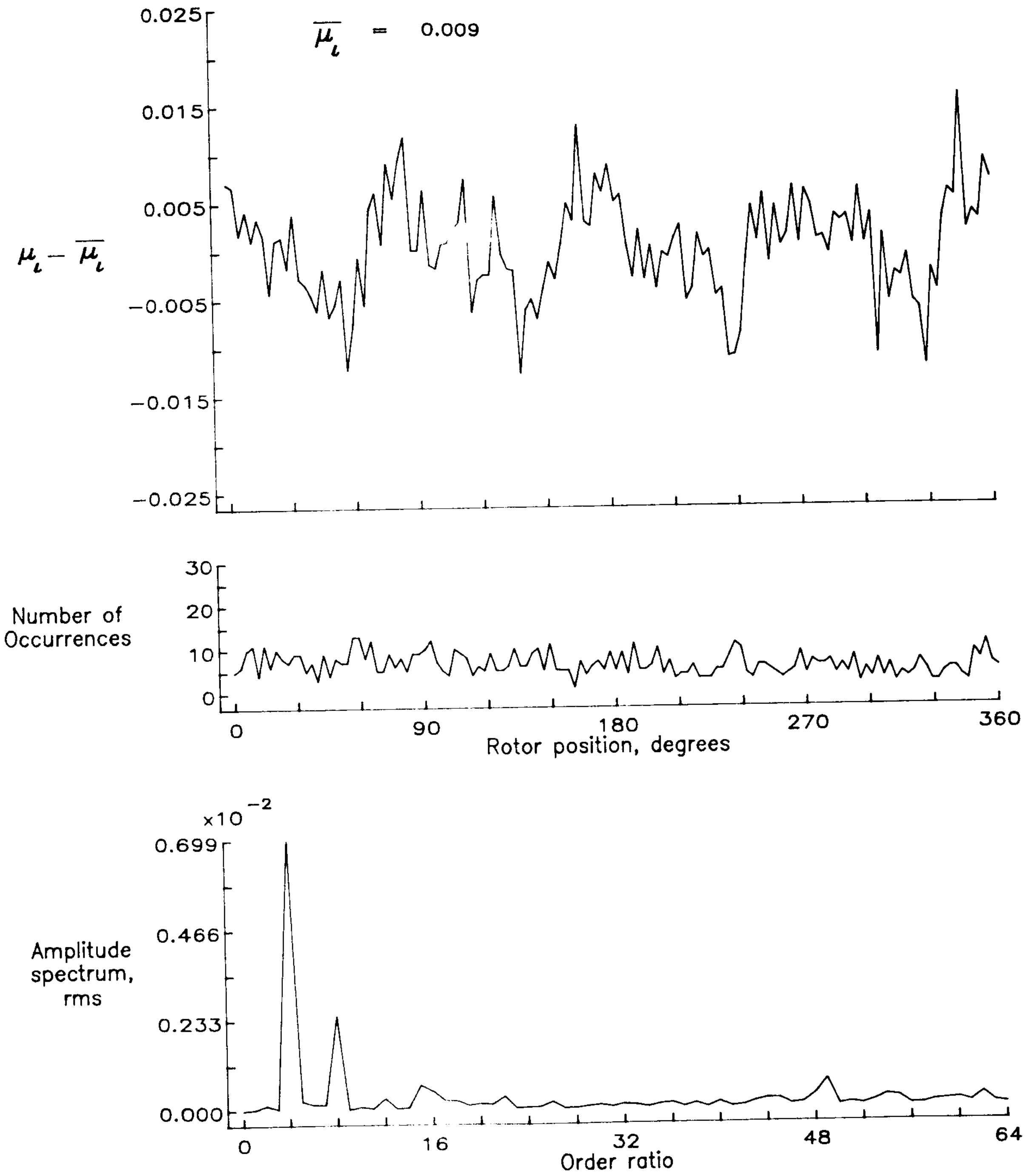

Figure 119.– Induced inflow velocity measured at 240 degrees and r/R of 0.98.

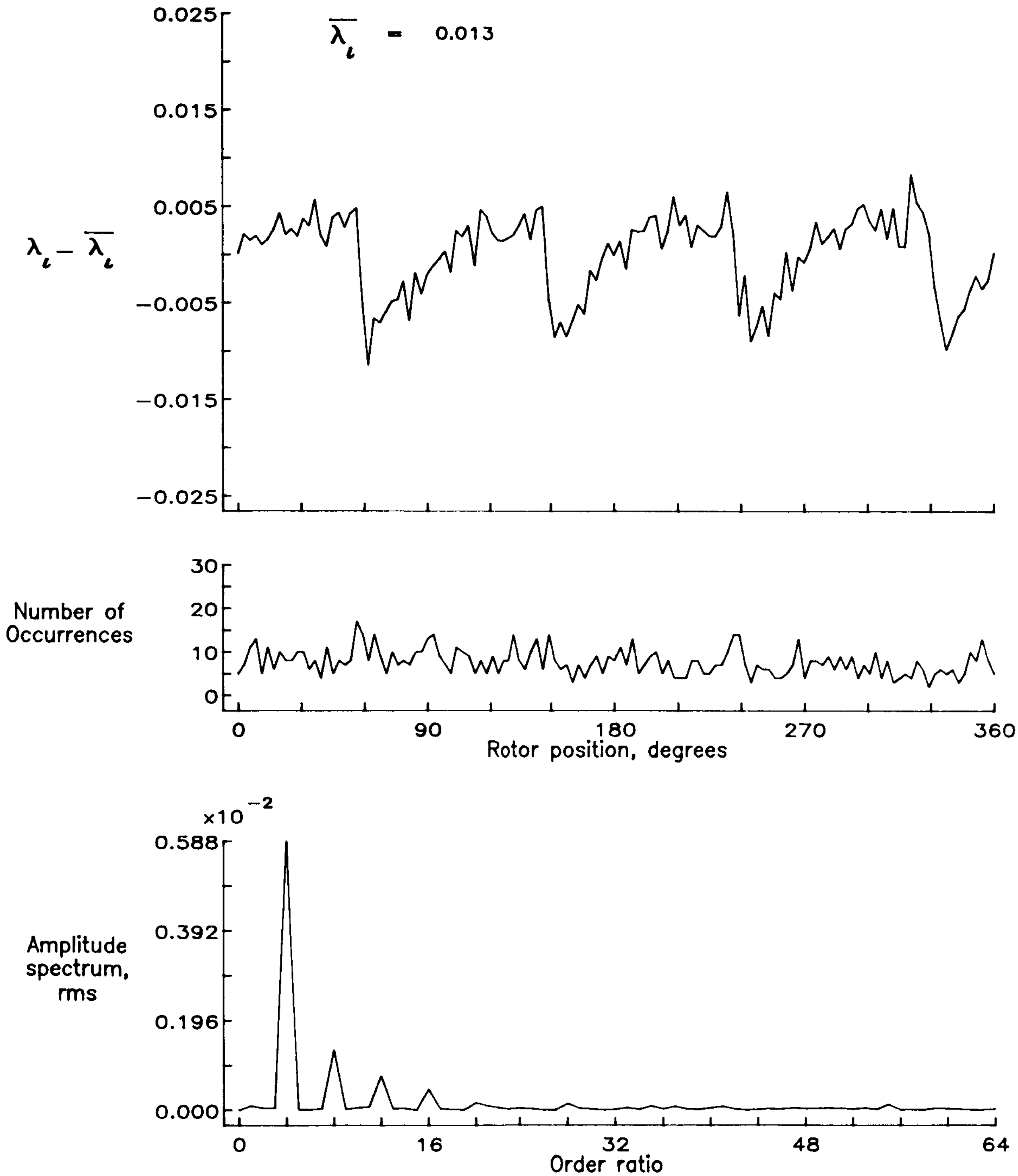

Figure 119.- Concluded.

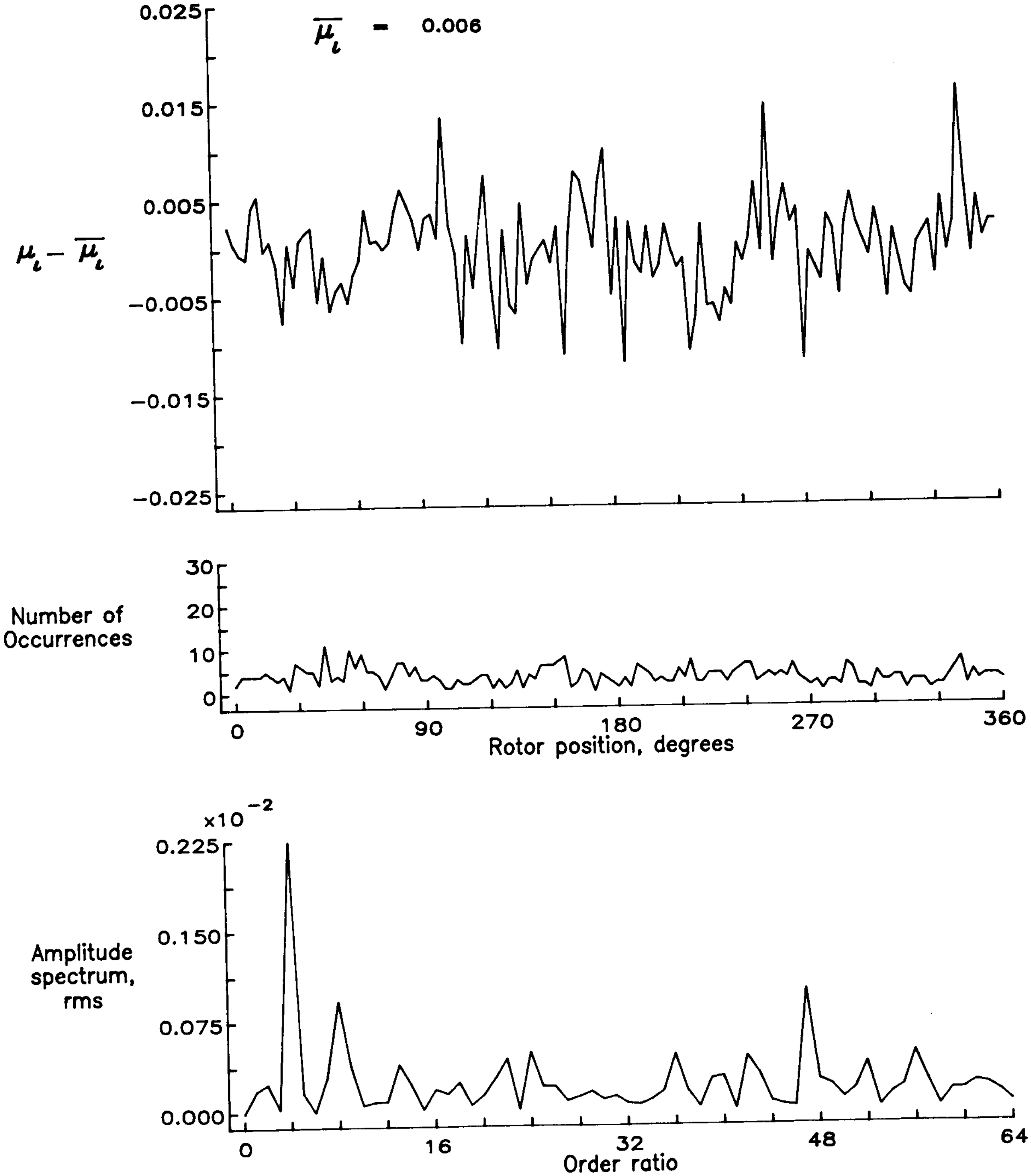

Figure 120.– Induced inflow velocity measured at 240 degrees and r/R of 1.04.

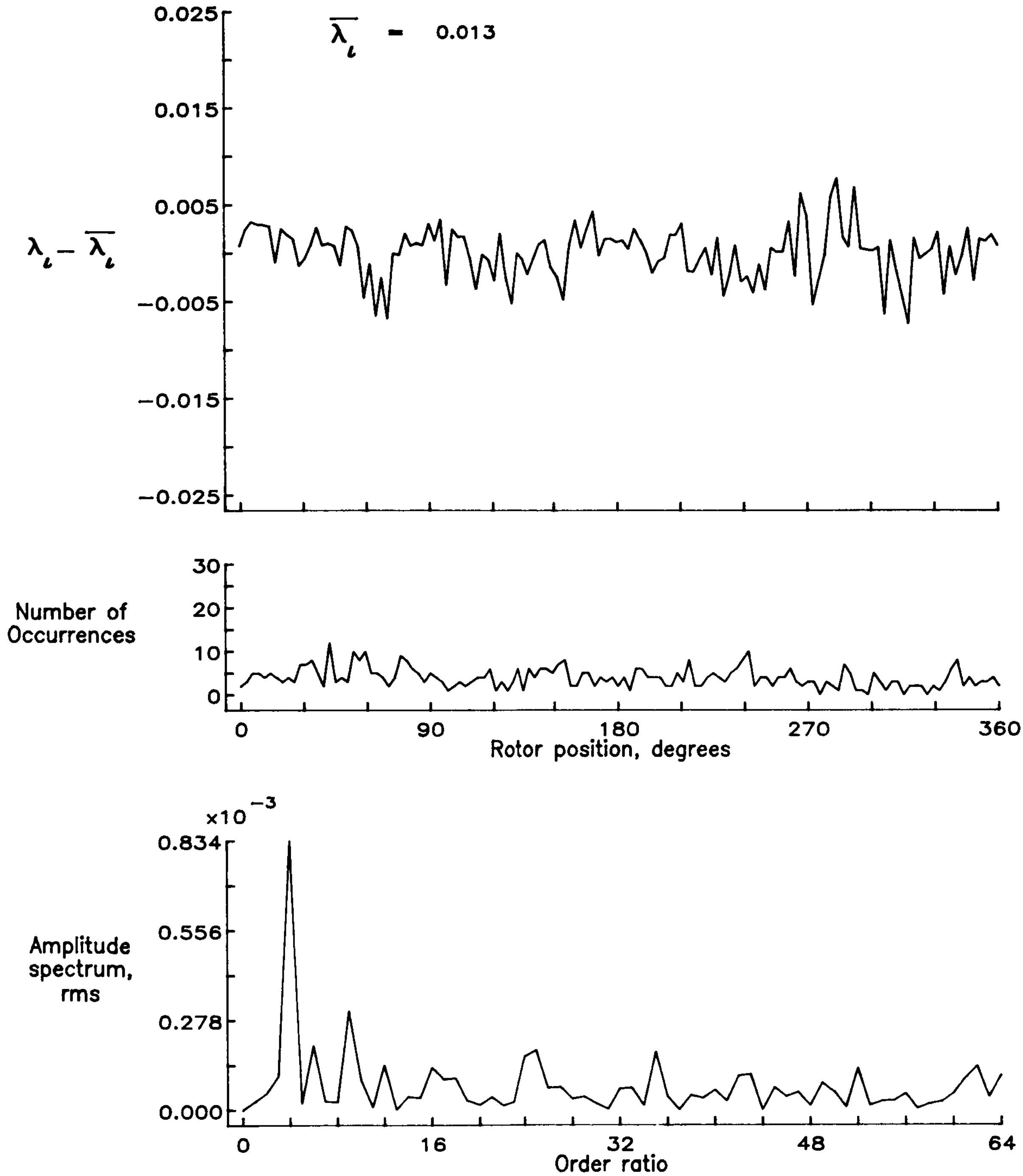

Figure 120.– Concluded.

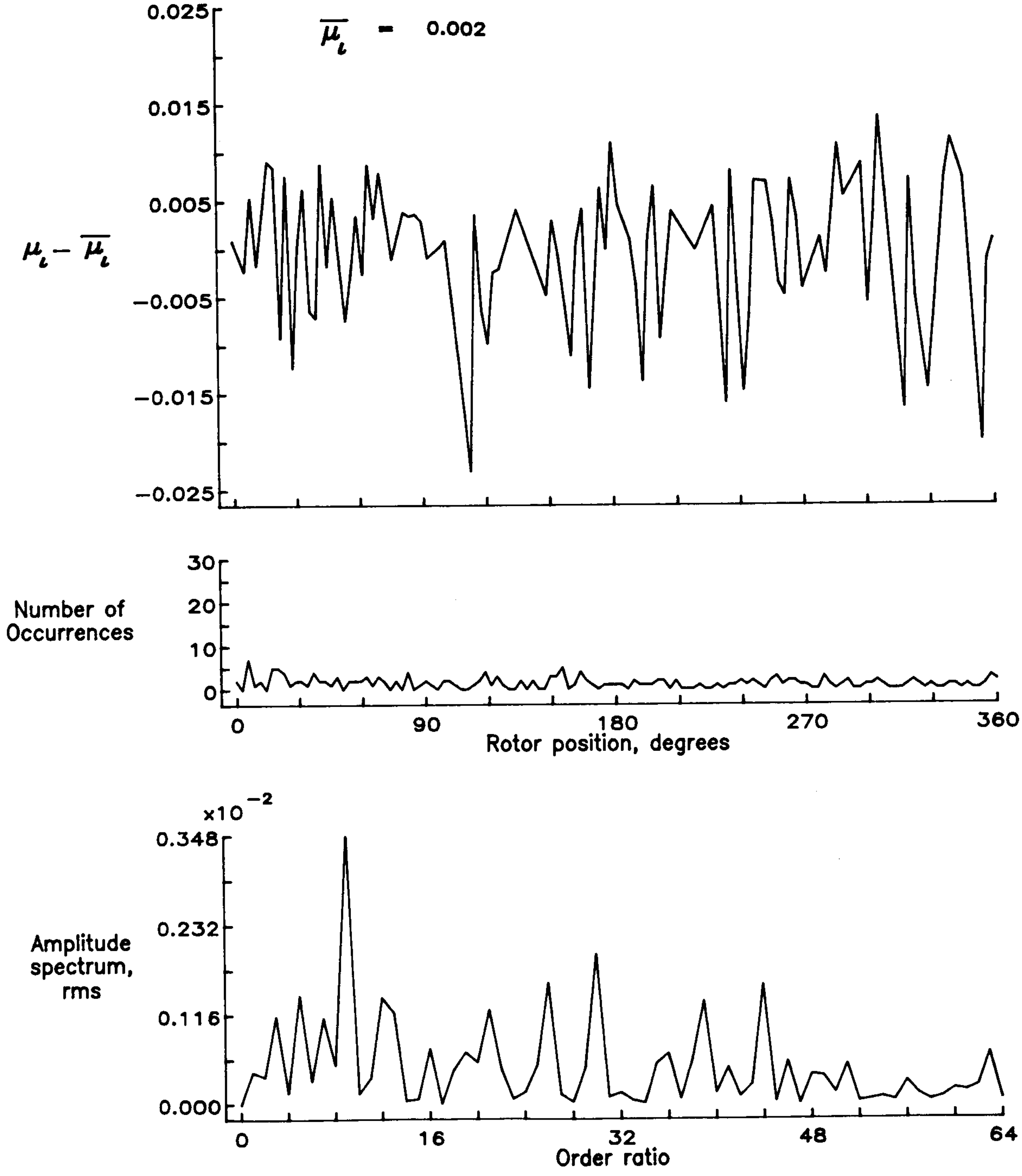

Figure 121.– Induced inflow velocity measured at 240 degrees and r/R of 1.10.

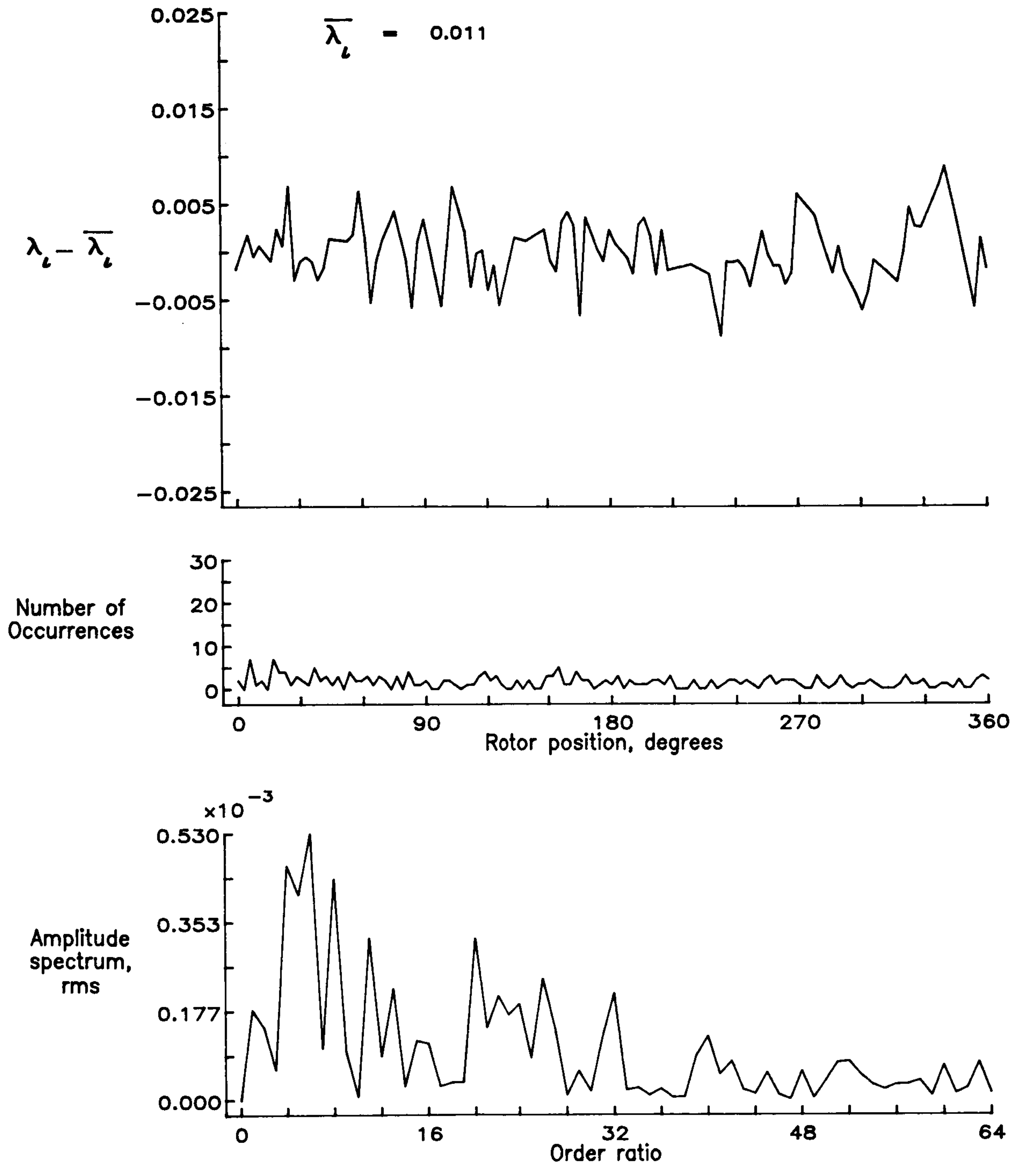

Figure 121.– Concluded.

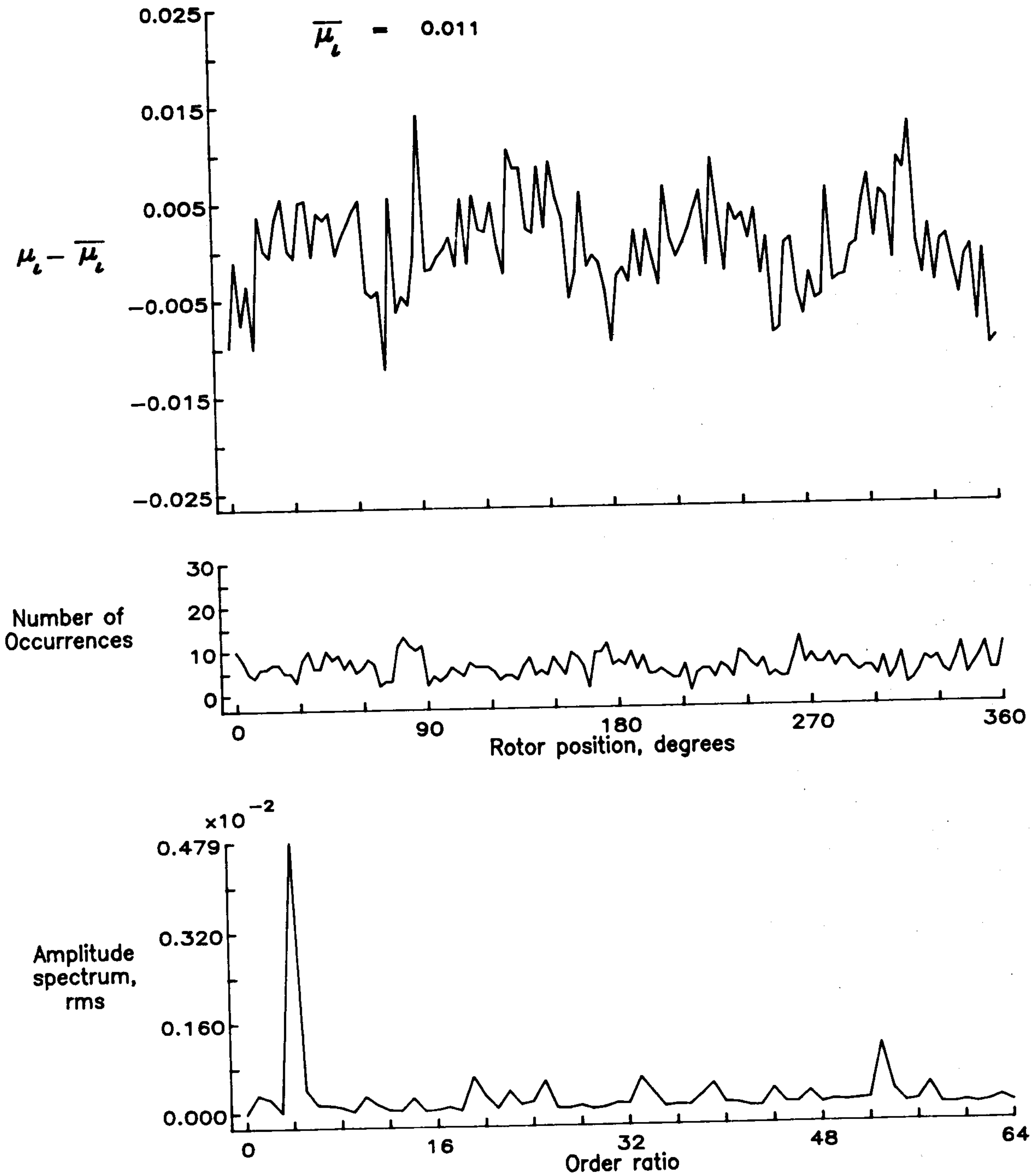

Figure 122.– Induced inflow velocity measured at 270 degrees and r/R of 0.40.

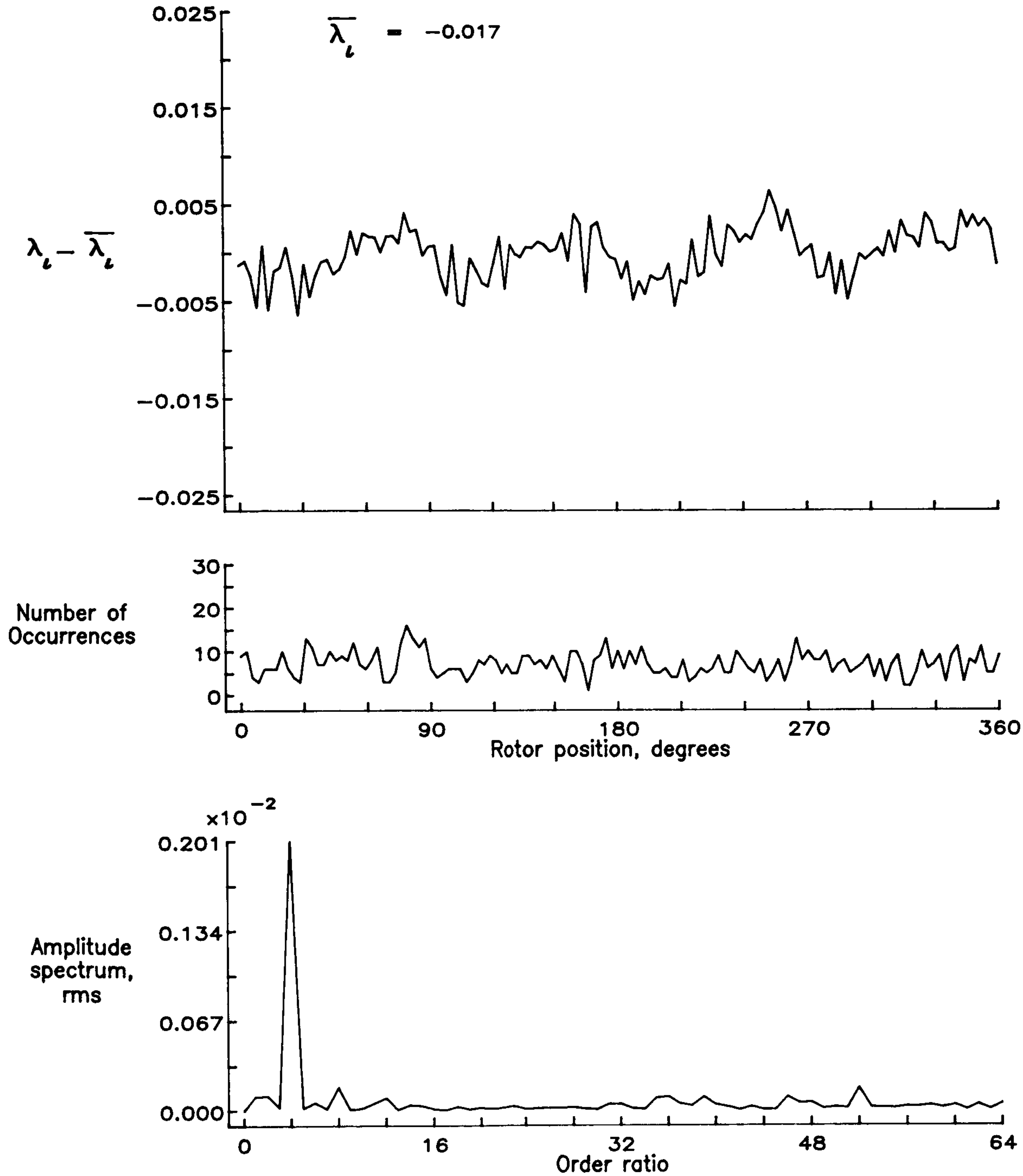

Figure 122.– Concluded.

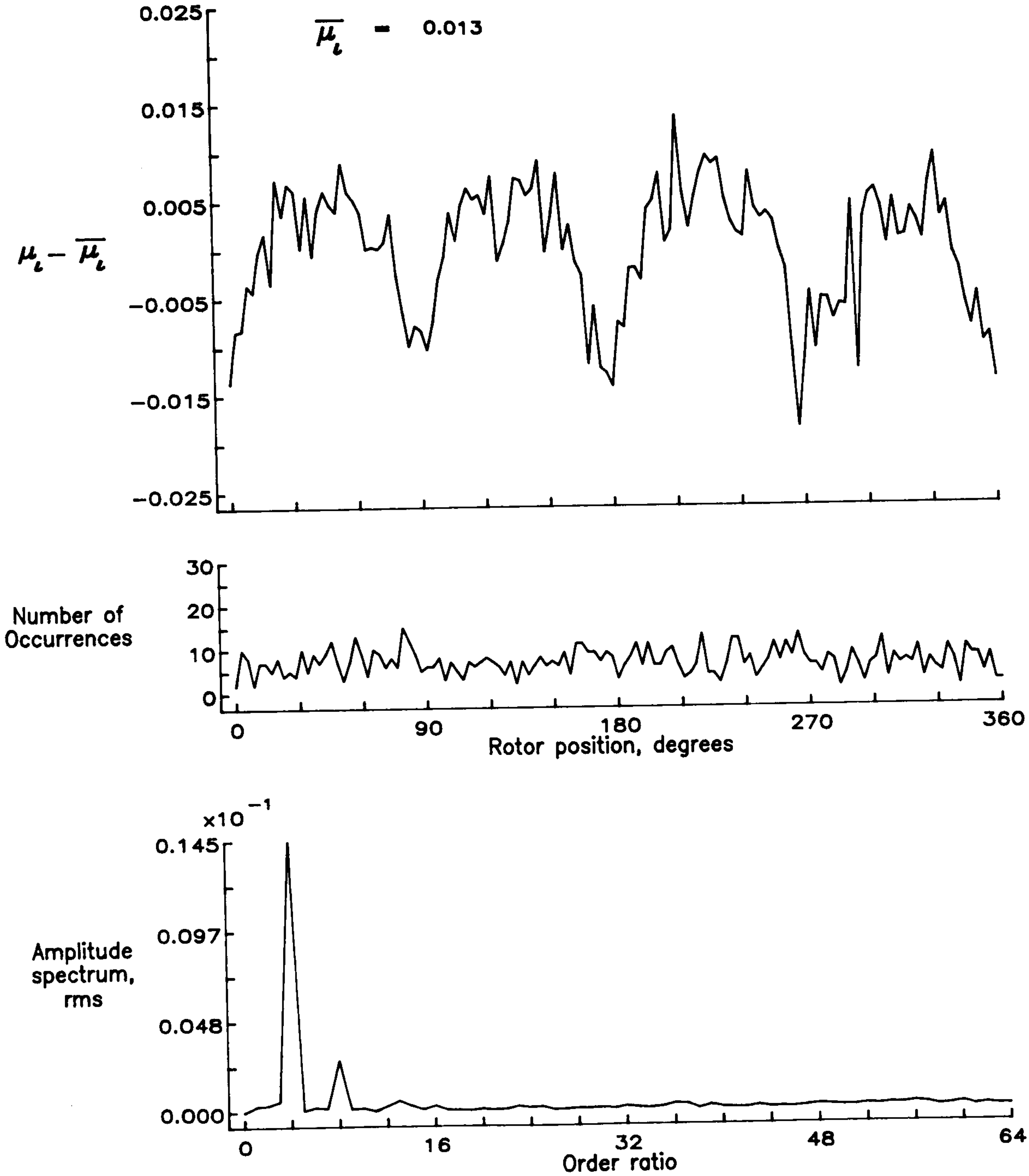

Figure 123.– Induced inflow velocity measured at 270 degrees and r/R of 0.50.

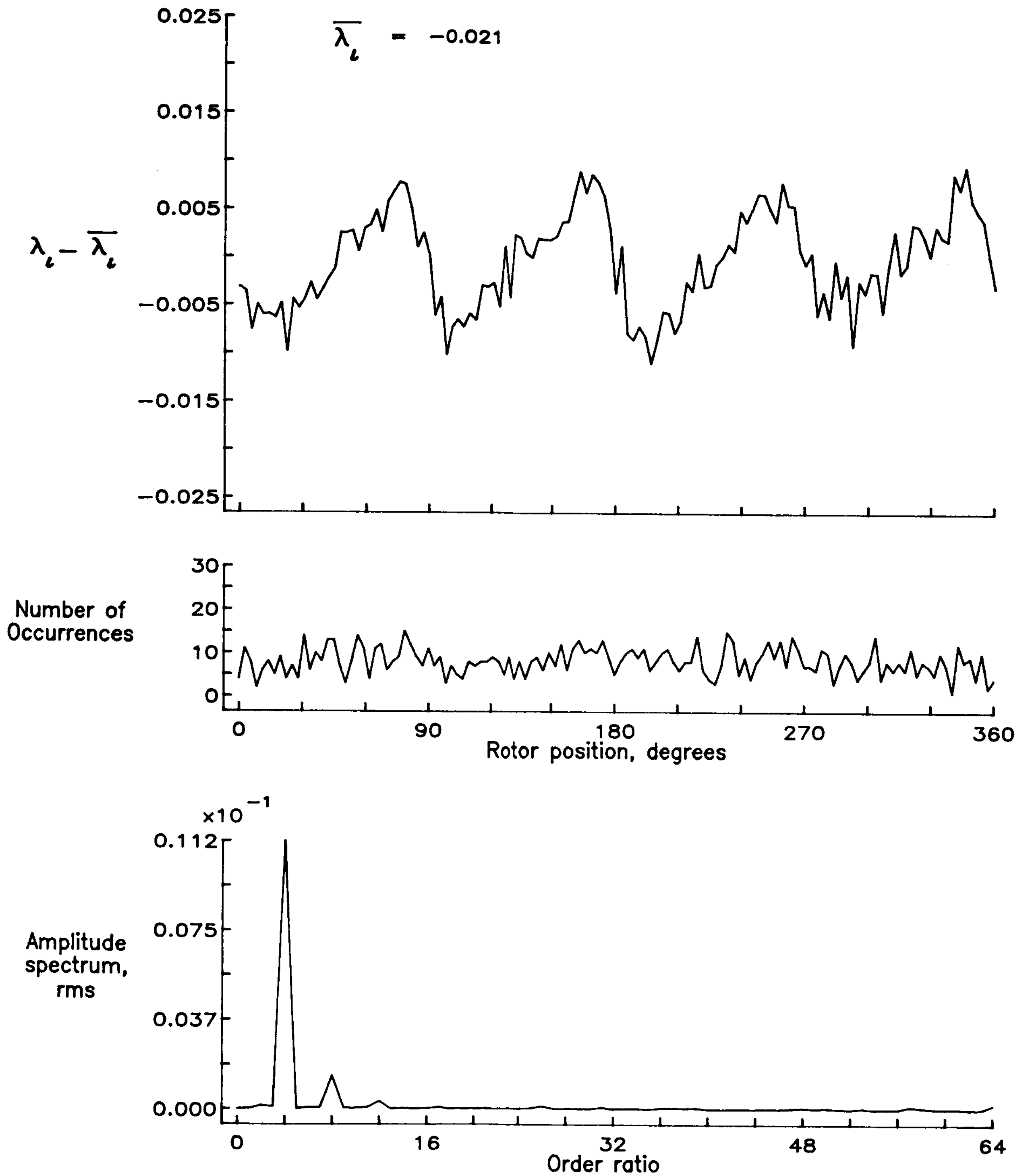

Figure 123.– Concluded.

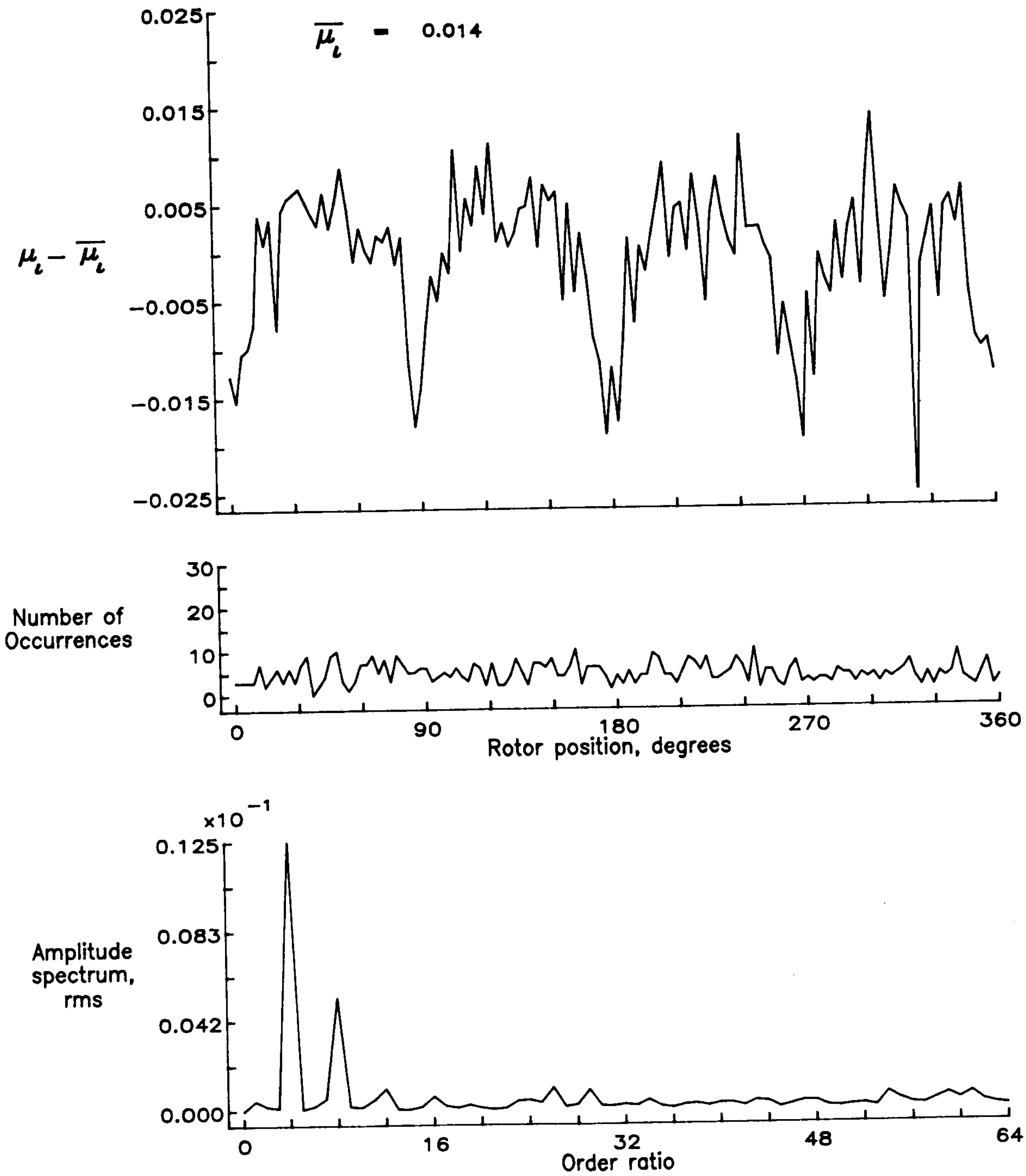

Figure 124.– Induced inflow velocity measured at 270 degrees and r/R of 0.60.

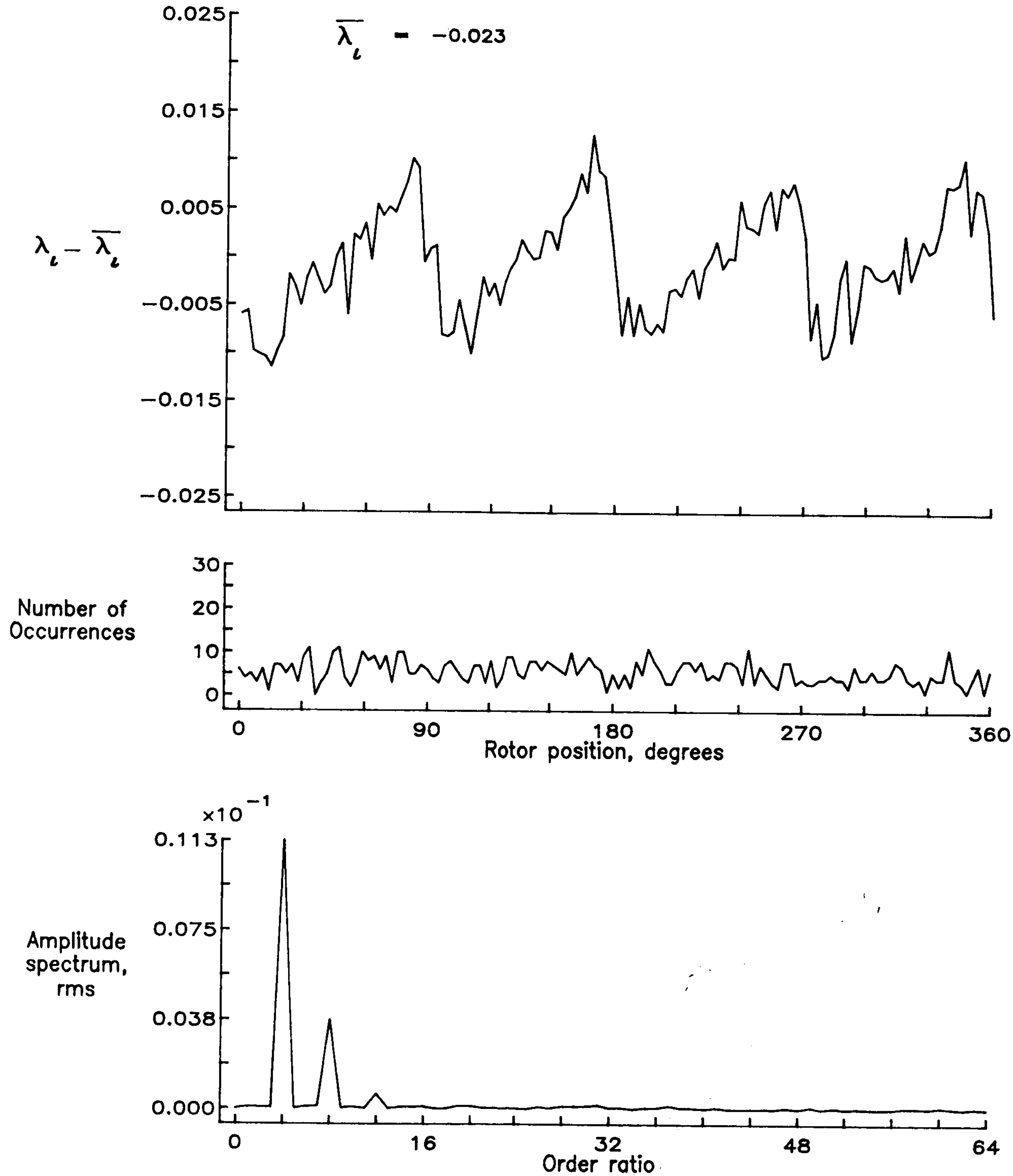

Figure 124.– Concluded.

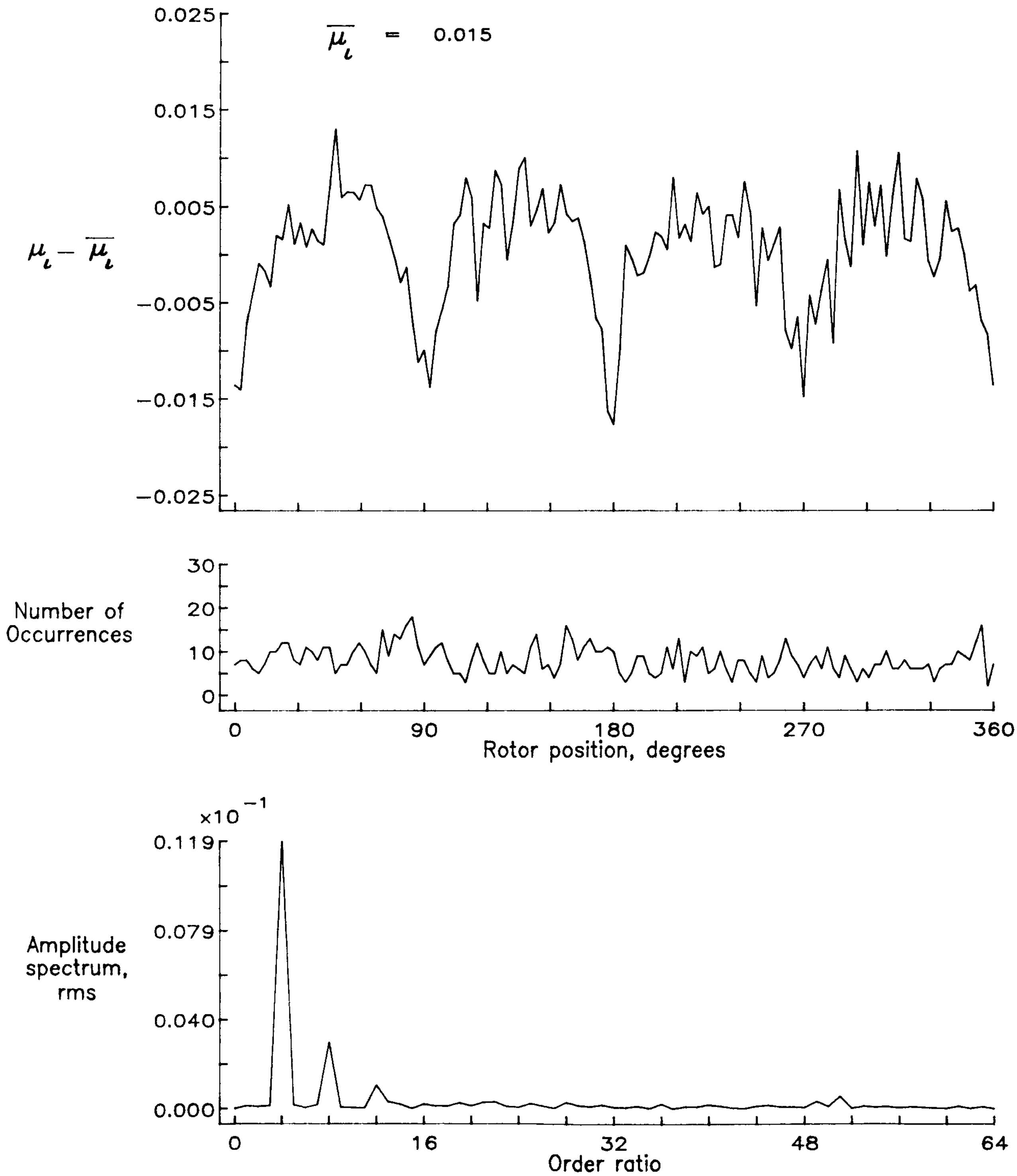

Figure 125.– Induced inflow velocity measured at 270 degrees and r/R of 0.70.

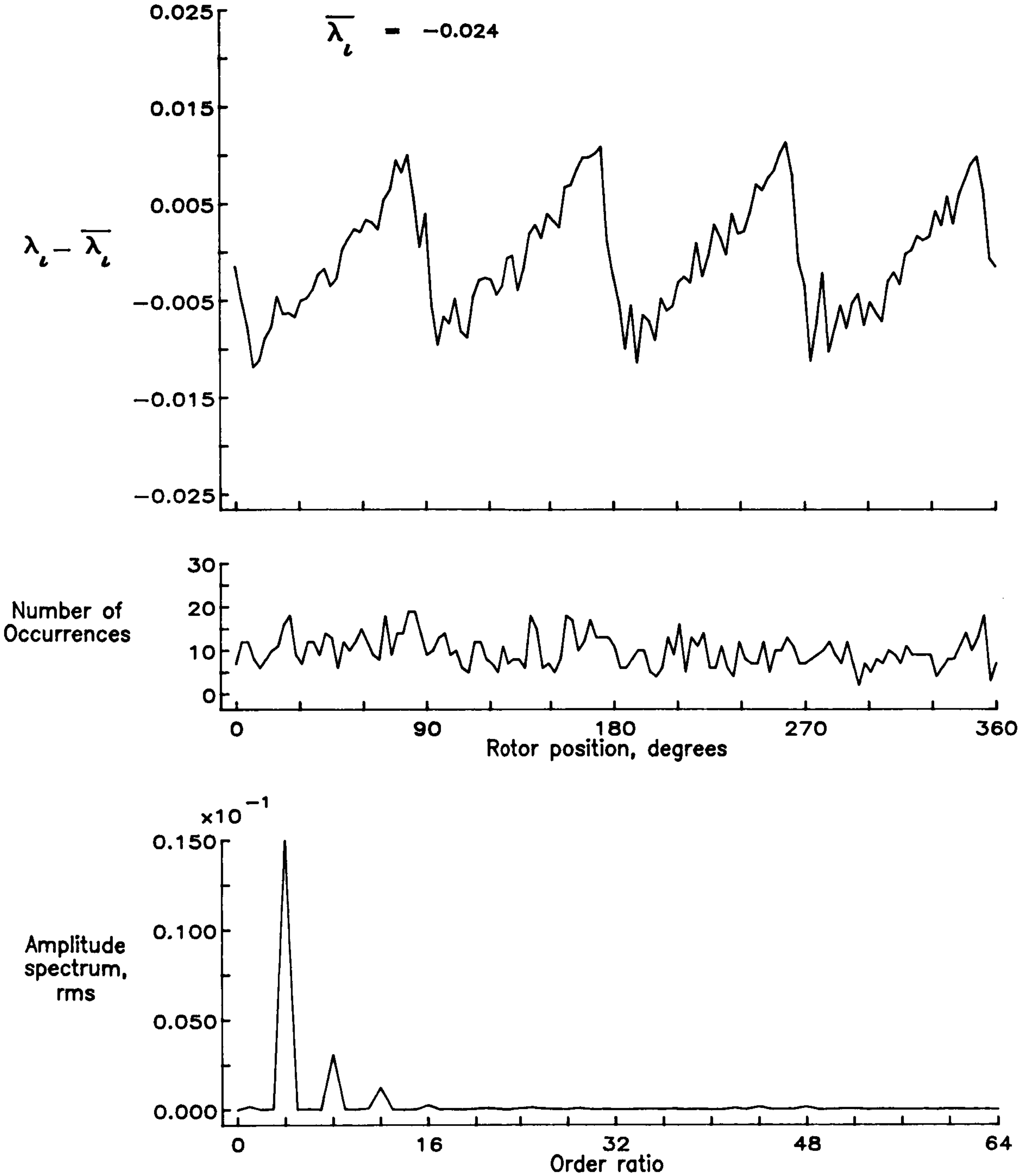

Figure 125.– Concluded.

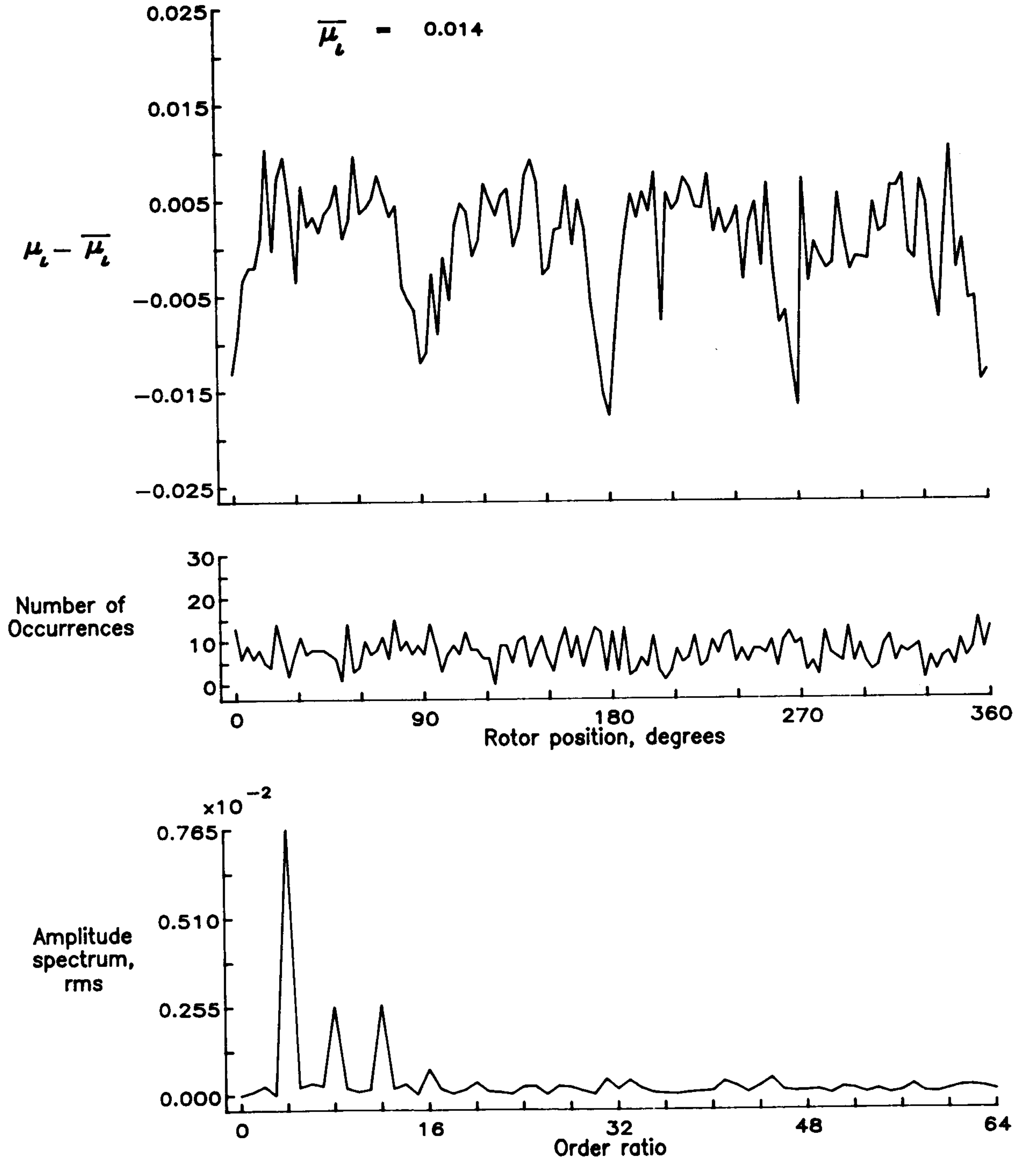

Figure 126.– Induced inflow velocity measured at 270 degrees and r/R of 0.74.

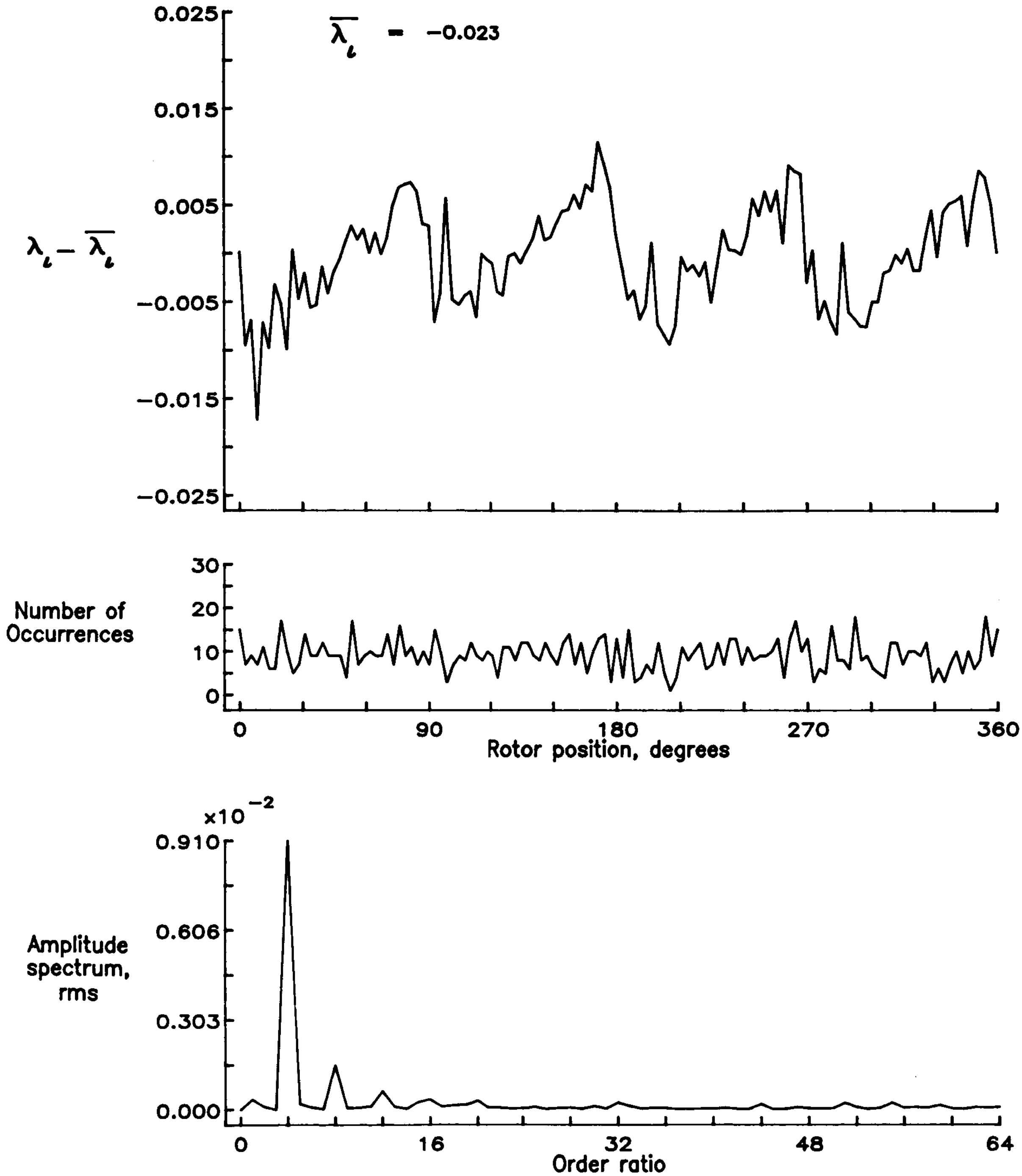

Figure 126.— Concluded.

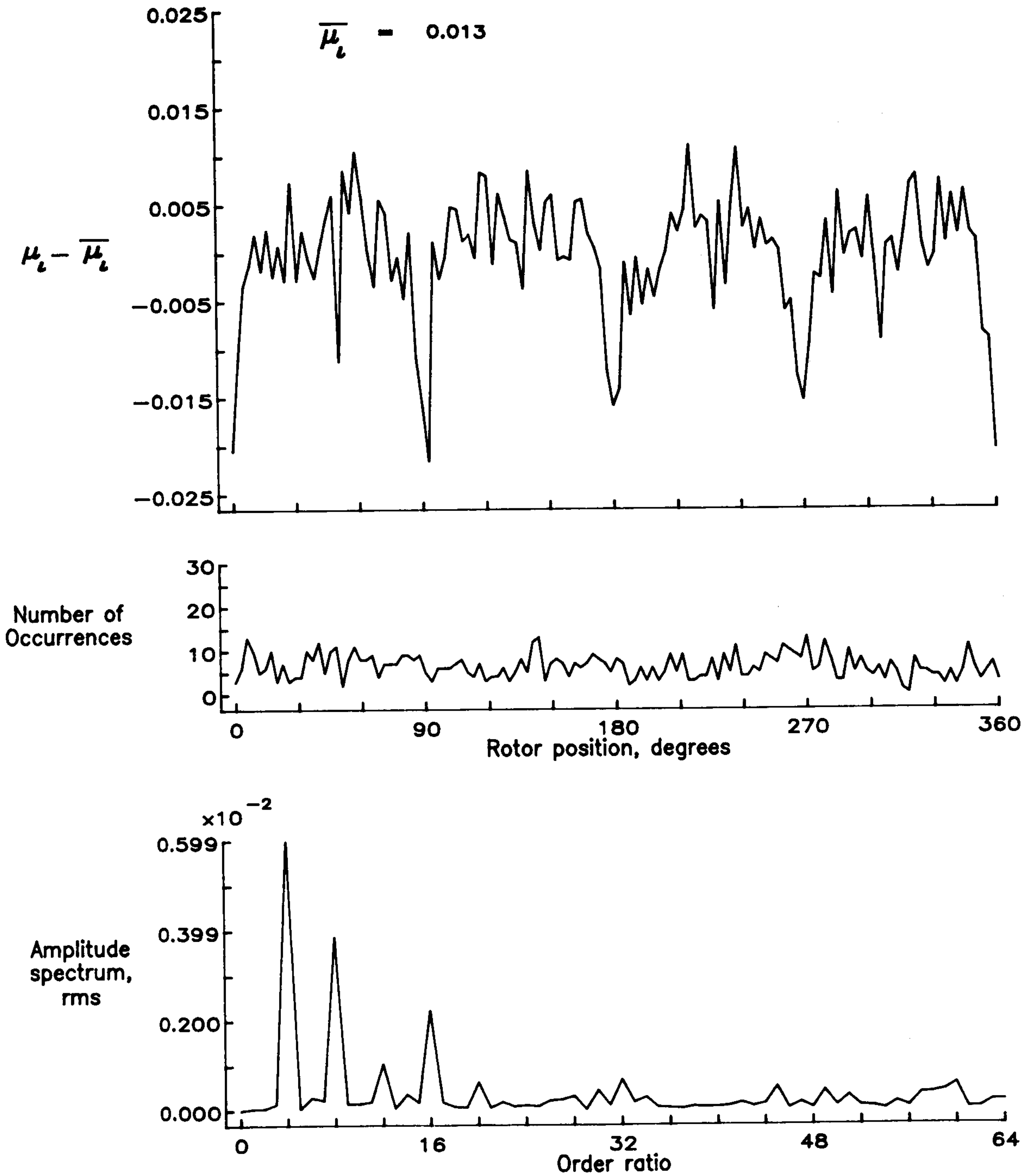

Figure 127.– Induced inflow velocity measured at 270 degrees and r/R of 0.78.

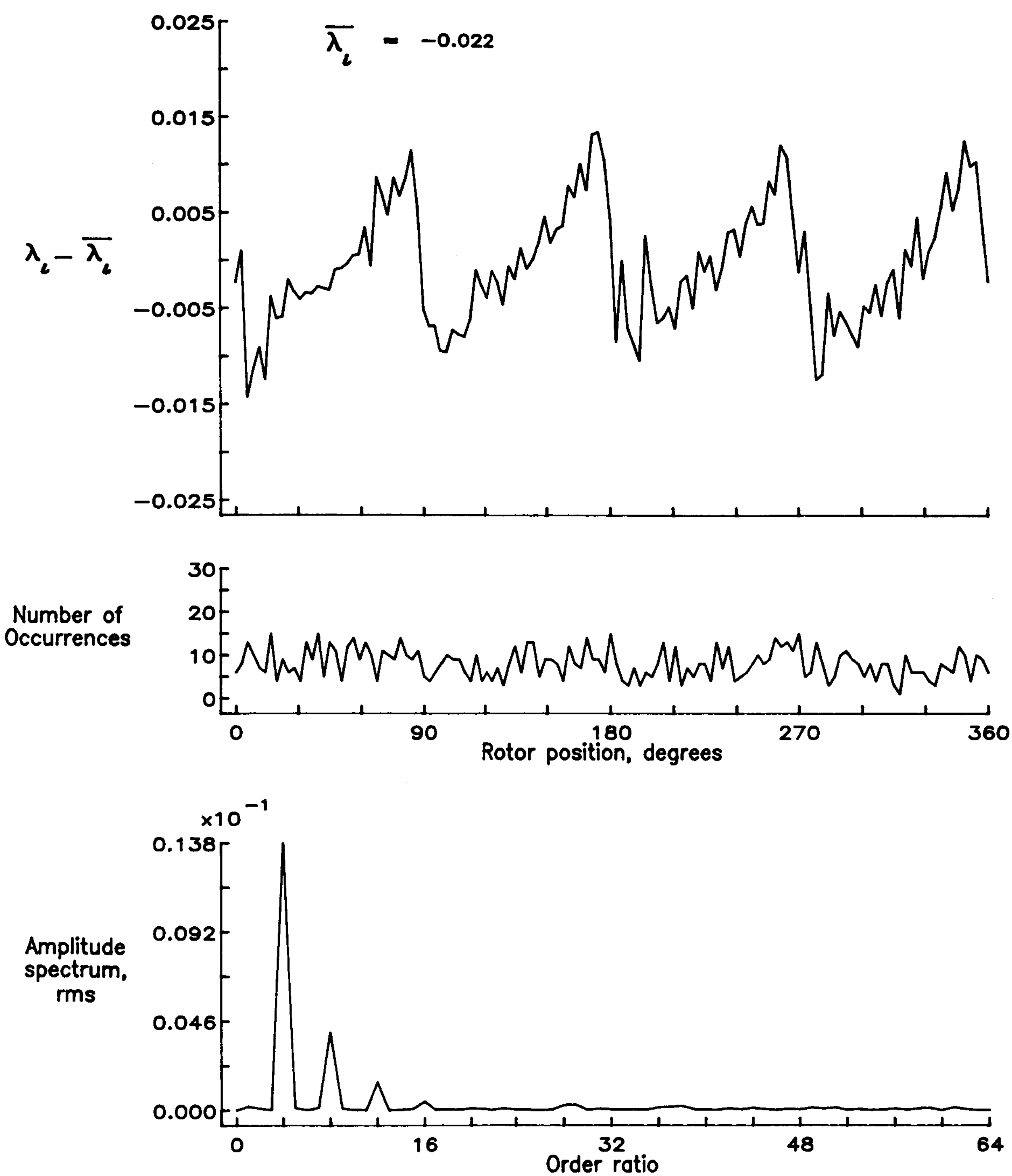

Figure 127.– Concluded.

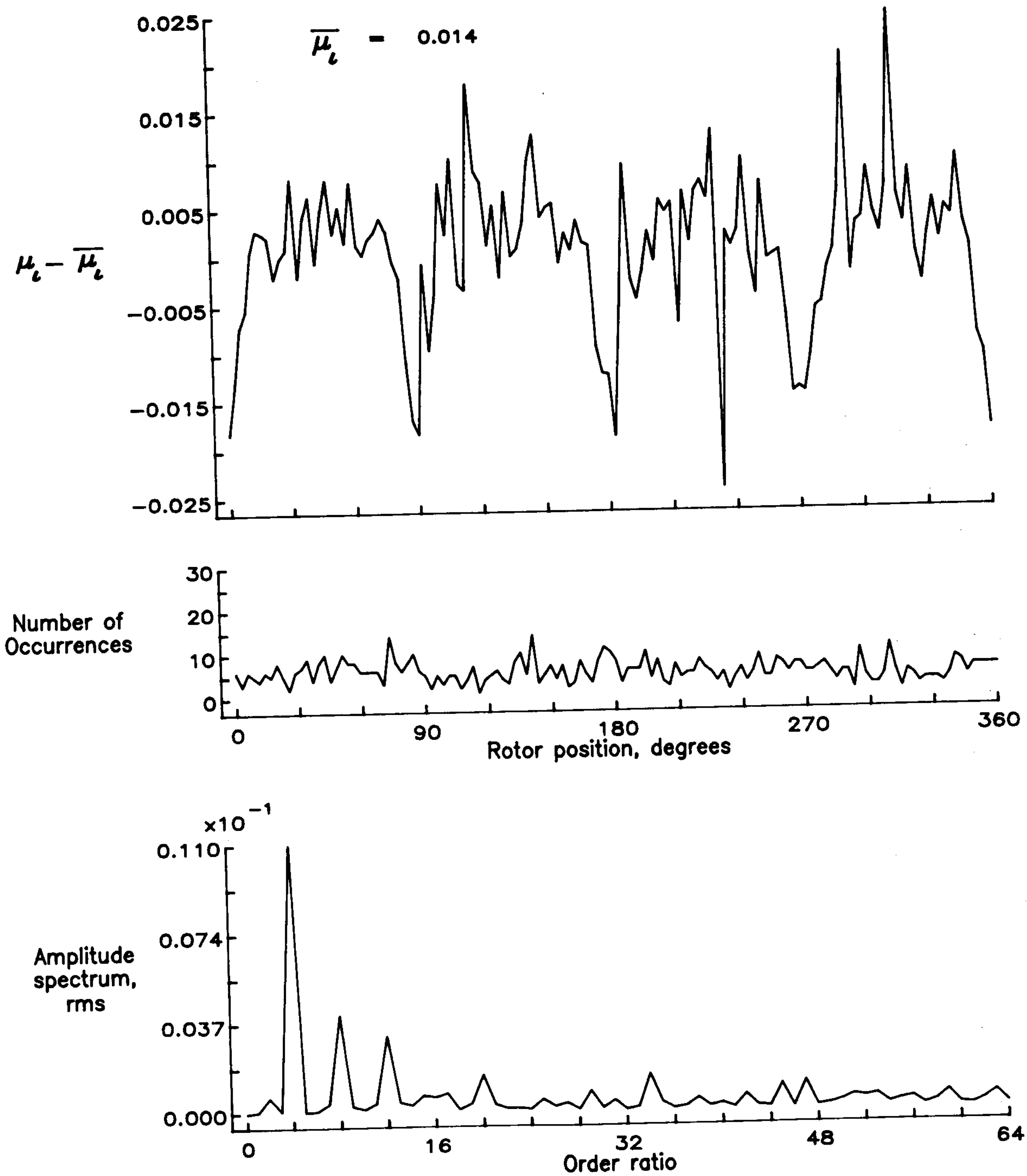

Figure 128.– Induced inflow velocity measured at 270 degrees and r/R of 0.82.

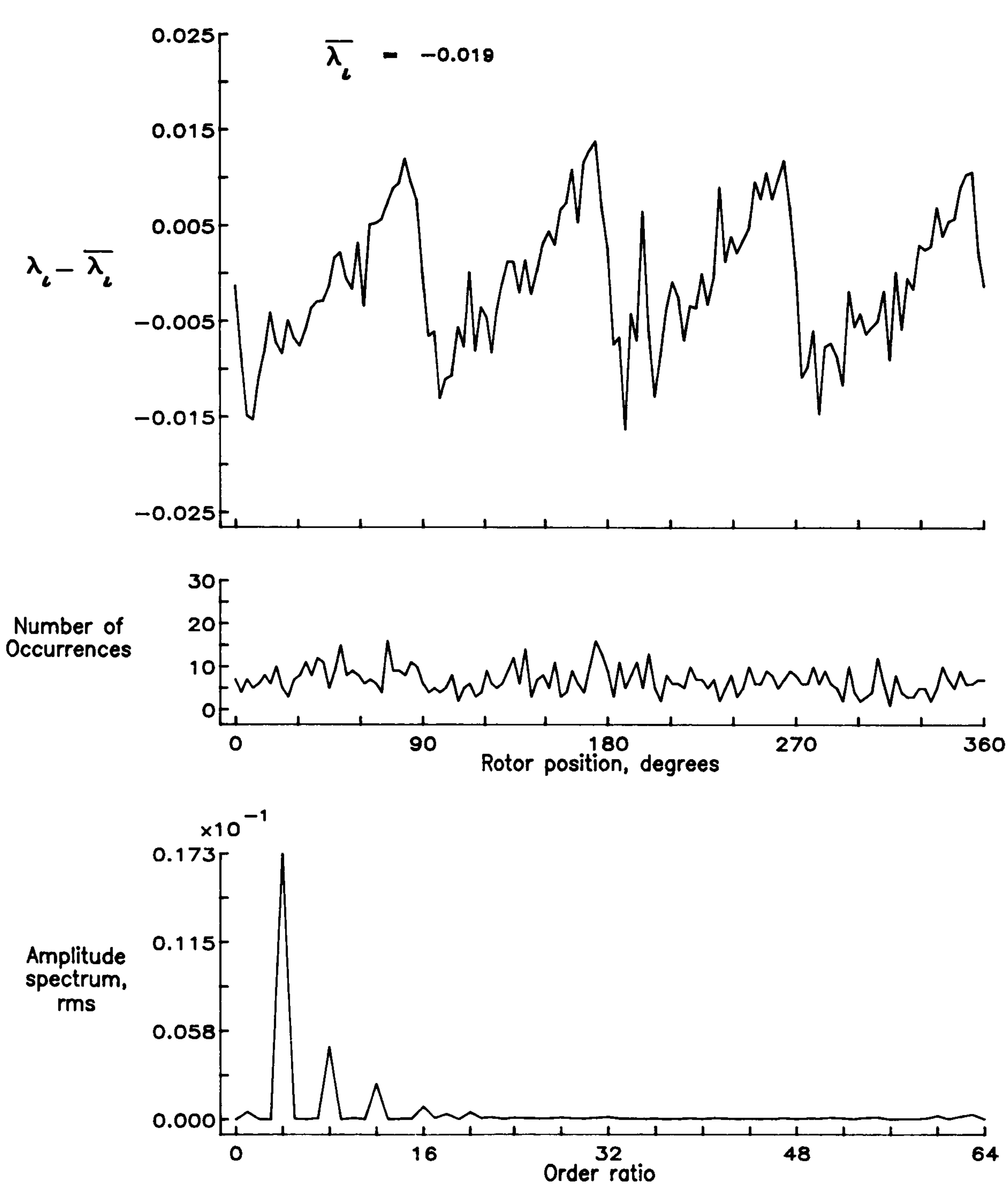

Figure 128.– Concluded.

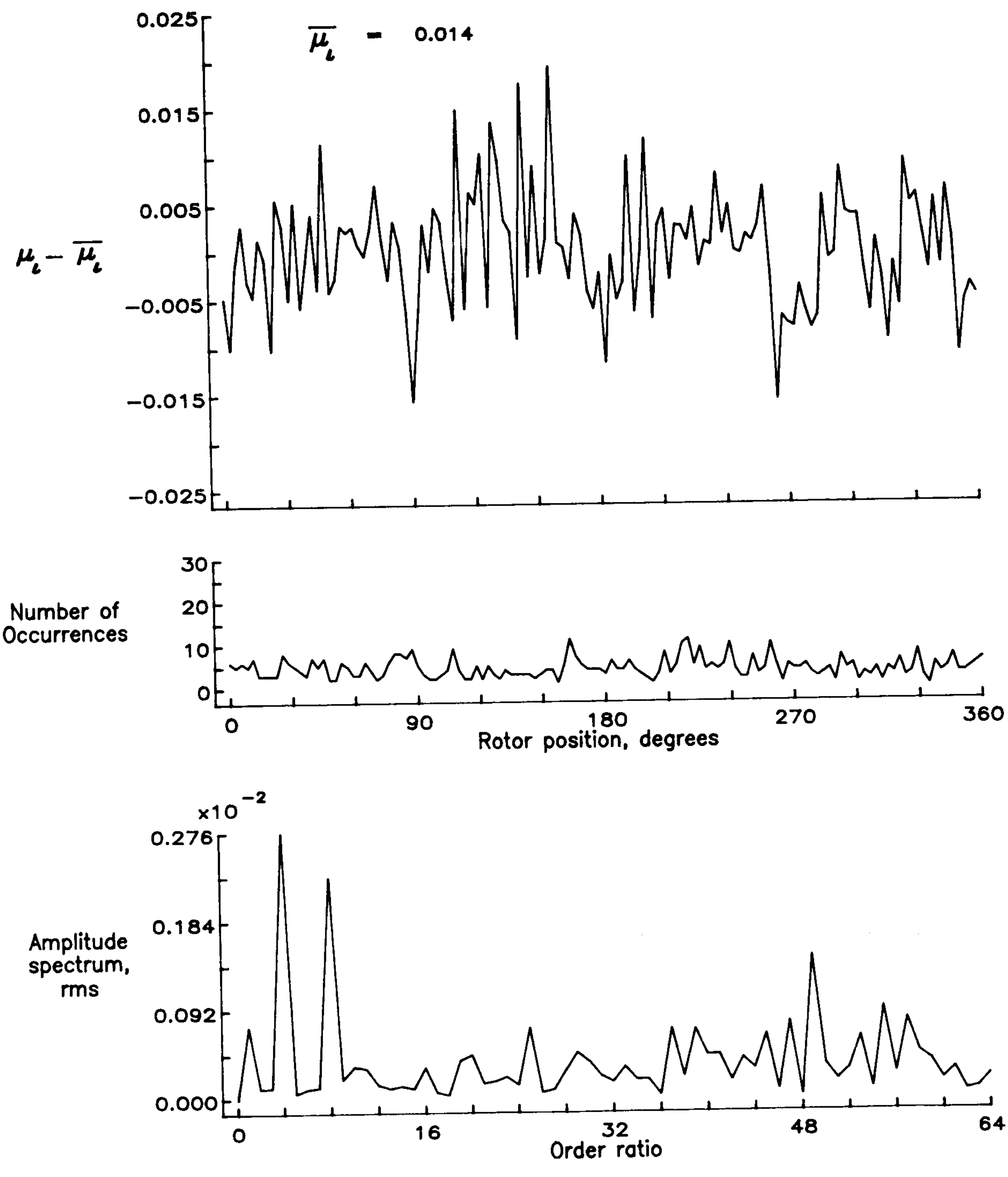

Figure 129.– Induced inflow velocity measured at 270 degrees and r/R of 0.86.

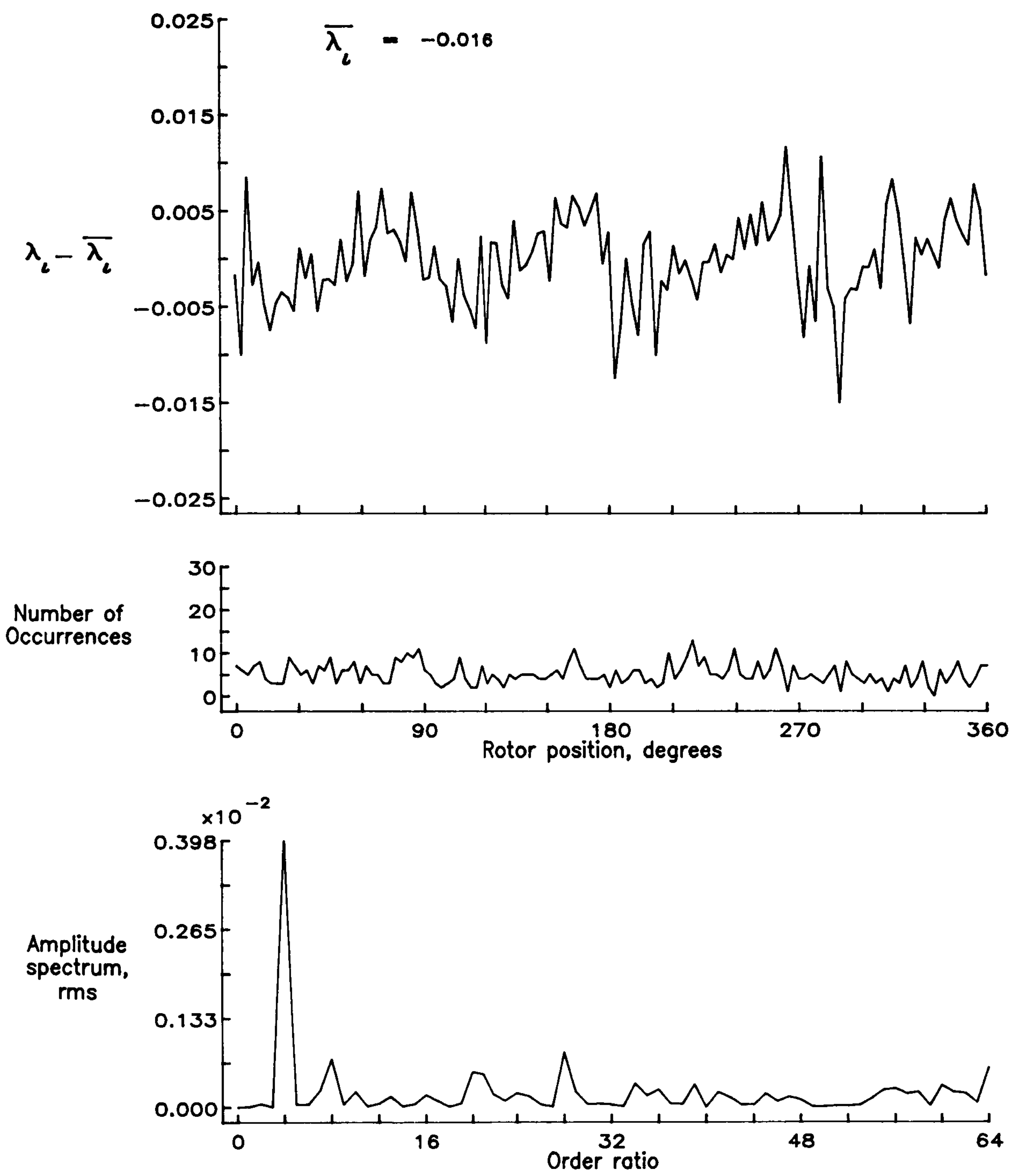

Figure 129.– Concluded.

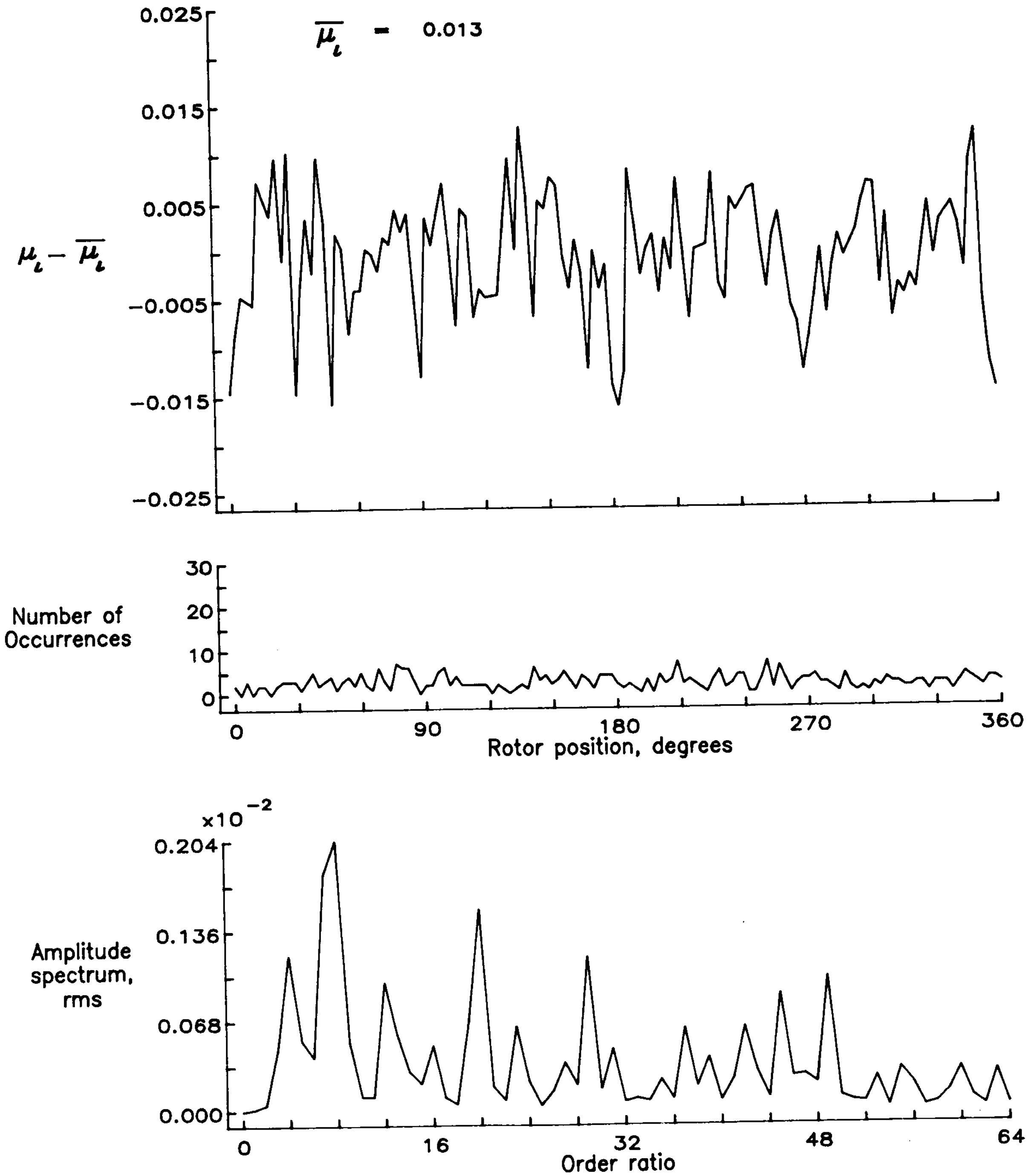

Figure 130.– Induced inflow velocity measured at 270 degrees and r/R of 0.90.

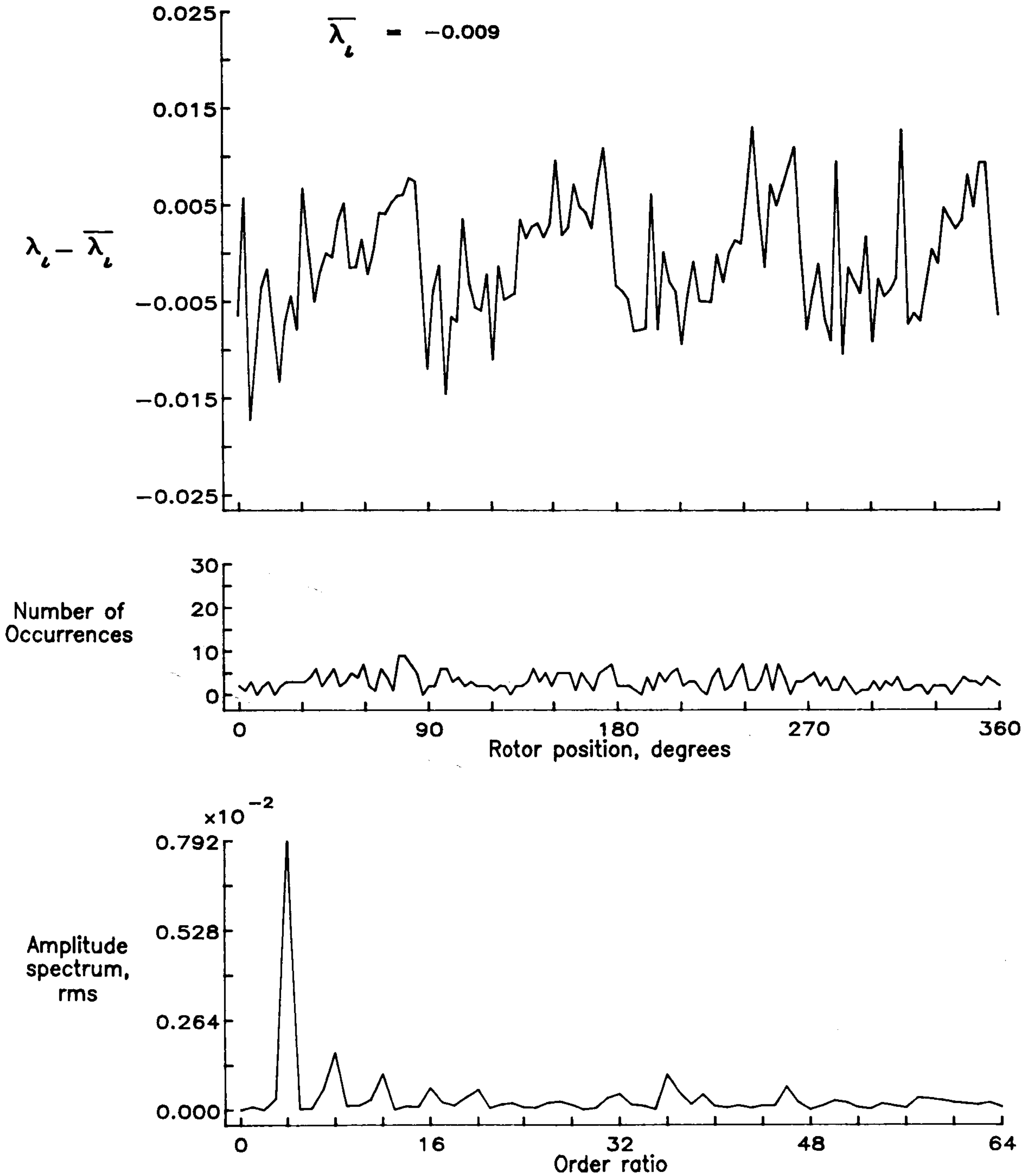

Figure 130.– Concluded.

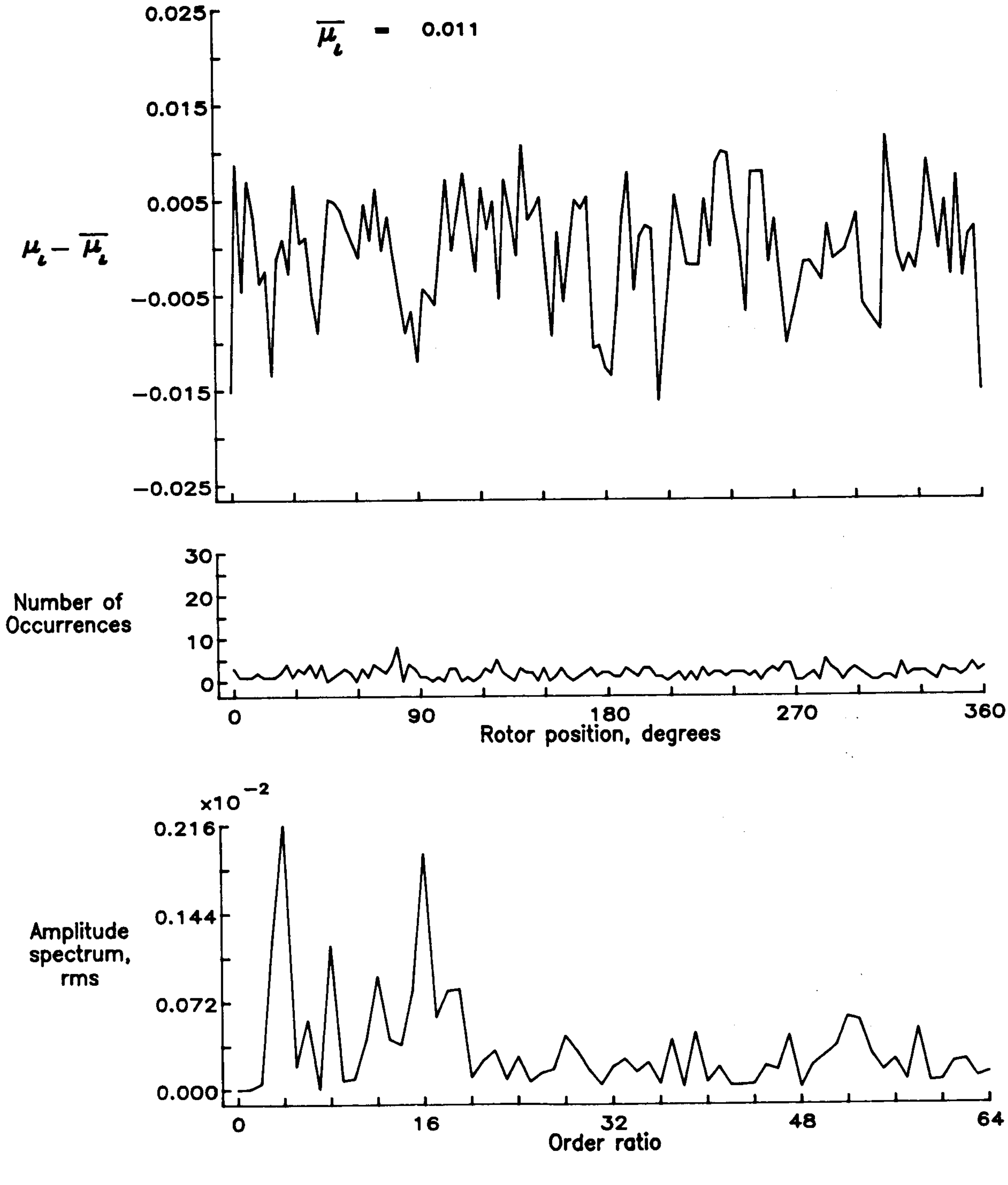

Figure 131.– Induced inflow velocity measured at 270 degrees and r/R of 0.94.

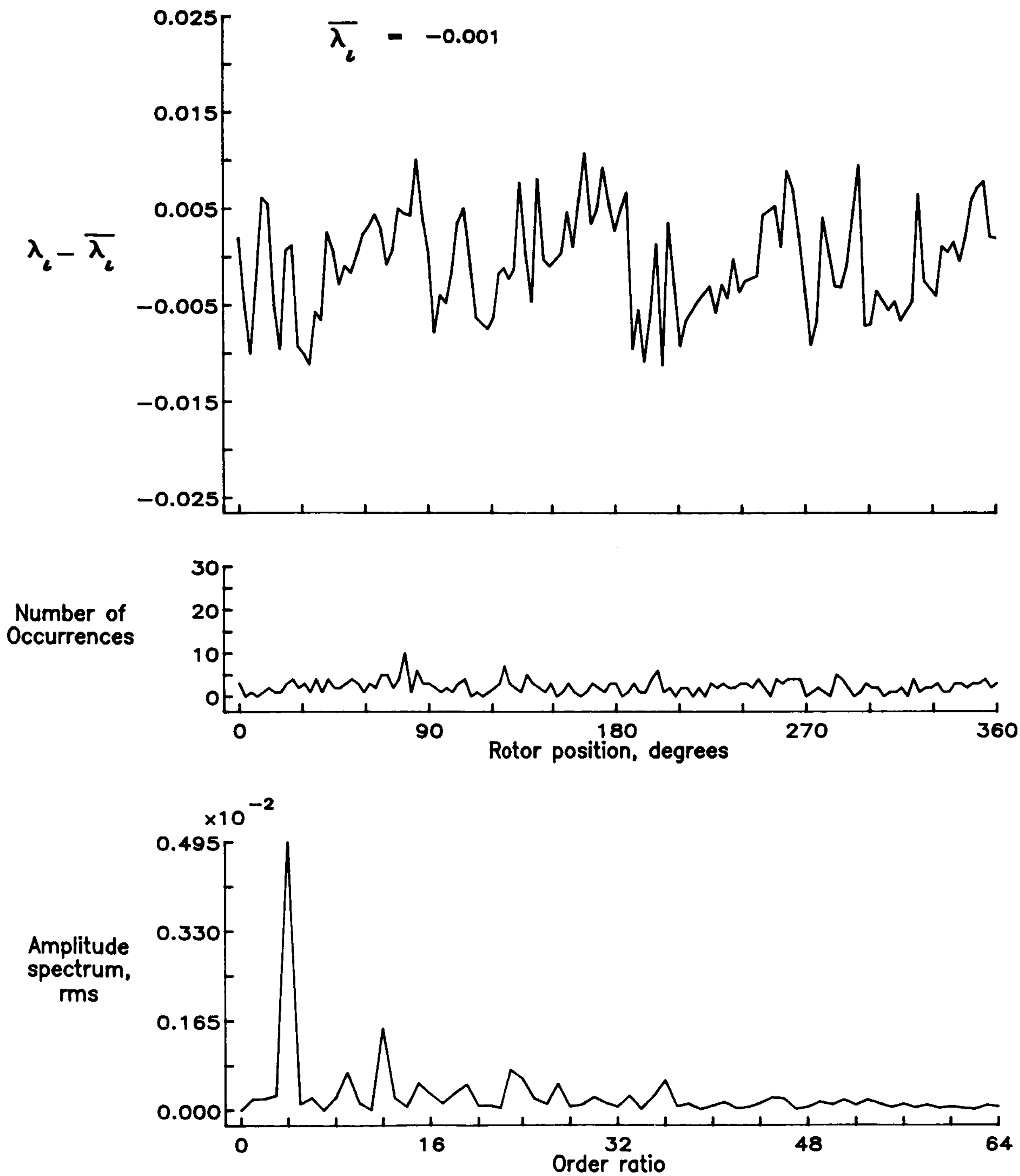

Figure 131.– Concluded.

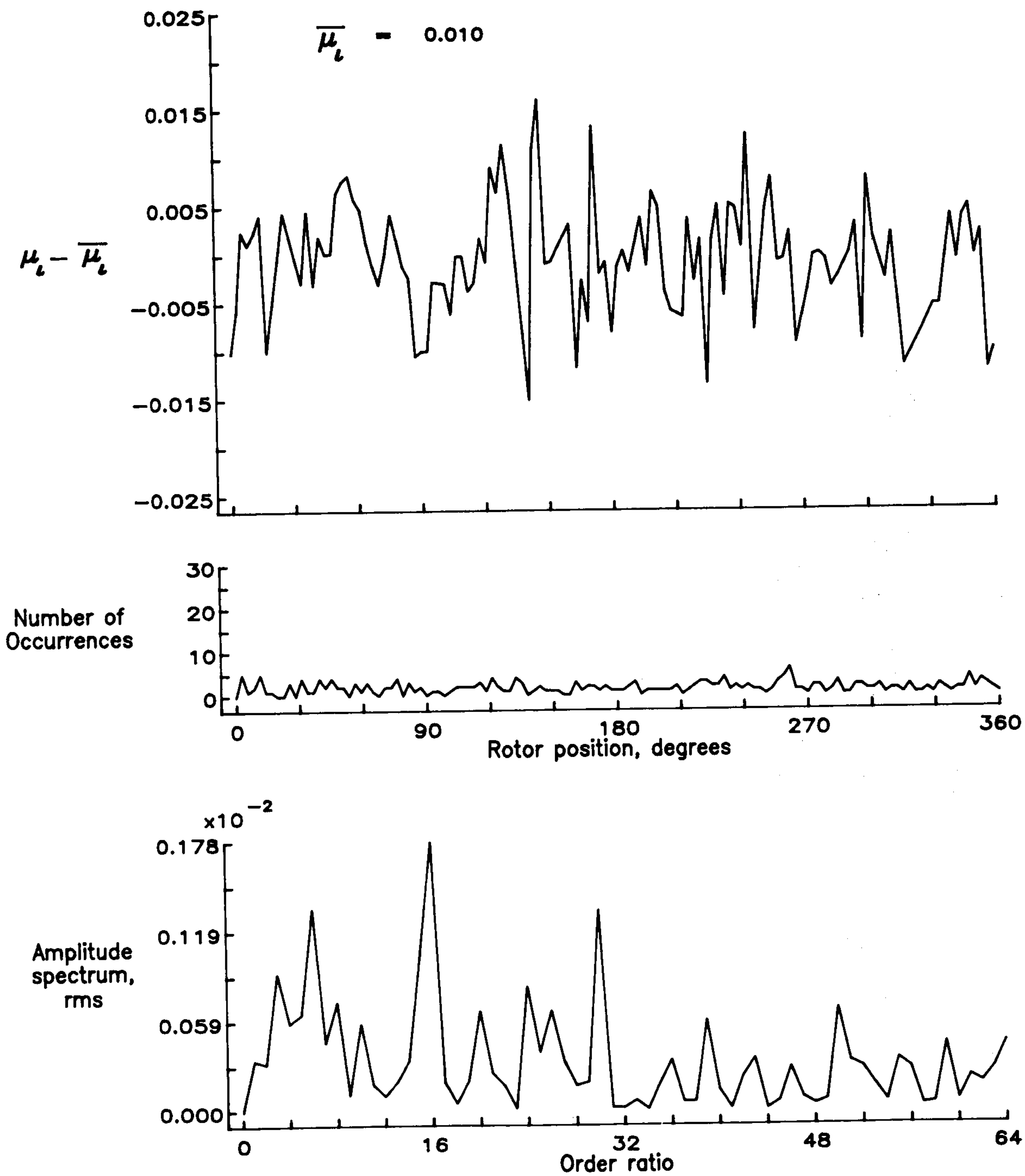

Figure 132.– Induced inflow velocity measured at 270 degrees and r/R of 0.98.

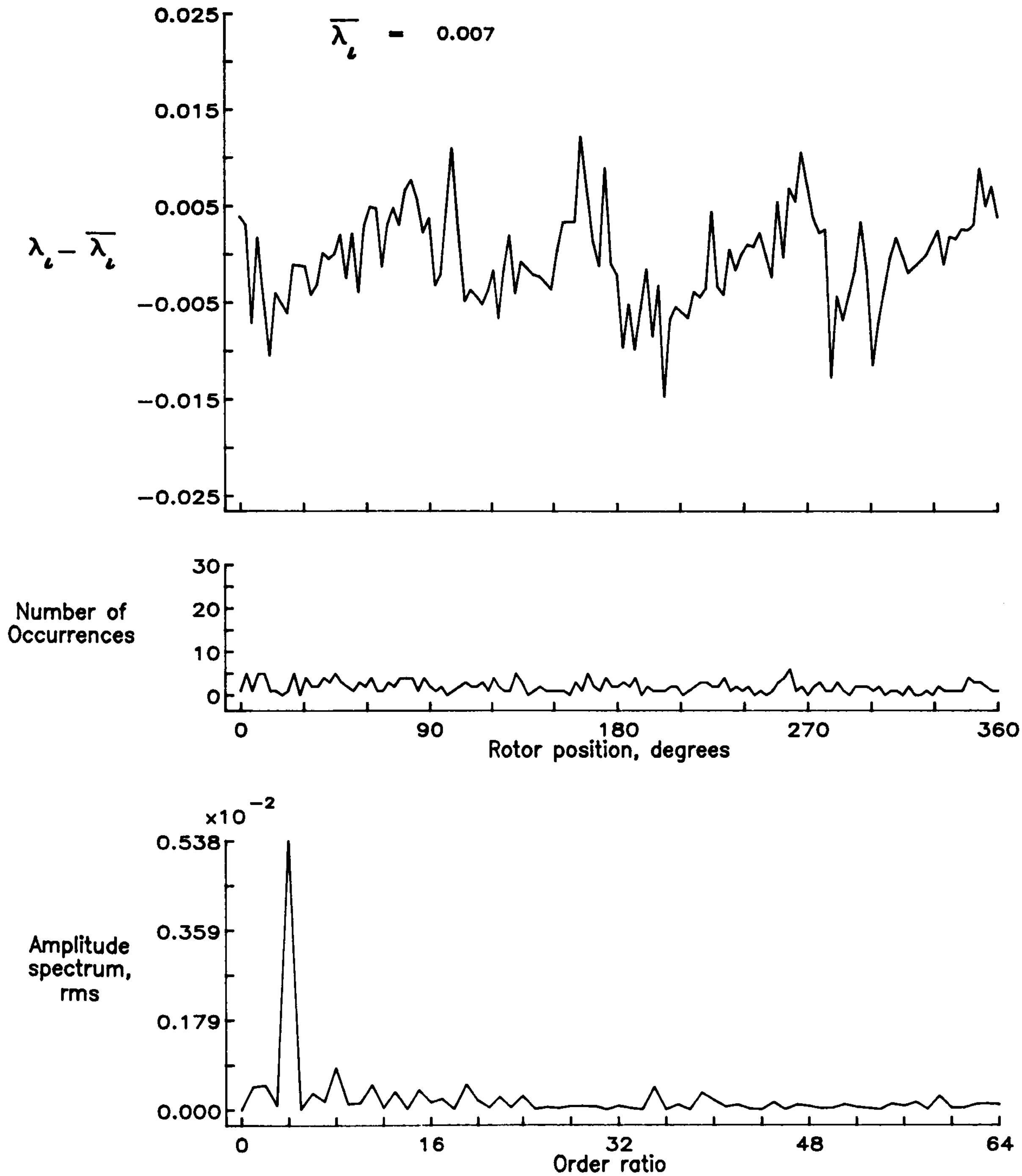

Figure 132.– Concluded.

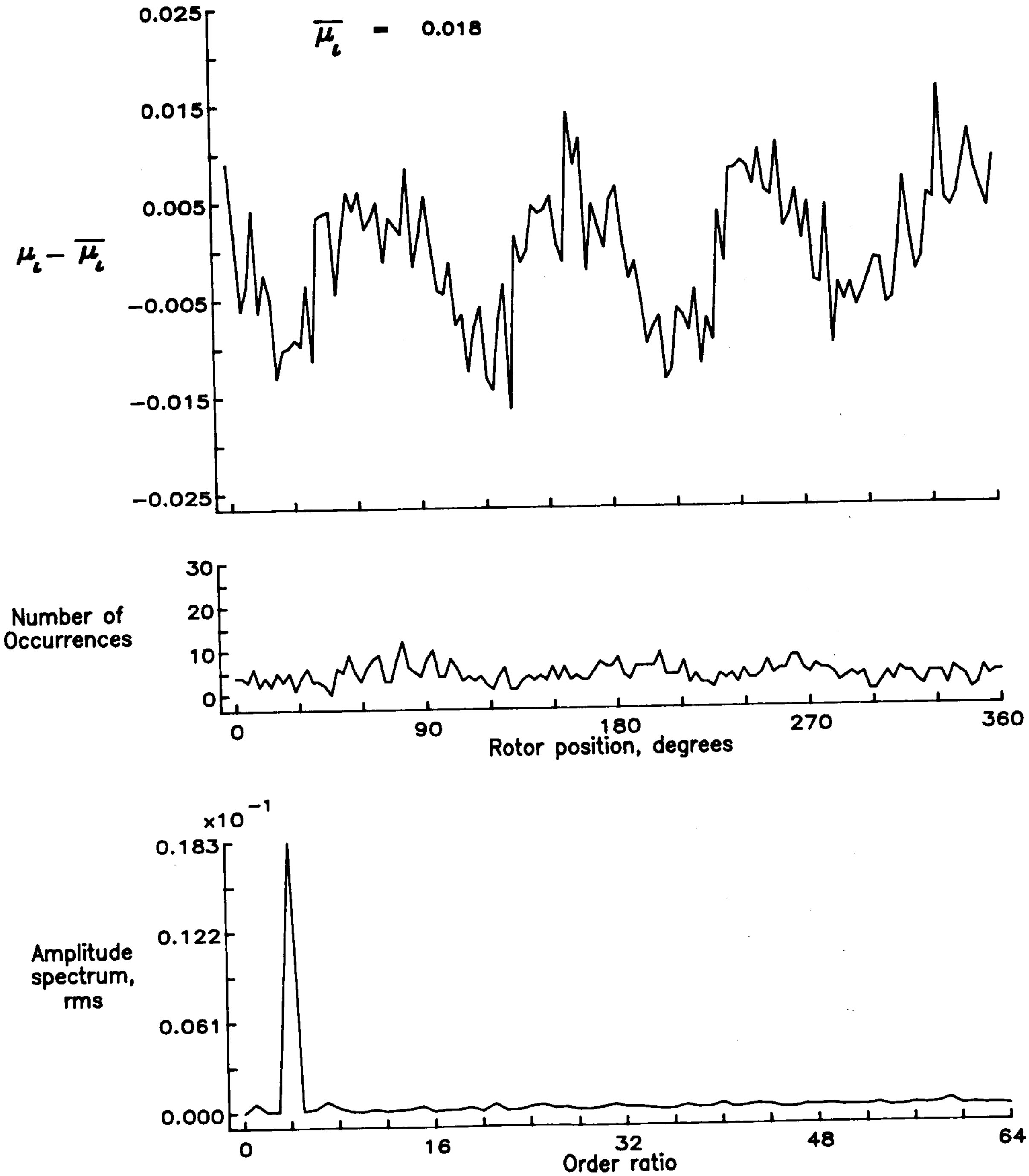

Figure 133.– Induced inflow velocity measured at 300 degrees and r/R of 0.40.

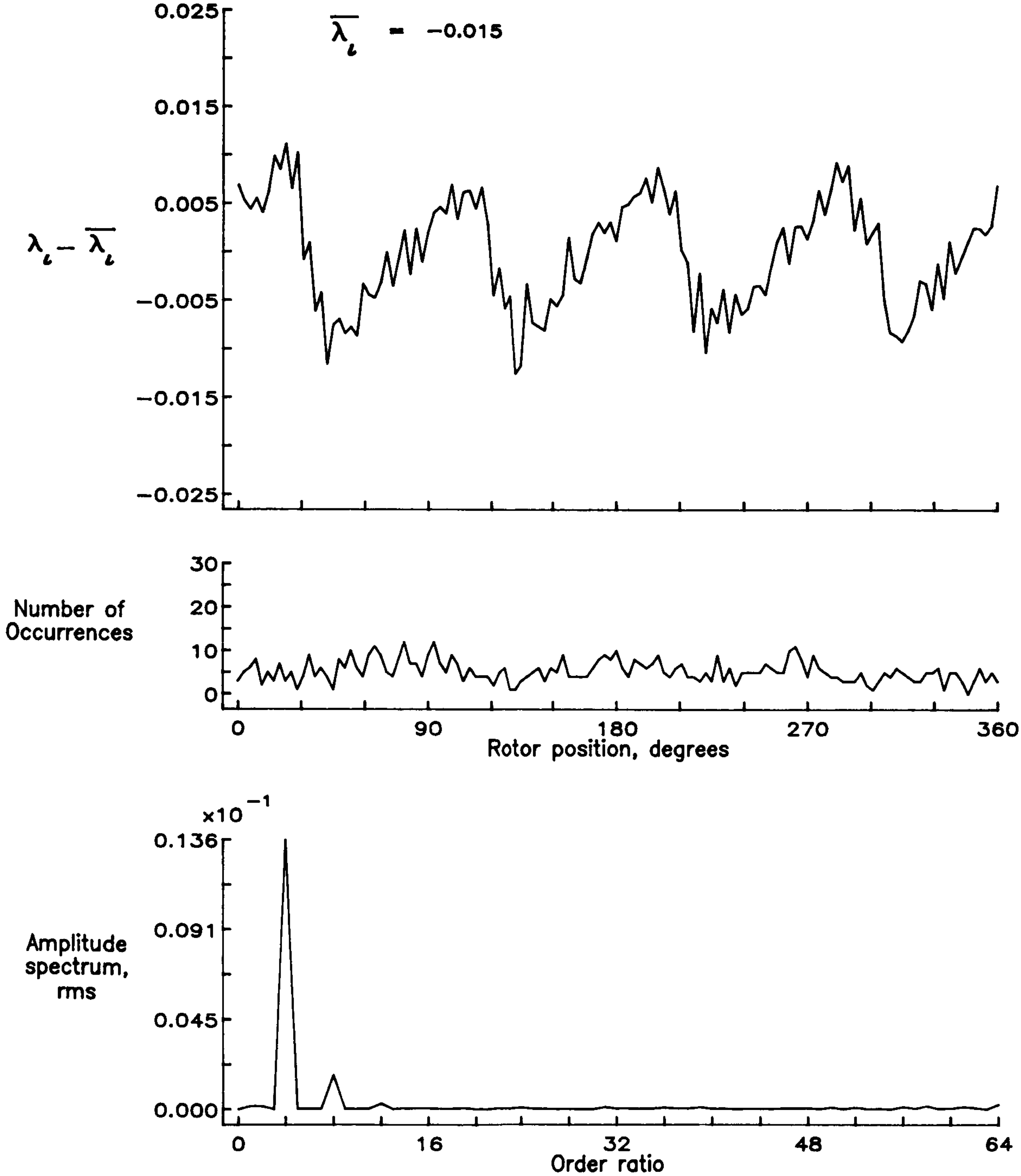

Figure 133.– Concluded.

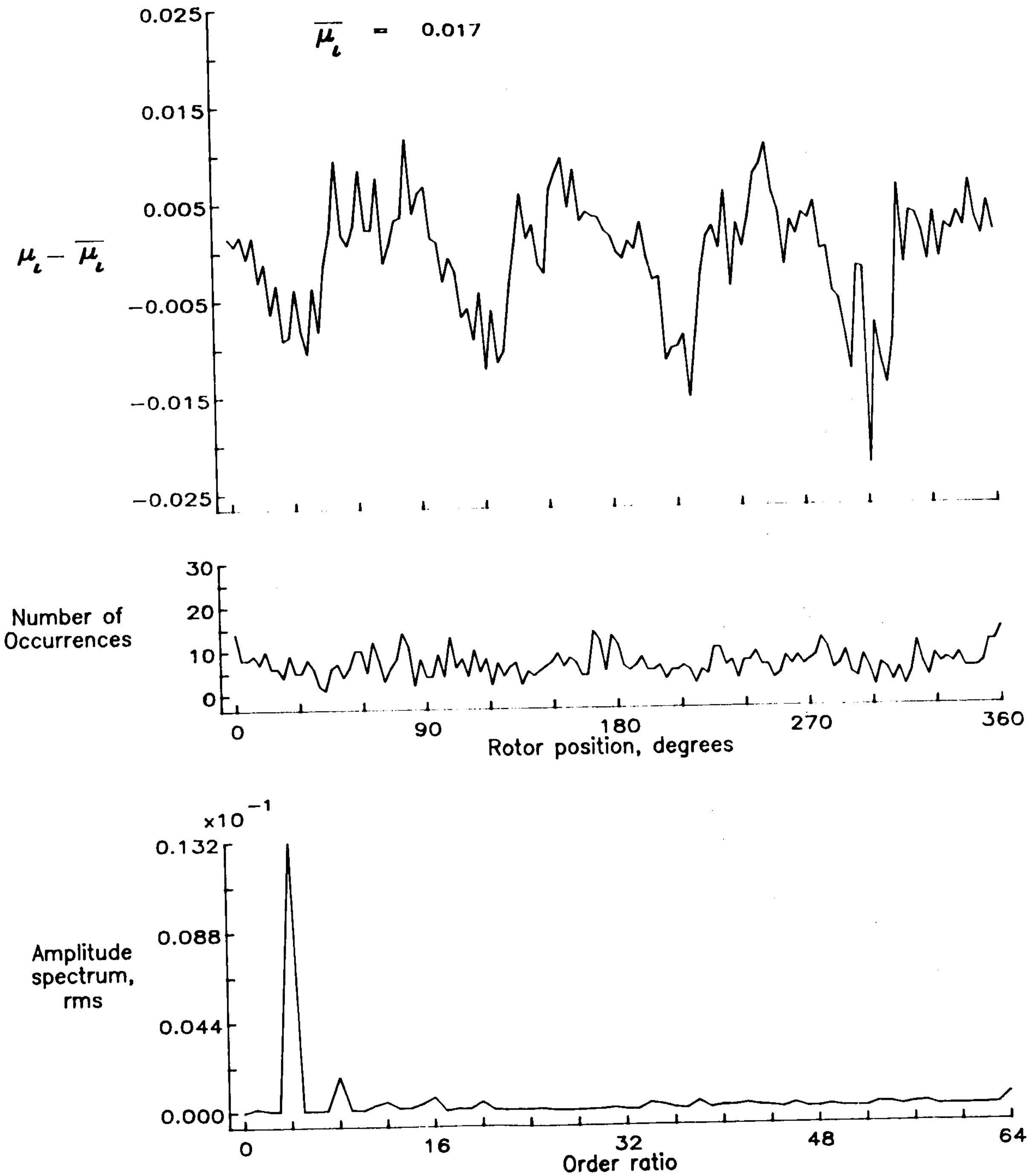

Figure 134.– Induced inflow velocity measured at 300 degrees and r/R of 0.50.

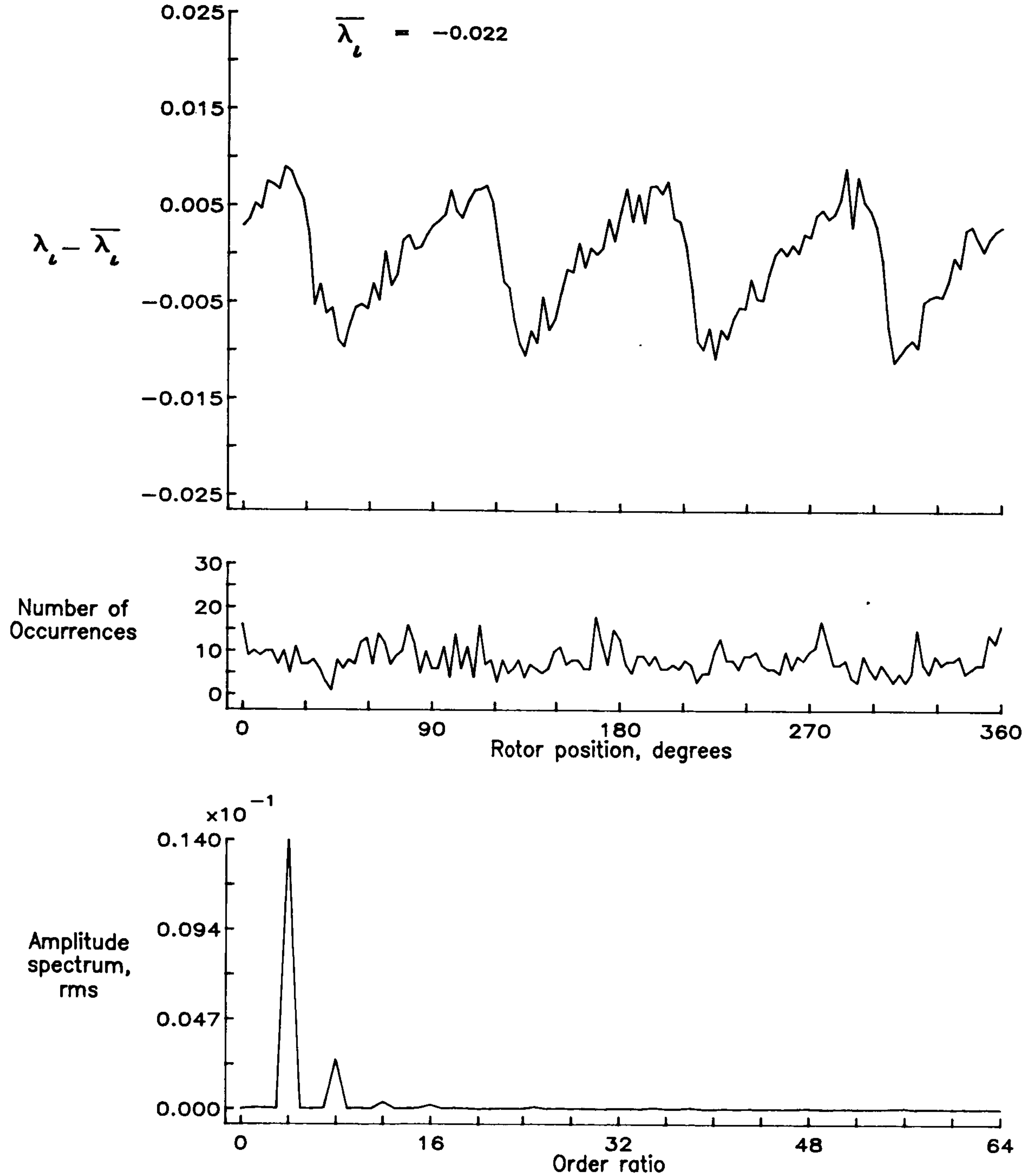

Figure 134.– Concluded.

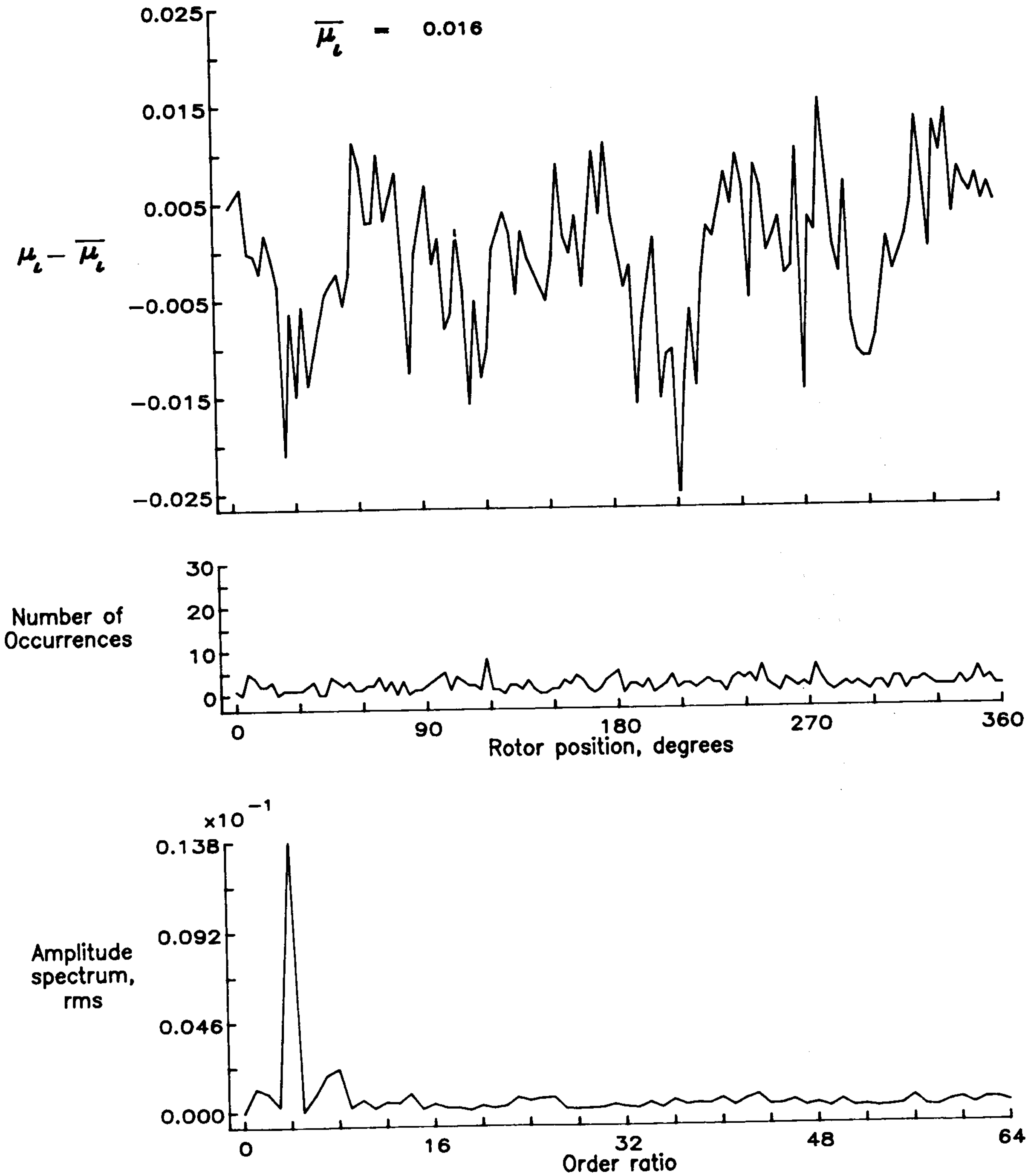

Figure 135.– Induced inflow velocity measured at 300 degrees and r/R of 0.60.

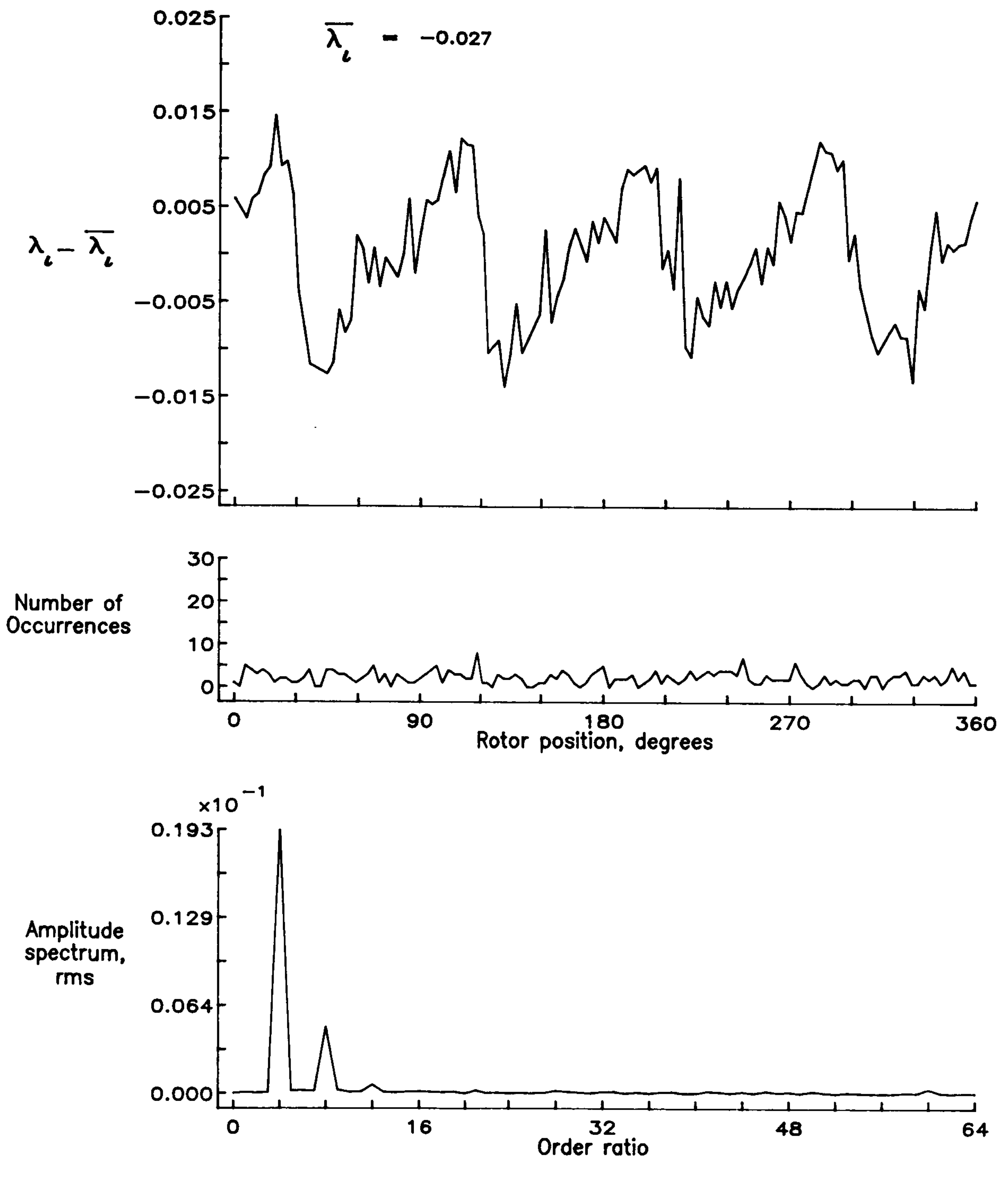

Figure 135.– Concluded.

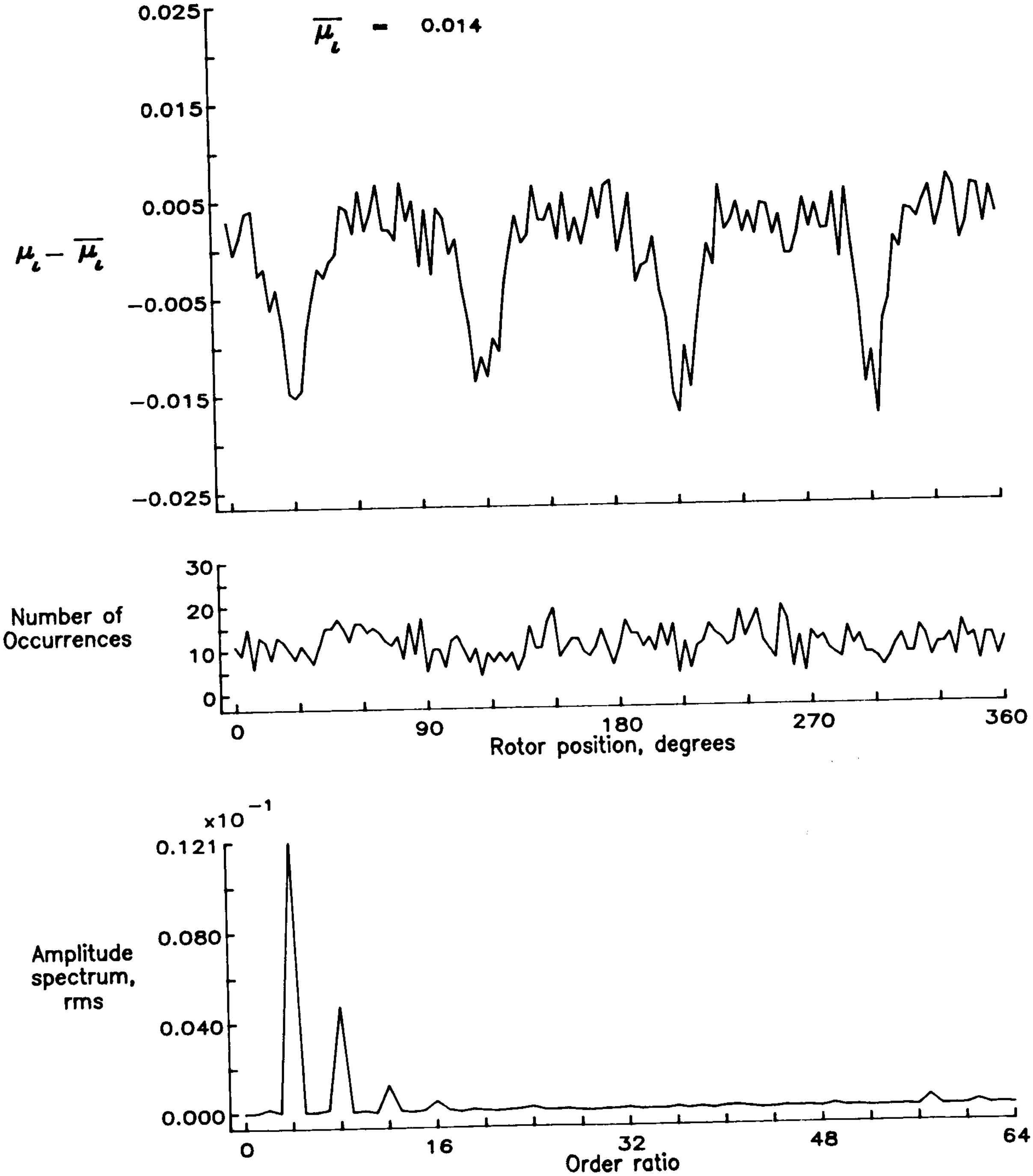

Figure 136.– Induced inflow velocity measured at 300 degrees and r/R of 0.70.

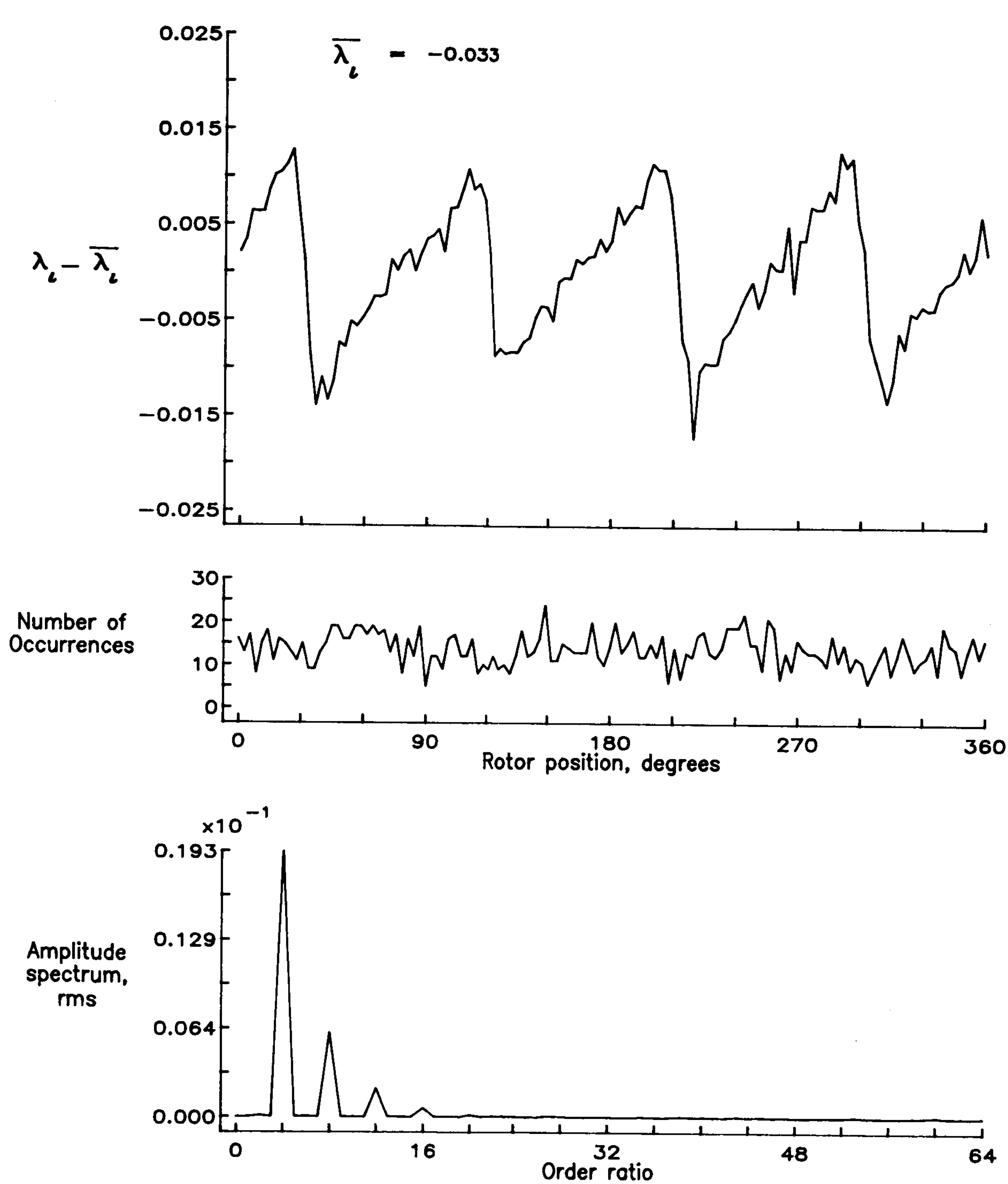

Figure 136.– Concluded.

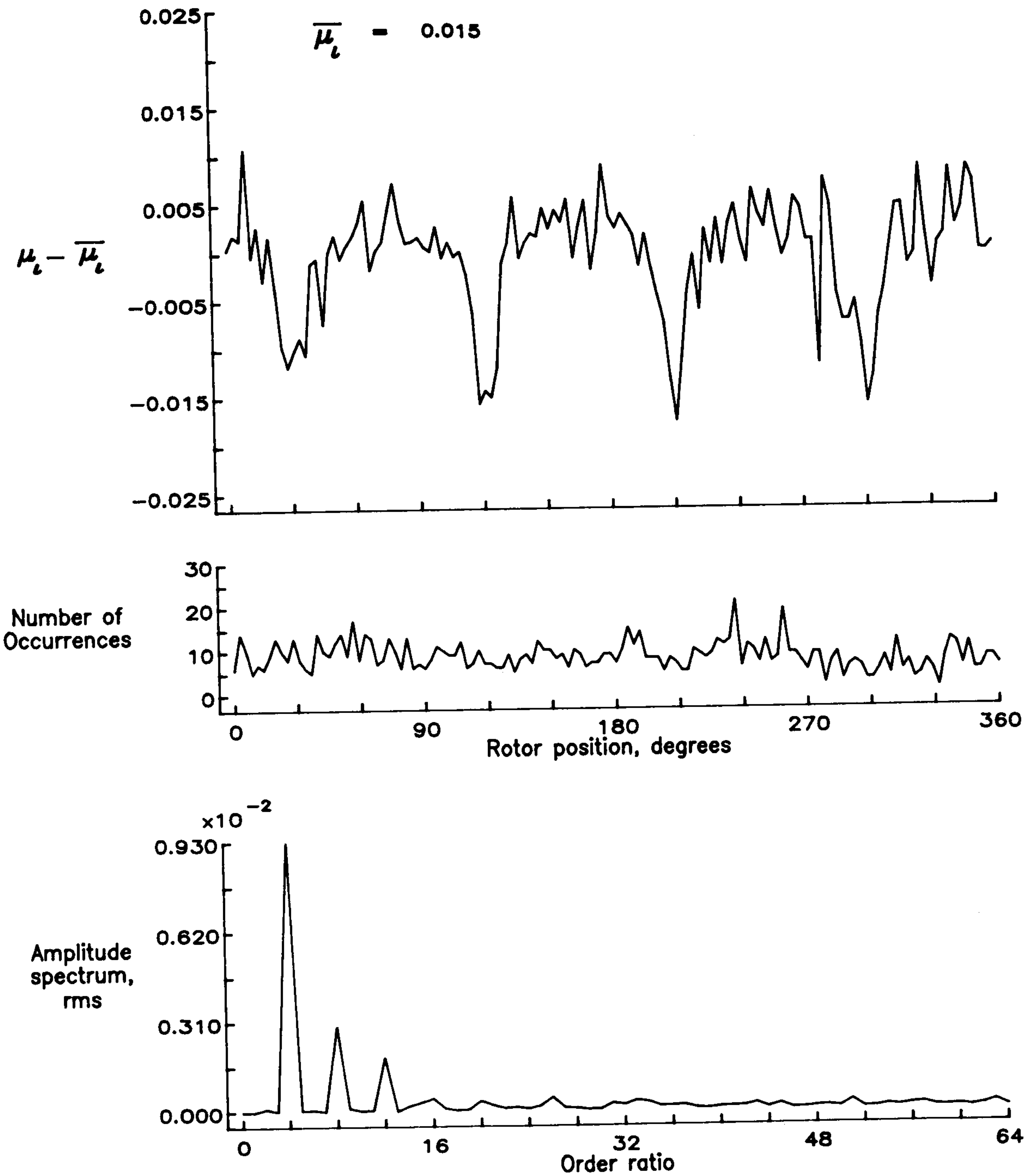

Figure 137.– Induced inflow velocity measured at 300 degrees and r/R of 0.74.

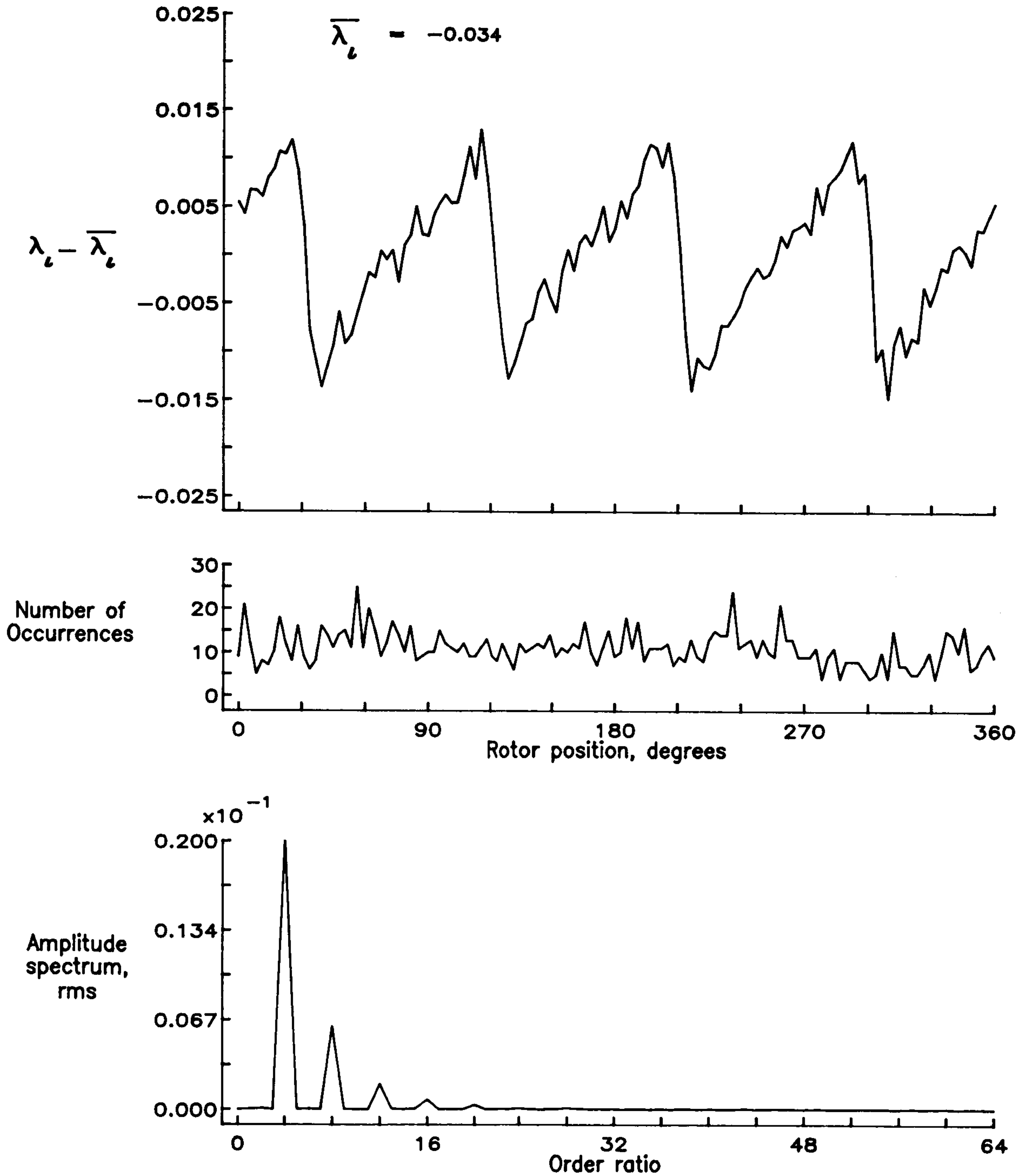

Figure 137.– Concluded.

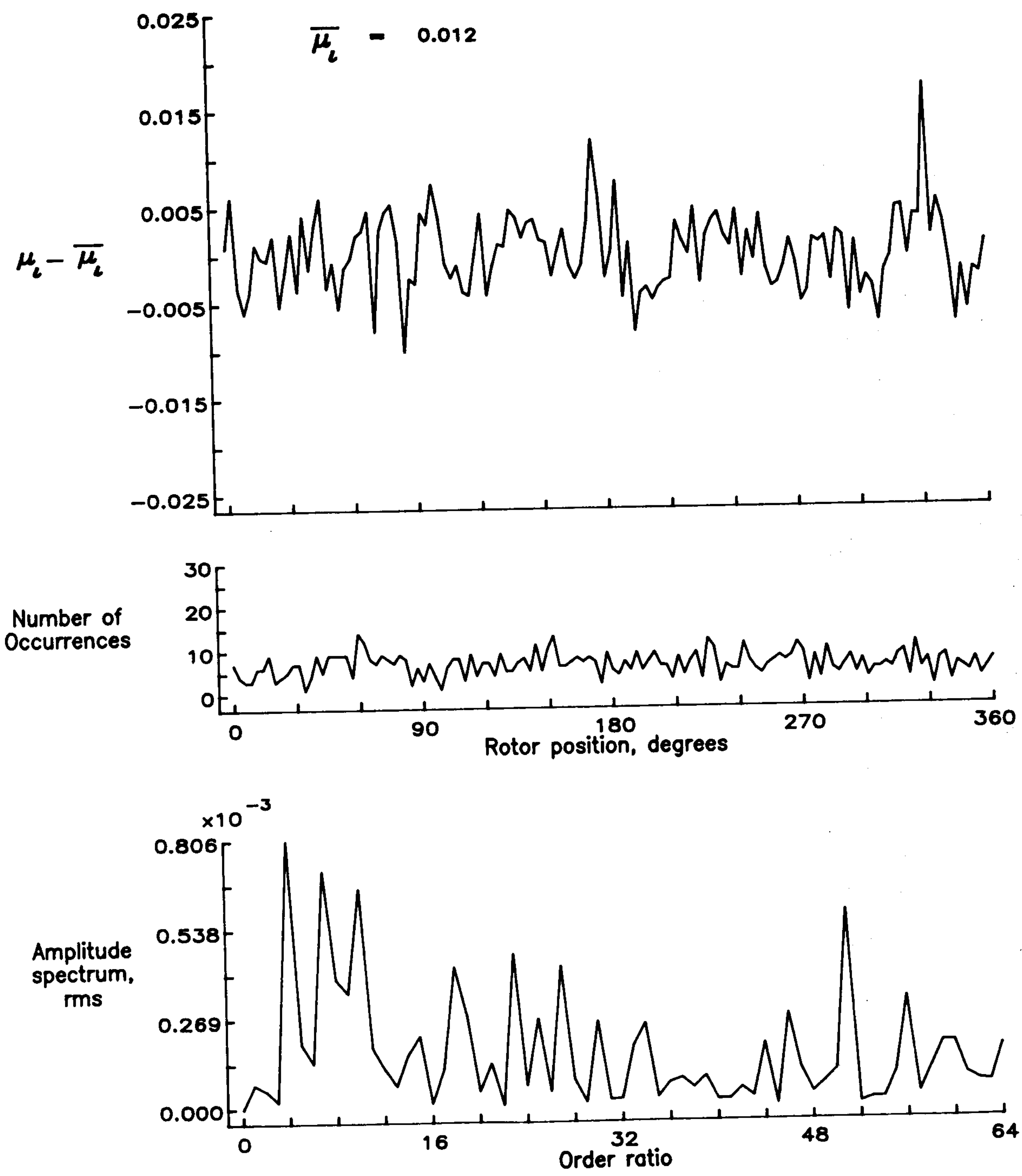

Figure 138.– Induced inflow velocity measured at 300 degrees and r/R of 0.78.

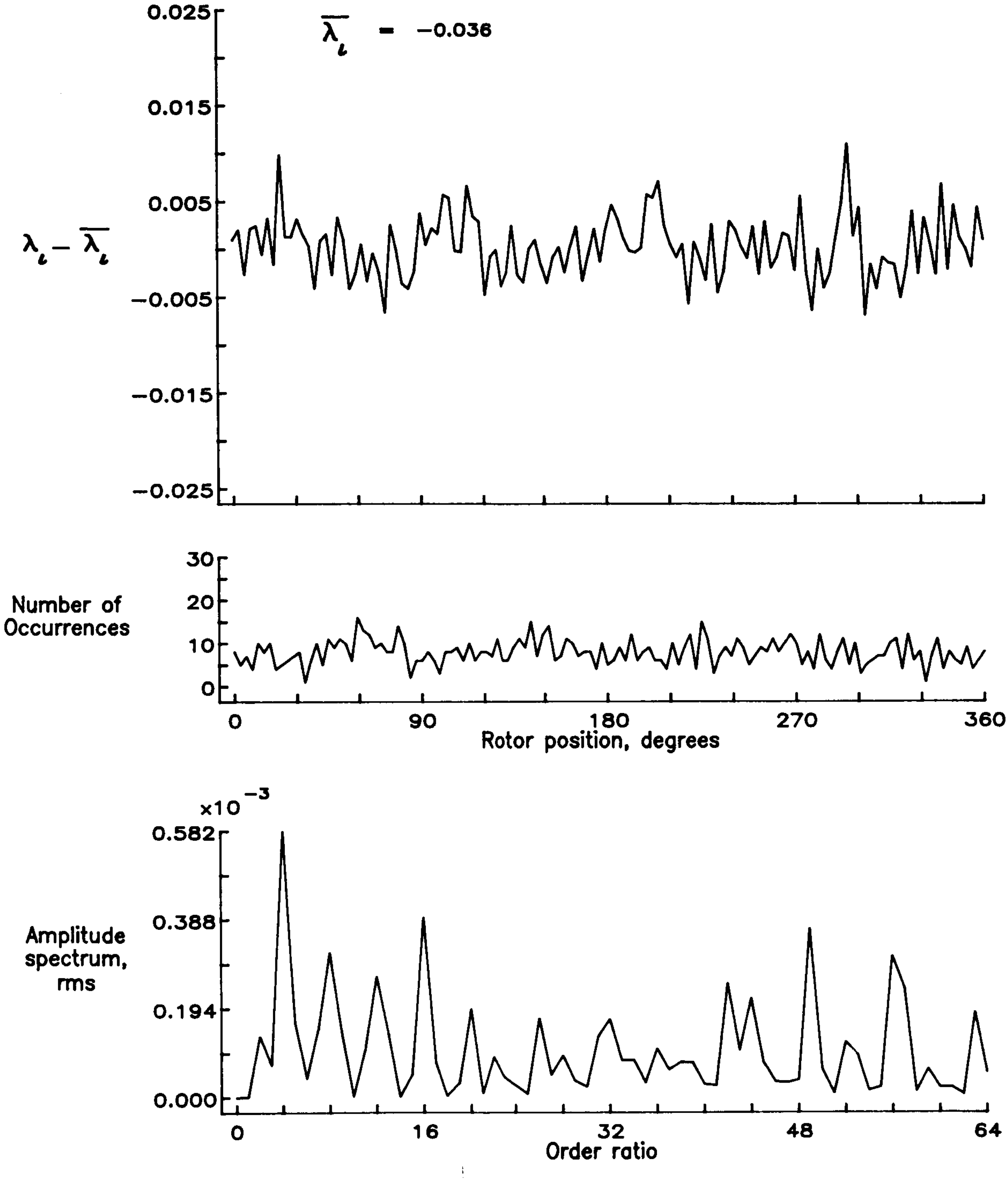

Figure 138.– Concluded.

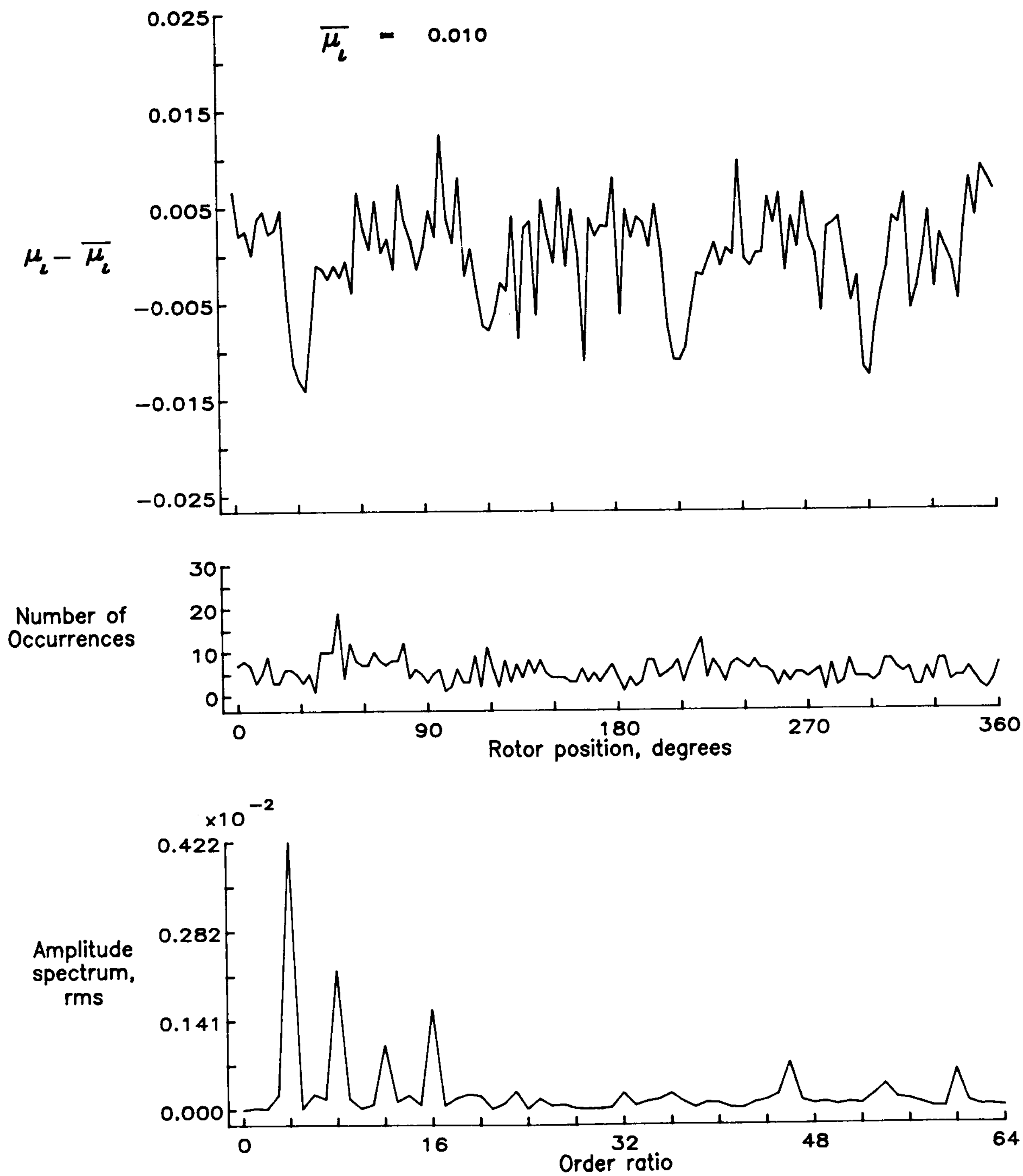

Figure 139.– Induced inflow velocity measured at 300 degrees and r/R of 0.82.

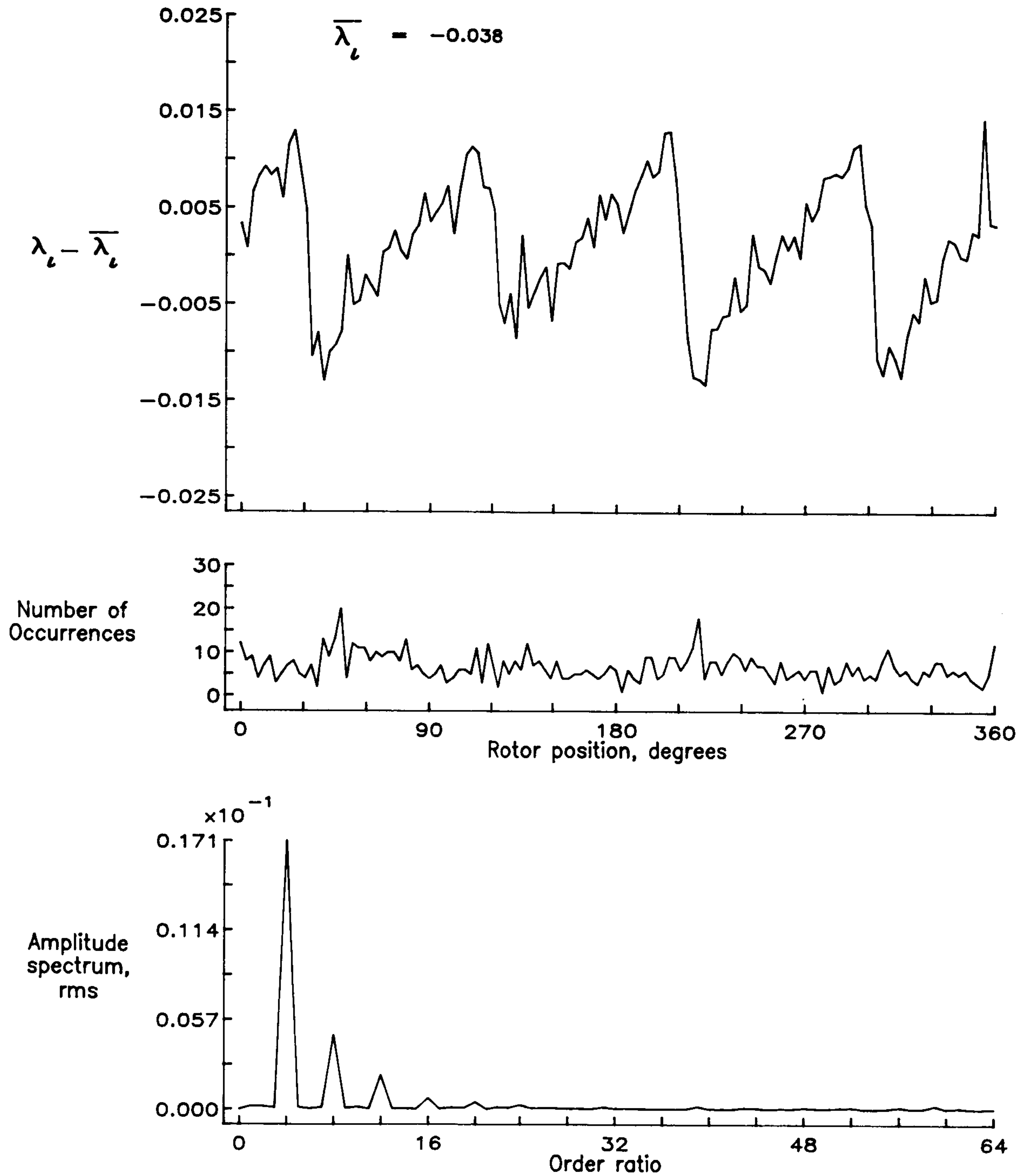

Figure 139.– Concluded.

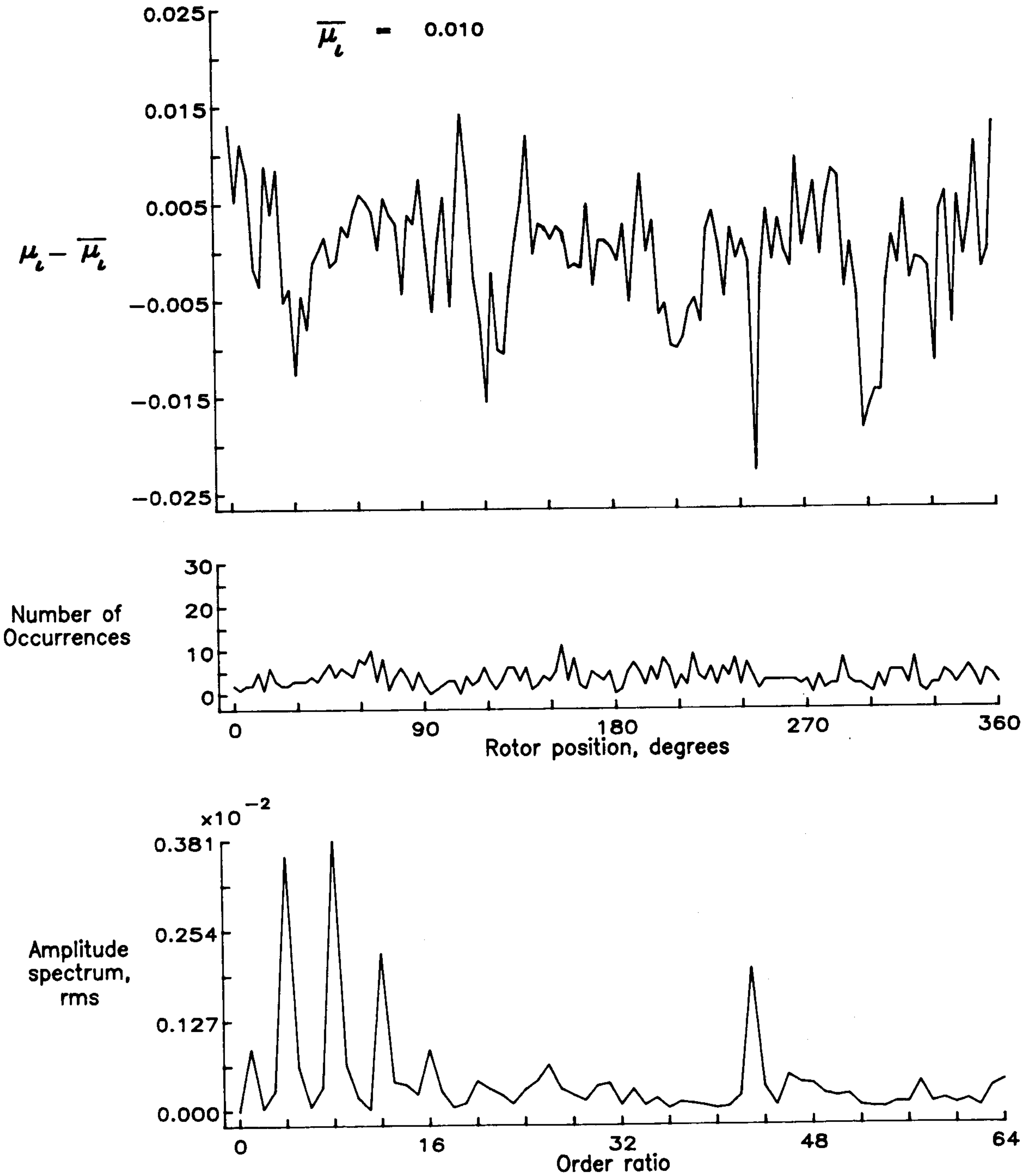

Figure 140.– Induced inflow velocity measured at 300 degrees and r/R of 0.86.

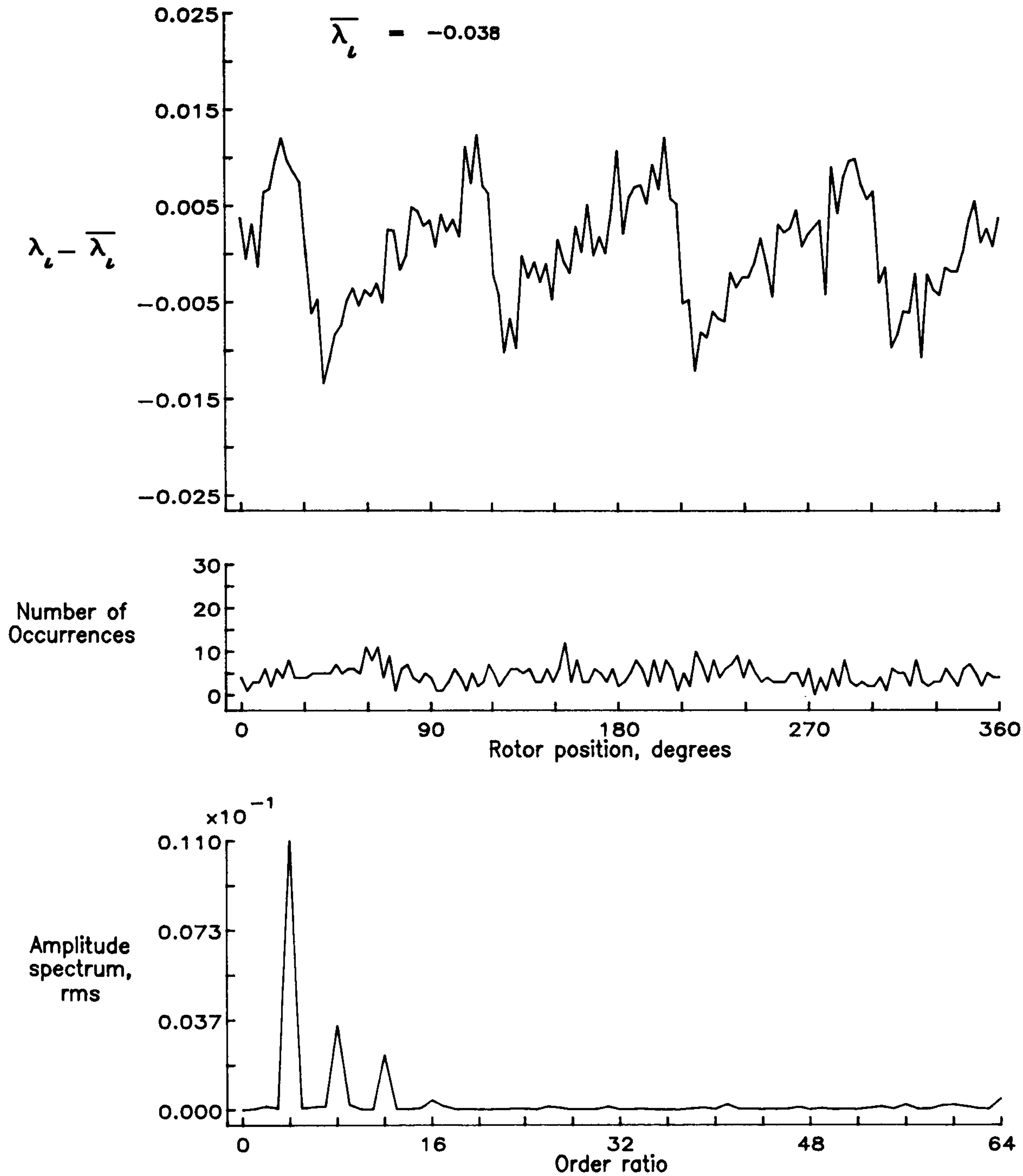

Figure 140.– Concluded.

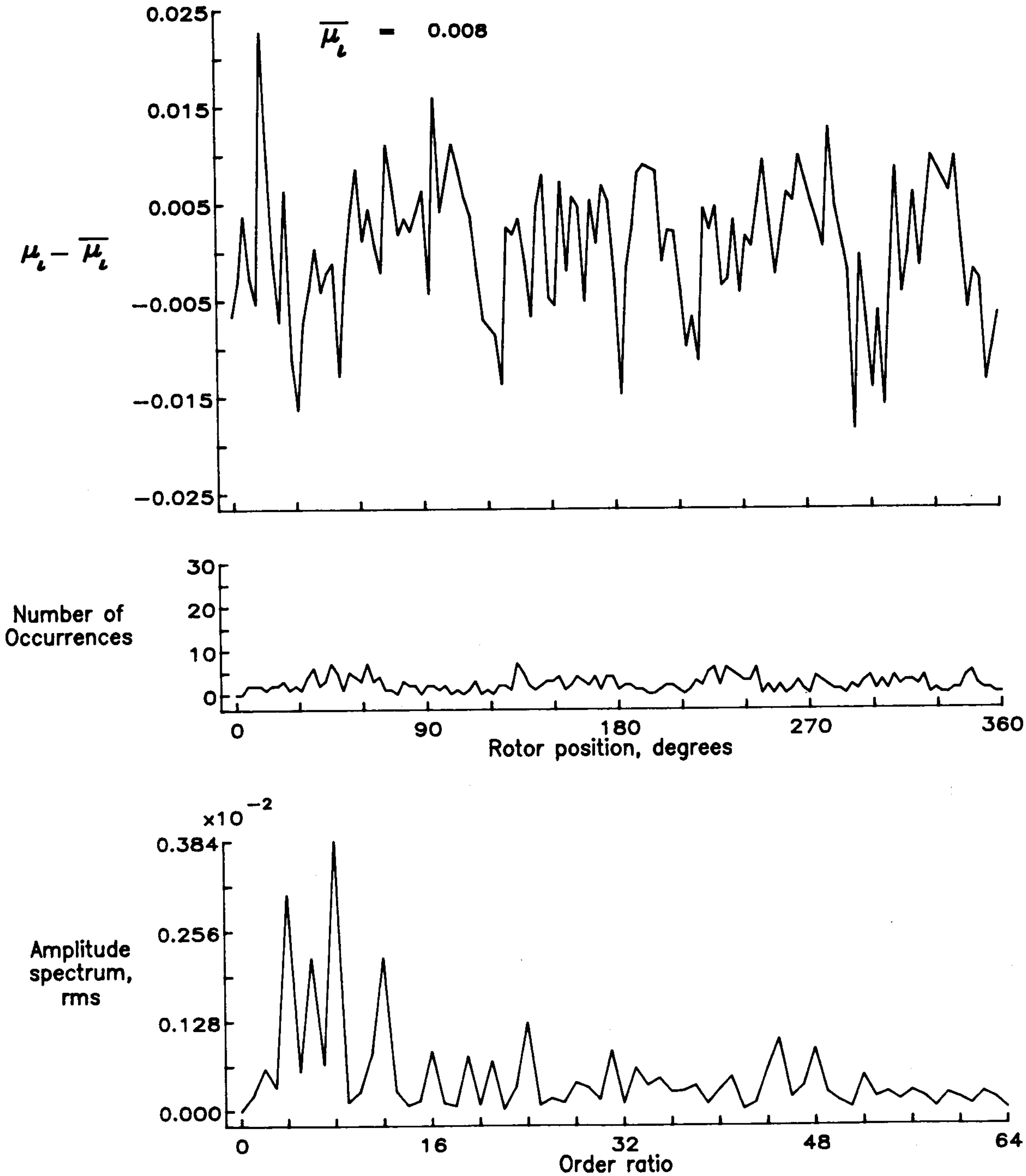

Figure 141.– Induced inflow velocity measured at 300 degrees and r/R of 0.90.

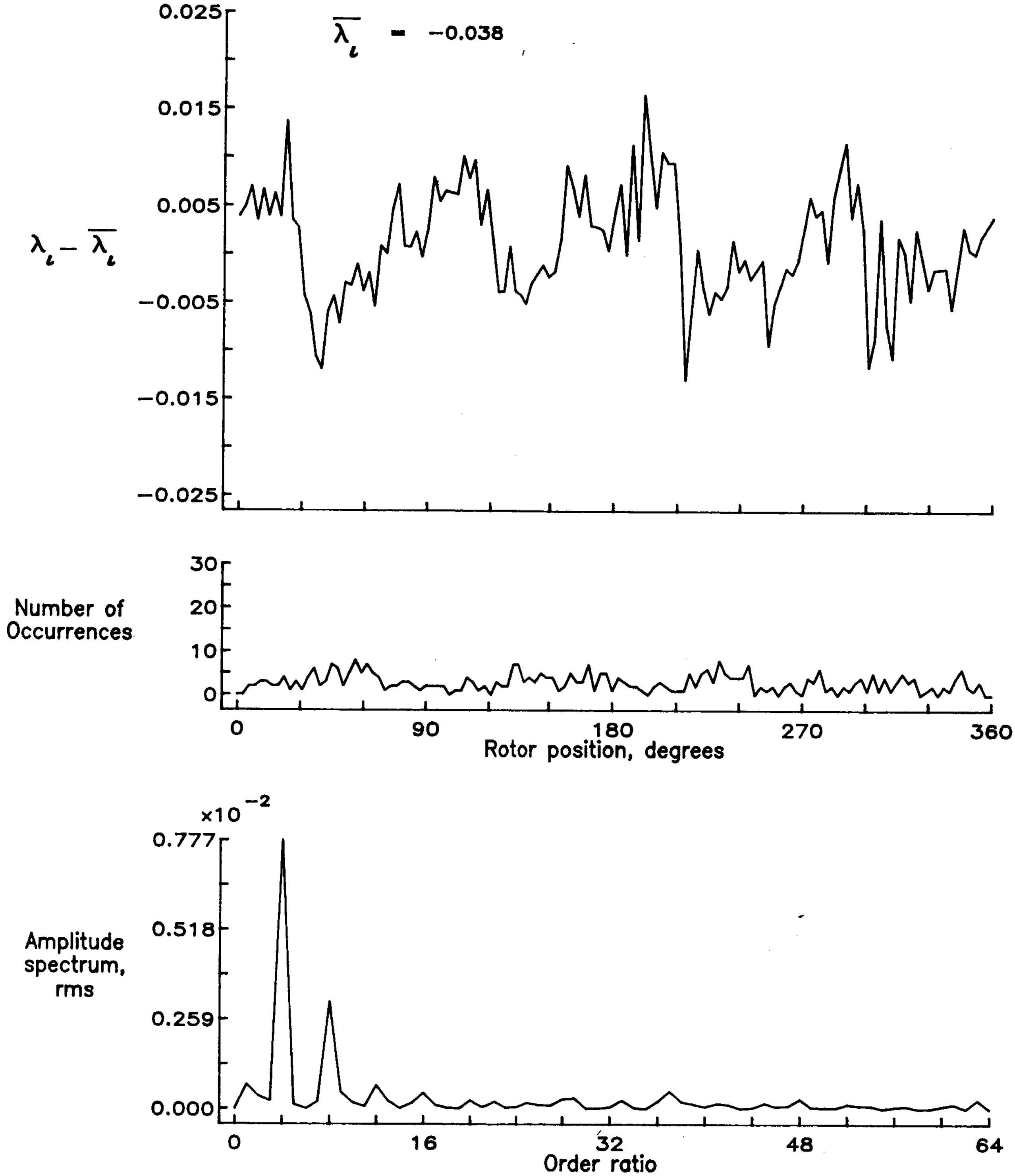

Figure 141.– Concluded.

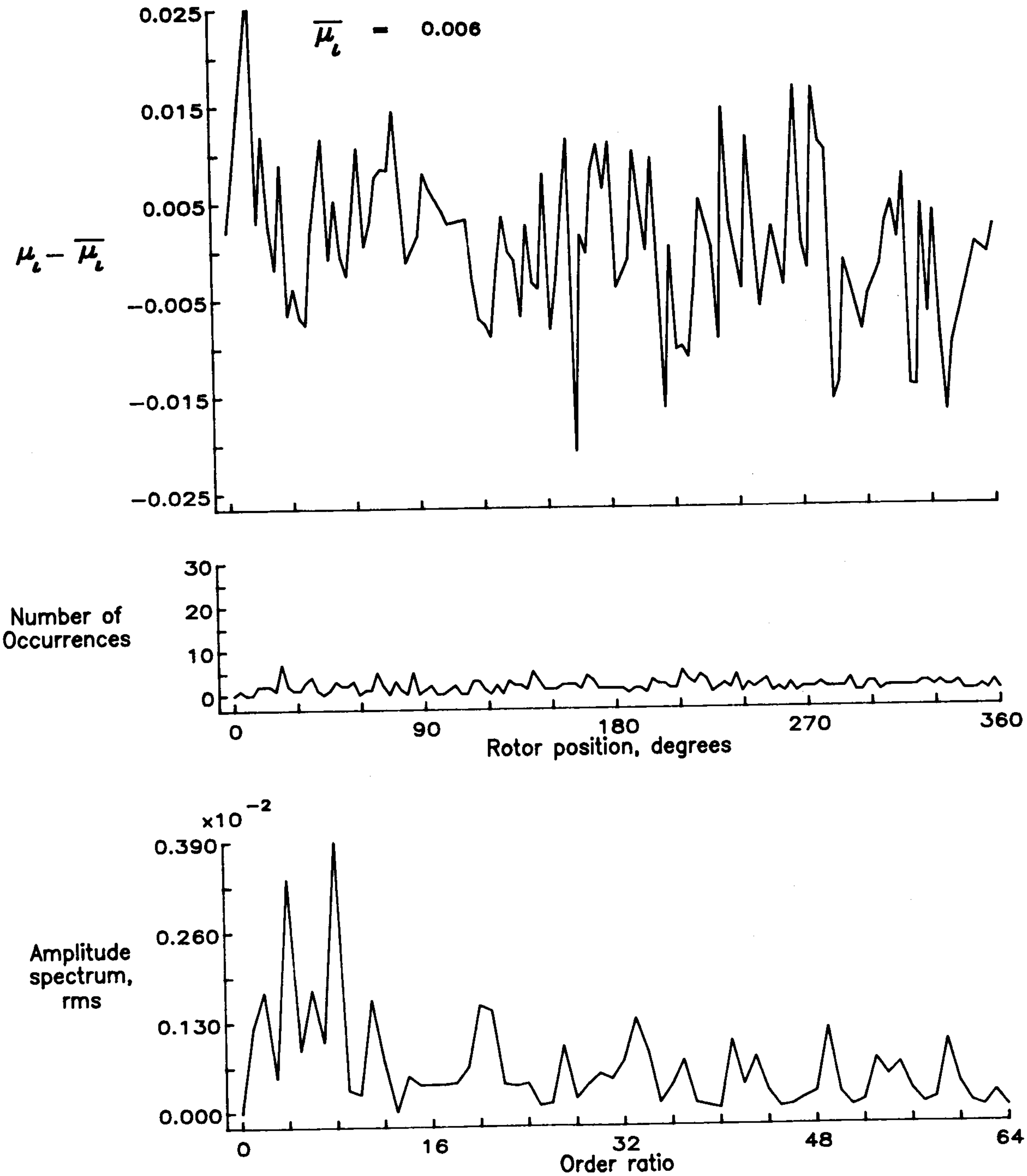

Figure 142.– Induced inflow velocity measured at 300 degrees and r/R of 0.94.

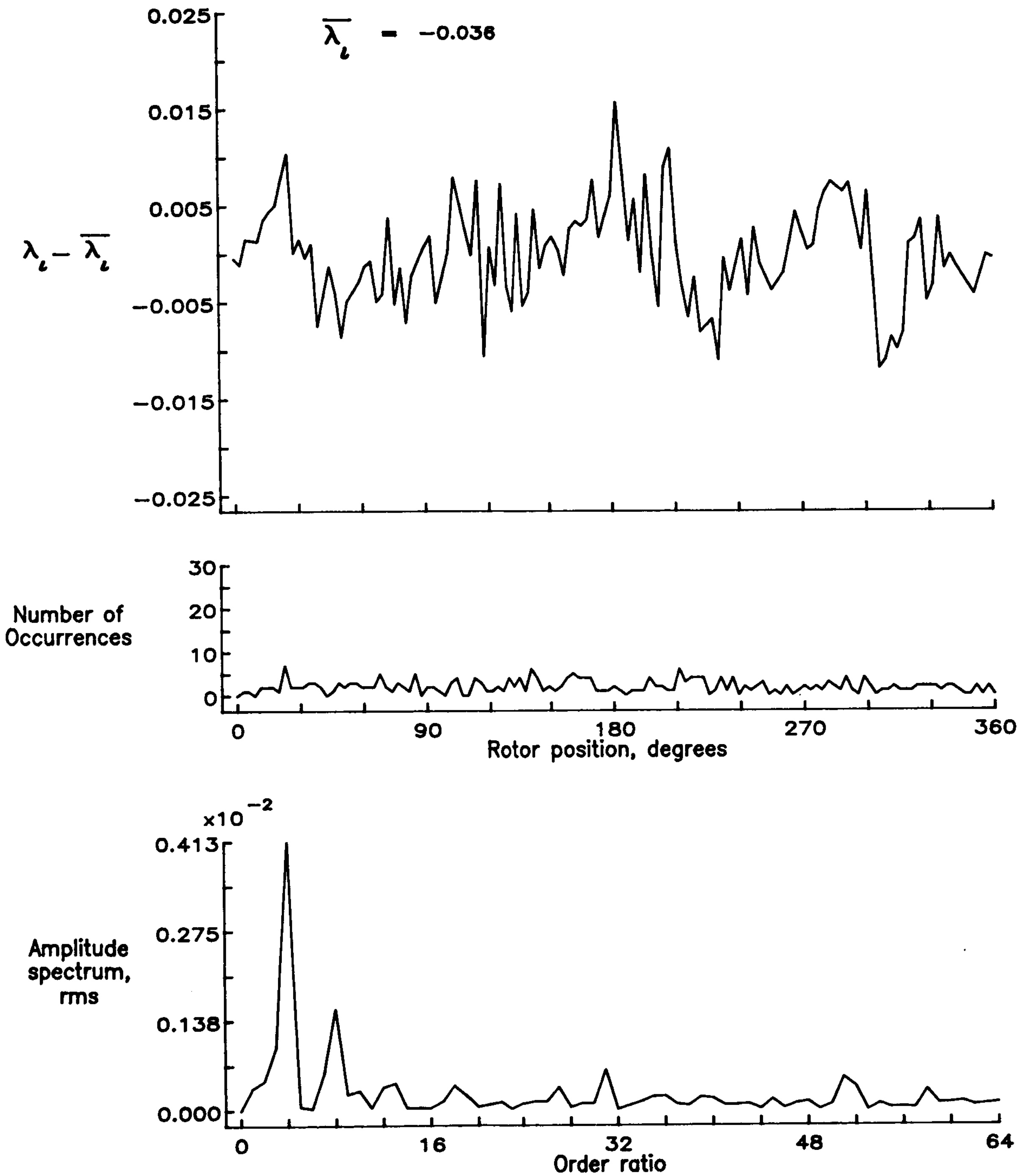

Figure 142.– Concluded.

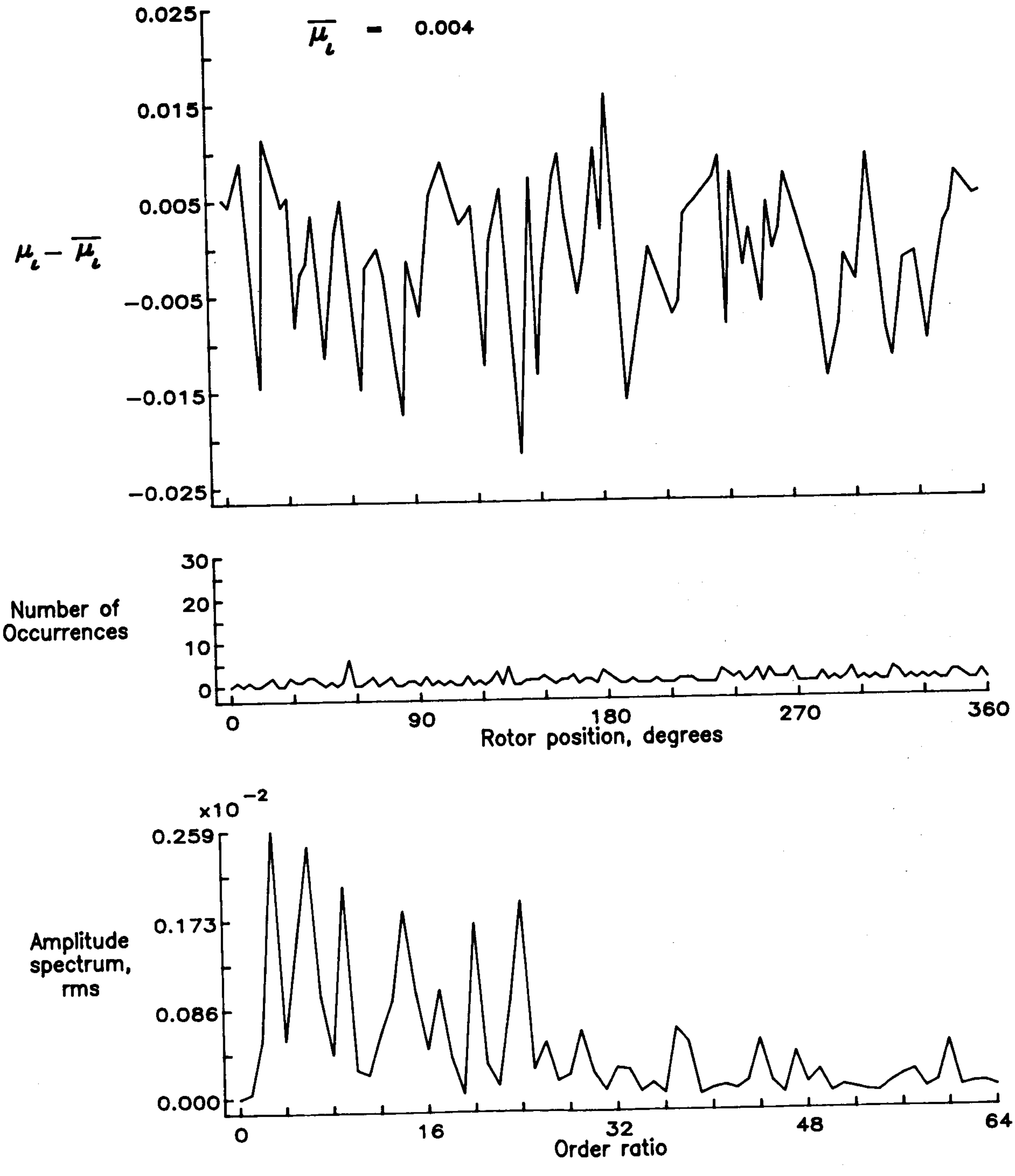

Figure 143.– Induced inflow velocity measured at 300 degrees and r/R of 0.98.

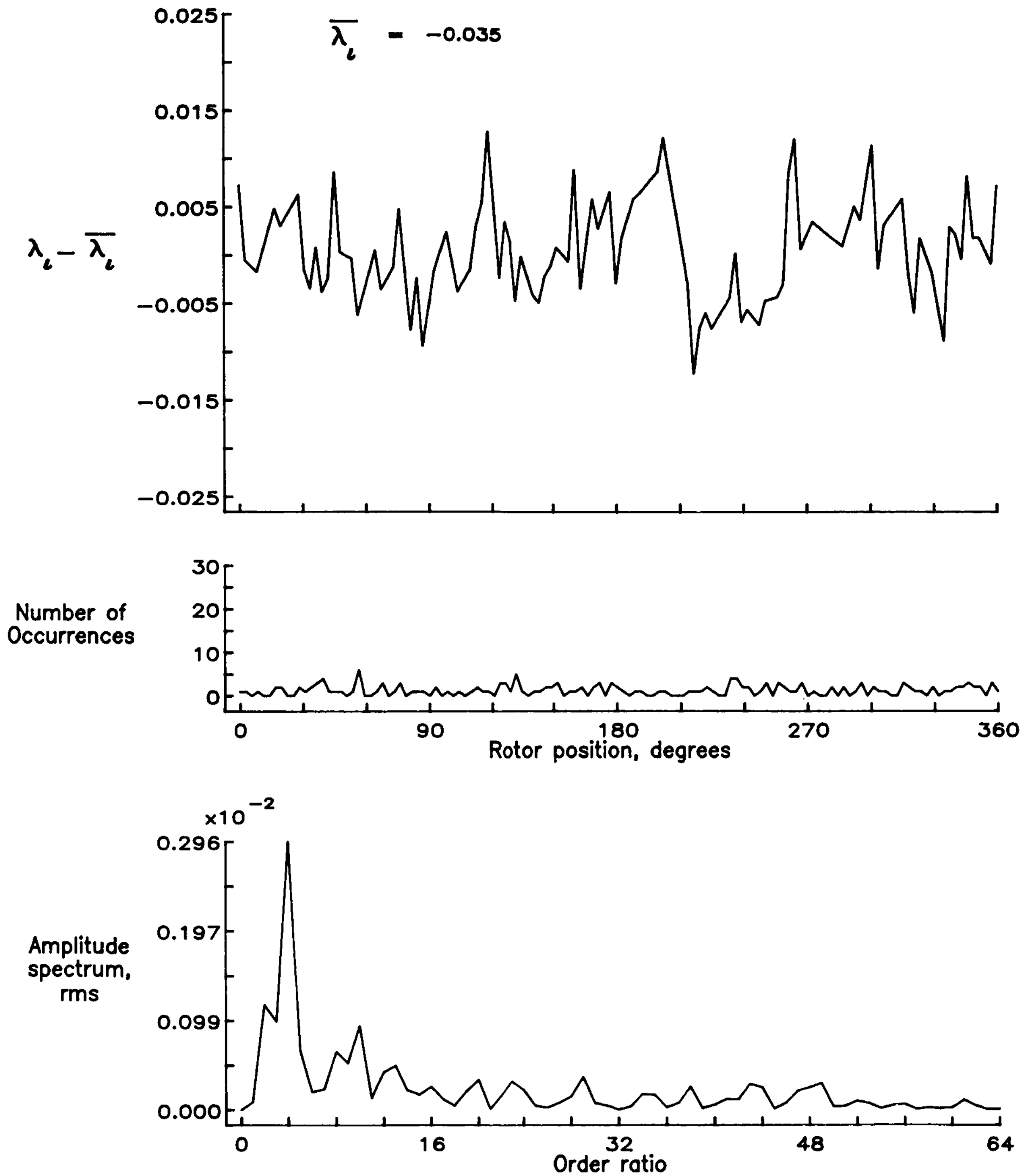

Figure 143.– Concluded.

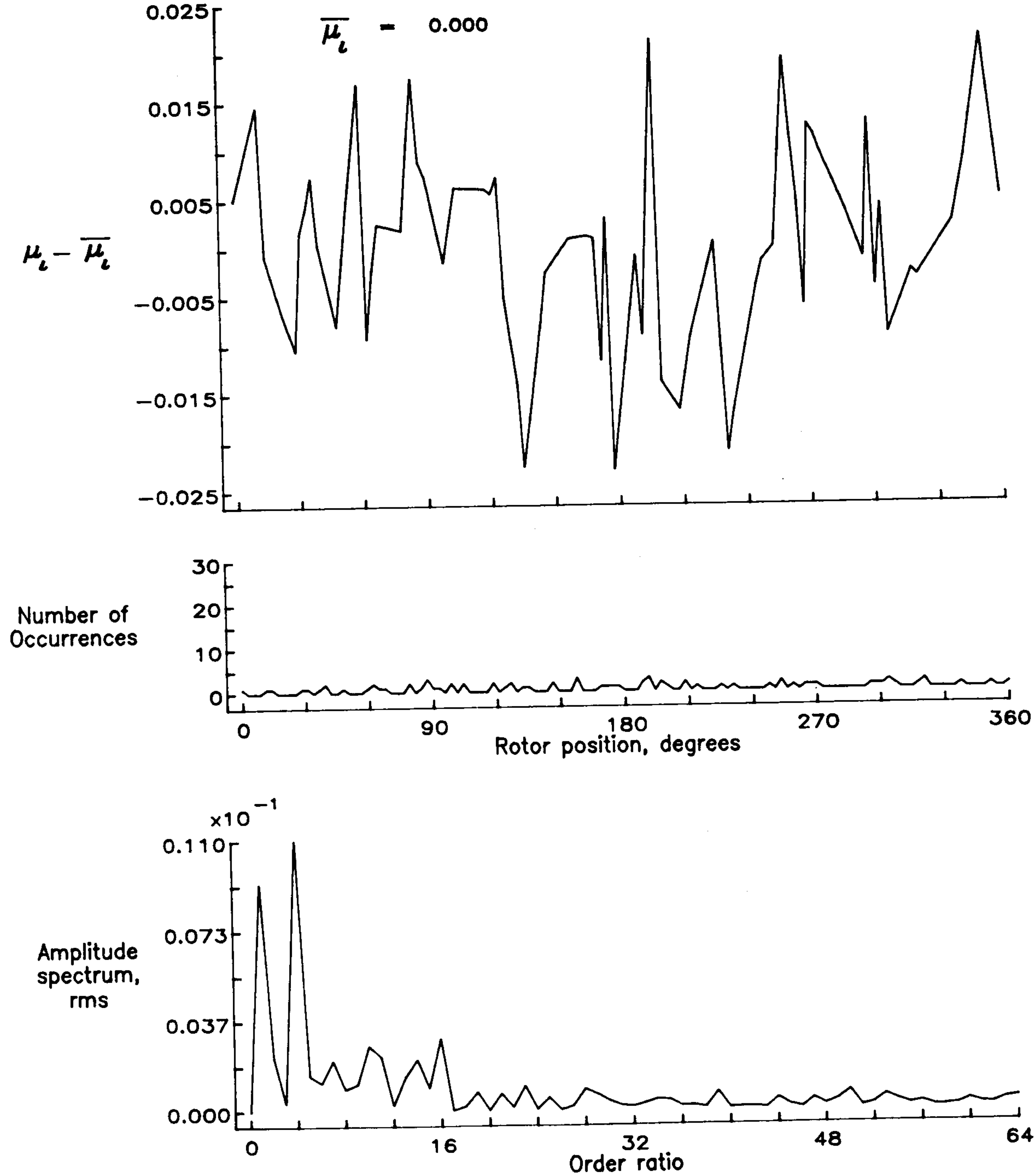

Figure 144.– Induced inflow velocity measured at 300 degrees and r/R of 1.04.

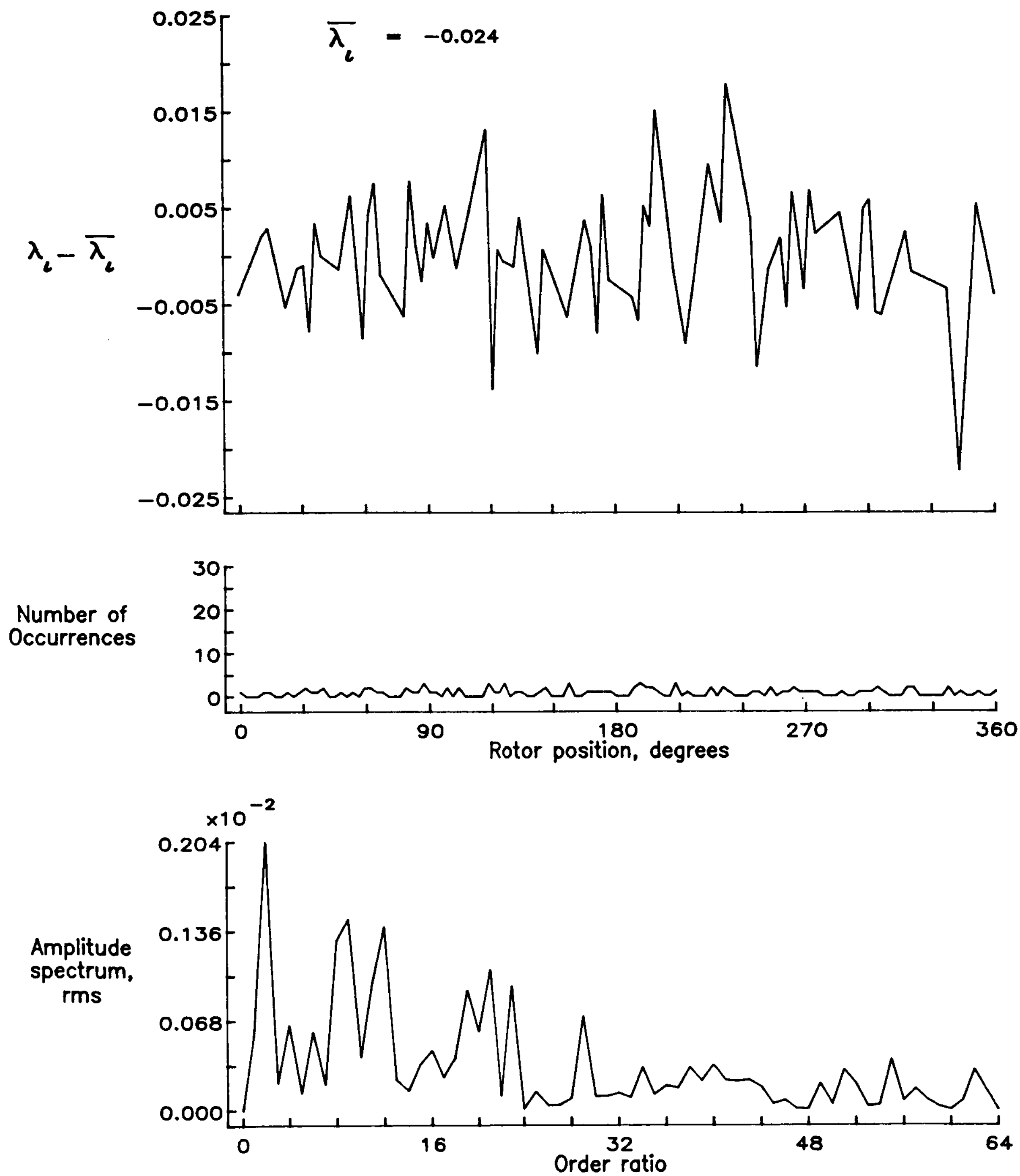

Figure 144.– Concluded.

c-4

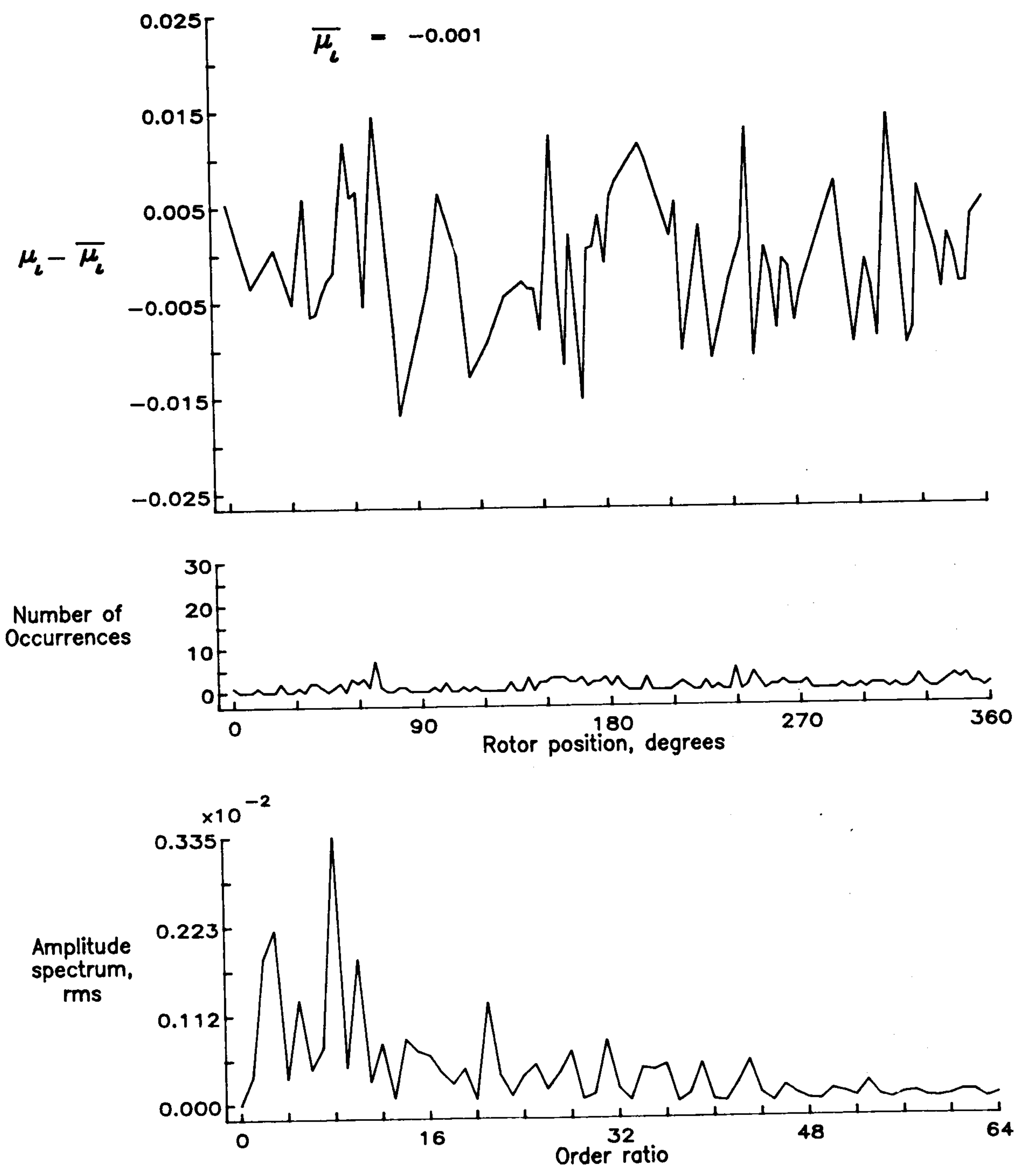

Figure 145.– Induced inflow velocity measured at 300 degrees and r/R of 1.10.

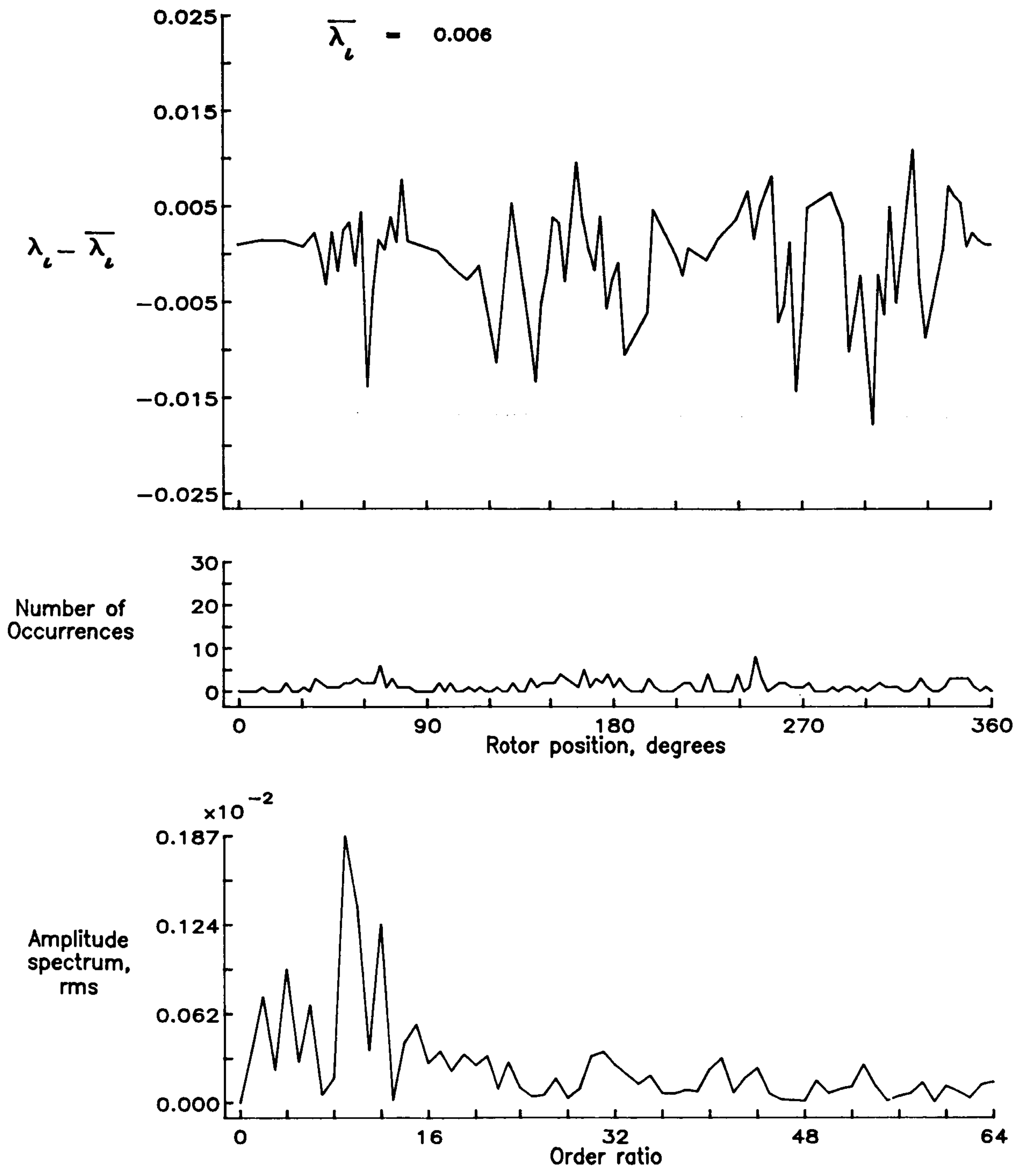

Figure 145.– Concluded.

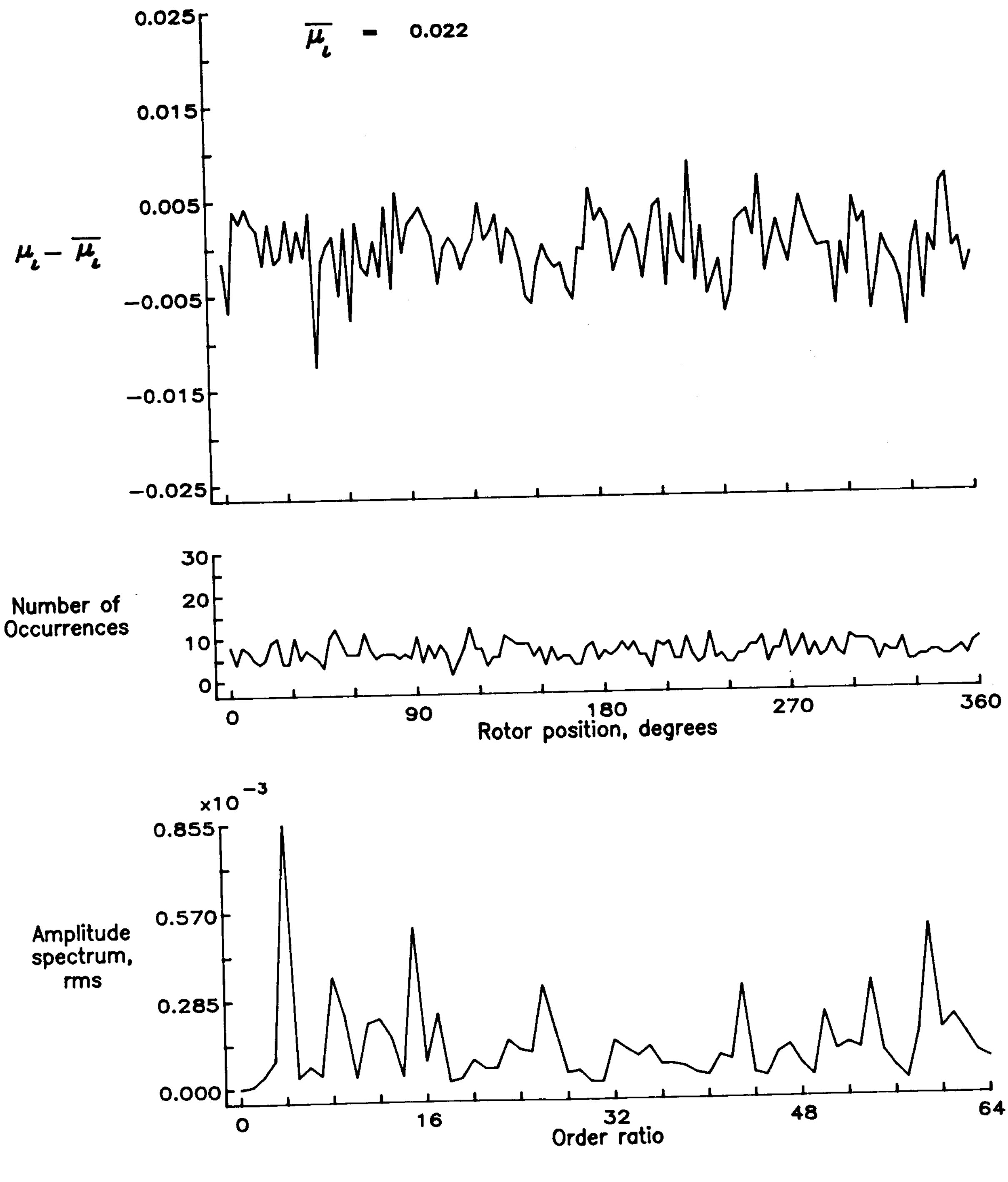

Figure 146.– Induced inflow velocity measured at 330 degrees and r/R of 0.40.

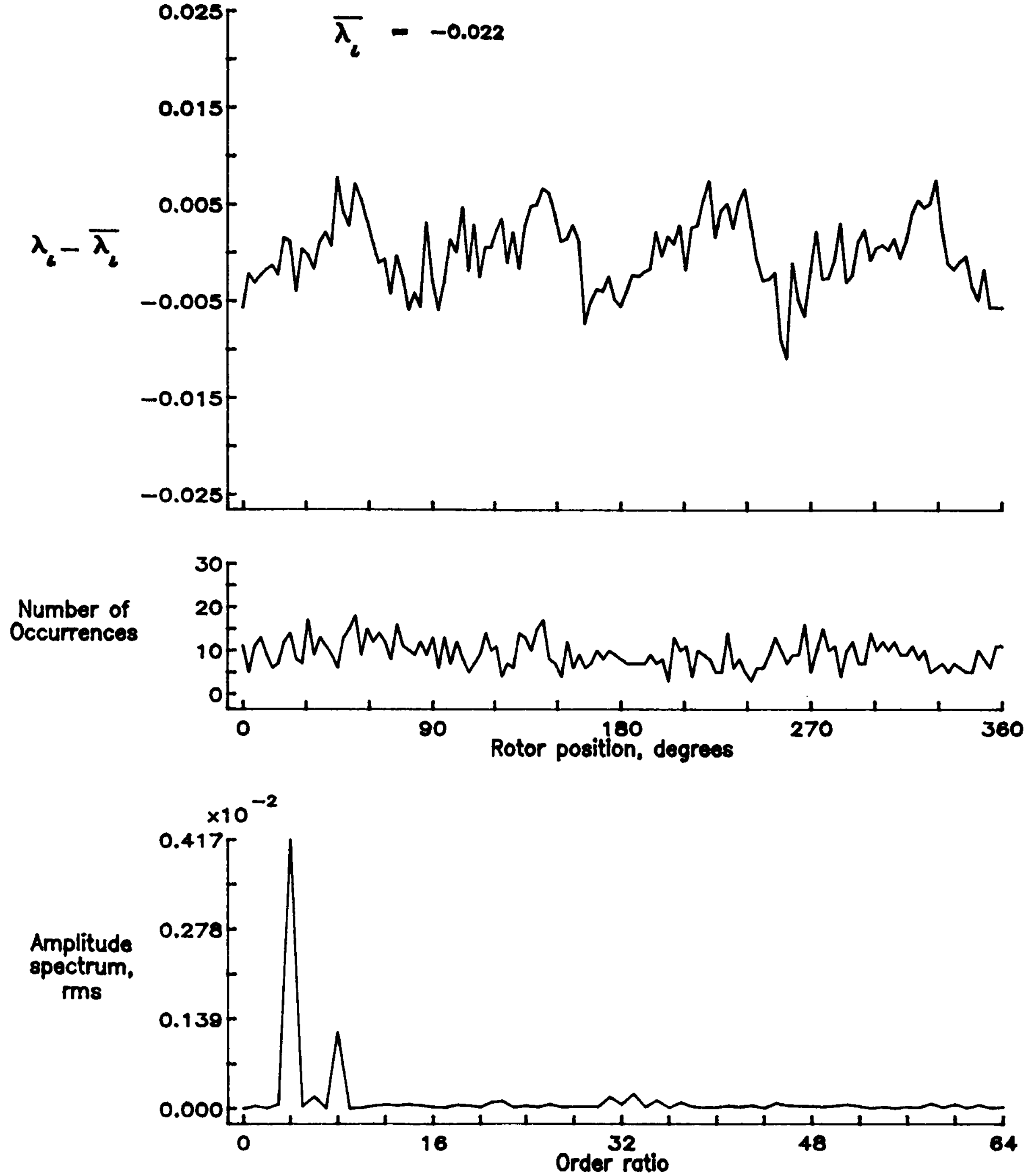

Figure 146.– Concluded.

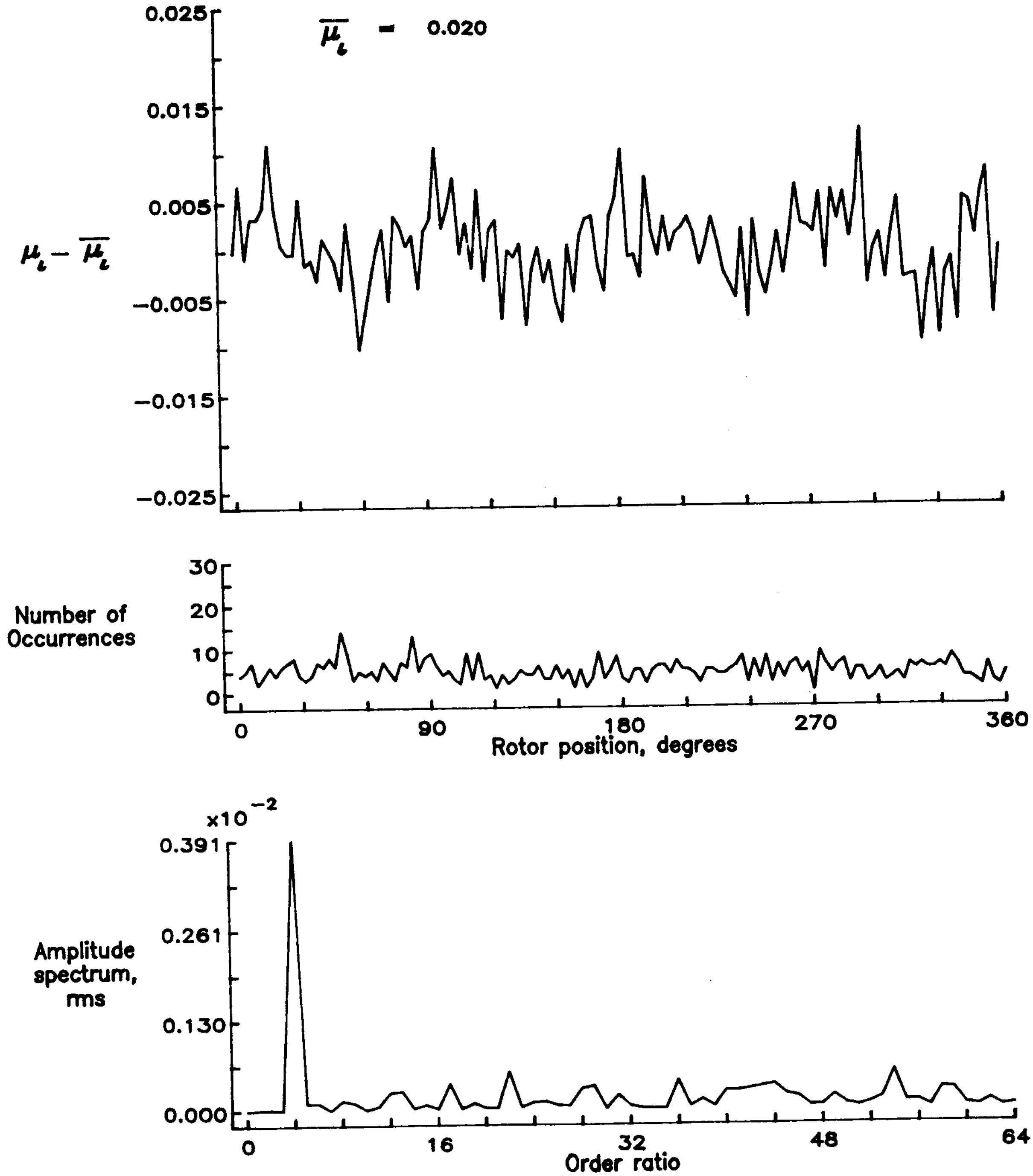

Figure 147.– Induced inflow velocity measured at 330 degrees and r/R of 0.50.

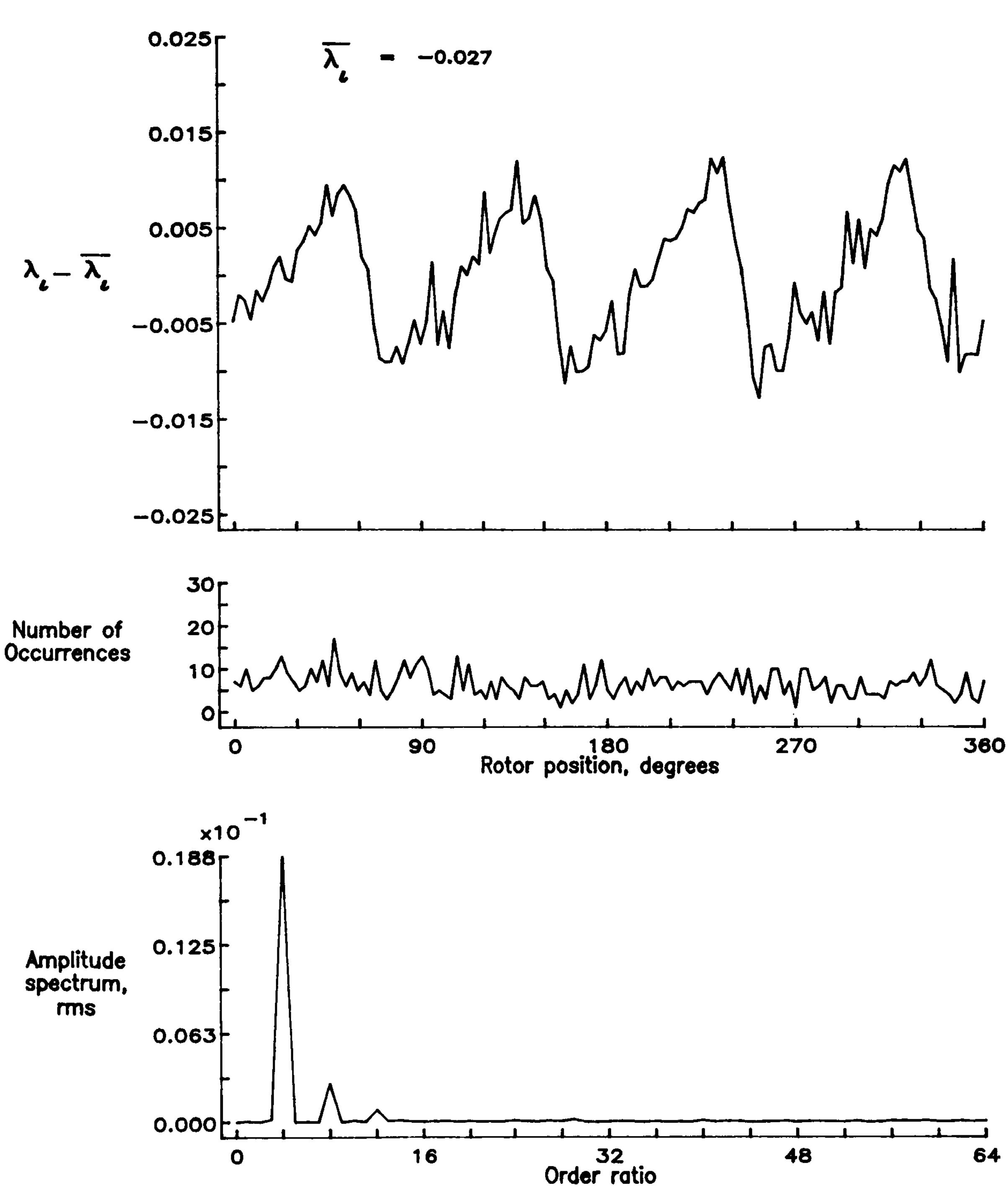

Figure 147.– Concluded.

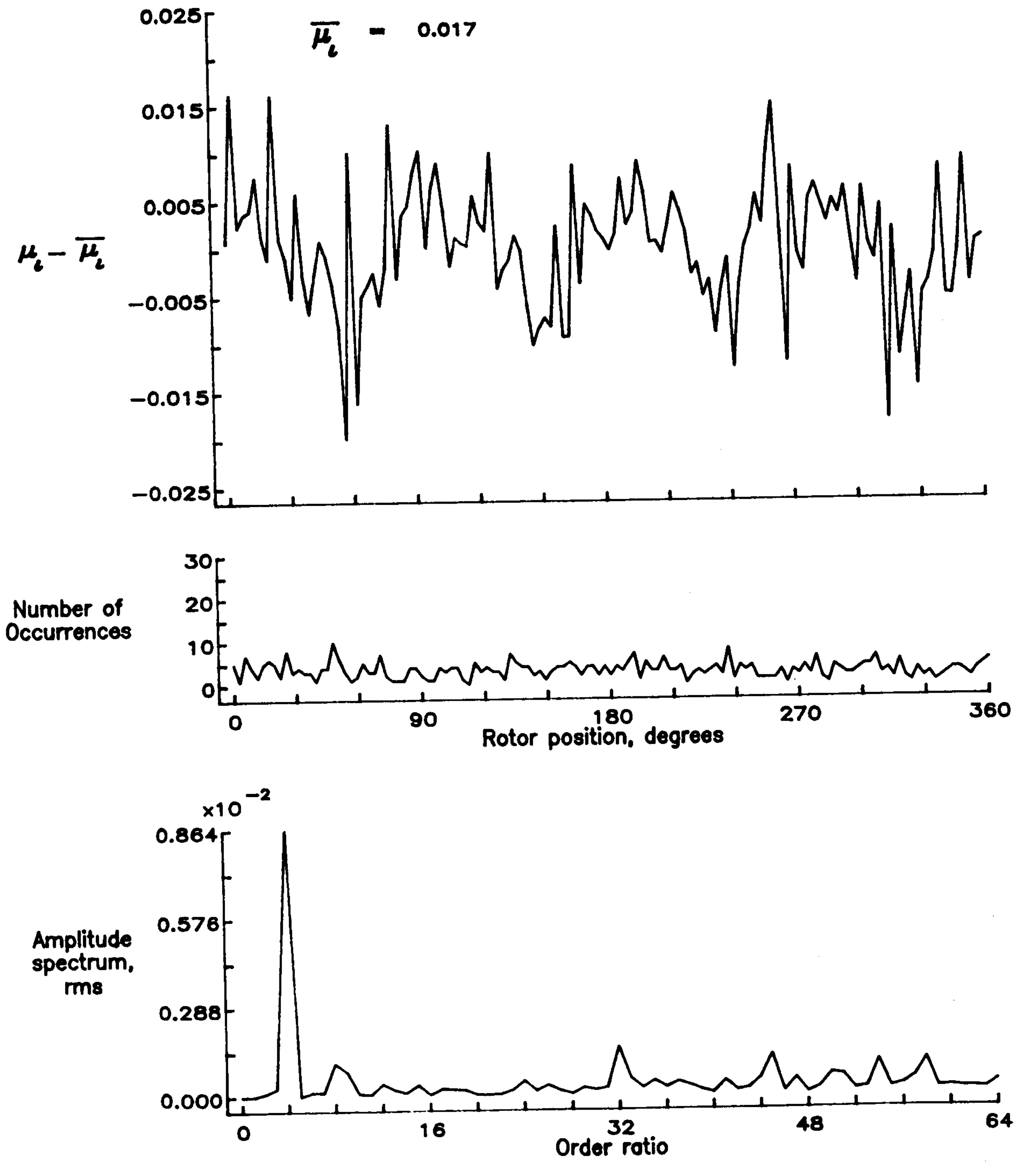

Figure 148.– Induced inflow velocity measured at 330 degrees and r/R of 0.60.

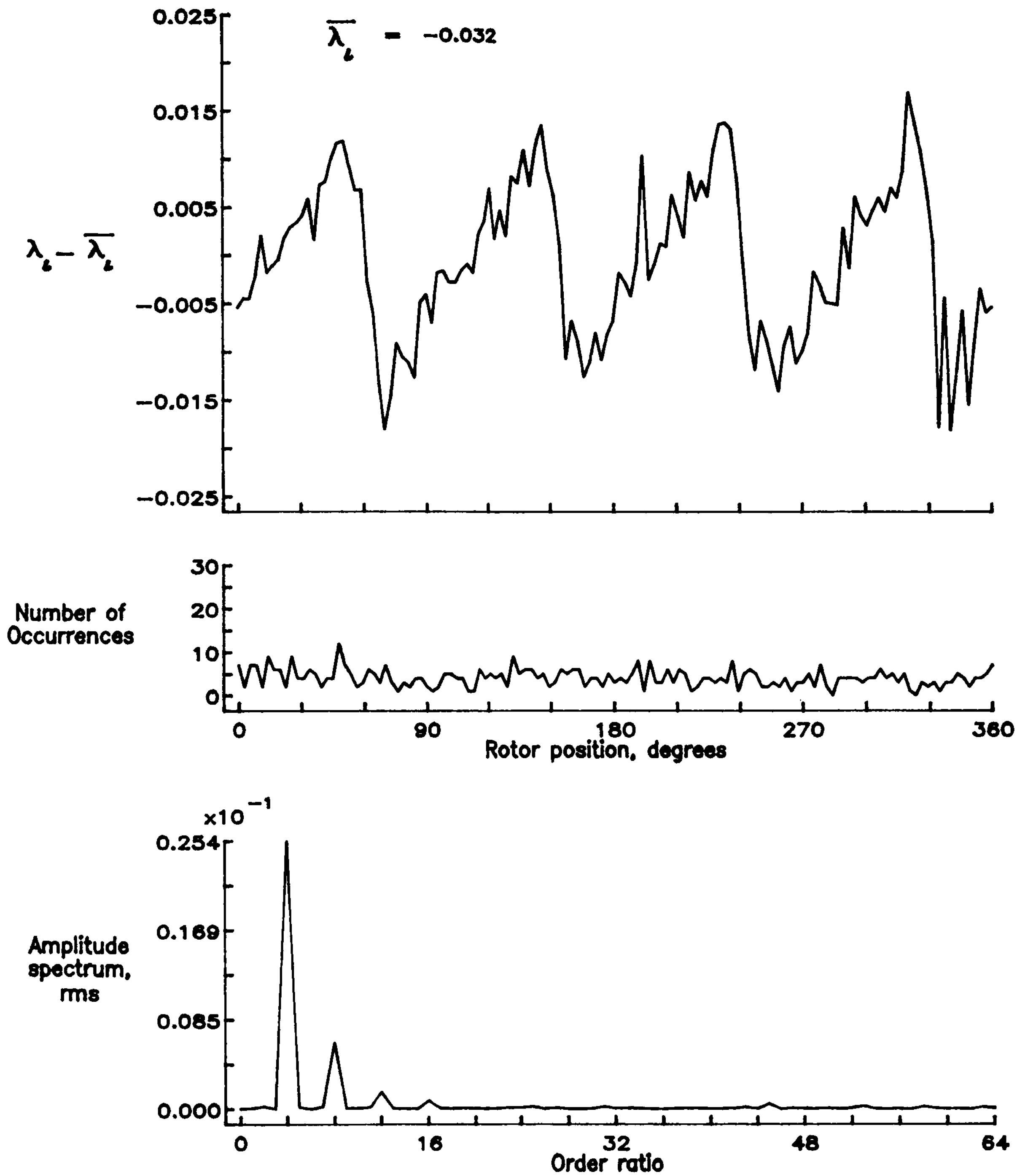

Figure 148.– Concluded.

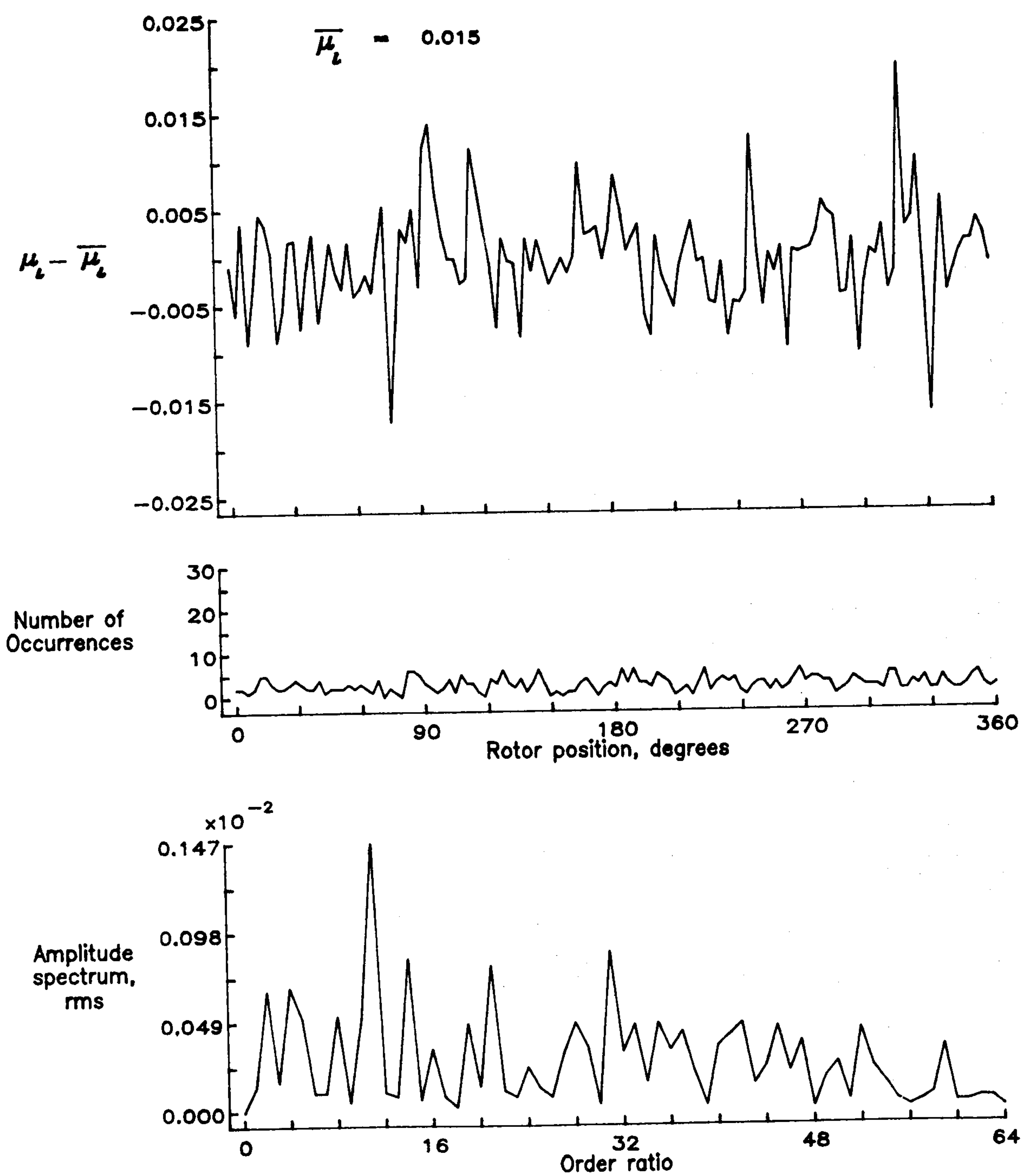

Figure 149.– Induced inflow velocity measured at 330 degrees and r/R of 0.70.

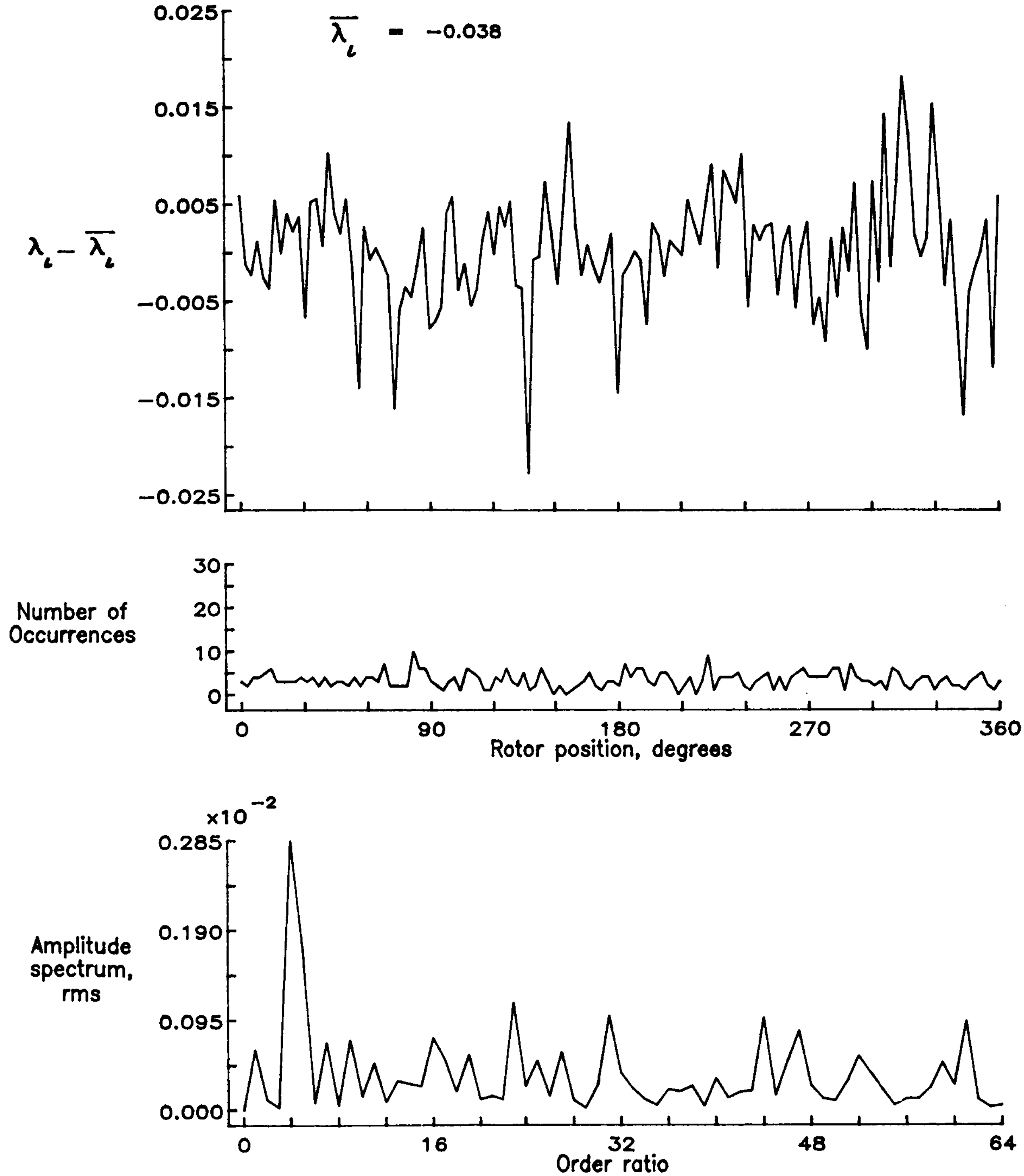

Figure 149.– Concluded.

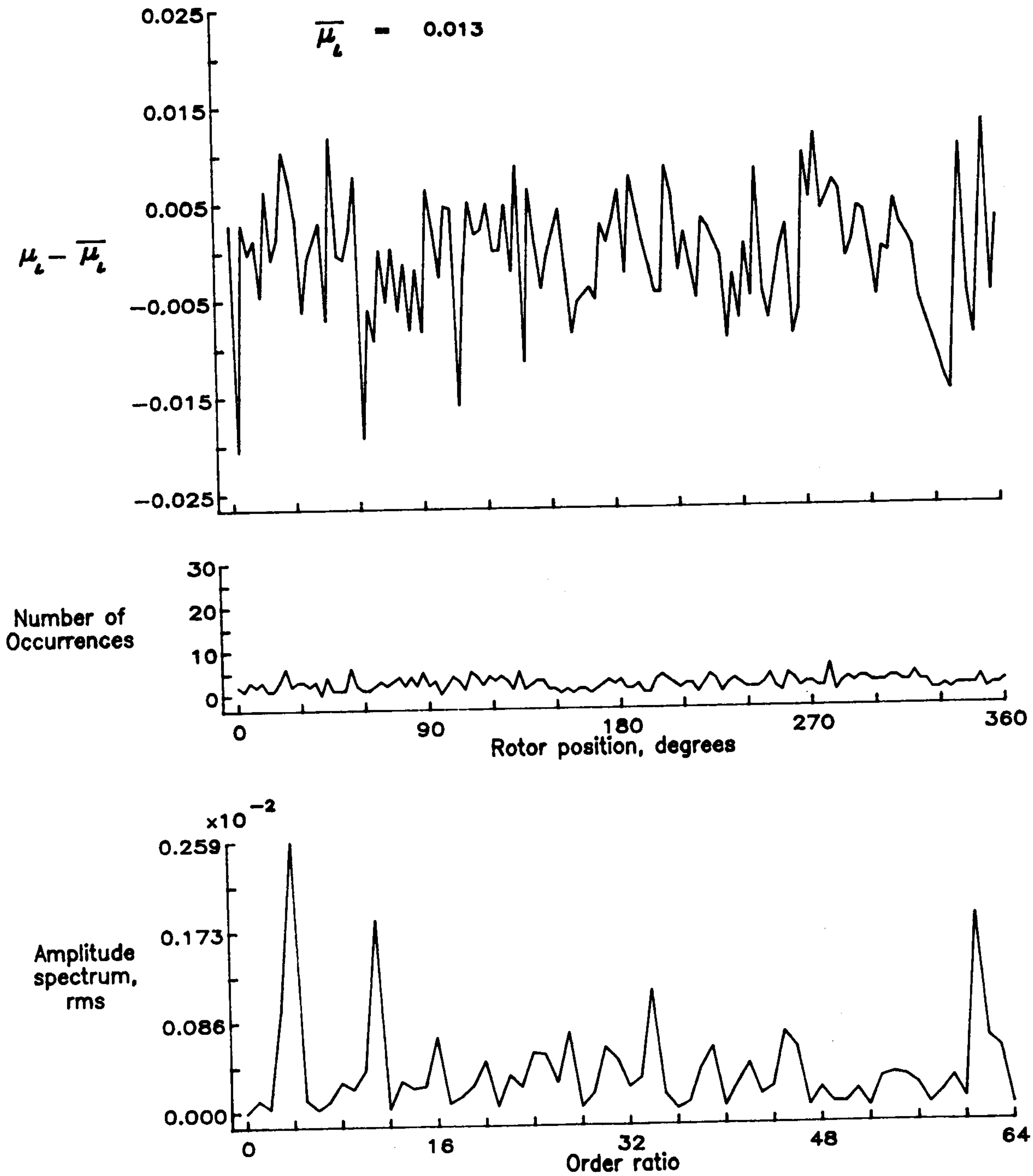

Figure 150.— Induced inflow velocity measured at 330 degrees and r/R of 0.74.

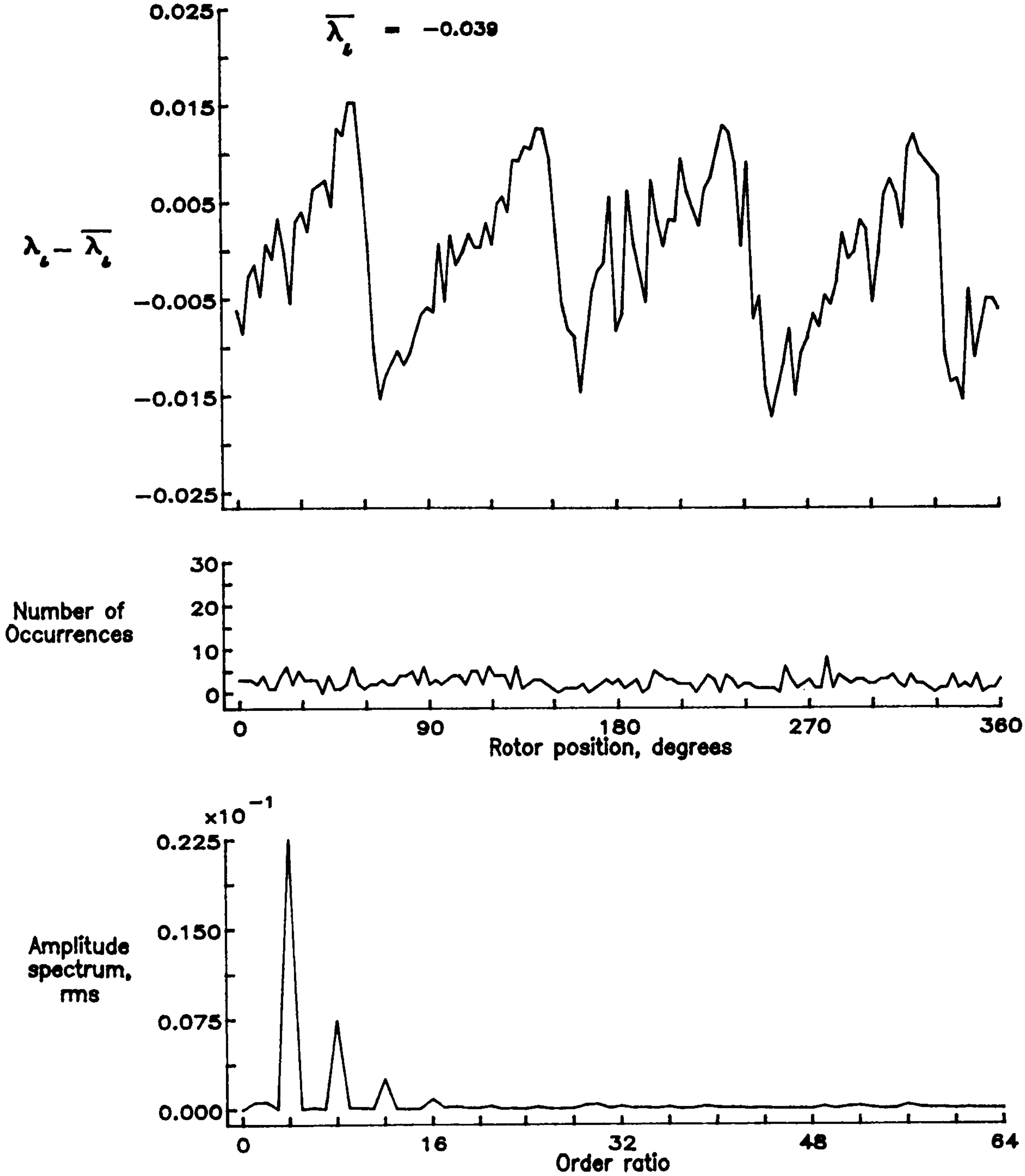

Figure 150.– Concluded.

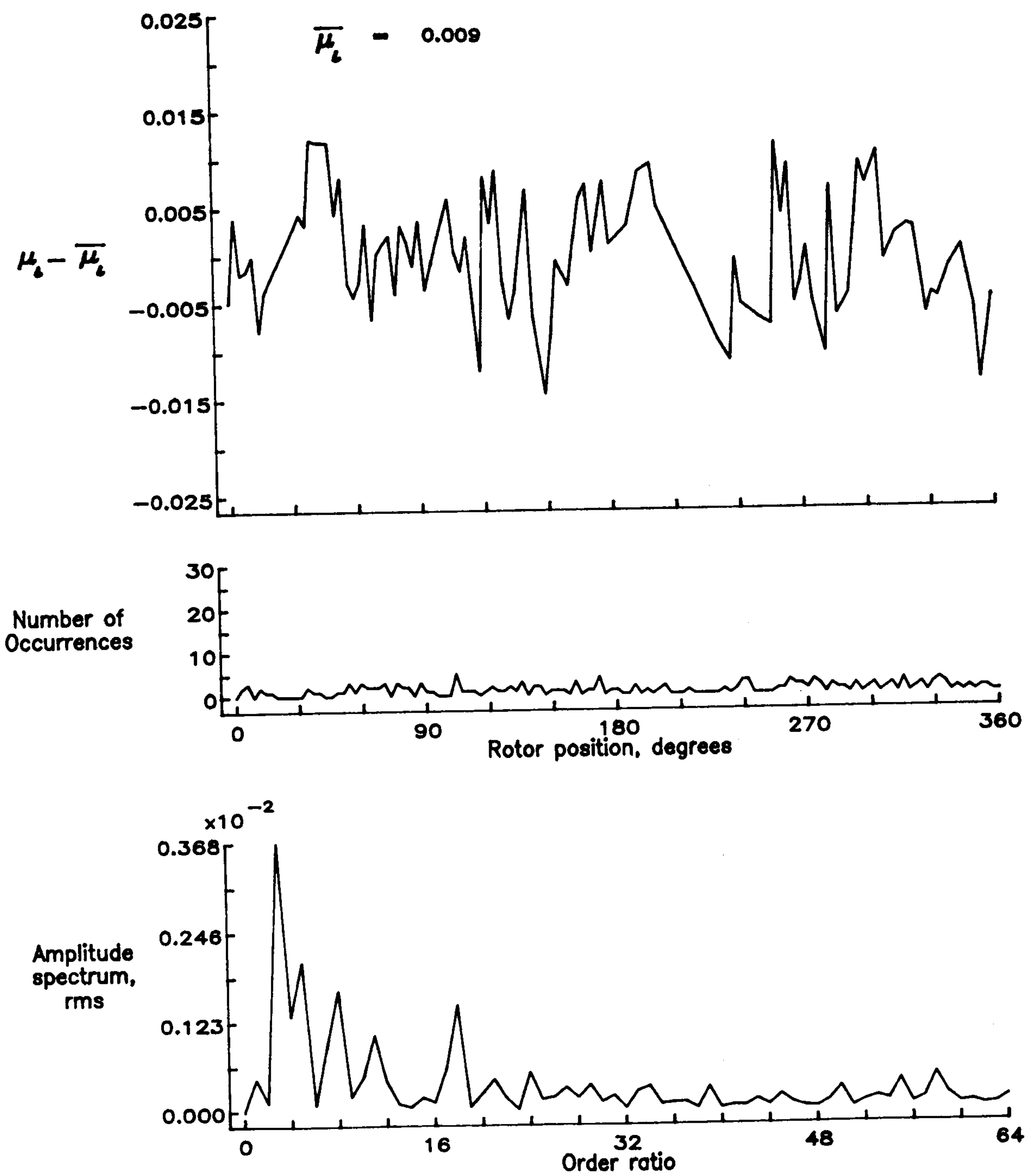

Figure 151.– Induced inflow velocity measured at 330 degrees and r/R of 0.78.

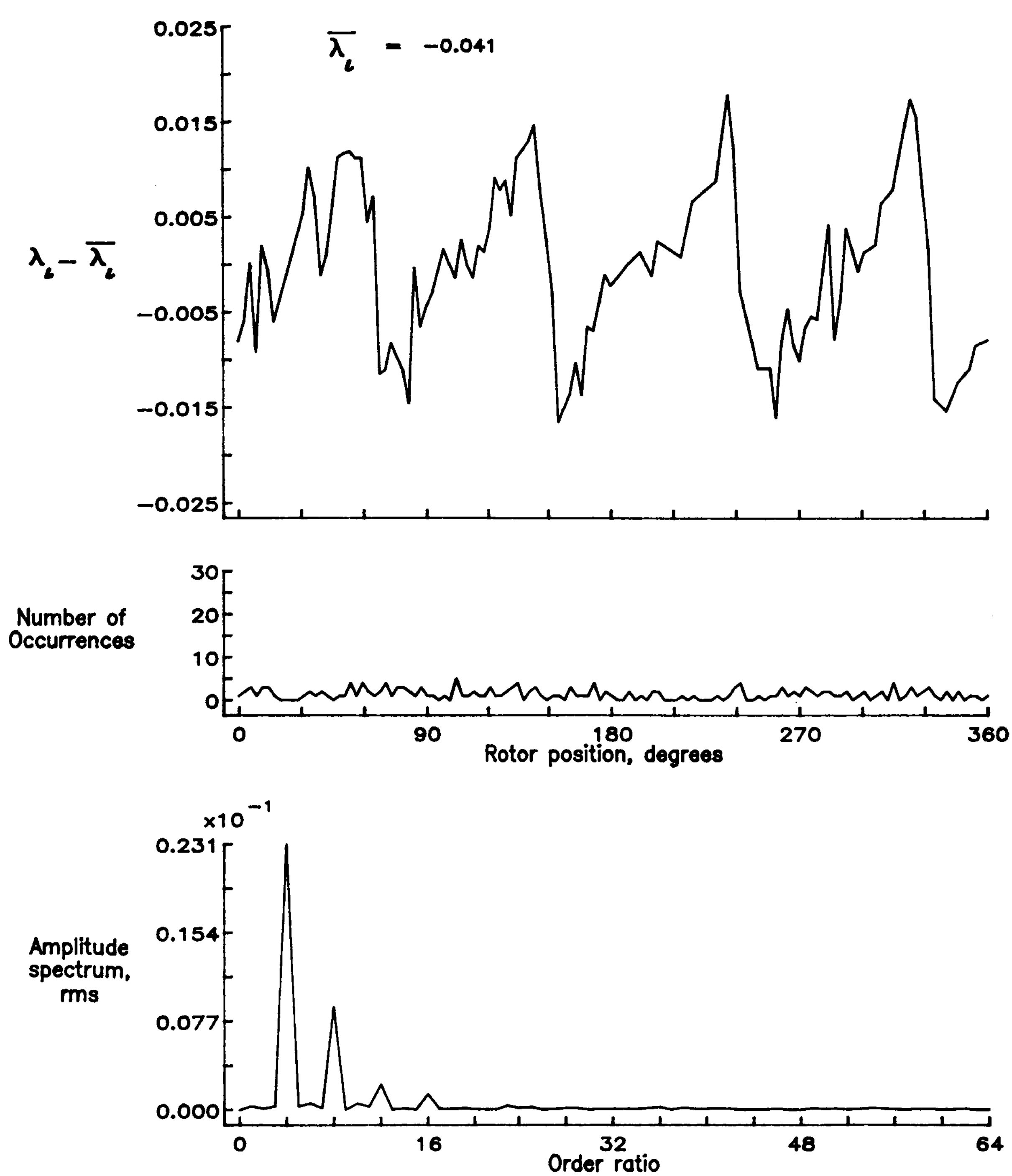

Figure 151.– Concluded.

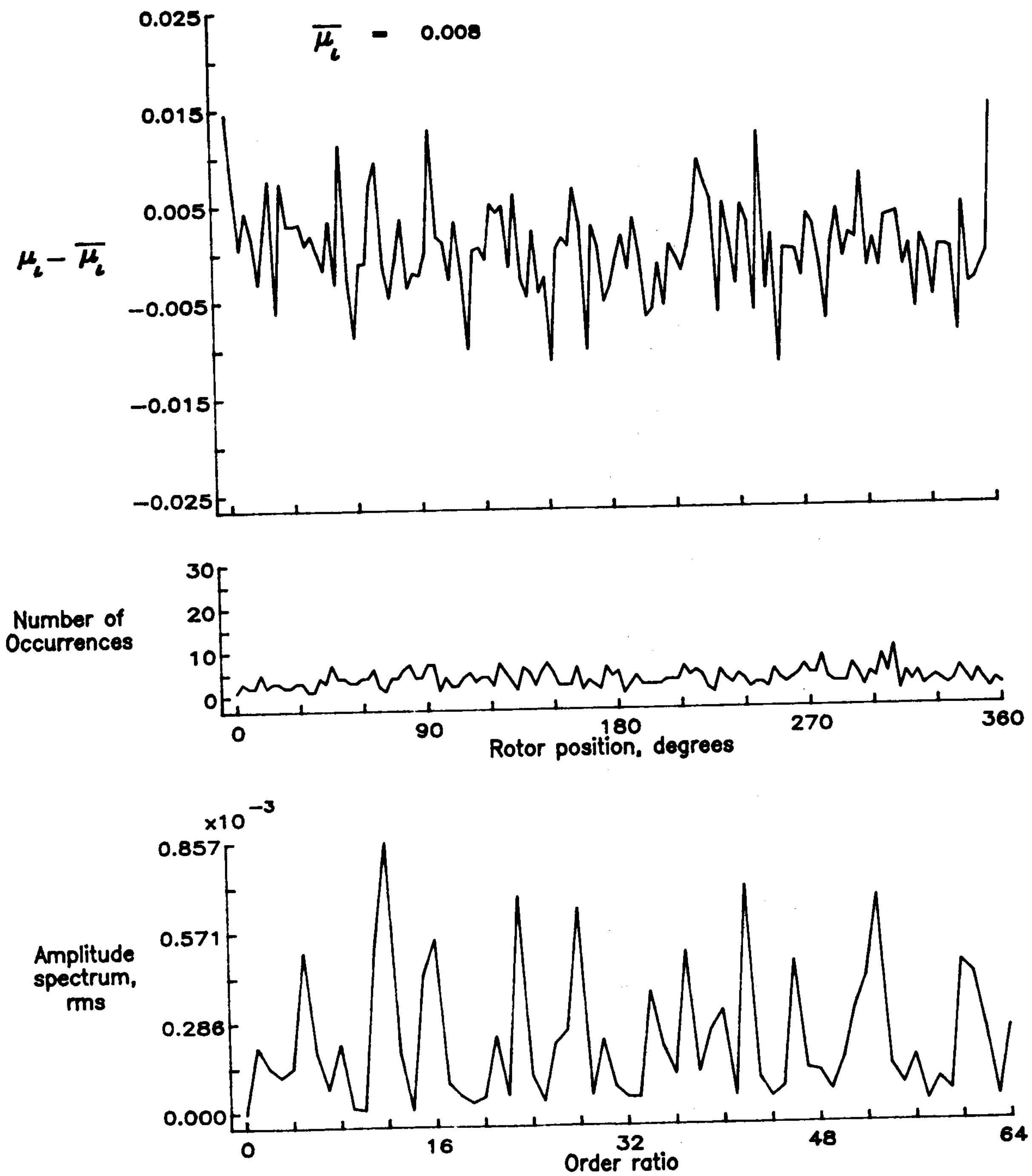

Figure 152.– Induced inflow velocity measured at 330 degrees and r/R of 0.82.

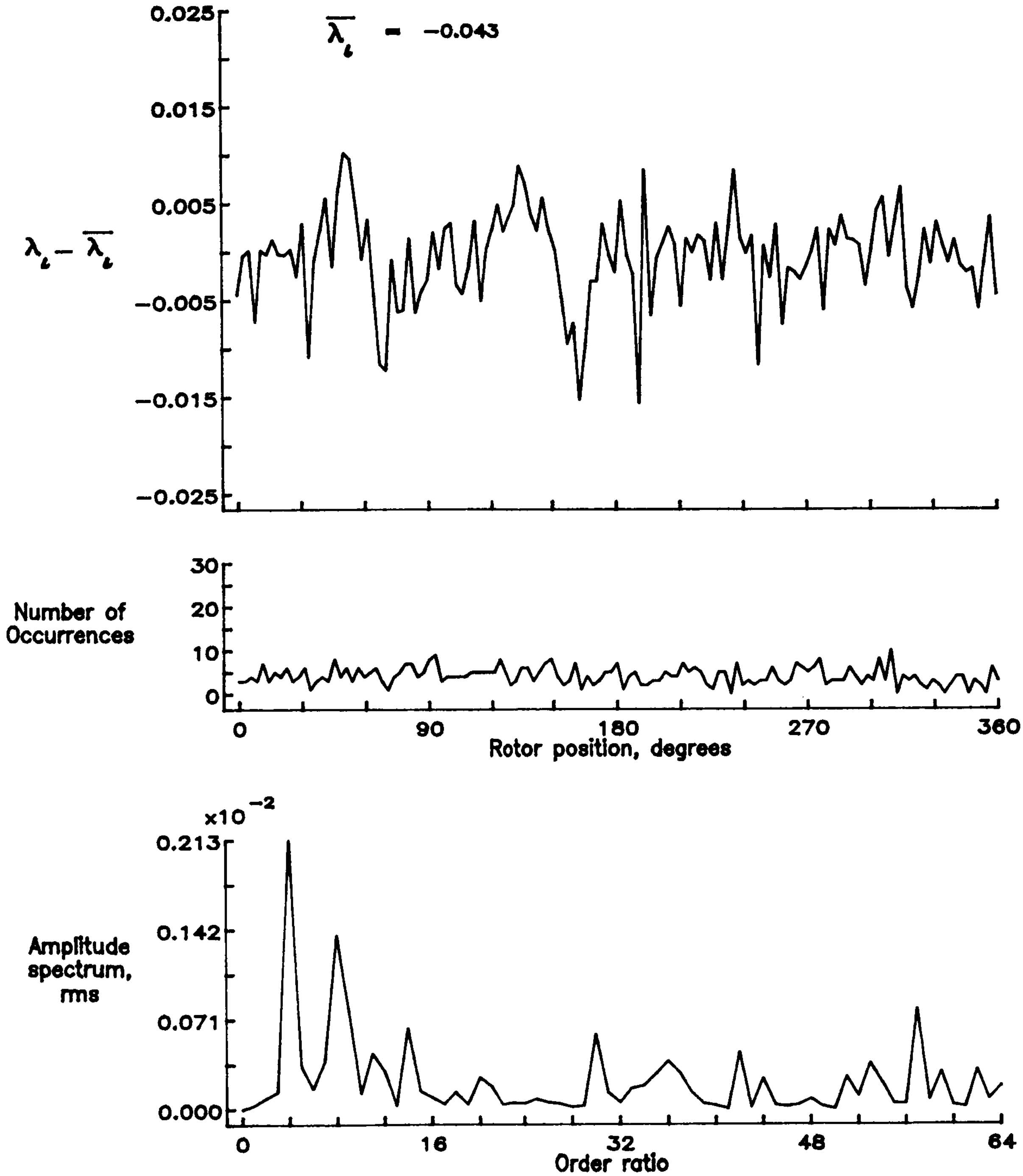

Figure 152.– Concluded.

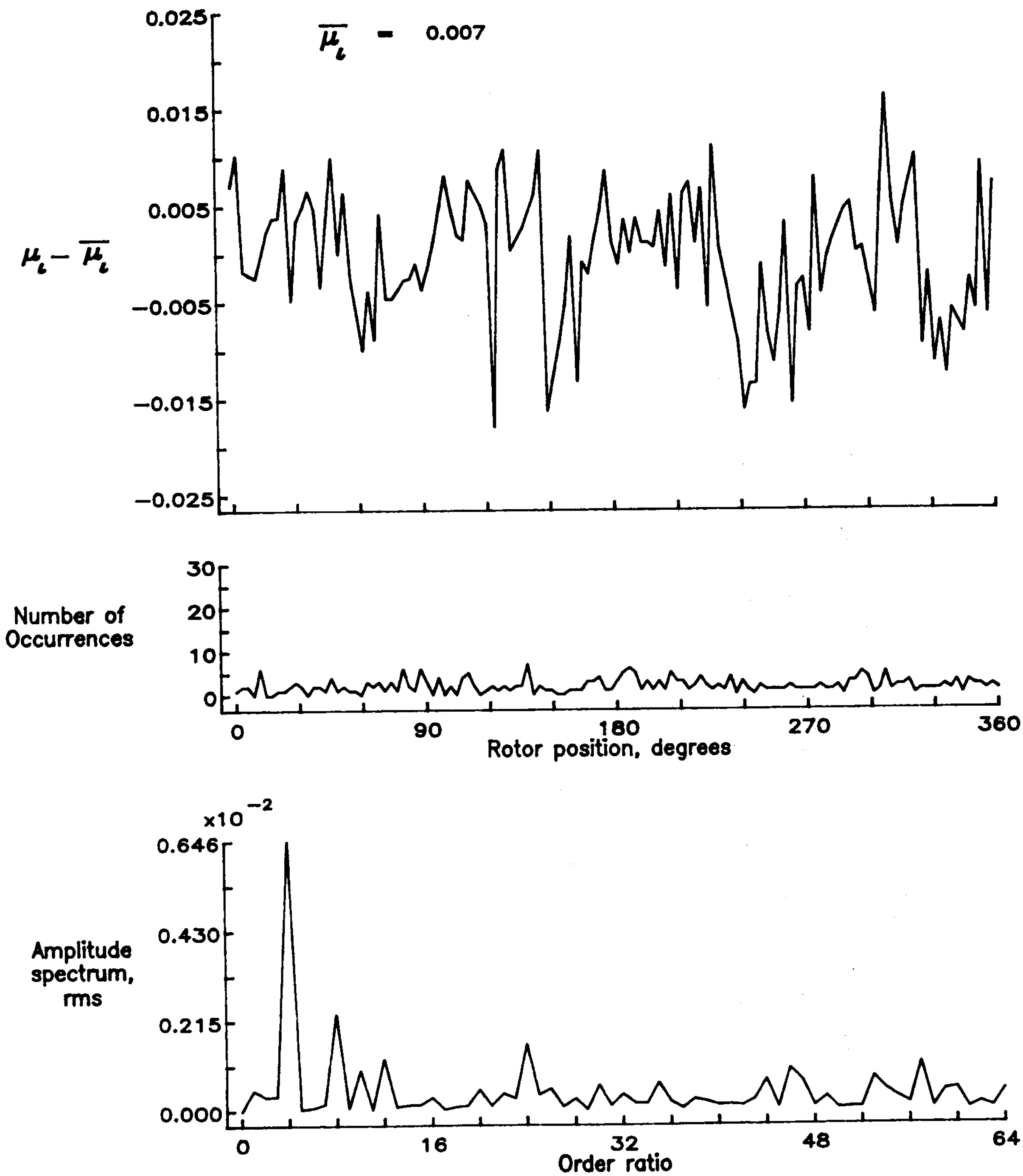

Figure 153.– Induced inflow velocity measured at 330 degrees and r/R of 0.86.

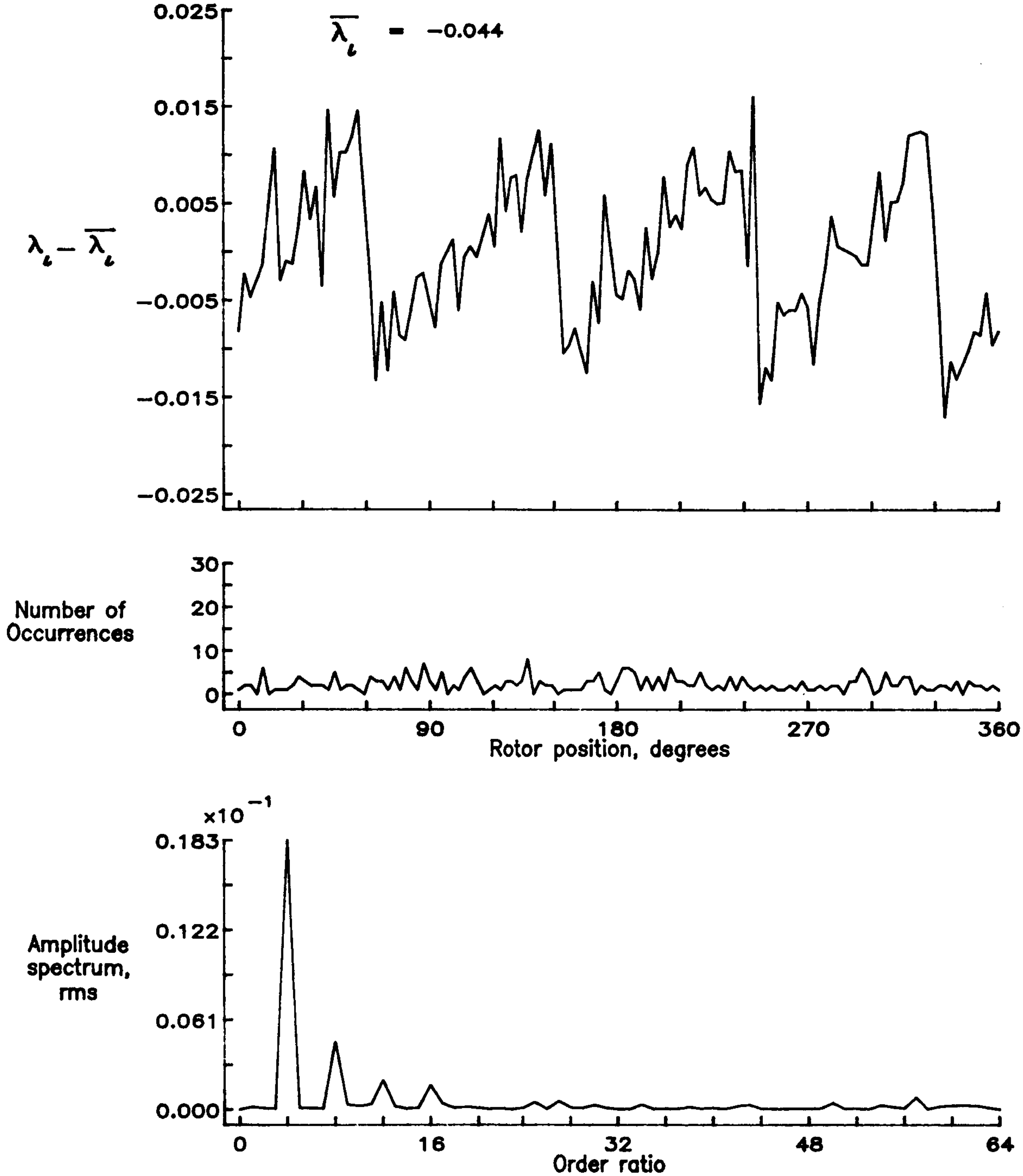

Figure 153.– Concluded.

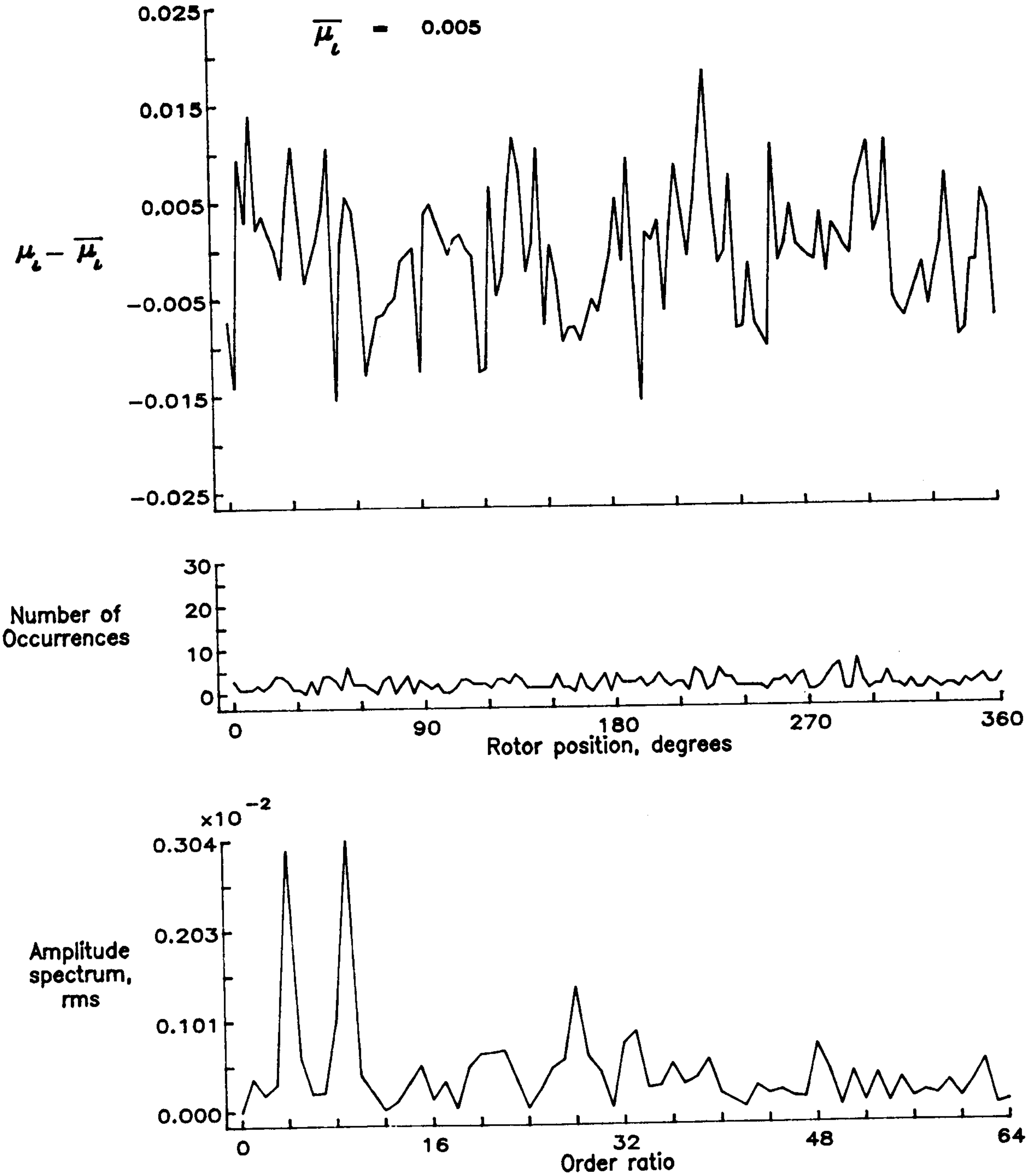

Figure 154.— Induced inflow velocity measured at 330 degrees and r/R of 0.90.

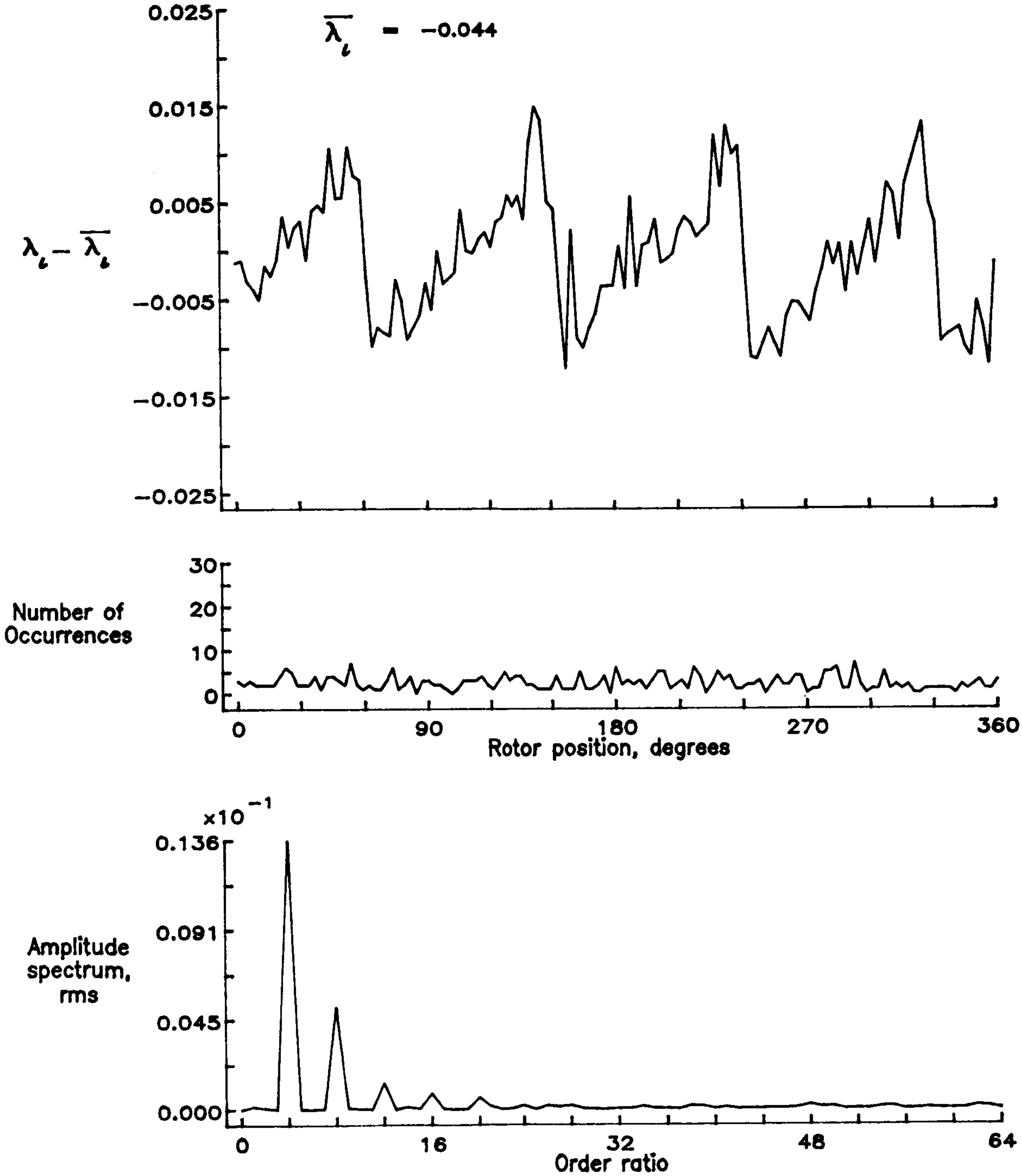

Figure 154.– Concluded.

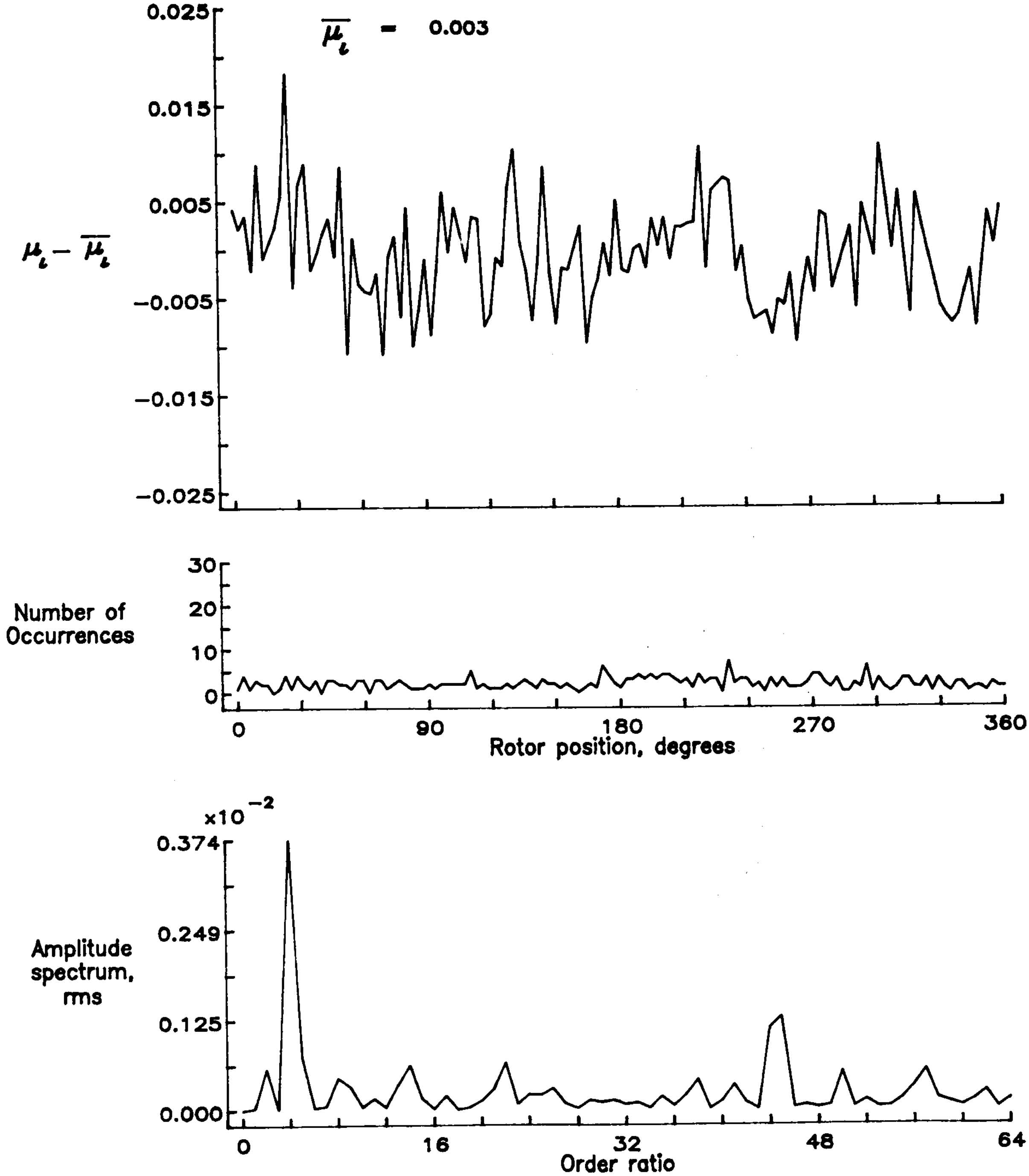

Figure 155.– Induced inflow velocity measured at 330 degrees and r/R of 0.94.

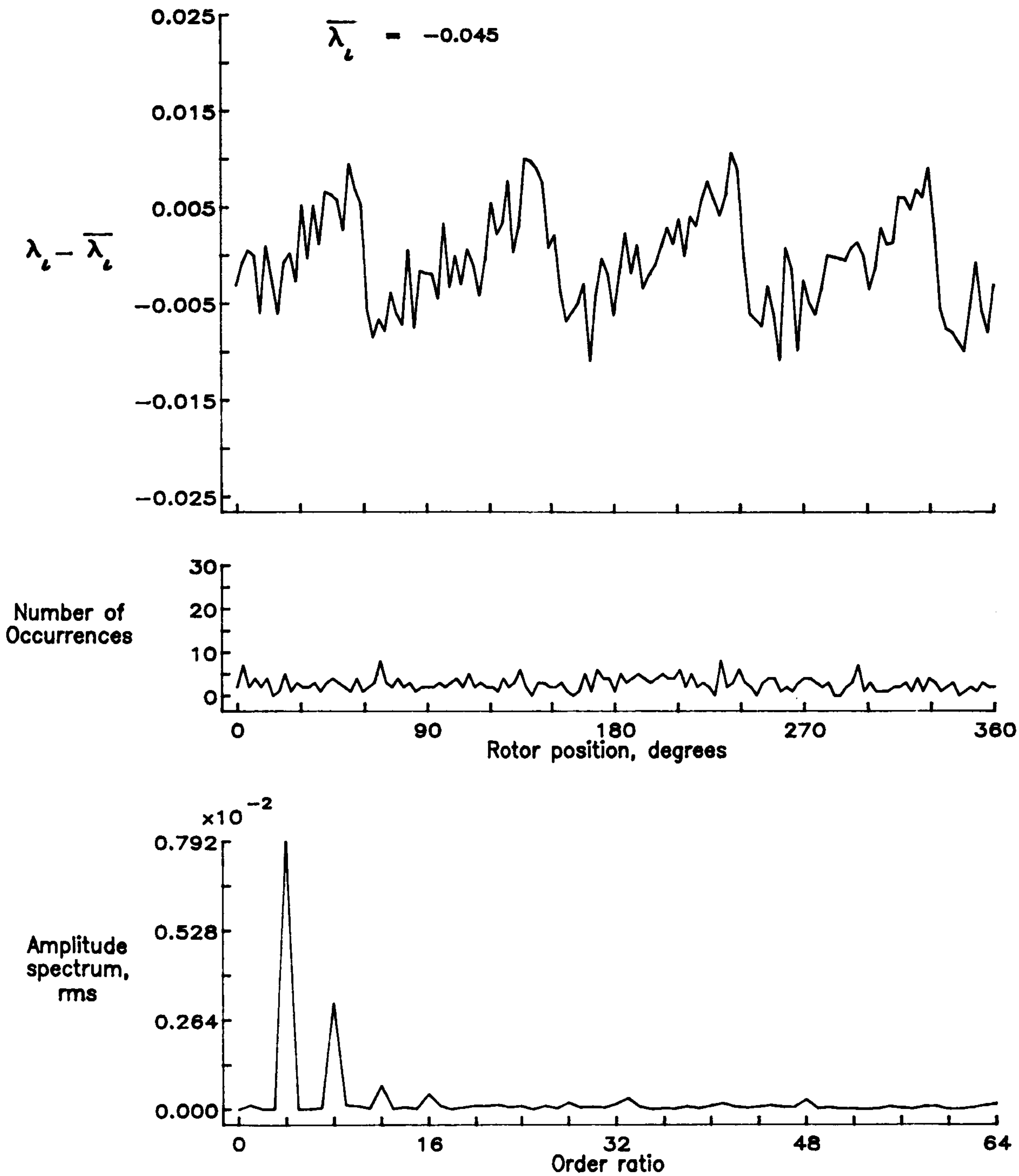

Figure 155.– Concluded.

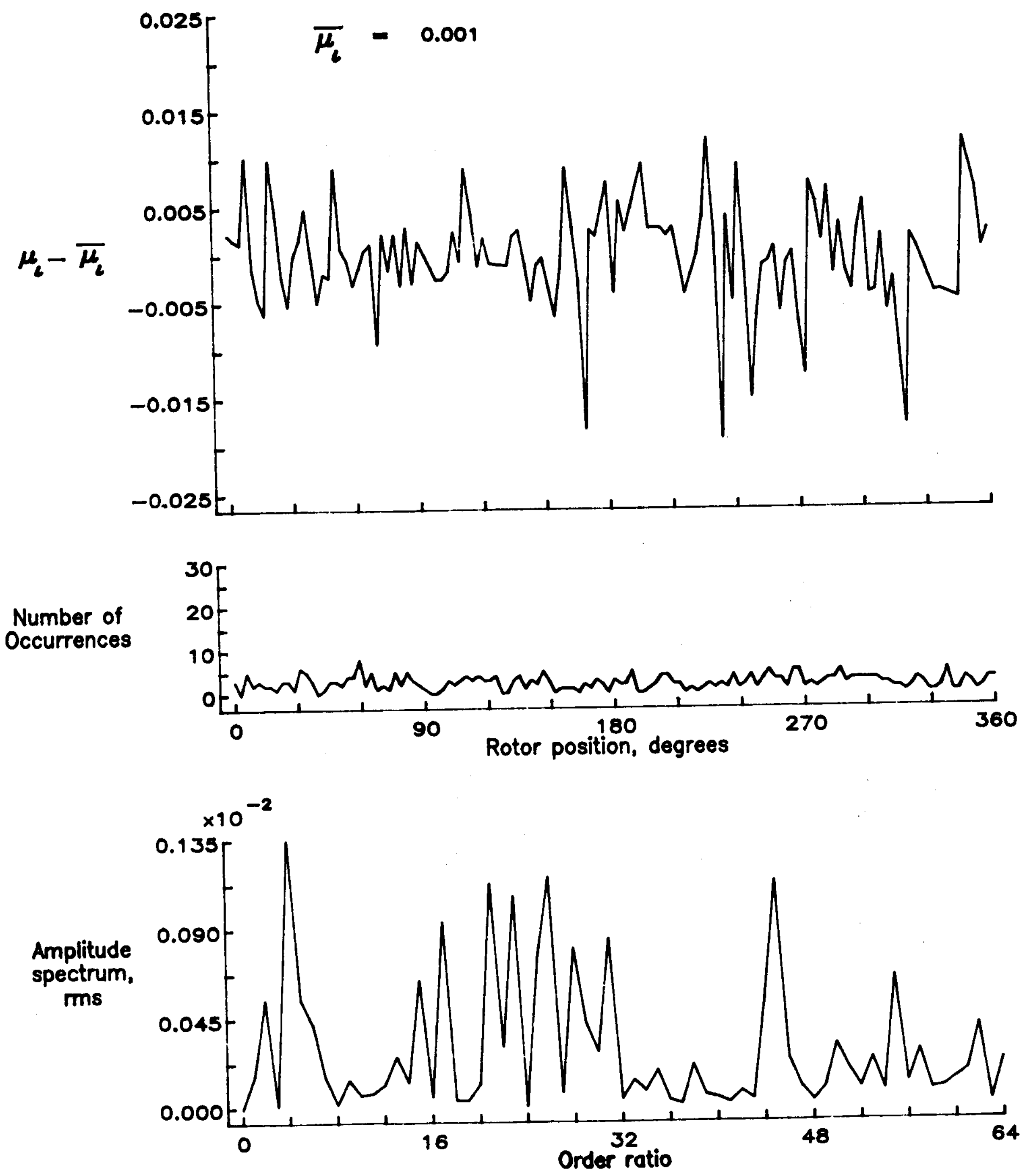

Figure 156.– Induced inflow velocity measured at 330 degrees and r/R of 0.98.

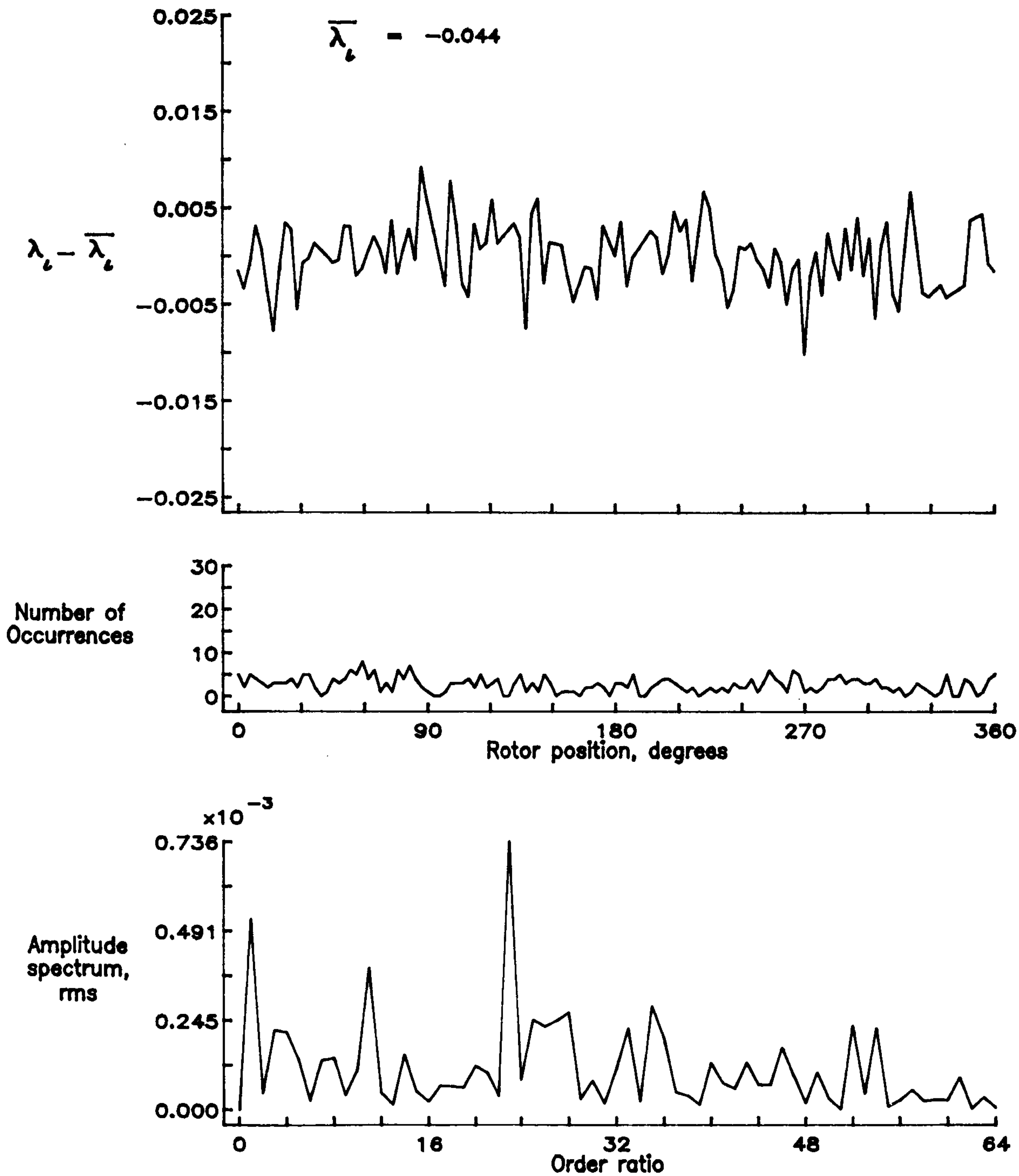

Figure 156.– Concluded.

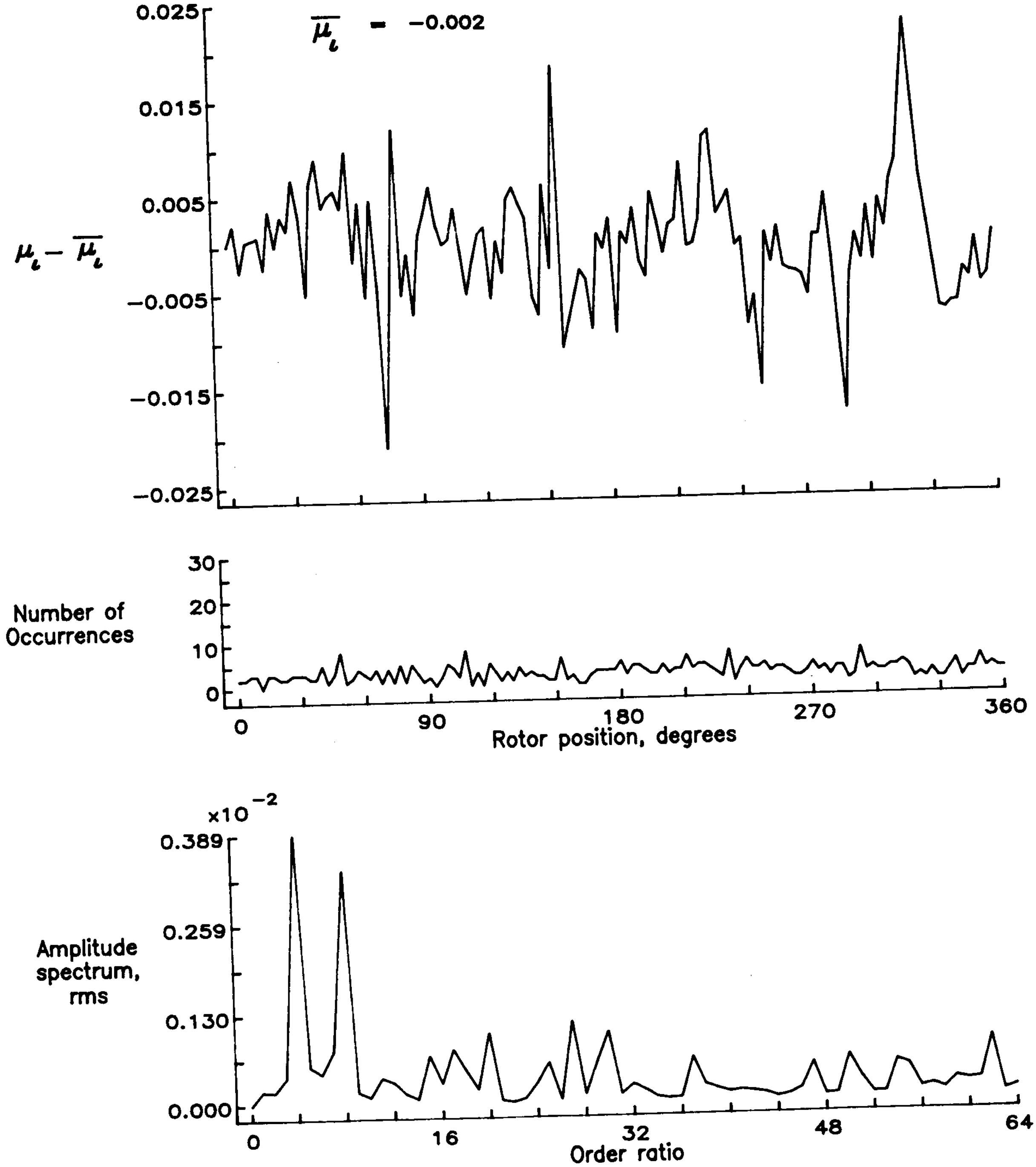

Figure 157.– Induced inflow velocity measured at 330 degrees and r/R of 1.04.

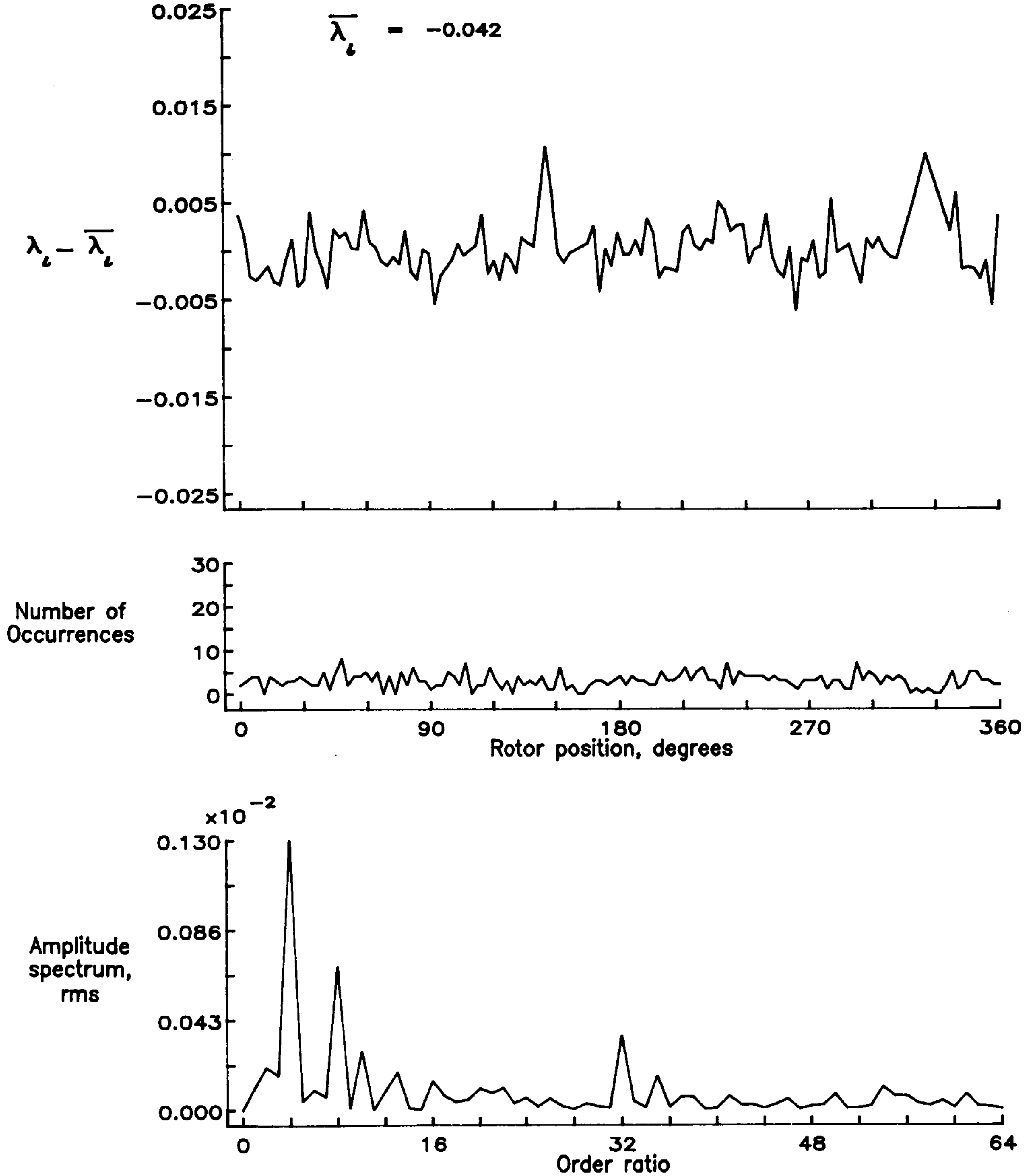

Figure 157.– Concluded.

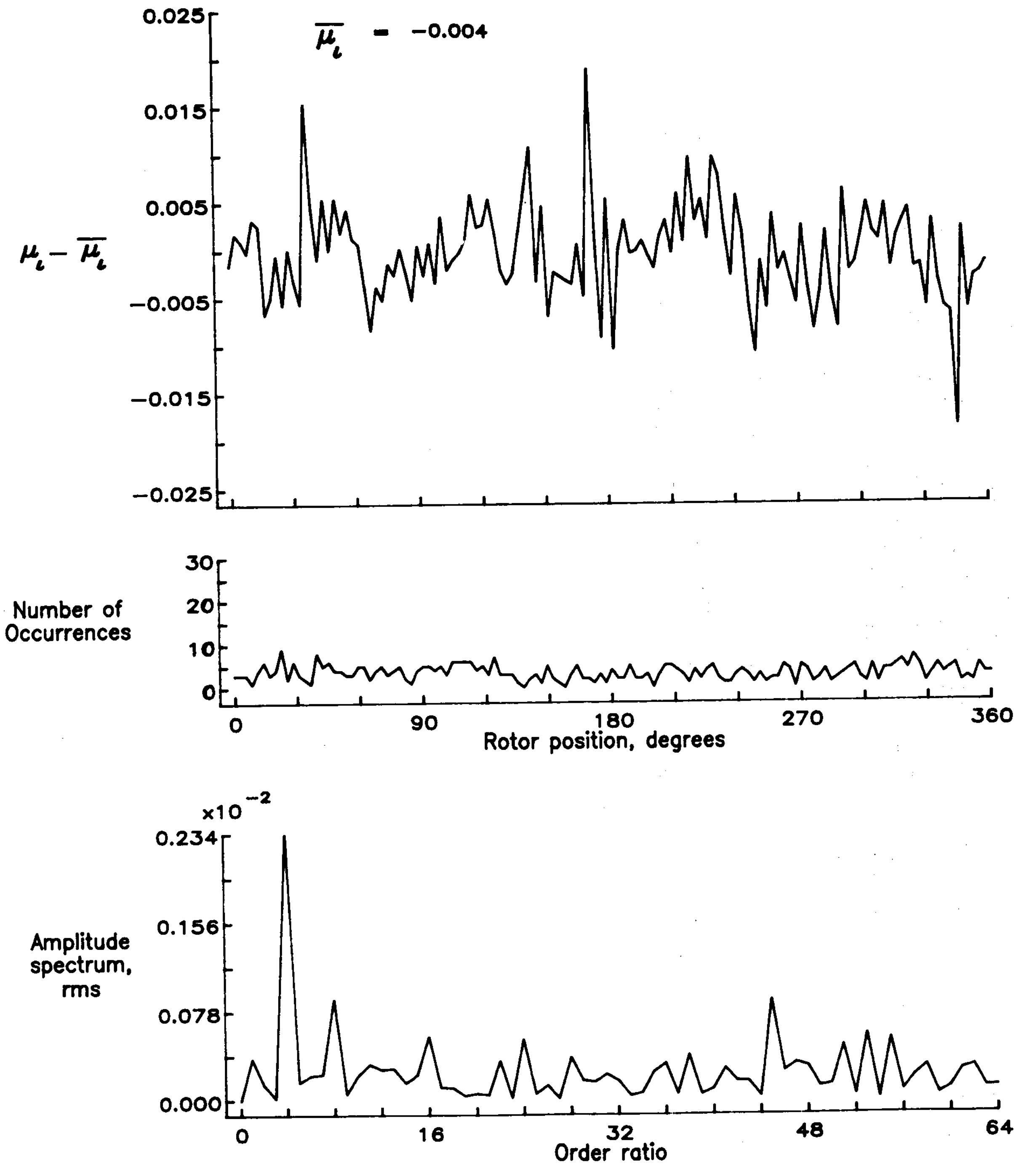

Figure 158.– Induced inflow velocity measured at 330 degrees and r/R of 1.10.

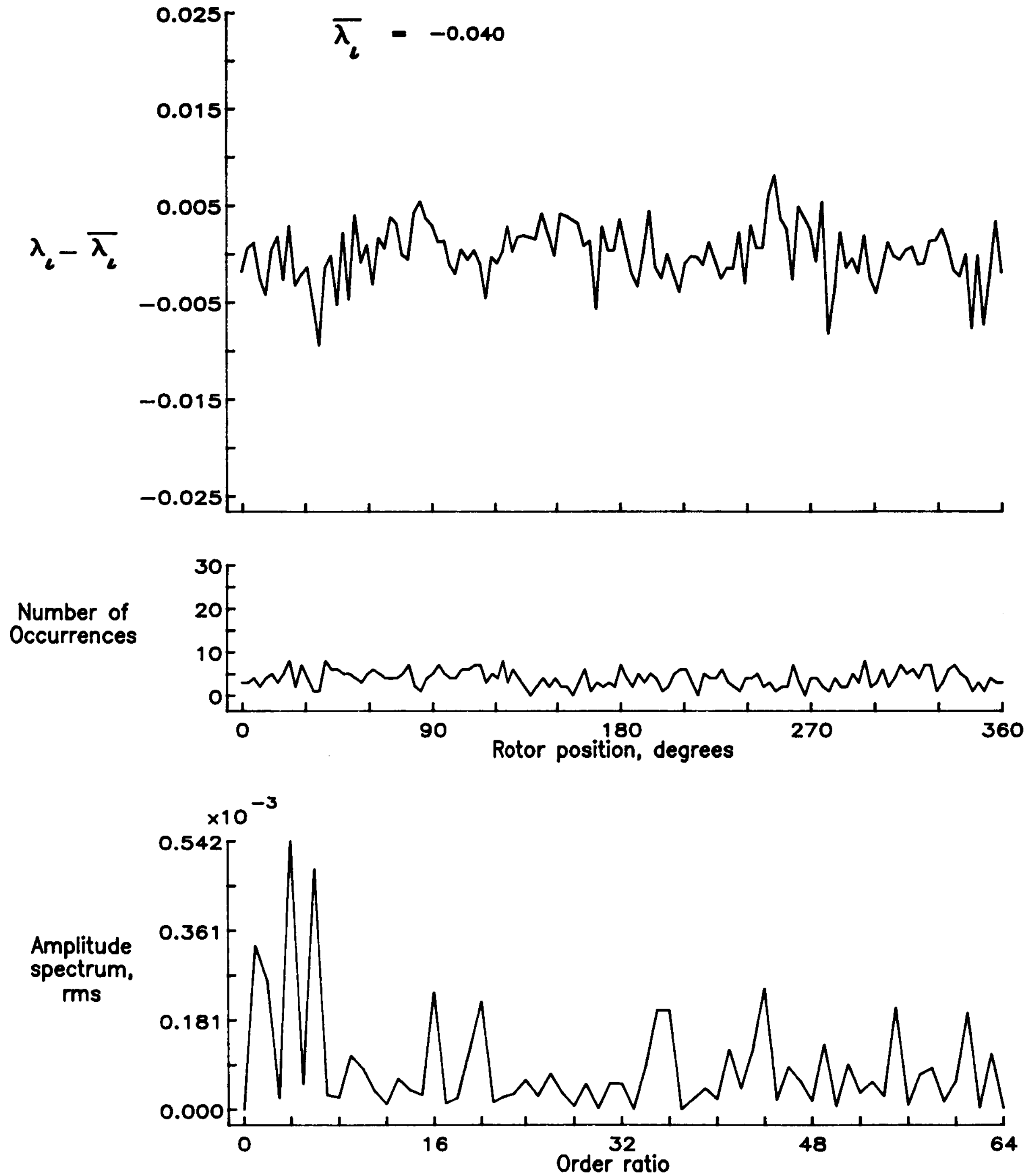

Figure 158.– Concluded.

NASA
National Aeronautics and Space Administration

Report Documentation Page

1. Report No.	2. Government Accession No.	3. Recipient's Catalog No.
NASA TM-100544 AVSCOM TM 88-B-007		

4. Title and Subtitle	5. Report Date
Inflow Measurements Made With A Laser Velocimeter On A Helicopter Model In Forward Flight, Volume IV Tapered Planform Blades at an Advance Ratio of 0.15	April 1988
	6. Performing Organization Code
7. Author(s)	8. Performing Organization Report No.
Susan L. Althoff, Joe W. Elliott, and Richard H. Sailey	
	10. Work Unit No.
9. Performing Organization Name and Address	11. Contract or Grant No.
Aerostructures Directorate USAARTA-AVSCOM Langley Research Center Hampton, VA 23665-5225	505-61-51-10
	13. Type of Report and Period Covered
12. Sponsoring Agency Name and Address	Technical Memorandum
National Aeronautics and Space Administration Washington, DC 20546-0001 and US Army Aviation Systems Command St. Louis, MO 63120-1798	14. Sponsoring Agency Code

15. Supplementary Notes

Susan L. Althoff and Joe W. Elliott: Aerostructures Directorate, USAARTA-AVSCOM, Langley Research Center, Hampton, VA
Richard H. Sailey: Planning Research Corporation, Hampton, VA

16. Abstract

An experimental investigation was conducted in the 14- by 22-Foot Subsonic Tunnel at NASA Langley Research Center to measure the inflow into a scale model helicopter rotor in forward flight ($\mu_\infty = 0.15$). The measurements were made with a two-component Laser Velocimeter (LV) one chord above the plane formed by the path of the rotor tips (tip path plane). A conditional sampling technique was employed to determine the position of the rotor at the time that each velocity measurement was made so that the azimuthal fluctuations in velocity could be determined. Measurements were made at a total of 146 separate locations in order to clearly define the inflow character. This data is presented herein without analysis. In order to increase the availability of the resulting data, both the mean and azimuthally dependent values are included as part of this report on two 5.25 inch floppy disks in Microsoft Corporation MS-DOS format.

17. Key Words (Suggested by Author(s))	18. Distribution Statement
Rotor model Inflow Laser Velocimetry	Unclassified - Unlimited Subject Category 02

19. Security Classif. (of this report)	20. Security Classif. (of this page)	21. No. of pages	22. Price
Unclassified	Unclassified	321	

NASA FORM 1626 OCT 86